НАЦІОНАЛЬНА АКАДЕМІЯ НАУК УКРАЇНИ
ІНСТИТУТ ФІЗІОЛОГІЇ ім. О.О. БОГОМОЛЬЦЯ

Кваліфікаційна наукова
праця на правах рукопису

КОПАЧ ОЛЬГА ВОЛОДИМИРІВНА

УДК 612.812:611.813.14

ДИСЕРТАЦІЯ

КЛІТИННІ ТА МОЛЕКУЛЯРНІ СПІНАЛЬНІ МЕХАНІЗМИ НОЦИЦЕПЦІЇ ЯК МІШЕНІ ДЛЯ КОРЕГУВАННЯ ХРОНІЧНИХ БОЛЬОВИХ СИНДРОМІВ

03.00.13 – Фізіологія людини і тварин
Біологічні науки

Подається на здобуття наукового ступеня доктора біологічних наук

Дисертація містить результати власних досліджень. Використання ідей, результатів і текстів інших авторів мають посилання на відповідне джерело
_____ О.В. Копач

Науковий консультант: Войтенко Нана Володимирівна
доктор біологічних наук,
професор

Київ – 2020

АНОТАЦІЯ

Копач О.В. Клітинні та молекулярні спільнальні механізми ноцицепції як мішені для корегування хронічних больових синдромів. – Кваліфікаційна наукова праця на правах рукопису за сукупністю наукових статей.

Дисертація на здобуття наукового ступеня доктора біологічних наук за спеціальністю 03.00.13 «Фізіологія людини і тварин». – Інститут фізіології ім. О.О. Богомольця НАН України, Київ, 2020.

У дисертаційній роботі представлено комплексне дослідження клітинних та молекулярних механізмів, що залучені у підтримання хронічного болю різного генезу, у сенсорних нейронах спинного мозку. Основна увага була зосереджена на встановленні ролі та регуляції функціювання AMPA-рецепторів у нейронах дорзального рогу (ДР) спинного мозку за наявності хронічних больових синдромів різного генезу, а саме периферичного запалення та травми спинного мозку.

Міжнародна асоціація з вивчення болю (IASP) розглядає хронічний або постійний біль як біль, що «відірвався» від основного захворювання і набув «надорганного» характеру; біль як багатофакторний патологічний феномен, часто автономний: такий, що сам себе підтримує. Хронічний біль може отримувати риси хвороби («біль як хвороба»); цей стан проявляється не лише болем, але й вегетативними, емоційними та психічними порушеннями і потребує серйозної терапії. Причиною невдачі при лікуванні хронічного болю, за висновками ВООЗ, є, найперше, відсутність повноцінної наукової концепції щодо фундаментальних механізмів виникнення та підтримання хронічного болю, основою якої були б результати ґрунтовних науково-експериментальних досліджень для подальшої розробки нових підходів до терапії болю. Відповідно, одним із фундаментальних завдань, які матимуть вагоме біомедичне (клінічне) значення, є з’ясування молекулярних та клітинних

механізмів розвитку хронічного болю – як у центральній нервовій системі (ЦНС), так і периферичній – для пошуку перспективних мішеней у терапії больових синдромів та можливості ефективного полегшення больових відчуттів.

Метою роботи було з'ясування спінальних механізмів ноцицепції для подальшого пошуку та обґрунтування новітніх біотехнологічних підходів для корекції хронічних больових синдромів.

У роботі було використано комплекс різноманітних **методів** для проведення **експериментальних досліджень** у галузі сучасної фізіології та біомедицини. Усі експерименти проводили на лабораторних тваринах із дотриманням міжнародних принципів Європейської конвенції про захист хребетних тварин, які використовуються в експериментальних та інших наукових цілях, та статті 26 Закону України «Про захист тварин від жорстокого поводження» (№3447-IV, 21.02.2006), а також усіх норм біоетики та біологічної безпеки, прийнятих в установах НАН України.

Моделювання хронічного болю різного генезу проводили шляхом а) індукування постійного периферичного запалення внаслідок підшкірної ін'єкції запального агента CFA у задню кінцівку тварин та б) травми спинного мозку при його половинній перерізці (гемісекції). У деяких експериментах проводили моделювання хронічного нейропатичного болю (нейропатії трійчастого лицевого нерва) шляхом перетяжки інфраорбітального нерву лігатурою.

Оцінку больових синдромів у тварин проводили із використанням низки поведінкових тестів для визначення порогу болю у відповідь на теплові (метод Харгрівса) та механічні (метод філаментів фон Фрея) стимули та кількісного міжгрупового порівняння досліджуваних показників (поведінкових проявів больових відчуттів) із застосуванням методів варіаційної статистики при кількісній обробці результатів.

Фізіологічні методи включали локальне введення тест-речовин в інтратекальний простір спинного мозку після хронічної імплантації катетеру у поперековий відділ спинного мозку через атланто-окципітальну мембрану, а також отримання зрізів спинного мозку.

Біофізичні підходи включали реєстрацію іонних струмів у режимі локальної фіксації мембранного потенціалу (patch-clamp) у конфігурації "ціла клітина" (whole-cell) та флуоресцентне вимірювання внутрішньоклітинної концентрації іонів кальцію ($[Ca^{2+}]_i$). У роботі були також використані молекулярно-біологічні методи (використання полімеразної ланцюгової реакції у реальному часі (real-time PCR) та визначення рівня експресії білка (Western-blot) у тканині), фармакологічні та математичні методи експериментальних досліджень (оцінка провідностей поодиноких каналів з використанням нестаціонарного флуктуаційного аналізу струмів, опосередкованих активацією AMPA-рецепторів), застосування підходів генної інженерії (нокдаун гену, що кодує PKCα, за допомогою антисенсових олігонуклеотидів) та нанотехнологій (полімерні мікросфери для депонування та контрольованого вивільнення тест-сполук).

Отримані експериментальні дані свідчать про низку нових аспектів у функціонуванні складного комплексу клітинних та молекулярних спінальних механізмів, що залучені у підтримання хронічного болю у нейронних мережах ДР спинного мозку. Виявлені у проведенних дослідженнях порушення трафікінгу AMPA-рецепторів у нейронах ДР вперше в світі демонструють причинно-наслідкові зв'язки між порушеннями регуляції функціювання AMPA-рецепторів на клітинному рівні та розвитком і підтриманням хронічного болю в експериментальних тварин.

Вперше встановлено молекулярний механізм порушеного обігу AMPA-рецепторів – інтерналізація GluR2-вмісних рецепторів із синапсів між первинними аферентами та ноцицептивними нейронами ДР спинного мозку – при тривалому периферичному запаленні. Охарактеризовано каскад

внутрішньоклітинних білків (старгазин, ABP/GRIP, PICK1), які залучені у регуляцію обігу AMPA-рецепторів між синаптичною та позасинаптичними мембранами за участю ключового ферменту протеїнкінази С підтипу α (PKCα).

Вперше експериментально продемонстровано, що в сенсорних нейронах ДР спинного мозку функціонує чисельна популяція позасинаптичних AMPA-рецепторів, які характеризуються змінною проникністю до іонів Ca^{2+}. Встановлено, що різні підтипи нейронів експресують за фізіологічних умов позасинаптичні AMPA-рецептори подібного складу, які містять домінуючу кількість GluR2-субодиниць; це визначає їх низьку проникність до Ca^{2+}. Вперше показано порушення обігу позасинаптичних AMPA-рецепторів при тривалому периферичному запаленні.

Вперше екпериментально показано, що порушення трафікінгу AMPA-рецепторів призводить до змін у балансі між синаптичним збудженням та гальмуванням у нейронних мережах ДР спинного мозку; це, в свою чергу, спричиняє довготривалу підвищену збудливість ДР, яка може самопідтримуватися – феномен центральної сенситизації. Останній, як вважається, опосередковує розвиток і підтримання хронічного болю різного генезу. Вперше продемонстровано клітиноспецифічність вищеназваних змін, а саме специфіку порушення обігу AMPA-рецепторів та зміщення балансу збудження-гальмування у сенсорних нейронах різних підтипів.

Розроблено та експериментально обґрунтувано новий підхід для потенційно нової терапії хронічних больових синдромів із врахуванням ключової ролі спінальних механізмів у підтриманні хронічного болю різного походження. В основі такого підходу лежить корегування порушень у ланці молекулярного каскаду, що опосередковує регулювання трафікінгу AMPA-рецепторів у сенсорних нейронах ДР спинного мозку. Уперше продемонстровано терапевтичні ефекти фармакологічного блокування Ca^{2+}-проникних AMPA-рецепторів високоселективними сполуками-інгібіторами нового покоління (активаційнозалежними блокаторами IEM-1460 та IEM-

1925) на полегшення больового синдрому із мінімальними побічними ефектами.

Вперше застосовано генну терапію хронічного болю у експериментальних моделях і продемонстровано істотний терапевтичний ефект блокування експресії спінальної PKCα на послаблення больового синдрому у тварин при тривалому периферичному запаленні. Доведено терапевтичну доцільність корегування порушень молекулярного механізму регуляції трафікінгу AMPA-рецепторів у нейронах ДР спинного мозку (із науковим обґрунтуванням на клітинному рівні) при тривалому периферичному запаленні.

Вперше застосовано новітні підходи у галузі наноінженерії для практичного впровадження з метою корекції хронічного больового синдрому, а також створено цільові системи доставки біологічно активних сполук для потенційного впровадження у терапію болю.

Ключові слова: хронічний біль, спінальні механізми ноцицепції, нейрони дорсального рогу, спинний мозок, AMPA-рецептори, периферичне запалення, травма спинного мозку.

SUMMARY

Kopach O.V. Targeting cellular and molecular spinal mechanisms of nociception for the treatment of chronic pain. – Qualifying scientific work, collection of scientific manuscripts.

The thesis for the Degree of Doctor of Biological Sciences in Human and Animal Physiology (03.00.13). – Bogomoletz Institute of Physiology, National Academy of Science of Ukraine. Kyiv, 2020.

The thesis presents the obtained data of a complex study of the intricate cellular and molecular mechanisms for the maintenance of chronic pain of different aetiology in sensory neurons of the spinal cord. The main focus of the research has been on establishing the role and regulation of AMPA receptor functioning in the dorsal horn (DR) neurons of the spinal cord in chronic pain syndromes of various origins, such as peripheral inflammation and spinal cord injury.

The International Association for the Study of Pain (IASP) defines chronic or persistent pain as pain that has "detached" from the original disease, by overcoming it; pain that represents a multicomponent pathophysiological phenomenon, often autonomous and self-sustaining. Chronic pain can become a disease on its own ("pain as a disease") that can be manifested not only by pain but also by autonomic, emotional and mental disorders and requires specialized treatment. The lack of the effective therapeutic interventions of chronic pain, according to the WHO, is due, first of all, to our incomplete understanding of the fundamental mechanisms underlying the development and maintenance of chronic pain and the absence of a common concept on how to treat pain, which will be based on comprehensive research to pave a way for the development of novel strategies to chronic pain therapy. Hence, among the fundamental issues of important significance in biomedicine (relevant in the clinic) remains deciphering the molecular and cellular mechanisms of chronic pain – both in the central nervous system (CNS) and peripheral one – to figure out perspective targets for the treatment of chronic pain and success in pain relief (alleviated pain behaviour).

The aim of this study has been to elucidate the spinal mechanisms of nociception for further development of novel approaches to alleviate chronic pain syndromes.

In this work, a set of various **methods** was utilized **to carry out research** using state-of-the-art approaches. All experiments were conducted using laboratory animals in full compliance with the international guidelines of the European Convention for the Protection of Vertebrate Animals Used for Experimental and

Other Scientific Purposes and Article 26 of the Law of Ukraine "On Protection of Animals from Cruelty" (№3447-IV, 21.02.2006), in full accord with the protocols approved by bioethics committee in Institutes of National Academy of Science of Ukraine.

For modelling of chronic pain of varied origins, it was utilized (i) persistent peripheral inflammation induced by subcutaneous injection of the inflammatory agent CFA into the hind limb of animals and (ii) spinal cord injury by hemisection of the spinal cord. In some experiments, modelling of chronic neuropathic pain (trigeminal neuropathy) was performed by carrying out ligation of the trigeminal nerve in mice.

For the assessment of pain syndromes, behavioural tests were performed in animals by employing a set of approaches for measuring the pain threshold in response to thermal (Hargreaves method) or mechanical (von Frey method) stimuli, followed by a quantitative comparison between the parameters (the behavioural outcome of pain) in experimental groups, using methods of variation statistics with a quantitative comparison between variables.

Physiological methods included (i) local delivery of test compounds intrathecally into the lumbar segments of the spinal cord through the surgically implanted catheter via the atlanto-occipital membrane; (ii) preparation of acute spinal cord slices for the experiments carried out in tissue.

Biophysical methods consisted of electrophysiology for the recordings of membrane currents in patch-clamp mode (“whole-cell” configuration) and fluorescent measurements of intracellular concentration of free calcium ($[Ca^{2+}]_i$). In the study, there were also used molecular biological methods (real-time polymerase chain reaction (PCR) and measurements of the protein expression level (Western-blot) in tissue), pharmacological and mathematical methods (the assessment of single channel conductance, by applying a non-stationary fluctuation analysis of AMPA receptor-mediated currents), genetic approaches (knockdown of the gene encoding PKCα with antisense oligonucleotides) and nanotechnology (fabrication

of the purpose-designed polymeric microspheres for local delivery and controlled release of a drug).

The obtained data indicate a range of new findings regarding the cellular and molecular spinal mechanisms contributing to the maintenance of chronic pain at the neuronal level in the spinal cord. The revealed changes in AMPA receptor trafficking in the DR neurons have demonstrated, for the first time, the causality between the AMPA receptor dysfunctions at the cellular level and the development and maintenance of chronic pain *in vivo*.

It has been first described the molecular mechanism of impaired AMPA receptor trafficking in persistent peripheral inflammatory conditions – internalization of GluR2-containing receptors from the synapses between primary afferents and nociceptive neurons of the DR of the spinal cord. The cascade of intracellular proteins involved in the molecular basis of dynamic AMPA receptor trafficking was characterized (stargazine, ABP / GRIP, PICK1), with the key role of protein kinase C subtype α (PKCα).

For the first time, it has been experimentally validated the functioning of a large pool of extrasynaptic AMPA receptors in sensory neurons of the spinal cord, which are characterized by variable permeability to Ca^{2+}. It was shown that different neuronal subtypes express extrasynaptic AMPA receptors of a similar composition, those in physiological conditions predominantly contain GluR2 subunits, hence are low permeable to Ca^{2+}. The inflammatory-induced changes in trafficking of extrasynaptic AMPA receptors were first found in the DH neurons during persistent peripheral inflammation.

For the first time, it has been experimentally confirmed that changes in AMPA receptor trafficking lead to a shift in the balance between synaptic excitation and inhibition within the sensory neuronal networks in the spinal cord, causing the hyperexcitability of the DR – central sensitization, a phenomenon that is considered to underlie the development and maintenance of chronic pain of various origins. It was fist demonstrated the cell-specificity of the aforementioned changes. The latter

includes the cell-type-specific changes in AMPA receptor trafficking and the shifted balance between synaptic excitation and inhibition in neuronal subtypes.

New approaches have been developed towards a potentially new strategy for the treatment of chronic pain, considering the key role of spinal mechanisms in the maintenance of chronic pain of various origins, and been experimentally validated. This relies on targeting the impaired molecular mechanism regulating the AMPA receptor trafficking in sensory neurons of the spinal cord. For the first time, there have been demonstrated the therapeutic effects of pharmacological inhibition of Ca^{2+}-permeable AMPA receptors by dicationic compounds (IEM-1460 and IEM-1925), a class of novel highly selective antagonists of these receptors acting in an activity-dependent manner, on the relief of persistent inflammatory pain. Importantly, no detectable detrimental effects were found for such treatment.

In this work, it has been first implemented gene therapy for the treatment of chronic pain. A significant therapeutic effect of knocking down the spinal PKCα expression level on pain relief was shown in animals with persistent peripheral inflammation. The efficacy of targeting the impaired molecular mechanism of spinal AMPA receptor trafficking for alleviating persistent pain has been proved both on pain behaviour in animals *in vivo* and the restored AMPA receptor functioning in sensory neurons of the spinal cord at the cellular level.

For the first time, novel approaches in nanoengineering and materials science have been probed for the treatment of chronic pain. The purposely-designed cargo systems were elaborated for delivery of biologically active compounds, aimed at their potential applications in pain therapy.

Keywords: chronic pain, spinal nociceptive mechanisms, dorsal horn neurons, spinal cord, AMPA receptors, peripheral inflammation, spinal cord injury.

СПИСОК ОПУБЛІКОВАНИХ ПРАЦЬ ЗА ТЕМОЮ ДИСЕРТАЦІЇ

Основні наукові результати дисертації, опубліковані у фахових виданнях, віднесених до першого і другого квартилів **(Q1 і Q2)** відповідно до класифікації SCImago Journal and Country Rank або Journal Citation Reports:

1. Park JS, Voitenko N, Petralia RS, Guan X, Xu JT, Steinberg JP, Takamiya K, Sotnik A, **Kopach O**, Huganir RL, Tao YX. Persistent inflammation induces GluR2 internalization via NMDA receptor-triggered PKC activation in dorsal horn neurons. (2009). *Journal of Neuroscience,* 29(10), 3206-3219. (*Особисто дисертантом проведено частину електрофізіологічних досліджень, статистичну обробку та інтерпретування результатів*).
2. **Kopach O**, Kao SC, Petralia RS, Belan P, Tao YX, Voitenko N. (2011). Inflammation alters trafficking of extrasynaptic AMPA receptors in tonically firing lamina II neurons of the rat dorsal horn. *Pain*, 152(4), 912-923. (*Особисто дисертантом проведено електрофізіологічні та флуоресцентні дослідження, статистичний аналіз та інтерпретування результатів, формулювання висновків та підготовку матеріалів до друку*).
3. **Kopach O**, Viatchenko-Karpinski V, Belan P, Voitenko N. (2012). Development of inflammatory-induced hyperalgesia and allodynia is accompanied by upregulation of extrasynaptic AMPA receptors in tonically firing lamina II dorsal horn neurons. *Frontiers in Physiology,* 3: 391. doi:10.3389/fphys.2012.00391 (*Особисто дисертантом проведено експериментальні дослідження, статистичний аналіз результатів та оформлення статті*).
4. **Kopach O**, Viatchenko-Karpinski V, Atianjoh FE, Belan P, Tao YX, Voitenko N. (2013). PKCα is required for inflammation-induced trafficking of extrasynaptic AMPA receptors in tonically firing lamina II dorsal horn neurons during the maintenance of persistent inflammatory pain. *Journal of Pain,* 14(2), 182-192. (*Особисто дисертантом проведено електрофізіологічні та частину*

поведінкових експериментів, статистичний аналіз та інтерпретування результатів, оформлення статті).

5. **Kopach O**, Voitenko N. (2013). Extrasynaptic AMPA receptors in dorsal horn: evidence and functional significance. *Brain Research Bulletin*. 93, 47-56. (*Особисто дисертантом проведено аналіз даних літератури, оформлення ілюстрацій та написання статті*).

6. **Kopach O**, Krotov V, Belan P, Voitenko N. (2015). Inflammatory-induced changes in synaptic drive and postsynaptic AMPARs in lamina II dorsal horn neurons are cell-type-specific. *Pain,* 156(3), 428-438. (*Особисто дисертантом проведено електрофізіологічні дослідження, інтерпретацію результатів та формулювання висновків, написання статті*).

7. Choi ML[1], Vernon J[1], **Kopach O**[1], Minett MS, Mills K, Clayton PT, Meert T, Wood JN. (2015). The Fabry disease-associated lipid Lyso-Gb3 enhances voltage-gated calcium currents in sensory neurons and causes pain. *Neuroscience Letters,* 594, 163-168. (*Особисто дисертантом проведено електрофізіологічні дослідження, їх аналіз та інтерпретування результатів, написання статті*). ([1] перший автор)

8. Luiz AP[1], **Kopach O**[1], Santana-Varela S, Wood JN. (2015). The role of Nav1.9 channels in the development of neuropathic orofacial pain associated with trigeminal neuralgia. *Molecular Pain,* 11(1), 72. (*Особисто дисертантом проведено частину експериментальних досліджень, аналіз отриманих результатів та написання статті*). ([1] перший автор)

9. **Kopach O**, Krotov V, Goncharenko J, Voitenko N. (2016). Inhibition of spinal Ca^{2+}-permeable AMPA receptors with dicationic compounds alleviates persistent inflammatory pain without adverse effects. *Frontiers in Cellular Neuroscience,* 10:50. (*Особисто дисертантом проведено частину експериментальнах досліджень, статистичний аналіз, формулювання*

висновків та написання статті).

10. **Kopach O**, Medvediev V, Krotov V, Borisyuk A, Tsymbaliuk V, Voitenko N. (2017). Opposite, bidirectional shifts in excitation and inhibition in specific types of dorsal horn interneurons are associated with spasticity and pain post-SCI. *Scientific Reports,* 7(1), 5884. doi: 10.1038/s41598-017-06049-7. (*Особисто дисертантом проведено електрофізіологічні дослідження, аналіз та інтерпретування результатів, написання статті*).

11. **Kopach O**, Krotov V, Voitenko N. (2017). Atlanto-occipital catheterization of young rats for long-term drug delivery into the lumbar subarachnoid space combined with in vivo testing and electrophysiology in situ. *Journal of Neuroscience Methods,* 290, 125-132. (*Особисто дисертантом проведено експериментальні дослідження, аналіз та інтерпретування отриманих результатів, оформлення статті*).

12. **Kopach O**, Zheng K, Dong L, Sapelkin A, Voitenko N, Sukhorukov GB, Rusakov DA. (2018). Nano-engineered microcapsules boost the treatment of peripheral pain. *Drug Delivery,* 25(1), 435-447. (*Особисто дисертантом проведено експериментальні дослідження, аналіз отриманих результатів та написання статті*).

13. **Kopach O**, Krotov V, Shysh A, Sotnic A, Viatchenko-Karpinski V, Dosenko V, Voitenko N. (2018). Spinal PKCα inhibition and gene-silencing for pain relief: AMPAR trafficking at the synapses between primary afferents and sensory interneurons. *Scientific Reports,* 8(1), 10285. doi: 10.1038/s41598-018-28512-9. (*Особисто дисертантом проведено електрофізіологічні дослідження та частину поведінкових експериментів, аналіз та інтерпретування отриманих результатів, написання статті*).

14. **Kopach O,** Zheng K, Sindeeva OA, Gai M, Sukhorukov GB, Rusakov DA. (2019). Polymer microchamber arrays for geometry-controlled drug release: a functional study in human cells of neuronal phenotype. *Biomaterials Science,*

7(6), 2358-2371. (*Особисто дисертантом проведено експериментальні дослідження, аналіз та інтерпретування отриманих результатів, оформлення статті*).

Наукові праці, які засвідчують апробацію матеріалів дисертації:

1. **Kopach O**, Sindeeva O.A., Zheng K., Sukhorukov GB, Rusakov DA. Microchamber arrays for delivery of bioactive compounds: functional testing of cargo release on demand. *Main Meeting of the Physiological Society*. July 8-10, 2019, Aberdeen (United Kingdom). Публікація тез, постерна доповідь.
2. **Kopach O**, Esteras N., Rusakov DA, Abramov AY. Human stem cell models of tau-related dementia: how much are they credible for functional studies of human brain neurodegeneration? *8th Annual Meeting of the Ukrainian Biophysical Society*, Nov. 12-15 2019, Kyiv-Lutsk (Ukraine). Публікація тез, усна доповідь.
3. **Kopach O**, Esteras N., Rusakov DA, Abramov AY. Targeting glutamate receptors: a novel approach to frontotemporal dementia? *10th IBRO World Congress of Neuroscience*, 21-25 September, 2019, Daegu (Korea). Публікація тез, постерна доповідь.
4. **Kopach O**, Esteras N., Rusakov DA, Abramov AY. Electrophysiological study of the iPSC-derived cortical neurons from patients with frontotemporal dementia. UCL Queen Square Institute of Neurology, London/ICM, *Paris Conference*, October 24-26, 2018, Paris (France). Публікація тез, усна доповідь.
5. **Kopach O.**, Esteras N., Rusakov DA, Abramov AY. Pathophysiological excitability of the iPSC-derived cortical neurons from patients with frontotemporal dementia: the role of ionotropic glutamate receptors. *11th FENS Forum of Neuroscience*, July 7-11, 2018, Berlin (Germany). Публікація тез, постерна доповідь.

6. **Kopach O**., Zheng K., Dong L., Sapelkin A., Voitenko N., Sukhorukov G.B., Rusakov D.A. Nano-engineered drug encapsulation: a long-lasting, localised drug delivery in chronic pain treatment. 47th Annual Meeting of Society for Neuroscience, November 11-15, 2017, Washington, DC, USA. Публікація тез, постерна доповідь.
7. **Kopach O**., Medvediev V, Krotov V, Borisyuk A, Tsymbaliuk V, Voitenko N. Reshuffle between synaptic excitation and inhibition in specific types of the DH interneurons mediates chronic pain in the spinal cord injury-induced spasticity. VII Congress of the Ukrainian Society for Neuroscience, June 7-11, 2017, Kyiv, Ukraine. Публікація тез, усна доповідь.
8. **Kopach O.**, Pavlov A., Sanders A., Sapelkin A., Sukhorukov G.B., Rusakov D.A. Cell-targeted drug delivery to neurons using purpose-designed microcapsules. 9th IBRO World Congress of Neuroscience, July 7–11, 2015, Rio de Janeiro (Brazil). Публікація тез, постерна доповідь.
9. Belan P., Krotov V., **Kopach O.**, Voitenko N. Cell-type-specific inflammatory-induced changes in dorsal horn synaptic transmission. 44th Annual Meeting of the Society for Neuroscience, Washington, DC, USA, November 15-19, 2014. Публікація тез, постерна доповідь.
10. **Kopach O.,** Krotov V., Belan P., Voitenko N. Persistent peripheral inflammation rearranges synaptic drive and postsynaptic ampars in lamina II dorsal horn neurons in a cell-type-specific manner. 6th Congress of the Ukrainian Society for Neuroscience, Kiev, Ukraine, 4 - 8 June 2014. Публікація тез, усна доповідь.
11. Voitenko N., **Kopach O.**, Viatchenko-Karpinski V., Belan P. AMPA receptor trafficking in persistent pain: a basis for pain therapies. 6th Congress of the Ukrainian Society for Neuroscience, Kiev, Ukraine, 4 - 8 June 2014. Публікація тез, усна доповідь.
12. **Kopach O.**, Krotov V., Belan P., Voitenko N. Chronic peripheral inflammation increases excitability of neuronal network in substantia gelatinosa of spinal

cord. *43nd Annual Meeting of SfN*, November 8-13, 2013, San Diego, CA (USA). Публікація тез, постерна доповідь.

13. Voitenko N., **Kopach O.**, Maistrenko A., Lushnikova I., Dosenko V., Skibo G. Anoxic preconditioning and blockage of HIF hydroxylation differently attenuates ischemia-induced changes in intracellular calcium signaling in CA1 and CA3 hippocampal neurons. *43nd Annual Meeting of SfN*, November 8-13, 2013, San Diego, CA (USA). Публікація тез, постерна доповідь.
14. **Kopach O.**, Sotnik A., Belan P., Voitenko N. Trafficking of AMPA receptors in dorsal horn neurons during persistent pain: the changes in synaptic and extrasynaptic receptor pools. *IUPS Congress 2013*. July 21-56, 2013, Birmingham (United Kingdom). Публікація тез, постерна доповідь.
15. Voitenko N., **Kopach O.**, Maistrenko A., Lushnikova I., Skibo G. Neuronal subtypes specificity of altered calcium signaling during ischemia, anoxia preconditioning, and blockage of HIF degradation in hippocampal organotypic slices. *42nd Annual Meeting of SfN*, October 13-17, 2012, New Orleans, LA (USA). Публікація тез.
16. Goncharenko Y., **Kopach O.**, Voitenko N. Selective inhibition of Ca^{2+}-permeable AMPA receptors attenuates persistent inflammatory pain and inflammatory-promoted AMPA receptors trafficking in dorsal horn neurons. *8th FENS Forum*, 14-18 July 2012, Barselona (Spain). Публікація тез, постерна доповідь.
17. **Kopach O.**, Maistrenko A., Lushnikova I., Skibo G., Voitenko N. Neuronal subtypes specificity of altered calcium signaling during ischemia, anoxia preconditioning, and blockage of HIF degradation in hippocampal organotypic slices. *8th FENS Forum*, 14-18 July 2012, Barselona (Spain). Публікація тез, постерна доповідь.
18. **Kopach O.**, Viatchenko-Karpinski V., Belan P., Tao Y.X., Voitenko N. Role of PKCα in adjusting of extrasynaptic AMPA receptors trafficking in dorsal horn neurons during persistent inflammatory pain. *Main Meeting of the*

Physiological Society. July 2-5, 2012, Edinburg (United Kingdom). Публікація тез, постерна доповідь.

19. **Kopach O**., Lipina C., Vats J., Irving A., Fedirko N. Salivary acinar cells: functional expression of different cannabinoid receptor subtypes. *Main Meeting of the Physiological Society*. July 2-5, 2012, Edinburg (United Kingdom). Публікація тез, постерна доповідь.
20. Гончаренко Ю., **Копач О.**, Войтенко Н. Використання селективних блокаторів Ca^{2+}-проникних АМПА-рецепторів для модуляції постійного периферичного болю. *VIII Міжнародна наукова конференція студентів і аспірантів "Молодь і поступ в біології"* 3-6 квітня 2012 року, Львів (Україна). Публікація тез, усна доповідь.
21. Іщенко Є., Вятченко-Карпінський В., **Копач О.**, Войтенко Н. Роль протеїн кінази Cα у підтриманні хронічного запального болю, викликаного тривалим периферичним запаленням. *VIII Міжнародна наукова конференція студентів і аспірантів "Молодь і поступ в біології"* 3-6 квітня 2012 року, Львів (Україна). Публікація тез, усна доповідь.
22. Sotnic A., **Kopach O.**, Viatchenko-Karpinski V., Belan P., Voitenko N. Spinal cord protein kinase C blocking attenuates nociceptive hypersensitivity and increased Ca^{2+}-permeability of AMPARs at the synapses in dorsal horn neurons during persistent inflammation. *Young Scientists Conference "Physiology from molecules to the organisms"*, 20-21 October 2011, Kiev (Ukraine). Публікація тез.
23. **Kopach O.**, Petralia R.S., Tao Y.-X., Belan P., Voitenko N. Trafficking of extrasynaptic AMPA receptors in lamina II neurons of the spinal dorsal horn as a molecular mechanism for the persistent pain maintenance. *Научные труды III Съезда физиологов СНГ,* 1-6 октября 2011, Ялта (Украина). Публікація тез, усна доповідь.
24. **Kopach O.**, Petralia R.S., Tao Y.-X., Belan P., Voitenko N. Trafficking of AMPA receptors at extrasynaptic plasma membrane of spinal lamina II neurons

during persistent inflammatory pain. *8th IBRO World Congress of Neuroscience 2011,* 14-18 July, 2011, Florence (Italy). Публікація тез, постерна доповідь.

25. Voitenko N., **Kopach O.**, Sotnic A., Viatchenko-Karpinski V., Tao Y.-X., Belan P. Trafficking of spinal AMPA receptors: a basis for future therapies of persistent pain. *8th IBRO World Congress of Neuroscience 2011,* 14-18 July, 2011, Florence (Italy). Публікація тез, постерна доповідь.
26. **Kopach O.**, Netsyk O., Voitenko N., Irving A., Fedirko N. Cannabinoid receptors activation: neurotransmition-related and unrelated peripheral effects. V Congress of the Ukrainian Society for Neuroscience. In memory of Platon Kostyuk, 6-10 June, 2011, Kiev (Ukraine). Публікація тез, постерна доповідь.
27. **Kopach O.**, Sotnic A., Viatchenko-Karpinski V., Tao Y.-X., Belan P., Voitenko N. *In vivo* silencing of spinal protein kinase Cα gene alleviates inflammation-induced hyperalgesia by adjusting a functional expression of $Ca2^{+}$-pearmeable AMPA receptors in Substantia Gelatinosa neurons. *40th Annual Meeting of SfN*, 12-17 November, 2010, San Diego (USA). 81.19/VV17. Публікація тез, постерна доповідь.
28. Voitenko N., **Kopach O.**, Sotnik A., Viatchenko-Karpinski V., Tao Y.-X., Belan P. AMPA receptor trafficking in persistent pain: a basis for future therapies. 9th International Conference on Fundamental Questions of Neuroscience “Gagra Talks”, October 13-16, 2010, Tbilisi (Georgia). Публікація тез, усна доповідь.
29. Нецик О.В., **Копач О.В.**, Федірко Н.В. Ендоканабіноїди регулюють процеси слиновиділення через модуляцію процесів кальцієвої сигналізації // *Матеріали X Українського біохімічного з’їзду*, 13-17 вересня 2010 р., м. Одеса. – *Укр. біохім. журн.* – 2010. – Т. 82, № 4 (додаток 1). – С.217–218. Публікація тез.
30. **Kopach O.,** Park J.-S., Petralia R.S., Belan P., Tao Y.-X., Voitenko N. Trafficking of extrasynaptic AMPA receptors in tonicaly firing dorsal horn

neurons is involved in the maintenance of inflammatory pain. *7th FENS Forum of European Neuroscience.* July 3-7, 2009, Amsterdam (Netherlands). Публікація тез, постерна доповідь.

31. **Kopach O.**, Voitenko N., Fedirko N. Impaired mitochondria calcium signalling contributes to the development of diabetes-induced xerostomia. *Main Meeting of the Physiological Society*. June 30-July 2, 2009, Manchester (United Kingdom). Публікація тез, постерна доповідь.
32. **Kopach O.,** Park J.-S., Petralia R.S., Sotnik A., Belan P., Tao Y.-X., Voitenko N. The extrasynaptic AMPA receptors functioning is altered under inflammatory pain. 39th Annual Meeting of SfN. Program #856.9. 17-21 October, 2009, Chicago (USA). Публікація тез, постерна доповідь.
33. Sotnik A., **Kopach O.,** Viatchenko-Karpinski V., Tao Y.-X., Belan P., Voitenko N. Protein kinase C α blocking or gene silencing in dorsal horn neurons demosntrates its major role in nociception. 39th Annual Meeting of SfN, Program #: 764.6. 17-21 October, 2009, Chicago (USA). Публікація тез, постерна доповідь.
34. **Kopach O.,** Sotnik A., Voitenko N. The extrasynaptic AMPA receptors functioning is altered under inflammatory pain. *9th International Congress of the Polish Neuroscience Society,* Warsaw, 9-12 Sept. 2009. Публікація тез, усна доповідь.
35. N. Voitenko, **O. Kopach**, A. Sotnik, X. Shang, P. Belan, Y.-X. Tao. Changes in Ca^{2+} permeability of AMPA receptors expressed on spinal dorsal horn neurons after peripheral inflammation. XXXVI Congress of Physiological Sciences, July 27-August 1, 2009, Kyoto (Japan). Публікація тез, постерна доповідь.
36. **Kopach O.,** Kruglikov I., Pivneva T., Voitenko N., Fedirko N. Mitochondria regulate Ca^{2+} influx and determine patterns of ER Ca^{2+} refilling in acinar cells. 7th European Biophysics Congress, July 11-15, 2009, Genoa, Italy. Публікація тез, постерна доповідь.

37. A. Sotnik, **O. Kopach**, P. Belan, X. Shang, Y.-X. Tao, N. Voitenko. Peripheral inflammation evokes an increase in Ca^{2+}-permeability of AMPA receptors of dorsal horn neurons due to GluR2 subunit loss. 6th FENS Forum, 12-16 July, 2008, Geneva, Switzerland. FENS Forum Abstract 189-26. Публікація тез, постерна доповідь.
38. **Kopach O.V.**, Kruglikov I.A., Voitenko N.V., Fedirko N.V. Neurotransmitter-induced store-operated calcium entry is strictly dependent on the mitochondria functioning. *6th FENS Forum,* July, 12-16, 2008, Geneva, Switzerland. Публікація тез, постерна доповідь.
39. **Kopach O.**, Pivneva T., Kruglikov I., Voitenko N., Fedirko N. Mitochondria are essential for maintaining of store-operated Ca^{2+} influx and ER refilling under prolonged cells` stimulation. *Physiological Society International Workshop "Latest advances in ion channel techniques applied to physiological problems".* – Sept. 12-16, 2008, Shanghai, China. Публікація тез, усна доповідь.
40. Sotnik A., **Kopach O.**, Viatchenko-Karpinski V., Voitenko N.. Inflammatory hyperalgesia are accompanied by changes in AMPA receptor function. *IBRO-advanced Workshop "T-type calcium channels: from discovery to channelopathies, 25 years of research".* June 5-7, 2008, Kiev, Ukraine. Публікація тез, усна доповідь.
41. Sotnik A., **Kopach O.,** Voitenko N. Changes in Ca^{2+}-permeability of AMPA receptors of dorsal horn neurons after peripheral inflammation. *Ukrainian-Poland Conference for Young Scientists in the frame Bogomoletz-Nencki collaboration*. Публікація тез, постерна доповідь.
42. Voitenko N., Shang X, **Kopach O.**, Sotnik A., Isaev D., Belan P., Tao Y.-X. "A switch of Ca^{2+}-impermeable AMPA receptors expressed on spinal dorsal horn neurons into Ca^{2+}-permeable AMPA receptors after peripheral inflammation", *SfN Meeting 2007* (Program #: 284.12). Публікація тез, постерна доповідь.

ЗМІСТ

ПЕРЕЛІК ОСНОВНИХ УМОВНИХ ПОЗНАЧЕНЬ

АМРА – α-аміно-3-гідрокси-5-метил-4-ізоксазолпропіонова кислота

ДР – дорсальний ріг спинного мозку

ЗПСС – збуджуючий постсинаптичний струм

ГПСС – гальмівний постсинаптичний струм

ІВ – індекс випрямлення струму

мЗПСС – мініатюрний збуджуючий постсинаптичний струм

мРНК – матрична рибонуклеїнова кислота

сЗПСС – спонтанний збуджуючий постсинаптичний струм

ПД – потенціал дії

ЦНС – центральна нервова система

AS ODN – антисенсові олігонуклеотиди

CFA – (від англ. Complete Freund's adjuvant), реагент для індукції хронічного запалення

$[Ca^{2+}]_i$ – концентрація вільного внутрішньоклітинного Ca^{2+}

GluR1-4 – субодиниці АМРА-рецепторів

IC50 – концентрація напівмаксимального інгібування

IEM-1460 – 1-trimethylammonio-5-1-adamantane-methyl-ammoniopentane dibromide, активаційнозалежний блокатор

IEM-1925 – N1-(1-phenylcyclohexyl)pentane-1,5-diaminium bromide, активаційнозалежний блокатор Ca^{2+}-проникних АМРА-рецепторів

I-V криві – вольт-амперні характеристики струмів

MS ODN – помилкові (міссенсові) олігонуклеотиди

Na_v – натрієві (Na^+) канали

NMDA – N-метил-D-аспартат

PCR – полімеразна ланцюгова реакція (polymerase chain reaction)

PKCα – протеїнкіназа С підтипу альфа

SCI – spinal cord injury, травма спинного мозку

TTX – тетродотоксин, блокатор натрієвих каналів

ВСТУП

Актуальність теми. Згідно зі статистичними даними ВООЗ, біль за масштабами свого поширення у розвинених країнах світу цілком порівнянний із пандемією – щонайменше кожний п’ятий житель Європи страждає від хронічного болю різноманітного походження, що становить близько 20% населення Європи. Це призводить до невідворотніх втрат внаслідок зниження працездатності, а також значних витрат на профілактику охорони здоров’я (Rice et al., 2016; Breivik et al., 2006). Міжнародна асоціація з вивчення болю (IASP) розглядає хронічний або постійний біль як біль, що «відірвався» від основного захворювання і набув «надорганного» характеру, який є багатофакторним патологічним феноменом та розвивається у випадках, коли неможливо вилучити вплив ініціюючого чинника, часто є автономним, таким, що сам себе підтримує (Treede et al., 2019, 2015; Scholz et al., 2019; Nicholas et al., 2019; Schug et al., 2019). Хронічний біль може отримувати риси хвороби («біль як хвороба»); цей стан проявляється не лише болем, але й вегетативними, емоційними та психічними порушеннями і потребує серйозної терапії (Goldberg, McGee, 2011; Jensen et al., 2007). Актуальність відповідних досліджень обумовлена відсутністю чіткої схеми ефективного лікування хронічного болю в більшості країн світу. Причиною невдачі при лікуванні хронічного болю, за висновками ВООЗ, є, найперше, відсутність повноцінної наукової концепції щодо фундаментальних механізмів виникнення та підтримання хронічного болю, основою якої були б результати ґрунтовних науково-експериментальних досліджень для подальшої розробки нових підходів до терапії болю. Відповідно, одним із фундаментальних завдань, які матимуть вагоме біомедичне (клінічне) значення, є з’ясування молекулярних та клітинних механізмів розвитку хронічного болю – як у центральній нервовій системі (ЦНС), так і периферичній – для пошуку перспективних

мішеней у терапії больових синдромів та можливості ефективного полегшення больових відчуттів.

На сьогодні основним механізмом, котрий, як вважається, опосередковує розвиток і підтримання хронічного болю, є так званий феномен центральної сенситизації (Treede, 2016; Kuner, 2010; Latremoliere, Woolf, 2009; Woolf, 1983). IASP характеризує центральну сенситизацію як «підвищену реакцію ноцицептивних нейронів у ЦНС на їх нормальні або підпорогові аферентні вхідні стимули». В основі цього феномену може лежати щонайменше три патофізіологічні процеси, а саме: постійна ектопічна активність як у пошкоджених, так і у здорових волокнах периферичних нервів та їх дорзальних гангліях, зміни внутрішніх властивостей нейронів та синаптичних мереж дорзального рогу (ДР) спинного мозку та порушення регуляції низхідних ноцицептивних шляхів. Ці процеси супроводжуються посиленням генерації спонтанних потенціалів дії (ПД) у спинному мозку та, як наслідок, посиленням та подовженням відповідей нейронів на периферичну стимуляцію. Активна увага останніми роками приділяється вивченню центральних механізмів ноцицепції, за яких патологічна активність поодиноких сенсорних нейронів може призводити до гіперзбудливості нейронних мереж, а відтак – патологічної гіперактивності нервової тканини (Kuner, 2010; Dubner, Basbaum, 1994). Така гіперактивність має здатність самопідтримуватися та призводити до незворотніх змін у функціюванні системи загалом (gain-of-function). Природа цих патологічних змін і закономірності, котрим вони підпорядковані на клітинному рівні, залишаються не з’ясованими, що обмежує поступ у розвитку ефективної терапії.

Для нейронів спинного мозку характерна складна морфологія, яка визначається насамперед різноманітністю дендритних розгалужень та їх проекцій як у латеральному, так і висхідному-нисхідному напрямках (Häring et al., 2018; Szucs et al., 2013; Todd, 2010; Lu, Perl, 2005). Наявність у нейронній

мембрані чисельних популяцій іонних каналів (потенціалзалежних та лігандкерованих) додатково ускладнює повноцінне розуміння деталізованої картини регулювання динаміки процесів збудження-гальмування сенсорних нейронів для детектування сенсорної інформації та її біофізичної обробки (процесінгу) у нейронних мережах ДР спинного мозку для подальшої передачі у вищі нервові центри емоційної діяльності, де формується усвідомлене (психофізіологічне) відчуття болю. Останнім часом активна увага приділяється регуляції функціювання іонотропних глутаматних рецепторів AMPA-типу, які активуються збуджуючим нейротрансмітером глутаматом і відіграють одну із ключових ролей у збуджувальній синаптичній передачі в ЦНС (Heine, Holcman, 2020; Choquet, 2018; Diering, Huganir, 2018; Bredt, Nicoll, 2003; Malinow, Malenka, 2002). Спинний мозок характеризується високим рівнем експресії AMPA-рецепторів; зокрема, нейрони ДР містять AMPA-рецептори, проникні для іонів Ca^{2+} (без GluR2 субодиниці у складі тетрамеру, що формує активний канал) та Ca^{2+}-непроникні (GluR2-вмісні) (Galan et al, 2004: Hartmann et al., 2004; Tong, MacDermott, 2006). Експериментальні дані свідчать, що цільове порушення експресії AMPA-рецепторів у спинному мозку сприяє проявам ноцицептивної пластичності і посилює довготривалу гіпералгезію, викликану периферичним запаленням (Han et al., 2019; Lin et al., 2015; Peng et al., 2012; Hartmann et al., 2004).

Представлена робота присвячена комплексному дослідженню клітинних та молекулярних спінальних механізмів, які лежать в основі феномену центральної сенситизації. Основна увага була зосереджена на встановленні ролі та регуляції функціювання AMPA-рецепторів у нейронах ДР спинного мозку за наявності хронічних больових синдромів різного генезу, а саме: периферичного запалення та травми спинного мозку. Оскільки відомості щодо динамічного регулювання функцій AMPA-рецепторів у спинному мозку практично відсутні, результати таких досліджень представлятимуть істотний фундаментальний інтерес, а виявлення терапевтичного ефекту модуляції

функціювання цих рецепторів на поведінкові прояви болю відкриє нові перпективи у пошуку новітніх біотехнологічних засобів для лікування хронічного болю та обґрунтування клінічних підходів до сучасної терапії больових синдромів (зокрема ефективності генної терапії).

Зв'язок роботи з науковими програмами, планами, темами. Робота виконана в рамках наукових програм відділу загальної фізіології нервової системи (пізніше відділу сенсорної сигналізації) Інституту фізіології ім. О.О. Богомольця НАН України: «Генетична корекція функцій глутаматних рецепторів спинного мозку як шлях лікування хронічного болю» (2011-2013 рр.; № державної реєстрації 0110U004750), «Розробка нових терапевтичних стратегій лікування хронічного болю з малою кількістю побічних ефектів, що базуються на генетичному регулюванні динамічних властивостей глутаматних рецепторів нейронів спинного мозку» (2010-2014 рр.; № державної реєстрації 0110U004761), у рамках гранту НАН України для молодих вчених «Функціонування нейрональних мереж спинного мозку при тривалому запаленні: участь AMPA-рецепторів у спонтанній активності нейронів» (2011-2012 рр.; № державної реєстрації 0111U007132), «Ендогенна та фармакологічна регуляція внутрішньоклітинної та міжклітинної сигналізації в клітинах нервової системи в нормі та патології» (2011-2013 рр.; № державної реєстрації 0110U004750), «Молекулярні та генетичні механізми клітинної сигналізації в нормі та патології» №UF45.2/001 (на базі державної ключової лабораторії молекулярної та клітинної біології) та «Розробка новітніх знеболюючих засобів на основі інгібіторів кальцій-проникних AMPA-рецепторів» (2015-2019 рр.; № державної реєстрації 0115U003632).

Мета дослідження: з’ясування спінальних механізмів ноцицепції для подальшого пошуку та обґрунтування новітніх біотехнологічних підходів для корекції хронічних больових синдромів.

Завдання дослідження:

1. Виявити порушення функціювання синаптичних AMPA-рецепторів у нейронах ДР спинного мозку при периферичному запаленні як потенційний механізм, що опосередковує феномен центральної сенситизації при больових синдромах.
2. З’ясувати молекулярні механізми порушення функціювання синаптичних AMPA-рецепторів та виявити участь інших клітинних білків, залучених у зміни функціювання цих рецепторів у синапсах ноцицептивних нейронів, при периферичному запаленні.
3. Встановити функціювання позасинаптичних AMPA-рецепторів у нейронах ДР спинного мозку за фізіологічних умов та охарактеризувати їх можливі зміни при тривалому периферичному запаленні.
4. Оцінити динамічний обіг AMPA-рецепторів між синаптичною та позасинаптичними ділянками мембрани у нейронах ДР спинного мозку при тривалому запальному болю.
5. Вивчити функціювання нейронних мереж ДР спинного мозку та встановити баланс між збудженням і гальмуванням за фізіологічних умов та при больовому синдромі.
6. Оцінити зміни функціювання нейронних мереж ДР спинного мозку при хронічному болю різного генезу (периферичного та центрального походження).
7. Розробити метод локальної цільової доставки інгібіторів нового покоління у поперековий відділ спинного мозку та з’ясувати терапевтичний вплив фармакологічного блокування AMPA-рецепторів на полегшення больового синдрому. Оцінити побічні ефекти такої терапії.
8. Охарактеризувати ефект фармакологічного блокування протеїнкінази С альфа (PKCα) як мішені для корегування порушеного обігу AMPA-рецепторів у нейронах ДР спинного мозку та модулювання хронічного болю при периферичному запаленні.

9. Застосувати генну терапію для корекції хронічного болю та оцінити терапевтичну ефективність генетичного вимкнення (нокдауну) PKCα у спинному мозку на експериментальній моделі периферичного запалення. Обґрунтувати застосування такого підходу на клітинному рівні.

Об'єкт дослідження – активність сенсорних нейронів і нейронних мереж дорзального рогу спинного мозку та поведінкові прояви больових відчуттів при експериментальному моделюванні хронічних больових синдромів.

Предмет дослідження – клітинні та молекулярні спінальні механізми виникнення та корегування хронічного болю у спинному мозку.

Методи дослідження включають біофізичні підходи, зокрема реєстрацію іонних струмів у режимі локальної фіксації мембранного потенціалу (patch-clamp) у конфігурації "ціла клітина" (whole-cell) та флуоресцентне вимірювання внутрішньоклітинної концентрації іонів кальцію ($[Ca^{2+}]_i$), фізіологічні (введення тест-речовин в інтратекальний простір спинного мозку, моделювання хронічного болю різного генезу), молекулярно-біологічні (real-time PCR та Western-blot), фармакологічні та математичні методи експериментальних досліджень (оцінка провідностей поодиноких каналів), застосування підходів генної інженерії, нанотехнологій, поведінкові тести на лабораторних тваринах і методи варіаційної статистики при кількісній обробці результатів.

Наукова новизна отриманих результатів. Отримані експериментальні дані свідчать про низку нових аспектів у функціонуванні складного комплексу клітинних та молекулярних спінальних механізмів, що залучені у підтримання хронічного болю у нейронних мережах ДР спинного мозку. Експериментально обґрунтуванний новий підхід для полегшення хронічних больових відчуттів шляхом селективного таргетування ланок молекулярного каскаду, що забезпечує регулювання динамічного обігу (трафікінгу) AMPA-рецепторів у сенсорних нейронах спинного мозку. Виявлені у проведенних експериментальних дослідженнях порушення трафікінгу AMPA-рецепторів у

нейронах ДР вперше в світі демонструють причинно-наслідкові зв'язки між порушеннями регуляції функціювання AMPA-рецепторів на клітинному рівні та розвитком і підтриманням хронічного болю у експериментальних тварин.

Вперше встановлено молекулярний механізм порушеного обігу AMPA-рецепторів – інтерналізація GluR2-вмісних рецепторів із синапсів між первинними аферентами та ноцицептивними нейроними ДР спинного мозку – при тривалому периферичному запаленні та охарактеризовано каскад внутрішньоклітинних білків, залучених у регуляцію трафікінгу синаптичного пулу рецепторів (старгазин, ABP/GRIP, PICK1 та PKCα як ключовий фермент-регулятор). Продемонстровано, що саме ці зміни є однією із необхідних передумов підтримання хронічного запального болю.

Вперше експериментально продемонстровано, що в сенсорних нейронах ДР спинного мозку функціонує чисельна популяція позасинаптичних AMPA-рецепторів, які характеризуються змінною проникністю до іонів Ca^{2+}, і що різні підтипи нейронів експресують за фізіологічних умов позасинаптичні AMPA-рецептори подібного складу, які містять домінуючу кількість GluR2-субодиниць; це визначає їх низьку проникність до Ca^{2+}. Вперше показано порушення обігу позасинаптичних AMPA-рецепторів при тривалому периферичному запаленні.

Вперше екпериментально показано, що порушення трафікінгу AMPA-рецепторів призводить до змін у балансі збудження та гальмування у нейронних мережах ДР спинного мозку; це, в свою чергу, спричиняє довготривалу підвищену збудливість ДР, яка може самопідтримуватися і опосередковувати хронічний біль різного генезу.

Вперше продемонстровано клітиноспецифічність вищеназваних змін, а саме: специфіку порушення обігу AMPA-рецепторів та зміщення балансу збудження-гальмування у сенсорних нейронах різних підтипів.

Розроблено метод цільової доставки терапевтичного матеріалу для локального таргетування нейронів поперекового відділу спинного мозку.

Вперше продемонстровано терапевтичний вплив фармакологічного блокування Ca^{2+}-проникних AMPA-рецепторів високоселективними сполуками-інгібіторами нового покоління (активаційнозалежними блокаторами IEM-1460 та IEM-1925) на полегшення больових синдромів із мінімальними побічними ефектами.

Вперше застосовано генну терапію для корекції хронічного болю у експериментальних моделях лабораторних тварин та продемонстровано істотний терапевтичний ефект блокування експресії PKCα на послаблення больового синдрому при тривалому периферичному запаленні (із науковим обґрунтуванням на клітинному рівні).

Вперше застосовано новітні підходи у галузі наноінженерії для практичного впровадження з метою корекції хронічного больового синдрому, а також у створенні цільових біоматеріалів для потенційного впровадження у терапію болю.

Практичне значення отриманих результатів. Результати дослідження мають фундаментальне значення для деталізованого розуміння каскаду молекулярних механізмів у нейронах ДР та порушень процесів збудження і гальмування на рівні нейронних мереж спинного мозку, які лежать в основі довготривалого підтримання больових синдромів. Вагомість роботи полягає найперше у формулюванні гіпотези щодо ключового вкладу центральних механізмів у підтримання хронічного болю та у науковому обґрунтуванні концепції нових підходів для терапії хронічного болю різного походження.

Практичне значення дослідження полягає в розробленні нових біотехнологічних підходів для полегшення хронічного болю. В основі такого напрямку лежить селективне таргетування виявленного фундаментального механізму больової пластичності ЦНС шляхом фармакологічної корекції порушень функціювання AMPA-рецепторів у нейронах ДР (із використанням інгібіторів нового покоління) та застосування генної терапії (нок-дауна PKCα за допомогою антисенсових олігонуклеотидів). Терапевтичні ефекти,

продемонстровані на експериментальних тваринах, відкривають нові можливості для розробки новітніх методів у боротьбі з хронічним запальним болем (патент на корисну модель № 94492 від 10.11.2014).

Розроблений інноваційний підхід із застосуванням нанотехнологій може бути використаний для цільової доставки локальних анестетиків та інших високоактивних сполук зі зменшенням їх потенційних побічних ефектів при використанні у клініці.

Особистий внесок здобувача. Автором проведено науковий пошук та критичний аналіз наявних даних літератури щодо обґрунтування ролі та вибраного таргетування AMPA-рецепторів для потенційної корекції хронічного болю. При проведенні досліджень автором особисто виконано основну частину експериментальної роботи, аналіз отриманих результатів, їх наукову інтерпретацію та узагальнення, формулювання висновків та написання статей. Деякі експерименти були проведені разом зі співавторами опублікованих робіт, зокрема співробітниками Інституту фізіології ім. О.О. Богомольця НАН України к.б.н. В.Ю. Вятченко-Карпінським, А.О. Сотником, к.б.н. В.В. Кротовим, Ю.В. Гончаренко, к.б.н. Є. Іщенко. Аналіз провідностей AMPA-рецепторів проведено у співпраці із співробітником інституту ім. О.О. Богомольця к.б.н. А.Л. Борисюк. Моделювання травми спинного мозку та оцінку ступеня дисфункцій у експериментальних тварин проводили разом із співробітником Національного Медичного Університету України імені О.О. Богомольця д.м.н. В.В. Медвєдєвим. Дослідження екпресії PKCα проводили у співробітництві із завідувачем відділом загальної та молекулярної патофізіології д.м.н. В.Є. Досенком та к.б.н. А. Шиш. Дослідження молекулярних механізмів порушення трафікінгу синаптичних AMPA-рецепторів було проведено на базі Школи Медицини Університету Джона Хопкінса (Балтимор, США) (керівник проф. Я.Х. Тао). Експерименти з моделювання травмування трійчастого нерва та периферичних ноцицепторних нейронів були проведені на базі Лабораторії ноцицепції Університетського Коледжу Лондона (керівник проф. Дж.Н. Вуд). Автор щиро вдячний керівнику

Лабораторії імиджингу синапсів Інституту Нейрології Університетського Коледжу Лондона (UCL, Великобританія) проф. Д.А. Русакову та професору Університету Королеви Марії (QMU, Лондон, Великобританія) Г.Б. Сухорукову за плідну співпрацю із використанням підходів у галузі нанотехнологій та застосуванням наноматеріалів для практичного впровадження, а також завідувачу відділом біофізики мембран Інституту фізіології ім. О.О. Богомольця проф. П.В. Білану за плідну співпрацю.

Автор висловлює подяку науковому консультанту проф. Н.В. Войтенко за допомогу у плануванні комплексного підходу та організації проведення досліджень, в обговоренні та підготовці матеріалів до публікацій.

Апробація результатів дисертації. Основні положення роботи доповідались на щорічних конференціях Американського Товариства Нейронаук (Сан Дієго, 2007, 2010 та 2013; Чікаго, 2009; Вашингтон, 2014 та 2017, США), щорічних з'їздах Фізіологічного Товариства Великобританії (Едінбург, 2012; Абердин, 2019), Конгресах Міжнародного Товариства Дослідження Мозку (Флоренція, 2011, Італія; Ріо-де-Жанейро, 2015, Бразилія), форумах Європейського Товариства Нейронаук (Женева, 2008, Швейцарія; Амстердам, 2010, Нідерланди; Барселона, 2012, Іспанія), Конгресах Фізіологічних Наук (Кіото, 2009, Японія; Бірмінгем, 2013, Великобританія), Товариства Нейронаук Польщі (Варшава, 2009) та Українського Товариства Нейронаук (Київ, 2014 та 2017, Україна), слухали та обговорювали на засіданнях сектору молекулярної фізіології Інституту фізіології ім. О.О. Богомольця НАН України.

Публікації. Результати дисертації викладено у 14 статтях (опублікованих у виданнях, віднесених до першого і другого квартилів (Q1 і Q2) відповідно до класифікації SCImago Journal and Country Rank або Journal Citation Reports) та 42 тезах міжнародних конференцій та з'їздів.

РОЗДІЛ 1

СИНАПТИЧНІ AMPA-РЕЦЕПТОРИ: МОЛЕКУЛЯРНИЙ МЕХАНІЗМ РЕГУЛЯЦІЇ ДИНАМІЧНОГО ОБІГУ РЕЦЕПТОРІВ РІЗНОГО СУБОДИНИЧНОГО СКЛАДУ ЗА ФІЗІОЛОГІЧНИХ УМОВ ТА ПРИ ХРОНІЧНОМУ БОЛЮ

1.1. Тривале периферичне запалення супроводжується інтерналізацією GluR2-вмісних AMPA-рецепторів із синапсів між первинними аферентами та ноцицептивними нейронами дорзального рогу спинного мозку за участі NMDA-рецептор-опосередкованої активації PKC

3206 • The Journal of Neuroscience, March 11, 2009 • 29(10):3206–3219

Neurobiology of Disease

Persistent Inflammation Induces GluR2 Internalization via NMDA Receptor-Triggered PKC Activation in Dorsal Horn Neurons

Jang-Su Park,[1]* Nana Voitenko,[2]* Ronald S. Petralia,[3] Xiaowei Guan,[1] Ji-Tian Xu,[1] Jordan P. Steinberg,[4] Kogo Takamiya,[4,5] Andrij Sotnik,[2] Olga Kopach,[2] Richard L. Huganir,[4,6] and Yuan-Xiang Tao[1]

[1]Department of Anesthesiology and Critical Care Medicine, Johns Hopkins University School of Medicine, Baltimore, Maryland 21205, [2]Department of General Physiology of Nervous System, Bogomoletz Institute of Physiology, Kiev 01024, Ukraine, [3]Laboratory of Neurochemistry, National Institute of Deafness and Other Communication Disorders, National Institutes of Health, Bethesda, Maryland 20892, and Departments of [4]Neuroscience and [5]Neurosurgery and [6]Howard Hughes Medical Institute, Johns Hopkins University School of Medicine, Baltimore, Maryland 21287

Spinal cord GluR2-lacking AMPA receptors (AMPARs) contribute to nociceptive hypersensitivity in persistent pain, but the molecular mechanisms underlying this event are not completely understood. We report that complete Freund's adjuvant (CFA)-induced peripheral inflammation induces synaptic GluR2 internalization in dorsal horn neurons during the maintenance of CFA-evoked nociceptive hypersensitivity. This internalization is initiated by GluR2 phosphorylation at Ser^{880} and subsequent disruption of GluR2 binding to its synaptic anchoring protein (GRIP), resulting in a switch of GluR2-containing AMPARs to GluR2-lacking AMPARs and an increase of AMPAR Ca^{2+} permeability at the synapses in dorsal horn neurons. Spinal cord NMDA receptor-mediated triggering of protein kinase C (PKC) activation is required for the induction and maintenance of CFA-induced dorsal horn GluR2 internalization. Moreover, preventing CFA-induced spinal GluR2 internalization through targeted mutation of the GluR2 PKC phosphorylation site impairs CFA-evoked nociceptive hypersensitivity during the maintenance period. These results suggest that dorsal horn GluR2 internalization might participate in the maintenance of NMDA receptor/PKC-dependent nociceptive hypersensitivity in persistent inflammatory pain.

Introduction

AMPA receptors (AMPARs) are responsible for the majority of excitatory synaptic transmission and play a critical role in synaptic plasticity in the mammalian CNS. They are heterotetrameric cation channels composed of a combinational assembly of four subunits, GluR1–GluR4 (Burnashev et al., 1992). In contrast to GluR1, GluR3, and GluR4 mRNA, GluR2 mRNA undergoes efficient editing at a critical residue in the pore-forming M2 segment (Burnashev et al., 1992). Incorporation of these edited GluR2 subunits into AMPARs (GluR2-containing AMPARs) reduces AMPAR conductance, hinders Ca^{2+} permeation through AMPARs, and confers a linear current–voltage (*I–V*) relationship. Conversely, AMPARs assembled without the edited GluR2 subunits (GluR2-lacking AMPARs) have higher conductance, are readily Ca^{2+} permeable, and exhibit inwardly rectifying *I–V* relationships. Therefore, the presence or absence of synaptic GluR2 in the AMPAR complex greatly influences AMPAR properties and synaptic functions.

In adult mammalian CNS, most AMPARs have low Ca^{2+} permeability because GluR2 is fully edited throughout development and widely expressed (Burnashev et al., 1992; Greger and Esteban, 2007). However, AMPAR Ca^{2+} permeability in adult CNS is not static. It can be modified dynamically by neuronal activity, sensory experience, and neuronal insults via changes in trafficking, expression, and RNA editing of the GluR2 subunit (Isaac et al., 2007; Liu and Zukin, 2007). These changes might underlie the central mechanisms during physiological and pathological processes, such as synaptic plasticity and stroke.

Although all four AMPAR subunits are found within the spinal dorsal horn, GluR1 and GluR2 are the most abundant and are highly concentrated on the postsynaptic neuronal membranes of the superficial dorsal horn (Kerr et al., 1998; Lu et al., 2002). Targeted disruption of GluR2 gene produces a deficiency of dorsal horn GluR2-containing AMPARs, facilitates dorsal horn nociceptive plasticity, enhances long-term potentiation of primary afferent neurotransmission, and increases inflammatory hyperalgesia (Hartmann et al., 2004; Youn et al., 2008). In contrast, GluR1 and GluR3 knock-out mice display intact responses to persistent inflammatory insult, although GluR1 deletion de-

Received Sept. 20, 2008; revised Feb. 4, 2009; accepted Feb. 5, 2009.

This work was supported by National Institutes of Health (NIH) Grants NS058886 and NS057345 and the Johns Hopkins University Blaustein Pain Research Fund (Y.-X.T.), Juvenile Diabetes Research Foundation Grant 1-2004-30 and INTAS Grant 8067 (N.V.), the Intramural Research Program of National Institute on Deafness and Other Communication Disorders (R.S.P.), and NIH Grant NS036715 and the Howard Hughes Medical Institute (R.L.H.). We thank N. Dubner, K. Ren, S. N. Raja, Y. Guan, and P. Belan for their consultation; D. Isaev and I. Galik for their electrophysiological technical support; F. X. Wang for her help with the immunogold labeling; and C. F. Levine for her editorial assistance.

*J.-S.P. and N.V. contributed equally to this work.

Correspondence should be addressed to Dr. Yuan-Xiang Tao, Department of Anesthesiology and Critical Care Medicine, Johns Hopkins University School of Medicine, 367 Ross, 720 Rutland Avenue, Baltimore, MD 21205. E-mail: ytao14@jhmi.edu.

J.-S. Park's present address: Department of Anesthesiology and Pain Medicine, Inje Paik Hospital, Inje University, Busyang 411706, South Korea.

DOI:10.1523/JNEUROSCI.4574-08.2009

 0270-6474/09/293206-14$15.00/0

creases expression of dorsal horn GluR2-lacking AMPARs (Hartmann et al., 2004). These genetic studies indicate that GluR2, as a key subunit in the AMPAR complex, determines activity-induced nociceptive hypersensitivity and suggest that removal (or internalization) of synaptic GluR2 in dorsal horn neurons might contribute to spinal central sensitization, a specific form of synaptic plasticity, in persistent inflammatory pain. However, whether and how GluR2 are trafficked away from the synaptic membrane in dorsal horn neurons under inflammatory pain conditions is unknown.

Here we show that complete Freund's adjuvant (CFA)-induced peripheral persistent inflammation causes a time-dependent increase in GluR2 phosphorylation at Ser^{880} (GluR2-p Ser^{880}) in dorsal horn. This phosphorylation is accompanied by reduced affinity of GluR2 to its synaptic anchoring protein (GRIP), internalization of synaptic GluR2, and a switch to synaptic GluR2-lacking AMPARs in dorsal horn neurons in the maintenance of CFA-induced inflammatory pain. GluR2-p Ser^{880} and its internalization are dependent on activation of the NMDA receptor (NMDAR)/protein kinase C (PKC) signaling cascade. Interfering with CFA-induced dorsal horn GluR2 internalization by preventing GluR2 PKC phosphorylation at Ser^{880} blunted CFA-evoked nociceptive hypersensitivity during the maintenance period. Together, our studies imply an involvement of dorsal horn GluR2 internalization in the maintenance of persistent inflammation-induced nociceptive hypersensitivity.

Materials and Methods

Animal preparation. Male Sprague Dawley rats (250–300 g) were purchased from Hilltop Lab Animals. For chronic intrathecal drug delivery, a polyethylene (PE-10) tube was inserted into the subarachnoid space at the rostral level of the spinal cord lumbar enlargement segment through an incision at the atlanto-occipital membrane according to the method described previously (Tao et al., 2000; Zhang et al., 2003). For persistent sciatic nerve conduction blockade, an indwelling perisciatic catheter system was developed based on previous studies (Chacur et al., 2001; Wei et al., 2007). Perisciatic catheters were constructed from sterile gelfoam (Upjohn) aseptically cut into 15 mm (L) × 5 mm (W) × 9 mm (H) strips. One end was bisected (3.5 mm W) to a depth of 1 cm to allow a 4 cm sterile PE-10 tube to be sutured inside. The assembly was implanted around the sciatic nerve at midthigh level. The animals were allowed to recover for 5–10 d before being used experimentally. Rats showing any neurologic deficits postoperatively were discarded from the study. The position of the PE-10 catheter was confirmed in each animal after behavioral testing.

GluR2K882A knock-in (KI) mice were created as described previously (Chung et al., 2003; Steinberg et al., 2006). Adult GluR2K882A KI mice and control wild-type (WT) littermates (10–12 weeks) were obtained by interbreeding GluR2K882A heterozygous mice. Genotypes were determined by PCR analysis on digested mouse tail samples (Chung et al., 2003; Steinberg et al., 2006). Male and female GluR2K882A KI mice are viable and fertile without any observable developmental defects (Steinberg et al., 2006). They also display normal locomotor functions (supplemental Table S1, available at www.jneurosci.org as supplemental material).

To produce inflammation and nociceptive hypersensitivity, CFA (*Mycobacterium tuberculosis*; Sigma; 0.1 ml for rats and 0.02 ml for mice) suspended in an oil–saline (1:1) emulsion was injected subcutaneously into the plantar side of one hindpaw. Naive animals and saline (0.9%; 0.1 ml for rats and 0.02 ml for mice) injections were used as controls. The animals were used in accordance with protocols that were approved by the Animal Care and Use Committee at Johns Hopkins University.

Behavioral testing. Animals were acclimatized to the experimental settings several times before the testing. The experimenters were blinded to the treatment groups and the mouse genotypes. Paw withdrawal responses to thermal and mechanical stimuli were measured in rats and mice as described previously (Tao et al., 2000, 2003; Zhang et al., 2003).

To measure paw withdrawal response to noxious heat stimuli, each animal was placed in a Plexiglas chamber on a glass plate located above a light box. Radiant heat from a Model 336 Analgesic Meter (ITTC/Life Science Instruments) was applied by aiming a beam of light through a hole in the light box through the glass plate to the middle of the plantar surface of each hindpaw. When the animal lifted its foot, the light beam was turned off. The length of time between the start of the light beam and the foot lift was defined as the paw withdrawal latency. Each trial was repeated five times at 5 min intervals for each paw. A cutoff time of 20 s was used to prevent paw tissue damage.

To measure paw withdrawal response to repeated mechanical stimuli, each animal was placed in a Plexiglas chamber on an elevated mesh screen. For rats, a single trial of mechanical stimuli consisted of eight applications of a calibrated von Frey filament (8.01 mN; Stoelting) within a 2–3 s period. Each trial was repeated 10 times at 5 min intervals on each hindpaw. For mice, two calibrated von Frey filaments (0.24 and 1.24 mN) were used. Each filament was applied to the hindpaw for ~1 s and repeated 10 times on each hindpaw. The occurrence of paw withdrawal in each of these 10 repeats was expressed as a percentage response frequency.

Locomotor function testing. Three reflexes (placing, grasping, and righting) were tested as described previously (Tao et al., 2000; Zhang et al., 2003). (1) Placing reflex: the experimenter held the mouse or rat with hindlimbs slightly lower than the forelimbs and brought the dorsal surfaces of the hindpaws into contact with the edge of a table. The experimenter recorded whether the hindpaws were placed on the table surface reflexively. (2) Grasping reflex: the experimenter placed the animal on a wire grid and recorded whether the hindpaws grasped the wire on contact. (3) Righting reflex: the experimenter placed the animal's back on a flat surface and noted whether it immediately assumed the normal upright position. Scores for placing, grasping, and righting reflexes were based on counts of each normal reflex exhibited in five trials. In addition, the animal's general behaviors, including spontaneous activity (e.g., walking and running), were observed.

Antibodies. The following antibodies were used: rabbit anti-GluR2 (Millipore Bioscience Research Reagents), mouse anti-GluR2 (Millipore Bioscience Research Reagents), rabbit anti-GluR2-p Ser^{880} (Chung et al., 2003; Steinberg et al., 2006), rabbit anti-PICK1 (Steinberg et al., 2006), rabbit anti-GRIP1 (Millipore), mouse anti-PSD-95 (Millipore), rabbit anti-PSD-93 (Alomone Labs), rabbit anti-NR2B (Millipore Bioscience Research Reagents), rabbit anti-NR1 (Millipore Bioscience Research Reagents), rabbit anti-NR2A/2B (Millipore Bioscience Research Reagents), rabbit anti-PKCα (Santa Cruz Biotechnology), rabbit anti-PKCβ (Santa Cruz Biotechnology), rabbit anti-PKCγ (Santa Cruz Biotechnology), rabbit anti-N-cadherin (BD Transduction Laboratories), rabbit anti-stargazin (Millipore), mouse anti-α-adaptin (Sigma), and mouse anti-β-actin (Sigma).

Surface expression assay. Surface biotinylation expression experiments were performed in dorsal horn neuronal culture and spinal cord slices as previously described (Tao et al., 2003). High-density cultured spinal dorsal horn neurons (1.5×10^6 cells/ml) and live transverse dorsal horn slices (400 μM) were prepared. Briefly, the cultured neurons or slices were incubated for 45 min on ice with artificial CSF (ACSF) containing 1.5 mg/ml sulfo-NHS-LC-biotin (Pierce) and then rinsed in ACSF to quench the biotin reaction. The cultured neurons were lysed and the slices homogenized in modified RIPA buffer (1% Triton X-100, 0.1% SDS, 0.5% deoxycholic acid, 50 mM $NaPO_4$, 150 mM NaCl, 2 mM NaF, 1 mM PMSF, 1 mg/ml leupeptin, and 10 mM sodium pyrophosphate). The homogenates were centrifuged at 10,000 × *g* for 15 min at 4°C, and the supernatant was harvested. After the measurement of protein concentration, 20% of the supernatant was removed to detect total expression of GluR2, NR1, and NR2B. The remaining supernatant was incubated with 50% NeutrAvidin agarose (Pierce) for 4 h at 4°C, and washed three times with RIPA buffer. Total and biotinylated surface proteins were detected using quantitative Western blots as described below. The surface/total ratio was calculated.

Subcellular fractionation. Subcellular fractionation was performed as

described previously (Matsuda et al., 2000) with minor modification. Briefly, the tissues were homogenized in homogenization buffer [250 mM sucrose, 10 mM Tris-HCl, pH 7.4, 1 mM EDTA, 1 mM PMSF, 1 mM benzamidine]. The homogenate was centrifuged at 1000 × *g* for 10 min at 4°C, and then the supernatant (S1, total soluble fraction) was collected. After centrifugation at 20,000 × *g* for 20 min at 4°C, the supernatant (S2, crude cytosolic fraction) and pellet (P1, crude plasma membrane fraction) were collected. The S2 was subsequently centrifuged at 150,000 × *g* for 1 h at 4°C, and the pellet was used as the 150,000 × *g* (150 k-g) fraction.

Immunoprecipitation and immunoblotting. The sample proteins from different fractions were prepared as described above. For immunoprecipitation, the affinity-purified antiserum, with or without preincubation with excess fusion protein, was incubated with 100 μl of a 1:1 slurry of protein A-Sepharose for 1 h, and the protein–antibody complex was spun down at 2000 rpm for 4 min. The solubilized fractions were then added to the Sepharose beads and the mixture incubated for 2–3 h at 4°C. The mixture was washed with the modified RIPA buffer. The proteins were separated on 4% stacking/7.5% polyacrylamide gels by SDS-PAGE and then electrophoretically transferred onto nitrocellulose membrane. The membrane was blocked with 3% nonfat dry milk and subsequently incubated with the primary antibody (see antibodies listed above) overnight. The proteins were detected with horseradish peroxidase-conjugated secondary antibody and visualized by chemiluminescence reagents provided with the ECL kit (GE Healthcare) and exposure to film. The intensity of blots was quantified with densitometry.

Postembedding immunogold labeling. Postembedding immunogold labeling was performed as described previously (Petralia et al., 1997; Tao et al., 2003; Ho et al., 2007). Briefly, rats were perfused transcardially with 4% paraformaldehyde + 0.5% glutaraldehyde 1 d after CFA or saline. Cryoprotected sections from the ipsilateral L_{4-5} superficial dorsal horns were frozen in Leica CPC and freeze-substituted into Lowicryl HM-20 in a Leica AFS freeze substitution instrument. Thin sections were labeled with monoclonal mouse (Ho et al., 2007) or polyclonal rabbit (Petralia et al., 1994) anti-GluR2 serum (Millipore Bioscience Research Reagents). Controls for specificity and selectivity of these antibodies were performed as described previously (Petralia et al., 1994; Ho et al., 2007). Areas for study were selected at random from the superficial dorsal horn at low magnification (i.e., synapses not visible) and then micrographs of synapses were taken at high magnification. Immunogold counts at synapses included all gold particles found in the synaptic cleft and postsynaptic density (Ho et al., 2007).

Electrophysiology. Transverse slices (300–400 μm thick) of the L_{4-5} spinal cord with attached long (8–15 mm) dorsal roots were prepared from 17- to 25-d-old male rats at 1 d after CFA or saline as described previously (Vikman et al., 2008). Whole-cell patch-clamp recordings were taken from neurons located in lamina II (substantia gelatinosa (SG)). Slices were continuously superfused with external solution [(in mM) 125 NaCl, 2.5 KCl, 1.25 NaH_2PO_4, 2 $CaCl_2$, 1 $MgCl_2$, 26 $NaHCO_3$, and 10 glucose (dextrose), pH 7.4; osmolarity adjusted to 310–320 mOsm/L with sucrose, equilibrated with 95% O_2, 5% CO_2]. Patch pipettes (6–9 MΩ) were filled with internal solution [(in mM) 130 Cs-methylsulfonate, 10 NaCl, 10 EGTA, 2 $CaCl_2$, 10 HEPES, 0.1 spermine tetrahydrochloride, 2 Mg-ATP, and 0.1 Na-GTP (pH adjusted to 7.2 with CsOH, osmolarity adjusted to 290 mOsm/L with sucrose)]. QX-314 (5 mM) was added to the internal solution to block voltage-activated sodium currents. Cells were held at −70 mV under voltage-clamp control. EPSCs were recorded at different membrane potentials from −70 mV to +50 mV using 20 mV steps. Dorsal roots were stimulated with a suction electrode. In most cases, stimulation intensities ranged from 70 to 400 μA (constant current output and consisting of 0.1 ms duration at frequency 0.1 Hz). Stimulus intensity was gradually increased until the maximal response was identified. The intensity was then adjusted slightly higher to ensure consistent axon activation under control conditions. Monosynaptic responses were selected based on the absence of synaptic failures and low variability of latency at a stimulation frequency of 10 Hz. At this frequency, polysynaptic responses tended to fail, and their latency markedly changed, but monosynaptic responses kept a constant latency. The latency was defined as the time interval between the stimulus artifact and the response onset. Latency values ranged from 5 to 20 ms. Neurons with high or low reversal potentials ($|E_{rev}| > 10$ mV) for AMPA evoked EPSCs (eEPSCs) were not included in the analysis.

To study eEPSCs at different voltages, the membrane potential was stepped to a new value 350 ms before the dorsal root was stimulated. Short hyperpolarizing voltage steps to −75 mV were applied every minute to monitor input and access resistance. To isolate the synaptic current, membrane currents recorded in the absence of dorsal root stimulation at each membrane potential were subtracted from the synaptic record. Peak amplitude measurement of synaptic currents was performed on averages of five eEPSCs. The rectification index (RI) of the AMPA eEPSC was determined by dividing the AMPA eEPSC amplitude at +40 mV by the AMPA eEPSC amplitude at −70 mV. In experiments that used the polyamine toxin philanthotoxin-433 (PhTx 433; Sigma), EPSCs were evoked at a stimulation frequency of 0.1 Hz, and PhTx 433 was bath applied after the baseline was recorded. Clampfit 8.0 software (Molecular Devices) was used to analyze evoked synaptic currents.

Statistics. All data are presented as mean ± SEM. Student's *t* tests or a one-way or two-way ANOVA followed by the *post hoc* Tukey tests were used to determine statistically significant differences ($p < 0.05$). The statistical software package SigmaStat (Systat) was used to perform all statistical analyses.

Results

CFA injection induces a time-dependent increase in dorsal horn GluR2 phosphorylation at Ser^{880}

Evidence from *in vitro* studies shows that GluR2-p Ser^{880} is required for GluR2 internalization (Perez et al., 2001; Dev et al., 2004). To characterize GluR2 internalization in dorsal horn neurons in persistent inflammatory pain, we first examined whether CFA-induced peripheral inflammatory insult induced GluR2-p Ser^{880} in dorsal horn. The ipsilateral and contralateral L_{4-5} dorsal horn tissues were collected from naive rats and rats at 0.5 h to 14 d after injection of CFA or saline into a hindpaw. Consistent with the previous studies (Guo et al., 2002; Zhang et al., 2003), CFA, but not saline, injection produced mechanical hypersensitivity on the ipsilateral side, which developed over 0.5–2 h, reached a peak level around day 1, lasted for at least 7 d, and disappeared at day 14 (Fig. 1*A*). A time-dependent change in the level of GluR2-p Ser^{880} in the ipsilateral dorsal horn was observed when compared with naive rats (0 h) (Fig. 1*B*) ($n = 5$/time point). A significant increase in GluR2-p Ser^{880} began at 2 h (160 ± 20% of naive group; $p < 0.05$) and was maintained for at least 7 d after CFA injection (Fig. 1*B*). No significant changes were observed at 0.5 h (120 ± 8%; $p > 0.05$) or 14 d (95 ± 10%; $p > 0.05$) after CFA. As expected, the expression level of GluR2-p Ser^{880} in the contralateral dorsal horn was not markedly altered during the observed period (supplemental Fig. S1*A*, available at www.jneurosci.org as supplemental material). Saline injection did not change the basal level of GluR2-p Ser^{880} in either side of dorsal horn (supplemental Fig. S1*B*, available at www.jneurosci.org as supplemental material). These results indicate that the increase in dorsal horn GluR2-p Ser^{880} is associated with CFA-induced peripheral inflammation.

We also examined whether persistent inflammatory insult affects total GluR2 protein expression in dorsal horn. Consistent with previous studies (Lee and Ro, 2007; Lu et al., 2008), quantitative Western blot analysis indicated that CFA injection did not lead to a significant change in the level of total GluR2 in either side of dorsal horn within a 14 d period (Fig. 1*B*; supplemental Fig. S1*A*, available at www.jneurosci.org as supplemental material), indicating that CFA-induced inflammation alters GluR2 phosphorylation status rather than total GluR2 protein expression in dorsal horn neurons.

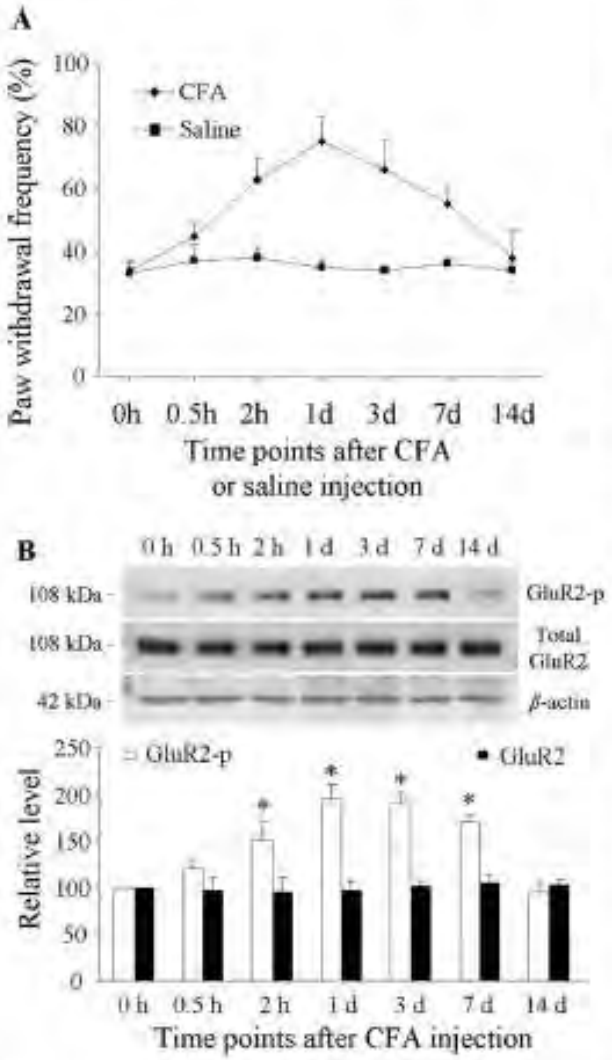

Figure 1. Increased mechanical hypersensitivity and dorsal horn GluR2 phosphorylation at Ser^{880} (GluR2-p) after CFA injection. *A*, Paw withdrawal frequency changed over time in response to mechanical stimulation on the ipsilateral side after CFA ($n = 10$/time point), but not saline ($n = 10$/time point), injection into a hindpaw. *B*, Top, Representative Western blots showing time-dependent changes of GluR2 phosphorylation at Ser^{880}, but not of total GluR2, in the ipsilateral dorsal horn after CFA injection; bottom, statistical summary of the densitometric analysis expressed relative to the naive animals (0 h). *$p < 0.05$ versus the naive group.

CFA injection disrupts binding of spinal GluR2 to GRIP1 and promotes synaptic GluR2 internalization in dorsal horn neurons

The C terminus of GluR2 contains a PDZ-binding motif that interacts with the PDZ domains of two scaffolding proteins, PICK1 and ABP/GRIP. ABP/GRIP anchors and stabilizes GluR2 at synaptic membranes (Dong et al., 1997, 1999a,b), whereas PICK1 presents PKC to ABP/GRIP–GluR2 complexes, leading to phosphorylation of GluR2 at Ser^{880} (Staudinger et al., 1997; Perez et al., 2001; Dev et al., 2004). GluR2 phosphorylated at Ser^{880} loses its ability to interact with ABP/GRIP, but the interaction of GluR2 with PICK1 remains intact (Chung et al., 2000; Perez et al., 2001). This differential effect may arise from the different structure of the ABP/GRIP and PICK1 PDZ domains (Chung et al., 2000). These *in vitro* results suggest that a CFA-induced increase in GluR2-p Ser^{880} might affect the binding affinity of GluR2 to ABP/GRIP (but not PICK1) and promote GluR2 internalization in *in vivo* dorsal horn neurons.

To test this hypothesis, we examined the interaction of spinal GluR2 with GRIP1 and PICK1 under CFA-induced inflammatory conditions. Coimmunoprecipitation was performed in ipsilateral L_{4-5} dorsal horn tissues at 1 d after CFA ($n = 4$) or saline ($n = 4$). In the saline-treated groups, GluR2 was immunoprecipitated with GRIP1 antibody or PICK1 antibody, indicating that GluR2 binds to both proteins in dorsal horn (Fig. 2). Interestingly, CFA injection significantly reduced the amount of GluR2 immunoprecipitated by GRIP1 antibody, although the amount of GRIP1 immunoprecipitated remained unchanged (Fig. 2*A*). The amount of GluR2 and PICK1 immunoprecipitated by PICK1 antibody in the tissues from CFA-treated rats was similar to that from the saline-treated rats (Fig. 2*B*). Total expression of GluR2, PICK1, and GRIP1 in dorsal horn from the CFA-treated rats was similar to that from the saline-treated groups (Fig. 2). These findings indicate a reduction in the binding affinity of GluR2 to GRIP, but not to PICK1, in dorsal horn neurons under persistent inflammatory pain conditions.

Next, we investigated whether this reduced affinity affects synaptic GluR2 membrane expression in dorsal horn neurons *in vivo*. Because GluR2 is transported away from the synaptic membrane mainly via clathrin-coated pit-dependent endocytosis (Matsuda et al., 2000), we used differential centrifugation to collect a 150 k-g spin fraction that contained abundant endocytosed, clathrin-coated vesicles (Matsuda et al., 2000) from the ipsilateral L_{4-5} dorsal horn tissues of naive rats (0 h) and rats at 2 h to 3 d after CFA ($n = 5$/time point) or saline ($n = 5$/time point). The crude membrane fraction was also fractionated. Consistent with previous studies (Matsuda et al., 2000; Tao et al., 2000), the 150 k-g spin proteins were effectively separated from the plasma membrane proteins (data not shown). We found that the amounts of GluR2 in the 150 k-g fraction were 195 ± 11% and 185 ± 5% higher than those of the naive group on days 1 and 3 after CFA, respectively, and correspondingly 67 ± 6% and 63 ± 8% lower in the membrane fraction at the same time points (Fig. 3*A*,*B*). Unexpectedly, the GluR2 level was not significantly changed in either the 150 k-g (96 ± 9% of the naive group; $p > 0.05$) or membrane (94 ± 4% of the naive group; $p > 0.05$) fractions at 2 h after CFA (Fig. 3*A*,*B*). No significant differences were observed between the saline-treated and naive groups in either the 150 k-g or membrane fractions at 2 h, 1 d, or 3 d after saline (Fig. 3*A*,*B*).

To further confirm GluR2 loss in the membranes of dorsal horn neurons, we used a surface biotinylation expression assay to compare the surface expression of GluR2 in adult dorsal horn neurons between the saline-treated and CFA-treated groups. Live slices were prepared from the ipsilateral L_{4-5} dorsal horn 1 d after CFA or saline. The surface receptors were labeled with biotin and then precipitated (Tao et al., 2003; Holman and Henley, 2007). The ratio of surface to total GluR2 was determined by quantitative Western blotting. The biochemical analysis showed that surface GluR2 in the CFA-treated group was 56% lower than that in the saline-treated group ($n = 5$/group; $p < 0.05$) (Fig. 3*C*). CFA injection had no effect on surface expression of NMDAR subunit NR1 in dorsal horn 1 d after CFA (Fig. 3*C*), ruling out the possibility of nonspecific changes.

To directly display the changes in synaptic expression of GluR2 in the superficial dorsal horn neurons in persistent inflammatory pain, we used a combined approach of postembedding immunogold labeling with electron microscopy. Ultrathin sections were prepared from rat ipsilateral L_{4-5} superficial dorsal

horn 1 d after CFA ($n = 2$) or saline ($n = 2$). Consistent with previous reports (Petralia et al., 1997; Morrison et al., 1998; Lu et al., 2002), GluR2 immunogold labeling was distributed mainly in postsynaptic profiles with few gold particles located presynaptically in the saline-treated group (Fig. 3*D*). CFA injection produced a decrease in the number of GluR2-labeled particles in the postsynaptic membrane and a corresponding increase in the cytoplasm (Fig. 3*D*). The number of GluR2-labeled particles/synapse in the CFA-treated group ($n = 99$ synapses) was 39% lower than that of the saline-treated group ($n = 109$ synapses) ($p < 0.05$). In addition, the ratio of the number of GluR2-labeled particles in the synapse to the number in the cytoplasm plus extrasynaptic membrane of the postsynaptic structure in the CFA-treated group was 54% lower than that in the saline-treated group ($n = 47–64$ profiles/group, $p < 0.05$). These findings further support the results obtained from the biochemical studies described above, indicating GluR2 internalization in dorsal horn neurons during the maintenance period of persistent inflammatory pain.

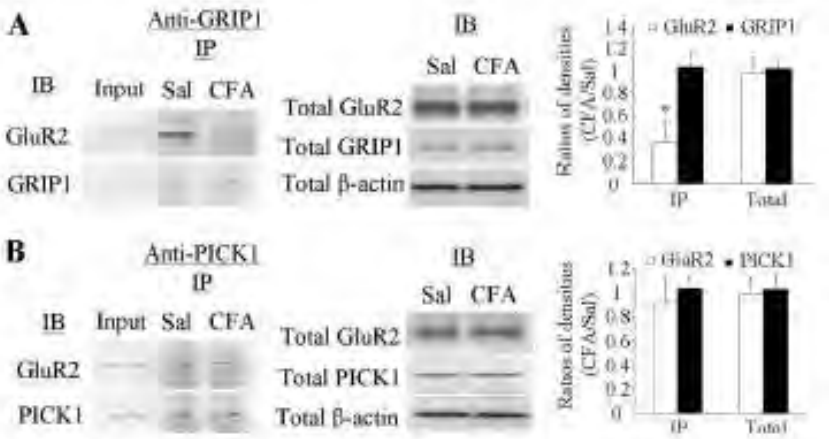

Figure 2. Reduced binding affinity of GluR2 to GRIP1, but not PICK1, in dorsal horn 1 d after CFA. ***A***, Left, Coimmunoprecipitation of GluR2 and GRIP1 with anti-GRIP1; middle, total expression of GluR2 and GRIP1; right, statistical summary for the ratios of the densities from the CFA-treated groups to those from the saline-treated groups. ***B***, Left, Coimmunoprecipitation of GluR2 and PICK1 with anti-PICK1; middle, total expression of GluR2 and PICK1; right, statistical summary for the ratios of the densities from the CFA-treated groups to those from the saline-treated groups. IB, Immunoblotting; IP, immunoprecipitation; Sal, saline. $^*p < 0.05$ versus the saline-treated groups. β-Actin was used as a loading control.

To examine whether CFA-induced inflammatory noxious input was required for dorsal horn GluR2 internalization, we infused vehicle (saline) or the nerve conduction blocker bupivacaine (0.5%; dissolved in saline; AstraZeneca) to the ipsilateral sciatic nerve for 1 d via an osmotic minipump (0.1 ml/h) beginning 3 h before or 2 d after CFA injection. The mechanical behavioral test was performed before infusion and on days 1, 2 or 3 after injection. L_{4-5} dorsal horns ipsilateral and contralateral to injection were collected on days 1 and 3 after behavioral tests, and the 150 k-g fraction was prepared. Consistent with previous reports (Beloeil et al., 2006; Wen et al., 2007), infusion of bupivacaine induced sensory (responses to pinch and von Frey filaments) and motor (responses to placing and grasping reflexes) blockade within 2.5–3 h. This effect lasted for at least 5–6 h, without signs of nerve damage, because all of these rats recovered to full sensory and motor responsiveness after the block wore off (data not shown). Therefore, none of the rats that were infused with bupivacaine for 1 d responded to ipsilateral mechanical stimulus on days 1 or 3 after CFA (Fig. 4*A*,*C*) ($n = 5$/group). Neither bupivacaine nor vehicle affected basal response to mechanical stimulus on the contralateral side (data not shown). Importantly, GluR2 protein expression in the ipsilateral dorsal horn 150 k-g fraction was significantly greater in the vehicle + CFA group than in the vehicle + saline group on days 1 and 3 after CFA (Fig. 4*B*,*D*) ($p < 0.01$; $n = 4$/group). CFA injection increased the amount of GluR2 by 1.75-fold on day 1 and by 1.9-fold on day 3 compared with saline injection. These increases were abolished in the bupivacaine + CFA group (94 ± 6.5% on day 1 and 90 ± 8% on day 3) (Fig. 4*B*,*D*). Bupivacaine treatment alone did not alter the expression of GluR2 in the 150 k-g fraction (data not shown). These findings indicate that peripheral inflammatory input is required to induce and maintain GluR2 internalization in dorsal horn neurons.

Synaptic GluR2-containing AMPARs in dorsal horn neurons of substantia gelatinosa decrease strikingly after CFA injection

GluR2 determines the properties of AMPARs, including Ca^{2+} permeability (Burnashev et al., 1992; Swanson et al., 1997). If CFA-induced inflammation drives synaptic GluR2 internalization, dorsal horn neurons would be expected to lose synaptic GluR2-containing AMPARs after CFA-induced inflammation. To test this hypothesis, we recorded EPSCs evoked by primary afferent stimulation from visually identified SG neurons of ipsilateral L_{4-5} dorsal horn 1 d after CFA or saline. The AMPAR component was isolated by application of 50 μM APV (an NMDAR antagonist), 10 μM bicuculline methiodide (a GABAR antagonist), and 2 μM strychnine hydrochloride (a glycine receptor antagonist). There were no significant differences between the saline-treated and CFA-treated groups in resting membrane potential (-60 ± 0.8 mV, $n = 38$ vs -58 ± 0.7 mV, $n = 31$, $p > 0.5$), neuronal input resistance (511.8 ± 49.9, $n = 38$ vs 586.1 ± 74.3, $n = 31$, $p > 0.5$), or threshold to evoked action potentials (-33.5 ± 0.9 mV, $n = 38$ vs -34.0 ± 1.4 mV, $n = 31$, $p > 0.5$). The eEPSCs were dramatically blocked by 95 ± 2% by an AMPAR antagonist, GYKI52466 (100 μM), but were not affected by a kainate receptor antagonist, SYM 2081 (3 μM), in either the saline-treated ($n = 4$) or CFA-treated ($n = 4$) rats (Fig. 5*A*), indicating that eEPSCs were mediated predominantly by AMPARs. Decay and rise times of eEPSCs revealed no significant differences between the saline-treated and CFA-treated rats (decay time: 1.3 ± 0.1 ms, $n = 11$ vs 1.2 ± 0.2 ms $n = 10$, $p > 0.5$; rise time: 4.7 ± 0.5 ms, $n = 11$ vs 5.7 ± 0.6 ms $n = 9$, $p > 0.2$).

Polyamine toxin PhTx-433 is a selective blocker of Ca^{2+}-permeable (GluR2-lacking) AMPARs (Tóth and McBain, 1998). Bath application of PhTx-433 (40 μM) inhibited AMPAR-mediated eEPSCs to a greater degree in SG neurons from the CFA-treated groups than in those from the saline-treated groups (Fig. 5*B*). Sixteen minutes after application of PhTx-433, eEPSC amplitude was inhibited by 51 ± 4% from baseline in the CFA-treated groups ($n = 4$) but only by 23 ± 3% from baseline in the saline-treated group ($n = 4$; $p < 0.01$). Given that AMPAR Ca^{2+} permeability is greatly influenced by the presence or absence of synaptic GluR2, this result indicates a reduction in the proportion of synaptic GluR2-containing AMPARs in SG neurons at 1 d after CFA.

As described above, another prominent feature of GluR2-lacking AMPARs is an inwardly rectifying *I–V* relationship

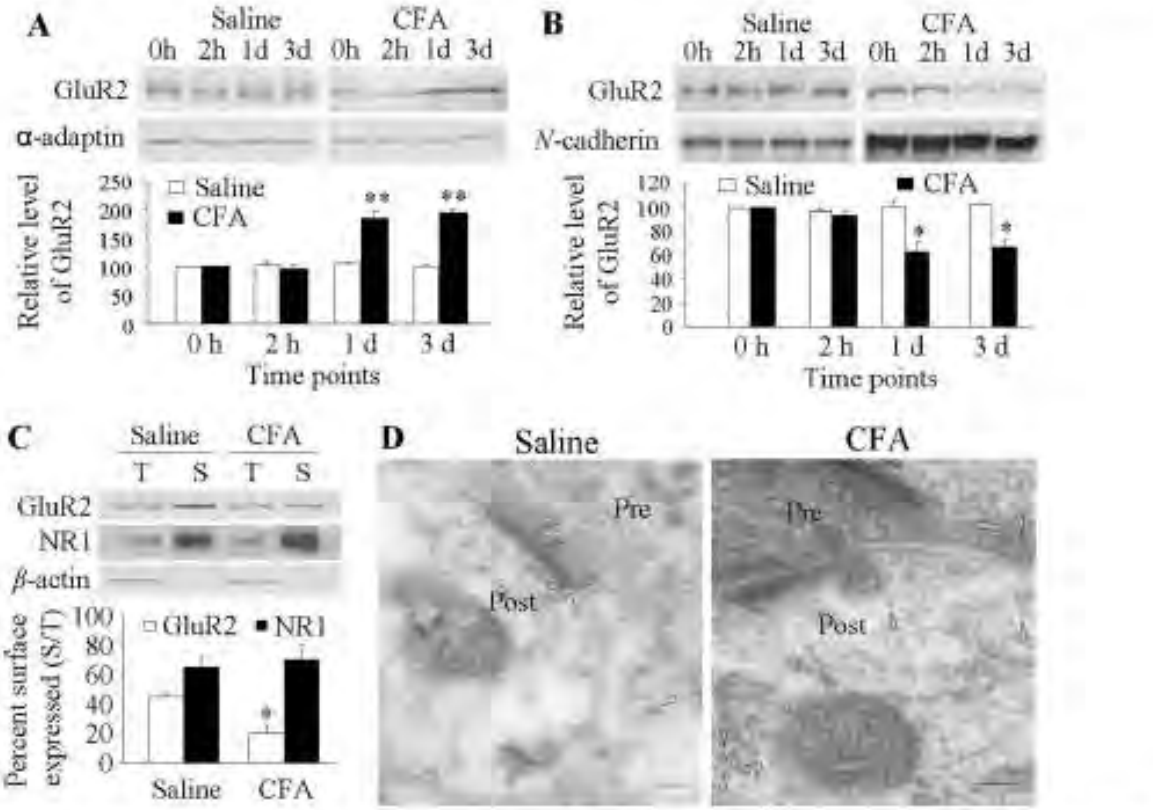

Figure 3. Dorsal horn GluR2 internalization after CFA injection. GluR2 expression in 150 k-g spin fraction (*A*) and plasma membrane fraction (*B*) from ipsilateral dorsal horn at 2 h, 1 d, and 3 d after saline or CFA. Top, Representative Western blots; bottom, statistical summaries of the densitometric analysis expressed relative to the naive animals (0 h). $^{*}p < 0.05$, $^{**}p < 0.01$ versus the naive group. *C*, Surface expression of GluR2 and NR1 in dorsal horn neurons at 1 d after CFA or saline. Top, Representative Western blot; bottom, statistical summary of the densitometric analysis. The amount of sample loaded for the total (T) was 10% of that for the biotinylated surface (S). $^{*}p < 0.05$ versus the saline-treated group. α-Actin, an unbiotinylated intracellular protein, was used as a control. *D*, Examples of postsynaptic immunogold labeling for GluR2 in superficial dorsal horn synapses illustrate labeling (arrowheads) in both the synapse and adjacent cytoplasmic structures 1 d after saline and only in cytoplasm 1 d after CFA. Pre, Presynaptic terminal; Post, postsynaptic structure. Scale bars, 100 nm.

(curve) of their eEPSCs, which can be quantitatively expressed as a RI. As shown in Figure 5*C*, *I–V* curves obtained from SG neurons of the saline-treated group had weak rectification at positive potentials, whereas a well marked inward rectification was observed in the SG neurons of the CFA-treated group. The SG neurons from the saline-treated animals had an average RI value of 0.26 ± 0.01 (range: 0.17–0.37, $n = 16$), whereas the average RI in SG neurons from the CFA-treated animals was 0.18 ± 0.02 (range: 0.08–0.29, $n = 12$; $p < 0.01$). Given that a reduced RI reflects the loss of synaptic GluR2-containing AMPARs (Tong and MacDermott, 2006), this finding further demonstrates CFA-induced synaptic GluR2 internalization in SG neurons of dorsal horn at 1 d after CFA.

Interestingly, the amplitudes of synaptic AMPAR-mediated eEPSCs at −70 mV (-191 ± 27 pA; $n = 10$) in the SG neurons of the CFA-treated animals were not markedly different from those of the saline-treated animals (-220 ± 45 pA; $n = 14$; $p > 0.6$). This suggests that the number of synaptic GluR2-lacking AMPARs in the SG neurons should be increased at 1 d after CFA. This increase may partially compensate for synaptic AMPAR EPSC reduction when synaptic GluR2-containing AMPARs are eliminated by synaptic GluR2 internalization. Indeed, the data from our laboratory and that of others showed that amount of GluR1 was increased in the postsynaptic density fraction from spinal cord 1 d after CFA (Katano et al., 2008; Park et al., 2008). These findings indicate a switch of GluR2-containing AMPARs to GluR2-lacking AMPARs at the synapses of dorsal horn neurons at 1 d after CFA.

Spinal NMDA receptor and PKC activation are involved in inflammation-induced phosphorylation and internalization of GluR2 in dorsal horn neurons

The increase of $[Ca^{2+}]_i$ that is required for PKC activation can result from an inflow through NMDAR channels (Basbaum and Woolf, 1999). Because spinal cord NMDARs and PKC are activated under persistent inflammatory pain conditions (Basbaum and Woolf, 1999), we hypothesized that spinal NMDAR-mediated triggering of PKC activation would induce GluR2-p Ser^{880} and GluR2 internalization in dorsal horn neurons during the maintenance of CFA-induced inflammatory pain.

To study this hypothesis, we challenged an *in vitro* spinal dorsal horn neuronal culture with NMDAR agonist (NMDA, 40 μM) and antagonist (APV, 50 μM) or with PKC activator (PMA/TPA, 1 μM) and inhibitor (chelerythrine chloride, 10 μM). The drug doses used were based on previous studies of *in vitro* cultured brain neurons (Chung et al., 2000, 2003; Tigaret et al., 2006). PMA significantly induced phosphorylation of GluR2 at Ser^{880} and GluR2 internalization in dorsal horn neurons (Fig. 6*A*, *B*). Compared with the control groups (GluR2-p Ser^{880}: 100%, $n = 4$; surface GluR2: 40 ± 5%, $n = 4$), the level of GluR2-p Ser^{880} increased by 2.3-fold ($n = 4$; $p < 0.01$) and surface GluR2 decreased by 75% ($n = 4$; $p < 0.01$). PMA-induced effects were

abolished by chelerythrine chloride (GluR2-p Ser^{880}: 110 ± 12.5%, $n = 4$; surface GluR2: 42 ± 4%, $n = 4$) (Fig. 6*A*,*B*). Chelerythrine chloride treatment alone did not affect basal expression of GluR2-p Ser^{880} ($n = 4$) or surface GluR2 ($n = 4$) (Fig. 6*A*,*B*). NMDA stimulation markedly increased the level of GluR2-p Ser^{880} (170 ± 6%, $n = 4$; $p < 0.01$) and reduced surface GluR2 (15 ± 6%, $n = 4$; $p < 0.01$) compared with the control groups (GluR2-p Ser^{880}: 100%, $n = 4$; surface GluR2: 50 ± 2%, $n = 4$) (Fig. 6*C*,*D*). Moreover, NMDA-stimulated effects were attenuated dramatically not only by APV (GluR2-p Ser^{880}: 107 ± 10%, $n = 4$; surface GluR2: 40 ± 8%, $n = 4$), but also by chelerythrine chloride (GluR2-p Ser^{880}: 105 ± 7%, $n = 4$; surface GluR2: 42 ± 2%, $n = 4$) (Fig. 6*C*,*D*). These findings suggest that NMDAR activation induces PKC-mediated GluR2-p Ser^{880} and GluR2 internalization in dorsal horn neurons. APV treatment alone did not affect basal expression of GluR2-p Ser^{880} ($n = 4$) or surface GluR2 ($n = 4$) (Fig. 6*C*,*D*). PMA, chelerythrine chloride, NMDA, APV, and their combined treatment failed to change total GluR2 protein or surface NMDAR subunit NR2B expression (used as a control) (Fig. 6).

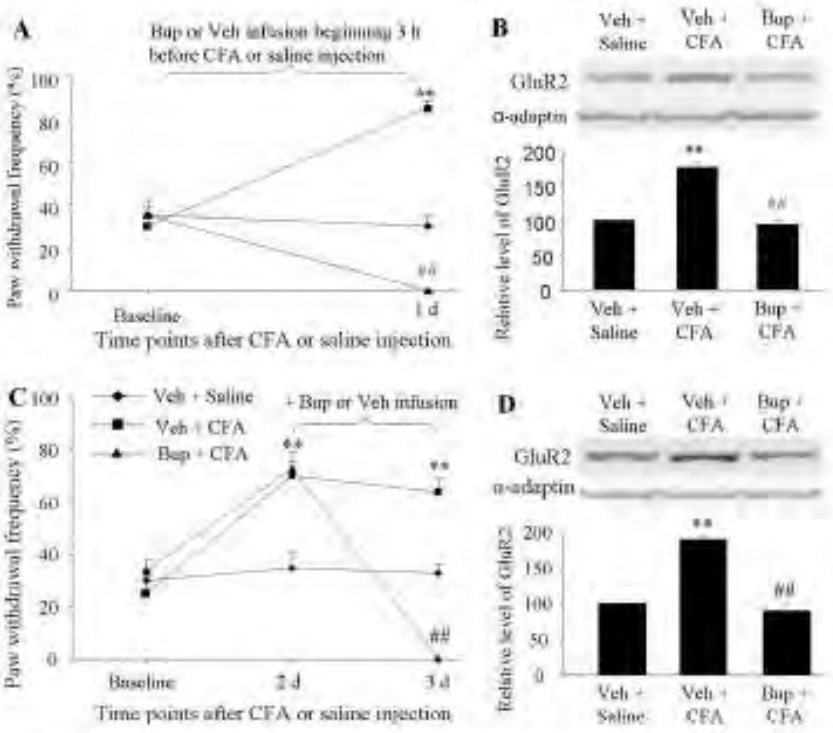

Figure 4. Requirement of CFA-induced inflammatory input for induction and maintenance of dorsal horn GluR2 internalization. Perisciatic nerve infusion of bupivacaine (Bup) for 1 d beginning 3 h before (*A*, *B*) or 2 d after (*C*, *D*) CFA injection blocked paw withdrawal responses to mechanical stimulation on the ipsilateral side at times shown (*A*, *C*). Bup also blocked CFA-induced increases in the amount of GluR2 in the 150 k-g fraction (*B*, *D*). $^{**}p < 0.01$ versus the vehicle (Veh) + saline group; $^{\#\#}p < 0.01$ versus the vehicle + CFA group.

Activation of AMPARs and group 1 metabotropic glutamate receptors (mGluRs) induced GluR2 internalization in cultured hippocampal neurons (Lin et al., 2000; Snyder et al., 2001). $[Ca^{2+}]_i$ may increase as a result of an inflow of extracellular Ca^{2+} through GluR2-lacking AMPARs and mobilization of intracellular stores through the activation of the IP3 pathway following group 1 mGluR activation. Thus, one might expect GluR2-lacking AMPAR and group 1 mGluR activation in dorsal horn neurons to induce PKC GluR2-p Ser^{880} and GluR2 internalization. To test this possibility, cultured dorsal horn and cortical neurons were treated with AMPA (100 μM), GYKI52466 (30 μM), DHPG (50 μM; agonist of group 1 mGluRs), and MPEP (100 μM; antagonist of group 1 mGluRs). The dosage of these drugs was based on previous *in vitro* studies (Lin et al., 2000; Snyder et al., 2001). In cultured cortical neurons, stimulation with AMPA and DHPG reduced surface GluR2 expression and was reversed by GYKI52466 and MPEP, respectively (supplemental Fig. S2*A*,*B*, available at www.jneurosci.org as supplemental material). However, in cultured dorsal horn neurons, these agonists did not significantly change basal levels of GluR2-p Ser^{880} or surface GluR2 expression (supplemental Fig. S3, available at www.jneurosci.org as supplemental material). These results suggest that in dorsal horn neurons, activation of AMPARs and group 1 mGluRs is not linked to induction of PKC GluR2-p Ser^{880} and GluR2 internalization.

Next we examined whether blocking spinal NMDAR and PKC activation affects CFA-induced increases in GluR2 internalization in dorsal horn during the maintenance of inflammatory pain. The rats were infused intrathecally with vehicle ($n = 30$), APV (25 nmol/μl/h, $n = 15$), or chelerythrine chloride (3 nmol/μl/h, $n = 15$) for 1 d via an osmotic minipump beginning 1 h before or 2 d after CFA (or saline) injection. The dosage of these two drugs was based on previous studies (McNally and Westbrook, 1998; Granados-Soto et al., 2000; Sun et al., 2006). The mechanical behavioral test was performed before drug infusion and on days 1, 2, or 3 after injection. L_{4-5} dorsal horns ipsilateral and contralateral to injection were collected on days 1 and 3 after behavioral tests, and the 150 k-g fraction was prepared. Pretreatment and posttreatment with APV or chelerythrine chloride significantly attenuated CFA-induced mechanical pain hypersensitivity on the ipsilateral side on days 1 and 3 after CFA; neither drug affected basal paw withdrawal responses to mechanical stimulation on either the ipsilateral or contralateral side (Fig. 7*A*,*B*,*E*). As expected, CFA injection markedly increased the amount of GluR2 in the 150 k-g fraction on days 1 and 3 after CFA compared with saline injection; these increases were markedly blocked by pretreatment or posttreatment with chelerythrine chloride (pretreatment: 105 ± 10% of the vehicle + saline group; posttreatment: 90 ± 7% of the vehicle + saline group) or APV (pretreatment: 116 ± 12% of the vehicle + saline group; posttreatment: 105 ± 4% of the vehicle + saline group) (Fig. 7*C*,*D*,*F*). Neither chelerythrine chloride (96 ± 6% of the vehicle + saline group) nor APV (110 ± 4% of the vehicle + saline group) treatment alone altered the expression of GluR2 in the 150 k-g fraction (Fig. 7*C*,*D*). These *in vivo* findings indicate that spinal NMDARs and PKC activation are required for induction and maintenance of CFA-induced GluR2 internalization in dorsal horn neurons.

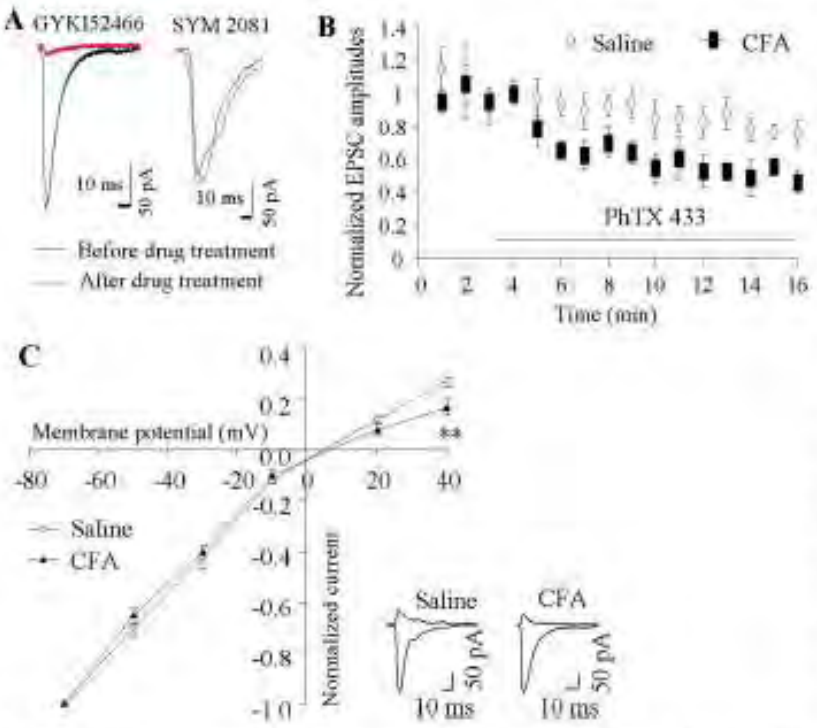

Figure 5. AMPAR-mediated evoked EPSCs at synapses between primary afferents and the SG neurons of dorsal horn. *A*, The evoked EPSCs were dramatically blocked by GYKI52466 ($n = 4$), but not by SYM 2081 ($n = 4$). Examples of EPSCs under control conditions and blockers. *B*, Pooled data for EPSC amplitude (normalized to mean amplitude before PhTx-433 application) versus time for experiments in which PhTx-433 (40 μM) was bath applied to spinal cord slices from rats 1 d after CFA ($n = 4$) or saline ($n = 4$). *C*, *I–V* curves at 1 d after saline or CFA. Inset at bottom, Examples of the eEPSCs at −70 mV and +40 mV holding potentials. $^{**}p < 0.01$ versus the saline-treated group.

NMDARs and PKCα are physically coupled to AMPARs in dorsal horn

The above findings suggest a physical link between AMPARs and NMDARs or PKC at synapses in spinal cord dorsal horn. Using a coimmunoprecipitation technique, we demonstrated a complex assembled by PICK1 with GluR2 and PKCα or by a PSD-95-stargazin linkage with GluR2 and NMDAR subunit NR2B in rat spinal cord dorsal horn. PICK1 antibody immunoprecipitated PICK1, GluR2, and PKCα, but not PKCβ1 and PKCγ (Fig. 8*A*). This finding is in agreement with previous *in vitro* studies demonstrating that, among PKC isoenzymes, only PKCα contains a unique PDZ ligand that binds to PICK1 PDZ domain (Staudinger et al., 1997). In addition, GluR2 antibody immunoprecipitated GluR2 as well as PICK1 and PKCα (Fig. 8*B*), indicating a triple GluR2-PICK1-PKCα complex in dorsal horn. Immunoprecipitation also revealed that NR2B and stargazin bind to PSD-95 and that PSD-95 and GluR2 bind to stargazin in dorsal horn (Fig. 8*C*,*D*), indicating that PSD-95 interaction with stargazin acts as a bridge to couple NMDARs and AMPARs. Our previous studies and those of others showed that NR2A/2B, PSD-95, GluR2, and stargazin are highly expressed in superficial dorsal horn and that GluR2 colocalizes with stargazin and PSD-95 in this region (Tao et al., 2000, 2003, 2006; Polgár et al., 2008). Under electron microscopy, superficial dorsal horn sections exhibited double labeling for GluR2 and NR1 in the synapse (Fig. 8*E*), indicating colocalization of AMPARs and NMDARs. Together, these findings present a molecular basis for the physical coupling of NMDARs and PKC to AMPARs in dorsal horn.

Targeted mutation of the GluR2 PKC phosphorylation site impairs pain hypersensitivity during the maintenance of CFA-induced inflammatory pain

Finally, we investigated whether inflammation-induced GluR2 internalization in dorsal horn neurons participates in pain hypersensitivity under persistent inflammatory pain conditions. Our findings presented above and previous studies (Chung et al., 2003; Steinberg et al., 2006) indicate that PKC GluR2-p Ser^{880} is the key initial regulatory step for induction of GluR2 internalization. Direct mutation of GluR2 Ser^{880} to alanine disrupts binding of GluR2 to GRIP (Dong et al., 1997; Osten et al., 2000), whereas mutation of GluR2 Ser^{882} to alanine (K882A) disrupts the PKC consensus site (S/T-T-K/R), prevents PKC phosphorylation of GluR2 at Ser^{880}, and interferes with GluR2 internalization (but does not interfere with GluR2 binding to PICK1 and GRIP) in central neurons (Chung et al., 2003; Steinberg et al., 2006). Therefore, we used GluR2K882A KI mice to investigate whether preventing CFA-induced spinal GluR2 internalization affects CFA-induced nociceptive hypersensitivity.

Basal levels of GluR2-p Ser^{880} and GluR2 in the 150 k-g fraction from either side of the dorsal horn were similar in WT and GluR2K882A KI mice (Fig. 9*A*; supplemental Fig. S4, available at www.jneurosci.org as supplemental material). Consistent with the findings in rats, CFA injection significantly increased the level of GluR2-p Ser^{880} ($170 \pm 5\%$, $n = 3$, $p < 0.05$) and the amount of GluR2 in the 150 k-g fraction ($180 \pm 7\%$, $n = 3$, $p < 0.05$) from the ipsilateral (but not contralateral) dorsal horn of WT mice 1 d after injection (Fig. 9*A*; supplemental Fig. S4, available at www.jneurosci.org as supplemental material). In contrast, those indices were unchanged in GluR2K882A KI mice at the same time point (Fig. 9*A*; supplemental Fig. S4, available at www.jneurosci.org as supplemental material). Saline injection did not alter basal levels of GluR2-p Ser^{880} or the amount of GluR2 in the 150 k-g fraction in WT or GluR2K882A KI mice (Fig. 9*A*; supplemental Fig. S4, available at www.jneurosci.org as supplemental material).

WT mice injected with CFA in one hindpaw developed long-term thermal nociceptive hypersensitivity (indicated by a significant decrease in paw withdrawal latency) and mechanical hypersensitivity (indicated by a marked increase in paw withdrawal frequency) on the ipsilateral side (Fig. 9*B–D*). The nociceptive hypersensitivity developed at 2 h, reached a peak on day 1, and persisted for at least 7 d after CFA injection (Tao et al., 2003; Chu et al., 2005). The basal paw withdrawal responses to thermal and mechanical stimuli were similar between WT ($n = 10$/test) and GluR2K882A KI ($n = 10$/test) mice (Fig. 9*B–D*). Although GluR2K882A KI mice developed intact thermal and mechanical nociceptive hypersensitivities 2 h after CFA, both types of hypersensitivity were impaired during the remainder of the observation period (Fig. 9*B–D*). The magnitude of response latencies to

thermal stimulation was significantly increased and the magnitude of response frequencies to mechanical stimuli markedly reduced from day 1 to day 7 after CFA in the GluR2K882A KI mice compared with those in the WT mice ($p < 0.05$). No significant changes in paw withdrawal responses to thermal and mechanical stimuli were seen on the contralateral side in either WT or GluR2K882A KI mice after CFA injection (Fig. 9*B–D*). These findings indicate that the GluR2K882A KI mice display blunted pain hypersensitivity during the maintenance phase (from day 1 to day 7 after CFA), but not during the development (2 h after CFA) of persistent inflammatory pain.

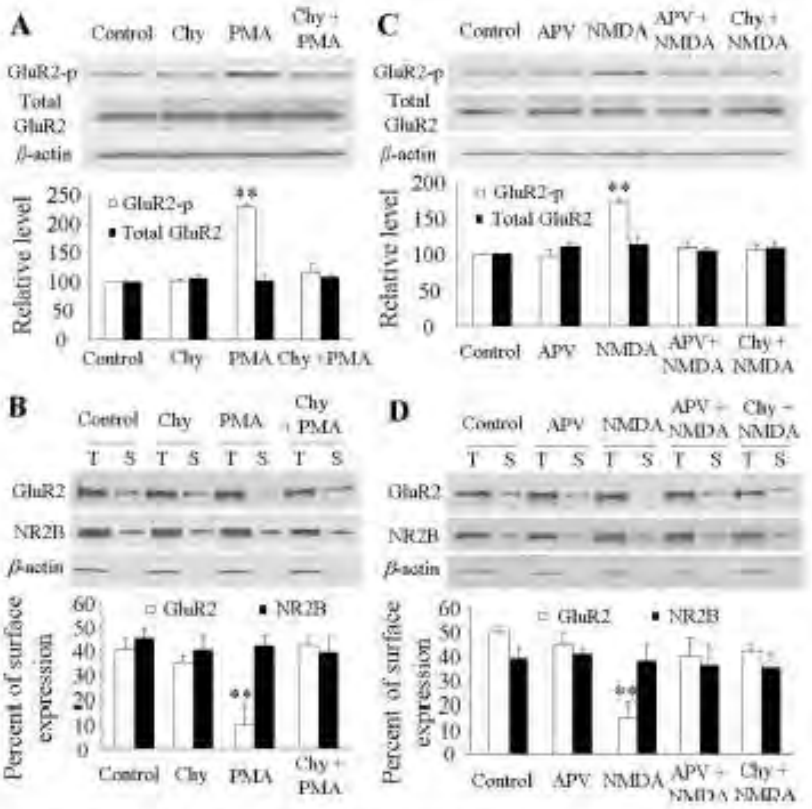

Figure 6. Induction of GluR2 phosphorylation at Ser^{880} (GluR2-p Ser^{880}) and GluR2 internalization in cultured dorsal horn neurons after NMDAR and PKC activation. PMA stimulation increased expression of GluR2-p Ser^{880} (but not total GluR2) (*A*) and reduced surface expression of GluR2 (but not NR2B) (*B*); these changes were abolished by chelerythrine chloride (Chy). NMDA stimulation increased expression of GluR2-p Ser^{880} (but not total GluR2) (*C*) and reduced surface expression of GluR2 (but not NR2B) (*D*); these changes were abolished by both APV and Chy. $^{**}p < 0.01$ versus control group.

Discussion

Cumulative evidence suggests that activity-dependent AMPAR trafficking at postsynaptic membranes is critical for synaptic plasticity and structural remodeling (Liu and Zukin, 2007; Santos et al., 2009). However, the role of regulated AMPAR trafficking in spinal central sensitization associated with persistent pain is much less understood. Here, we show that AMPAR subunit GluR2 is internalized in dorsal horn neurons after CFA-induced inflammation. This internalization is dependent on spinal cord NMDAR/PKC activation and is causally linked to CFA-inflammatory pain.

Normally, AMPAR subunits are constitutively recycled between the synaptic membrane and the intracellular compartment via membrane insertion (exocytosis) and clathrin-mediated internalization (endocytosis). The number of subunits expressed on the synaptic membrane is dependent on the balance between these two processes (Adesnik et al., 2005; Greger and Esteban, 2007). Using biochemical and morphological approaches, we found that GluR2 is internalized in dorsal horn neurons during days 1–3 after CFA. These findings indicate that inflammatory insult breaks the balance of GluR2 recycling between membrane insertion and internalization and promotes GluR2 trafficking away from synaptic membrane. Moreover, this inflammatory noxious input may be indispensable for induction and maintenance of dorsal horn GluR2 internalization because this event could not be induced by preinfusion and postinfusion of bupivacaine to the sciatic nerve or by saline injection.

Our results suggest that dorsal horn GluR2 internalization requires PKC phosphorylation of GluR2 at Ser^{880} in persistent inflammatory pain. Consistent with previous studies on cultured brain neurons (Perez et al., 2001; Hanley and Henley, 2005), PMA increased the level of GluR2-p Ser^{880} and reduced surface expression of GluR2 in the cultured dorsal horn neurons; these responses were blocked by chelerythrine chloride. Moreover, intrathecal preinfusion and postinfusion of chelerythrine chloride or prevention of GluR2 PKC phosphorylation at Ser^{880} attenuated the CFA-induced increase in the level of GluR2 in the dorsal horn 150 k-g fraction on days 1 and 3 after CFA. In addition, the binding affinity of GluR2 to GRIP1 in dorsal horn neurons was reduced on day 1 after CFA. These findings suggest that peripheral inflammatory insult activates spinal PKC and induces PKC phosphorylation of GluR2 Ser^{880} in dorsal horn. This phosphorylation disrupts GluR2 binding to ABP/GRIP and promotes dorsal horn GluR2 internalization under inflammatory pain conditions (Fig. 10).

Interestingly, we found no significant change in the amount of GluR2 in the dorsal horn 150 k-g spin fraction 2 h after CFA injection, although the level of GluR2-p Ser^{880} at 2 h after CFA was significantly increased compared with the naive group. This unexpected result is most likely attributable to the limited sensitivity of Western blot analysis. GluR2 internalization in dorsal horn neurons might be insufficient to be detectable at 2 h after CFA injection. Another possibility is that there may be a long timescale of synaptic AMPAR exchange for intracellular receptors in dorsal horn neurons because synaptic AMPAR trafficking events *in vitro* and in intact brains have a slow rate time constant of ~15–18 h (Adesnik et al., 2005; McCormack et al., 2006).

Our findings also suggest that spinal cord NMDAR activation, as an upstream trigger, leads to PKC phosphorylation of GluR2 Ser^{880} and GluR2 internalization in dorsal horn in persistent inflammatory pain. The AMPARs form multiprotein complexes with postsynaptic density proteins, including receptors, adaptor proteins, and protein kinases, at synapses (Derkach et al., 2007; Santos et al., 2009). These complexes allow for efficient intracellular signaling. The finding that NMDARs and PKCα are coupled

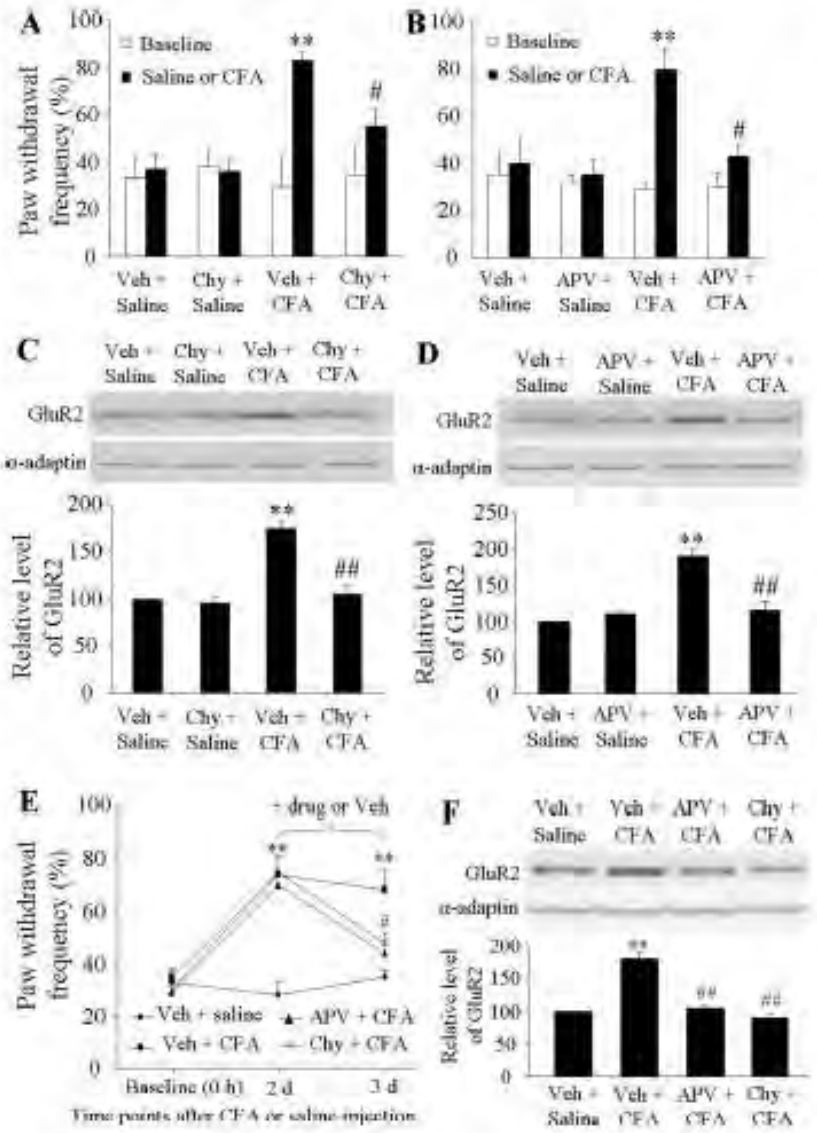

Figure 7. NMDAR/PKC-dependent mechanical hypersensitivity and dorsal horn GluR2 internalization on days 1 and 3 after CFA. Intrathecal infusion of Chy (*A*) or APV (*B*) for 1 d beginning 1 h before CFA injection attenuated CFA-induced ipsilateral mechanical hypersensitivity. $^{**}p < 0.01$ versus the saline + vehicle group; $^{\#}p < 0.05$ versus the CFA + vehicle group. Intrathecal infusion of Chy (*C*) or APV (*D*) for 1 d beginning 1 h before CFA injection abolished CFA-induced increases in the amount of GluR2 in the 150 k-g fraction. $^{**}p < 0.01$ versus the saline + vehicle group; $^{\#\#}p < 0.01$ versus the CFA + vehicle group. Intrathecal infusion of APV and Chy for 1 d beginning on day 2 after CFA reduced CFA-induced mechanical hypersensitivity (*E*) and increased the amount of GluR2 in the 150 k-g fraction (*F*). $^{**}p < 0.01$ versus the vehicle + saline group; $^{\#}p < 0.05$, $^{\#\#}p < 0.01$ versus the vehicle + CFA group.

with AMPARs via PICK1, PSD-95, and stargazin in the postsynaptic density of dorsal horn neurons provides a molecular basis for an NMDAR-PKC-AMPAR signal cascade (Fig. 10). Moreover, NMDA stimulation increased the level of GluR2-p Ser^{880} and reduced GluR2 surface expression in cultured dorsal horn neurons; these responses could be significantly attenuated by both APV and chelerythrine chloride. *In vivo*, intrathecal pretreatment and posttreatment with APV at the dose that significantly attenuated CFA-induced mechanical hypersensitivity markedly suppressed CFA-induced increases in the amount of GluR2 in the dorsal horn 150 k-g fraction at 1 and 3 d after CFA. Given that spinal cord NMDARs are activated after CFA injection (Dubner and Basbaum, 1997; Basbaum and Woolf, 1999), we propose that, after receiving strong primary afferent drive generated from peripheral nociceptors by inflammation, dorsal horn NMDARs are activated, increasing Ca^{2+} influx. The Ca^{2+} promptly activates PKC to phosphorylate GluR2 at Ser^{880} and to promote GluR2 internalization at postsynaptic dorsal horn neurons (Fig. 10). This conclusion is strongly supported by previous *in vitro* studies (Iwakura et al., 2001; Tigaret et al., 2006) which showed that NMDAR-triggered GluR2 internalization requires Ca^{2+} influx directly through NMDARs.

GluR2 internalization may result in an increase in synaptic AMPAR Ca^{2+} permeability in dorsal horn neurons after CFA injection. Under normal conditions, most dorsal horn AMPARs are Ca^{2+} impermeable. Our patch-clamp recording demonstrated a marked increase in the number of synaptic GluR2-lacking AMPARs in the SG neurons of dorsal horn 1 d after CFA. A previous study also reported an increase of synaptic GluR2-lacking AMPARs in neurokinin 1 receptor-positive lamina I neurons of dorsal horn on day 3 after CFA (Vikman et al., 2008). These results indicate a switch of GluR2-containing AMPARs expressed on many dorsal horn neurons to GluR2-lacking AMPARs (that is, an increase of Ca^{2+}-permeable AMPARs) after CFA injection. Although the cell types were not identified in our study or those of others (Katano et al., 2008; Vikman et al., 2008), it is very likely that this switch occurs on excitatory (but not inhibitory) neurons in the superficial dorsal horn, because most neurons in rat superficial dorsal horn (particularly in SG) are excitatory (Todd and Sullivan, 1990; Santos et al., 2007). It should be noted that our electrophysiological recording showed no changes in the amplitudes of synaptic AMPAR-mediated eEPSCs 1 d after CFA compared with the saline-treated groups. Since single-channel conductance of GluR2-lacking AMPARs is higher than that of GluR2-containing AMPARs (Burnashev et al., 1992; Swanson et al., 1997), it is very likely that after CFA injection, there are fewer GluR2-lacking AMPARs inserted in the synaptic membrane than internalized GluR2-containing AMPARs in dorsal horn neurons. Indeed, we found that the number of internalized GluR2 subunits is greater than the number of GluR1 subunits inserted in the membrane on day 1 after CFA (Park et al., 2008). Thus, GluR2 internalization may be a major player in CFA-induced increase of Ca^{2+}-permeable AMPARs in dorsal horn neurons.

Dorsal horn GluR2 internalization may be involved in the maintenance of CFA-induced inflammatory pain. We found that CFA-induced time-dependent changes in dorsal horn GluR2 internalization correlated with the time course of changes in CFA-

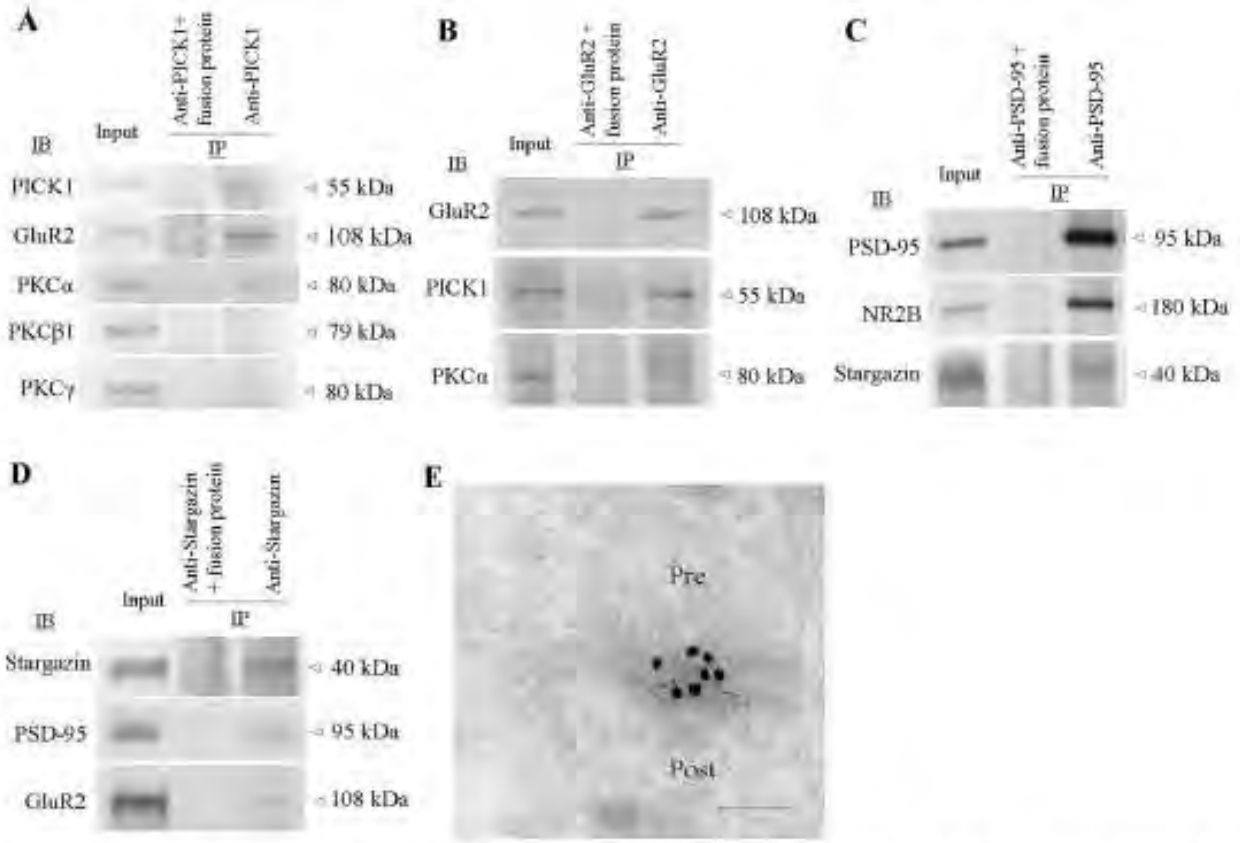

Figure 8. NMDARs and PKC couple to AMPAR complex in dorsal horn. *A*, PICK1 coimmunoprecipitates with GluR2 and PKCα (but not PKCβ or PKCγ). *B*, GluR2 coimmunoprecipitates with PICK1 and PKCα. *C*, PSD-95 coimmunoprecipitates with NR2B and stargazin. *D*, Stargazin coimmunoprecipitates PSD-95 and GluR2. *E*, NR1 (5 nm gold, arrowheads) and GluR2 (15 nm gold) colocalize at superficial dorsal horn synapses. Pre, Presynaptic terminal; Post, postsynaptic structure. Scale bar, 100 nm.

induced pain hypersensitivity during the maintenance period. Peripheral inflammatory input was required for induction and maintenance of dorsal horn GluR2 internalization. This finding indicates that dorsal horn GluR2 internalization might be a marker for inflammation-induced pain hypersensitivity during the maintenance period. We also showed that CFA-induced dorsal horn GluR2 internalization during the maintenance period is dependent on spinal cord NMDAR/PKC activation. Given that spinal cord NMDAR/PKC activation plays a critical role in inflammatory pain (Dubner and Basbaum, 1997; Basbaum and Woolf, 1999), dorsal horn GluR2 internalization may contribute to the mechanism by which NMDAR/PKC activation maintains inflammatory pain. As indicated above, GluR2 internalization leads to an increase in AMPAR Ca^{2+} permeability in dorsal horn neurons. Because the increase in $[Ca^{2+}]_i$ should initiate or potentiate a variety of Ca^{2+}-dependent intracellular cascades that are associated with the mechanisms of pain hypersensitivity during inflammatory pain states, GluR2 internalization may participate in the maintenance of CFA-induced pain hypersensitivity by increasing synaptic Ca^{2+}-permeable AMPARs in dorsal horn neurons (Fig. 10). More importantly, our behavioral study with GluR2K882A KI mice demonstrated that preventing CFA-induced dorsal horn GluR2 internalization through targeted mutation of the GluR2 PKC phosphorylation site attenuated CFA-evoked mechanical and thermal hypersensitivity during the maintenance period. This finding provides strong evidence that dorsal horn GluR2 internalization may underlie the mechanism of persistent inflammatory pain maintenance. It bears noting that the GluR2K882A KI mice, like conventional gene knock-out mice, might generate compensatory mechanisms during development. Thus, it will be necessary to confirm the role of dorsal horn GluR2 internalization in the maintenance of inflammatory pain by interfering with other mechanisms that determine GluR2 internalization (e.g., by inhibiting spinal PKCα and targeting disruption of the PICK1 gene).

Emerging evidence suggests that AMPAR subunit trafficking is critically involved in activity-induced synaptic plasticity (Liu and Zukin, 2007; Santos et al., 2009). Our study demonstrated GluR2 internalization and GluR1 membrane insertion in dorsal horn neurons after CFA-induced inflammation (Park et al., 2008). Previous studies reported that acute inflammatory insult (e.g., capsaicin) led to a significant increase in amount of GluR1, without altering GluR2 level, in the dorsal horn plasma membrane fraction (Galan et al., 2004; Larsson and Broman, 2008). We recently found that neither GluR1 nor GluR2 expression levels changed in either the cytosolic or plasma membrane fractions of dorsal horn after mouse hindpaw incision (data not shown). These findings suggest that different peripheral nociceptive insults may induce distinct changes of spinal AMPAR subunit trafficking. Thus, it will be very important to further examine whether GluR2 is internalized in dorsal horn neurons under other persistent pain conditions (e.g., neuropathic pain) and to investigate additional potential molecular mechanisms to fully understand the role of spinal AMPAR trafficking in spinal central sensitization that underlies persistent pain.

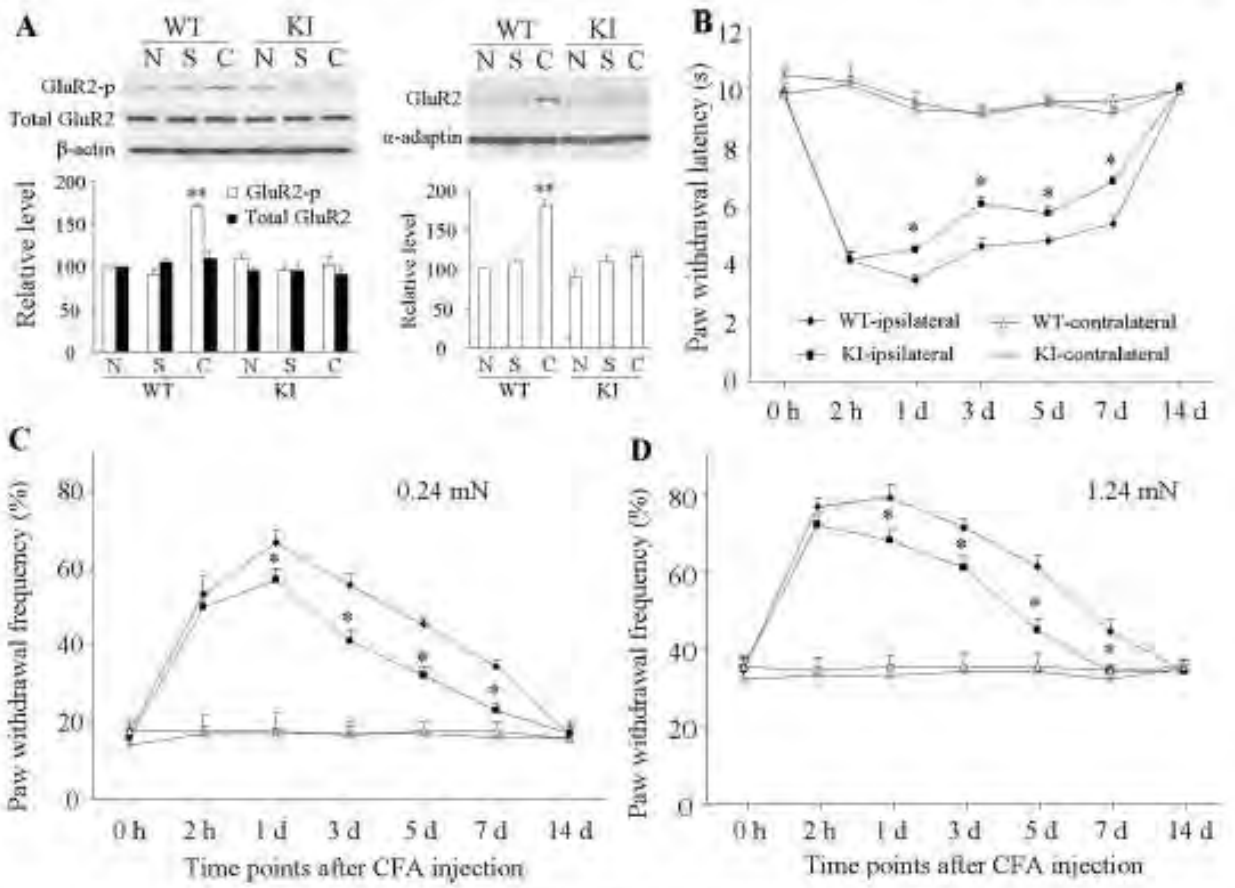

Figure 9. Biochemical and behavioral characterization of GluR2 K882A KI mice after CFA injection. *A*, Level of GluR2 phosphorylation at Ser[880] (GluR2-p Ser[880], left) and amount of GluR2 in a 150 k-g fraction (right) from ipsilateral dorsal horns of naive (N), wild-type (WT), and GluR2 K882A KI mice 1 d after CFA (C) or saline (S). $^{**}p < 0.01$ versus naive WT mice. *B*, Paw withdrawal response to thermal stimulation at times shown. $^{*}p < 0.05$ versus the corresponding time points on the ipsilateral side in WT mice. *C*, *D*, Paw withdrawal responses to 0.24 mN (*C*) and 1.24 mN (*D*) mechanical stimuli at times shown. $^{*}p < 0.05$ versus the corresponding time points on the ipsilateral side in WT mice.

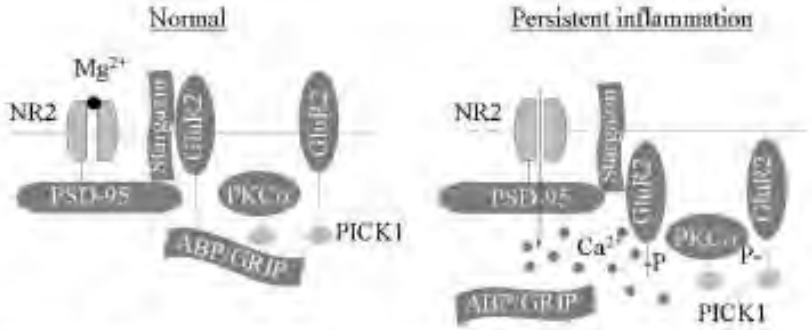

Figure 10. Proposed model for the NMDAR/PKC-dependent dorsal horn GluR2 internalization under persistent inflammatory pain conditions. NMDARs couple to AMPARs through PSD-95 (which binds to NR2A/2B1 interaction with stargazin (which binds to GluR1, GluR2, and GluR4). Under normal conditions, ABP/GRIP binds to and anchors GluR2 at synapses. Under persistent inflammatory pain conditions, NMDAR activation causes Ca^{2+} influx and PKCα activation. The latter phosphorylates GluR2 at Ser[880] and disrupts GluR2 binding to ABP/GRIP, which leads to GluR2 internalization. GluR2 internalization results in an increase of AMPAR Ca^{2+} permeability. The increase in $[Ca^{2+}]_i$ in dorsal horn neurons should initiate or potentiate a variety of Ca^{2+}-dependent intracellular cascades that are associated with the maintenance of persistent inflammatory pain.

References

Adesnik H, Nicoll RA, England PM (2005) Photoinactivation of native AMPA receptors reveals their real-time trafficking. Neuron 48:977–985.

Basbaum AI, Woolf CJ (1999) Pain. Curr Biol 9:R429–R431.

Beloeil H, Ji RR, Berde CB (2006) Effects of bupivacaine and tetrodotoxin on carrageenan-induced hind paw inflammation in rats (Part 2): cytokines and p38 mitogen-activated protein kinases in dorsal root ganglia and spinal cord. Anesthesiology 105:139–145.

Burnashev N, Monyer H, Seeburg PH, Sakmann B (1992) Divalent ion permeability of AMPA receptor channels is dominated by the edited form of a single subunit. Neuron 8:189–198.

Chacur M, Milligan ED, Gazda LS, Armstrong C, Wang H, Tracey KJ, Maier SF, Watkins LR (2001) A new model of sciatic inflammatory neuritis (SIN): induction of unilateral and bilateral mechanical allodynia following acute unilateral peri-sciatic immune activation in rats. Pain 94:231–244.

Chu YC, Guan Y, Skinner J, Raja SN, Johns RA, Tao YX (2005) Effect of genetic knockout or pharmacologic inhibition of neuronal nitric oxide synthase on complete Freund's adjuvant-induced persistent pain. Pain 119:113–123.

Chung HJ, Xia J, Scannevin RH, Zhang X, Huganir RL (2000) Phosphorylation of the AMPA receptor subunit GluR2 differentially regulates its interaction with PDZ domain-containing proteins. J Neurosci 20:7258–7267.

Chung HJ, Steinberg JP, Huganir RL, Linden DJ (2003) Requirement of

AMPA receptor GluR2 phosphorylation for cerebellar long-term depression. Science 300:1751–1755.
Derkach VA, Oh MC, Guire ES, Soderling TR (2007) Regulatory mechanisms of AMPA receptors in synaptic plasticity. Nat Rev Neurosci 8:101–113.
Dev KK, Nakanishi S, Henley JM (2004) The PDZ domain of PICK1 differentially accepts protein kinase C-alpha and GluR2 as interacting ligands. J Biol Chem 279:41393–41397.
Dong H, O'Brien RJ, Fung ET, Lanahan AA, Worley PF, Huganir RL (1997) GRIP: a synaptic PDZ domain-containing protein that interacts with AMPA receptors. Nature 386:279–284.
Dong H, Zhang P, Liao D, Huganir RL (1999a) Characterization, expression, and distribution of GRIP protein. Ann N Y Acad Sci 868:535–540.
Dong H, Zhang P, Song I, Petralia RS, Liao D, Huganir RL (1999b) Characterization of the glutamate receptor-interacting proteins GRIP1 and GRIP2. J Neurosci 19:6930–6941.
Dubner R, Bushnell MC (1997) Spinal dorsal horn plasticity following tissue or nerve injury. In: The textbook of pain (Wall PD, Melzack R, eds), pp 225–241. London: Churchill-Livingstone.
Galan A, Laird JM, Cervero F (2004) In vivo recruitment by painful stimuli of AMPA receptor subunits to the plasma membrane of spinal cord neurons. Pain 112:315–323.
Granados-Soto V, Kalcheva I, Hua X, Newton A, Yaksh TL (2000) Spinal PKC activity and expression: role in tolerance produced by continuous spinal morphine infusion. Pain 85:395–404.
Greger IH, Esteban JA (2007) AMPA receptor biogenesis and trafficking. Curr Opin Neurobiol 17:289–297.
Guo W, Zou S, Guan Y, Ikeda T, Tal M, Dubner R, Ren K (2002) Tyrosine phosphorylation of the NR2B subunit of the NMDA receptor in the spinal cord during the development and maintenance of inflammatory hyperalgesia. J Neurosci 22:6208–6217.
Hanley JG, Henley JM (2005) PICK1 is a calcium-sensor for NMDA-induced AMPA receptor trafficking. EMBO J 24:3266–3278.
Hartmann B, Ahmadi S, Heppenstall PA, Lewin GR, Schott C, Borchardt T, Seeburg PH, Zeilhofer HU, Sprengel R, Kuner R (2004) The AMPA receptor subunits GluR-A and GluR-B reciprocally modulate spinal synaptic plasticity and inflammatory pain. Neuron 44:637–650.
Ho MT, Pelkey KA, Topolnik L, Petralia RS, Takamiya K, Xia J, Huganir RL, Lacaille JC, McBain CJ (2007) Developmental expression of Ca^{2+}-permeable AMPA receptors underlies depolarization-induced long-term depression at mossy fiber CA3 pyramid synapses. J Neurosci 27:11651–11662.
Holman D, Henley JM (2007) A novel method for monitoring the cell surface expression of heteromeric protein complexes in dispersed neurons and acute hippocampal slices. J Neurosci Methods 160:302–308.
Isaac JT, Ashby M, McBain CJ (2007) The role of the GluR2 subunit in AMPA receptor function and synaptic plasticity. Neuron 54:859–871.
Iwakura Y, Nagano T, Kawamura M, Horikawa H, Ibaraki K, Takei N, Nawa H (2001) *N*-methyl-D-aspartate-induced alpha-amino-3-hydroxy-5-methyl-4-isoxazolepropionic acid (AMPA) receptor down-regulation involves interaction of the carboxyl terminus of GluR2/3 with Pick1. Ligand-binding studies using Sindbis vectors carrying AMPA receptor decoys. J Biol Chem 276:40025–40032.
Katano T, Furue H, Okuda-Ashitaka E, Tagaya M, Watanabe M, Yoshimura M, Ito S (2008) N-ethylmaleimide-sensitive fusion protein (NSF) is involved in central sensitization in the spinal cord through GluR2 subunit composition switch after inflammation. Eur J Neurosci 27:3161–3170.
Kerr RC, Maxwell DJ, Todd AJ (1998) GluR1 and GluR2/3 subunits of the AMPA-type glutamate receptor are associated with particular types of neurone in laminae I-III of the spinal dorsal horn of the rat. Eur J Neurosci 10:324–333.
Larsson M, Broman J (2008) Translocation of GluR1-containing AMPA receptors to a spinal nociceptive synapse during acute noxious stimulation. J Neurosci 28:7084–7090.
Lee I, Ro JY (2007) Differential regulation of glutamate receptors in trigeminal ganglia following masseter inflammation. Neurosci Lett 421:91–95.
Lin JW, Ju W, Foster K, Lee SH, Ahmadian G, Wyszynski M, Wang YT, Sheng M (2000) Distinct molecular mechanisms and divergent endocytotic pathways of AMPA receptor internalization. Nat Neurosci 3:1282–1290.
Liu SJ, Zukin RS (2007) Ca2+-permeable AMPA receptors in synaptic plasticity and neuronal death. Trends Neurosci 30:126–134.
Lu CR, Hwang SJ, Phend KD, Rustioni A, Valtschanoff JG (2002) Primary afferent terminals in spinal cord express presynaptic AMPA receptors. J Neurosci 22:9522–9529.
Lu Y, Sun YN, Wu X, Sun Q, Liu FY, Xing GG, Wan Y (2008) Role of alpha-amino-3-hydroxy-5-methyl-4-isoxazolepropionate (AMPA) receptor subunit GluR1 in spinal dorsal horn in inflammatory nociception and neuropathic nociception in rat. Brain Res 1200:19–26.
Matsuda S, Launey T, Mikawa S, Hirai H (2000) Disruption of AMPA receptor GluR2 clusters following long-term depression induction in cerebellar Purkinje neurons. EMBO J 19:2765–2774.
McCormack SG, Stornetta RL, Zhu JJ (2006) Synaptic AMPA receptor exchange maintains bidirectional plasticity. Neuron 50:75–88.
McNally GP, Westbrook RF (1998) Effects of systemic, intracerebral, or intrathecal administration of an *N*-methyl-D-aspartate receptor antagonist on associative morphine analgesic tolerance and hyperalgesia in rats. Behav Neurosci 112:966–978.
Morrison BM, Janssen WG, Gordon JW, Morrison JH (1998) Light and electron microscopic distribution of the AMPA receptor subunit, GluR2, in the spinal cord of control and C86R mutant superoxide dismutase transgenic mice. J Comp Neurol 395:523–534.
Osten P, Khatri L, Perez JL, Köhr G, Giese G, Daly C, Schulz TW, Wensky A, Lee LM, Ziff EB (2000) Mutagenesis reveals a role for ABP/GRIP binding to GluR2 in synaptic surface accumulation of the AMPA receptor. Neuron 27:313–325.
Park JS, Yaster M, Guan X, Xu JT, Shih MH, Guan Y, Raja SN, Tao YX (2008) Role of spinal cord alpha-amino-3-hydroxy-5-methyl-4-isoxazolepropionic acid receptors in complete freund's adjuvant-induced inflammatory pain. Mol Pain 4:67.
Perez JL, Khatri L, Chang C, Srivastava S, Osten P, Ziff EB (2001) PICK1 targets activated protein kinase Calpha to AMPA receptor clusters in spines of hippocampal neurons and reduces surface levels of the AMPA-type glutamate receptor subunit 2. J Neurosci 21:5417–5428.
Petralia RS, Yokotani N, Wenthold RJ (1994) Light and electron microscope distribution of the NMDA receptor subunit NMDAR1 in the rat nervous system using a selective anti-peptide antibody. J Neurosci 14:667–696.
Petralia RS, Wang YX, Mayat E, Wenthold RJ (1997) Glutamate receptor subunit 2-selective antibody shows a differential distribution of calcium-impermeable AMPA receptors among populations of neurons. J Comp Neurol 385:456–476.
Polgár E, Watanabe M, Hartmann B, Grant SG, Todd AJ (2008) Expression of AMPA receptor subunits at synapses in laminae I-III of the rodent spinal dorsal horn. Mol Pain 4:5.
Santos SD, Carvalho AL, Caldeira MV, Duarte CB (2009) Regulation of AMPA receptors and synaptic plasticity. Neuroscience 158:105–125.
Santos SF, Rebelo S, Derkach VA, Safronov BV (2007) Excitatory interneurons dominate sensory processing in the spinal substantia gelatinosa of rat. J Physiol 581:241–254.
Snyder EM, Philpot BD, Huber KM, Dong X, Fallon JR, Bear MF (2001) Internalization of ionotropic glutamate receptors in response to mGluR activation. Nat Neurosci 4:1079–1085.
Staudinger J, Lu J, Olson EN (1997) Specific interaction of the PDZ domain protein PICK1 with the COOH terminus of protein kinase C-alpha. J Biol Chem 272:32019–32024.
Steinberg JP, Takamiya K, Shen Y, Xia J, Rubio ME, Yu S, Jin W, Thomas GM, Linden DJ, Huganir RL (2006) Targeted in vivo mutations of the AMPA receptor subunit GluR2 and its interacting protein PICK1 eliminate cerebellar long-term depression. Neuron 49:845–860.
Sun H, Kawahara Y, Ito K, Kanazawa I, Kwak S (2006) Slow and selective death of spinal motor neurons in vivo by intrathecal infusion of kainic acid: implications for AMPA receptor-mediated excitotoxicity in ALS. J Neurochem 98:782–791.
Swanson GT, Kamboj SK, Cull-Candy SG (1997) Single-channel properties of recombinant AMPA receptors depend on RNA editing, splice variation, and subunit composition. J Neurosci 17:58–69.
Tao F, Skinner J, Su Q, Johns RA (2006) New role for spinal Stargazin in alpha-amino-3-hydroxy-5-methyl-4-isoxazolepropionic acid receptor-mediated pain sensitization after inflammation. J Neurosci Res 84:867–873.
Tao YX, Huang YZ, Mei L, Johns RA (2000) Expression of PSD-95/SAP90 is critical for *N*-methyl-D-aspartate receptor-mediated thermal hyperalgesia in the spinal cord. Neuroscience 98:201–206.
Tao YX, Rumbaugh G, Wang GD, Petralia RS, Zhao C, Kauer FW, Tao F,

Zhuo M, Wenthold RJ, Raja SN, Huganir RL, Bredt DS, Johns RA (2003) Impaired NMDA receptor-mediated postsynaptic function and blunted NMDA receptor-dependent persistent pain in mice lacking postsynaptic density-93 protein. J Neurosci 23:6703–6712.

Tigaret CM, Thalhammer A, Rast GF, Specht CG, Auberson YP, Stewart MG, Schoepfer R (2006) Subunit dependencies of *N*-methyl-D-aspartate (NMDA) receptor-induced alpha-amino-3-hydroxy-5-methyl-4-isoxazolepropionic acid (AMPA) receptor internalization. Mol Pharmacol 69:1251–1259.

Todd AJ, Sullivan AC (1990) Light microscope study of the coexistence of GABA-like and glycine-like immunoreactivities in the spinal cord of the rat. J Comp Neurol 296:496–505.

Tong CK, MacDermott AB (2006) Both Ca2+-permeable and -impermeable AMPA receptors contribute to primary synaptic drive onto rat dorsal horn neurons. J Physiol 575:133–144.

Tóth K, McBain CJ (1998) Afferent-specific innervation of two distinct AMPA receptor subtypes on single hippocampal interneurons. Nat Neurosci 1:572–578.

Vikman KS, Rycroft BK, Christie MJ (2008) Switch to Ca2+-permeable AMPA and reduced NR2B NMDA receptor-mediated neurotransmission at dorsal horn nociceptive synapses during inflammatory pain in the rat. J Physiol 586:515–527.

Wei XH, Zang Y, Wu CY, Xu JT, Xin WJ, Liu XG (2007) Peri-sciatic administration of recombinant rat TNF-alpha induces mechanical allodynia via upregulation of TNF-alpha in dorsal root ganglia and in spinal dorsal horn: the role of NF-kappa B pathway. Exp Neurol 205:471–484.

Wen YR, Suter MR, Kawasaki Y, Huang J, Pertin M, Kohno T, Berde CB, Decosterd I, Ji RR (2007) Nerve conduction blockade in the sciatic nerve prevents but does not reverse the activation of p38 mitogen-activated protein kinase in spinal microglia in the rat spared nerve injury model. Anesthesiology 107:312–321.

Youn DH, Royle G, Kolaj M, Vissel B, Randić M (2008) Enhanced LTP of primary afferent neurotransmission in AMPA receptor GluR2-deficient mice. Pain 136:158–167.

Zhang B, Tao F, Liaw WJ, Bredt DS, Johns RA, Tao YX (2003) Effect of knock down of spinal cord PSD-93/chapsin-110 on persistent pain induced by complete Freund's adjuvant and peripheral nerve injury. Pain 106:187–196.

1.2. Фармакологічне інгібування та генетичне вимкнення експресії PKCα у поперековому відділі спинного мозку супроводжується корекцією порушеного обігу синаптичних AMPA-рецепторів між первинними аферентами і ноцицептивними нейронами дорзального рогу спинного мозку та полегшенням болю

www.nature.com/scientificreports

SCIENTIFIC REPORTS

OPEN

Spinal PKCα inhibition and gene-silencing for pain relief: AMPAR trafficking at the synapses between primary afferents and sensory interneurons

Received: 24 August 2017
Accepted: 22 June 2018
Published online: 06 July 2018

Olga Kopach[1,2], Volodymyr Krotov[1], Angela Shysh[1], Andrij Sotnic[1], Viacheslav Viatchenko-Karpinski[1,3], Victor Dosenko[3,4] & Nana Voitenko[1,4]

Upregulation of Ca^{2+}-permeable AMPA receptors (CP-AMPARs) in dorsal horn (DH) neurons has been causally linked to persistent inflammatory pain. This upregulation, demonstrated for both synaptic and extrasynaptic AMPARs, depends on the protein kinase C alpha (PKCα) activation; hence, spinal PKC inhibition has alleviated peripheral nociceptive hypersensitivity. However, whether targeting the spinal PKCα would alleviate both pain development and maintenance has not been explored yet (essential to pharmacological translation). Similarly, if it could balance the upregulated postsynaptic CP-AMPARs also remains unknown. Here, we utilized pharmacological and genetic inhibition of spinal PKCα in various schemes of pain treatment in an animal model of long-lasting peripheral inflammation. Pharmacological inhibition (pre- or post-treatment) reduced the peripheral nociceptive hypersensitivity and accompanying locomotive deficit and anxiety in rats with induced inflammation. These effects were dose-dependent and observed for both pain development and maintenance. Gene-therapy (knockdown of PKCα) was also found to relieve inflammatory pain when applied as pre- or post-treatment. Moreover, the revealed therapeutic effects were accompanied with the declined upregulation of CP-AMPARs at the DH synapses between primary afferents and sensory interneurons. Our results provide a new focus on the mechanism-based pain treatment through interference with molecular mechanisms of AMPAR trafficking in central pain pathways.

Targeting the mechanisms underlying impairments for disease treatment is a concept of precision medicine for emerging advanced therapeutics with limited side effects. Over decades of exploring the mechanisms of pain development and maintenance for effective interception of persistent pain at the cellular and molecular levels, glutamate AMPA receptors (AMPAR) are of a particular interest among various systems being outlined. This is due to the principal role of AMPARs in fast transmission and because of AMPAR upregulation causing central sensitization of the dorsal horn (DH), a specific form of spinal plasticity mediating pain[1–3]. Changes in the activity-dependent trafficking of AMPARs have been well documented in the DH interneurons in chronic pain conditions where two mechanisms take place: internalization of GluA2-containing, Ca^{2+}-impermeable AMPARs away from the synapses between primary afferents and DH interneurons[4–6], while insertion of GluA1-containing, Ca^{2+}-permeable (CP) AMPARs into the extrasynaptic sites[7,8]. Either mechanism increases the AMPAR-mediated Ca^{2+}-conductance in sensory interneurons, triggering the long lasting hyperexcitability of central nociceptors[9] and, hence, Ca^{2+}-dependent pain chronification[2]. Our recent study has demonstrated that spinal administration of the activity-dependent antagonists of CP-AMPARs had alleviated inflammatory pain hypersensitivity at the

[1]Department of Sensory Signalling, Bogomoletz Institute of Physiology, Kyiv, Ukraine. [2]Department of Clinical and Experimental Epilepsy, Institute of Neurology, University College London, London, UK. [3]Department of General and Molecular Pathophysiology, Bogomoletz Institute of Physiology, Kyiv, Ukraine. [4]Kyiv Academic University, Kyiv, Ukraine. [5]Present address: The University of Alabama at Birmingham, Birmingham, United States. Correspondence and requests for materials should be addressed to O.K. (email: o.kopach@ucl.ac.uk) or N.V. (email: nana@biph.kiev.ua)

periphery without any detectable side effects that further supports the role of spinal CP-AMPARs in chronic pain[20].

Predominantly, upregulation of CP-AMPARs depends on the protein kinase C alpha (PKCα) activation. This molecular mechanism includes phosphorylation of GluA2 subunit by PKCα that disrupts binding of the receptor to its synaptic anchoring protein, causing, thereby, the receptor's internalization away from the postsynaptic density[9]. Our previous studies demonstrated that PKC antagonists[5,10] or genetic targeting the PKCα[8] alleviated the inflammatory-induced nociceptive hypersensitivity. Though it provides a proof-of-concept of targeting the spinal PKCα for pain relief, there has been, however, no systematic exploration of the therapeutic profile of such targeting to addressing both development and maintenance of persistent pain (essential for preclinical translation). Furthermore, whether PKCα inhibition has an effect on balancing the inflammation-induced upregulation of CP-AMPARs at the synapses between primary afferents and nociceptive interneurons also remains unknown.

In this study, we combined behavioural testing *in vivo* with electrophysiology in the spinal cord *in situ* to determine the therapeutic potential of targeting the spinal PKCα in relieving persistent inflammatory pain through pharmacological inhibition or a gene-silencing approach (knockdown). Gene targeting holds great promise as a therapy that could feasibly replace repeatedly injected drugs, gaining an ever-increasing interest for its therapeutic potential in persistent pain treatment. Moreover, the gene-silencing approach does not involve permanent gene modification and, thereby, could provide long-lasting, still reversible, effects on neurons. Therefore, one of our goals was to examine the effect of different experimental schemes for gene-therapy: pre- and post-treatment of persistent inflammatory pain in an animal model of long-lasting peripheral inflammation. The outcome of either pharmacological inhibition or gene-silencing approach on the inflammation-induced upregulation of CP-AMPARs at the DH synapses was also demonstrated through recordings of the AMPAR-mediated postsynaptic currents evoked with primary afferent (dorsal root) stimulation in the superficial DH interneurons.

Results

For targeting the spinal PKCα we have utilized two different approaches: pharmacological inhibition and gene silencing through local delivery of a drug into the lumbar spinal cord. The CFA-induced model of long lasting peripheral inflammation was used to produce persistent nociceptive hypersensitivity in rats, which could persist for over several weeks after the induction of inflammation if left untreated[5,8,10]. Different experimental schemes (pre- or post-treatment) were probed to figure out the therapeutic effects of spinal PKCα inhibition on the developing inflammatory pain and its maintenance. Next, the effects on locomotive deficit and anxiety of animals with peripheral inflammation were determined. Ultimately, the postsynaptic AMPAR-mediated currents were recorded in DH interneurons to assess whether PKCα inhibition arrested the inflammatory upregulation of CP-AMPARs at the DH synapses between primary afferents and sensory interneurons.

Spinal PKC inhibition declines the development of both nociceptive hypersensitivity and locomotive deficit in animals with induced peripheral inflammation. For PKC inhibition, a potent, cell-permeable PKC inhibitor, chelerythrine, was initially used. In untreated animals (no pre-treatment with chelerythrine), an intraplantar injection of CFA produced a robust peripheral thermal hypersensitivity, which could be detected on the ipsilateral hindpaw within as short time period as half an hour, being severely developed further (Fig. 1b). Chelerythrine given shortly prior to the induction of peripheral inflammation (30 min in advance; Fig. 1a) alleviated the thermal hypersensitivity with a high potency. We detected the antinociceptive effect of chelerythrine at 660 nM (IC_{50} for PKC inhibition), which emerged rapidly (within 30 min after i.l. injection) as a decline in the CFA-induced drop of the nociceptive threshold on the ipsilateral (inflamed) hindpaw (the threshold increased by ~168%, $n = 5$ rats/group, $p < 0.001$ compared with the corresponding time-point in the inflamed group without chelerythrine; Fig. 1b). The effect was time-dependent and weakened following the next 2 days (Fig. 1c). Increasing the concentration of chelerythrine resulted in the antinociceptive effect of longer duration. At 39 μM, chelerythrine produced an approximate two-fold rise in the thermal threshold (n = 5 rats/group, $p < 0.01$ compared with the CFA-inflamed group without chelerythrine; Fig. 1b). The effect remained for the next 2 days (increase in the threshold by ~46% and ~41%, $p < 0.05$ on the days 1 and 2, respectively; Fig. 1c). Chelerythrine at 396 μM completely abolished the peripheral nociceptive hypersensitivity that the threshold in inflamed rats at 5 h post-CFA became reversing to control level (before inflammation, $n = 4$ rats/group, $p > 0.2$ paired comparison; Fig. 1b). The effect remained steady when re-determined on the days 1 and 2 post-CFA (increase in the threshold by ~105%, $p < 0.001$ and ~81%, $p < 0.01$, respectively, compared with the corresponding latency in CFA-inflamed group without chelerythrine; Fig. 1c).

We probed the time-dependence of the antinociceptive effects produced by chelerythrine through modifying the experimental scheme of pre-treatment by extending the time of a drug administration up to 3 h in advance (Supplementary Fig. S1a). However, the antinociceptive effect was minor, if any, for both micromolar and millimolar concentrations of chelerythrine ($p > 0.05$; Supplementary Fig. S1b). Some effect was observed for higher chelerythrine concentrations on the day 1 post-CFA (the thermal threshold increased by ~47%, n = 8, $p < 0.05$ for 39 μM chelerythrine and by ~36%, n = 3, $p < 0.05$ for 3.96 mM chelerythrine compared with the inflamed group without chelerythrine; Supplementary Fig. S1c).

Peripheral nociceptive hypersensitivity was associated with a robust locomotive deficit that inflamed animals exhibited rapidly after the induction of inflammation (within an hour), which could persist for over days (Fig. 2a). Inhibition of spinal PKC with chelerythrine given 30 min before the induction of peripheral inflammation abolished the development of locomotive deficit in rats after CFA injection. The total distance of animal movements within the open-field arena was similar to control ("0" time, pre-inflammatory level) over the time-course of testing for all groups of CFA-inflamed animals treated with different concentrations of chelerythrine ($p > 0.1$; Fig. 2b).

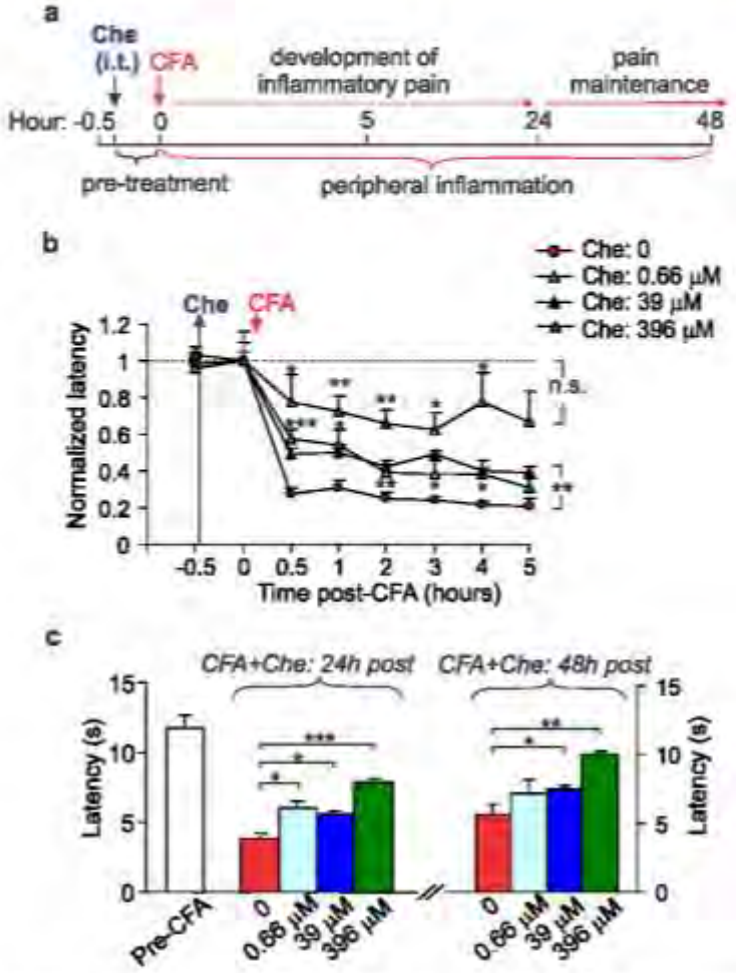

Figure 1. Pharmacological inhibition of spinal PKC alleviates the peripheral nociceptive hypersensitivity in rats. (**a**) A cartoon depicting experimental scheme of pre-treatment with chelerythrine (Che, 10 µl/rat), given intrathecally (i.t.) prior to the induction of peripheral inflammation with an intraplantar injection of CFA (30 min in advance). (**b**) The time course of changes in the thermal nociceptive threshold following i.t. administration of chelerythrine at different concentrations. The threshold (the paw withdrawal latency) normalized to the time of CFA injection ("0" time; induction of inflammation). (**c**) Summary of the nociceptive threshold (the paw withdrawal latency) in CFA-inflamed animals on the days 1 and 2 post-CFA after pre-treatment with chelerythrine at different concentrations. All data are shown as mean ± SEM. $^{*}P < 0.05$, $^{**}p < 0.01$, $^{***}p < 0.001$, n.s., non-significant vs. the corresponding time-point in the CFA-inflamed group without chelerythrine.

Animals with locomotive deficit often exhibited the anxiety-like behaviour. Consistent with our previous studies[10,11], animals with peripheral inflammation and pain hypersensitivity typically sat within the arena corners, preferably not moving across the open area of the arena (Fig. 2a). However, neither signs of anxiety were observed in animals with peripheral inflammation those received pre-treatment with chelerythrine at different concentrations – animals displayed a common exploratory behaviour pattern by moving freely across the open field arena and through the centre (Fig. 2c).

Spinal PKC inhibition shortens the pain maintenance and recovers both locomotive deficit and anxiety of animals with peripheral inflammation: chelerythrine and PKCα (C2-4) inhibitor peptide. Thus far, the observed effects of spinal PKC inhibition demonstrate the therapeutic potential of such a targeting in pain treatment and against animal anxiety when applied shortly in advance before the induction of inflammation. However, therapy implemented as a post-treatment is more preferable towards clinical relevance. Therefore, we next examined the therapeutic effects of spinal PKC inhibition used as a post-treatment of persistent inflammatory pain. Post-treatments were initiated 1 d post-CFA (Fig. 3a), the time-point representing the inflammatory pain maintenance[9,10,12].

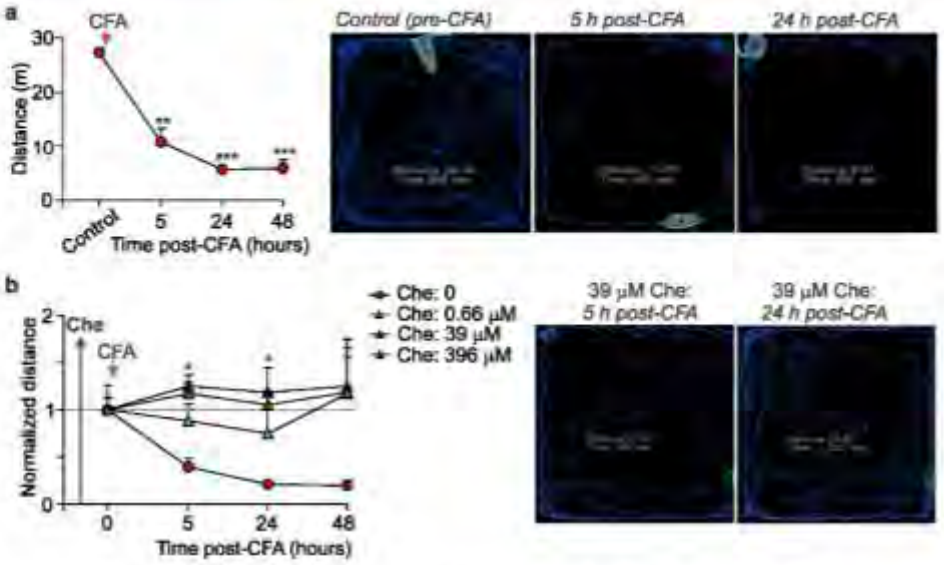

Figure 2. Spinal PKC inhibition declines locomotive deficit in animals with induced peripheral inflammation. (**a**) Summary of the total distance travelled by animals before and after the induction of CFA-induced peripheral inflammation (left graph) and representative snapshots of the analysed open-field test recordings (taken from the same animal over the time of testing) depicting animal's movement for the 5-min duration (images on the right). $^{**}P < 0.01$, $^{***}p < 0.001$ vs. control (before CFA injection); n = 9 animals/group. (**b**) Summary of the average distance travelled by CFA-inflamed animals those received pre-treatment with chelerythrine at different concentrations (left graph) and representative snapshots of the analysed open-field test recordings taken from a CFA-inflamed animal after pre-treatment with chelerythrine (39 µM, treatment scheme as shown in Fig. 1a). All data are shown as mean ± SEM. $^{*}P < 0.05$ vs. the corresponding time-point in the CFA-inflamed group without chelerythrine.

Chelerythrine markedly alleviated the thermal nociceptive hypersensitivity following its post-treatment administration, with a high efficiency. The antinociceptive effect was observed following i.t. injection of chelerythrine at the concentration of 660 nM (IC_{50} for PKC inhibition), which appeared shortly (within 2 h, an increase in the threshold was by ~25%, n = 5, $p < 0.05$; Fig. 3b). The antinociceptive effect further augmented with increasing the chelerythrine concentration – the effect has been also longer persisted. At 39 µM of chelerythrine, an increase in the thermal latency has been detected within 30 min (by ~57%, n = 12, $p < 0.05$) and gradually raised up (by ~110% at 1 h and by ~128% at 1.5 h, $p < 0.01$ compared with the corresponding time-point in CFA-inflamed animals without chelerythrine; Fig. 3b); also, it remained steady for over the next days (Fig. 3c).

In addition to the antinociceptive effect, chelerythrine markedly reduced the locomotive deficit in animals with persistent peripheral inflammation. Such an effect, being rapidly emerging (within hours), was concentration-dependent and progressive (Fig. 4a). At higher concentrations, chelerythrine recovered impaired locomotion of CFA-inflamed animals back to control (pre-inflammatory) level. In particular, the mean distance travelled by rats was: 24.6 ± 1.7 m in control (non-inflamed group) but 15 ± 1.5 m in the inflamed animals 1 d post-CFA and 22.9 ± 3.5 m in the inflamed, Che-treated animals at 1 d post-CFA, 5 h after 396 µM chelerythrine (n = 6/group). Chelerythrine produced a decrease in anxiety of animals with persistent peripheral inflammation (Fig. 4b,c). Animals with peripheral inflammation showed recovery in their explorative behaviour following treatment with chelerythrine at different concentrations – inflamed animals increasingly crossed the open-field arena by freely entering the arena centre (Fig. 4c) that reflects a lack of anxiety.

For the selective pharmacological inhibition of PKCα subtype, the antinociceptive effects of PKCα (C2-4) inhibitor peptide were also examined, which use has not been yet reported *in vivo*. Although there was no clear effect of C2-4 peptide administered at the concentration of 1 µM (n = 4, $p > 0.05$), the peptide at 10 µM concentration produced a significant increase in the nociceptive threshold in CFA-inflamed rats, which was appeared within half an hour ($p < 0.05$; Fig. 5a) and remained on the days 1 and 2 post-CFA (increase in the threshold by ~26% and ~17%, respectively, $p < 0.05$; Fig. 5b). Increasing the C2-4 peptide concentration from 100 µM (n = 5) to 1 mM (n = 4) produced further increase in the threshold (by ~50% to 60%, $p < 0.05$ for each concentration tested; Fig. 5b), resulting in pain alleviation observed within 0.5–1 h after i.t. administration and persisted for over few days ($p < 0.05$; Fig. 5c).

Gene silencing of spinal PKCα for antinociception. To ultimately determine whether genetic inhibition of spinal PKCα would produce a marked and lasting alleviation of inflammatory pain at the periphery, the gene therapy – gene silencing with AS ODN specific to PKCα – was next implemented. The reduced expression of PKCα protein at the DH of the spinal cord after i.t. administration of AS ODN, but not MS ODN, was

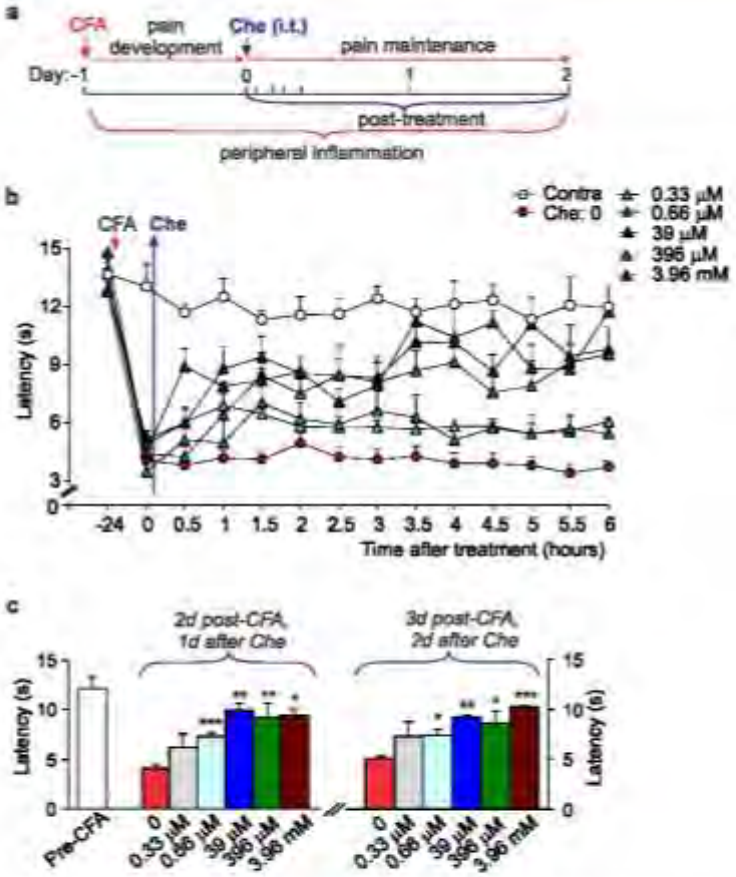

Figure 3. Spinal PKC inhibition shortens the maintenance of persistent inflammatory pain in rats. (**a**) A cartoon depicting experimental scheme of post-treatment of the CFA-induced peripheral hypersensitivity with chelerythrine (Che, intrathecal, i.t., administration, 10 µl/rat) for the assessment of inflammatory pain maintenance. (**b**) The time course of changes in the thermal nociceptive threshold (the paw withdrawal latency) in CFA-inflamed rats treated with chelerythrine at different concentrations ("0" is the time of chelerythrine injection, a start of treatment). (**c**) Summary of the thermal nociceptive threshold in CFA-inflamed rats on the days 1 and 2 following post-treatment with chelerythrine at different concentrations. All data are mean ± SEM. $^{*}P<0.05$, $^{**}p<0.01$, $^{***}p<0.001$ vs. the CFA-inflamed group without chelerythrine.

confirmed with Western blot analysis (by ~23%, n = 6 rats/group, $p < 0.01$; Fig. 6a), fully consistent with our previous observations[5]. Gene silencing of the DH PKCα produced a reduction in the thermal nociceptive hypersensitivity of inflamed rats when applied as either pre- or post-treatment of the CFA-induced inflammatory pain. Gene-therapy initiated before the induction of peripheral inflammation resulted in a profound antinociception; its therapeutic effect, nevertheless, was not strictly determined by duration of the therapy (Fig. 6b,c). After daily i.t. administration of AS ODN for 3 days, the thermal nociceptive threshold in CFA-inflamed rats increased by ~64% (n = 8, $p < 0.001$) and by ~70% ($p < 0.05$ compared with the MS ODN-treated group) on the days 1 and 2 post-CFA, respectively (Fig. 6c). Such administration of AS ODN for 4 days produced the increase by ~84% (n = 6, $p < 0.001$) and ~98% ($p < 0.05$), respectively (Fig. 6c).

Gene-therapy initiated as a post-treatment of persistent inflammatory pain (Fig. 7a) also alleviated the thermal nociceptive hypersensitivity at the periphery. Initiation of the therapy shortly after the induction of inflammation (4 h post-CFA) resulted in the increased thermal latency in rats with peripheral inflammation by ~48% (n = 8, $p < 0.05$) on the day 2 post-CFA and by ~43% ($p < 0.01$ compared with the MS ODN-treated group) on the day 3 (Fig. 7b).

PKCα-dependent inflammatory upregulation of CP-AMPARs in the DH synapses between primary afferents and sensory interneurons: pharmacological inhibition and gene silencing. Finally, for the assessment that antinociception produced by the spinal PKCα inhibition relates to changes in the PKCα-dependent AMPAR trafficking at the DH synapses, we recorded the AMPAR-mediated EPSCs evoked by primary afferent stimulation in DH interneurons. The recorded currents were solely mediated

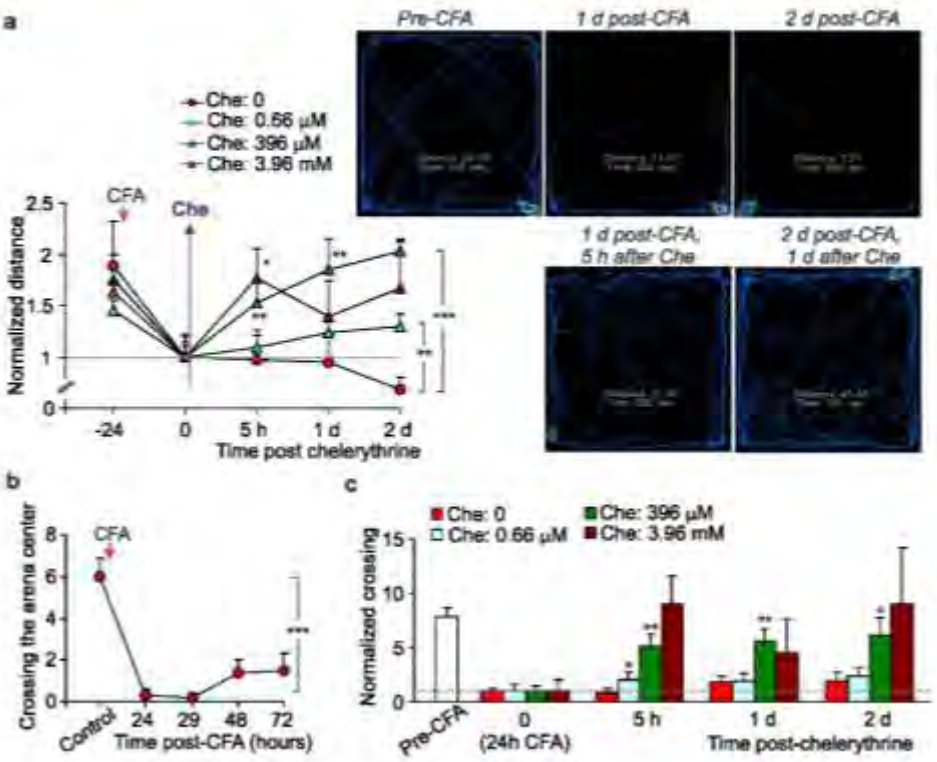

Figure 4. Pharmacological inhibition of spinal PKC with chelerythrine restores both locomotive deficit and anxiety of animals with peripheral inflammation. (**a**) Summary of the total distance travelled by CFA-inflamed animals before and following post-treatment with chelerythrine at different concentrations (left graph) and representative snapshots of the analysed open-field test recordings taken from the same animal at different time-points of testing. Upper row: images depicting movements of a CFA-inflamed animal with no chelerythrine treatment. Lower row: images of a CFA-inflamed animal following post-treatment with 396µM chelerythrine. Images are taken from the same rats over the time of testing. The average distance normalized to the time of chelerythrine administration ("0" time, a start of treatment); experimental scheme for post-treatment was as in Fig. 3a. (**b**) The time course of changes in animal explorative behaviour as readout of anxiety produced by persistent peripheral inflammation. (**c**) Summary of changes in animal explorative behaviour following post-treatment with chelerythrine at different concentrations. The number of crossing the arena centre normalized to chelerythrine administration ("0" time that is 24h post-CFA). All data are mean ± SEM. $^{*}P < 0.05$, $^{**}p < 0.01$, $^{***}p < 0.001$ vs. the corresponding time-point in CFA-inflamed group without chelerythrine or vs. control (before CFA injection) for Fig. b.

by AMPAR activation since were entirely eliminated by AMPAR antagonists, NBQX (20µM) and GYKI 52466 (100µM) (Fig. 8a).

We established that, in consistence with our previous results[7], the CFA-induced peripheral hypersensitivity led to upregulation of postsynaptic CP-AMPARs at the DH synapses between primary afferents and sensory interneurons. This was demonstrated by the inwardly rectified AMPAR-mediated eEPSCs at positive membrane potentials when recorded in DH interneurons 1 d post-CFA (Fig. 8b,c): the average RI dropped from 0.29 ± 0.04 (n = 20) in control to 0.18 ± 0.02 (n = 12) 1 d post-CFA ($p < 0.01$; Fig. 8b). Pharmacological inhibition of spinal PKC in rats with the developed peripheral pain hypersensitivity completely abolished that rectification 1 d post-CFA when recorded in DH interneurons at 3 to 5 h after i.t. injection of 39µM chelerythrine. The average RI was 0.25 ± 0.03 (n = 12) in DH interneurons from CFA-inflamed rats treated with chelerythrine, demonstrating a great similarity with that value in control (non-inflamed animals, $p = 0.44$ compared to control; Fig. 8b,c). Having such effect in CFA-inflamed animals, chelerythrine influenced neither RI nor *I-V* shape of the AMPAR-mediated EPSCs in the DH neurons from non-inflamed animals (the average RI: 0.27 ± 0.02, n = 17 in non-inflamed chelerythrine-treated group and 0.29 ± 0.04, n = 20, $p = 0.5$ in non-inflamed group without chelerythrine, control; Supplementary Fig.S2). The latter indicates no effect of chelerythrine *per se* on the postsynaptic AMPARs at the DH synapses (wherein no inflammation).

Genetic targeting of the spinal PKCs arrested the inflammatory upregulation of CP-AMPARs at the DH synapses between primary afferents and sensory interneurons. Analysis of the AMPAR-mediated EPSCs recorded in DH interneurons from the AS ODN-and MS ODN-treated CFA-inflamed animals (4 days of gene-therapy)

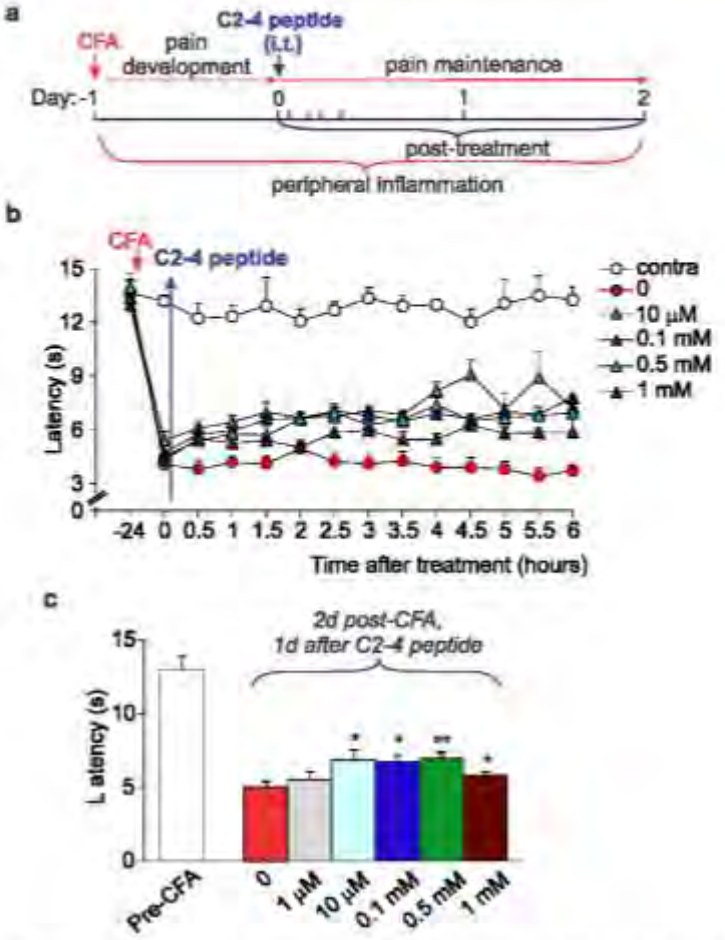

Figure 5. The antinociceptive effect of PKCα (C2-4) inhibitor peptide in rats with induced peripheral inflammation. (**a**) A cartoon depicting experimental scheme of post-treatment of the CFA-induced peripheral hypersensitivity with PKCα (C2-4) inhibitor peptide (intrathecal administration, i.t., 10μl/rat). (**b**) The time course of changes in the thermal nociceptive threshold (the paw withdrawal latency) in the CFA-inflamed rats treated with C2-4 peptide at different concentrations. "0" time is 24 h post-CFA when treatment had been initiated. (**c**) Summary of the thermal nociceptive threshold in CFA-inflamed rats on the day 2 post-CFA after treatment with C2-4 peptide at different concentrations (that is the day 1 after initiating post-treatment). All data are mean ± SEM. $^{*}P < 0.05$, $^{**}p < 0.01$ vs. the CFA-inflamed group without C2-4 peptide.

revealed that the average RI 1 d post-CFA was 0.18 ± 0.02 (n = 6) for the MS ODN-treated (a decrease by ~62%, $p < 0.01$ compared with non-inflamed group; Fig. 8e) but 0.25 ± 0.02 (n = 11) for the AS ODN-treated animals ($p < 0.05$ compared with the MS ODN-treated, CFA-inflamed group and $p = 0.5$ compared with non-inflamed group; Fig. 8e). Altogether this indicates that antinociception produced by targeting the spinal PKCα (pharmacological or genetic inhibition) is causally linked to the PKCα-dependent inflammatory upregulation of postsynaptic CP-AMPARs at the DH synapses between primary afferents and sensory interneurons and, hence, peripheral nociceptive hypersensitivity in persistent inflammatory conditions.

Discussion

Despite the latest improvements in pain medication emerged from fundamental and clinical studies, treating persistent pain remains quite challenging. For effective treatment of persistent pain it appears that the development of new approaches is required, aimed specifically at targeting the molecular mechanisms to provide benefits of preventing (or at least minimizing) side effects, commonly associated with the repeatedly injected existing drug medications.

Fundamental studies of the central mechanisms underlying chronic pain unveiled that CP-AMPARs play a crucial role in maintaining of persistent inflammatory pain[2,3,6,12]. This role originates from the activity-dependent trafficking of AMPARs, which balance has been broken in the DH interneurons in chronic pain conditions[3,7,8,12].

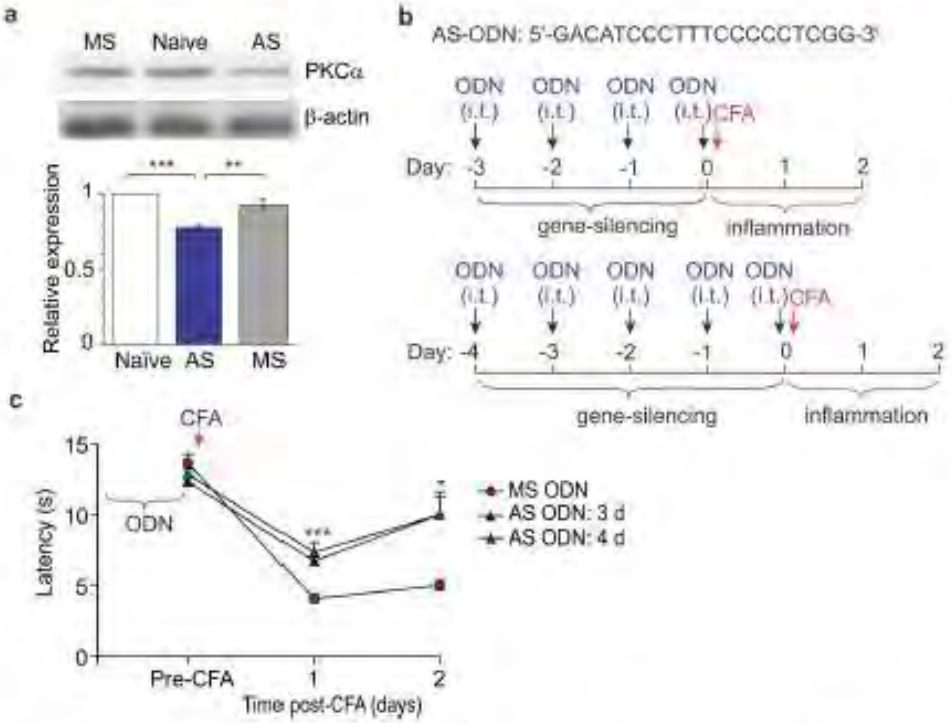

Figure 6. Gene-silencing of spinal PKCα reduces the inflammatory pain maintenance. (**a**) Western blot analysis of the PKCα protein expression level in the dorsal horn of spinal cord in rats after intrathecal injections of AS ODN specific to PKCα, but not MS ODN. Top: Western blot examples for PKCα protein (80 kDa) and beta-actin (43 kDa). The examples are original images taken using the same exposition. Bottom: Summary of the PKCα protein expression level in experimental groups (n = 6 rats/group) relative to naïve. The PKCα protein expression was normalized to the corresponding beta-actin. (**b**) Cartoons of the experimental schemes of gene-therapy (gene-silencing of spinal PKCα) with AS ODN of the indicated sequence (upper row) administered intrathecally (i.t., 10 μl/rat). (**c**) The time-course of changes in the thermal nociceptive threshold (the paw withdrawal latency) in rats with persistent peripheral inflammation those received gene therapy with oligodeoxynucleotides (AS ODN, MS ODN) in accord with the experimental schemes as above. All data are mean ± SEM. *$P < 0.05$, **$p < 0.01$, ***$p < 0.001$ *vs.* the corresponding time-point in the CFAinflamed group treated with MS ODN or as indicated in (**a**).

As a result, upregulated CP-AMPARs (both synaptic and extrasynaptic receptors) cause the hyperexcitability of DH interneurons and hyperexcitation of the DH circuitry, linked to pain chronification in central pathways[9]. Our recent study demonstrated that inhibition of spinal CP-AMPARs with the activity-dependent antagonists produced a marked alleviation of inflammatory pain at the periphery without any detectable side effects[10]. Cumulatively, it argues that a decline in upregulation of spinal CP-AMPARs would represent a promising strategy for pain treatment in preventing the long lasting pain. Based on our previous studies of the molecular mechanism of inflammatory pain development and maintenance, a mechanism-based treatment was utilized in this study, which focuses on preventing upregulation of CP-AMPARs through inhibiting an upstream trigger of such upregulation in central pain pathways, namely PKCα[5,8]. We probed two different strategies for targeting the spinal PKCα – pharmacological inhibition or gene-silencing – through local delivery of a drug (genetic material) into the lumbar spinal cord. To build-up the therapeutic profile of such targeting, we designed and examined different experimental schemes, pre- and post-treatment of peripheral inflammatory hypersensitivity, for thorough testing of any effects emerging acutely (within hours) and/or with a delay following treatment (over days) by measuring the nociceptive threshold in animals twice an hour for 5 to 6-h time window and then each day for over the next few days. The time-courses that we built up for pain relief have demonstrated a high potency of PKC antagonists in relieving thermal inflammatory pain following spinal administration. A broad, cell-permeable PKC antagonist chelerythrine effectively alleviated peripheral inflammatory pain when used as either pre- or post-treatment, whose therapeutic effects were detectable even at nanomolar concentrations (330 nM, 660 nM), the range close to IC_{50} for PKC inhibition (established as 660 nM). The antinociceptive effects of chelerythrine were time-dependent – pain relief to last for few days required higher drug concentrations (at the micromolar range). High potency of chelerythrine for reliving inflammatory pain via spinal administration is consistent with the alleviation of inflammatory hyperalgesia by chelerythrine injections into the hypothalamus[14], one of the brain structures for pain modulation, and through intracerebroventricular injections[15]. Importantly that in addition

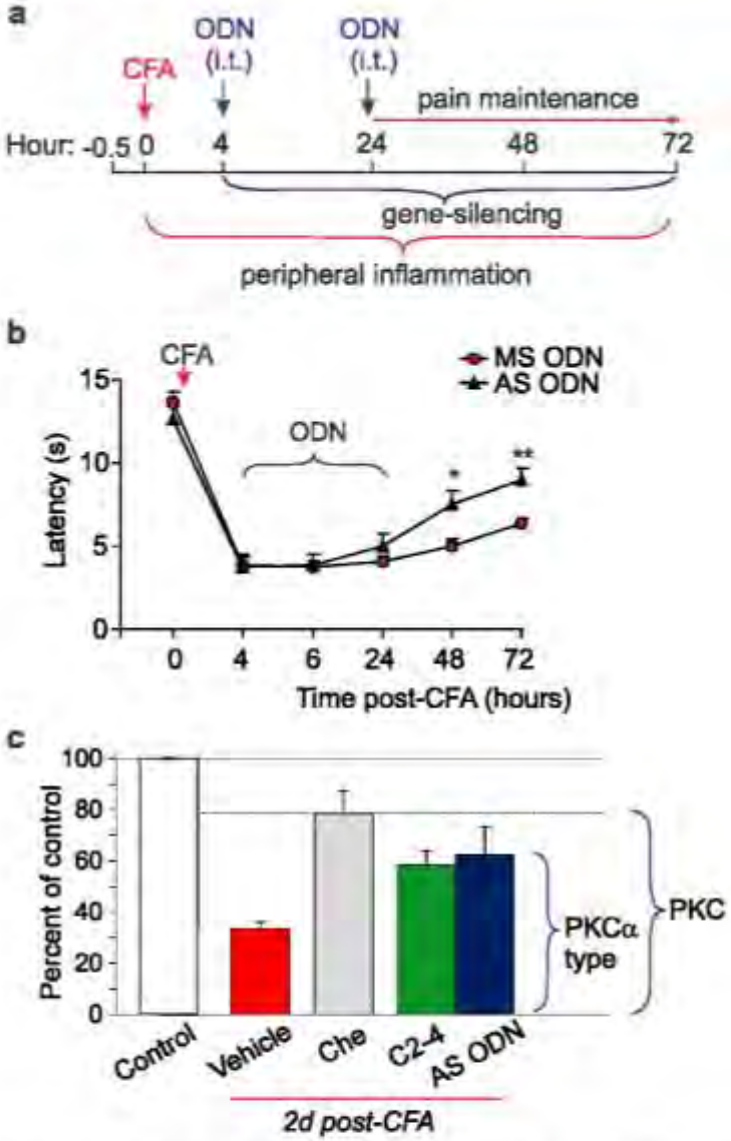

Figure 7. Gene-therapy produces alleviation in the persistent inflammatory pain. (**a**) A cartoon of the experimental scheme of gene-therapy with oligodeoxynucleotides specific to PKCα administered intrathecally (i.t., 10 µl/rat) after the peripheral nociceptive hypersensitivity had developed. (**b**) The time-course of changes in the thermal nociceptive threshold (the paw withdrawal latency) in the CFA inflamed rats those received treatment with oligodeoxynucleotides (AS ODN, MS ODN) as indicated above. (**c**) Summary of changes in the thermal nociceptive threshold in control and CFA-inflamed groups those received different post-treatment for estimation of the spinal PKCα contribution into the peripheral inflammatory pain maintenance. The relative thermal threshold is the maximum efficiency for each antagonist tested. Control is non-inflamed animals. All data are mean ± SEM. $^{*}P < 0.05$, $^{**}p < 0.001$ vs. the corresponding time-point in the CFA-inflamed group treated with MS ODN.

to its antinociceptive effect, chelerythrine recovered locomotive deficit in CFA-inflamed animals; moreover, it declined anxiety, a common sign of painful states. The latter is consistent with the PKC involvement in memory formation and anxiety status[34] and suggests a complex link between locomotion, anxiety-like behaviour and nociceptive processing in central pathways[35]. Our behavioral studies provide for the first time evidence of the antinociceptive effect produced by PKCα (C2–4) inhibitor peptide. The effects of C2–4 peptide were tested out for different peptide concentrations administered i.t. after the peripheral hypersensitivity had been developed (post-treatment). Although PKCα (C2–4) inhibitor peptide produced the antinociceptive effects at high potency (10 µM) and being emerged rapidly (within half an hour), its effect was markedly lower than that produced by

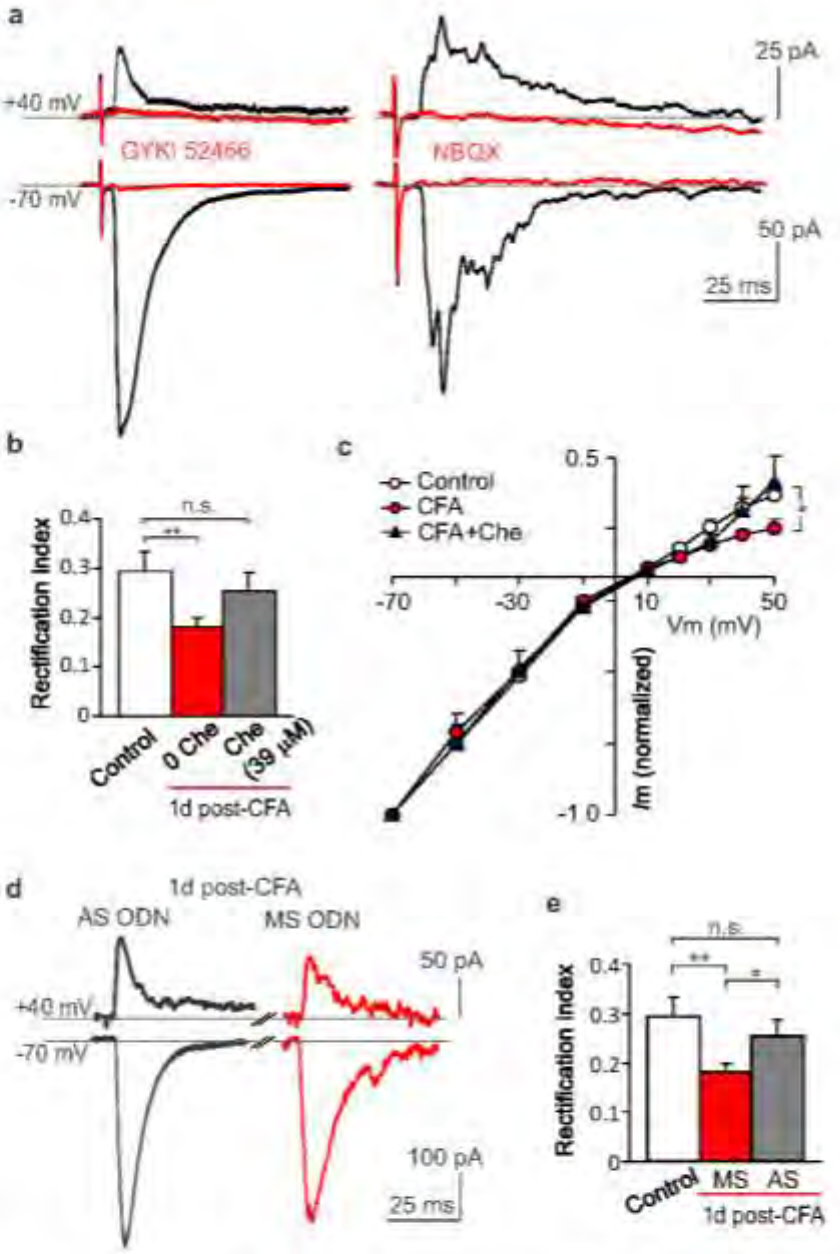

Figure 8. Targeting the spinal PKCα results in ablating the upregulated CP-AMPARs at the DH synapses between primary afferents and sensory interneurons in persistent inflammatory conditions. (**a**) Examples of the AMPAR-mediated excitatory postsynaptic currents (EPSCs) evoked by primary afferent stimulation in DH interneurons recorded at different membrane potentials. The AMPAR blockers GYKI 52466 and NBQX eliminated the currents at −70 mV and +40 mV (red traces). (**b**,**c**) Summary of the rectification index of the AMPAR-mediated EPSCs (**b**) and their *I-V* relationship (**c**) in DH neurons from control (no inflammation), the CFA-inflamed, non-treated and the CFA-inflamed animals given 39 μM chelerythrine (experimental scheme as in Fig. 3a). The rectification index was calculated as the ratio of the current amplitude at +40 mV to that at −70 mV. (**d**) Examples of the AMPAR-mediated EPSCs recorded at −70 mV and +40 mV in DH interneurons from the CFA-inflamed groups after gene-therapy (experimental scheme as in Fig. 6b). (**e**) Summary of the rectification index of the AMPAR-mediated EPSCs in DH neurons from control (non-inflamed) and CFA-inflamed groups after gene-therapy (experimental scheme of gene-therapy as in Fig. 6b). The rectification index was calculated as above. All data are mean ± SEM. **P* < 0.05, **p < 0.01, n.s., non-significant vs. control (non-inflamed) group or as indicated.

chelerythrine (Fig. 7c). This represents the next line in support for the role of other PKC isoforms in maintaining of persistent pain of inflammatory origin. The PKC enzyme family includes at present at least twelve isoforms, few of those were recognized as being particularly involved in pain. In the first instance, PKCβ and PKCγ were both upregulated in inflammation[18–20], thereby, implicated into the development of CFA-induced hypersensitivities[8,20], while atypical spinal PKCs (e.g. PKMζ) were reported to undergo activation in both development and maintenance of pain states[21]. Apart from the inflammatory pain, a bulk of experimental studies on rodents demonstrated that PKC isoforms, especially gamma subtype[22], play the important role in allodynia and hyperalgesia of different etiology[23–26]. Our results of gene-silencing of spinal PKCα have confirmed the therapeutic potential of acute genetic inhibition (knockdown) of PKCα in the treatment of persistent inflammatory pain. A downregulation of the PKCα protein expression in the DH of the spinal cord after spinal administration of AS ODN specific for PKCα has been confirmed by Western blot analysis, in full compliance with a use of such approach in our earlier studies[8]. The antinociceptive effects of gene-therapy, confirmed for either pre- or post-treatment of persistent inflammatory pain, were the most promising in shortening the pain maintenance.

Numerous signalling cascades are coupled to PKCα, hence, its inhibition can trigger modifications of various proteins. Nevertheless, our patch-clamp recordings of the AMPAR-mediated EPSCs in DH interneurons evoked by primary afferent stimulation clearly stated that pharmacological inhibition of spinal PKC with chelerythrine declined the inward rectification of postsynaptic AMPAR-mediated currents at positive membrane potentials in DH neurons from CFA-inflamed animals (under persistent inflammatory conditions). Given that the inwardly rectified currents featured CP-AMPARs[5,6,13], this indicates a decline in inflammatory upregulation of the postsynaptic CP-AMPARs following inhibition of spinal PKC *in vivo*. As a functional outcome, we have observed alleviation of inflammatory pain hypersensitivity at the periphery. Similar ablation of the upregulated CP-AMPARs at the DH synapses between primary afferents and DH interneurons was found following gene-therapy (gene-silencing of spinal PKCα). These findings further argue towards a causal link between pain relief at the periphery and arrested upregulation of the postsynaptic CP-AMPARs at DH synapses by targeting the spinal PKCα. The molecular mechanism of PKCα-dependent upregulation of CP-AMPARs includes the activation of PKCα under painful conditions as an upstream trigger for the AMPAR protein phosphorylation, a subsequent disrupting of the receptor binding to its synaptic anchoring protein, followed by receptor's internalization[5]. Multiple sites for the PKC-mediated phosphorylation of AMPAR subunits have been distinguished: serine residue S880 for GluA2[5], S831[27], S818, and S816 for GluA1[28–30] that opens considerations for multiple involvement of different PKC enzyme isoforms in both inflammatory pain development and maintenance.

Summartzing, the PKCα-dependent upregulation of CP-AMPARs in DH interneurons is causally linked to the persistent inflammatory pain hypersensitivity at the periphery. Targeting the spinal PKCα, either through pharmacological inhibition or gene-silencing, produced relief in persistent inflammatory pain via ablation of the inflammatory-induced upregulation of postsynaptic AMPARs at the DH synapses between primary afferents and sensory interneurons. This treatment, mechanism-based on targeting the spinal PKCα, will minimize a risk of damage to interneurons not involved in nociceptive processing, thus, reducing side effects on the cellular and systemic levels as one being tailored to nociceptive interneurons only. Such strategy may open a new route towards cutting-edge approaches to treat chronic pain states through targeting the mechanism-based chronification in central pain pathways.

Methods

Animals. Animals were 18- to 30-day-old male Wistar rats. All animal procedures were approved by the Animal Ethics Committee in Bogomoletz Institute of Physiology (Kyiv, Ukraine) and were in accordance with the European Commission Directive (86/609/EEC) and ethical guidelines of the International Association for the Study of Pain. The efforts were made to minimize animal suffering and to reduce the number of animals used.

Intrathecal catheter implantation. For local delivery of a drug into the spinal cord, a catheter was implanted into the lumbar spinal segment, as we have described in details earlier[10,11]. Briefly, after a rat was anesthetized with a mixture of ketamine (70 mg kg^{-1}) and xylazine (15 mg kg^{-1}), a catheter (PE-10) was inserted into the subarachnoid space at the rostral level of the spinal cord lumbar region through incision at the atlanto-occipital membrane, using a stereotaxic frame system. Animals received postoperatively bicillin (0.6 million U kg^{-1}) and dexamethazon (60 mg kg^{-1}). Catheterized animals were taken into experiments after complete healing of surgical incision (typically 3 to 5 days postoperatively). The position of the catheter was confirmed for each animal after termination of behavioural studies or prior to the spinal cord preparation.

Induction of peripheral inflammation. Unilateral peripheral inflammation was induced in rats by an intraplantar injection of complete Freund's adjuvant (CFA, 50 µl of an oil-saline (1:1) emulsion) given subcutaneously into one hind paw as described previously[7,9,10]. Saline (0.9%) injection was used as a control.

Intrathecal drug administration. For pharmacological inhibition, a potent inhibitor of PKC chelerythrine chloride and PKCalpha (C2–4) inhibitor peptide were used. An animal received a single i.t. injection of a drug (10 µl) given at various concentrations. For i.t. injections, a 25-gauge needle connected to a 25 µl Hamilton syringe were both used. Injection of a drug was followed by administration of saline to flush the catheter.

For gene-silencing approach we used the antisense (AS) oligodeoxynucleotides (ODN) specific to PKCα with the following sequence: 5′-GACATCCCTTTCCCCCTCGG-3′. Missense (MS) oligodeoxynucleotides with the sequence of 5′-CGTCCTCAGTCGTCCCTCAC-3′ were used as a control. Animals received a daily injection of AS ODN or MS ODN (10 µg/10 µl) as indicated in the text.

Western blot analysis. The PKCα protein expression level was determined in the spinal cord of the rats injected with AS- or MS ODNs (n = 6/group). The tissue from the dorsal spinal cord was dissected out and

immediately frozen in liquid nitrogen. The tissue was then homogenized in an ice-cold RIPA-buffer (1:3) that contained 20 mM Tris–HCl, 150 mM NaCl, 1 mM EDTA, 1% NP-40, 1% sodium deoxycholate, 0.1% SDS, 1 μM leupeptin and 1 mM protease inhibitor PMSF (pH 7.5). The homogenate was centrifuged (15 min at 11,000 × *g*, 4 °C) and the supernatant was collected. After measuring the protein concentration, the protein fraction was separated using 10% polyacrylamide gel with 0.1% SDS and then electrophoretically transferred onto a nitrocellulose membrane (90 min at 200 mA). For the Western blot analysis human/mouse/rat affinity purified polyclonal antibody for PKCα (1:1000, incubation for overnight, 4°C, CAF5340-SP, R&D Systems Inc, UK) and monoclonal mouse primary antibody for β-actin (1:1000, 2 h incubation, A1978, Sigma, USA) were used. The proteins were detected with anti-goat or anti-mouse secondary antibodies and visualized with chemiluminescence reagents provided with the ECL kit (Amersham Pharmacia Biotech, Piscataway, NJ) and exposured to film. The PKCα protein level, normalized to the corresponding β-actin value, was calculated for each individual sample as the relative expression (to naïve group).

Hargreaves plantar test for the thermal nociceptive threshold measurement. Behavioural testing was performed to measure the peripheral nociceptive threshold to the thermal (heat) stimulus in rats, using the Hargreaves technique, as we have described previously[10,12]. Briefly, after an animal habituated to the Plexiglas chamber located above a light box (Ugo Basile Model 7370 Plantar Test), a radiant heat was applied to the middle of the plantar surface of one hind paw. The light beam was automatically turned off when animal lifted its paw. The trial was repeated 3–5 times with an interval between measurements 3 to 5 minutes. The time between the start of stimulus and animal lifted its paw, the withdrawal latency, was measured, which represents the thermal nociceptive threshold.

Open-field test for the assessment of animal locomotion and anxiety. The open-field test was performed to assess the locomotive behaviour of the animals before and following experimental treatment, as described in details in our previous studies[10,11]. Briefly, a tested animal was placed in the open-field arena representing a 75 × 75 × 40 cm wooden box with a digital camera (Logitech C270) attached above the arena to record the animal relocations. The total distance travelled by an animal for the defined period of time (5 minutes) was calculated.

Anxiety is a commonly used readout of side effects that could rise following treatment. Since animal anxiety is characterized by a reduced exploratory behaviour – animals avoid entering an open area (centre of the arena) by keeping close to the walls and corners (closed area) – for the assessment of anxiety, we analysed the number of crossings by animals the centre of the arena. Testing was performed in a quiet room by the same experimenter carrying out a given test in a blind to drug treatment condition manner.

Spinal cord slice preparation. Spinal cord slices of the lumbar spinal cord region (L_{4-5}) were prepared as described previously[8,9]. Briefly, the spinal cord was quickly removed and placed in an ice-cold dissection solution that contained (in mM) 250 sucrose, 2 KCl, 1.2 NaH_2PO_4, 0.5 $CaCl_2$, 7 $MgCl_2$, 26 $NaHCO_3$, 11 glucose, oxygenated with 95% O_2 and 5% CO_2. Transverse slices (350-μm thick) with attached dorsal roots (8–15 mm) were cut with an HA 752 vibratome (Campden Instruments, Loughborough, UK). Slices were maintained at room temperature in a physiological Krebs bicarbonate solution that contained (in mM) 125 NaCl, 2.5 KCl, 1.25 NaH_2PO_4, 2 $CaCl_2$, 1 $MgCl_2$, 26 $NaHCO_3$, 10 glucose, oxygenated with 95% O_2 and 5% CO_2 (pH 7.4).

Electrophysiology. Whole-cell recordings of the AMPAR-mediated EPSCs were made from DH interneurons of the superficial dorsal horn (lamina I-II), using an Axopatch 200B amplifier controlled with pClamp 9.2 software (Molecular Devices, USA). Neurons were visualized with an infrared optics using a ×60.09 water-immersion objective on an Olympus BX50WI upright microscope (Olympus, Japan). Patch pipettes had the resistance of 5–6.5 MΩ when filled with an internal solution containing (in mM) 130 Cs-methylsulfonate, 10 NaCl, 10 EGTA, 2 CaCl2, 10 HEPES, 5 QX-314, 0.1 spermine tetrahydrochloride, 2 Mg-ATP, and 0.1 Na-GTP (pH 7.2). The dorsal root (afferent fibres) was stimulated with a suction electrode by applying the current pulses of an increased stimulus intensity (70 to 400 μA, 0.1-ms-duration) at a low frequency (0.1 Hz). Only stable EPSCs were selected if they displayed the same latency (the interval between the stimulus artefact and the evoked current). The recordings (3 to 5 trials) were averaged and the peak current amplitude was estimated for each tested neuron. The membrane resistance was constantly monitored by applying a short hyperpolarizing pulse (−5 mV). To isolate the AMPAR-mediated component, EPSCs were recorded in the continuous presence of APV (50 μM), bicuculline methiodide (10 μM), and strychnine hydrochloride (2 μM). For the *I-V* relationship, the membrane potential was held from −70 mV to +50 mV (in a 10- to 20-mV increment). For the *I-V* rectification of the AMPAR-mediated EPSCs, the rectification index (RI) was calculated as the peak current amplitude at +40 mV to that peak amplitude at −70 mV.

Statistical analysis. All data are presented as mean ± SEM with *n* referring to the number of animals tested or the number of cells recorded. For behavioural studies, a statistical difference was analysed using one-way or two-way analysis of variance (ANOVA) followed by Bonferroni *post hoc* test where appropriate. For electrophysiological recordings and Western blot analysis Student's t-test (two-tailed unpaired) was used. A *P* value of less than 0.05 was considered as statistically significant for either test.

Experimental drugs. CFA was purchased from Sigma Chemical Co. (St. Louis, MO, USA), chelerythrine chloride– from Tocris Bioscience (Ellisville, MO). AS ODN and MS ODN were purchased from ISIS Pharmaceuticals Inc. (Carlsbad, CA) or Sigma-Aldrich (UK).

References

1. Kohno, T. *et al.* Bradykinin enhances AMPA and NMDA receptor activity in spinal cord dorsal horn neurons by activating multiple kinases to produce pain hypersensitivity. *The Journal of neuroscience: the official journal of the Society for Neuroscience* **28**, 4533–4540, https://doi.org/10.1523/jneurosci.5349-07.2008 (2008).
2. Kopach, O. & Voitenko, N. Extrasynaptic AMPA receptors in the dorsal horn: evidence and functional significance. *Brain research bulletin* **93**, 47–56, https://doi.org/10.1016/j.brainresbull.2012.11.004 (2013).
3. Latremoliere, A. & Woolf, C. J. Central sensitization: a generator of pain hypersensitivity by central neural plasticity. *The journal of pain: official journal of the American Pain Society* **10**, 895–926, https://doi.org/10.1016/j.jpain.2009.06.012 (2009).
4. Katano, T. *et al.* N-ethylmaleimide-sensitive fusion protein (NSF) is involved in central sensitization in the spinal cord through GluR2 subunit composition switch after inflammation. *The European journal of neuroscience* **27**, 3161–3170, https://doi.org/10.1111/j.1460-9568.2008.06293.x (2008).
5. Park, J. S. *et al.* Persistent inflammation induces GluR2 internalization via NMDA receptor-triggered PKC activation in dorsal horn neurons. *The Journal of neuroscience: the official journal of the Society for Neuroscience* **29**, 3206–3219, https://doi.org/10.1523/jneurosci.4514-08.2009 (2009).
6. Vikman, K. S., Rycroft, B. K. & Christie, M. J. Switch to Ca2+-permeable AMPA and reduced NR2B NMDA receptor-mediated neurotransmission at dorsal horn nociceptive synapses during inflammatory pain in the rat. *The Journal of physiology* **586**, 515–527, https://doi.org/10.1113/jphysiol.2007.145581 (2008).
7. Kopach, O. *et al.* Inflammation alters trafficking of extrasynaptic AMPA receptors in tonically firing lamina II neurons of the rat spinal dorsal horn. *Pain* **152**, 912–923, https://doi.org/10.1016/j.pain.2011.01.016 (2011).
8. Kopach, O. *et al.* PKCalpha is required for inflammation-induced trafficking of extrasynaptic AMPA receptors in tonically firing lamina II dorsal horn neurons during the maintenance of persistent inflammatory pain. *The journal of pain: official journal of the American Pain Society* **14**, 182–192, https://doi.org/10.1016/j.jpain.2012.10.015 (2013).
9. Kopach, O., Krotov, V., Belan, P. & Voitenko, N. Inflammatory-induced changes in synaptic drive and postsynaptic AMPARs in lamina II dorsal horn neurons are cell-type specific. *Pain* **156**, 428–438, https://doi.org/10.1097/01.j.pain.0000460318.65734.00 (2015).
10. Kopach, O., Krotov, V., Goncharenko, J. & Voitenko, N. Inhibition of Spinal Ca(2+)-Permeable AMPA Receptors with Dicationic Compounds Alleviates Persistent Inflammatory Pain without Adverse Effects. *Frontiers in cellular neuroscience* **10**, 50, https://doi.org/10.3389/fncel.2016.00050 (2016).
11. Kopach, O., Krotov, V. & Voitenko, N. Atlanto-occipital catheterization of young rats for long-term drug delivery into the lumbar subarachnoid space combined with *in vivo* testing and electrophysiology *in situ*. *Journal of neuroscience methods* **290**, 125–132, https://doi.org/10.1016/j.jneumeth.2017.08.001 (2017).
12. Kopach, O., Viatchenko-Karpinski, V., Belan, P. & Voitenko, N. Development of inflammation-induced hyperalgesia and allodynia is associated with the upregulation of extrasynaptic AMPA receptors in tonically firing lamina II dorsal horn neurons. *Frontiers in physiology* **3**, 391, https://doi.org/10.3389/fphys.2012.00391 (2012).
13. Hartmann, B. *et al.* The AMPA receptor subunits GluR-A and GluR-B reciprocally modulate spinal synaptic plasticity and inflammatory pain. *Neuron* **44**, 637–650, https://doi.org/10.1016/j.neuron.2004.10.029 (2004).
14. Bu, F. *et al.* Phosphorylation of NR2B NMDA subunits by protein kinase C in arcuate nucleus contributes to inflammatory pain in rats. *Scientific reports* **5**, 15945, https://doi.org/10.1038/srep15945 (2015).
15. Matsushita, Y. *et al.* Involvement of the protein kinase Cgamma isoform in development of tolerance to nitrous oxide-induced antinociception in mice. *Neuroscience* **148**, 541–547, https://doi.org/10.1016/j.neuroscience.2007.06.019 (2007).
16. Lei, Z., Liu, B. & Wang, J. H. Reward memory relieves anxiety-related behavior through synaptic strengthening and protein kinase C in dentate gyrus. *Hippocampus* **26**, 502–516, https://doi.org/10.1002/hipo.22540 (2016).
17. Schorscher-Petcu, A., Austin, J. S., Mogil, J. S. & Quirion, R. Role of central calcitonin gene-related peptide (CGRP) in locomotor and anxiety- and depression-like behaviors in two mouse strains exhibiting a CGRP-dependent difference in thermal pain sensitivity. *Journal of molecular neuroscience: MN* **39**, 125–136, https://doi.org/10.1007/s12031-009-9201-x (2009).
18. Igwe, O. J. & Chronwall, B. M. Hyperalgesia induced by peripheral inflammation is mediated by protein kinase C betaII isozyme in the rat spinal cord. *Neuroscience* **104**, 875–890 (2001).
19. Martin, W. J., Liu, H., Wang, H., Malmberg, A. B. & Basbaum, A. I. Inflammation-induced up-regulation of protein kinase Cgamma immunoreactivity in rat spinal cord correlates with enhanced nociceptive processing. *Neuroscience* **88**, 1267–1274 (1999).
20. Zhao, C. & Lettges, M. & Gereau, R. W. t. *Isozyme-specific effects of protein kinase C in pain modulation*. *Anesthesiology* **115**, 1261–1270, https://doi.org/10.1097/ALN.0b013e3182390785 (2011).
21. Laferriere, A. *et al.* PKMzeta is essential for spinal plasticity underlying the maintenance of persistent pain. *Molecular pain* **7**, 99, https://doi.org/10.1186/1744-8069-7-99 (2011).
22. Malmberg, A. B., Chen, C., Tonegawa, S. & Basbaum, A. I. Preserved acute pain and reduced neuropathic pain in mice lacking PKCgamma. *Science (New York, N.Y.)* **278**, 279–283 (1997).
23. Alra, Z. *et al.* Transient, 5-HT2B receptor-mediated facilitation in neuropathic pain: Up-regulation of PKCgamma and engagement of the NMDA receptor in dorsal horn neurons. *Pain* **154**, 1865–1877, https://doi.org/10.1016/j.pain.2013.06.009 (2013).
24. Matsuo, H. *et al.* Early transcutaneous electrical nerve stimulation reduces hyperalgesia and decreases activation of spinal glial cells in mice with neuropathic pain. *Pain* **155**, 1888–1901, https://doi.org/10.1016/j.pain.2014.06.022 (2014).
25. Peirs, C., Bourgois, N., Artola, A. & Dallel, R. Protein Kinase C gamma Interneurons Mediate C-fiber-Induced Orofacial Secondary Static Mechanical Allodynia, but Not C-fiber-Induced Nociceptive Behavior. *Anesthesiology* **124**, 1136–1152, https://doi.org/10.1097/aln.0000000000001080 (2016).
26. Shumilla, J. A., Limin, T., Mochly-Rosen, D., Kendig, J. J. & Sweitzer, S. M. Ethanol withdrawal-associated allodynia and hyperalgesia: age-dependent regulation by protein kinase C epsilon and gamma isoenzymes. *The journal of pain: official journal of the American Pain Society* **6**, 535–549, https://doi.org/10.1016/j.jpain.2005.03.005 (2005).
27. Wang, Y. *et al.* Surgical incision induces phosphorylation of AMPA receptor GluR1 subunits at Serine-831 sites and GluR1 trafficking in spinal cord dorsal horn via a protein kinase Cgamma-dependent mechanism. *Neuroscience* **240**, 361–370, https://doi.org/10.1016/j.neuroscience.2013.02.051 (2013).
28. Boehm, J. *et al.* Synaptic incorporation of AMPA receptors during LTP is controlled by a PKC phosphorylation site on GluR1. *Neuron* **51**, 213–225, https://doi.org/10.1016/j.neuron.2006.06.013 (2006).
29. Lin, D. T. *et al.* Regulation of AMPA receptor extrasynaptic insertion by 4.1N, phosphorylation and palmitoylation. *Nature neuroscience* **12**, 879–887, https://doi.org/10.1038/nn.2351 (2009).
30. Miletic, G., Hermes, J. L., Bosscher, G. L., Meier, B. M. & Miletic, V. Protein kinase C gamma-mediated phosphorylation of GluA1 in the postsynaptic density of spinal dorsal horn neurons accompanies neuropathic pain, and dephosphorylation by calcineurin is associated with prolonged analgesia. *Pain* **156**, 2514–2520, https://doi.org/10.1097/j.pain.0000000000000323 (2015).

Acknowledgements

This work was supported by the Biotechnology grant of the National Academy of Science of Ukraine to N.V.

Author Contributions

O.K.: research concept and expertmental design, animal surgeries, electrophysiological recordings and behavioural testing, data analysis and interpretation, manuscript preparation and revision. V.K.: animal surgeries and behavioural testing, data analysis and interpretation. A.M.S., V.D.: Western blot. A.S.: electrophysiological recordings. V.V.K.: animal surgeries and behavioural testing. N.V.: conceiving the study, manuscript revision.

Additional Information

Supplementary information accompanies this paper at https://doi.org/10.1038/s41598-018-28512-9.

Competing Interests: The authors declare no competing interests.

Publisher's note: Springer Nature remains neutral with regard to jurisdictional claims in published maps and institutional affiliations.

РОЗДІЛ 2

ПОЗАСИНАПТИЧНІ AMPA-РЕЦЕПТОРИ: ФУНКЦІОНУВАННЯ ТА Ca^{2+}-ПРОВІДНІСТЬ У НОРМІ ТА ПРИ ТРИВАЛОМУ ПЕРИФЕРИЧНОМУ ЗАПАЛЕННІ

2.1. Периферичне запалення призводить до змін трафікінгу позасинаптичних AMPA-рецепторів у сенсорних нейронах дорзального рогу спинного мозку

PAIN® 152 (2011) 912–923

PAIN®

www.elsevier.com/locate/pain

Inflammation alters trafficking of extrasynaptic AMPA receptors in tonically firing lamina II neurons of the rat spinal dorsal horn

Olga Kopach [a], Sheng-Chin Kao [b,c], Ronald S. Petralia [d], Pavel Belan [a], Yuan-Xiang Tao [b,*], Nana Voitenko [a,*]

[a] Department of General Physiology of Nervous System, Bogomoletz Institute of Physiology, Kiev 01024, Ukraine
[b] Department of Anesthesiology and Critical Care Medicine, Johns Hopkins University School of Medicine, Baltimore, MD 21205, USA
[c] Department of Anesthesiology, Lin-Kou Medical Center, Chung Gung Memorial Hospital, Taoyuan County, Taiwan 333, ROC
[d] Laboratory of Neurochemistry, National Institute of Deafness and Other Communication Disorders, National Institutes of Health, Bethesda, MD 20892, USA

Sponsorships or competing interests that may be relevant to content are disclosed at the end of this article.

ARTICLE INFO

Article history:
Received 24 June 2010
Received in revised form 2 November 2010
Accepted 10 January 2011

Keywords:
Extrasynaptic AMPA receptors
GluR1 and GluR2 subunits
Peripheral inflammation
Receptor trafficking
Substantia gelatinosa neurons

ABSTRACT

Peripheral inflammation alters AMPA receptor (AMPAR) subunit trafficking and increases AMPAR Ca^{2+} permeability at synapses of spinal dorsal horn neurons. However, it is unclear whether AMPAR trafficking at extrasynaptic sites of these neurons also changes under persistent inflammatory pain conditions. Using patch-clamp recording combined with Ca^{2+} imaging and cobalt staining, we found that, under normal conditions, an extrasynaptic pool of AMPARs in rat substantia gelatinosa (SG) neurons of spinal dorsal horn predominantly consists of GluR2-containing Ca^{2+}-impermeable receptors. Maintenance of complete Freund's adjuvant (CFA)-induced inflammation was associated with a marked enhancement of AMPA-induced currents and $[Ca^{2+}]_i$ transients in SG neurons, while, as we previously showed, the amplitude of synaptically evoked AMPAR-mediated currents was not changed 24 h after CFA. These findings indicate that extrasynaptic AMPARs are upregulated and their Ca^{2+} permeability increases dramatically. This increase occurred in SG neurons characterized by intrinsic tonic firing properties, but not in those exhibited strong adaptation. This increase was also accompanied by an inward rectification of AMPA-induced currents and enhancement of sensitivity to a highly selective Ca^{2+}-permeable AMPAR blocker, IEM-1460. Electron microcopy and biochemical assays additionally showed an increase in the amount of GluR1 at extrasynaptic membranes in dorsal horn neurons 24 h post-CFA. Taken together, our findings indicate that CFA-induced inflammation increases functional expression and proportion of extrasynaptic GluR1-containing Ca^{2+}-permeable AMPARs in tonically firing excitatory dorsal horn neurons, suggesting that the altered extrasynaptic AMPAR trafficking might participate in the maintenance of persistent inflammatory pain.

1. Introduction

α-Amino-3-hydroxy-5-methyl-4-isoxazolepropionic acid receptors (AMPARs) mediate fast excitatory transmission and play a critical role in synaptic plasticity in the central nervous system. AMPARs are present in multiple locations throughout neurons, including the extrasynaptic plasma membrane, where they have been identified within spines, dendrites, and somata. Numerous *in vitro* and *in vivo* studies have shown clearly that extrasynaptic AMPARs are highly mobile at the plasma membrane [8,38]. They rapidly move between the plasma membrane and intracellular compartments by exocytosis and endocytosis and can migrate laterally to and from synaptic sites [7,15,16]. Such receptor trafficking alters the number of synaptic AMPARs and might participate in synaptic plasticity under different cell conditions [8,13, 44,47]. Extrasynaptic AMPARs can also contribute to glutamate-mediated signaling at nonsynaptic locations by responding to glutamate spillover or glial glutamate release [2,30,56]. Although it has been shown definitively that AMPARs are critically involved in activity-dependent changes of nociceptive inputs [23,28,41,54], most studies in this field have concentrated on elucidating the role of synaptic AMPARs, leaving possible involvement of extrasynaptic receptors open for consideration.

The functional properties of AMPARs, such as conduction and trafficking behavior, are determined by the subunit composition. AMPARs are heterotetramers composed of different combinations of the subunits GluR1–GluR4. Among these subunits, GluR1 and GluR2 are highly expressed in spinal dorsal horn. The ratio

* Corresponding authors. Address: Department of Anesthesiology and Critical Care Medicine, Johns Hopkins University School of Medicine, 720 Rutland Ave., 370 Ross, Baltimore, MD 21205, USA. Tel.: +1 443 287 5490; fax: +1 410 502 5554 (Y.X. Tao). Department of General Physiology of Nervous System, Bogomoletz Institute of Physiology, 4 Bogomoletz Str., Kiev 01024, Ukraine. Tel.:+380 44 256 2049; fax: +380 44 256 2053 (N. Voitenko).
E-mail addresses: ytao1@jhmi.edu (Y.-X. Tao), nana@biph.kiev.ua (N. Voitenko).

0304-3959/$36.00 © 2011 International Association for the Study of Pain. Published by Elsevier B.V. All rights reserved.
doi:10.1016/j.pain.2011.01.016

of GluR1/GluR2 determines Ca^{2+} permeability of AMPARs and rectification property of AMPAR-mediated currents in dorsal horn neurons [11,26,49]. Both Ca^{2+}-permeable and Ca^{2+}-impermeable AMPARs are expressed in substantia gelatinosa (SG) of the spinal cord, where primary afferents carrying nociceptive inputs to the spinal second-order neurons terminate [1,18,23,52]. In contrast to other parts of the central nervous system, a substantial proportion of SG neurons in adult rat dorsal horn densely express Ca^{2+}-permeable homomeric GluR1 AMPARs [1,9,18,23].

The changes in synaptic trafficking of AMPARs and their Ca^{2+}-permebility have been causally linked to multiple neuropathologic conditions, including excitotoxic vulnerability, neuronal injury [14,19,31,32], and persistent inflammatory pain [23,37,50]. It has been shown recently that neuroinflammatory factors promote lateral diffusion of GluR1/GluR2 heteromers from the extrasynaptic sites to synaptic sites, and enhance recycling of intracellular GluR1 homomers back to extrasynaptic membrane via exocytosis [19,32]. In spite of the functional significance of extrasynaptic AMPARs in modulation of spinal nociception, their trafficking during persistent inflammatory pain has not yet been studied.

Here we show that complete Freund's adjuvant (CFA)-induced inflammation causes an increase in functional expression of Ca^{2+}-permeable extrasynaptic AMPARs in rat SG neurons during the maintenance period of inflammatory pain. This increase occurred in neurons characterized by intrinsic tonic firing properties, but not in those that exhibited a strong adaptation. The change in AMPAR Ca^{2+} permeability might be related to a CFA-induced increase in GluR1 membrane insertion at extrasynaptic sites during the maintenance period of inflammatory pain.

2. Materials and methods

2.1. Animal preparation

Male rats were housed in cages on a standard 12:12 h light/dark cycle. Water and food were available *ad libitum* until rats were transported to the laboratory for experiments. The animals were used in accordance with protocols that were approved by the Animal Care and Use Committee at the Bogomoletz Institute of Physiology and Johns Hopkins University and were consistent with the ethical guidelines of the National Institutes of Health and the International Association for the Study of Pain. All efforts were made to minimize animal suffering and to reduce the number of animals used.

2.2. Experimental drugs

CFA was purchased from Sigma Chemical Co. (St. Louis, MO). Fura-2 was obtained from Invitrogen (Carlsbad, CA, USA). Tetrodotoxin (TTX) was obtained from Alomone Labs Ltd. (Israel). CNQX, NBQX, APV, AMPA, SYM 2206, cyclothiazide (CTZ), GYKI 52466, bicuculline, strychnine, and 1-trimethylammonio-5-(1-adamantane-methyl-ammoniopentane dibromide) (IEM-1460) were purchased from Tocris Bioscience (Ellisville, MO).

2.3. Induction of peripheral inflammation

Persistent peripheral inflammation was induced in rats by injecting 100 μl of CFA (*Mycobacterium tuberculosis*) suspended in an oil–saline (1:1) emulsion subcutaneously into the plantar side of one hind paw. Because studies from our laboratory and those of others showed that CFA produces a significant change in synaptic AMPAR trafficking in dorsal horn neurons 24 h post-injection [41,42], we focused on this time point. Saline (0.9%; 100 μl) injection into age-matched rats was used as a control.

2.4. Spinal cord slice preparation

Spinal cord slices were prepared from 18- to 35-day-old male rats as described previously [41,54,57]. Briefly, after rats were deeply anesthetized with an overdose of isoflurane, the L_{4-5} spinal segments were removed. Transverse slices (300 μm thick) were cut on a vibratome in an ice-cold solution containing (in mM) 250 sucrose, 2 KCl, 1.2 NaH_2PO_4, 0.5 $CaCl_2$, 7 $MgCl_2$, 26 $NaHCO_3$, 11 glucose (pH 7.4) and continuously bubbled with 95% O_2, 5% CO_2. Slices were maintained at room temperature (RT) in a physiologic Krebs bicarbonate solution that contained (in mM) 125 NaCl, 2.5 KCl, 1.25 NaH_2PO_4, 2 $CaCl_2$, 1 $MgCl_2$, 26 $NaHCO_3$, 10 glucose (pH 7.4, osmolarity 310–320 mOsM) and was equilibrated with 95% O_2, 5% CO_2.

2.5. Co^{2+} uptake labeling

The slices were labeled by Co^{2+} uptake as described previously [18]. Briefly, the slices from 25- to 35-day-old rats were transferred into a six-well plate containing oxygenated low-sodium and low-calcium Krebs solution containing (in mM) 50 NaCl, 2.5 KCl, 0.5 $CaCl_2$, 2 $MgCl_2$, 26 $NaHCO_3$, 25 glucose, and 135 sucrose at RT. This solution always contained 0.5 μM TTX and either 100 μM D-APV, 50 μM CNQX, or 50 μM GYKI 52466 or an equal volume of the appropriate vehicle (DMSO or saline). The stimulation solution was identical but also contained 250 μM kainate and 1.5 mM $CoCl_2$. After being exposed to the stimulation solution at RT for 20 min, slices were rinsed for 10 min in physiologic Krebs solution containing 5 mM EDTA to remove non-specifically bound Co^{2+}, and then for 5 min in physiologic Krebs solution. Cobalt ions were then precipitated by incubating the slices for 5 min in physiologic Krebs solution containing 0.12% $(NH_4)_2S$. Slices were rinsed again in physiologic Krebs solution and then fixed overnight in 4% paraformaldehyde in 0.1 M PBS at 4 °C. They were cryoprotected in 30% sucrose in 0.1 M PBS and sectioned at a thickness of 25 μm on a cryostat. Silver enhancement of cobalt precipitates was carried out as described [18].

Cobalt-labeled sections were quantified with an Olympus microscope (Olympus, Tokyo, Japan) linked to a Toshiba 3CCD camera (Toshiba, Japan) and I-Cube computer image analysis system (I-Cube, Cambridge, MA). The dorsal horn was divided into two regions: (1) the superficial laminae (laminae I and II) and (2) the nucleus proprius and neck of the dorsal horn (laminae III–VI). Five sections randomly selected from a total of 15 sections from each animal were analyzed. Two experimenters independently counted the number of Co^{2+}-labeled cells in two regions of the dorsal horn, with results that were consistent within 10%.

2.6. Immunohistochemistry

To define whether the Co^{2+}-labeled cells were neurons, some Co^{2+}-labeled sections were blocked for 1 h in PBS containing 10% goat serum and 0.3% TritonX-100 and then incubated with primary rabbit polyclonal antibody to NeuN (1:500, Chemicon, Temecula, CA) overnight at 4 °C. Immunofluorescence histochemistry was carried out with goat anti-rabbit IgG conjugated with Rhodamine Red-X (1:300, Jackson ImmunoResearch, West Grove, PA). Control sections lacking primary antiserum were stained in parallel. All immunofluorescence-labeled sections were rinsed in 0.01 M PBS and mounted onto gelatin-coated glass slides. Cover slips were applied with a mixture of 50% glycerin and 2.5% triethylene diamine in 0.01 M PBS. The labeled sections were observed with an epifluorescence microscope under appropriate filter for Rhodamine Red-X (excitation 545–580 nm; emission ⩾610 nm).

2.7. Synaptosomal membrane fraction

Biochemical fractionation was carried out according to previous studies with minor modification [48]. Briefly, 25–35-day-old rats were sacrificed by decapitation. The L_{4-5} spinal segments ipsilateral to CFA (n = 4 rats) or saline (n = 4 rats) injection were collected. The dorsal part of the spinal cord was separated from the ventral part. The tissues were homogenized in homogenization buffer [in mM, 10 Tris–HCl (pH 7.4), 5 NaF, 1 sodium orthovanadate, 320 sucrose, 1 EDTA, 1 EGTA, 0.1 phenylmethylsulfonyl fluoride, 0.04 leupeptin, and 0.02 pepstatin A]. After centrifugation at 1000g for 20 min at 4 °C, the supernatant (S1, total soluble fraction) was collected and the pellet (P1, nuclei and debris fraction) discarded. The supernatant was centrifuged at 10,000g for 20 min to produce a pellet (P2) and supernatant (S2). The P2 was lysed hypo-osmotically in water and centrifuged at 25,000g to produce a pellet (P3). The S2 was considered to be the crude cytosolic fraction and the P3 the crude synaptosomal membrane fraction.

2.8. Surface biotinylation expression assay

Surface biotinylation expression experiments were performed in spinal cord slices as previously described [51]. Live transverse dorsal horn slices were prepared as described above from 25–35-day-old rats. Briefly, the slices were incubated with Krebs solution containing 1.5 mg/ml Sulfo-NHS-LC-biotin (Pierce, Rockford, IL) for 45 min on ice and rinsed in Krebs solution to quench the biotin reaction. The slices were homogenized in modified RIPA buffer (1% Triton X-100, 0.1% SDS, 0.5% deoxycholic acid, 50 mM $NaPO_4$, 150 mM NaCl, 2 mM NaF, 1 mM PMSF, 1 mg/ml leupeptin, 10 mM sodium pyrophosphate). The homogenates were centrifuged at 10,000g for 15 min at 4 °C, and the supernatant was collected. After the measurement of protein concentration, 20% of the supernatant was removed to detect total expression of GluR1. The remaining supernatant was incubated with 50% NeutrAvidin agarose (Pierce) for 4 h at 4 °C and washed three times with RIPA buffer. Total and biotinylated surface proteins were detected by Western blotting analysis as described previously [40,41]. The surface/total ratio was calculated.

2.9. Postembedding immunogold labeling

Postembedding immunogold labeling was performed as described previously [25,41]. Briefly, 25–35-day-old rats were perfused transcardially with 4% paraformaldehyde +0.5% glutaraldehyde 24 h after CFA or saline injection. Sections from ipsilateral

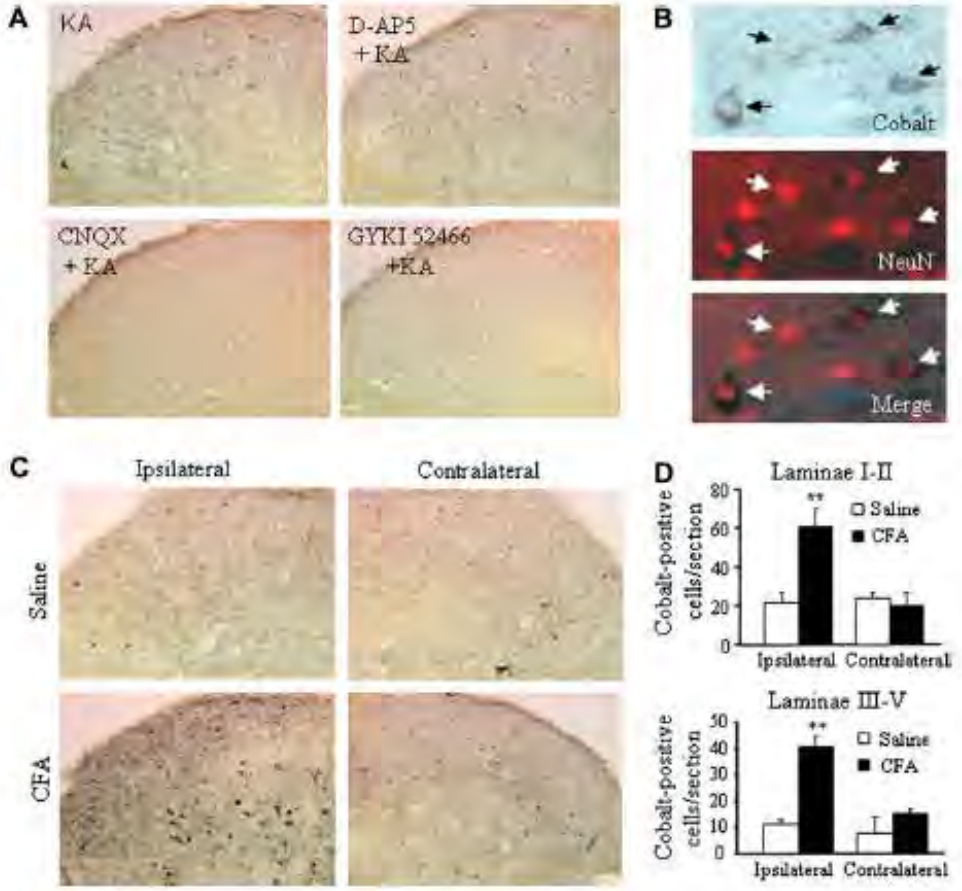

Fig. 1. Increased kainate-induced cobalt loading in the dorsal horn after CFA injection. (A) Representative examples of kainate-induced cobalt loading in live spinal cord slices in the absence or presence of the NMDA receptor antagonist APV (500 μM) or AMPAR antagonists CNQX (250 μM) and GYKI 52466 (250 μM). (B) The neuronal marker NeuN overlaps with cobalt-uptake in the superficial dorsal horn. (C) CFA (but not saline) injection increased cobalt uptake in dorsal horn neurons on the ipsilateral, but not contralateral, side. (D) Statistical summary of the number of cobalt-positive dorsal horn neurons in laminae I–II (top graph) and laminae III–VII (bottom graph) 24 h after saline and CFA.

L_5 superficial dorsal horn were cryoprotected and frozen in a Leica CPC cryopreparation chamber and freeze-substituted into Lowicryl HM-20 in a Leica AFS freeze substitution instrument. Thin sections were labeled with monoclonal mouse GluR2 and polyclonal rabbit GluR1, and controls were treated as described previously [25]. Areas for study were selected at random from the superficial dorsal horn at low magnification (i.e., synapses were not visible) and then micrographs of synapses were taken at high magnification. In the analyses, "synaptic" corresponded to the synaptic cleft and postsynaptic density, and "extrasynaptic" referred to the surface of the cell membrane to 20 nm deep and more than 100 nm from the edge of the active zone.

2.10. Simultaneous Ca^{2+} imaging and patch-clamp recording

Simultaneous Ca^{2+} imaging and whole-cell electrophysiological recordings were obtained from SG neurons of the spinal L_{4-5} dorsal horn from 18–21-day-old rats as described previously [55]. Briefly, the neurons were visually identified with a video microscopy system (Olympus, Japan). The patch pipettes with resistance of 6–10 MΩ were filled with an internal solution containing (in mM) 133 K-gluconate, 5 NaCl, 0.5 $MgCl_2$, 10 HEPES-Na, 2 MgATP, 0.1 GTP-Na, and 0.2 fura-2 pentapotassium salt (pH 7.2, osmolarity 290 mOsM). The membrane potential of SG neurons was held at −60 mV by a patch-clamp amplifier PC-505B (Warner Instruments, Hamden, CT) and Digidata board 1320A (Molecular Devices, Union City, CA) controlled by pCLAMP 8.2 software (Axon Instruments, USA) in current or voltage-clamp mode. Only data from neurons that exhibited a resting membrane potential negative to −60 mV were included in the analysis.

SG neurons that were localized mainly in the mediolateral SG were chosen at random and categorized on the basis of their discharge pattern in response to a series of 1-s current pulses (Fig. 2). Of the 70 neurons tested, 35 were "tonically firing," and 28 exhibited strong adaptation and were considered "transient" neurons. We also encountered a few neurons that exhibited a sustained delay prior to the action potential's discharge or that discharged action potentials followed by firing accommodation. We characterized those neurons as transient if the number of spikes was dependent on the pulse strength, and the neuron exhibited an adaptation when the applied depolarizing current (20–30 pA) was increased [36,46]. Other unclassified neurons that were not characterized by any aforementioned categories were excluded from the analysis.

To isolate the AMPAR-mediated membrane current and the associated $[Ca^{2+}]_i$ increase, recordings were made in the continuous presence of D-APV (50 μM), bicuculline (5 μM), and strychnine (2 μM) to block NMDA, $GABA_A$, and glycine receptors respectively. In addition, TTX (0.5 μM) and cadmium chloride (100 μM) were added to Krebs bicarbonate solution to block corresponding voltage-activated sodium and calcium channels. To prevent a desensitization of AMPARs during bath application of agonist to slices, AMPA was applied in the continuous presence of CTZ (20 μM). Typically, one neuron was studied per slice. Simultaneous fura-2 fluorescence was measured by using a 60× water-immersion objective and a 12-bit cooled CCD camera and capturing board (Sensicam, PCO, Germany). Fluorescent signals from SG neurons were collected between 50 and 100 μm below the surface of the slice. Calcium changes were detected by a PolyChrome IV monochromator (Till Photonics, Germany) as the change in fluorescence of fura-2 dye measured at wavelengths > 510 nm when excitation light was 380 nm. The monochromator was attenuated with neutral density filters to avoid bleaching of fura-2. Imaging Workbench software (INDEC System, USA) was used to measure changes in fura-2 fluorescence. When AMPA was applied exogenously to SG neurons, fluorescence changes in soma and dendrites were measured simultaneously and expressed as changes in the ratio of fura-2 fluorescence at 340 and 380 nm, which is proportional to $[Ca^{2+}]_i$. The background closest to the area of interest was subtracted. The amplitude of AMPA-induced $[Ca^{2+}]_i$ signal was estimated as the difference between the fura-2 fluorescence ratio prior to AMPA application and that at the maximum $[Ca^{2+}]_i$ rise after AMPA stimulation.

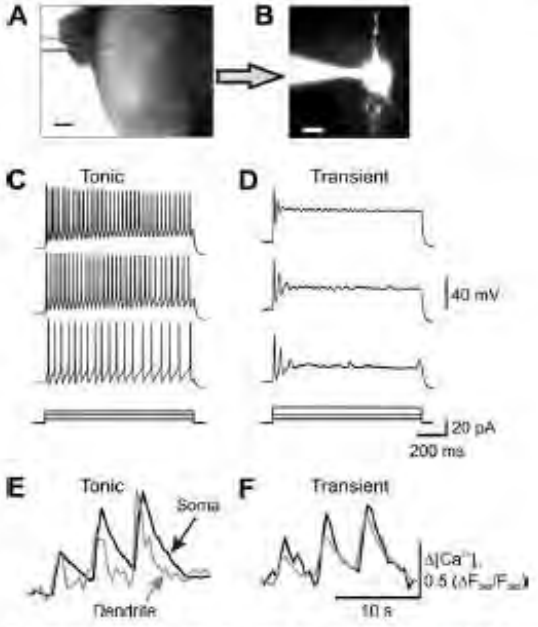

Fig. 2. Sustained membrane depolarization revealed two groups of SG neurons exhibiting different discharge patterns. (A) Transmitted light image of patch electrode position (square) in the SG of a transverse dorsal horn slice; scale bar = 200 μm. (B) A fluorescent image of a neuron loaded with fura-2 (200 μM); scale bar = 20 μm. (C and D) Current-clamp recordings of typical firing patterns for tonic (C) and transient (D) groups of neurons in response to three different intensities of depolarizing currents shown at the bottom of each panel. (E and F) Recordings of depolarizing current-induced changes in the cytosolic free calcium concentration ($[Ca^{2+}]_i$) in the soma (black traces) and dendrites (grey traces) in tonic (E) and transient (F) groups of neurons.

To study the current–voltage (*I–V*) relationship, we recorded membrane currents using an internal solution that contained (in mM) 130 Cs-methylsulphonate, 10 NaCl, 0.5 EGTA, 10 HEPES, 0.2 spermine tetrahydrochloride, 2 Mg-ATP, and 0.1 Na-GTP; pH was adjusted to 7.2 with CsOH (osmolarity 290 mOsM) at RT. *I–V* curves were constructed by holding neurons at −70 mV in a voltage clamp and ramping for 100–300 ms every 5 s initially to +50 mV and then to −70 mV. We applied short hyperpolarizing voltage steps to −75 mV before every ramp to monitor input and access resistance. To inhibit K^+-channel currents, we recorded the AMPA-induced currents after at least 10 min perfusion of patched neurons with an internal solution. To isolate the extrasynaptic AMPAR-mediated current, we subtracted the ramp currents recorded before AMPA application from the currents recorded during the bath AMPA application at each membrane potential. The rectification index (RI) of the extrasynaptic AMPAR-mediated current was determined by dividing the AMPA-induced current amplitude at +30 mV by the current amplitude at −50 mV.

To block Ca^{2+}-permeable AMPARs, we used IEM-1460 which was applied before (3–5 min) or after establishing the steady-state level of AMPA-induced current.

2.11. Statistical analysis

All data are presented as mean ± SEM with *n* referring to the number of cells analyzed. Student's *t*-tests (two-tailed unpaired) were used to determine statistically significant differences. A *p* value of less than 0.05 was considered as statistically significant.

3. Results

3.1. Peripheral inflammation increases AMPAR-mediated Ca^{2+} permeability in dorsal horn neurons

Kainate-induced cobalt uptake has been used to visualize Ca^{2+}-permeable AMPARs in dorsal horn neurons [18]. To determine whether CFA-induced peripheral inflammation alters the expression of spinal Ca^{2+}-permeable AMPARs, we analyzed kainate-induced cobalt uptake in spinal cord transverse slices derived from adult rats (25–35 days) 24 h after saline or CFA injection. Although the dorsal horns of adult saline-treated rats contained fewer cobalt-positive cells than those of younger naïve rats (P6–14) [18,23], their distribution patterns were similar (Fig. 1A). Cobalt-positive cells were predominantly observed in laminae I and II; few were distributed in laminae III–VII (Fig. 1A). To assess whether this pattern reflected selective cobalt uptake through AMPARs, we pre-incubated the slices with GYKI 52466, CNQX, or APV. AMPAR antagonists, CNQX and GYKI 52466 entirely abolished kainate-induced cobalt uptake in the slices, whereas NMDAR antagonist APV had no effect (Fig. 1A). To determine whether kainate-induced cobalt uptake occurred in neurons rather than in other cell types, we incubated the sections with a primary antibody against neuronal marker NeuN after kainate-induced cobalt uptake. In the dorsal horn, most cells that took up cobalt (90 ± 7%, n = 4) were positive for NeuN (Fig. 1B). We found that CFA (but not saline) injection significantly increased cobalt uptake loading in dorsal horn on the ipsilateral, but not contralateral, side (Fig. 1C). After 24 h, the number of cobalt-positive cells was 2.77-fold greater ($p < 0.01$, n = 4) in laminae I–II and 3.73-fold greater ($p < 0.01$, n = 4) in laminae III–VII of CFA-injected rats than in those regions of saline-treated rats (Fig. 1D). However, some NeuN-labeled cells in the superficial and deep dorsal horn were still not cobalt-positive (Fig. 1C), indicating that this group of dorsal horn neurons fails to alter AMPAR Ca^{2+} permeability in response to peripheral inflammatory stimulation.

3.2. Peripheral inflammation augments extrasynaptic AMPAR-mediated currents and $[Ca^{2+}]_i$ transients in "tonic" but not in "transient" lamina II neurons

The fact that CFA-induced increase in cobalt uptake was observed predominantly in neuronal bodies of dorsal horn suggests that Ca^{2+}-permeable AMPARs are upregulated in dorsal horn neurons during CFA-induced peripheral inflammation. By simultaneously recording AMPA-induced membrane current and associated $[Ca^{2+}]_i$ changes in soma and dendrites of superficial lamina II neurons of the spinal L_{4-5} dorsal horn, we directly evaluated upregulation of AMPARs and their Ca^{2+} permeability 24 h after saline or CFA injection. According to intrinsic firing properties during sustained membrane depolarization, lamina II neurons were predominantly divided into two groups: "tonic" and "transient" (Fig. 2). Tonic neurons (n = 35) were defined as those able to support continued discharge of action potentials during 1-s depolarizing inward current and an increased frequency of discharge with increasing current intensity (Fig. 2C). Transient neurons (n = 28) were those that exhibited a strong adaptation by generating short bursts of spikes or just a single spike regardless of depolarizing current intensity (Fig. 2D). Tonic and transient neurons demonstrated similar changes in $[Ca^{2+}]_i$ after depolarizing inward currents (Fig. 2E and F), indicating that the contribution of voltage-gated Ca^{2+} channels to spike generation was similar in the two groups.

To activate the total pool of AMPARs and mimic excessive glutamate release from presynaptic neurons and glia during dorsal horn injuries or inflammation [2,30,56], we bath applied AMPA to the slices. Bath administration of AMPA (5 μM, 60 s) evoked an inward current at a holding potential of −60 mV in both tonic and transient neurons (Fig. 3A, bottom trace). It was characterized by a slow rising phase and desensitization to a plateau level. This current is predominantly mediated by extrasynaptic AMPARs due to their relative abundance compared to synaptic ones in the neuronal plasma membrane [3,22]. No significant difference was observed between the amplitudes of the AMPA-induced currents in the tonic (−204 ± 18 pA, n = 35) and transient (−173 ± 19 pA, n = 28) neurons (Fig. 3D; $p = 0.24$). The current activation was associated with a synchronous rise in $[Ca^{2+}]_i$ in both the soma and dendrites in all examined neurons (Fig. 3A, upper traces). A typical calcium response to AMPA application consisted of a fast initial transient rise in $[Ca^{2+}]_i$ followed by a slow decay to the baseline within several minutes. A comparison of $[Ca^{2+}]_i$ transient amplitudes, expressed as an increase in the ratio of fura-2 fluorescence at 340 and 380 nm, ΔR (see Methods), showed no significant differences in the amplitudes between tonic and transient groups of neurons. Average amplitudes of AMPA-induced $[Ca^{2+}]_i$ transients were 0.47 ± 0.10 (n = 21, tonic) vs 0.48 ± 0.09 (n = 22, transient; $p > 0.1$) for soma and 0.60 ± 0.12 (n = 14, tonic) vs 0.52 ± 0.09 (n = 18, transient; $p > 0.1$) for dendrites (Fig. 3D). These findings indicate that the two groups of neurons have similar levels of AMPAR expression.

The observed AMPA-induced currents and $[Ca^{2+}]_i$ transients were mediated by AMPAR activation, as NBQX, a non-selective AMPAR antagonist, and GYKI 52466, a selective AMPAR antagonist, significantly inhibited the currents. NBQX inhibited AMPA-induced current amplitudes by 97 ± 9% (n = 3, $p < 0.0001$) and 98 ± 11% (n = 3, $p < 0.0001$) in tonic and transient neurons, respectively. GYKI 52466 inhibited the amplitudes by 75 ± 15% (n = 5, $p < 0.05$) and by 86 ± 15% (n = 7, $p < 0.01$) in the tonic and transient neurons, respectively. NBQX inhibited somatic and dendritic $[Ca^{2+}]_i$ transients in tonic neurons by 93 ± 20% and 88 ± 12%, respectively (n = 3, $p < 0.05$) and somatic $[Ca^{2+}]_i$ transients in transient neurons by 92 ± 17% (n = 3, $p < 0.05$). GYKI 52466 inhibited somatic and dendritic $[Ca^{2+}]_i$ transients in tonic neurons by 94 ± 20% (n = 5, $p < 0.05$) and 92 ± 18% (n = 5, $p < 0.01$), respectively, and inhibited somatic and dendritic $[Ca^{2+}]_i$ transients of the transient group by 83 ± 15% (n = 3, $p < 0.05$) and 92 ± 15% (n = 3, $p < 0.05$), respectively.

CFA-induced inflammation significantly increased AMPA-induced currents and associated $[Ca^{2+}]_i$ transients in tonically firing group of neurons (Fig. 4A, B and D). The amplitude of AMPA-induced inward current was increased by 125 ± 13% (n = 20; $p < 0.001$) 24 h post-CFA compared to post-saline (Fig. 4A and D). The increase in AMPA-induced current was associated with an augmentation in amplitudes of somatic and dendritic $[Ca^{2+}]_i$ transients. Twenty-four hours after CFA injection, the amplitude of $[Ca^{2+}]_i$ transients increased by 92 ± 11% and 96 ± 17% in soma and dendrites, respectively (n = 11; $p < 0.05$; average amplitude in soma: 0.47 ± 0.10 post-saline vs 0.91 ± 0.10 post-CFA; average amplitude in dendrites: 0.60 ± 0.12 post-saline vs 1.17 ± 0.21 post-CFA; Fig. 4A and D). At the same time, we found no significant differences between the tonic neurons from the saline- and CFA-treated animals in electrophysiological properties such as input resistance (saline: 612 ± 111 MΩ, n = 25; CFA: 604 ± 75 MΩ, n = 25, $p > 0.5$), capacitance (saline: 22 ± 1 pF, n = 26; CFA: 24 ± 1 pF, n = 30, $p = 0.2$) as well as a series resistance (saline: 28 ± 2 MΩ, n = 25; CFA: 30 ± 2 MΩ, n = 25, $p = 0.4$). These findings clearly

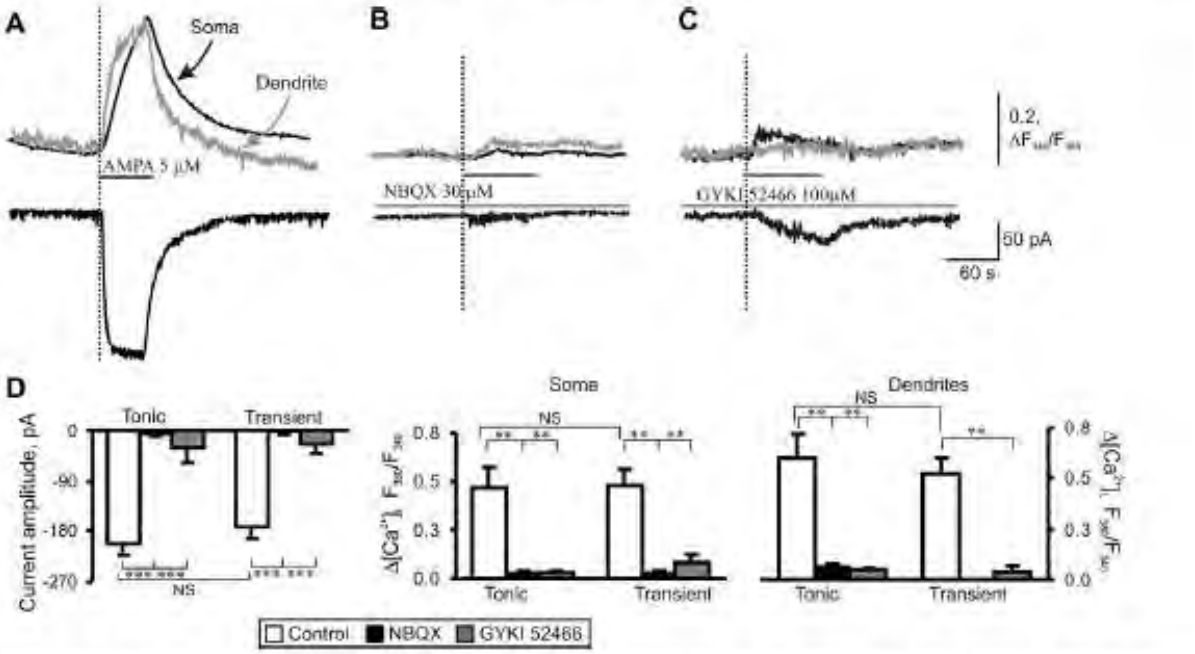

Fig. 3. AMPAR-mediated currents and $[Ca^{2+}]_i$ transients are similar in tonic and transient neurons of naïve rats. (A) Representative traces of a somatic membrane current (bottom trace) and associated $[Ca^{2+}]_i$ transients (upper traces) recorded from the soma (black trace) and dendrites (grey trace) in tonic neurons during AMPA bath application (5 μM, 60 s). (B, C) Pre-application of AMPAR antagonists NBQX (30 μM, B) and GYKI 52466 (100 μM, C) abolished AMPA-induced current (lower traces) and associated somatic (upper black traces) and dendritic (upper grey traces) $[Ca^{2+}]_i$ transients. (D) Pooled results demonstrate that AMPA-induced current amplitudes (left graph) and $[Ca^{2+}]_i$ transients (center and right graphs) recorded from soma and dendrites of different groups of SG neurons are similar. $^{**}p < 0.001$, $^{***}p < 0.0001$ versus the control; NS, not significant.

indicate a marked increase in functional expression of AMPARs in the dendrites and soma of tonically firing SG neurons during the maintenance of persistent inflammation. The data from our laboratory [41] and those of others [28,54] have demonstrated that CFA-induced inflammatory input does not significantly alter the amplitude of synaptically evoked AMPAR-mediated excitatory post-synaptic currents (eEPSCs) in the superficial dorsal horn neurons at 24 h post-CFA. Thus, the increase in AMPA-induced currents in the tonically firing SG neurons that we observed after inflammation can be attributed to upregulation of an extrasynaptic pool of AMPARs. In addition, a marked increase in the amplitudes of $[Ca^{2+}]_i$ transients suggests that this upregulation of AMPA-induced current is accounted for by an increase in the number of extrasynaptic Ca^{2+}-permeable AMPARs.

Interestingly, CFA-induced inflammation did not produce significant changes in AMPAR-mediated currents and associated somatic and dendritic $[Ca^{2+}]_i$ transients in transient neurons. The amplitudes of AMPA-induced currents were −173 ± 19 pA in the saline-treated group (n = 28) and −150 ± 17 pA in the CFA-treated group (n = 21; $p > 0.37$; Fig. 4C and D). The amplitudes of AMPA-induced $[Ca^{2+}]_i$ transients in soma were 0.48 ± 0.09 (n = 21) and 0.47 ± 0.08 (n = 8) in the saline- and CFA-treated groups, respectively ($p > 0.9$; Fig. 4 D). The amplitudes of AMPA-induced $[Ca^{2+}]_i$ transients in dendrites were 0.52 ± 0.09 (n = 18) and 0.59 ± 0.1 (n = 6) in the saline- and CFA-treated groups, respectively ($p > 0.6$; Fig. 4D). Additionally, inflammation did not significantly change series resistance (saline: 27 ± 1 MΩ, n = 38; CFA: 29 ± 1 MΩ, n = 32. $p = 0.2$), input resistance (saline: 682 ± 92 MΩ, n = 38; CFA: 663 ± 91 MΩ, n = 37. $p > 0.5$), or capacitance (saline: 17 ± 2 pF, n = 38; CFA: 19 ± 1 pF, n = 37. $p = 0.5$) in the transient neurons. These results indicate that the total pool of extrasynaptic and synaptic AMPARs in dendrites and somata was not changed in the transient group of SG neurons during maintenance of persistent inflammation.

3.3. Peripheral inflammation increases the proportion of Ca^{2+}-permeable AMPARs in the total pool of extrasynaptic AMPARs

Persistent inflammation changes a proportion of Ca^{2+}-permeable AMPARs to Ca^{2+}-impermeable AMPARs at synapses in dorsal horn neurons during the maintenance period of CFA-induced inflammatory pain [28,41,54]. To establish whether inflammation also changes this parameter for extrasynaptic populations of AMPARs, we first examined the effect of selective Ca^{2+}-permeable AMPAR blocker on AMPA-induced currents. IEM-1460, a polyamine derivative, rapidly and reversibly blocks Ca^{2+}-permeable AMPARs [10]. In the saline-treated rats, IEM-1460 (40 μM) produced a small, insignificant effect on amplitudes of AMPA-induced currents when it was applied to slices before AMPA (5–7 min, Fig. 5A, left graph) or when it was applied during a steady-state period of AMPA-induced current (Fig. 5A, right graph). In tonic neurons from the saline-treated group, the inhibitory effect of IEM-1460 on AMPA-induced current amplitude was small and insignificant (7 ± 2%, n = 7; $p > 0.45$; Fig. 5B), indicating that Ca^{2+}-permeable extrasynaptic AMPARs only slightly contribute to the total AMPA-induced current under normal conditions. On the contrary, sensitivity of synaptic AMPAR-mediated eEPSCs in SG neurons to Ca^{2+}-permeable AMPAR blockers was substantially greater (~23% inhibition [41,54]), further indicating that synaptic AMPARs do not contribute substantially to the generation of AMPA-induced currents. In contrast, in the CFA-treated group, the inhibitory effect of IEM-1460 on AMPA-induced current amplitude was substantially enhanced in the tonic neurons (26 ± 5%; n = 10; $p < 0.01$, Fig. 5A and B). This finding suggests that persistent

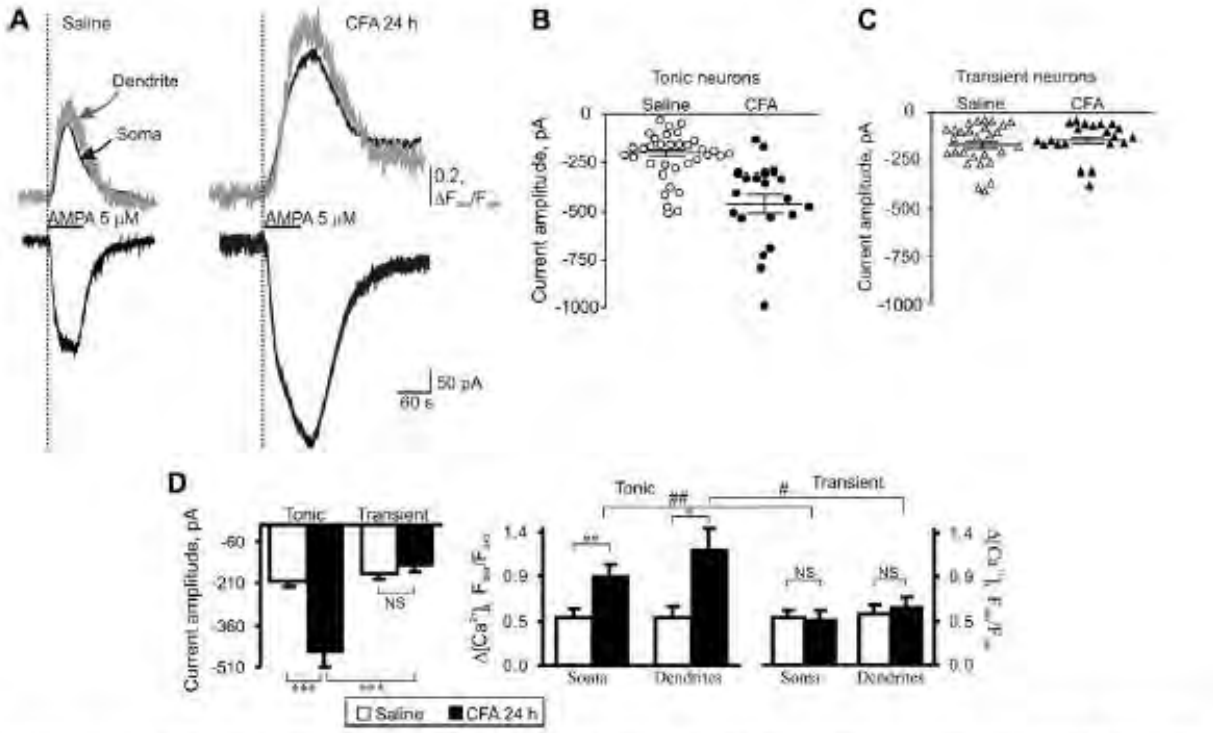

Fig. 4. AMPAR-mediated currents and associated $[Ca^{2+}]_i$ transients are markedly potentiated in tonic but not in transient SG neurons during persistent inflammation. (A) Representative examples of AMPA-induced currents (lower traces) and $[Ca^{2+}]_i$ transients (upper traces) in soma (black traces) and dendrites (grey traces) in tonic neurons 24 h after saline (control) or CFA. (B and C) Scatter dot plots illustrate a spread in extrasynaptic AMPAR-mediated currents in tonic (B) and transient (C) neurons 24 h after saline or CFA. (D) A statistical summary of current amplitudes (left graph) and $[Ca^{2+}]_i$ transients (right two graphs) in soma and dendrites of different groups of SG neurons 24 h post-saline and post-CFA. $^*p < 0.05$, $^{**}p < 0.001$, $^{***}p < 0.0001$ versus the saline-treated group; $^{\#}p < 0.05$, $^{\#\#}p < 0.001$ versus the transient SG neurons; NS, not significant.

peripheral inflammation not only increases the number of Ca^{2+}-permeable AMPARs at extrasynaptic sites in the tonic SG neurons but also increases their proportion in the total pool of extrasynaptic AMPARs. IEM-1460 had no significant effect on the amplitude of AMPA-induced current in the transient neurons from saline- or CFA-treated groups (saline: 7 ± 3%, n = 5, CFA: 15 ± 5%, n = 5, $p = 0.22$, Fig. 5B).

The proportion of extrasynaptic Ca^{2+}-permeable AMPARs in the somatic and dendritic pools was also examined based on the unique rectification properties of AMPAR-mediated currents. To obtain an *I–V* relationship of the AMPA-induced currents, we held neurons at −70 mV and ramped every 5 s initially to +50 mV and then to −70 mV before and during bath application of AMPA (Fig. 5C, upper panel). To isolate an AMPAR-mediated component of a current, we subtracted the ramp currents recorded before AMPA application from those recorded during the agonist application (see Methods for details). In the tonic neurons, the *I-V* curves showed weak rectification at positive membrane potentials in the saline-treated group that differed from the strong rectification of synaptic eEPSCs [41]. However, a significant inward rectification was observed in the CFA-treated group (Fig. 5C). To estimate the rectification of AMPA-induced currents, we calculated a rectification index expressed as a ratio of the current amplitudes at positive and negative membrane potentials ($RI_{+50/-50}$). RI was 0.74 ± 0.07 (n = 11) in the saline-treated group and 0.27 ± 0.05 (n = 12; $p < 0.001$, Fig. 5D) in the CFA-treated group. In contrast, RI for synaptic AMPAR-mediated eEPSCs was 0.26 and 0.18 in SG neurons from saline-treated and CFA-inflamed rats, respectively [41], further confirming that synaptic and extrasynaptic AMPA receptors have different properties.

CFA-induced inward rectification of AMPA-induced currents could be reversed by IEM-1460 (Fig. 5C). The RI value was significantly increased to 0.91 ± 0.05 after IEM-1460 treatment (n = 5; $p < 0.001$, Fig. 5D and E). These findings further indicate an increased proportion of extrasynaptic Ca^{2+}-permeable AMPARs in dorsal horn neurons during the maintenance of peripheral inflammation.

3.4. Peripheral inflammation induces GluR1 membrane insertion at extrasynaptic sites of dorsal horn neurons

To further validate whether extrasynaptic Ca^{2+}-permeable AMPARs are increased in plasma membrane of dorsal horn neurons under persistent inflammatory conditions, we used a combined approach of post-embedding immunogold labeling with electron microscopy (EM) to compare ultrastructural distribution of GluR1 and GluR2 in superficial dorsal horn 24 h after saline (n = 2) or CFA (n = 2) injection. We focused on these two subunits because they are more abundant in dorsal horn than are GluR3 and GluR4 [9,18,29]. We counted the immunogold-labeled particles at synapses, in extrasynaptic membranes, and in cytoplasm in both saline- and CFA-treated groups. Consistent with previous reports [41,43], we observed GluR1 and GluR2 immunogold labeling in post-synaptic membranes, cytoplasm, and extrasynaptic membranes in the saline-treated group (Fig. 6A). CFA injection produced a tendency toward an increase in the number of GluR1-labeled particles in extrasynaptic membranes and a decrease in synaptic membranes and cytoplasm (Fig. 6B). The ratio of the number of GluR1-labeled particles in the CFA-treated group to the number in the saline-treated group was 0.62 at synapses, 2.54 at

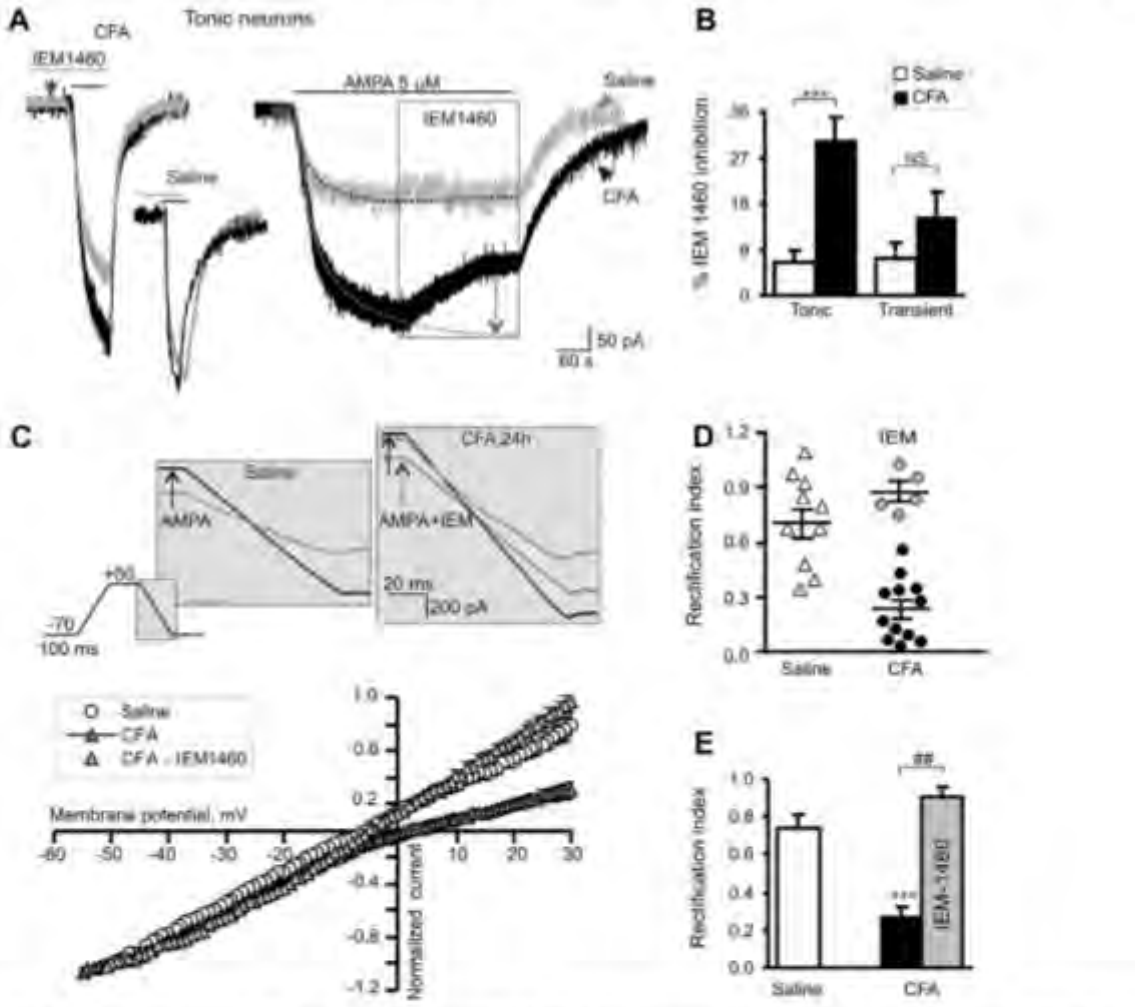

Fig. 5. Persistent peripheral inflammation increases the proportion of Ca^{2+}-permeable AMPARs in the extrasynaptic plasma membrane of tonic SG neurons. (A) A selective blocker of Ca^{2+}-permeable AMPARs, IEM-1460 (40 μM), substantially inhibited AMPA-induced currents in tonic neurons of CFA-treated but not of saline-treated rats. Left, an overlay of AMPA-induced currents recorded in the absence (black traces) and presence (pre-incubation for 5 min; grey traces) of IEM-1460 24 h after saline or CFA. Right, IEM-1460 was both applied during a steady-state phase of AMPA-induced current. Dotted lines represent exponential fitting of the currents; dotted arrow indicates the value of IEM-1460 inhibition. (B) A statistical summary of IEM-1460 inhibition of extrasynaptic AMPARs in tonic and transient SG neurons. ***$p < 0.0001$ versus the saline-treated group. (C) The top panel illustrates the protocol for reconstruction of the *I–V* relationship from ramp recordings. The bottom panel shows *I–V* curves obtained in tonic neurons at 24 h post-saline or post-CFA. Note that IEM-1460 reverses the rectification of AMPA-induced currents recorded from neurons of CFA-treated rats. (D, E) The scatter plot illustrates the spread in rectification index ($RI = I_{+50mV}/I_{-70mV}$) (D), and the bar graph shows the statistical summary for RI (E) in tonic neurons 24 h post-saline and post-CFA before (black) and after (grey) IEM-1460 application. ***$p = 0.0001$ versus the saline-treated group, **$p < 0.001$ versus the CFA-treated group.

extrasynaptic membranes, and 0.79 in the cytoplasm (n = 57; Fig. 6B). In agreement with our previous report [41], CFA injection led to a decrease in the number of GluR2-labled particles at synapses and a tendency toward an increase in the cytoplasm (Fig. 6B). The ratio of the number of GluR2-labeled particles in the CFA-treated group to the number in the saline-treated group was 0.61 at synapses, 1.05 at extrasynaptic membranes, and 1.2 in the cytoplasm (n = 47; Fig. 6B). These findings indicate that peripheral inflammation might induce GluR1 membrane insertion at extrasynaptic membranes and GluR2 internalization at synapses in superficial dorsal horn.

EM immunogold study of low-density extrasynaptic receptors has spatial and sample size limitations. To further confirm our observation, we used a surface biotinylation expression assay and synaptosomal fractionation approach to compare the expression of GluR1 in surface plasma membranes and in synaptic membranes derived from the dorsal horn. For the surface biotinylation expression assay, live slices were prepared from the ipsilateral L_{4-5} dorsal horn 24 h after saline (n = 4) or CFA (n = 4) injection. The surface receptors were labeled with biotin and then precipitated [41,51]. The amount of surface GluR1 was 33% greater in the CFA-treated group than in the saline-treated group ($p < 0.05$) (Fig. 7A). In control experiments, β-actin, an intracellular protein, could not be precipitated by biotin (Fig. 7A). Using differential centrifugation [49], we collected synaptosomal fractions that contained abundant synaptic receptors from the ipsilateral L_{4-5} dorsal horn tissues 24 h after saline (n = 4) or CFA (n = 4) injection. Western blot analysis showed that the level of GluR1 in the synaptosomal fraction of the CFA-treated group was similar to that of the saline-treated group ($p > 0.05$; Fig. 7B). Taken together, our findings suggest that the amount of GluR1 in extrasynaptic membranes is increased in dorsal horn under persistent inflammatory conditions.

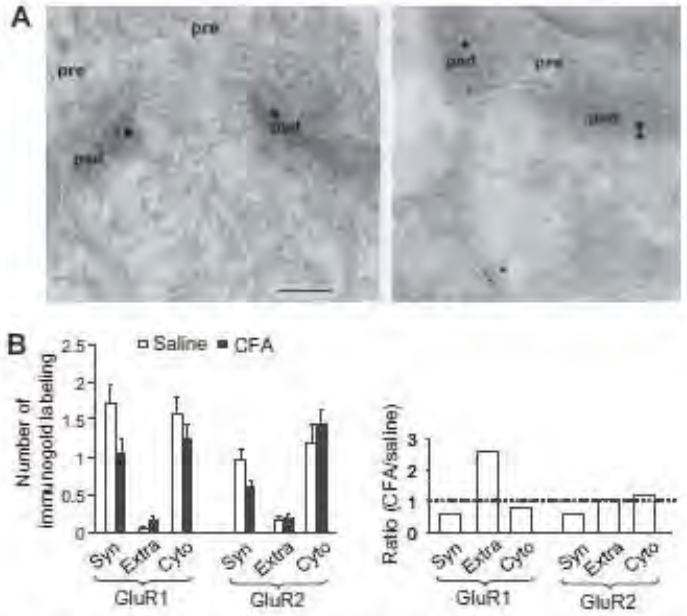

Fig. 6. Ultrastructural distribution of GluR1 and GluR2 in the superficial dorsal horn 24 h after saline (left) or CFA (right) injection. (A) Representative micrographs of postembedding immunogold labeling for GluR1 (5 nm) and GluR2 (15 nm). In these representative images, the synapses are marked by the presence of GluR2; GluR1 is more prevalent at synapses in the saline-treated group. In the CFA-treated group, GluR1 is evident in the extrasynaptic membrane (asterisk). PSD, postsynaptic density; pre, presynaptic terminal; scale bar = 100 nm. (B) The left bar graph shows the number of GluR1- and GluR2-labeled immunogold particles at synapses (Syn), at extrasynaptic membranes (Extra), and in cytoplasm (Cyto) of superficial dorsal horn neurons 24 h after CFA or saline injection. The right bar graph shows ratios of the number of GluR1- and GluR2-labeled particles in the CFA-treated group to those in the saline-treated group at synapses, extrasynaptic membranes, and cytoplasm of superficial dorsal horn neurons 24 h after injections.

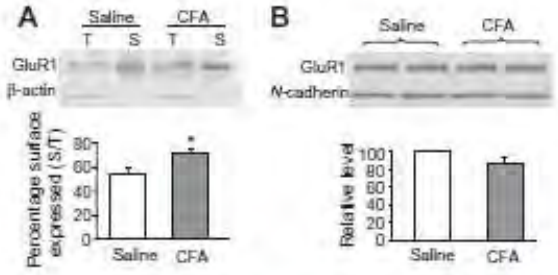

Fig. 7. GluR1 membrane insertion in dorsal horn neurons 24 h after CFA injection. (A) Surface expression of GluR1 in dorsal horn neurons 24 h after CFA or saline injection. Top, representative Western blot; bottom, statistical summary of the densitometric analysis. The level of sample loaded for the total (T) expression was 10% of that for the biotinylated surface (S) expression. $^{*}p < 0.05$ versus the saline-treated group. β-Actin, an unbiotinylated intracellular protein, was used as a control. (B) Expression of GluR1 in the synaptosomal fraction from dorsal horn 1 day after CFA or saline injection. Top, representative Western blot; bottom, statistical summary of the densitometric analysis. *N*-cadherin, a membrane marker, was used as a control.

4. Discussion

In the present study, we have demonstrated that peripheral inflammation markedly increases the absolute number of, as well as the proportion of Ca^{2+}-permeable AMPARs in the extrasynaptic membrane of tonically firing SG neurons during the maintenance period of inflammatory pain. Our morphological and biochemical results further showed increased membrane insertion of extrasynaptic GluR1 at 24 h post-CFA. This inflammation-associated increase in functional expression of extrasynaptic GluR1-containing Ca^{2+}-permeable AMPARs in the tonically firing dorsal horn neurons might contribute to the maintenance of persistent inflammatory pain.

4.1. Composition of extrasynaptic AMPARs under normal conditions

A high level of extrasynaptic AMPAR immunoreactivity has been detected throughout the central nervous system, including the dorsal horn [39–42]. By using electrophysiological, imaging, and immunochemical approaches, we demonstrated the presence of functional AMPARs at extrasynaptic sites of dorsal horn neurons. Their functional properties are distinct from those of synaptic AMPARs [28,41,52,54]. AMPA-induced currents in the neurons of naïve rats displayed roughly linear current–voltage relationships (RI = 0.74) and were not significantly suppressed by the specific Ca^{2+}-permeable AMPAR blocker IEM-1460 (Fig. 5). In contrast, we observed that AMPAR-mediated EPSCs (RI = 0.26) had prominent rectification and were substantially inhibited by polyamine blockers (23%) [41]. These findings suggest that synaptic AMPA receptors did not significantly contribute to AMPA-induced currents, which were mediated mainly by AMPARs located at extrasynaptic sites. These results also indicate that most extrasynaptic AMPARs in SG neurons consist of GluR2 subunits and are Ca^{2+}-impermeable under normal conditions. Consistently, immunogold labeling showed more GluR2 than GluR1 in the extrasynaptic profiles of the superficial dorsal horn neurons (Fig. 6B). At the same time, the AMPA-induced currents did evoke $[Ca^{2+}]_i$ transients, implying that a minor proportion of Ca^{2+}-permeable AMPARs are located in the plasma membrane of SG neurons (Fig. 3). Our findings indicate that GluR2-containing Ca^{2+}-impermeable AMPARs are dominant at extrasynaptic sites in normal superficial dorsal horn. Similar differences in synaptic and extrasynaptic AMPAR channel composition have been reported in other brain regions [6,35].

4.2. Trafficking of extrasynaptic AMPARs during persistent pain

Extrasynaptic AMPAR trafficking in dorsal horn during inflammatory pain has not been well studied. Previous studies have shown that persistent inflammation induces synaptic GluR2 internalization. This internalization results in a switch from Ca^{2+}-impermeable to Ca^{2+}-permeable AMPAR-mediated neurotransmission at synapses in dorsal horn, although the amplitude of eEPSCs was not changed [28,41,54]. In the present study, we found a significant increase in the amplitudes of AMPAR-mediated current (evoked by bath application of AMPA) and the associated $[Ca^{2+}]_i$ transients recorded in soma and dendrites of the tonically firing SG neurons at 24 h post-CFA (Fig. 4). These data indicate that the number of extrasynaptic Ca^{2+}-permeable AMPARs is substantially increased in the tonic SG neurons after inflammation. Moreover, the *I-V* curves obtained in SG neurons from rats with peripheral inflammation were inwardly rectified, and sensitivity to the selective inhibition of Ca^{2+}-permeable AMPARs was significantly increased at 24 h post-CFA (Fig. 6). Our results indicate that peripheral inflammation might increase the number of Ca^{2+}-permeable AMPARs at extrasynaptic sites as well as the proportion of them in the total pool of extrasynaptic AMPARs in dorsal horn neurons during the maintenance period. In line with these results, previous studies have demonstrated that the amount of GluR1 was increased (by 23%) and that the amount of GluR2 was correspondingly decreased (by 25%) in the crude membrane fraction of ipsilateral dorsal horn 1 day after intraplantar CFA injection [28,42]. In the present study, we also showed that surface membrane expression of GluR1 in dorsal horn from the CFA-treated group was 33% greater than that in the saline-treated group (Fig. 7A). Since we found no significant difference in the levels of GluR1 in the synaptosomal fraction of the ipsilateral dorsal horn between the CFA- and saline-treated groups (Fig. 7B), the observed increase in surface membrane GluR1 mostly reflects an increase in the extrasynaptic pool of receptors. Our findings suggest that persistent inflammation promotes marked insertion of GluR1-containing Ca^{2+}-permeable AMPARs at extrasynaptic membrane sites. The data from our laboratory and those of others [28,41] showed that the amount of GluR2 decreased at surface plasma membranes and synapses while correspondingly increasing in the cytoplasm in dorsal horn at 24 h post-CFA. Therefore, it is evident that peripheral inflammation might produce a reciprocal rearrangement of GluR1-containing Ca^{2+}-permeable and GluR2-containing Ca^{2+}-impermeable AMPARs in different cellular pools of dorsal horn neurons.

4.3. Functional significance of increased extrasynaptic Ca^{2+}-permeable AMPARs

Our findings suggest that persistent inflammatory insult alters trafficking of extrasynaptic AMPARs in dorsal horn and induces delivery of spinal GluR1-containing Ca^{2+}-permeable AMPARs to extrasynaptic sites. Although it is well established that Ca^{2+}-permeable AMPARs facilitate nociceptive plasticity and enhance long-lasting inflammatory hyperalgesia [23,27,37], molecular mechanisms that underlie these events are still unclear. Surface AMPARs represent a mobile population that traffics between synaptic and extrasynaptic sites [24]. Since the extrasynaptic AMPARs are subjected to Brownian-like unrestricted mobility, the dynamic equilibrium between synaptic and extrasynaptic receptor pools determines the number of synaptic receptors and synaptic strength [53]. We found that inflammatory insult promotes insertion of GluR1-containing Ca^{2+}-permeable AMPARs at extrasynaptic membranes. These extrasynaptic Ca^{2+}-permeable receptors can diffuse laterally in the plasma membrane to the postsynaptic density [17] where they might be trapped at synapses [41,50]. It is very likely that an inflammation-induced increase in extrasynaptic Ca^{2+}-permeable AMPARs may be involved in the mechanisms that underlie a persistent increase in synaptic Ca^{2+}-permeable AMPARs in the dorsal horn neurons that has been reported recently [28,41,54]. Persistent inflammatory insult also induces PKC-dependent disruption of GluR2 binding to its synaptic anchoring proteins [4], promotes GluR2 internalization from synapses, and decreases the number of synaptic GluR2-containing AMPARs [28,41,54]. All of these events finally result in an increase of synaptic [28,41,54] and extrasynaptic AMPAR Ca^{2+} permeability. This conclusion is supported by inflammation-induced potentiation of $[Ca^{2+}]_i$ transients evoked in SG neurons by dorsal root stimulation [37,55]. The related increase in intracellular Ca^{2+} concentration should initiate or potentiate a variety of Ca^{2+}-dependent intracellular cascades that are associated with the mechanisms of pain hypersensitivity during inflammatory pain maintenance.

AMPARs can also contribute to glutamate-mediated signaling at non-synaptic locations. Strong primary afferent inputs generated from peripheral nociceptors by persistent inflammation may produce glutamate spillover from nearby primary afferent terminals [30]. In addition, excessive glutamate is released from glia during dorsal horn injuries or inflammation [2,30,56]. This endogenously released glutamate may activate not only post-synaptic AMPARs [45] but also extrasynaptic glutamate receptors. The latter may further strengthen glutamatergic transmission under persistent inflammatory conditions.

4.4. Tonic excitatory SG neurons likely contribute to the maintenance of inflammatory pain

Peripheral inflammation alters AMPAR trafficking in the SG neurons characterized by intrinsic tonic firing properties, but not in those that exhibit strong adaptation. In the transient neurons, CFA injection did not change the amplitudes of AMPA-induced current and associated $[Ca^{2+}]_i$ transients 24 h post-injection (Fig. 4). Taking into account that AMPA-induced current and $[Ca^{2+}]_i$ transients did not differ between tonic and transient neurons from the saline-treated group, we suggest that the total receptor pool is stable in the transient neurons even at the peak of inflammation. Our cobalt staining results also showed that a proportion of NeuN-marked neurons in superficial dorsal horn 24 h post-CFA were not cobalt-positive (Fig. 2). Thus, it is evident that inflammation-induced changes in AMPAR trafficking occur specifically in a subpopulation of SG neurons. It is known that the population of SG neurons is not homogeneous and displays distinct immunohistochemical [18,29], electrophysiological [5,20,21], and functional properties. The superficial dorsal horn neurons are characterized by different patterns of AMPAR subunit expression [18,29]. Under normal conditions, surface GluR1 protein expression is particularly associated with inhibitory dorsal horn neurons, whereas GluR2, mainly observed in this work, is associated with excitatory neurons [1,29]. Furthermore, in the SG, most tonic interneurons are excitatory [46]. These neurons make synaptic connections not only within lamina II, but also in lamina I, a region where the most nociceptive projection neurons are localized [12,33,34]. It is therefore reasonable to conclude that altered AMPAR trafficking in excitatory tonic SG neurons might be a key component in spinal central sensitization that underlies the maintenance of persistent inflammatory pain.

In conclusion, our study has shown that CFA-induced peripheral inflammation increases the number of extrasynaptic Ca^{2+}-permeable AMPARs as well as their proportion within the entire pool of extrasynaptic AMPARs in tonically firing SG neurons during the maintenance period. Thus, tonically firing SG neurons may represent a specific population of spinal neurons that carry out nociceptive inputs and contribute to spinal central sensitization. Since the total amount of GluR1 remains constant under CFA-induced inflammatory pain conditions [42], the observed increase in extra-

synaptic Ca^{2+}-permeable AMPARs is likely attributable to CFA-promoted GluR1 membrane insertion at extrasynaptic membranes. Although the molecular mechanisms that underlie this GluR1 trafficking are still unclear, our study suggests that extrasynaptic GluR1-containing Ca^{2+}-permeable AMPARs in the dorsal horn may be used as a new target in preventing and treating persistent inflammatory pain.

Acknowledgements

This work was supported by NASU Biotechnology and INTAS 8061 Grants (N.V.), NIH Grant NS058886, Mr. David Koch and the Patrick C. Walsh Prostate Cancer Research Fund, and the Johns Hopkins University Blaustein Pain Research Fund (Y.X.T.), and the Intramural Research Program of NIDCD (R.S.P.). We thank Mrs. Ya-Xian Wang for help with the immunogold experiments. The authors thank Claire F. Levine, MS, for her editorial assistance. The authors declare no conflict of interests.

References

[1] Albuquerque C, Lee CJ, Jackson AC, MacDermott AB. Subpopulations of GABAergic and non-GABAergic rat dorsal horn neurons express Ca^{2+}-permeable AMPA receptors. Eur J Neurosci 1999;11:2758–66.
[2] Allan SM, Rothwell NJ. Cytokines and acute neurodegeneration. Nat Rev Neurosci 2001;2:734–44.
[3] Arendt KL, Royo M, Fernandez-Monreal M, Knafo S, Petrok CN, Martens JR, Esteban JA. PIP3 controls synaptic function by maintaining AMPA receptor clustering at the postsynaptic membrane. Nat Neurosci 2010;13:36–44.
[4] Atianjoh FE, Yaster M, Zhao X, Takamiya K, Xia J, Gauda EB, Huganir RL, Tao YX. Spinal cord protein interacting with C kinase 1 is required for the maintenance of complete Freund's adjuvant-induced inflammatory pain but not for incision-induced post-operative pain. Pain 2010;151:226–34.
[5] Balasubramanyan S, Stemkowski PL, Stebbing MJ, Smith PA. Sciatic chronic constriction injury produces cell-type-specific changes in the electrophysiological properties of rat substantia gelatinosa neurons. J Neurophysiol 2006;96:579–90.
[6] Beique JC, Huganir RL. AMPA receptor subunits get their share of the pie. Neuron 2009;62:165–8.
[7] Borgdorff AJ, Choquet D. Regulation of AMPA receptor lateral movements. Nature 2002;417:649–53.
[8] Bredt DS, Nicoll RA. AMPA receptor trafficking at excitatory synapses. Neuron 2003;40:361–79.
[9] Brown KM, Wrathall JR, Yasuda RP, Wolfe BB. Quantitative measurement of glutamate receptor subunit protein expression in the postnatal rat spinal cord. Brain Res Dev Brain Res 2002;137:127–33.
[10] Buldakova SL, Kim KK, Yikhonov DB, Magazanik LG. Selective blockade of Ca^{2+} permeable AMPA receptors in CA1 area of rat hippocampus. Neuroscience 2007;144:88–99.
[11] Burnashev N, Monyer H, Seeburg PH, Sakmann B. Divalent ion permeability of AMPA receptor channels is dominated by the edited form of a single subunit. Neuron 1992;8:189–98.
[12] Burstein R, Cliffer KD, Giesler Jr GJ. Direct somatosensory projections from the spinal cord to the hypothalamus and telencephalon. J Neurosci 1987;7:4159–64.
[13] Carroll RC, Lissin DV, von ZM, Nicoll RA, Malenka RC. Rapid redistribution of glutamate receptors contributes to long-term depression in hippocampal cultures. Nat Neurosci 1999;2:454–60.
[14] Choi JI, Svensson CI, Koehrn FJ, Bhuskute A, Sorkin LS. Peripheral inflammation induces tumor necrosis factor dependent AMPA receptor trafficking and Akt phosphorylation in spinal cord in addition to pain behavior. Pain 2010;149:243–53.
[15] Choquet D, Triller A. The role of receptor diffusion in the organization of the postsynaptic membrane. Nat Rev Neurosci 2003;4:251–65.
[16] Cognet L, Groc L, Lounis B, Choquet D. Multiple routes for glutamate receptor trafficking: surface diffusion and membrane traffic cooperate to bring receptors to synapses. Sci STKE 2006;2006:e13.
[17] Derkach VA, Oh MC, Guire ES, Soderling TR. Regulatory mechanisms of AMPA receptors in synaptic plasticity. Nat Rev Neurosci 2007;8:101–13.
[18] Engelman HS, Allen TB, MacDermott AB. The distribution of neurons expressing calcium-permeable AMPA receptors in the superficial laminae of the spinal cord dorsal horn. J Neurosci 1999;19:2081–9.
[19] Ferguson AR, Christensen RN, Gensel JC, Miller BA, Sun F, Beattie EC, Bresnahan JC, Beattie MS. Cell death after spinal cord injury is exacerbated by rapid TNF alpha-induced trafficking of GluR2-lacking AMPARs to the plasma membrane. J Neurosci 2008;28:11391–400.
[20] Graham BA, Brichta AM, Callister RJ. In vivo responses of mouse superficial dorsal horn neurones to both current injection and peripheral cutaneous stimulation. J Physiol 2004;561:749–63.
[21] Grudt TJ, Perl ER. Correlations between neuronal morphology and electrophysiological features in the rodent superficial dorsal horn. J Physiol 2002;540:189–207.
[22] Guire ES, Oh MC, Soderling TR, Derkach VA. Recruitment of calcium-permeable AMPA receptors during synaptic potentiation is regulated by CaM-kinase I. J Neurosci 2008;28:6000–9.
[23] Hartmann B, Ahmadi S, Heppenstall PA, Lewin GR, Schott C, Borchardt T, Seeburg PH, Zeilhofer HU, Sprengel R, Kuner R. The AMPA receptor subunits GluR-A and GluR-B reciprocally modulate spinal synaptic plasticity and inflammatory pain. Neuron 2004;44:637–50.
[24] Heine M, Groc L, Frischknecht R, Beique JC, Lounis B, Rumbaugh G, Huganir RL, Cognet L, Choquet D. Surface mobility of postsynaptic AMPARs tunes synaptic transmission. Science 2008;320:201–5.
[25] Ho MT, Pelkey KA, Topolnik L, Petralia RS, Takamiya K, Xia J, Huganir RL, Lacaille JC, McBain CJ. Developmental expression of Ca^{2+}-permeable AMPA receptors underlies depolarization-induced long-term depression at mossy fiber CA3 pyramid synapses. J Neurosci 2007;27:11651–62.
[26] Hollmann M, O'Shea-Greenfield A, Rogers SW, Heinemann S. Cloning by functional expression of a member of the glutamate receptor family. Nature 1989;342:643–8.
[27] Jones TL, Activated SorkinLS, PKA PKC. But not CaMKIIalpha, are required for AMPA/kainate-mediated pain behavior in the thermal stimulus model. Pain 2005;117:258–70.
[28] Katano T, Furue H, Okuda-Ashitaka E, Tagaya M, Watanabe M, Yoshimura M, Ito S. N-ethylmaleimide-sensitive fusion protein (NSF) is involved in central sensitization in the spinal cord through GluR2 subunit composition switch after inflammation. Eur J Neurosci 2008;27:3161–70.
[29] Kerr RC, Maxwell DJ, Todd AJ. GluR1 and GluR2/3 subunits of the AMPA-type glutamate receptor are associated with particular types of neurone in laminae I-III of the spinal dorsal horn of the rat. Eur J Neurosci 1998;10:324–33.
[30] Kullmann DM. Spillover and synaptic cross talk mediated by glutamate and GABA in the mammalian brain. Prog Brain Res 2000;125:339–51.
[31] Kwak S, Weiss JH. Calcium-permeable AMPA channels in neurodegenerative disease and ischemia. Curr Opin Neurobiol 2006;16:281–7.
[32] Leonoudakis D, Zhao P, Beattie EC. Rapid Tumor Necrosis Factor (alpha)-induced Exocytosis of Glutamate Receptor 2-Lacking AMPA Receptors to Extrasynaptic Plasma Membrane Potentiates Excitotoxicity. J Neurosci 2008;28:2119–30.
[33] Lima D. Anatomical basis for the dynamic processing of nociceptive input. Eur J Pain 1998;2:195–202.
[34] Lima D, Coimbra A. The spinothalamic system of the rat: structural types of retrogradely labelled neurons in the marginal zone (lamina I). Neuroscience 1988;27:215–30.
[35] Lu W, Shi Y, Jackson AC, Bjorgan K, During MJ, Sprengel R, Seeburg PH, Nicoll RA. Subunit Composition of Synaptic AMPA Receptors Revealed by a Single-Cell Genetic Approach. Neuron 2009;62:254–68.
[36] Lu Y, Perl ER. Modular organization of excitatory circuits between neurons of the spinal superficial dorsal horn (laminae I and II). J Neurosci 2005;25:3900–7.
[37] Luo C, Seeburg PH, Sprengel R, Kuner R. Activity-dependent potentiation of calcium signals in spinal sensory networks in inflammatory pain states. Pain 2008;140:358–67.
[38] Malinow R, Malenka RC. AMPA receptor trafficking and synaptic plasticity. Annu Rev Neurosci 2002;25:103–26.
[39] Masugi-Tokita M, Shigemoto R. High-resolution quantitative visualization of glutamate and GABA receptors at central synapses. Curr Opin Neurobiol 2007;17:387–93.
[40] Masugi-Tokita M, Tarusawa E, Watanabe M, Molnar E, Fujimoto K, Shigemoto R. Number and Density of AMPA Receptors in Individual Synapses in the Rat Cerebellum as Revealed by SDS-Digested Freeze-Fracture Replica Labeling. J Neurosci 2007;27:2135–44.
[41] Park JS, Voitenko N, Petralia RS, Guan X, Xu JT, Steinberg JP, Takamiya K, Sotnik A, Kopach O, Huganir RL, Tao YX. Persistent inflammation induces GluR2 internalization via NMDA receptor-triggered PKC activation in dorsal horn neurons. J Neurosci 2009;29:3206–19.
[42] Park JS, Yaster M, Guan X, Xu JT, Shih MH, Guan Y, Raja SN, Tao YX. Role of spinal cord alpha-amino-3-hydroxy-5-methyl-4-isoxazolepropionic acid receptors in complete freund's adjuvant-induced inflammatory pain. Mol Pain 2008;4:67.
[43] Petralia RS, Wang YX, Mayat E, Wenthold RJ. Glutamate receptor subunit 2-selective antibody shows a differential distribution of calcium-impermeable AMPA receptors among populations of neurons. J Comp Neurol 1997;385:456–76.
[44] Petrini EM, Lu J, Cognet L, Lounis B, Ehlers MD, Choquet D. Endocytic trafficking and recycling maintain a pool of mobile surface AMPA receptors required for synaptic potentiation. Neuron 2009;63:92–105.
[45] Russo RE, Delgado-Lezama R, Hounsgaard J. Dorsal root potential produced by a TTX-insensitive micro-circuitry in the turtle spinal cord. J Physiol 2000;528:115–22.
[46] Santos SF, Rebelo S, Derkach VA, Safronov BV. Excitatory interneurons dominate sensory processing in the spinal substantia gelatinosa of rat. J Physiol 2007;581:241–54.
[47] Shi SH, Hayashi Y, Petralia RS, Zaman SH, Wenthold RJ, Svoboda K, Malinow R. Rapid spine delivery and redistribution of AMPA receptors after synaptic NMDA receptor activation. Science 1999;284:1811–6.

[48] Singh OV, Yaster M, Xu JT, Guan Y, Guan X, Dharmarajan AM, Raja SN, Zeitlin PL, Tao YX. Proteome of synaptosome-associated proteins in spinal cord dorsal horn after peripheral nerve injury. Proteomics 2009;9:1241–53.
[49] Sommer B, Keinanen K, Verdoorn TA, Wisden W, Burnashev N, Herb A, Kohler M, Takagi T, Sakmann B, Seeburg PH. Flip and flop: a cell-specific functional switch in glutamate-operated channels of the CNS. Science 1990;249:1580–5.
[50] Tao YX. Dorsal horn alpha-amino-3-hydroxy-5-methyl-4-isoxazolepropionic acid receptor trafficking in inflammatory pain. Anesthesiology 2010;112:1259–65.
[51] Tao YX, Rumbaugh G, Wang GD, Petralia RS, Zhao C, Kauer FW, Tao F, Zhuo M, Wenthold RJ, Raja SN, Huganir RL, Bredt DS, Johns RA. Impaired NMDA receptor-mediated postsynaptic function and blunted NMDA receptor-dependent persistent pain in mice lacking postsynaptic density-93 protein. J Neurosci 2003;23:6703–12.
[52] Tong CK, MacDermott AB. Both Ca^{2+}-permeable and -impermeable AMPA receptors contribute to primary synaptic drive onto rat dorsal horn neurons. J Physiol 2006;575:133–44.
[53] Triller A, Choquet D. New concepts in synaptic biology derived from single-molecule imaging. Neuron 2008;59:359–74.
[54] Vikman KS, Rycroft BK, Christie MJ. Switch to Ca^{2+}-permeable AMPA and reduced NR2B NMDA receptor-mediated neurotransmission at dorsal horn nociceptive synapses during inflammatory pain in the rat. J Physiol 2008;586:515–27.
[55] Voitenko N, Gerber G, Youn D, Randic M. Peripheral inflamation-induced increase of AMPA-mediated currents and Ca^{2+} transients in the presence of cyclothiazide in the rat substantia gelatinosa neurons. Cell Calcium 2004;35:461–9.
[56] Weng HR, Chen JH, Cata JP. Inhibition of glutamate uptake in the spinal cord induces hyperalgesia and increased responses of spinal dorsal horn neurons to peripheral afferent stimulation. Neuroscience 2006;138:1351–60.
[57] Youn DH, Voitenko N, Gerber G, Park YK, Galik J, Randic M. Altered long-term synaptic plasticity and kainate-induced Ca^{2+} transients in the substantia gelatinosa neurons in GLU(K6)-deficient mice. Brain Res Mol Brain Res 2005;142:9–18.

2.2. Розвиток больового синдрому супроводжується збільшенням Ca2+-провідних AMPA-рецепторів у позасинаптичних мембранах нейронів дорзального рогу спинного мозку

frontiers in PHYSIOLOGY

ORIGINAL RESEARCH ARTICLE
published: 02 October 2012
doi: 10.3389/fphys.2012.00391

Development of inflammation-induced hyperalgesia and allodynia is associated with the upregulation of extrasynaptic AMPA receptors in tonically firing lamina II dorsal horn neurons

Olga Kopach, Viacheslav Viatchenko-Karpinski, Pavel Belan and Nana Voitenko*

State Key Laboratory of Molecular and Cellular Biology, Bogomoletz Institute of Physiology, Kiev, Ukraine

Edited by:
Francisco F De-Miguel, Universidad Nacional Autonoma de Mexico, Mexico

Reviewed by:
Alberto Lopez-Avila, Instituto Nacional de Psiquiatria Ramon de la Fuente Muñiz, Mexico
Leonardo Rodriguez-Sosa, UNAM, Mexico

***Correspondence:**
Nana Voitenko, Department of General Physiology of Nervous System, Bogomoletz Institute of Physiology, Bogomoletz Str. 4, Kiev 01024, Ukraine.
e-mail: nana@biph.kiev.ua

Persistent peripheral inflammation changes AMPA receptor (AMPAR) trafficking in dorsal horn neurons by promoting internalization of GluR2-containing, Ca^{2+}-impermeable AMPARs from the synapses and by increasing insertion of GluR1-containing, Ca^{2+}-permeable AMPARs in extrasynaptic plasma membrane. These changes contribute to the maintenance of persistent inflammatory pain. However, much less is known about AMPAR trafficking during development of persistent inflammatory pain and direct studies of extrasynaptic AMPARs functioning during this period are still lacking. Using Complete Freund's adjuvant (CFA)-induced model of long-lasting peripheral inflammation, we showed that remarkable hyperalgesia and allodynia developes in 1–3 h after intraplantar CFA injection. By utilizing patch-clamp recording combined with Ca^{2+} imaging, we found a significant upregulation of extrasynaptic AMPARs in substantia gelatinosa (SG) neurons of the rat spinal cord 2–3 h after CFA injection. This upregulation was manifested as a robust increase in the amplitude of AMPAR-mediated currents 2–3 h post-CFA. These changes were observed specifically in SG neurons characterized by intrinsic tonic firing properties, but not in those that exhibited strong adaptation. Our results indicate that CFA-induced inflammation increases functional expression of extrasynaptic AMPARs in tonically firing SG neurons during development of pain hypersensitivity and that this increase may contribute to the development of peripheral persistent pain.

Keywords: extrasynaptic AMPA receptors, development of inflammatory pain, substantia gelatinosa neurons, hyperalgesia, allodynia

INTRODUCTION

Persistent or chronic pain is a public health problem worldwide and may result from infection, inflammation, peripheral injury to tissue or nerve. Understanding the molecular mechanisms underlying development and maintenance of chronic pain ensures success of its treatment by developing alternative strategies, which target specific molecules precisely, and would therefore be of potential benefit in treatment or even prevention of persistent pain. Cumulative evidence demonstrates that altered AMPAR trafficking in dorsal horn neurons is required for the persistent inflammatory pain maintenance. However, a role of AMPARs in persistent inflammatory pain development is not completely understood. Besides, current studies in this field are predominantly concentrated on synaptic AMPARs, leaving functioning of extrasynaptic AMPARs population out of direct investigation.

α-amino-3-hydroxy-5-methyl-4-isoxazolepropionic acid receptors (AMPARs) expression level at extrasynaptic sites of neuronal plasma membrane is high throughout the central nervous system (CNS). Extrasynaptic AMPARs are localized within spines, dendrites, and somata (Malinow and Malenka, 2002; Bredt and Nicoll, 2003). They are mobile and rapidly move between the plasma membrane and intracellular compartments by exocytosis and endocytosis, and can migrate laterally to and from synaptic sites adjusting synaptic strength (Borgdorff and Choquet, 2002; Choquet and Triller, 2003; Adesnik et al., 2005; Cognet et al., 2006). Extrasynaptic AMPARs may also contribute to glutamatergic signaling at nonsynaptic locations. Glutamate, released from the presynaptic neurons and from astrocytes, can bath the extrasynaptic plasma membrane by the glutamate spillover and activates extrasynaptic AMPARs, thus strengthening glutamatergic transmission. During neuropathological conditions, when a primary afferent input is strong, glutamate spillover is excessive (Allan and Rothwell, 2001) and results in increased excitotoxic vulnerability and neurons injury (Kullmann, 2000; Allan and Rothwell, 2001; Weng et al., 2006).

The changes in AMPAR subunit trafficking, subunit composition, phosphorylation of AMPAR subunits or their interaction with partner proteins may contribute to spinal nociceptive transmission (Santos et al., 2009; Wang et al., 2010; He et al., 2011). In a spinal cord, AMPAR trafficking has been suggested as one of key mechanisms for central sensitization, a specific form of plasticity underlying induction and maintenance of pain (Hartmann et al., 2004; Park et al., 2008, 2009; Latremoliere and Woolf, 2009; Tao, 2010; Kopach et al., 2011).

Recent studies demonstrated that altered AMPAR trafficking in dorsal horn neurons is causally linked to peripheral inflammatory pain maintenance (Hartmann et al., 2004; Katano et al., 2008; Park et al., 2009). Persistent peripheral inflammation promotes internalization of GluR2-containing, Ca^{2+}-impermeable AMPARs from the synapses (Park et al., 2009) and insertion of GluR1-containing, Ca^{2+}-permeable AMPARs at extrasynaptic membrane of lamina II dorsal horn neurons (Kopach et al., 2011) during inflammatory pain maintenance. However, much less is known about extrasynaptic AMPAR trafficking in dorsal horn neurons during development of inflammatory pain. So far as inflammation-induced peripheral hypersensitivity develops rapidly (2–3 h) after intraplantar complete Freund's adjuvant (CFA) injection and is comparable to one observed during the period of inflammatory pain maintenance (Zhang et al., 2003; Park et al., 2009), the same peripheral inflammatory insult may also potentially alter AMPAR trafficking in dorsal horn neurons when hypersensitivity is being developed. The altered AMPAR trafficking may in turn contribute to the observed hypersensitivity and strength pain development and maintenance.

In this work, we used electrophysiology combined with $[Ca^{2+}]_i$ imaging to study extrasynaptic AMPAR functioning in dorsal horn substantia gelatinosa (SG) neurons during the development period of peripheral inflammatory pain. We show that development of inflammation-induced hyperalgesia and allodynia is associated with the upregulation of extrasynaptic AMPA receptors (AMPARs) in specific subtype of lamina II dorsal horn neuron.

MATERIALS AND METHODS

ANIMAL PREPARATION

Male rats were housed in cages on a standard 12:12 h light/dark cycle. Water and food were available ad libitum until rats were transported to the laboratory for experiments. The animals were used in accordance with protocols that were approved by the Animal Care and Use Committee at the Bogomoletz Institute of Physiology and were consistent with the ethical guidelines of the National Institutes of Health and the International Association for the Study of Pain. All efforts were made to minimize animal suffering and to reduce the number of animals used.

EXPERIMENTAL DRUGS

CFA was purchased from Sigma Chemical Co. (St. Louis, MO). Fura-2 was obtained from Invitrogen (Carlsbad, CA, USA). Tetrodotoxin (TTX) was obtained from Alomone Labs Ltd. (Jerusalem, Israel). NBQX, APV, AMPA, cyclothiazide (CTZ), bicuculline, and strychnine were purchased from Tocris Bioscience (Ellisville, MO).

INDUCTION OF PERIPHERAL INFLAMMATION

To produce unilateral peripheral inflammation and nociceptive hypersensitivity, 100 µl of CFA (*Mycobacterium tuberculosis*) suspended in an oil-saline (1:1) emulsion was injected subcutaneously into the plantar side of one hind paw of the rats. Saline injection (0.9%; 100 µl) was used as a control.

BEHAVIORAL TESTING

Animals were acclimatized to the experimental setup before the testing. The experimenters were blinded to the treatment groups during behavioral testing.

Paw withdrawal responses to thermal stimuli were measured in rats by using the Hargreaves technique (Hargreaves et al., 1988). For measurement of paw withdrawal responses to noxious heat stimuli, the animal was placed in a Plexiglas chamber on a glass plate located above a light box (Bioseb, Italy). Radiant heat was applied by focused infrared beam through a hole in the light box through the glass plate to the middle of the plantar surface of each hind paw. When the animal lifted its foot, the light beam was automatically turned off. The length of time between the start of the beam and the foot lift was defined as the paw withdrawal latency. Each trial was repeated five times at 5-min intervals for each paw. A cut-off time of 30 s was used to avoid tissue damage. Behavioral tests were performed before and after CFA injection.

To measure paw withdrawal responses to repeated mechanical stimuli, we used von Frey method. A rat was placed in a Plexiglas chamber on an elevated mesh screen and each von Frey monofilament (Bioseb, Italy) was applied to the hind paw for approximately 1–2 s. Trials of each hind paw were repeated 10 times at 1-min intervals. The occurrence of paw withdrawal in each of these trials was expressed as a percentage response frequency.

SPINAL CORD SLICE PREPARATION

Spinal cord slices were prepared from 18–21-day-old male rats subjected to saline or CFA injection as described previously (Voitenko et al., 2004; Kopach et al., 2011). Briefly, after rats were deeply anesthetized with an overdose of isoflurane, the L_{4-5} spinal segments were removed. Transverse slices (300 µm thick) were cut on a vibratome (Campden Instrument, UK) in an ice-cold solution that was continuously bubbled with 95% O_2 and 5% CO_2 and contained (in mM) 250 sucrose, 2 KCl, 1.2 NaH_2PO_4, 0.5 $CaCl_2$, 7 $MgCl_2$, 26 $NaHCO_3$, and 11 glucose (pH 7.4). Slices were maintained at room temperature in a physiologic Krebs bicarbonate solution that contained (in mM) 125 NaCl, 2.5 KCl, 1.25 NaH_2PO_4, 2 $CaCl_2$, 1 $MgCl_2$, 26 $NaHCO_3$, and 10 glucose (pH 7.4, osmolarity 310–320 mOsM) and was equilibrated with 95% O_2 and 5% CO_2.

SIMULTANEOUS CA^{2+} IMAGING AND PATCH-CLAMP RECORDING

Simultaneous Ca^{2+} imaging and whole-cell electrophysiologic recordings were obtained from SG neurons of the spinal L_{4-5} dorsal horn as described previously (Voitenko et al., 2004; Kopach et al., 2011). Briefly, the neurons were visually identified with a video microscope (Olympus, Japan). The patch pipettes with resistance of 6–10 MΩ were filled with an internal solution containing (in mM) 133 K-gluconate, 5 NaCl, 0.5 $MgCl_2$, 10 HEPES-Na, 2 MgATP, 0.1 GTP-Na, and 0.2 fura-2 pentapotassium salt (pH 7.2, osmolarity 290 mOsM). The membrane potential of SG neurons was held at –60 mV by a patch-clamp amplifier PC-505B (Warner Instruments, Hamden, CT) and Digidata board 1320A (Molecular Devices, Union City, CA) controlled by pCLAMP 8.2 software (Axon Instruments, USA) in current or voltage-clamp

mode. Only data from neurons that exhibited a resting membrane potential negative to –60 mV were included in the analysis.

Neurons were randomly chosen in the SG, but were mainly localized in its media-lateral part (**Figure 3A**). All SG neurons were categorized according to their discharge pattern in response to the series of 1-s current pulses, as described previously (Kopach et al., 2011).

To isolate AMPAR-mediated membrane current and associated increase in free calcium concentration in cytosol ($[Ca^{2+}]_i$), we performed recordings in the continuous presence of D-APV (50 μM), bicuculline (5 μM), and strychnine (2 μM) to block NMDA, $GABA_A$, and glycine receptors, respectively. In addition, TTX (0.5 μM) and cadmium chloride (100 μM) were added to Krebs bicarbonate solution to block corresponding voltage-activated sodium and calcium channels. To prevent a desensitization of AMPARs during bath application of the agonist, we applied AMPA to the slices in the continuous presence of CTZ (20 μM). Typically, one neuron was studied per slice.

Fura-2 fluorescence from SG neurons, located between 50 and 100 μm below the surface of the slice, was measured by using a 60×, NA 0.9 water-immersion objective (Olympus, Japan) and a 12-bit cooled CCD camera and capturing board (Sensicam, PCO, Germany). Fluorescence intensity was measured at wavelengths >510 nm when excited at 380 and 340 nm by a PolyChrome IV monochromator (Till Photonics, Germany) using Imaging Workbench software (INDEC System, USA). Fura-2 fluorescence were measured in soma and dendrites of SG neurons and expressed as changes in the ratio of fluorescence at 340–380 nm. The background area closest to the areas of interest was subtracted for each wavelength. The amplitude of the AMPA-induced $[Ca^{2+}]_i$ transient was calculated as the difference between the fura-2 fluorescence ratio before AMPA application and the ratio at the maximum $[Ca^{2+}]_i$ rise during AMPARs activation.

STATISTICAL ANALYSIS

All data are presented as mean ± SEM with n referring to the number of cells analyzed. Student's *t*-tests (two-tailed unpaired) were used to determine statistically significant differences. A *p*-value of less than 0.05 was considered statistically significant.

RESULTS

DEVELOPMENT OF CFA-INDUCED PERIPHERAL HYPERSENSITIVITY

Our previous studies (Park et al., 2009) and those of others (Zhang et al., 2003; Park et al., 2008) show that subcutaneous injection of CFA into a hind paw led to development of robust hypersensitivity on the ipsilateral side. This inflammation-induced hypersensitivity reached a peak around 24 h after the injection of CFA and maintained for a few days, representing the maintenance period of persistent pain. Here, we examined how persistent pain develops. For this, we thoroughly measured paw withdrawal responses to both thermal and mechanical stimuli. before CFA injection, and then at 0.5, 1, 2, 3, 4, 5, 6, 7, and 8 h after CFA injection. Consistent with previous reports (Zhang et al., 2003), CFA injection produced a rapid development of thermal hypersensitivity, as evidenced by a decrease in ipsilateral paw withdrawal latency (**Figure 1**). This hypersensitivity was observed even at 0.5 h after CFA injection and further progressed in following 2–4 h ($n = 6$; $p < 0.01$; **Figure 1**). After 4–8 h, this hypersensitivity was maintained at the similar level for a few days after CFA injection, representing maintenance period of CFA-induced inflammatory pain (**Figure 1**).

CFA (but not saline) injection led also to development of mechanical hypersensitivity that manifested as a marked increase in paw withdrawal frequencies in response to von Frey filaments applied to the injected hind paw (**Figure 2**). As with the paw withdrawal latency, a significant increase in paw withdrawal frequency started at 0.5 h after CFA injection and further progressed

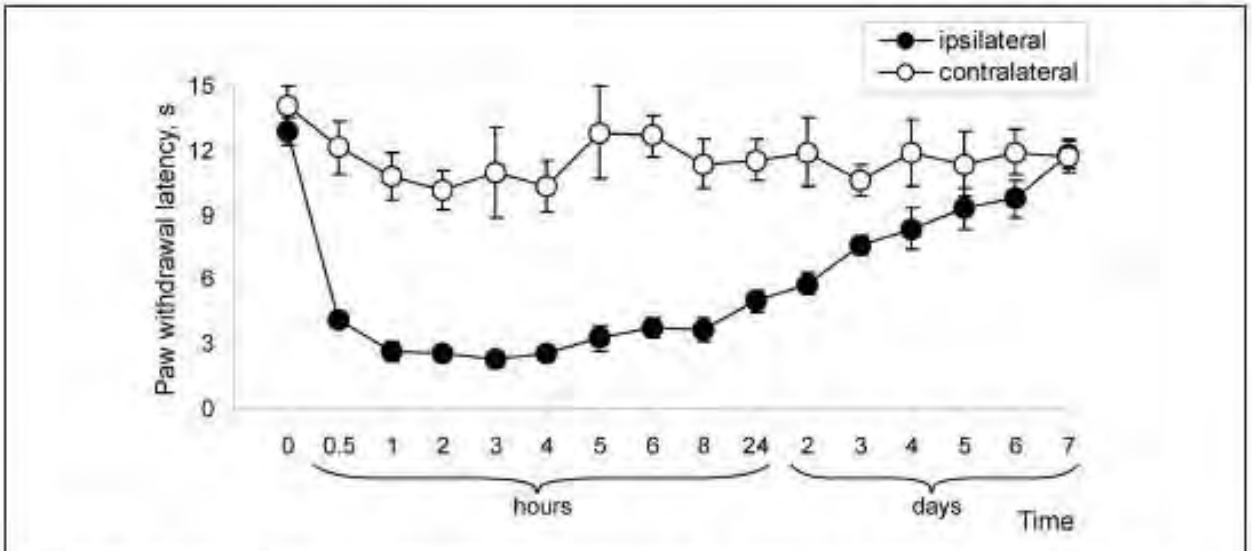

FIGURE 1 | Development of CFA-induced peripheral thermal hypersensitivity in rats. CFA injection induced a decrease in paw withdrawal latency (i response to thermal stimulation (n = 6/time point).

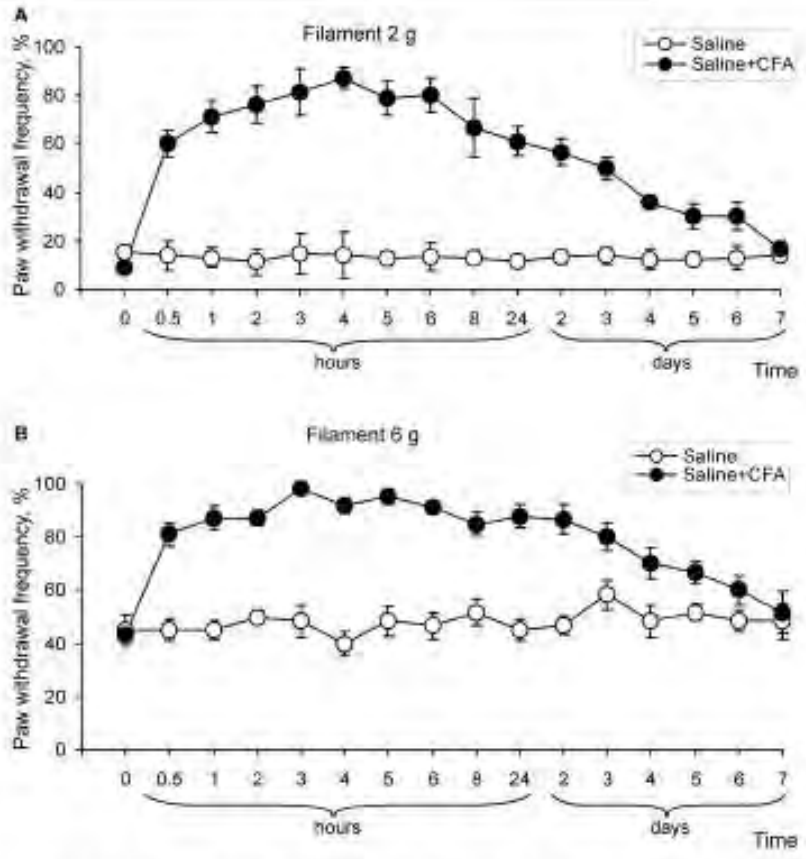

FIGURE 2 | Development of mechanical hypersensitivity after CFA injection. (A,B) Paw withdrawal frequency in response to 2 g **(A)** and 6 g **(B)** von Frey filaments changed over time on the ipsilateral side after CFA, but not after saline injection into a hind paw ($n = 6$/time point for saline and CFA).

over 2–4 h ($n = 8$; $p < 0.01$), then was maintained for a few days (**Figure 2**). In addition, CFA injection significantly increased the paw withdrawal frequencies in response to innoxious (2 and 4 g) and noxious (6 and 8 g) von Frey filaments, indicating development of mechanical allodynia and hyperalgesia, respectively ($n = 6$; $p < 0.01$; **Figures 2A,B**; data for 4 and 8 g are not shown). These results indicate that remarkable thermal and mechanical hypersensitivities develop in a time interval of 1–6 h after CFA injection and these changes of peripheral sensitivity are comparable to the changes observed during the maintenance period of chronic inflammatory pain (1–7 days after CFA injection).

CFA-INDUCED INFLAMMATION UPREGULATES EXTRASYNAPTIC AMPARs IN TONICALLY FIRING SG NEURONS RATHER THAN IN TRANSIENT NEURONS

Previously we showed that CFA-induced peripheral inflammation substantially increases functional expression of Ca^{2+}-permeable AMPARs in the extrasynaptic plasma membrane of lamina II dorsal horn neurons during the maintenance period of persistent inflammatory pain (Kopach et al., 2011) and altered AMPAR trafficking is necessary for the maintenance of inflammatory pain (Park et al., 2009). In this work, we studied whether CFA-induced peripheral inflammation affects extrasynaptic AMPARs functioning in these neurons during the development phase of persistent inflammatory pain. Because of our behavioral results and those of others (Zhang et al., 2003) have shown that CFA-induced robust thermal and mechanical hypersensitivities develop over 2–4 h after CFA injection, we chose the time point of 3 h after CFA injection to represent the development phase of CFA-induced persistent inflammatory pain. To directly evaluate CFA-induced changes in functional expression of extrasynaptic AMPARs during inflammatory pain development, we performed simultaneous recordings of membrane current and associated $[Ca^{2+}]_i$ transients produced by a selective agonist of AMPARs, AMPA, 3 h after saline or CFA injection (**Figures 3A,B**). We recorded AMPA-induced $[Ca^{2+}]_i$ transients in both the soma and dendrites of SG neurons.

Consistent with our previous reports (Voitenko et al., 2004; Kopach et al., 2011), bath application of AMPA (5 μM, 60 s) to the spinal cord slices evoked an inward current in all SG neurons at a holding potential of –60 mV. This current was characterized

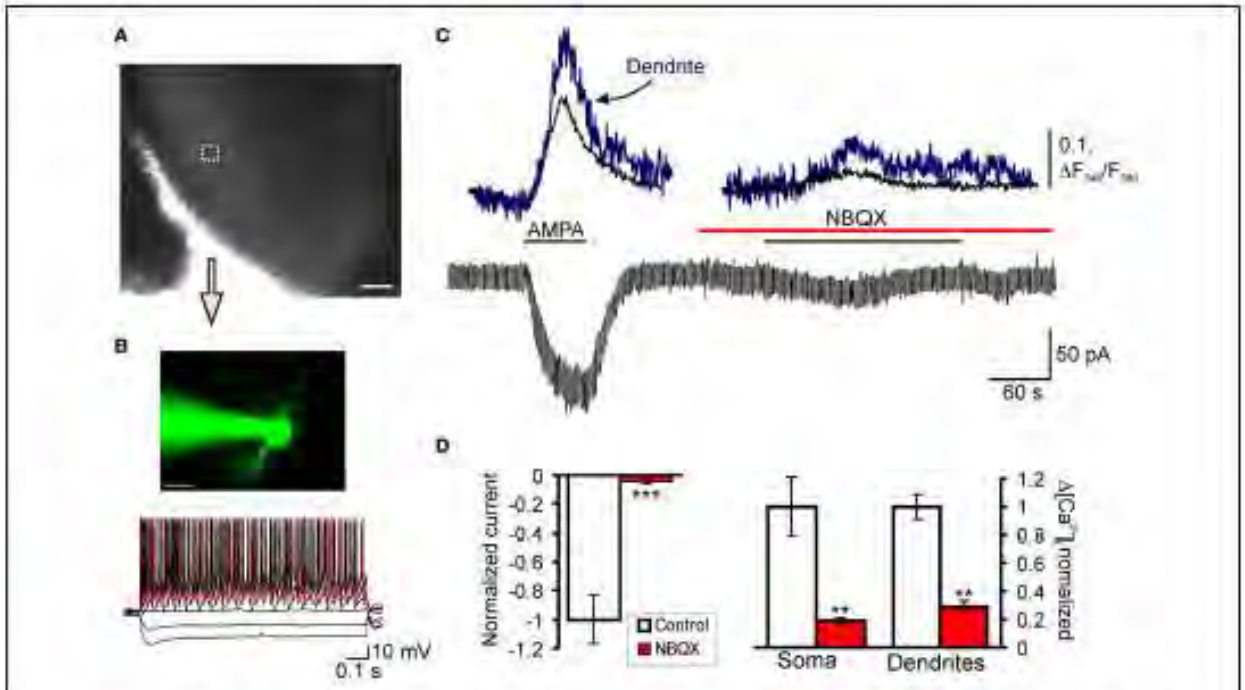

FIGURE 3 | AMPAR-mediated currents and associated $[Ca^{2+}]_i$ transients in SG neurons of spinal cord slices. **(A)** Transmitted light image of patch electrode position (square) in the SG of a transverse spinal cord slice; scale bar = 200 μm. **(B)** A fluorescent image of SG neuron loaded with fura-2 (200 μM) and current-clamp recording of typical firing pattern for tonic neurons; scale bar = 20 μm. **(C)** Representative trace of a membrane current recorded from the soma in tonic neurons during AMPA bath application (5 μM) before and after pre-application of AMPAR antagonist NBQX (30 μM). **(D)** A statistical summary of the AMPA-induced current amplitudes (left graph) and $[Ca^{2+}]_i$ transients (right graph) in soma and dendrites of SG neurons before and after pre-application of AMPAR antagonists NBQX. $^{**}p < 0.01$, $^{***}p < 0.001$ versus control.

by a slow rising phase and subsequent plateau, reached within 20–60 seconds (**Figure 3C**). Although bath applied AMPA activates a total pool of plasma membrane AMPARs, the extrasynaptic receptors are the predominant contributor to AMPA-induced current because they are relatively more abundant in neuronal plasma membrane and have weaker desensitization than synaptic AMPARs (Guire et al., 2008; Arendt et al., 2010; Vizi et al., 2010). In addition, substantial differences in a rectification index and a sensitivity to polyamine blockers between AMPA-induced currents (Kopach et al., 2011) and AMPAR-mediated excitatory postsynaptic currents evoked by dorsal root stimulation in SG neurons (Katano et al., 2008; Viikman et al., 2008; Park et al., 2009) further confirm a major contribution of extrasynaptic receptors to AMPA-induced currents.

The AMPA-induced current was associated with a synchronous rise in $[Ca^{2+}]_i$ observed in both soma and dendrites of examined neurons (**Figure 3C**). The observed current and associated $[Ca^{2+}]_i$ transients were mediated by an activation of AMPARs, as a potent AMPAR antagonist NBQX (30 μM) almost completely inhibited both the current and $[Ca^{2+}]_i$ transients (**Figures 3C,D**). Other selective AMPAR antagonist, GYKI 52466, also inhibited both the current and associated $[Ca^{2+}]_i$ transients similar to NBQX (Kopach et al., 2011), further indicating an activation of AMPARs.

Taking into account that the population of SG neurons is not homogeneous and displays distinct immunohistochemical (Engelman et al., 1999), electrophysiological (Grudt and Perl, 2002) and functional properties (Graham et al., 2004), we divided all neurons accordingly to their firing pattern in a response to sustained depolarizing current. Furthermore, our previous results have shown that persistent peripheral inflammation changes extrasynaptic AMPAR trafficking specifically in subpopulation of SG neurons characterized by intrinsic tonic firing properties, but not in those that exhibited strong adaptation (Kopach et al., 2011). Therefore, we divided all SG neurons tested into two main groups: "tonic" and "transient." Tonic neurons were those that supported continued discharge of action potentials during 1-s depolarizing inward current with increased frequency of discharge in a response to increased current intensity (**Figure 3B**). Transient neurons were those that exhibited a strong adaptation by generating short bursts of spikes or just a single spike regardless of depolarizing current intensity (**Figure 5A**).

In tonically firing SG neurons, the average amplitude of AMPA-induced currents comprised 236 ± 39 pA ($n = 23$) in the saline-treated group; the amplitude of associated $[Ca^{2+}]_i$ transients, expressed as an increase in the ratio of fura-2 fluorescence at 340–380 nm, ΔR (see "Materials and Methods"), were

0.47 ± 0.10 ($n = 21$) for soma and 0.60 ± 0.12 ($n = 14$) for dendrites (**Figures 4A,B**). CFA-induced inflammation significantly increased the amplitude of AMPA-induced current in the tonic SG neurons 3 h after CFA injection (**Figure 5C**). In particular, the average amplitude of AMPA-induced current was -236 ± 39 pA ($n = 23$) in 3 h post-saline group, but -437 ± 41 pA ($n = 23$; $p < 0.001$) in 3 h post-CFA group (**Figure 4B**). CFA-induced inflammation led to a tendency toward an increase in the amplitude of associated $[Ca^{2+}]_i$ transients in soma and dendrites of tonic SG neurons 3 h after injection (**Figures 4A,B**). In soma, the average amplitudes of AMPA-induced $[Ca^{2+}]_i$ transients were 0.47 ± 0.10 ($n = 21$) vs 0.54 ± 0.10 ($n = 20$) in the post-saline and post-CFA groups, respectively (**Figure 4B**). In dendrites, the average amplitudes of $[Ca^{2+}]_i$ transients were 0.60 ± 0.12 ($n = 14$) 3 h after saline vs 0.84 ± 0.23 ($n = 15$) 3 h after CFA (**Figure 4B**). However, these changes were not significant ($p > 0.05$).

These findings indicate that CFA-induced peripheral inflammation significantly upregulates functional expression of extrasynaptic AMPARs in tonically firing SG neurons during the development period of inflammatory pain.

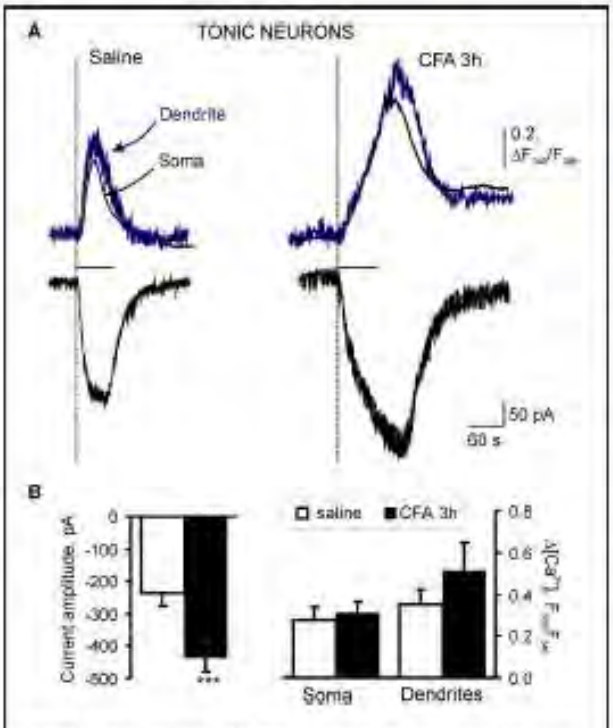

FIGURE 4 | Extrasynaptic AMPARs are markedly upregulated in tonic SG neurons during development of CFA-induced inflammatory pain. **(A)** Representative examples of AMPA-induced membrane current (bottom traces) and associated $[Ca^{2+}]_i$ transients in soma (upper black traces) and dendrites (upper blue traces) in tonic neurons 3 h after saline (left traces) or CFA injection (right traces). **(B)** A statistical summary of current amplitudes (left graph) and $[Ca^{2+}]_i$ transients (right graph) in soma and dendrites of tonic SG neurons 3 h after saline or CFA injection. AMPA-induced currents were significantly increased during chronic pain development. Despite the tendency toward an increase in $[Ca^{2+}]_i$ transients in SG neurons 3 h after CFA injection, no significant change in their amplitudes was observed. ***$p < 0.001$ versus the saline-treated group.

CFA-induced inflammation did not significantly change the AMPA-induced current and associated $[Ca^{2+}]_i$ transients in the transient subtype of SG neurons during the development period of inflammatory pain. In the saline-treated group, average amplitude of AMPA-induced current was -177 ± 22 pA ($n = 24$) in the transient SG neurons that was not significantly different from that in the tonic neurons ($p > 0.05$). In the transient SG neurons from the CFA-treated group, the current amplitude was -259 ± 35 pA at 3 h after CFA injection ($n = 34$; $p > 0.05$ compared to the saline-treated group; **Figures 5A–C**). No significant differences were observed also in the average amplitudes of AMPA-induced $[Ca^{2+}]_i$ transients in soma and dendrites of transient SG neurons between the saline- and CFA-treated groups 3 h after injection. In soma, average amplitudes of $[Ca^{2+}]_i$ transients were: 0.48 ± 0.09 ($n = 22$) and 0.39 ± 0.04 ($n = 31$) for the saline- and CFA-treated groups, respectively ($p > 0.05$; **Figure 5B**). In dendrites, average amplitudes of $[Ca^{2+}]_i$ transients were 0.52 ± 0.09 ($n = 18$) for the saline-treated and 0.54 ± 0.09 ($n = 18$) for the CFA-treated groups 3 h after injection ($p > 0.05$; **Figure 5B**). These results demonstrate that in the transient type of SG neurons extrasynaptic AMPARs functioning is not significantly altered during development of CFA-induced inflammatory pain.

DISCUSSION

In this work, we have demonstrated that extrasynaptic AMPARs are significantly upregulated in tonically firing dorsal horn SG neurons during the development of persistent inflammatory pain. This upregulation of AMPARs in dorsal horn neurons is associated with inflammation-induced hyperalgesia and allodynia and might contribute to the development and maintenance of persistent inflammatory pain.

Our findings and those of others (Zhang et al., 2003; Park et al., 2009) show that CFA-induced peripheral inflammation produces rapid development of peripheral hyperalgesia and allodynia (2–3 h after CFA injection) that represents developmental period of persistent inflammatory pain, whereas pain hypersensitivities observed during 1–7 d post-CFA reflects the maintenance phase of inflammatory pain (**Figures 1** and **2**). Spinal cord dorsal horn sensitization is considered to be a central mechanism that underlies the induction and maintenance of pain hypersensitivities (Woolf and Salter, 2000; Latremoliere and Woolf, 2009; Wang et al., 2010). Central sensitization produces a substantial prolongation and enhancement of responses to both noxious and innocuous stimuli (hyperalgesia and allodynia) and is a specific form of synaptic plasticity in spinal cord, which depends crucially on recruitment of glutamate receptors (Woolf and Salter, 2000; Latremoliere and Woolf, 2009; Wang et al., 2010). Activation of particularly NMDA receptors and AMPARs in dorsal horn neurons is required for the development and maintenance of spinal sensitization and hyperalgesia (Woolf and Salter, 2000; Hartmann et al., 2004; Katano et al., 2008; Vikman et al., 2008; Latremoliere and Woolf, 2009; Park et al., 2009).

Previously we and others showed that persistent inflammation produces a switch of Ca^{2+}-impermeable to Ca^{2+}-permeable AMPAR-mediated neurotransmission at synapses in dorsal horn

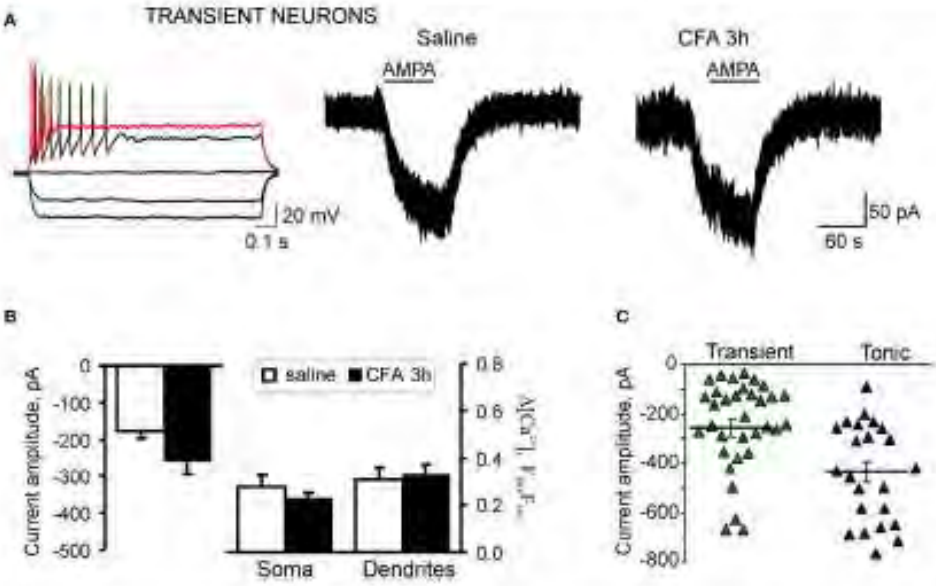

FIGURE 5 | Extrasynaptic AMPARs functioning is not altered in the transient SG neurons during development of CFA-induced inflammatory pain. (A) Typical firing pattern (left traces) and representative examples of AMPA-induced somatic currents (right traces) in the transient SG neurons 3 h after saline (control) or CFA injection. **(B)** A statistical summary of the current amplitudes (left graphs) and $[Ca^{2+}]_i$ transients (right graphs) in soma and dendrites of transient SG neurons 3 h after injection of saline or CFA. No significant difference was found in all measured parameters. **(C)** The scatter plot illustrates a spread in AMPA-induced currents in the tonic (blue) and transient (green) neurons 3 h after CFA injection. Difference in the amplitudes of AMPA-induced currents between the transient and tonic SG neurons was significant in the CFA-inflamed group ($p < 0.01$), but not significant 3 h post-saline ($p > 0.05$).

during the maintenance of inflammatory pain (Katano et al., 2008; Vikman et al., 2008; Park et al., 2009) and these changes are necessary for the peripheral inflammatory pain maintenance (Park et al., 2009). Peripheral inflammatory insult also increases functional expression of extrasynaptic Ca^{2+}-permeable AMPARs in the tonically firing SG neurons during the maintenance period of inflammatory pain, as we reported recently (Kopach et al., 2011). Our current work illustrates that CFA-induced inflammation substantially upregulates extrasynaptic AMPARs in tonically firing SG neurons during the inflammatory pain development (3 h after CFA injection). Our electrophysiological results suggest that the number of extrasynaptic AMPARs is substantially increased in the SG neurons during development of CFA-induced peripheral hyperalgesia and allodynia. This upregulation of AMPARs may contribute to the observed hypersensitivities during pain development, as altered AMPAR trafficking is necessary for the persistent pain maintenance (Park et al., 2009). In contrast to the maintenance of inflammatory pain, AMPAR-mediated Ca^{2+} signaling in the tonic firing SG neurons was not significantly changed during the inflammatory pain development. We suggest that the upregulation of extrasynaptic AMPARs during pain development may be mediated mainly by an increase in GluR2-containing, Ca^{2+}-impermeable AMPARs followed by a subsequent upregulation of GluR2-lacking, Ca^{2+}-permeable extrasynaptic AMPARs, which was observed during the maintenance period of persistent inflammation (Kopach et al., 2011). Phosphorylation of AMPAR subunits may underlie the observed CFA-induced upregulation of extrasynaptic AMPARs in dorsal horn SG neurons during inflammatory pain development. As we have demonstrated previously, CFA injection significantly changes the level of GluR2 phosphorylation 2 h after CFA injection (Park et al., 2009), supporting our current electrophysiological results. However, the precise mechanisms of AMPARs regulation are not completely clear because of their complexity (Santos et al., 2009; Wang et al., 2010; He et al., 2011).

Other important finding of this study is the fact that extrasynaptic AMPAR upregulation during development of persistent inflammatory pain was observed specifically in a subpopulation of SG neurons that exhibit intrinsic tonic firing properties, with no significant changes in the neurons that exhibit strong adaptation (transient neurons). This indicates that CFA alters extrasynaptic AMPARs in tonic firing SG neurons, whereas the pool of extrasynaptic AMPAR in the transient neurons is stable during the development of inflammatory pain and even during the persistent pain maintenance (Kopach et al., 2011). Taking into account similar patterns of extrasynaptic AMPAR expression in tonic and transient SG neurons under normal conditions (Kopach et al., 2011), these findings suggest different contribution of neuronal subtypes to the detection and/or transmission of nociceptive stimuli, resulting in different involvement in persistent inflammatory pain development and maintenance.

In conclusion, our study shows that CFA-induced peripheral inflammation upregulates extrasynaptic AMPARs specifically in tonic firing SG neurons during the development of inflammatory pain. These neurons may represent a specific population of neurons that carry out nociceptive inputs and

contribute to spinal central sensitization during development and maintenance of persistent inflammatory pain. The upregulated extrasynaptic AMPARs in dorsal horn neurons during the inflammatory pain development might contribute to persistent pain hypersensitivities.

ACKNOWLEDGMENTS

This work was supported by DFFD F46.2/001, NASU Biotechnology Grants (Nana Voitenko), by STCU/NASU Project #5510 (Pavel Belan), and by NASU Grant for Young Scientists (Olga Kopach).

REFERENCES

Adesnik, H., Nicoll, R. A., and England, P. M. (2005). Photoinactivation of native AMPA receptors reveals their real-time trafficking. *Neuron* 48, 977–985.

Allan, S. M., and Rothwell, N. J. (2001). Cytokines and acute neurodegeneration. *Nat. Rev. Neurosci.* 2, 734–744.

Arendt, K. L., Royo, M., Fernandez-Monreal, M., Knafo, S., Petrok, C. N., Martens, J. R., et al. (2010). PIP3 controls synaptic function by maintaining AMPA receptor clustering at the postsynaptic membrane. *Nat. Neurosci.* 13, 36–44.

Borgdorff, A. J., and Choquet, D. (2002). Regulation of AMPA receptor lateral movements. *Nature* 417, 649–653.

Bredt, D. S., and Nicoll, R. A. (2003). AMPA receptor trafficking at excitatory synapses. *Neuron* 40, 361–379.

Choquet, D., and Triller, A. (2003). The role of receptor diffusion in the organization of the postsynaptic membrane. *Nat. Rev. Neurosci.* 4, 251–265.

Cognet, L., Groc, L., Lounis, B., and Choquet, D. (2006). Multiple routes for glutamate receptor trafficking: surface diffusion and membrane traffic cooperate to bring receptors to synapses. *Sci. STKE* 2006, e13.

Engelman, H. S., Allen, T. B., and MacDermott, A. B. (1999). The distribution of neurons expressing calcium-permeable AMPA receptors in the superficial laminae of the spinal cord dorsal horn. *J. Neurosci.* 19, 2081–2089.

Graham, B. A., Brichta, A. M., and Callister, R. J. (2004). *In vivo* responses of mouse superficial dorsal horn neurones to both current injection and peripheral cutaneous stimulation. *J. Physiol.* 561, 749–763.

Grudt, T. J., and Perl, E. R. (2002). Correlations between neuronal morphology and electrophysiological features in the rodent superficial dorsal horn. *J. Physiol.* 540, 189–207.

Guire, E. S., Oh, M. C., Soderling, T. R., and Derkach, V. A. (2008). Recruitment of calcium-permeable AMPA receptors during synaptic potentiation is regulated by CaM-kinase I. *J. Neurosci.* 28, 6000–6009.

Hargreaves, K., Dubner, R., Brown, F., Flores, C., and Joris, J. (1988). A new and sensitive method for measuring thermal nociception in cutaneous hyperalgesia. *Pain* 32, 77–88.

Hartmann, B., Ahmadi, S., Heppenstall, P. A., Lewin, G. R., Schott, C., Borchardt, T., et al. (2004). The AMPA receptor subunits GluR-A and GluR-B reciprocally modulate spinal synaptic plasticity and inflammatory pain. *Neuron* 44, 637–650.

He, K., Goel, A., Ciarkowski, C. E., Song, L., and Lee, H. K. (2011). Brain area specific regulation of synaptic AMPA receptors by phosphorylation. *Commun. Integr. Biol.* 4, 569–572.

Katano, T., Furue, H., Okuda-Ashitaka, E., Tagaya, M., Watanabe, M., Yoshimura, M., et al. (2008). N-ethylmaleimide-sensitive fusion protein (NSF) is involved in central sensitization in the spinal cord through GluR2 subunit composition switch after inflammation. *Eur. J. Neurosci.* 27, 3161–3170.

Kopach, O., Kao, S. C., Petralia, R. S., Belan, P., Tao, Y. X., and Voitenko, N. (2011). Inflammation alters trafficking of extrasynaptic AMPA receptors in tonically firing lamina II neurons of the rat spinal dorsal horn. *Pain* 152, 912–923.

Kullmann, D. M. (2000). Spillover and synaptic cross talk mediated by glutamate and GABA in the mammalian brain. *Prog. Brain Res.* 125, 339–351.

Latremoliere, A., and Woolf, C. J. (2009). Central sensitization: a generator of pain hypersensitivity by central neural plasticity. *J. Pain* 10, 895–926.

Malinow, R., and Malenka, R. C. (2002). AMPA receptor trafficking and synaptic plasticity. *Annu. Rev. Neurosci.* 25, 103–126.

Park, J. S., Voitenko, N., Petralia, R. S., Guan, X., Xu, J. T., Steinberg, J. P., et al. (2009). Persistent inflammation induces GluR2 internalization via NMDA receptor-triggered PKC activation in dorsal horn neurons. *J. Neurosci.* 29, 3206–3219.

Park, J. S., Yaster, M., Guan, X., Xu, J. T., Shih, M. H., Guan, Y., et al. (2008). Role of spinal cord alpha-amino-3-hydroxy-5-methyl-4-isoxazolepropionic acid receptors in complete Freund's adjuvant-induced inflammatory pain. *Mol. Pain* 4, 67.

Santos, S. D., Carvalho, A. L., Caldeira, M. V., and Duarte, C. B. (2009). Regulation of AMPA receptors and synaptic plasticity. *Neuroscience* 58, 105–125.

Tao, Y. X. (2010). Dorsal horn alpha-amino-3-hydroxy-5-methyl-4-isoxazolepropionic acid receptor trafficking in inflammatory pain. *Anesthesiology* 112, 1259–1265.

Vikman, K. S., Rycroft, B. K., and Christie, M. J. (2008). Switch to Ca^{2+}-permeable AMPA and reduced NR2B NMDA receptor-mediated neurotransmission at dorsal horn nociceptive synapses during inflammatory pain in the rat. *J. Physiol.* 586, 515–527.

Viti, E. S., Fekete, A., Karoly, R., and Mike, A. (2010). Non-synaptic receptors and transporters involved in brain functions and targets of drug treatment. *Br. J. Pharmacol.* 160, 785–809.

Voitenko, N., Gerber, G., Youn, D., and Randic, M. (2004). Peripheral inflammation-induced increase of AMPA-mediated currents and Ca^{2+} transients in the presence of cyclothiazide in the rat substantia gelatinosa neurons. *Cell Calcium* 35, 461–469.

Wang, Y., Wu, J., Wu, Z., Lin, Q., Yue, Y., and Fang, L. (2010). Regulation of AMPA receptors in spinal nociception. *Mol. Pain* 6, 5.

Weng, H. R., Chen, J. H., and Cata, J. P. (2006). Inhibition of glutamate uptake in the spinal cord induces hyperalgesia and increased responses of spinal dorsal horn neurons to peripheral afferent stimulation. *Neuroscience* 138, 1351–1360.

Woolf, C. J., and Salter, M. W. (2000). Neuronal plasticity: increasing the gain in pain. *Science* 288, 1765–1769.

Zhang, B., Tan, E., Liaw, W. J., Bredt, D. S., Johns, R. A., and Tao, Y. X. (2003). Effect of knock down of spinal cord PSD-93/chapsin-110 on persistent pain induced by complete Freund's adjuvant and peripheral nerve injury. *Pain* 106, 187–196.

Conflict of Interest Statement: The authors declare that the research was conducted in the absence of any commercial or financial relationships that could be construed as a potential conflict of interest.

Received: 15 April 2012; accepted: 13 September 2012; published online: 02 October 2012.

Citation: Kopach O, Viatchenko-Karpinski V, Belan P and Voitenko N (2012) Development of inflammation-induced hyperalgesia and allodynia is associated with the upregulation of extrasynaptic AMPA receptors in tonically firing lamina II dorsal horn neurons. Front. Physio. 3:391. doi: 10.3389/fphys.2012.00391

This article was submitted to Frontiers in Membrane Physiology and Biophysics, a specialty of Frontiers in Physiology.

2.3. Екстрасинаптичні AMPA-рецептори у дорзальному розі спинного мозку: функціонування та значимість у підтриманні хронічного болю

Brain Research Bulletin 93 (2013) 47–56

Contents lists available at SciVerse ScienceDirect

Brain Research Bulletin

journal homepage: www.elsevier.com/locate/brainresbull

Review

Extrasynaptic AMPA receptors in the dorsal horn: Evidence and functional significance

Olga Kopach[a], Nana Voitenko[a,b,*]

[a] State Key Laboratory of Molecular and Cellular Biology, Bogomoletz Institute of Physiology, Kiev, Ukraine
[b] Molecular Physiology and Biophysics Department, Moscow Institute of Physics and Technology, Moscow, Russian Federation

ARTICLE INFO

Article history:
Received 14 September 2012
Received in revised form
15 November 2012
Accepted 19 November 2012
Available online 26 November 2012

Keywords:
Extrasynaptic AMPA receptors
AMPAR trafficking
AMPAR subunits
Dorsal horn
Inflammatory pain

ABSTRACT

Extrasynaptic AMPA receptors (AMPARs) are widely expressed in the brain, spinal cord and periphery. These receptors are critically involved in activity-dependent synaptic transmission and changes in their functioning are causally linked to multiple neuropathologies in the central nervous system (CNS). However, most studies in this field have been concentrated on elucidating synaptic AMPAR functioning, leaving a possible involvement of an extrasynaptic pool of AMPARs in normal and pathological signaling open for consideration.

Here, we review the present evidence for extrasynaptic AMPAR function in the dorsal horn neurons of the spinal cord, linking these receptors to neurotransmission and non-synaptic signaling in this part of the CNS. In addition, we summarize current knowledge about the role of extrasynaptic AMPARs in the development and maintenance of pain states during inflammation. This knowledge potentially suggests the development of alternative therapies to prevent and/or treat inflammatory pain.

Contents

1. Introduction

During the last 100 years and until recently most attention in neuroscience was directed toward the study of synaptic connections in the central nervous system (CNS), being considered as the intrinsic and the most important component of neuronal network functioning. However, a number of experimental studies over the last decades have indicated that, in addition to synaptic transmission, there is another way to transmit information between the cells, based upon diffusion of neurotransmitters into the extracellular space and the activation of extrasynaptic receptors (Kullmann, 2000; Makani and Zagha, 2007). Such routes of intercellular communication have been termed non-synaptic (Vizi, 1980, 1984), parasynaptic (Schmitt, 1984), "volume" (Agnati et al., 1991) or extrasynaptic transmission (Kopanitsa, 1997).

Glutamate is the major excitatory neurotransmitter in the CNS, since over half of 100 billion neurons release glutamate (van der Zeyden et al., 2008; Vizi et al., 2010). Furthermore, almost all neurons express receptors sensitive to this neurotransmitter (van der Zeyden et al., 2008). Glutamate is not only involved in most normal aspects of brain function, including cognition, memory and learning, but also in multiple brain pathologies.

* Corresponding author at: Department of General Physiology of Nervous System, Sensory Signaling Laboratory, Bogomoletz Institute of Physiology, 4 Bogomoletz Str., Kiev 01024, Ukraine. Tel.: +380 44 256 2049; fax: +380 44 256 2053.
E-mail address: nana@biph.kiev.ua (N. Voitenko).

0361-9230/$ – see front matter © 2012 Elsevier Inc. All rights reserved.
http://dx.doi.org/10.1016/j.brainresbull.2012.11.004

such as epilepsy (Albrecht et al., 2010), cancer (de Groot and Sontheimer, 2011), schizophrenia (Rotaru et al., 2012), neurodegenerative disorders (Kwak and Weiss, 2006) excitotoxicity and ischemic damage (Kostandy, 2012). In the spinal cord, altered glutamatergic transmission is associated with central sensitization and pain (Latremoliere and Woolf, 2009). Enhanced glutamate release from primary afferents in the dorsal horn (DH) and upregulated glutamate receptor functioning in DH neurons result in increased pain sensation following tissue or nerve injury (Xu and Yaksh, 2011). In addition to synaptically localized receptors for glutamate, the extrasynaptic receptors provide an extra route for the local regulation of synaptic signals under physiological and pathological conditions (Camire et al., 2012).

Glutamate receptors of the AMPA type (AMPARs) are present in multiple locations throughout DH neurons, including the extrasynaptic plasma membrane, where they are apparently involved in physiological and pathological processing of sensory information (Triller and Choquet, 2005). Extrasynaptic AMPARs, identified within spines, dendrites, and somata, possess high mobility and rapidly move between the plasma membrane and intracellular compartments by exocytosis and endocytosis, and diffuse laterally to and from synaptic sites (Borgdorff and Choquet, 2002; Choquet and Triller, 2003; Cognet et al., 2006; Bredt and Nicoll, 2003; Malinow and Malenka, 2002). Such continuous AMPAR exchange between synapses and different cellular pools (AMPAR trafficking) ensures dynamic fitting of synaptic AMPAR number and participates in synaptic plasticity under different cell conditions (Bredt and Nicoll, 2003; Carroll et al., 2001). The induction of long-term potentiation (LTP) is mediated by an increase in the number of extrasynaptic AMPARs that can then be translocated to synapses (Nusser, 2000), and conversely, for long-term depression (LTD), a decrease in the number of extrasynaptic AMPARs has been reported (Carroll et al., 2001; Triller and Choquet, 2005). It has been shown in hippocampal neurons that lateral diffusion of extrasynaptic AMPARs allows fast exchange of desensitized receptors with fresh functional ones at synapses upon fast synaptic stimulation (Heine et al., 2008). Therefore, extrasynaptic AMPARs contributed to the precise and fine regulation of synaptic efficacy. Besides, extrasynaptic AMPARs also contribute to glutamate-induced signaling at nonsynaptic locations (Rossi et al., 2008) due to spillover of glutamate (Kullmann, 2000) or glutamate release from glia (Araque et al., 1999).

Here, we review recent key findings in molecular and cellular mechanisms of extrasynaptic AMPARs functioning in DH neurons and their role in peripheral hypersensitivity and inflammatory pain syndromes.

2. AMPAR structure, subunits expression and localization in the DH

AMPAR channel consists of four subunits, GluA1–GluA4 (or GluR1–GluR4), identified by molecular cloning in the late 1980s (Hollmann et al., 1989). Four different genes (GluR1, GluR2, GluR3, and GluR4) encode AMPAR subunits. Each subunit includes an N-terminal extracellular amino domain, a ligand-binding domain, a receptor-channel domain, and an intracellular C-terminal domain (Song and Huganir, 2002). GluR1, GluR4, and GluR2L (a long splice form of GluR2) have a long cytoplasmic carboxy-terminal tail (C-tail), whereas GluR2, GluR3, and GluR4c (a short splice form of GluR4) have short and structurally similar C-tails (Kessels and Malinow, 2009). The C-terminal domain contains multiple protein phosphorylation sites for various protein kinases, and several binding sites (motifs) for various membrane-related and intracellular proteins, such as scaffolding proteins. The receptor-channel domain consists of three transmembrane segments (M1, M3, and M4) crossing the membrane, and one re-entrant loop within the membrane (M2), which forms part of the ion-channel pore and controls the flow of calcium ions through the channel (Song and Huganir, 2002).

The functional properties of AMPAR are dependent on the subunit composition. Functional AMPARs are homomeric or heteromeric tetramers. Mutational analysis demonstrated that the Ca^{2+} permeability of the channel is strictly determined by the R/Q position in the pore-forming M2 segment: Ca^{2+} permeability of the channel assembled from GluR1, GluR3, and GluR4 subunits, in which the arginine is replaced by glutamine (R586Q), is high, whereas the Ca^{2+} permeability of the channel assembled from GluR2 subunits, in which the glutamine is replaced by arginine (Q587R), is low (Burnashev et al., 1992). Therefore, incorporation of GluR2 subunit into heteromeric AMPARs dramatically reduces their Ca^{2+} permeability and changes the current properties and channel conductance (Burnashev et al., 1992; Song and Huganir, 2002).

All four GluR subunits are expressed in the DH of the spinal cord. Among these subunits, GluR1 and GluR2 were found to be highly expressed in the superficial DH (laminae I–II), where primary afferents carrying nociceptive inputs make synapses to the spinal second-order nociceptive neurons. GluR3 and GluR4 are weakly expressed in the DH (Furuyama et al., 1993), although GluR4 was recently detected in large neurokinin-1 receptor-expressing projection neurons in lamina I (Polgar et al., 2010). Thus, GluR1 and GluR2 represent the two most abundant subunits forming the AMPAR channel in the DH.

Most GluR1 and GluR2 immunoreactivity in the superficial DH is restricted to the postsynaptic density (PSD) (Petralia et al., 1997). Nonetheless, a high level of extrasynaptic AMPAR expression has been also detected in the DH within neuronal dendrites and somata (Kopach et al., 2011). Electron microscopy of the spinal cord shows substantial staining for GluR1 and GluR2 in the extrasynaptic membranes of the superficial DH. Analysis of electrophysiological recordings and Ca^{2+} influx using Ca^{2+}-sensitive dyes further indicated that GluR2-containing, Ca^{2+}-impermeable AMPARs and GluR2-lacking, Ca^{2+}-permeable AMPARs are both expressed extrasynaptically in the soma and dendrites of lamina II DH neurons (Kopach et al., 2011; Kyrozis et al., 1995). In contrast to other parts of the CNS, in the adult rat DH, a majority of the neurons densely express Ca^{2+}-permeable homomeric GluR1 AMPARs (Albuquerque et al., 1999; Engelman et al., 1999; Hartmann et al., 2004). Interestingly, in laminae III–IV of the DH, synaptic AMPARs located on the dendrites of neurokinin 1 receptor-expressing projection neurons contain GluR2, GluR3 and GluR4 subunits, but not GluR1 (Todd et al., 2009). All these data suggest that extrasynaptic AMPAR channel composition differs from the channel assembly of the synaptic receptor. However, the precise subunit composition of synaptic and extrasynaptic AMPARs has not been determined in DH neurons as yet. To the best of our knowledge, the only region where the subunit composition for synaptic and extrasynaptic AMPA has been described is the hippocampus where synaptic receptors contain both GluR1R2 and GluR2R3 heteromers, whereas the extrasynaptic AMPARs mainly consist of only GluR1R2 heteromers (Beique and Huganir, 2009; Lu et al., 2009). Homomeric GluA1 AMPARs are found in the extrasynaptic membranes of adult rat nucleus accumbens (Ferrario et al., 2011). By using a gene knockout approach the GluR1 subunit has been revealed as an obligatory component of extrasynaptic AMPARs, because extrasynaptic AMPARs were almost totally absent in hippocampal neurons of the GluR1 knockout mice (Andrasfalvy et al., 2003).

The density of the extrasynaptic AMPARs detected in different parts of the CNS varies among the neuron types. A high AMPAR immunolabeling in the extrasynaptic sites of the plasma membrane (~100 particles μm^{-2}) was shown in the dentate gyrus of the hippocampus, whereas it was much lower (~10 particles μm^{-2}) in the

neurons of the molecular layer of the cerebellum (Masugi-Tokita et al., 2007; Momiyama et al., 2003). Thus, the density of extrasynaptic AMPARs (10–100 receptors μm^{-2}) is much lower than that of the synaptic ones, which may exceed 1000 receptors μm^{-2}. Despite the much lower density of extrasynaptic AMPARs (10^1–10^2 times), they are relatively more abundant in the neuronal plasma membrane than the synaptic receptors, because a total area of plasma membrane is about 10^4 times larger than the area of synaptic zones (Arendt et al., 2010; Guire et al., 2008; Momiyama et al., 2003). The density of functional extrasynaptic AMPARs also increases with distance from the soma (Andrasfalvy and Magee, 2001).

Recent studies demonstrate that the AMPAR is associated with auxiliary subunits, which strictly modulate AMPAR function, including their surface expression, synaptic targeting, gating properties and pharmacology (Nicoll et al., 2006). There are at least three families of protein auxiliary subunits: transmembrane AMPAR regulatory proteins (TARP), cornichon proteins (CNIH) and cystein-knot AMPAR modulating protein (CKAMP44). Six TARP isoforms have been identified: γ-2 (stargazin), γ-3, γ-4, γ-5, γ-7, and γ-8 (Kato et al., 2010). The functional properties of AMPARs associated with the TARPs are different from those of AMPARs devoid of auxiliary subunits: TARPs increase single channel conductance and open probability, slow down deactivation, and reduce desensitization of the receptors (Kato et al., 2007; Traynelis et al., 2010). The TARP isoform γ-5, for instance, increases glutamate potency and glutamate-evoked peak currents, and accelerates the time course of deactivation and desensitization only in GluR2-containing receptors, but does not affect regulation of GluR2 surface expression (Kato et al., 2010). The γ-7 isoform shares many of these properties but is not selective for GluR2-containing receptors, enhancing peak currents in GluR1-containing receptors (Kato et al., 2007). Transmembrane protein CNIH was thought to be necessary for protein export from the endoplasmic reticulum. Recently, cornichon homologs 2 and 3 (CNIH-2 and CNIH-3) were identified by proteomic analysis as AMPAR-interacting proteins, which assemble with and regulate AMPARs at the cell surface of various neurons and glia (Schwenk et al., 2009). Co-expression of recombinant AMPARs with CNIH proteins, as with TARPs, has been demonstrated to increase the surface expression of receptors, slow their deactivation and desensitization (Shi et al., 2010; Coombs et al., 2012) and to markedly increase single-channel conductance of GluR2-lacking, Ca^{2+}-permeable AMPARs (Coombs et al., 2012). The role of these proteins in AMPAR regulation is not yet completely understood.

3. Functional properties of extrasynaptic AMPARs in DH neurons

The functional properties of extrasynaptic AMPARs in DH neurons are distinct from those of synaptic AMPARs, as demonstrated using electrophysiological, imaging, and immunochemical approaches (Li and Baccei, 2009; Katano et al., 2008; Kopach et al., 2011; Park et al., 2009; Tong and MacDermott, 2006; Vikman et al., 2008). Immunogold labeling and electron microscopy of the spinal cord showed substantial GluR2 staining in the postsynaptic profiles of DH neurons (Petralia et al., 1997; Furuyama et al., 1993). Hence, a majority of AMPARs at the synapses in DH neurons would display low permeability to Ca^{2+} ions entering a neuron through the channel. However, electrophysiological studies in the superficial DH neurons demonstrated a prominent rectification of AMPARs-mediated evoked excitatory postsynaptic currents (eEPSCs) and their high sensitivity to polyamine derivatives (Katano et al., 2008; Li and Baccei, 2009; Park et al., 2009; Tong and MacDermott, 2006; Vikman et al., 2008), which are both obvious features of GluR2-lacking, Ca^{2+}-permeable AMPARs (Burnashev et al., 1992).

Recent studies of extrasynaptic AMPARs showed that AMPA-induced currents in lamina II DH neurons displayed roughly linear current–voltage relationship (*I–V* curves) with a rectification index of 0.74 (Kopach et al., 2011) versus 0.26 for synaptic AMPARs-mediated eEPSCs in these neurons (Park et al., 2009), indicating the presence of a higher proportion of Ca^{2+}-impermeable AMPARs in the extrasynaptic membrane compared to the synapses. Further evidence that extrasynaptic AMPARs in lamina II DH neurons contain more Ca^{2+}-impermeable AMPARs than synaptic ones is the fact that AMPA-induced extrasynaptic currents were not significantly suppressed by specific blockers of Ca^{2+}-permeable AMPARs (Kopach et al., 2011), as opposed to the AMPAR-mediated eEPSCs, which were more sensitive to polyamine derivatives (from 20% to 60% inhibition) (Park et al., 2009; Vikman et al., 2008; Katano et al., 2008). Consistently, immunogold labeling showed that GluR2 staining exceeds GluR1 staining in the extrasynaptic profiles of the superficial DH neurons, whereas GluR1 staining exceeds GluR2 staining at synapses (Kopach et al., 2011). Patch-clamp recording combined with Ca^{2+} imaging revealed a functional activity of extrasynaptic Ca^{2+}-permeable AMPARs, since AMPA-induced currents were accompanied by $[Ca^{2+}]_i$ transients, evoked both in soma and dendrites of lamina II DH neurons (Kopach et al., 2011). Thus, the extrasynaptic pool of AMPARs in the superficial DH neurons consists of both GluR2-containing, Ca^{2+}-impermeable AMPARs and GluR2-lacking, Ca^{2+}-permeable AMPARs. A mixed population of AMPARs in both synaptic and extrasynaptic plasma membrane was also reported for other brain regions (Beique and Huganir, 2009; Liu and Cull-Candy, 2000; Lu et al., 2009).

The subunit composition of the AMPAR determines receptor binding affinity for an agonist and the rate of desensitization (Stein et al., 1992; Jackson et al., 2003). However, determination of subunit composition for different receptor pools in order to predict their relative affinity and desensitization is a very complicated task. It has been shown for recombinant AMPAR that the binding affinities for glutamate (measured as EC_{50} values) of GluR3 and GluR4 homomers are about 1 mM, (Pei et al., 2007; Sekiguchi et al., 2002) and that of GluR2 is about 1.4 mM (Koike et al., 2000; Pei et al., 2009). A much higher affinity for glutamate has been demonstrated for GluR1 homomers, with a corresponding value for the EC_{50} about 0.5 mM (Pei et al., 2009; Li and Niu, 2004). Taking into account that persistent inflammatory pain as well as LTP promotes insertion of relatively high-affinity GluR1 subunits at extrasynaptic sites (Lin et al., 2009; Kopach et al., 2011), we may suggest that this activity-dependent GluR1 insertion increases the affinity of extrasynaptic AMPARs as compared to the normal conditions.

The rate of desensitization of AMPARs varies from 1 to 5 ms dependently upon splicing and subunit composition (Sekiguchi et al., 2002; Mosbacher et al., 1994). A slower rate of desensitization of the extrasynaptic AMPARs may be suggested from experimental studies where AMPA-induced current has not desensitized during minutes of AMPA bath application (Voitenko et al., 2004; Billa et al., 2010).

4. Functional significance of extrasynaptic AMPARs in the DH

Extrasynaptic AMPARs substantially contribute to excitatory glutamatergic transmission in the DH by tuning synaptic efficacy and mediating activity-dependent plasticity in DH neurons. The implication of extrasynaptic AMPARs in synaptic plasticity is determined by the trafficking behavior of AMPARs. AMPAR trafficking represents a dynamic process of constitutive receptor diffusion between the different cellular pools and synaptic and extrasynaptic sites of the neuronal plasma membrane. Although the mechanisms of AMPAR trafficking have been better studied in

hippocampal neurons than in spinal neurons, they are in general similar in all regions of the CNS.

Numerous in vitro and in vivo studies demonstrated that extrasynaptic AMPARs are highly mobile at the plasma membrane and rapidly and continuously move between the membrane surface and intracellular compartments by exocytosis and endocytosis (Bredt and Nicoll, 2003; Malinow and Malenka, 2002) as well as laterally diffusing to and from synaptic sites (Bats et al., 2007; Borgdorff and Choquet, 2002; Choquet and Triller, 2003; Cognet et al., 2006). AMPAR subunits are synthesized and assembled in the rough endoplasmic reticulum and Golgi apparatus of the cell bodies and then undergo insertion into the plasma membrane at the soma. The subunits can also be synthesized locally in dendrites. Subunit messenger RNA is trafficked into dendrites via an RNA–protein complex that travels along the cytoskeleton. Messenger RNA can be further translated by local polyribosomes in response to neuronal activity (Shepherd and Huganir, 2007). Proteins translated in the dendrites are processed via the dendrite Golgi apparatus and then travel to extrasynaptic sites (Tao, 2010). Membrane insertion of AMPARs appears at the extrasynaptic sites exclusively followed by AMPARs delivery to the PSD by lateral diffusion in the plasma membrane (a two-step delivery model) (Adesnik et al., 2005; Leonoudakis et al., 2008; Oh et al., 2006, Lin et al., 2009). In the PSD, AMPARs are trapped by interactions with PSD scaffold proteins and cytoskeletal elements that reduce their mobility and stabilizes AMPARs at the PSD during synaptic activity (the third step of AMPAR delivery model) (Opazo and Choquet, 2011; Choquet and Triller, 2003; Cognet et al., 2006). Stabilization of AMPARs at the PSD requires the interaction between numerous scaffolding proteins including the most prominent members of the MAGUK family (PSD95, PSD93, SAP97, and SAP102), TARPs, proteins interacting with protein kinase C (PICK) or AMPA binding protein/glutamate receptor interacting protein (ABP/GRIP) (Bats et al., 2007; Elias and Nicoll, 2007; Lu and Ziff, 2005). The interactions occur at the end of AMPAR C-tail that contains multiple phosphorylation sites and protein binding motifs, which ensure AMPAR immobilization during synaptic activity and very likely modulate the receptors properties. The large proportion of mobile AMPARs continuously diffusing between synaptic and extrasynaptic compartments is not trapped at the synaptic sites and easily exits the synapse after a short dwell time (Heine et al., 2008; Petrini et al., 2009). These receptors then can be recycled to the intracellular stores via endocytosis (internalization) (Fig. 1). The internalized receptors are either recycled back to the plasma membrane via exocytosis or targeted to the lysosome for degradation (Carroll et al., 2001). Thus, the extrasynaptic pool of AMPARs supplies the AMPARs at the synapses, the number of which is tightly correlated with synaptic efficacy during different cell conditions such as synaptic maturation, activity and disease.

Another functional significance of extrasynaptic AMPARs is their contribution to glutamate-mediated signaling at non-synaptic locations. Glutamate released from a presynaptic terminal following exocytosis can leak out of a synaptic cleft and reach the extrasynaptic receptors on the same neuron or at a neighboring synapse (where exocytosis does not take place); this process is termed "spillover" (Kullmann, 2000). To reach and activate the extrasynaptic receptors, glutamate must spill out of the synaptic cleft and overcome the barrier of glutamate uptake. To detect glutamate spillover, extrasynaptic AMPARs must possess higher binding affinity for glutamate than synaptic ones concomitant with lower desensitization to sense the diluted agonist continuously present in the extracellular space (Fig. 2).

Glutamate released from a presynaptic terminal is not metabolized extracellularly: its clearance in the synaptic cleft is ensured by a family of glutamate transporters located in both glial cells and neurons that take up glutamate from the extracellular space into the cells, ultimately maintaining extracellular glutamate homeostasis. In the spinal cord, three subtypes of glutamate transporter exist, including two glial and one neuronal glutamate transporters. The highest expression of glial glutamate transporters is concentrated in laminae I and II of the DH, whereas in the deeper dorsal and ventral horns glutamate transporters are expressed

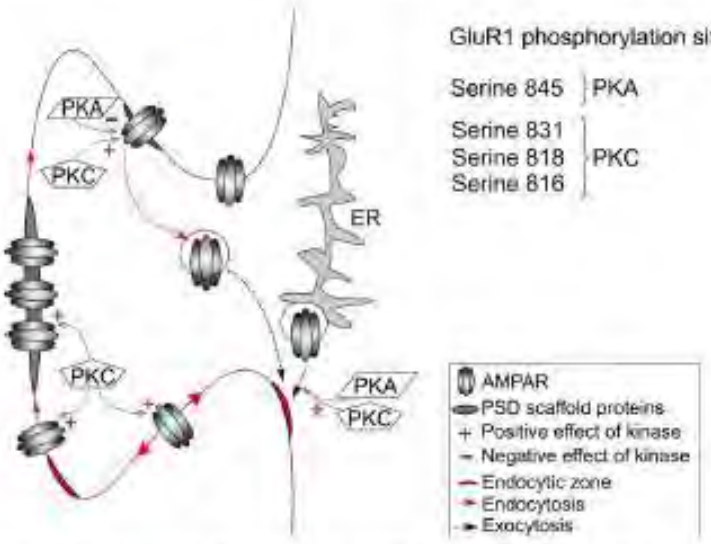

Fig. 1. Regulation of AMPAR trafficking in the DH neurons by the phosphorylation of GluR1 subunit. Trafficking of GluR1-containing, Ca^{2+}-permeable AMPARs in the DH neurons is regulated by two protein kinases: PKA and PKC, which phosphorylate GluR1 subunit at different serine residues. AMPAR are synthesized in the rough endoplasmic reticulum (ER) and inserted in the plasma membrane via exocytosis. This insertion is positively regulated via GluR1 phosphorylation by PKA and PKC during neuronal activity. Newly inserted (or pre-existing) GluR1-containing AMPARs laterally diffuse to synaptic sites (a process promoted by PKC), where they are trapped in the postsynaptic density (PSD) by interactions with numerous scaffolding proteins and cytoskeletal elements due to phosphorylation events triggered by CaMKII and PKC. If AMPARs are not trapped in the PSD, they diffuse out of the synapse and may be endocytosed (internalized) at endocytic zones. This process is triggered by PKC-mediated phosphorylation of GluR1 and downregulated by PKA.

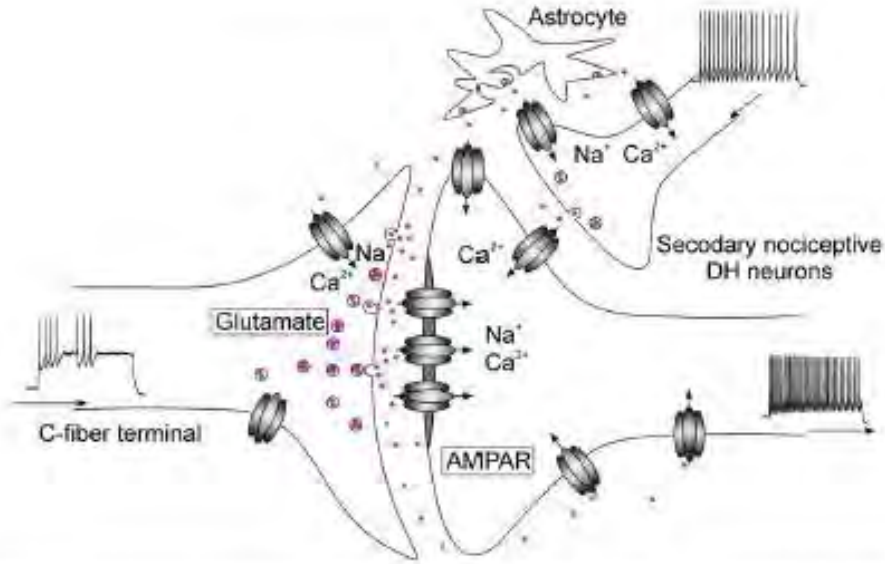

Fig. 2. Extrasynaptic AMPAR signaling in the secondary nociceptive DH neurons. AMPARs are localized in the DH secondary nociceptive neurons at the postsynaptic densities, at extrasynaptic sites and at presynaptic terminals of primary nociceptors. Strong afferent nociceptive inputs generated by peripheral primary nociceptors produce an extensive glutamate release from the primary afferent terminals. This may result in glutamate spillover from synaptic cleft and activation of extrasynaptic AMPARs in secondary nociceptive neurons in the DH. The extrasynaptic pool of AMPARs consists of both GluR2-containing, Ca^{2+}-impermeable AMPARs and GluR1-containing, Ca^{2+}-permeable AMPARs. Under persistent pain the extrasynaptic pool of AMPARs is enriched with GluR1-containing, Ca^{2+}-permeable AMPARs. Thus, their activation produces enhanced Na^+ and Ca^{2+} influx into the secondary DH neuron that may lead to increased neuronal excitability and strengthened glutamatergic transmission. In pathological conditions, excessive glutamate is also released from the glial cells, representing an additional source of extrasynaptic glutamate being able to activate extrasynaptic AMPARs in the DH neurons.

diffusely (Weng et al., 2005; Mao et al., 2002; Sung et al., 2003). Substantial down-regulation of the glial glutamate transporters in the DH, observed during the pathogenesis of pain, results in extrasynaptic glutamate spillover (Nie and Weng, 2009, 2010; Mao et al., 2002; Sung et al., 2003), which may further activate the extrasynaptic AMPARs.

Glutamate-mediated nonsynaptic transmission appears to be a consequence of the high frequency discharge of DH neurons, which receive and process both extrinsic nociceptive inputs from primary afferents and intrinsic inputs from spinal interneurons and supraspinal centers (Furue et al., 2004). This type of transmission is also possible in the case of the synchronous discharge of many primary afferent terminals, when glutamate released from one synapse may act at neighboring neurons.

Another source of glutamate that can act on extrasynaptic AMPARs is glutamate released from astrocytes (Araque et al., 1999). Responding to glial glutamate release, extrasynaptic AMPARs may mediate a possible "cross-talk" between glial cells and neurons in the spinal processing of sensory information during normal signaling and/or pathogenesis of pain.

5. Extrasynaptic AMPARs function in the DH neurons during inflammatory pain

Extrasynaptic AMPARs are implicated in both normal glutamatergic neurotransmission and excitotoxicity. Over the last decade many studies have demonstrated that altered AMPAR trafficking is causally linked to numerous pathologies of the CNS by altering neuronal excitability (Choi et al., 2010; Ferguson et al., 2008; Kwak and Weiss, 2006; Leonoudakis et al., 2008). In the spinal cord, activity-regulated AMPAR trafficking is thought to be one of key mechanisms for central sensitization, a phenomenon considered to underlie the development and maintenance of pain (Greger and Esteban, 2007; Latremoliere and Woolf, 2009; Hartmann et al., 2004). Central sensitization is believed to be a specific form of synaptic plasticity in the spinal cord.

Current evidence indicates the involvement of extrasynaptic AMPARs in spinal nociception (Voitenko et al., 2004; Kopach et al., 2011, 2012a) (Fig. 3). In a model of acute peripheral inflammation induced by intraplantar injection of capsaicin, inflammatory insult increases the number of GluR1 subunits in the membranes of DH neurons and decreases it simultaneously in the cytosolic fraction, with no changes in the GluR2 level in either the membrane or cytosolic fraction (Galan et al., 2004; Larsson and Broman, 2008). A similar increase in the GluR1 level, but not GluR2, in the plasma membrane of DH neurons was observed after the injection of carrageenan or formalin (Choi et al., 2010; Pezet et al., 2008). In a model of persistent peripheral inflammation, induced by complete Freund's adjuvant (CFA) injection, the subcellular distribution of both GluR1 and GluR2 subunits was changed in DH neurons by increasing the amount of GluR1 and decreasing GluR2 in the plasma membrane (Park et al., 2008) Thus, it seems likely that nociceptive insult promotes insertion of GluR1-containing AMPARs in the plasma membrane, and persistent pain produces a reciprocal rearrangement of GluR1-containing, Ca^{2+}-permeable and GluR2-containing, Ca^{2+}-impermeable AMPARs in different cellular pools of DH neurons.

Our recent electrophysiological studies combined with Ca^{2+}-imaging demonstrate that persistent inflammation increases the peak amplitude of AMPAR-mediated currents (evoked by bath application of AMPA) and the associated $[Ca^{2+}]_i$ transients in the soma and dendrites of lamina II neurons during the maintenance period of CFA-induced inflammatory pain (Kopach et al., 2011). Furthermore, the AMPA-induced currents were inwardly rectifying in the neurons of inflamed rats, and the sensitivity of these currents to the selective inhibition of Ca^{2+}-permeable AMPARs was

Fig. 3. AMPAR-mediated central sensitization in the DH. Tissue or nerve injury promotes an insertion of GluR1-containing, Ca^{2+}-permeable AMPARs at the extrasynaptic sites followed by their increase in the synapses of the DH neurons with simultaneous internalization of GluR2-containing, Ca^{2+}-impermeable AMPARs from the same synapses. Both of these processes lead to an increased Ca^{2+} influx into DH neurons, modulate neuronal signaling and finally result in spinal central sensitization and pain. Protein kinases (PKA and PKC) promote membrane insertion and internalization of AMPARs by phosphorylation of GluR1 and GluR2 receptor subunits.

significantly increased. These findings indicate that persistent inflammation up-regulates extrasynaptic AMPARs by increasing the functional expression of extrasynaptic Ca^{2+}-permeable AMPARs. Interestingly, peripheral inflammation alters extrasynaptic AMPAR trafficking in lamina II DH neurons, which were characterized by their intrinsic tonic firing properties ("tonic" neurons), but not in those that exhibit strong adaptation ("transient" neurons). In the "transient" neurons, inflammation did not significantly change the extrasynaptic AMPAR-mediated currents and associated $[Ca^{2+}]_i$ transients. Cobalt staining also demonstrated that some of the NeuN-marked neurons in the superficial DH 1 day post-CFA were not cobalt-positive (Kopach et al., 2011). Thus, inflammation apparently changes extrasynaptic AMPARs in a specific subpopulation of lamina II DH neurons. Indeed, DH neurons are not homogeneous and display distinct immunohistochemical (Engelman et al., 1999; Kerr et al., 1998), electrophysiological (Balasubramanyan et al., 2006; Grudt and Perl, 2002), and functional properties (Lima, 1998). The superficial DH neurons are also characterized by different patterns of AMPAR subunits expression. It has been reported that under normal conditions, surface GluR1 protein expression is particularly associated with inhibitory DH neurons, whereas GluR2 is associated with excitatory neurons (Albuquerque et al., 1999; Kerr et al., 1998). It is therefore reasonable to suggest that peripheral inflammatory insult may alter AMPAR trafficking in a specific subpopulation of DH neurons, involved in spinal central sensitization during persistent inflammation. It is still not completely clear in which type of lamina II neurons, inhibitory or excitatory, Ca^{2+}-permeable AMPARs are upregulated, since "tonic" lamina II neurons represent both inhibitory and excitatory interneurons, as has been demonstrated in different studies (Lu and Perl, 2003; Yasaka et al., 2010). However, the study by Safronov's group clearly demonstrated that most of "tonic" neurons are excitatory interneurons and that these neurons dominate sensory processing in the spinal substantia gelatinosa of rat (Santos et al., 2007). This suggests that inflammatory-induced changes in AMPAR trafficking in excitatory neurons would be the most plausible explanation of increased pain sensitivity.

The up-regulation of Ca^{2+}-permeable AMPARs, observed within the extrasynaptic AMPARs pool during persistent inflammation, is mediated by an increased surface expression of GluR1 in extrasynaptic membranes 1 day post-CFA (Kopach et al., 2011). These GluR1-containing, Ca^{2+}-permeable AMPARs can then diffuse laterally through the plasma membrane to the PSD (Derkach et al., 2007), where they may be trapped (Park et al., 2009). Indeed, it was reported that neuroinflammatory factors promote lateral diffusion of GluR1/GluR2 heteromers from the extrasynaptic sites to the synapses and enhance recycling of intracellular GluR1 homomers back to extrasynaptic membrane via exocytosis (Ferguson et al., 2008; Leonoudakis et al., 2008). The upregulation of extrasynaptic GluR1-containing, Ca^{2+}-permeable AMPARs may further contribute to an increase of Ca^{2+}-permeable AMPARs in the synapses, as has been observed in the DH neurons during persistent inflammation by different groups of researchers (Katano et al., 2008; Park et al., 2009; Vikman et al., 2008). Concomitant internalization of GluR2 from the synapses (Park et al., 2008, 2009) further increases the number of synaptic GluR2-lacking, Ca^{2+}-permeable AMPARs in the DH neurons. Targeted disruption of GluR1 gene resulted in a reduction of Ca^{2+}-permeable AMPARs and was accompanied by a loss of nociceptive plasticity in DH neurons and by a reduction of inflammatory pain in GluR1-deficient mice (Hartmann et al., 2004). In contrast, disruption of the gene encoding GluR2 produced an increase in spinal Ca^{2+}-permeable AMPARs, facilitated nociceptive plasticity and increased inflammatory hyperalgesia (Hartmann et al., 2004; Youn et al., 2008).

The molecular mechanisms which underlie inflammatory-induced insertion of GluR1-containing, Ca^{2+}-permeable AMPARs into extrasynaptic membranes of DH neurons are still elusive, as opposed to the mechanism of synaptic GluR2 internalization

described by Park et al. (2009). The latter includes protein kinase C (PKC)-dependent phosphorylation of GluR2 subunit at the serine (S) residue S880 that disrupts interaction between GluR2 and its synaptic anchoring protein, ABP/GRIP, and promotion of GluR2 endocytosis from the postsynaptic membrane (Park et al., 2009). Preventing GluR2 internalization through targeted mutation of the GluR2 PKC phosphorylation site impaired nociceptive hypersensitivity during the maintenance period of inflammatory pain (Park et al., 2009). Also, genetic knockout of protein interacting with C kinase 1 (PICK1), a scaffolding protein that interacts with GluR2 and PKCα and recruits intracellular PKCα to synaptic GluR2, prevented PKCα-mediated GluR2 phosphorylation at S880 and GluR2 internalization in DH, and impaired mechanical and thermal pain hypersensitivities induced by persistent inflammation, but not by a hind paw incision (a model of post-operative pain) (Atianjoh et al., 2010).

Phosphorylation of GluR1 subunits by protein kinases may also underlie the insertion of GluR1-containing AMPARs at the extrasynaptic sites. The c-terminus of GluR1 contains several sites for phosphorylation, and a phosphorylation status of the GluR1 at these sites directly affects electrophysiological properties, subunit composition, and AMPAR subunit trafficking. In the DH neurons GluR1 can be specifically phosphorylated by two protein kinases: PKA and PKC (Fig. 1). Phosphorylation of GluR1 at the site of S845 by PKA increases the AMPAR channel open probability and current amplitude, enhances the incorporation of GluR1-containing AMPARs in plasma membrane, stabilizes GluR1 in the membrane, and also decreases AMPAR internalization (Man et al., 2007; Oh et al., 2006). A few serine residue sites on GluR1 in hippocampal neurons are phosphorylated by PKC: S831, S818, and S816 (Barria et al., 1997; Boehm et al., 2006; Hayashi et al., 2000; Lin et al., 2009). GluR1 S831 is a substrate for both PKC and CaMKII. It undergoes phosphorylation during LTP (Barria et al., 1997), increasing the single channel conductance of synaptic AMPARs (Luthi et al., 2004), by binding of GluR1 to its scaffolding protein (Hayashi et al., 2000). Phosphorylation of S831 does not influence membrane insertion (Hayashi et al., 2000). In contrast, phosphorylation at S818 by PKC promotes synaptic incorporation of GluR1-containing AMPARs and facilitates AMPAR interaction with protein 4.1 N, a downstream actin-binding protein; this interaction stabilizes GluR1 (Boehm et al., 2006). Recent studies have also shown that protein 4.1 N is required for activity-dependent GluR1 insertion at extrasynaptic sites. Phosphorylation of GluR1 at S816 and S818 enhances 4.1 N binding and facilitates GluR1-containing AMPAR insertion in extrasynaptic plasma membrane (Lin et al., 2009). Thus, CFA-promoted insertion of GluR1-containing, Ca^{2+}-permeable AMPARs in the extrasynaptic membranes of DH neurons (Kopach et al., 2011) may result from PKCα-dependent phosphorylation of GluR1 at S816 and S818 and subsequent receptor insertion in extrasynaptic sites of DH neurons. This conclusion could be directly confirmed if specific and selective antibodies against GluR1 S816 and S818 phosphorylation sites were available. By utilizing transient knockdown of PKCα locally in spinal cord with the antisense oligodeoxynucleotides, we recently found that PKCα is required for the inflammation-induced upregulation of extrasynaptic Ca^{2+}-permeable AMPARs, as its knockdown was able to attenuate CFA-induced augmentation of both the extrasynaptic AMPAR-mediated current and $[Ca^{2+}]_i$ transients in the DH neurons, and to reverse the inward rectification of these currents (Kopach et al., 2012b). Peripheral inflammation, induced by capsaicin or CFA, increases phosphorylation of GluR1 both at S845 (PKA site) (Choi et al., 2010; Jones and Sorkin, 2005) and S831 (PKC/CaMKII site) in DH neurons (Fang et al., 2002, 2003; Lu et al., 2008; Jones and Sorkin, 2005). This effect was not observed following spinal nerve ligation (Lu et al., 2008). Thus, GluR1 phosphorylation at S845 and S831 might play a role in both acute (capsaicin) and persistent (CFA) inflammatory pain but not in neuropathic pain. In capsaicin-induced model of acute pain, the increased phosphorylation of GluR1 at both S845 and S831 was blocked by spinal pretreatment with an inhibitor of CaMKII (Fang et al., 2002; Roche et al., 1996). In contrast, the thermal stimulus model does not involve CaMKII-dependent GluR1 phosphorylation, but requires the activation of spinal PKA and PKC (Jones and Sorkin, 2005).

6. Extrasynaptic AMPARs implications for antinociceptive therapy: future perspectives

Pain syndromes, which may persist for a long time, disturb about 10% of the population of developed countries and cause the loss of about $100 billion per year for health care spending. That is why approaches for the therapy of persistent pain are under active investigation.

Cumulative evidence indicates that altered AMPAR trafficking in DH neurons is necessary for the development and maintenance of persistent pain (Park et al., 2008, 2009; Kopach et al., 2012a). Knockout of the gene encoding GluR1 subunit was accompanied by a reduction of the hyperalgesia induced by inflammation, due to a decrease in the amount of GluR1-containing, Ca^{2+}-permeable AMPARs in the spinal cord (Hartmann et al., 2004), thus indicating a key role of this AMPARs subtype in nociceptive plasticity and in the maintenance of long-lasting pain. However, a gene knockout approach is limited by the development of multiple compensatory mechanisms, leaving knockdown strategies to be a more reliable alternative way to perform inducible and localized blockade in nociceptive pathways. Many studies have reported that intrathecal or epidural administration of AMPAR and kainate receptor antagonists alleviates pain symptoms in animals produced by inflammation or nerve damage (Jin et al., 2007; Lee et al., 2006; Zahn et al., 2005; Kopach et al., 2012b). Intrathecal administration of these antagonists also reduces the increased background activity of DH neurons induced by different mechanical stimuli (Zahn et al., 2005).

Inasmuch as existing AMPAR/kainate antagonists produce side effects, other alternative strategies to alleviate painful syndromes are necessary, based on the thorough understanding of molecular and cellular mechanisms of pain development and maintenance. This will ensure the successful treatment of pain by precise targeting of specific molecules, and would therefore be of potential benefit for the treatment, or even prevention, of long-lasting pain. Extrasynaptic AMPARs in the DH neurons may be a potential target for antinociceptive therapy since they possess multiple phosphorylation sites on C-tails of their subunits that allows fine tuning of AMPAR trafficking at multiple stages and consequently the precise regulation of both synaptic and non-synaptic transmission in the DH.

7. Conclusions

In conclusion we can state that two features of extrasynaptic AMPARs may position them as important players in dorsal horn functioning. First, a subunit composition of the extrasynaptic AMPARs may be dynamically changed leading to the remodeling of synaptic receptor composition. Second, this pool of extrasynaptic AMPARs may also directly contribute to glutamatergic signaling at nonsynaptic locations due to glutamate spillover or glial glutamate release, which are potentially increased during pain states. Altogether, this may lead to the strengthening of glutamatergic transmission in the dorsal horn and result in the induction and maintenance of pain syndroms. Thus, extrasynaptic AMPAR trafficking may be considered as a potential mechanism of central sensitization and a promising target for analgesia.

Conflict of interests

The authors declare no conflict of interests.

Acknowledgements

This work was funded by The State Fund Fundamental Research (DFFD) F46.2/001 and the National Academy of Sciences of Ukraine (NASU) Biotechnology and Young Doctor of Sciences Grants to Nana Voitenko, and by NASU Grant for Young Scientists to Olga Kopach.

References

Adesnik, H., Nicoll, R.A., England, P.M., 2005. Photoinactivation of native AMPA receptors reveals their real-time trafficking. Neuron 48, 977–985.
Agnati, L.F., Tiengo, M., Ferraguti, F., Biagini, G., Benfenati, F., Benedetti, C., Rigoli, M., Fuxe, K., 1991. Pain, analgesia, and stress: an integrated view. Clinical Journal of Pain 7 (Suppl. 1), S23–S37.
Albrecht, J., Sidoryk-Wegrzynowicz, M., Zielinska, M., Aschner, M., 2010. Roles of glutamine in neurotransmission. Neuron Glia Biology 6, 263–276.
Albuquerque, C., Lee, C.J., Jackson, A.C., MacDermott, A.B., 1999. Subpopulations of GABAergic and non-GABAergic rat dorsal horn neurons express Ca^{2+}-permeable AMPA receptors. European Journal of Neuroscience 11, 2758–2766.
Andrasfalvy, B.K., Magee, J.C., 2001. Distance-dependent increase in AMPA receptor number in the dendrites of adult hippocampal CA1 pyramidal neurons. Journal of Neuroscience 21, 9151–9159.
Andrasfalvy, B.K., Smith, M.A., Borchardt, T., Sprengel, R., Magee, J.C., 2003. Impaired regulation of synaptic strength in hippocampal neurons from GluR1-deficient mice. Journal of Physiology 552, 35–45.
Araque, A., Parpura, V., Sanzgiri, R.P., Haydon, P.G., 1999. Tripartite synapses: glia, the unacknowledged partner. Trends in Neurosciences 22, 208–215.
Arendt, K.L., Royo, M., Fernandez-Monreal, M., Knafo, S., Petrok, C.N., Martens, J.R., Esteban, J.A., 2010. PIP3 controls synaptic function by maintaining AMPA receptor clustering at the postsynaptic membrane. Nature Neuroscience 13, 36–44.
Atianjoh, F.E., Yaster, M., Zhan, X., Takamiya, K., Xia, J., Gaiska, E.B., Huganir, R.L., Tao, Y.X., 2010. Spinal cord protein interacting with C kinase 1 is required for the maintenance of complete Freund's adjuvant-induced inflammatory pain but not for incision-induced post-operative pain. Pain 151, 226–234.
Balasubramanyan, S., Stemkowski, P.L., Stebbing, M.J., Smith, P.A., 2006. Sciatic chronic constriction injury produces cell-type-specific changes in the electrophysiological properties of rat substantia gelatinosa neurons. Journal of Neurophysiology 96, 579–590.
Barria, A., Muller, D., Derkach, V., Griffith, L.C., Soderling, T.R., 1997. Regulatory phosphorylation of AMPA-type glutamate receptors by CaM-KII during long-term potentiation. Science 276, 2042–2045.
Bats, C., Groc, L., Choquet, D., 2007. The interaction between stargazin and PSD-95 regulates AMPA receptor surface trafficking. Neuron 53, 719–734.
Beique, J.C., Huganir, R.L., 2009. AMPA receptor subunits get their share of the pie. Neuron 62, 165–168.
Billa, S.K., Liu, J., Bjorklund, N.L., Sinha, N., Fu, Y., Shimizu-Gallagher, R., Morón, J.A., 2010. Increased insertion of glutamate receptor 2-lacking alpha-amino-3-hydroxy-5-methyl-4-isoxazole propionic acid (AMPA) receptors at hippocampal synapses upon repeated morphine administration. Molecular Pharmacology 77, 874–883.
Boehm, J., Kang, M.G., Johnson, R.C., Esteban, J., Huganir, R.L., Malinow, R., 2006. Synaptic incorporation of AMPA receptors during LTP is controlled by a PKC phosphorylation site on GluR1. Neuron 51, 213–225.
Borgdorff, A.J., Choquet, D., 2002. Regulation of AMPA receptor lateral movements. Nature 417, 649–653.
Bredt, D.S., Nicoll, R.A., 2003. AMPA receptor trafficking at excitatory synapses. Neuron 40, 361–379.
Burnashev, N., Monyer, H., Seeburg, P.H., Sakmann, B., 1992. Divalent ion permeability of AMPA receptor channels is dominated by the edited form of a single subunit. Neuron 8, 189–198.
Camire, O., Lacaille, J.C., Topolnik, L., 2012. Dendritic signaling in inhibitory interneurons: local tuning via group I metabotropic glutamate receptors. Frontiers in Physiology 3, 259.
Carroll, R.C., Beattie, E.C., von, Z.M., Malenka, R.C., 2001. Role of AMPA receptor endocytosis in synaptic plasticity. Nature Reviews Neuroscience 2, 315–324.
Choi, J.I., Svensson, C.I., Koehrn, F.J., Bhuskute, A., Sorkin, L.S., 2010. Peripheral inflammation induces tumor necrosis factor dependent AMPA receptor trafficking and Akt phosphorylation in spinal cord in addition to pain behavior. Pain 149, 243–253.
Choquet, D., Triller, A., 2003. The role of receptor diffusion in the organization of the postsynaptic membrane. Nature Reviews Neuroscience 4, 251–265.
Cognet, L., Groc, L., Lounis, B., Choquet, D., 2006. Multiple routes for glutamate receptor trafficking: surface diffusion and membrane traffic cooperate to bring receptors to synapses. Science's STKE 2006, e13.
Coombs, I.D., Soto, D., Zonouzi, M., Renzi, M., Shelley, C., Farrant, M., Cull-Candy, S.G., 2012. Cornichons modify channel properties of recombinant and glial AMPA receptors. Journal of Neuroscience 32, 9796–9804.
de Groot, J., Sontheimer, H., 2011. Glutamate and the biology of gliomas. Glia 59, 1181–1189.
Derkach, V.A., Oh, M.C., Guire, E.S., Soderling, T.R., 2007. Regulatory mechanisms of AMPA receptors in synaptic plasticity. Nature Reviews Neuroscience 8, 101–113.
Elias, G.M., Nicoll, R.A., 2007. Synaptic trafficking of glutamate receptors by MAGUK scaffolding proteins. Trends in Cell Biology 17, 343–352.
Engelman, H.S., Allen, T.B., MacDermott, A.B., 1999. The distribution of neurons expressing calcium-permeable AMPA receptors in the superficial laminae of the spinal cord dorsal horn. Journal of Neuroscience 19, 2083–2089.
Fang, L., Wu, J., Lin, Q., Willis, W.D., 2002. Calcium-calmodulin-dependent protein kinase II contributes to spinal cord central sensitization. Journal of Neuroscience 22, 4196–4204.
Fang, L., Wu, J., Zhang, X., Lin, Q., Willis, W.D., 2003. Increased phosphorylation of the GluR1 subunit of spinal cord alpha-amino-3-hydroxy-5-methyl-4-isoxazole propionate receptor in rats following intradermal injection of capsaicin. Neuroscience 122, 237–245.
Ferguson, A.R., Christensen, R.N., Gensel, J.C., Miller, B.A., Sun, F., Beattie, E.C., Bresnahan, J.C., Beattie, M.S., 2008. Cell death after spinal cord injury is exacerbated by rapid TNF alpha-induced trafficking of GluR2-lacking AMPARs to the plasma membrane. Journal of Neuroscience 28, 11391–11400.
Ferrario, C.R., Loweth, J.A., Milovanovic, M., Wang, X., Wolf, M.E., 2011. Distribution of AMPA receptor subunits and TARPs in synaptic and extrasynaptic membranes of the adult rat nucleus accumbens. Neuroscience Letters 490, 180–184.
Furue, H., Katafuchi, T., Yoshimura, M., 2004. Sensory processing and functional reorganization of sensory transmission under pathological conditions in the spinal dorsal horn. Neuroscience Research 48, 361–368.
Furuyama, T., Kiyama, H., Sato, K., Park, H.T., Maeno, H., Takagi, H., Tohyama, M., 1993. Region-specific expression of subunits of ionotropic glutamate receptors (AMPA-type, KA-type and NMDA receptors) in the rat spinal cord with special reference to nociception. Brain Research: Molecular Brain Research 18, 141–151.
Galan, A., Laird, J.M., Cervero, F., 2004. In vivo recruitment by painful stimuli of AMPA receptor subunits to the plasma membrane of spinal cord neurons. Pain 112, 315–323.
Greger, I.H., Esteban, J.A., 2007. AMPA receptor biogenesis and trafficking. Current Opinion in Neurobiology 17, 289–297.
Grudt, T.J., Perl, E.R., 2002. Correlations between neuronal morphology and electrophysiological features in the rodent superficial dorsal horn. Journal of Physiology 540, 189–207.
Guire, E.S., Oh, M.C., Soderling, T.R., Derkach, V.A., 2008. Recruitment of calcium-permeable AMPA receptors during synaptic potentiation is regulated by CaM-kinase I. Journal of Neuroscience 28, 6000–6009.
Hartmann, B., Ahmadi, S., Heppenstall, P.A., Lewin, G.R., Schott, C., Borchardt, T., Seeburg, P.H., Zeilhofer, H.U., Sprengel, R., Kuner, R., 2004. The AMPA receptor subunits GluR-A and GluR-B reciprocally modulate spinal synaptic plasticity and inflammatory pain. Neuron 44, 637–650.
Hayashi, Y., Shi, S.H., Esteban, J.A., Piccini, A., Poncer, J.C., Malinow, R., 2000. Driving AMPA receptors into synapses by LTP and CaMKII: requirement for GluR1 and PDZ domain interaction. Science 287, 2262–2267.
Heine, M., Groc, L., Frischknecht, R., Beique, J.C., Lounis, B., Rumbaugh, G., Huganir, R.L., Cognet, L., Choquet, D., 2008. Surface mobility of postsynaptic AMPARs tunes synaptic transmission. Science 320, 201–205.
Hollmann, M., O'Shea-Greenfield, A., Rogers, S.W., Heinemann, S., 1989. Cloning by functional expression of a member of the glutamate receptor family. Nature 342, 643–648.
Jackson, M.F., Joo, D.T., Al-Mahrouki, A.A., Orser, B.A., Macdonald, J.F., 2003. Desensitization of alpha-amino-3-hydroxy-5-methyl-4-isoxazolepropionic acid (AMPA) receptors facilitates use-dependent inhibition by pentobarbital. Molecular Pharmacology 64, 395–406.
Jin, H.C., Keller, A.J., Jung, J.K., Sobieta, A., Brennan, T.J., 2007. Epidural lorazepam, an AMPA/kainate receptor antagonist, produces postoperative analgesia in rats. Anesthesia and Analgesia 105, 1152–1159, table.
Jones, T.L., Sorkin, L.S., 2005. Activated PKA and PKC, but not CaMKIIalpha, are required for AMPA/kainate-mediated pain behavior in the thermal stimulus model. Pain 117, 259–270.
Katano, T., Furue, H., Okuda-Ashitaka, E., Tagaya, M., Watanabe, M., Yoshimura, M., Ito, S., 2008. N-ethylmaleimide-sensitive fusion protein (NSF) is involved in central sensitization in the spinal cord through GluR2 subunit composition switch after inflammation. European Journal of Neuroscience 27, 3161–3170.
Kato, A.S., Gill, M.B., Yu, H., Nisenbaum, E.S., Bredt, D.S., 2010. TARPs differentially decorate AMPA receptors to specify neuropharmacology. Trends in Neurosciences 33, 241–248.
Kato, A.S., Zhou, W., Milstein, A.D., Knierman, M.D., Siuda, E.R., Dotzlaf, J.E., Yu, H., Hale, J.E., Nisenbaum, E.S., Nicoll, R.A., et al., 2007. New transmembrane AMPA receptor regulatory protein isoform, gamma-7, differentially regulates AMPA receptors. Journal of Neuroscience 27, 4969–4977.
Kerr, R.C., Maxwell, D.J., Todd, A.J., 1998. GluR1 and GluR2/3 subunits of the AMPA-type glutamate receptor are associated with particular types of neurone in laminae I–III of the spinal dorsal horn of the rat. European Journal of Neuroscience 10, 324–333.
Kessels, H.W., Malinow, R., 2009. Synaptic AMPA receptor plasticity and behavior. Neuron 61, 340–350.
Kolke, M., Tsukada, S., Tsuzuki, K., Kijima, H., Ozawa, S., 2000. Regulation of kinetic properties of GluR2 AMPA receptor channels by alternative splicing. Journal of Neuroscience 20, 2166–2174.

Kopach, O., Kao, S.C., Petralia, R.S., Belan, P., Tao, Y.X., Voitenko, N., 2011. Inflammation alters trafficking of extrasynaptic AMPA receptors in tonically firing lamina II neurons of the rat spinal dorsal horn. Pain 152, 912–923.

Kopach, O., Viatchenko-Karpinski, V., Belan, P., Voitenko, N., 2012a. Development of inflammation-induced hyperalgesia and allodynia is associated with the upregulation of extrasynaptic AMPA receptors in tonically firing lamina II dorsal horn neurons. Frontiers in Physiology 3, 1–8.

Kopach, O., Viatchenko-Karpinski, V., Atianjoh, F.E., Belan, P., Tao, Y.H.L., Voitenko, N., 2012b. PKCα is required for inflammation-induced trafficking of extrasynaptic AMPA receptors in tonically firing lamina II dorsal horn neurons during the maintenance of persistent inflammatory pain. Journal of Pain.

Kopnitsa, M.V., 1997. Extrasynaptic receptors of neurotransmitters: distribution, mechanisms of activation, and physiological role. Neurophysiology 29, 357–365.

Kostandy, B.B., 2012. The role of glutamate in neuronal ischemic injury: the role of spark in fire. Neurological Sciences 33, 223–237.

Kullmann, D.M., 2000. Spillover and synaptic cross talk mediated by glutamate and GABA in the mammalian brain. Progress in Brain Research 125, 339–351.

Kwak, S., Weiss, J.H., 2006. Calcium-permeable AMPA channels in neurodegenerative disease and ischemia. Current Opinion in Neurobiology 16, 281–287.

Kyrozis, A., Goldstein, P.A., Heath, M.J., MacDermott, A.B., 1995. Calcium entry through a subpopulation of AMPA receptors desensitized neighbouring NMDA receptors in rat dorsal horn neurons. Journal of Physiology 485 (Pt 2), 373–381.

Larsson, M., Broman, J., 2008. Translocation of GluR1-containing AMPA receptors to a spinal nociceptive synapse during acute noxious stimulation. Journal of Neuroscience 28, 7084–7090.

Latremoliere, A., Woolf, C.J., 2009. Central sensitization: a generator of pain hypersensitivity by central neural plasticity. Journal of Pain 10, 895–926.

Lee, H.J., Pogatzki-Zahn, E.M., Brennan, T.J., 2006. The effect of the AMPA/kainate receptor antagonist LY293558 in a rat model of postoperative pain. Journal of Pain 7, 768–777.

Lemmudakis, D., Zhan, P., Beattie, E.C., 2008. Rapid tumor necrosis factor (alpha)-induced exocytosis of glutamate receptor 2-lacking AMPA receptors to extrasynaptic plasma membrane potentiates excitotoxicity. Journal of Neuroscience 28, 2119–2130.

Li, G., Nie, L., 2004. How fast does the GluR1 flip channel open? Biological Chemistry 279, 3990–3997.

Li, J., Baccei, M.L., 2009. Excitatory synapses in the rat superficial dorsal horn are strengthened following peripheral inflammation during early postnatal development. Pain 143, 56–64.

Lima, D., 1998. Anatomical basis for the dynamic processing of nociceptive input. European Journal of Pain 2, 195–202.

Lin, D.T., Makino, Y., Sharma, K., Hayashi, T., Neve, R., Takamiya, K., Huganir, R.L., 2009. Regulation of AMPA receptor extrasynaptic insertion by 4.1 N, phosphorylation and palmitoylation. Nature Neuroscience 12, 879–887.

Liu, S.Q., Cull-Candy, S.G., 2000. Synaptic activity at calcium-permeable AMPA receptors induces a switch in receptor subtype. Nature 405, 454–458.

Lu, W., Shi, Y., Jackson, A.C., Bjorgan, K., During, M.J., Sprengel, R., Seeburg, P.H., Nicoll, R.A., 2009. Subunit composition of synaptic AMPA receptors revealed by a single-cell genetic approach. Neuron 62, 254–268.

Lu, W., Ziff, E.B., 2005. PICK1 interacts with ABP/GRIP to regulate AMPA receptor trafficking. Neuron 47, 407–421.

Lu, Y., Perl, E.R., 2003. A specific inhibitory pathway between substantia gelatinosa neurons receiving direct C-fiber input. Journal of Neuroscience 23, 8752–8758.

Lu, Y., Sun, Y.N., Wu, X., Sun, Q., Liu, F.Y., Xing, G.G., Wan, Y., 2008. Role of alpha-amino-3-hydroxy-5-methyl-4-isoxazole propionate (AMPA) receptor subunit GluR1 in spinal dorsal horn in inflammatory nociception and neuropathic nociception in rat. Brain Research 1200, 19–26.

Luthi, A., Wikstrom, M.A., Palmer, M.J., Matthews, P., Benke, T.A., Isaac, J.T., Collingridge, G.L., 2004. Bi-directional modulation of AMPA receptor unitary conductance by synaptic activity. BMC Neuroscience 5, 44.

Makara, S., Zagha, E., 2007. Out of the cleft: the source and target of extra-synaptic glutamate in the CA1 region of the hippocampus. Journal of Physiology 582, 479–480.

Malinow, R., Malenka, R.C., 2002. AMPA receptor trafficking and synaptic plasticity. Annual Review of Neuroscience 25, 103–126.

Man, H.Y., Sekine-Aizawa, Y., Huganir, R.L., 2007. Regulation of {alpha}-amino-3-hydroxy-5-methyl-4-isoxazolepropionic acid receptor trafficking through PKA phosphorylation of the Glu receptor 1 subunit. Proceedings of the National Academy of Sciences of the United States of America 104, 3579–3584.

Mao, J., Sung, B., Ji, R.R., Lim, G., 2002. Chronic morphine induces downregulation of spinal glutamate transporters: implications in morphine tolerance and abnormal pain sensitivity. Journal of Neuroscience 22, 8312–8323.

Masugi-Tokita, M., Tarusawa, E., Watanabe, M., Molnar, E., Fujimoto, K., Shigemoto, R., 2007. Number and density of AMPA receptors in individual synapses in the rat cerebellum as revealed by SDS-digested freeze-fracture replica labeling. Journal of Neuroscience 27, 2135–2144.

Momiyama, A., Silver, R.A., Hausser, M., Notomi, T., Wu, Y., Shigemoto, R., Cull-Candy, S.G., 2003. The density of AMPA receptors activated by a transmitter quantum at the climbing fibre–Purkinje cell synapse in immature rats. The Journal of Physiology 549, 75–92.

Mosbacher, J., Schmoller, R., Monyer, H., Burnashev, N., Seeburg, P.H., Ruppersberg, J.P., 1994. A molecular determinant for submillisecond desensitization in glutamate receptors. Science 266, 1059–1062.

Nicoll, R.A., Tomita, S., Bredt, D.S., 2006. Auxiliary subunits assist AMPA-type glutamate receptors. Science 311 (5765), 1253–1256.

Nie, H., Weng, H.R., 2009. Glutamate transporters prevent excessive activation of NMDA receptors and extrasynaptic glutamate spillover in the spinal dorsal horn. Journal of Neurophysiology 101, 2041–2051.

Nie, H., Weng, H.R., 2010. Impaired glial glutamate uptake induces extrasynaptic glutamate spillover in the spinal sensory synapses of neuropathic rats. Journal of Neurophysiology 103, 2570–2580.

Nusser, Z., 2000. AMPA and NMDA receptors: similarities and differences in their synaptic distribution. Current Opinion in Neurobiology 10, 337–341.

Oh, M.C., Derkach, V.A., Guire, E.S., Soderling, T.R., 2006. Extrasynaptic membrane trafficking regulated by GluR1 serine 845 phosphorylation primes AMPA receptors for long-term potentiation. Journal of Biological Chemistry 281, 752–758.

Opazo, P., Choquet, D., 2011. A three-step model for the synaptic recruitment of AMPA receptors. Molecular and Cellular Neurosciences 46, 1–8.

Park, J.S., Voitenko, N., Petralia, R.S., Guan, X., Xu, J.T., Steinberg, J.P., Takamiya, K., Sotnik, A., Kopach, O., Huganir, R.L., Tao, Y.X., 2009. Persistent inflammation induces GluR2 internalization via NMDA receptor-triggered PKC activation in dorsal horn neurons. Journal of Neuroscience 29, 3206–3219.

Park, J.S., Yaster, M., Guan, X., Xu, J.T., Shih, M.H., Guan, Y., Raja, S.N., Tao, Y.X., 2008. Role of spinal cord alpha-amino-3-hydroxy-5-methyl-4-isoxazolepropionic acid receptors in complete Freund's adjuvant-induced inflammatory pain. Molecular Pain 4, 67.

Pei, W., Huang, Z., Niu, L., 2007. GluR3 flip and flop: differences in channel opening kinetics. Biochemistry 46, 2027–2036.

Pei, W., Huang, Z., Wang, C., Han, Y., Park, J.S., Niu, L., 2009. Flip and flop: a molecular determinant for AMPA receptor channel opening. Biochemistry 48, 3767–3777.

Petralia, R.S., Wang, Y.X., Mayat, E., Wenthold, R.J., 1997. Glutamate receptor subunit 2-selective antibody shows a differential distribution of calcium-impermeable AMPA receptors among populations of neurons. Journal of Comparative Neurology 385, 456–476.

Petrini, E.M., Lu, J., Cognet, L., Lounis, B., Ehlers, M.D., Choquet, D., 2009. Endocytic trafficking and recycling maintain a pool of mobile surface AMPA receptors required for synaptic potentiation. Neuron 63, 92–105.

Pezet, S., Marchand, F., D'Mello, R., Grist, J., Clark, A.K., Malcangio, M., Dickenson, A.H., Williams, R.J., McMahon, S.B., 2008. Phosphatidylinositol 3-kinase is a key mediator of central sensitization in painful inflammatory conditions. Journal of Neuroscience 28, 4261–4270.

Polgar, E., Al Ghamdi, K.S., Todd, A.J., 2010. Two populations of neurokinin 1 receptor-expressing projection neurons in lamina I of the rat spinal cord that differ in AMPA receptor subunit composition and density of excitatory synaptic input. Neuroscience 167, 1192–1204.

Roche, K.W., O'Brien, R.J., Mammen, A.L., Bernhardt, J., Huganir, R.L., 1996. Characterization of multiple phosphorylation sites on the AMPA receptor GluR1 subunit. Neuron 16, 1179–1188.

Rossi, B., Maton, G., Collin, T., 2008. Calcium-permeable presynaptic AMPA receptors in cerebellar molecular layer interneurones. Journal of Physiology 586, 5125–5145.

Rotaru, D.C., Lewis, D.A., Gonzalez-Burgos, G., 2012. The role of glutamatergic inputs onto parvalbumin-positive interneurons: relevance for schizophrenia. Reviews in the Neurosciences 23, 97–109.

Santos, S.F., Rebelo, S., Derkach, V.A., Safronov, B.V., 2007. Excitatory interneurons dominate sensory processing in the spinal substantia gelatinosa of rat. Journal of Physiology 581, 241–254.

Schmitt, F.O., 1984. Molecular regulators of brain function: a new view. Neuroscience 13, 991–1001.

Schwenk, J., Harmel, N., Zolles, G., Bildl, W., Kulik, A., Heimrich, B., Chisaka, O., Jonas, P., Schulte, U., Fakler, B., et al., 2009. Functional proteomics identify cornichon proteins as auxiliary subunits of AMPA receptors. Science 323, 1313–1319.

Sekiguchi, M., Nishikawa, K., Aoki, S., Wada, K., 2002. A desensitization-selective potentiator of AMPA-type glutamate receptors. British Journal of Pharmacology 136, 1033–1041.

Shepherd, J.D., Huganir, R.L., 2007. The cell biology of synaptic plasticity: AMPA receptor trafficking. Annual Review of Cell and Developmental Biology 23, 613–643.

Shi, Y., Suh, Y.H., Milstein, A.D., Isozaki, K., Schmid, S.M., Roche, K.W., Nicoll, R.A., 2010. Functional comparison of the effects of TARPs and cornichons on AMPA receptor trafficking and gating. Proceedings of the National Academy of Sciences of the United States of America 107, 16315–16319.

Song, I., Huganir, R.L., 2002. Regulation of AMPA receptors during synaptic plasticity. Trends in Neurosciences 25, 578–588.

Stein, E., Cox, J.A., Seeburg, P.H., Verdoorn, T.A., 1992. Complex pharmacological properties of recombinant alpha-amino-3-hydroxy-5-methyl-4-isoxazole propionate receptor subtypes. Molecular Pharmacology 42, 864–871.

Sung, B., Lim, G., Mao, J., 2003. Altered expression and uptake activity of spinal glutamate transporters after nerve injury contribute to the pathogenesis of neuropathic pain in rats. Journal of Neuroscience 23, 2899–2910.

Tao, Y.X., 2010. Dorsal horn alpha-amino-3-hydroxy-5-methyl-4-isoxazolepropionic acid receptor trafficking in inflammatory pain. Anesthesiology 112, 1259–1265.

Todd, A.J., Polgar, E., Watt, C., Bailey, M.E., Watanabe, M., 2009. Neurokinin 1 receptor-expressing projection neurons in laminae III and IV of the rat spinal cord have synaptic AMPA receptors that contain GluR2, GluR3 and GluR4 subunits. European Journal of Neuroscience 29, 718–726.

Tong, C.K., MacDermott, A.B., 2006. Both Ca^{2+}-permeable and -impermeable AMPA receptors contribute to primary synaptic drive onto rat dorsal horn neurons. Journal of Physiology 575, 133–144.
Traynelis, S.F., Wollmuth, L.P., McBain, C.J., Menniti, F.S., Vance, K.M., Ogden, K.K., Hansen, K.B., Yuan, H., Myers, S.J., Dingledine, R., 2010. Glutamate receptor ion channels: structure, regulation, and function. Pharmacological Reviews 62, 405–496.
Triller, A., Choquet, D., 2005. Surface trafficking of receptors between synaptic and extrasynaptic membranes: and yet they do move! Trends in Neurosciences 28, 133–139.
van der Zeyden, M., Oldenziel, W.H., Rea, K., Cremers, T.I., Westerink, B.H., 2008. Microdialysis of GABA and glutamate: analysis, interpretation and comparison with microsensors. Pharmacology Biochemistry and Behavior 90, 135–147.
Vikman, K.S., Rycroft, B.K., Christie, M.J., 2008. Switch to Ca^{2+}-permeable AMPA and reduced NR2B NMDA receptor-mediated neurotransmission at dorsal horn nociceptive synapses during inflammatory pain in the rat. Journal of Physiology 586, 515–527.
Vizi, E.S., Fekete, A., Karoly, R., Mike, A., 2010. Non-synaptic receptors and transporters involved in brain functions and targets of drug treatment. British Journal of Pharmacology 160, 785–809.
Vizi, E.S., 1980. Non-synaptic modulation of transmitter release: pharmacological implication. Trends in Pharmacological Sciences 1, 172–175.
Vizi, E.S., 1984. Non-synaptic Interactions Between Neurons: Modulation of Neurochemical Transmission. Pharmacological and Clinical Aspects. John Wiley and Sons, Chichester, New York.
Voitenko, N., Gerber, G., Youn, D., Randic, M., 2004. Peripheral inflamation-induced increase of AMPA-mediated currents and Ca^{2+} transients in the presence of cyclothiazide in the rat substantia gelatinosa neurons. Cell Calcium 35, 461–469.
Weng, H.R., Aravindan, N., Cata, J.P., Chen, J.H., Shaw, A.D., Dougherty, P.M., 2005. Spinal glial glutamate transporters downregulate in rats with taxol-induced hyperalgesia. Neuroscience Letters 386, 18–22.
Xu, Q., Yaksh, T.L., 2011. A brief comparison of the pathophysiology of inflammatory versus neuropathic pain. Current Opinion in Anesthesiology 24, 400–407.
Yasaka, T., Tiong, S.Y., Hughes, D.I., Riddell, J.S., Todd, A.J., 2010. Populations of inhibitory and excitatory interneurons in lamina II of the adult rat spinal dorsal horn revealed by a combined electrophysiological and anatomical approach. Pain 151, 475–488.
Youn, D.H., Royle, G., Kolaj, M., Vissel, B., Randić, M., 2008. Enhanced LTP of primary afferent neurotransmission in AMPA receptor GluR2-deficient mice. Pain 136, 158–167.
Zahn, P.K., Pogatzki-Zahn, E.M., Brennan, T.J., 2005. Spinal administration of MK-801 and NBQX demonstrates NMDA-independent dorsal horn sensitization in incisional pain. Pain 114, 499–510.

РОЗДІЛ 3

ФЕНОМЕН ЦЕНТРАЛЬНОЇ СЕНСИТИЗАЦІЇ ПРИ ХРОНІЧНИХ БОЛЬОВИХ СИНДРОМАХ РІЗНОГО ГЕНЕЗУ: ВКЛАД ПОРУШЕНЬ ОБІГУ AMPA-РЕЦЕПТОРІВ У ГІПЕРЗБУЛИВІСТЬ НЕЙРОНАЛЬНИХ МЕРЕЖ СПИННОГО МОЗКУ

3.1. Порушення трафікінгу AMPA-рецепторів у нейронах дорзального рогу при тривалому периферичному запаленні призводить до клітинноспецифічних змін у балансі між синаптичним збудженням та гальмуванням у нейронних мережах спинного мозку

Research Paper

PAIN

Inflammatory-induced changes in synaptic drive and postsynaptic AMPARs in lamina II dorsal horn neurons are cell-type specific

Olga Kopach, Volodymyr Krotov, Pavel Belan, Nana Voitenko*

Abstract

Persistent peripheral inflammation alters trafficking of AMPA receptors (AMPARs) at the synapses between primary afferents and dorsal horn (DH) neurons that contribute to the maintenance of inflammatory pain. However, whether peripheral inflammation changes the synaptic activity within the DH circuitry and how it modulates synaptic AMPARs in different neuronal types still remain unknown. We find that complete Freund adjuvant (CFA)-induced peripheral inflammation prominently augments excitatory neurotransmission in rat lamina II neurons characterized by intrinsic adapting firing properties and apparently decreases it in the tonic firing lamina II neurons, suggesting different roles of these types of interneurons in pain processing. Peripheral inflammation also differentially changes inhibitory neurotransmission in these neuronal types, shifting the balance between neuronal excitation and inhibition toward excitation of the adapting firing, but toward inhibition of the tonic firing lamina II neurons. Synaptic AMPARs were differentially changed in the adapting firing and the tonic firing neurons, implying different mechanisms of AMPAR adjustment at the synapses in these types of interneurons during persistent inflammation. The inflammatory-induced, neuron-type specific changes in synaptic drive within the DH circuitry and synaptic AMPAR functioning in lamina II neurons may contribute to the persistent pain maintenance.

Keywords: Synaptic AMPARs, Excitatory and inhibitory transmission, Persistent peripheral inflammation, Lamina II dorsal horn neurons

1. Introduction

Persistent or chronic pain presents a significant burden to both society and economies with direct and indirect costs that run into billions of dollars. In spite of this, the awareness, understanding and treatment of chronic pain are limited. Persistent or chronic pain can be provoked by peripheral or spinal cord injury, inflammation, infection, or neuropathies of various origins. Even after termination of an apparent initial trigger, persistent pain can be sustained by intrinsic mechanisms, giving rise to a chronic pain syndrome. Intensive studies of painful syndromes over many years have revealed severe impairments of function in the peripheral nervous system. However, central mechanisms of persistent pain remain less clear. Central sensitization is considered to be the central mechanism in the dorsal horn (DH) that underlies persistent pain. Dorsal horn hypersensitivity is initiated by enhanced glutamate release from both damaged and undamaged primary afferents that augments glutamatergic transmission within the circuits and alters activity of DH neurons.[2,15,23,52] Reduced GABAergic and/or glycinergic inhibitory transmissions[31,39,45,47] may result in disinhibition of certain types of DH neurons, as was reported for chronic neuropathic pain,[12] that further augments DH hypersensitivity. However, little is known about the balance between excitatory and inhibitory transmissions, determining ectopic activity of particular subsets of DH neurons that process nociceptive information, during chronic inflammatory pain.

Central sensitization depends on trafficking of AMPA receptor (AMPAR) subunits in DH neurons.[21,23] Altered AMPAR trafficking in DH neurons is associated with increased pain sensation during the development and maintenance of persistent inflammatory pain and may be mediated by internalization of GluR2-containing AMPARs, shown in the first-order synapses between primary afferents and DH neurons,[14,17,32,49] and by insertion of GluR2-lacking AMPARs in extrasynaptic membranes.[18,19] Although the type of neurons where GluR2-containing AMPARs undergo internalization remains unidentified, inflammatory-induced insertion of GluR1-containing AMPARs into extrasynaptic sites was observed in the lamina II neurons characterized by intrinsic tonic firing properties.[18,19] This raises a physiologically relevant hypothesis of neuron type–specific changes of AMPAR trafficking in pathological conditions.

Cumulative evidence indicates that most lamina II neurons revealing the tonic firing pattern are GABAergic, whereas those exhibiting A-type potassium channel–related patterns apparently represent excitatory glutamatergic interneurons[13,28,37,55] (although see Refs. 10,40,46). During injury-related neuropathic pain, increased excitatory synaptic activity was found in different types of DH neurons, but not in those with tonic firing pattern.[2,4,12] However, neuron type–specific changes in DH

Sponsorships or competing interests that may be relevant to content are disclosed at the end of this article.

Department of General Physiology of Nervous System, Bogomoletz Institute of Physiology, Kyiv, Ukraine

**Corresponding author. Address: Department of General Physiology of Nervous System, Bogomoletz Institute of Physiology, 4 Bogomoletz St, Kyiv 01024, Ukraine. Tel.: +38044-256-2049; fax: +38044-256-2053. E-mail address: nana@biph.kiev.ua (N. Voitenko).*

PAIN 156 (2015) 428–438

http://dx.doi.org/10.1097/01.j.pain.0000460318.65734.00

neurotransmission during persistent inflammatory pain still remain unknown. Furthermore, neuron type–specific changes in AMPAR trafficking at the secondary-order DH synapses have not been studied before.

We demonstrate increased synaptic excitation within the DH circuitry in persistent inflammatory pain conditions that is associated with differentially shifted balance between neuronal excitation and inhibition and changed postsynaptic AMPAR functioning in different types of lamina II neurons. Taken together, these findings suggest neuron type–specific, activity-dependent adjustment of synaptic strength within the DH circuitry.

2. Materials and methods

2.1. Animal care

Male Wistar rats were used throughout the study and were treated in accordance with the guidelines approved by the Animal Care and Use Committee at Bogomoletz Institute of Physiology and consistent with ethical guidelines of the International Association for the Study of Pain. All efforts were made to minimize animal suffering and to reduce the number of animals used.

2.2. Induction of peripheral inflammation

To produce unilateral peripheral inflammation and nociceptive hypersensitivity, 100 μL of complete Freund adjuvant (CFA, *Mycobacterium tuberculosis*) suspended in an oil–saline (1:1) emulsion was injected subcutaneously into the plantar side of a hind paw of the rats. Electrophysiological studies were undertaken 24 hours after injection of CFA, the time point representing maintenance of persistent inflammatory pain.[18,20,32] Saline (0.9%; 100 μL) injection in a separate cohort of animals was used as a control.

2.3. Spinal cord slice preparation

Spinal cord slices were prepared from 18- to 24-day-old rats as described previously.[18,50] Briefly, after rats were deeply anesthetized, L_{4-5} spinal segments were removed. Transverse slices (300-350 μm thick) were cut on an HA 752 vibratome (Campden Instruments, Loughborough, United Kingdom) in an ice-cold solution containing (in millimolars) 250 sucrose, 2 KCl, 1.2 NaH_2PO_4, 0.5 $CaCl_2$, 7 $MgCl_2$, 26 $NaHCO_3$, 11 glucose and continuously bubbled with 95% O_2 and 5% CO_2. Slices were then maintained at room temperature in physiologic Krebs solution that contained (in millimolars) 125 NaCl, 2.5 KCl, 1.25 NaH_2PO_4, 2 $CaCl_2$, 1 $MgCl_2$, 26 $NaHCO_3$, and 10 glucose (osmolarity 310-320 mOsM) and was equilibrated with 95% O_2 and 5% CO_2.

2.4. Electrophysiology

Whole-cell patch-clamp recordings of lamina II (*Substantia gelatinosa*) (SG) DH neurons were performed in spinal cord slices as described previously.[18] Dorsal horn neurons were patched under visual control with infrared optics using a ×60 water-immersion objective on Olympus BX50WI upright microscope equipped with a video system (Olympus, Tokyo, Japan). Recording pipettes had a resistance of 3 to 5 MΩ when filled with an internal solution containing (in millimolars) 133 K-gluconate, 5 NaCl, 0.5 $MgCl_2$, 10 HEPES-Na, 2 MgATP, 0.1 GTP-Na, and 0.5 EGTA (pH 7.2, osmolarity 290 mOsM). Recordings were made using a Multipatch 700B amplifier under control of pClamp 9.2 software (Molecular Devices, Sunnyvale, CA).

All tested SG neurons were categorized according to their discharge patterns of action potentials in response to the series of 0.5- to 1-s current pulses.[18,37] Hyperpolarizing current with an amplitude of −20 pA or −10 pA was injected in the current-clamp mode into a tested neuron, followed by a set of depolarizing currents of the same duration and increment (**Fig. 1A** bottom). Tonic firing, adapting firing, transient (initial burst) firing, and single-spiking discharge patterns of SG neurons were recorded from neurons within SG (**Fig. 1A**). Given that all of these patterns, except the tonic firing, are considered to be adapting because of the A-type potassium current–related pattern of discharge,[29,46,55] neurons were grouped together and divided into 2 main groups: "adapting firing" and "tonic firing." Tonic firing neurons were defined as those able to support continuous discharge of action potentials and to increase the frequency of discharge with increasing depolarizing current intensity (**Fig. 1A**). The resting membrane potential was −58 ± 1 mV ($n = 26$) for the tonic firing and −58 ± 2 mV ($n = 40$) for the adapting firing lamina II neurons. Only data from neurons that exhibited low resting membrane potentials, nonjittering through the recording, were included in the analysis.

Spontaneous excitatory postsynaptic currents (sEPSCs) were recorded at a holding potential of −70 mV for at least 5 minutes to thoroughly evaluate the synaptic activity within the DH circuitry. The holding potential was then switched to 0 mV, and spontaneous inhibitory postsynaptic currents (sIPSCs) were recorded from the same neuron for at least 5 minutes after stabilization of baseline at 0 mV. To isolate miniature excitatory postsynaptic currents (mEPSCs) mediated by activation of AMPARs exclusively, a cocktail of blockers that contained (in micromolars) 0.3 tetrodotoxin (TTX), 50 APV, 5 bicuculline, 2 strychnine, and 100 $CdCl_2$ was used. AMPAR-mediated mEPSCs were recorded at −70 mV in the continuous presence of cocktail of blockers typically after 10 minutes after bath administration of blockers. One neuron was studied per slice, and only recordings from neurons with a stable baseline through the entire experiment were used for analysis.

2.5. Data analysis

The Mini Analysis Program (Synaptosoft, Decatur, GA) was used to detect and analyze excitatory and inhibitory synaptic events off-line. Postsynaptic currents were automatically distinguished from baseline noise by setting an appropriate amplitude and area threshold for each neuron. All events were then visually re-examined to eliminate false-positive events. The Mini Analysis Program was used to generate the cumulative probability plots. Only neurons that revealed linear cumulative time histograms of recorded events were included in the analysis. To accurately calculate the kinetics of postsynaptic currents within baseline noise, the time frame of 10% to 90% of current for rise time and 100% to 37% of current for decay time were analyzed. The area of current was calculated as an integral within the time frame of current initiation until 37% of current decay.

The data sets of synaptic events were probed for normality within each experimental group using a Shapiro–Wilk test. Data sets were compared using a nonparametric statistical Mann–Whitney *U* test, if not normally distributed, and results were presented as medians with interquartile ranges (IQR) and *n* referring to the number of cells analyzed. Data sets of miniature synaptic events were normally distributed and satisfied distributional symmetry criteria and were therefore analyzed using an unpaired Student *t* test; the results were presented as mean with standard error of the mean and *n* referring to the number of cells

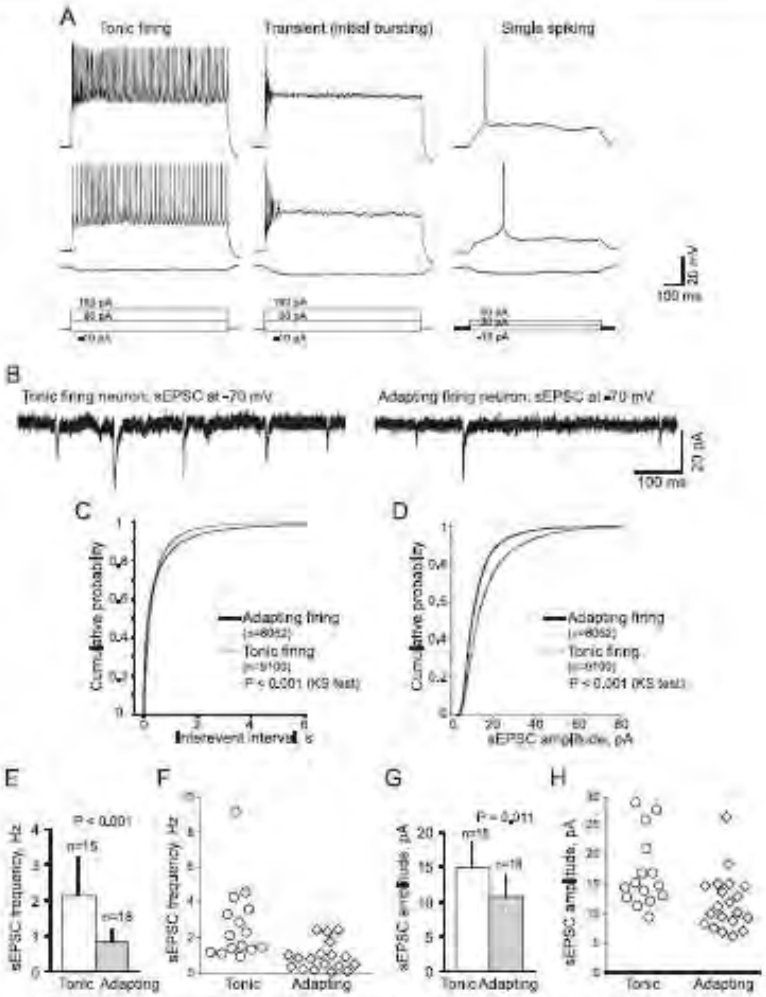

Figure 1. Different types of lamina II DH neurons show different excitatory synaptic activity. (A) Typical action potential discharges (3 top rows) for the tonic firing, transient (initial bursting), and single-spike *Substantia gelatinosa* (SG) neurons in response to sustained depolarizing currents (bottom). Transient and single-spike neurons were considered to be adapting because of A type potassium current–related pattern of discharge. (B) Representative examples of spontaneous excitatory postsynaptic currents (sEPSCs) recorded at −70 mV in the tonic firing (left) and the adapting firing (right) SG neurons. (C and D) Cumulative probability plots for the interevent interval (C) and the amplitude (D) of sEPSCs in the tonic firing (9100 events from 15 cells) and the adapting firing SG neurons (8052 events from 18 cells) demonstrate the difference in both parameters between neuronal types. The Kolmogorov–Smirnov test significance is indicated. (E and F) A statistical summary (E) and a scatter plot (F) of sEPSC frequency, analyzed for the tonic firing (15 cells) and the adapting firing SG neurons (18 cells), validate the difference in sEPSC frequency in different neuronal types. Data are expressed as median and interquartile ranges (IQR). Mann–Whitney *U* test significance is indicated. (G and H) A statistical summary (G) and a scatter plot (H) of sEPSC amplitude, analyzed for the tonic firing (15 cells) and the adapting firing neurons (18 cells), validate the difference in sEPSC amplitude in different neuronal types. Data are expressed as median and IQR. Mann–Whitney *U* test significance is indicated.

analyzed. Cumulative probability curves were plotted for the entire population of events pooled from all recorded neurons in each experimental group. The Kolmogorov–Smirnov 2-sample test was used to compare the distributions of either interevent intervals or amplitudes of synaptic events between experimental groups. A *P* value less than 0.05 was considered as statistically significant for each test used.

2.6. Experimental drugs

Complete Freund adjuvant was purchased from Sigma Chemical Co (St Louis, MO). Tetrodotoxin was obtained from Alomone Labs Ltd (Jerusalem, Israel), and APV, bicuculline, and strychnine from Tocris Bioscience (Ellisville, MO).

3. Results

3.1. Persistent peripheral inflammation leads to hyperexcitability of the dorsal horn by increasing excitatory synaptic drive to different types of lamina II neurons

The first study investigated how persistent peripheral inflammation changes excitatory synaptic drive within the DH neuronal circuitry and how these changes may depend on the type of lamina II neurons. For this, spontaneous excitatory synaptic activity in lamina II neurons characterized by intrinsic adapting firing and tonic firing properties (**Fig. 1A**) was studied in a control and 1 day after induction of peripheral inflammation.

Even in control conditions, both the interevent intervals and the amplitudes of sEPSCs were significantly different between the

tonic firing and the adapting firing SG neurons when the entire pools of events were compared by the Kolmogorov–Smirnov test ($P < 0.001$; **Fig. 1B–D**). Moreover, the median values of both frequency and amplitude of sEPSCs calculated for each type of neurons were significantly different. The median sEPSC frequency was 2.1 s^{-1} ($n = 15$) for the tonic firing, while 0.8 s^{-1} ($n = 19$) for the adapting firing SG neurons (difference − 62%, $P < 0.001$ Mann–Whitney U test; **Fig. 1E–F**). The median sEPSC amplitude was 14.8 pA ($n = 15$) for the tonic firing and 10.8 pA ($n = 20$) for the adapting firing SG neurons (difference − 27%, $P = 0.011$ Mann–Whitney U test; **Fig. 1G–H**). Meanwhile, the rise and decay kinetics of sEPSCs were similar in these neuronal types. The rise time was 1.3 milliseconds ($n = 15$) and 1.5 milliseconds ($n = 20$, $P = 0.45$ Mann–Whitney U test), and the decay time was 3.4 milliseconds ($n = 15$) and 2.8 milliseconds ($n = 20$, $P = 0.39$ Mann–Whitney U test) for the tonic firing and the adapting firing SG neurons, respectively (data not shown). Substantial difference in the sEPSC frequencies along with the sEPSC amplitudes in SG neurons that exhibited different discharge patterns reflects distinct excitatory drive that these types of neurons receive within the DH circuitry and suggests their diverse roles in processing of sensory information.

Persistent peripheral inflammation increased excitatory synaptic activity within the DH. In total, 17,162 spontaneous excitatory events were recorded in 33 lamina II neurons of the control group and 19,653 events in 32 neurons of CFA-inflamed animals. The interevent interval of sEPSCs was 532 milliseconds in the control, but 386 milliseconds in 1 day after CFA (difference −27%, $P < 0.001$, the Kolmogorov–Smirnov test), reflecting CFA-induced increase in the sEPSC frequency and indicating boosted excitability within the DH circuitry during persistent peripheral inflammation.

The changes in spontaneous excitatory synaptic activity in lamina II DH neurons during persistent inflammation were cell-type specific. The interevent interval of sEPSCs was decreased by 39% ($P < 0.001$, the Kolmogorov–Smirnov test; **Fig. 2Ba**) in the adapting firing SG neurons 1 day after CFA (that reflects increased sEPSC frequency), but it was only slightly decreased in the tonic firing SG neurons (by 13%, $P < 0.05$; **Fig. 2Bb**, the Kolmogorov–Smirnov test) when the entire pools of events from tested neurons were compared between control and inflamed groups. The median sEPSC frequency was substantially increased (by 177%) in the adapting firing SG neurons (0.8 s^{-1}, $n = 19$ in control vs 2.3 s^{-1}, $n = 21$ in 1 day after CFA, $P < 0.001$, Mann–Whitney U test; **Fig. 2Ca–b**), but was not significantly changed in the tonic firing SG neurons (2.1 s^{-1}, $n = 15$ in control vs 1.6 s^{-1}, $n = 11$ in 1 day after CFA, $P = 0.47$, Mann–Whitney U test; **Fig. 2Co–d**). The amplitude of sEPSCs was also changed in persistent inflammatory pain conditions in a cell-type specific manner. It was increased in the adapting firing SG neurons (by 12%, $P < 0.001$, the Kolmogorov–Smirnov test; **Fig. 2Da**), although decreased in the tonic firing (by 13%, $P < 0.05$, the Kolmogorov–Smirnov test; **Fig. 2Db**) 1 day after CFA.

Thus, different types of lamina II DH neurons have distinct patterns of spontaneous synaptic activity, indicating nonidentical synaptic drives that they receive within the circuitry and suggesting their contrasting functional roles in processing of nociceptive information. Persistent peripheral inflammation increases DH excitability by predominantly boosting spontaneous excitatory drive to the lamina II neurons exhibiting intrinsic adaptation and slightly modulating this drive to the tonic firing interneurons. Prominently increased excitatory neurotransmission in the adapting firing lamina II neurons during persistent inflammation reflects the major contribution of these interneurons to the DH hyperexcitability in persistent pain conditions and is consistent with the suggestion of their excitatory role in processing of nociceptive inputs from primary afferents and/or from spinal interneurons.

3.2. Persistent inflammation differentially shifts the balance between excitation and inhibition of different types of lamina II neurons

Also studied were whether inhibitory neurotransmission is changed in different types of lamina II neurons in persistent inflammatory pain conditions and whether the changes in both excitatory and inhibitory synaptic inputs, received by different types of lamina II neurons within the circuitry, affect the balance between their excitation and inhibition.

As in the case of excitatory synaptic activity, persistent peripheral inflammation changed inhibitory synaptic activity in lamina II DH neurons in a cell type–specific manner (**Fig. 3A**). However, the interevent interval of sIPSCs was increased in the adapting firing SG neurons 1 day after CFA, reflecting the decreased sIPSC frequency (by 22%, $P < 0.05$, the Kolmogorov–Smirnov test; **Fig. 3Ba**), but was decreased in the tonic firing SG neurons 1 day after CFA, mirroring the increased sIPSC frequency in these neurons (by 59%, $P < 0.05$, the Kolmogorov–Smirnov test; **Fig. 3Bb**). An analysis of the median sIPSC frequency showed a tendency toward its increase in the tonic firing SG neurons 1 day after CFA (by 433%, $P = 0.12$ Mann–Whitney U test), whereas no changes were found in the adapting firing SG neurons (0.06 s^{-1}, $n = 15$ and 0.06 s^{-1}, $n = 17$ in the control and 1 day after CFA, respectively, $P = 0.91$ Mann–Whitney U test). At the same time, the sIPSC amplitude was changed in an opposite manner than the frequency. The amplitude was increased in the tonic firing SG neurons (by 28%, $P < 0.05$, the Kolmogorov–Smirnov test; **Fig. 3Cb**), but decreased in the adapting firing SG neurons (by 21%, $P < 0.05$, the Kolmogorov–Smirnov test; **Fig. 3Ca**) 1 day after CFA when the entire pools of events were compared. An analysis of the median amplitudes of sIPSCs further showed a tendency toward the amplitude increase (by 37%, $P = 0.057$ Mann–Whitney U test) in the tonic firing SG neurons and toward slight decrease (by −15%, $P = 0.39$ Mann–Whitney U test) in the adapting firing SG neurons 1 day after CFA (22.6 pA, $n = 15$ and 19.2 pA, $n = 17$ in control and 1 day after CFA, respectively).

Thus, peripheral inflammation augments inhibitory neurotransmission in the tonic firing SG neurons, although reduces this neurotransmission in the adapting firing SG neurons. This implies boosted inhibition of the tonic firing neurons with concomitant disinhibition of the adapting firing lamina II neurons in persistent inflammatory pain conditions.

To evaluate how the inflammatory-induced changes in both excitatory and inhibitory neurotransmissions affect the balance between neuronal excitation and inhibition, the ratio of excitatory synaptic inputs that individual lamina II neurons receive within the circuitry to inhibitory inputs recorded in the same SG neuron was estimated. In the adapting firing SG neurons, the ratio of the median sEPSC frequency to the median sIPSC frequency was 21 ($n = 13$) in the control, but 65 ($n = 15$) in CFA-inflamed conditions (**Fig. 3D–E**), indicating that peripheral inflammation markedly (~3-fold, $P < 0.05$ Mann–Whitney U test) shifts the balance between synaptic excitation and inhibition of this type of neurons toward their excitation. In contrast, this ratio in the tonic firing SG neurons was 92 ($n = 11$) in the control and 21 ($n = 7$) in CFA-inflamed conditions, demonstrating a substantial (~4-fold), yet nonsignificant ($p = 0.085$ Mann–Whitney U test), shift in the

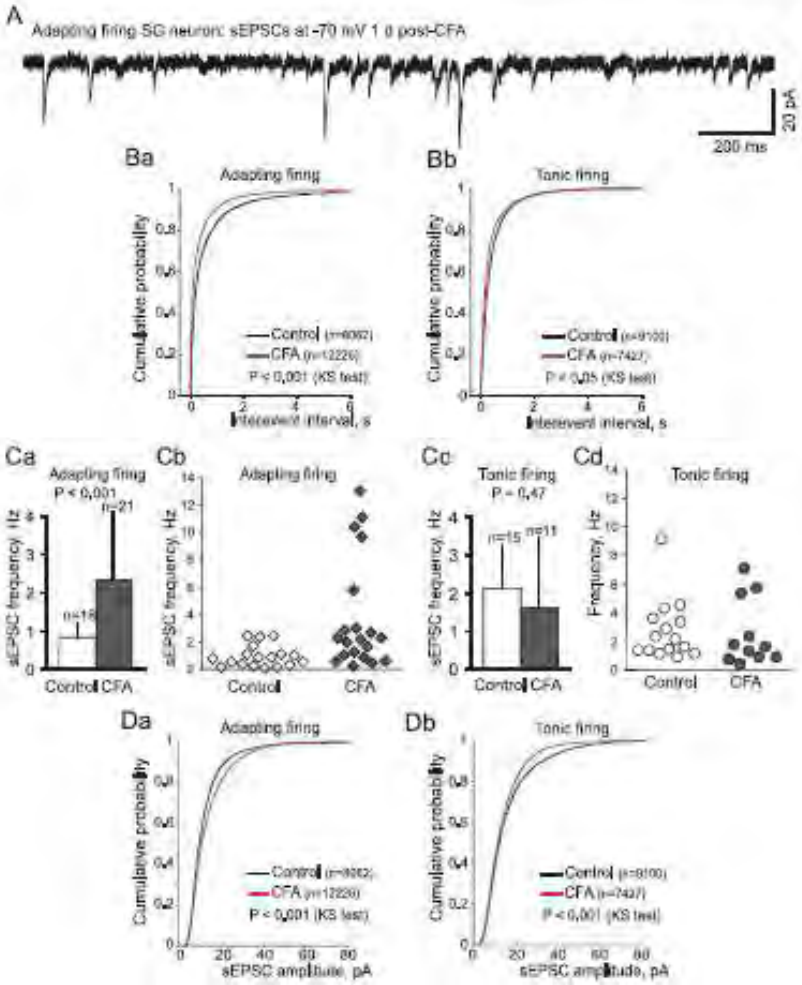

Figure 2. Persistent peripheral inflammation increases excitatory synaptic drive to different types of lamina II DH neurons. (A) An example of spontaneous excitatory postsynaptic currents (sEPSCs) recorded at −70 mV in the adapting firing *Substantia gelatinosa* (SG) neurons 1 day after CFA. Note the substantially increased sEPSC frequency 1 day after CFA compared with that in the control shown in Fig. 1B (right example). (B) Cumulative probability plots for the interevent interval of sEPSCs show the difference between control and persistent inflammatory conditions for the adapting firing (Ba) and the tonic firing SG neurons (Bb). The Kolmogorov–Smirnov test significance is indicated. (C) Statistical summaries (Ca and Cc) and scatter plots (Cb and Cd) of the sEPSC frequency in the adapting firing (18 cells in control and 21 cells 1 day after CFA) and the tonic firing SG neurons (15 cells in control and 11 cells 1 day after CFA) demonstrate the increased sEPSC frequency in the adapting firing neurons 1 day after CFA. Data are expressed as median and interquartile ranges. Mann–Whitney *U* test significance is indicated. (D) Cumulative probability plots for the sEPSC amplitude in the adapting firing (Da) and the tonic firing SG neurons (Db) demonstrate the opposite changes of sEPSC amplitude in these types of neurons during persistent inflammation. The Kolmogorov–Smirnov test significance is indicated.

balance between excitation and inhibition of this subset of neurons toward their inhibition during persistent inflammation (**Fig. 3D, F**).

Together, these data indicate that persistent peripheral inflammation substantially shifts the balance between neuronal excitation and inhibition within the DH circuitry in reciprocal manner: toward excitation of the adapting firing SG neurons, although toward inhibition of the tonic firing SG neurons.

3.3. Inflammatory-induced changes in synaptic AMPAR functioning are neuron-type specific

Finally, we investigated how persistent inflammation changes the AMPAR-mediated neurotransmission and synaptic AMPAR functioning in different types of DH neurons. Previous studies[14,17,32,49] showed the changed AMPAR trafficking at the first-order synapses between primary afferents and DH neurons during persistent peripheral inflammation due to promoted internalization of GluR2-containing AMPARs that resulted in a switch of GluR2-containing AMPARs to GluR2-lacking AMPARs at these synapses.[14,32] Nevertheless, the neuronal type where synaptic GluR2-containing AMPARs undergo internalization remains unknown. Moreover, functioning of synaptic AMPARs during persistent peripheral inflammation has not been studied in different types of lamina II interneurons throughout the DH circuitry.

To reveal how persistent inflammation changes functioning of postsynaptic AMPARs in various types of lamina II DH neurons, AMPAR-mediated miniature postsynaptic currents were studied in the adapting firing and in the tonic firing SG neurons. A cocktail of blockers consisting of APV, bicuculline, strychnine, TTX, and $CdCl_2$ (see Methods) was used to block ionotropic NMDA,

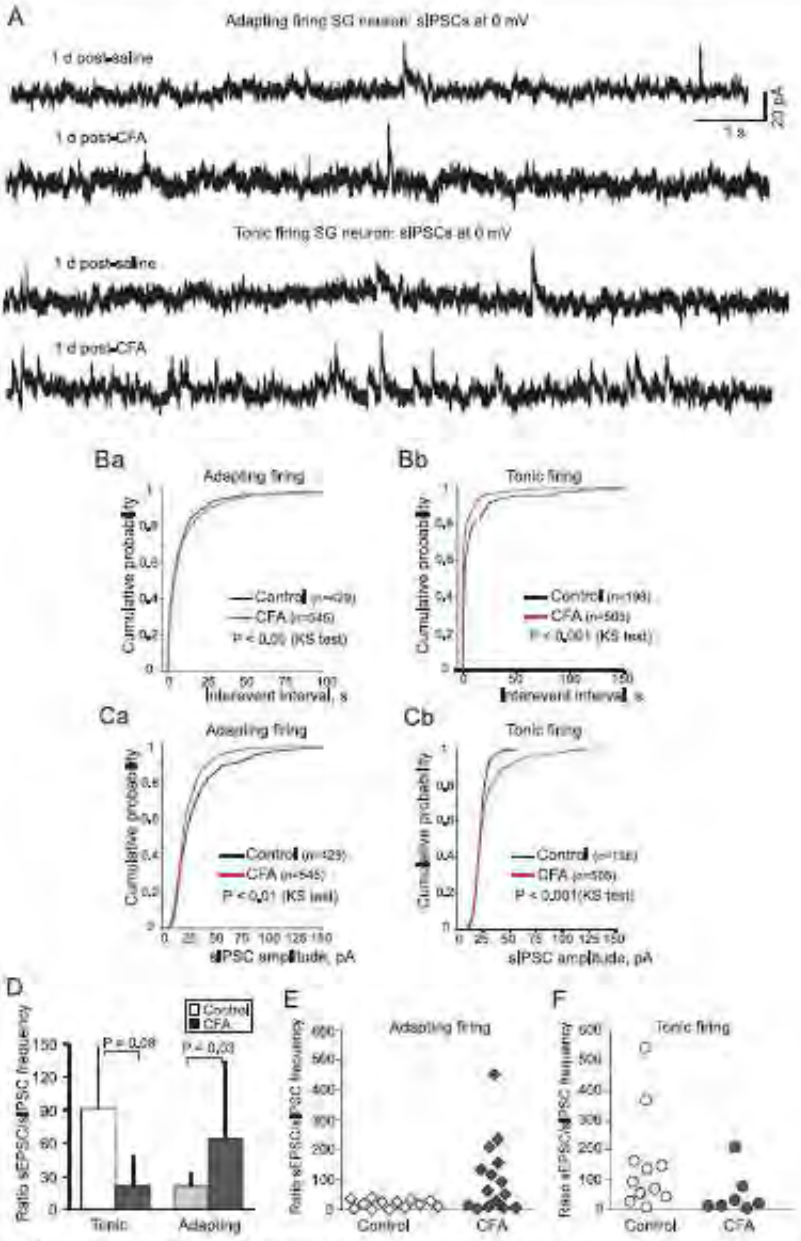

Figure 3. Persistent peripheral inflammation shifts the balance between synaptic excitation and inhibition of lamina II-OH neurons in a cell type–specific manner. (A) Typical recordings of spontaneous inhibitory postsynaptic currents (sIPSCs) obtained at 0 mV after recordings of spontaneous excitatory postsynaptic currents (sEPSCs) at −70 mV in individual adapting firing and the tonic firing *Substantia gelatinosa* (SG) neurons in control and persistent inflammatory conditions. (B) Cumulative probability plots for the sIPSC interevent intervals in the adapting firing (Ba) and the tonic firing (Bb) SG neurons demonstrate the opposite changes in the interevent intervals in different neuronal types during persistent inflammation. The Kolmogorov–Smirnov test significance is indicated. (C) Cumulative probability plots for the amplitudes of sIPSCs in the adapting firing (Ca) and the tonic firing (Cb) SG neurons demonstrate the opposite changes in different neuronal types during persistent inflammation. The Kolmogorov–Smirnov test significance is indicated. (D–F) A statistical summary (D) and scatter plots for the ratio of sEPSC frequency to sIPSC frequency calculated for individual adapting firing (E) and the tonic firing (F) SG neurons in the control and 1 day after CFA (15 adapting firing neurons in the control and 17 in 1 day after CFA; 11 tonic firing neurons in the control and 7 in 1 day after CFA). Note substantial changes in the balance between neuronal excitation and inhibition during persistent inflammation that was shifted in a cell type–specific and reciprocal manner. Data are expressed as median and interquartile ranges. Mann–Whitney *U* test significance is indicated.

$GABA_A$, and glycine receptors, and voltage-gated sodium and calcium channels that contribute to spontaneous glutamate release. First, the parameters of sEPSCs recorded before cocktail administration with those of mEPSCs recorded after prolonged (about 10 minutes) presence of blockers were compared for each type of neurons. The mEPSC frequency was lower than that of sEPSCs in the adapting firing SG neurons (by 69%, $P < 0.0001$, the Kolmogorov–Smirnov test) and was not significantly different in the tonic firing SG neurons ($P > 0.05$, the Kolmogorov–Smirnov test). The mEPSC amplitude was smaller than that of

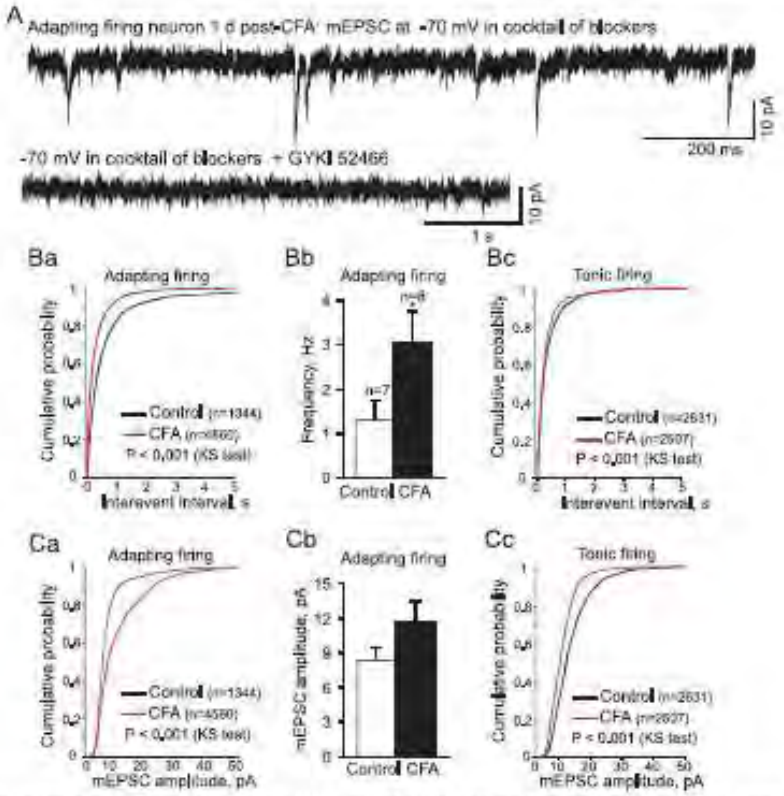

Figure 4. Persistent peripheral inflammation differentially changes AMPA receptor (AMPAR)-mediated miniature excitatory postsynaptic currents (mEPSCs) in different types of lamina II DH neurons. (A) Typical recording of AMPAR-mediated mEPSCs at −70 mV in the presence of TTX, $CdCl_2$, and blockers of ligand gated channels (APV, bicuculline, strychnine) in the adapting firing SG neuron 1 day after CFA (top). Note that selective AMPAR blocker GYKI52466 completely inhibited mEPSCs (bottom). (B) Cumulative probability plots for the mEPSC interevent interval in the adapting firing (Ba) and the tonic firing (Bc) SG neurons demonstrate the opposite changes in mEPSC frequency in different neuronal types during persistent inflammation. The Kolmogorov–Smirnov test significance is indicated. (Bb) A statistical summary of the mEPSC frequency calculated for 7 adapting firing SG neurons in the control and 8 cells 1 day after CFA validates the increased frequency in the adapting firing SG neurons during persistent inflammation. Data are expressed as a mean with SEM. *$P < 0.05$ (unpaired t test). (C) Cumulative probability plots for the mEPSC amplitude in the adapting firing (Ca) and the tonic firing (Cc) SG neurons show the opposite changes in mEPSC amplitude in these neuronal types during persistent inflammation. The Kolmogorov–Smirnov test significance is indicated. (Cb) A statistical summary of the mEPSC amplitude calculated as the mean of amplitude for each of 7 adapting firing SG neurons tested in control and 8 in 1 day after CFA validates the increased amplitude in the adapting firing SG neurons during persistent inflammation. Data are expressed as a mean with SEM.

sEPSCs in both the adapting firing (by 34%, $P < 0.001$, the Kolmogorov–Smirnov test) and the tonic firing SG neurons (by 26%, $P < 0.001$, the Kolmogorov–Smirnov test). Differences in both frequencies and amplitudes between sEPSCs and mEPSCs reflect an impact of action potential-dependent postsynaptic currents to synaptic events. A selective blocker of AMPARs GYKI52466 completely inhibited mEPSCs, confirming that the currents were solely mediated by AMPARs (**Fig. 4A**).

Persistent peripheral inflammation increased the AMPAR-mediated synaptic activity throughout the DH circuitry. In total, 3975 AMPAR-mediated mEPSCs were recorded in 13 SG neurons in control and 7067 mEPSCs in 14 SG neurons 1 day after CFA. The interevent interval of mEPSCs was 646 milliseconds in the control and 376 milliseconds 1 day after CFA reflecting the increased mEPSC frequency during persistent inflammation (by 72%, $P < 0.001$, the Kolmogorov–Smirnov test). Given that changes in the mEPSC frequency mainly reflect presynaptic alterations, this increase indicates that inflammation boosts the probability of presynaptic neurotransmitter release within the DH circuitry.

Changes in the AMPAR-mediated synaptic activity during persistent inflammation were neuron-type specific. The mEPSC frequency was substantially increased in the adapting firing SG neurons (by 230%, $P < 0.001$, the Kolmogorov–Smirnov test; **Fig. 4Ba**), although slightly decreased in the tonic firing SG neurons 1 day after CFA (by 9%, $P < 0.001$, the Kolmogorov–Smirnov test; **Fig. 4Bc**) when the entire pools of events were compared between control and inflammatory conditions. An analysis of the mean mEPSC frequencies calculated for each tested neuron further showed a marked increase of the mEPSC frequency in the adapting firing SG neurons (by 137 ± 31%, $P < 0.05$ unpaired t test; **Fig. 4Bb**) and the absence of changes in the tonic firing SG neurons 1 day after CFA (2.1 ± 0.7 s^{-1}, n = 6 and 2.1 ± 0.8 s^{-1}, n = 6 in the control and 1 day after CFA, respectively, $P > 0.9$ unpaired t test). These data demonstrate that CFA-induced inflammation prominently increases the neurotransmitter release probability at the synapses of adapting firing SG neurons, whereas moderately decreases this probability at the synapses of tonic firing SG neurons. The mEPSC amplitudes were also changed in a cell type-specific manner. The amplitude was increased in the adapting firing SG neurons (by 42%, $P < 0.001$, the Kolmogorov–Smirnov test; **Fig. 4Ca**), but it was decreased in the tonic firing SG neurons (by 23%, $P < 0.001$, the

Kolmogorov–Smirnov test; **Fig. 4Cc**). An analysis of the mean of mEPSC amplitude calculated for individual neurons further showed a tendency toward the increased amplitude in the adapting firing SG neurons (by 39%, $P = 0.14$ unpaired t test; **Fig. 4Cb**), but not in the tonic firing ones 1 day after CFA (11.0 ± 1.5 pA, n = 6 and 9.6 ± 1.3 pA, n = 5 in the control and 1 day after CFA, respectively, $P > 0.5$ unpaired t test). The differentially changed AMPAR-mediated mEPSC amplitudes in both types of DH neurons might reflect distinct modulation in either AMPAR properties and/or the receptor subunit composition and imply opposite changes in trafficking of synaptic AMPARs in these neuronal types. This is reasonable given the dissimilarly changed synaptic drive in the tonic firing and the adapting firing SG neurons during persistent inflammation.

The subunit composition of AMPARs can be distinguished based on deactivation kinetics of AMPAR-mediated currents.[3,9,27] Taking into account that currents mediated by GluR2-containing AMPARs possess markedly slow deactivation kinetics, the decay kinetics of AMPAR-mediated mEPSCs and the probability density function of decay kinetics were analyzed to assess the inflammatory-induced changes in the proportion of GluR2-containing AMPARs at the synapses in different types of lamina II interneurons. The decay kinetics of mEPSCs were significantly changed between control and inflamed conditions when the entire pools of events were compared by the Kolmogorov–Smirnov test for the adapting firing ($P < 0.001$; **Fig. 5Aa**) and the tonic firing SG neurons ($P < 0.001$; **Fig. 5Ab**), which indicate altered subunit composition of synaptic AMPARs in either neuronal type during persistent inflammation. The averaged decay time of mEPSCs was increased in either the adapting firing (by 23%, $P < 0.001$, the Kolmogorov–Smirnov test) or the tonic firing SG neurons (by 23%, $P < 0.001$, the Kolmogorov–Smirnov test) 1 day after CFA. The prolonged decay kinetics along with the increased amplitude of mEPSCs resulted in the increased area of currents in the adapting firing SG neurons (by 40%, $P < 0.001$, the Kolmogorov–Smirnov test; **Fig. 5Ba**), while the area of currents was slightly, but significantly, decreased in the tonic firing SG neurons (by 7%, $P < 0.001$, the Kolmogorov–Smirnov test; **Fig. 5Bb**). Having in mind slower deactivation kinetics of currents mediated by GluR2-containing AMPARs,[3,9,27] the prolonged decay time of mEPSCs might reflect the increased proportion of GluR2-containing receptors at synapses. An analysis of the probability density function of mEPSC decay kinetics further supported this increase for the adapting firing SG neurons showing the substantial decrease in the proportion of mEPSCs with fast decay in favor of currents with prolonged decay kinetics 1 day after CFA (**Fig. 5C**). These findings along with the increased mEPSC amplitude cumulatively indicate the increased proportion of GluR2-containing AMPARs at the synapses of adapting firing neurons during persistent inflammation. This might be attributed to promoted incorporation of GluR2-containing AMPARs in the conditions of augmented excitatory drive to these neurons. At the same time, the probability density of mEPSC decay kinetics was rearranged in the tonic firing SG neurons in a different manner. In contrast to the adapting firing neurons, the probability density of decay kinetics was shifted toward slower decay, still keeping its basic profile (**Fig. 5D**). The latter along with the opposite changes in mEPSC amplitude and area in the tonic firing SG neurons 1 day after CFA directs at principally different mechanism mediating synaptic AMPAR changes in this neuronal population. A decrease in the mEPSC amplitude very likely reflects a decrease in the number of postsynaptic receptors that might mediate changes in AMPAR trafficking at the first-order synapses between primary afferents and DH neurons in persistent inflammatory pain conditions.[14,32]

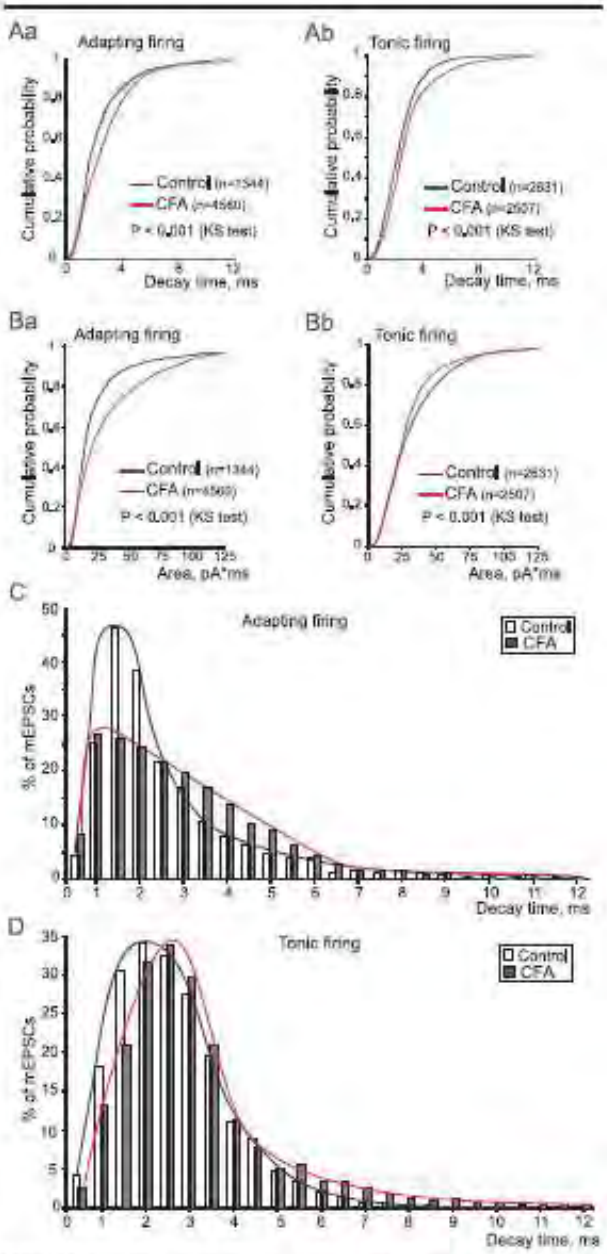

Figure 5. Persistent peripheral inflammation rearranges the distributions of AMPA receptor (AMPAR)-mediated miniature excitatory postsynaptic currents (mEPSC) decay kinetics in a neuronal type–specific manner. (A and B) Cumulative probability plots for the mEPSC decay time (A) and the integrated current area (B) of the entire pool of AMPAR-mediated mEPSCs in the adapting firing (Aa and Ba) and the tonic firing (Ab and Bb) *Substantia gelatinosa* (SG) neurons in the control and 1 day after CFA. The Kolmogorov–Smirnov test significance is indicated. (C and D) The probability density functions of mEPSC decay kinetics in the adapting firing (C) and the tonic firing (D) SG neurons in control and 1 day after CFA show distinct profile of changes in different neuronal types during inflammation. Blue (control) and red (CFA) lines are spline lines for the corresponding functions.

4. Discussion

The balance between excitatory and inhibitory transmissions in the DH is critical for normal sensory transduction. Changes in this balance can result in abnormal pain sensation and be a basis for development of chronic pain. We studied excitatory and inhibitory

transmissions in different types of lamina II neurons and found that persistent peripheral inflammation increases excitability of the DH circuitry and differentially shifts neuronal excitation and inhibition toward excitation of lamina II neurons characterized by intrinsic adapting firing properties, while toward inhibition of those revealing the tonic firing pattern of discharge. The changes in DH circuitry were accompanied by the cell type–specific changes in synaptic AMPARs.

4.1. Inflammatory-induced dorsal horn hyperexcitability

Persistent peripheral inflammation augments the DH excitability and alters excitatory AMPAR-mediated transmission throughout the circuitry. Given that changes in mEPSC frequency directly evidence the changes in presynaptic mechanisms of neurotransmitter release, while changes in sEPSCs also reflect changes in presynaptic action potential–dependent activity, the augmented frequency of both sEPSCs and mEPSCs in DH neurons 1 day after CFA indicates that inflammation potentiates both action potential–dependent and -independent glutamate release from primary afferents and/or spinal interneurons. Meanwhile, altered mEPSC amplitude and kinetics argue for the reorganization in postsynaptic receptor pools during persistent inflammation. Consistently, increased excitatory transmission in DH neurons was observed during injury-related neuropathies[2,4,8,15,53] and is thought to be responsible for the development and maintenance of long-lasting pain.[38,42,48] A physiologically plausible scenario of persistent pain consists of the initiation of hypersensitivity by repeated bursts of action potentials, produced by peripheral tissue inflammation or nerve injury, that provoke ectopic firing of sensory afferents.[26,51] This is accompanied by enhanced glutamate release from the active primary afferent terminals over highly interconnected DH circuits,[23] which subsequently increases excitability of DH interneurons that may be sustainable because of complex postsynaptic changes.

4.2. Neuron type–specific changes in excitatory transmission

Lamina II neurons receive synaptic inputs from primary afferents and from both excitatory and inhibitory interneurons within the DH. The proportion of these inputs could, in principle, differ between neuronal populations and our results provide evidence supporting that. Both sEPSC frequencies and amplitudes vary between neuronal populations in control conditions. Furthermore, the ratio of excitatory and inhibitory synaptic inputs received by 2 types of neurons was found to vary prominently (up to 8 times). The aforementioned suggests their distinct functional roles in DH circuitry.

Although there is currently a lack of unique classification able to cover a high diversity of DH neurons, some classifications of neuronal morphology, neurochemical phenotype, and electrophysiological properties are widely used.[10,11,54,55] Among them, a firing pattern is generally consistent with the type of released neurotransmitter, although there is still little correlation with neuronal morphology.[11,12] Cumulative evidence indicates that DH neurons exhibiting A type potassium channel–related patterns are most probably excitatory glutamatergic interneurons, whereas neurons revealing tonic firing pattern are inhibitory interneurons.[1,10,13,28,37,55] Although firing pattern does not indisputably reflect neurochemical phenotype as a number of excitatory neurons (expressing VGLUT2 [55] or generating evoked EPSCs[40]) still showed a tonic firing pattern, whereas some inhibitory cells (expressing VGAT) revealed adapting firing pattern,[55] most tonic firing neurons are very likely inhibitory interneurons, whereas the adapting firing ones predominantly represent a population of excitatory glutamatergic interneurons. Moderate excitatory drive received by the adapting firing neurons in control and its prominent increase during persistent inflammation also support the excitatory role of these neurons.

4.3. Neuron type–specific changes in inhibitory transmission

The inflammatory-induced DH hyperexcitability originates from the changes in both excitatory and inhibitory transmissions. These changes were distinct in different types of DH neurons that process nociceptive information. Moreover, the changes in inhibitory transmission were opposite to those in an excitatory one. The inhibitory drive was decreased in the adapting firing, but increased in the tonic firing neurons, whilst excitatory drive was increased in both neuronal populations in different proportions. These results are consistent with the cell type–specific changes in inhibitory transmission in DH neurons observed during chronic neuropathic pain.[12,24] The reciprocal changes in both frequency and amplitude of sIPSCs indicate different presynaptic and postsynaptic mechanisms mediating them. A reduced presynaptic GABA release in the superficial DH, reported for peripheral pain conditions,[31] may underlie the decreased sIPSC amplitude in the adapting firing neurons, whereas shifted transmembrane chloride gradient[6] might be considered as alternative postsynaptic mechanism because the $GABA_A$ receptor expression was not altered during neuropathic pain.[31,34,36]

The inflammatory-induced changes in both excitatory and inhibitory drives shifted the balance between neuronal excitation and inhibition, indicating a rearrangement of synaptic excitation and inhibition within the circuitry. In the context of firing pattern correlation to neurochemical phenotype,[1,10,13,37,55] persistent inflammation boosts excitatory drive to the adapting firing, presumably excitatory, DH interneurons while concomitantly lowers it to the tonic firing, most likely inhibitory, interneurons. A loss of inhibition within the DH circuits was accompanied by abnormal pain sensation and development of chronic pain, associated with allodynia, hyperalgesia, and spontaneous pain.[6,31,33,39,47] Increased inhibitory drive observed specifically in the tonic firing, apparently inhibitory, interneurons could, in principle, contribute to this phenomenon and is consistent with concomitantly reduced excitatory drive to these neurons. Decreased tone of inhibitory interneurons may affect local neuronal circuits being a prerequisite for disinhibition of excitatory interneurons within nociceptive pathways. Inflammatory-induced decrease of sIPSC frequency in the adapting firing, presumably excitatory, interneurons also supports this suggestion.

4.4. Neuron type–specific changes in synaptic AMPAR functioning

The inflammatory-induced DH hyperexcitability was accompanied by the augmented AMPAR-mediated transmission and changed postsynaptic AMPAR functioning in different types of DH neurons. Both AMPAR-mediated mEPSC amplitude and kinetics profile were changed in the tonic firing and the adapting firing neurons in a distinct manner, suggesting different mechanisms of synaptic AMPAR trafficking. This difference could be related to the apparently nonidentical constitutive mechanisms of AMPAR trafficking in excitatory and inhibitory interneurons assumed from the higher surface expression of GluR1 in inhibitory DH interneurons, while GluR2 in excitatory ones.[1,7,36,44] The promoted insertion of

GluR1-containing AMPARs into extrasynaptic membranes of DH neurons during persistent inflammation was cell-type specific,[18,19] further suggesting different activity-dependent AMPAR trafficking between neuronal types.

The increased mEPSC amplitude in the adapting firing neurons implies an increased number of AMPARs at their synapses apparently due to additional receptor insertion. In addition, (1) the mEPSC decay kinetics was prolonged, and (2) the proportion of currents with fast decay was decreased in the adapting firing neurons, suggesting the increased proportion of GluR2-containing AMPARs at synapses.[9,27] The inflammatory-promoted incorporation of synaptic GluR2-containing AMPARs in the adapting firing neurons may represent a physiologically relevant mechanism of intrinsic adaptation of excitatory interneurons, enabling to increase action potential firing[27,41] and concomitantly avoid Ca^{2+}-induced excitotoxicity, provoked by extended activation of GluR2-lacking Ca^{2+}-permeable AMPARs.[25] This may adjust synaptic strength within the circuitry in the conditions of augmented afferent drive during persistent inflammation.

In the tonic firing neurons, the mEPSC decay kinetics were also prolonged 1 day after CFA, implying an increase in the proportion of GluR2-containing AMPARs at these synapses. However, the mEPSC amplitude was decreased, and the distribution profile of mEPSC decay kinetics was changed in a distinct manner than in the adaptive firing neurons, suggesting principally different mechanism mediating AMPAR changes. Notably, AMPAR trafficking varies not only between neuronal subtypes but also between different synapses in individual interneurons because the increased proportion of GluR2-containing AMPARs shown here for the entire pool of synapses coincides with internalization of GluR2-containing AMPARs from the first-order synapses between C-fiber afferents and lamina II neurons during inflammation.[14,32,40] This internalization and increased number of Ca^{2+}-permeable AMPARs at the first-order synapses[32,40] may lead to an increased cytoplasmic Ca^{2+} concentration and Ca^{2+}-induced excitotoxicity[25] causing the loss of these neurons within the circuitry. The decreased inhibitory synaptic drive to the adapting firing (presumably excitatory) but not to the tonic firing neurons (**Fig. 3**) suggests this loss that contributes to the DH hyperexcitability. Increased cytoplasmic $[Ca^{2+}]$ level may also promote release of inhibitory retrograde messenger[24] that, in turn, would cause presynaptic depression of excitatory drive to the tonic firing neurons, retarding them within the circuitry. The retrograde-dependent presynaptic inhibition in glutamatergic synapses has recently been found to depend on postsynaptic Ca^{2+} rise in GABAergic DH interneurons in chronic neuropathic pain.[24] Nevertheless, this is rather unlikely because the AMPAR-mediated mEPSC frequency was increased in the tonic firing neurons in persistent inflammatory pain (**Fig. 4**).

Changes in AMPAR properties also might be provoked by altered AMPAR binding to auxiliary proteins, eg, transmembrane AMPAR regulatory proteins (TARPs), which were found to prolong the current kinetics[5,16,30] and increase the single channel conductance.[43] The contribution of TARPs to AMPAR properties in DH neurons remains unknown, although the abundant TARP expression reported in spinal cord[22] may associate possible TARP involvement to mEPSC changes as one of molecular mechanisms mediating altered AMPAR properties and/or trafficking during persistent inflammation.

Cumulatively, synaptic AMPAR functioning was differentially changed in the adapting firing and the tonic firing DH neurons during persistent peripheral inflammation, implying neuron type–specific adjustment of synaptic strength within the DH circuitry that may contribute to the maintenance of DH hyperexcitability and chronic inflammatory pain.

Conflict of interest statement

The authors have no conflicts of interest to declare.

This work was supported by NASU Biotechnology, SFFR F50/090 Grants (N.V), STCU #5510, SFFR F46.2/001 Grants (P.B), and NASU Grant for Young Scientists (O.K).

Acknowledgments

The authors thank V. Cherkas for technical assistance. The authors thank Anne E. King, Professor of Translational Neuroscience, for her editorial assistance.

Article history:
Received 15 April 2014
Received in revised form 28 November 2014
Accepted 2 December 2014
Available online 14 January 2015

References

[1] Albuquerque C, Lee CJ, Jackson AC, MacDermott AB. Subpopulations of GABAergic and non-GABAergic rat dorsal horn neurons express Ca2+-permeable AMPA receptors. Eur J Neurosci 1999;11:2758–66.
[2] Balasubramanyan S, Stemkowski PL, Stebbing MJ, Smith PA. Sciatic chronic constriction injury produces cell-type-specific changes in the electrophysiological properties of rat substantia gelatinosa neurons. J Neurophysiol 2006;96:579–90.
[3] Burnashev N, Monyer H, Seeburg PH, Sakmann B. Divalent ion permeability of AMPA receptor channels is dominated by the edited form of a single subunit. Neuron 1992;8:189–98.
[4] Chen Y, Balasubramanyan S, Lai AY, Todd KG, Smith PA. Effects of sciatic nerve axotomy on excitatory synaptic transmission in rat substantia gelatinosa. J Neurophysiol 2009;102:3203–15.
[5] Cho CH, St-Gelais F, Zhang W, Tomita S, Howe JR. Two families of TARP isoforms that have distinct effects on the kinetic properties of AMPA receptors and synaptic currents. Neuron 2007;55:890–904.
[6] Coull JAM, Boudreau D, Bachand K, Prescott SA, Nault F, Sik A, De Koninck P, De Koninck Y. Trans-synaptic shift in anion gradient in spinal lamina I neurons as a mechanism of neuropathic pain. Nature 2003;424:938–42.
[7] Engelman HS, Allen TB, MacDermott AB. The distribution of neurons expressing calcium-permeable AMPA receptors in the superficial laminae of the spinal cord dorsal horn. J Neurosci 1999;19:2081–9.
[8] Fukushima T, Takasusuki T, Tomitori H, Hori Y. Possible involvement of syntaxin 1A downregulation in the late phase of allodynia induced by peripheral nerve injury. Neuroscience 2011;175:344–57.
[9] Geiger JR, Melcher T, Koh DS, Sakmann B, Seeburg PH, Jonas P, Monyer H. Relative abundance of subunit mRNAs determines gating and Ca2+ permeability of AMPA receptors in principal neurons and interneurons in rat CNS. Neuron 1995;15:193–204.
[10] Graham BA, Brichta AM, Callister RJ. Moving from an averaged to specific view of spinal cord pain processing circuits. J Neurophysiol 2007;98:1057–63.
[11] Grudt TJ, Perl ER. Correlations between neuronal morphology and electrophysiological features in the rodent superficial dorsal horn. J Physiol 2002;540:189–207.
[12] Gustafson-Vickers SL, Lu VB, Lai AY, Todd KG, Balanyi K, Smith PA. Long-term actions of interleukin-1beta on delay and tonic firing neurons in rat superficial dorsal horn and their relevance to central sensitization. Mol Pain 2008;4:63.
[13] Hantman AW, van den Pol AN, Perl ER. Morphological and physiological features of a set of spinal substantia gelatinosa neurons defined by green fluorescent protein expression. J Neurosci 2004;24:836–42.
[14] Hartmann B, Ahmadi S, Heppenstall PA, Lewin GR, Schott C, Bordoni T, Seeburg PH, Zeilhofer HU, Sprengel R, Kuner R. The AMPA receptor subunits GluR-A and GluR-B reciprocally modulate spinal synaptic plasticity and inflammatory pain. Neuron 2004;44:637–50.
[15] Inquimbert P, Bartels K, Babaniyi OB, Barrett LB, Tegeder I, Scholz J. Peripheral nerve injury produces a sustained shift in the balance between

glutamate release and uptake in the dorsal horn of the spinal cord. PAIN 2012;153:2422–31.
[16] Jackson AC, Nicoll RA. Stargazin (TARP gamma-2) is required for compartment-specific AMPA receptor trafficking and synaptic plasticity in cerebellar stellate cells. J Neurosci 2011;31:3939–52.
[17] Katano T, Furue H, Okuda-Ashitaka E, Tagaya M, Watanabe M, Yoshimura M, Ito S. N-ethylmaleimide-sensitive fusion protein (NSF) is involved in central sensitization in the spinal cord through GluR2 subunit composition switch after inflammation. Eur J Neurosci 2008;27:3161–70.
[18] Kopach O, Kao SC, Petralia RS, Belan P, Tao YX, Voitenko N. Inflammation alters trafficking of extrasynaptic AMPA receptors in tonically firing lamina II neurons of the rat spinal dorsal horn. PAIN 2011;152:912–23.
[19] Kopach O, Valchenko-Karpinski V, Allanjon FE, Belan P, Tao YX, Voitenko N. PKCα is required for inflammation-induced trafficking of extrasynaptic AMPA receptors in tonically firing lamina II dorsal horn neurons during the maintenance of persistent inflammatory pain. J Pain 2013;14:182–92.
[20] Kopach O, Valchenko-Karpinski V, Belan P, Voitenko N. Development of inflammation-induced hyperalgesia and allodynia is associated with the upregulation of extrasynaptic AMPA receptors in tonically firing lamina II dorsal horn neurons. Front Physiol 2012;3:391.
[21] Kopach O, Voitenko N. Extrasynaptic AMPA receptors in the dorsal horn: evidence and functional significance. Brain Res Bull. 2013;93:47–56.
[22] Larsson M, Agalave N, Watanabe M, Svensson CI. Distribution of transmembrane AMPA receptor regulatory protein (TARP) isoforms in the rat spinal cord. Neuroscience 2013;248C:180–93.
[23] Latremoliere A, Woolf CJ. Central sensitization: a generator of pain hypersensitivity by central neural plasticity. J Pain 2009;10:895–926.
[24] Leitner J, Westerholz S, Heinke B, Forsthuber L, Wunderbaldinger G, Jäger T, Gruber-Schoffnegger D, Braun K, Sandkühler J. Impaired excitatory drive to spinal GABAergic neurons of neuropathic mice. PLoS One 2013;8:e73370.
[25] Leonoudakis D, Zhao P, Beattie EC. Rapid tumor necrosis factor alpha-induced exocytosis of glutamate receptor 2-lacking AMPA receptors to extrasynaptic plasma membrane potentiates excitotoxicity. J Neurosci 2008;28:2119–30.
[26] Liu H, Mantyh PW, Basbaum AI. NMDA-receptor regulation of substance P release from primary afferent nociceptors. Nature 1997;386:721–4.
[27] Liu SQ, Cull-Candy SG. Synaptic activity at calcium-permeable AMPA receptors induces a switch in receptor subtype. Nature 2000;405:454–8.
[28] Lu Y, Perl ER. A specific inhibitory pathway between substantia gelatinosa neurons receiving direct C-fiber input. J Neurosci 2003;23:8752–8.
[29] Melnick IV, Santos SFA, Safronov BV. Mechanism of spike frequency adaptation in substantia gelatinosa neurones of rat. J Physiol 2004;559:383–95.
[30] Milstein AD, Zhou W, Karimzadegan S, Bredt DS, Nicoll RA. TARP subtypes differentially and dose-dependently control synaptic AMPA receptor gating. Neuron 2007;55:905–18.
[31] Moore KA, Kohno T, Karchewski LA, Scholz J, Baba H, Woolf CJ. Partial peripheral nerve injury promotes a selective loss of GABAergic inhibition in the superficial dorsal horn of the spinal cord. J Neurosci 2002;22:6724–31.
[32] Park JS, Voitenko N, Petralia RS, Guan X, Xu JT, Steinberg JP, Takamiya K, Sotnik A, Kopach O, Huganir RL, Tao YX. Persistent inflammation induces GluR2 internalization via NMDA receptor-triggered PKC activation in dorsal horn neurons. J Neurosci 2009;29:3206–19.
[33] Polgár E, Hughes DI, Arham AZ, Todd AJ. Loss of neurons from laminas I–III of the spinal dorsal horn is not required for development of tactile allodynia in the spared nerve injury model of neuropathic pain. J Neurosci 2005;25:6658–66.
[34] Polgár E, Hughes DI, Riddell JS, Maxwell DJ, Puskár Z, Todd AJ. Selective loss of spinal GABAergic or glycinergic neurons is not necessary for development of thermal hyperalgesia in the chronic constriction injury model of neuropathic pain. PAIN 2003;104:229–39.
[35] Polgár E, Todd AJ. Tactile allodynia can occur in the spared nerve injury model in the rat without selective loss of GABA or GABA(A) receptors from synapses in laminae I–II of the ipsilateral spinal dorsal horn. Neuroscience 2008;156:193–202.
[36] Polgár E, Watanabe M, Hartmann B, Grant SG, Todd AJ. Expression of AMPA receptor subunits at synapses in laminae I–III of the rodent spinal dorsal horn. Mol Pain 2008;4:5.
[37] Punnakkal P, von Schoultz C, Haenraets K, Wildner H, Zeilhofer HU. Morphological, Biophysical and Synaptic Properties of Glutamatergic Neurons of the Mouse Spinal Dorsal Horn. J Physiol 2014;592:759–76.
[38] Sandkühler J. Understanding LTP in pain pathways. Mol Pain 2007;3:9.
[39] Sandkühler J. Models and mechanisms of hyperalgesia and allodynia. Physiol Rev 2009;89:707–58.
[40] Santos SFA, Rebelo S, Derkach VA, Safronov BV. Excitatory interneurons dominate sensory processing in the spinal substantia gelatinosa of rat. J Physiol 2007;581:241–54.
[41] Savtchouk I, Liu SJ. Remodeling of synaptic AMPA receptor subtype alters the probability and pattern of action potential firing. J Neurosci 2011;31:501–11.
[42] Scholz J, Woolf CJ. The neuropathic pain triad: neurons, immune cells and glia. Nat Neurosci 2007;10:1361–8.
[43] Shelley C, Farrant M, Cull-Candy SG. TARP-associated AMPA receptors display an increased maximum channel conductance and multiple kinetically distinct open states. J Physiol 2012;590:5723–38.
[44] Spike R, Kerr R, Maxwell DJ, Todd AJ. GluR1 and GluR2/3 subunits of the AMPA-type glutamate receptor are associated with particular types of neurone in laminae I–III of the spinal dorsal horn of the rat. Eur J Neurosci 1998;10:324–33.
[45] Takazawa T, MacDermott AB. Synaptic pathways and inhibitory gates in the spinal cord dorsal horn. Ann N Y Acad Sci 2010;1198:153–8.
[46] Todd AJ. Neuronal circuitry for pain processing in the dorsal horn. Nat Rev Neurosci 2010;11:823–36.
[47] Torsney C, MacDermott AB. Disinhibition opens the gate to pathological pain signaling in superficial neurokinin 1 receptor-expressing neurons in rat spinal cord. J Neurosci 2006;26:1833–43.
[48] Tsuda M, Inoue K, Salter MW. Neuropathic pain and spinal microglia: a big problem from molecules in "small" glia. Trends Neurosci 2005;28:101–7.
[49] Vikman KS, Rycroft BK, Christie MJ. Switch to Ca2+-permeable AMPA and reduced NR2B NMDA receptor-mediated neurotransmission at dorsal horn nociceptive synapses during inflammatory pain in the rat. J Physiol 2008;586:515–27.
[50] Voitenko N, Gerber G, Youn D, Randic M. Peripheral inflammation-induced increase of AMPA-mediated currents and Ca2+ transients in the presence of cyclothiazide in the rat substantia gelatinosa neurons. Cell Calcium 2004;35:461–9.
[51] Xie W, Strong JA, Meij JTA, Zhang JM, Yu L. Neuropathic pain: early spontaneous afferent activity is the trigger. PAIN 2005;116:243–56.
[52] Xu Q, Yaksh TL. A brief comparison of the pathophysiology of inflammatory versus neuropathic pain. Curr Opin Anaesthesiol 2011;24:400–7.
[53] Yan X, Weng HR. Endogenous interleukin-1β in neuropathic rats enhances glutamate release from the primary afferents in the spinal dorsal horn through coupling with presynaptic N-methyl-D-aspartic acid receptors. J Biol Chem 2013;288:30544–57.
[54] Yasaka T, Kato G, Furue H, Rashid MH, Sonohata M, Tamae A, Murata Y, Masuko S, Yoshimura M. Cell-type-specific excitatory and inhibitory circuits involving primary afferents in the substantia gelatinosa of the rat spinal dorsal horn in vitro. J Physiol 2007;581:603–18.
[55] Yasaka T, Tiong SYX, Hughes DI, Riddell JS, Todd AJ. Populations of inhibitory and excitatory interneurons in lamina II of the adult rat spinal dorsal horn revealed by a combined electrophysiological and anatomical approach. PAIN 2010;151:475–88.

3.2. Клітинноспецифічні зміни у балансі між синаптичним збудженням та гальмуванням у нейронних мережах дорзального рогу внаслідок травми спинного мозку призводять до спастичності та хронічного болю

www.nature.com/scientificreports

SCIENTIFIC REPORTS

OPEN

Received: 1 November 2016
Accepted: 1 June 2017
Published online: 19 July 2017

Opposite, bidirectional shifts in excitation and inhibition in specific types of dorsal horn interneurons are associated with spasticity and pain post-SCI

Olga Kopach[1,2], Volodymyr Medvediev[3], Volodymyr Krotov[1], Anya Borisyuk[1], Vitaliy Tsymbaliuk[3] & Nana Voitenko[1]

Spasticity, a common complication after spinal cord injury (SCI), is frequently accompanied by chronic pain. The physiological origin of this pain (critical to its treatment) remains unknown, although spastic motor dysfunction has been related to the hyperexcitability of motoneurons and to changes in spinal sensory processing. Here we show that the pain mechanism involves changes in sensory circuits of the dorsal horn (DH) where nociceptive inputs integrate for pain processing. Spasticity is associated with the DH hyperexcitability resulting from an increase in excitation and disinhibition occurring in two respective types of sensory interneurons. In the tonic-firing inhibitory lamina II interneurons, glutamatergic drive was reduced while glycinergic inhibition was potentiated. In contrast, excitatory drive was boosted to the adapting-firing excitatory lamina II interneurons while GABAergic and glycinergic inhibition were reduced. Thus, increased activity of excitatory DH interneurons coupled with the reduced excitability of inhibitory DH interneurons post-SCI could provide a neurophysiological mechanism of central sensitization and chronic pain associated with spasticity.

Spasticity is one of the most severe complications after spinal cord injury (SCI) or trauma, representing chronic motor deficit attributed with muscle spasms, hyperreflexia and impaired locomotion, which develops in up to 80% of the SCI patients[1–4]. With the irreversible motor dysfunctions, spasticity remains with limited options for an effective treatment focused primarily on reducing negative influences on an individual's quality of life[5]. However, chronic pain often progressively develops within months after SCI and could expand to severe and unceasing pain syndrome either rapidly or through various patterns of delayed appearance[5,6]. This pain is poorly treatable, which is, at least partly, due to poorly understood mechanisms of pain chronification.

It has emerged that the central mechanism of spasticity – hyperexcitability of motoneurons below lesion mediated by the plateau potentials and self-sustained firing – is causally related to changes in sensory processing in the spinal cord[7,8]. The primary afferent inputs and activity of the wide dynamic range interneurons in response to either noxious or innocuous stimuli were both augmented post-SCI[9–11], arguing for the hyperexcitability of the dorsal horn (DH), the area for sensory input integration and processing. Pathological signalling in sensory interneurons could involve a variety of impairments related to SCI, such as an upregulation of sodium channels[12,13], an increase in the extracellular glutamate level[14], a reduced GAD expression[15] and a shift in chloride gradient[16]. Notwithstanding the reported impairments at the cellular level, a neurophysiological explanation of pain remains elusive. Here we test the hypothesis that the pain mechanism involves changes in the DH circuitry with the key question how the overall hyperexcitability post-SCI relates to a high heterogeneity of DH interneurons.

To address this we combined electrophysiology with behavioural testing in experimental modelling of SCI in rats. Our findings proposed two complementary mechanisms contributing to the hyperexcitability of the DH

[1]Bogomoletz Institute of Physiology, Kyiv, Ukraine. [2]Institute of Neurology, University College London, London, UK. [3]Romodanov Institute of Neurosurgery, Kyiv, Ukraine. Correspondence and requests for materials should be addressed to O.K. (email: o.kopach@ucl.ac.uk) or N.V. (email: nana@biph.kiev.ua)

post-SCI – increased excitability of excitatory lamina II interneurons and suppressed activity of inhibitory lamina II interneurons – that provide novel insights into neurophysiological mechanisms underlying chronic pain.

Results

Spasticity and pain post-SCI. The SCI-injured rats were examined for the motor deficit of hindlimb and chronic pain postoperatively. Each animal displayed severe motor dysfunction of the hindlimb ipsilateral to hemisection side (n = 32), including impaired joint movements with increased muscle tone (Table 1, see Methods Section), impaired coordination between corpus and the hindlimb, resulting in paralytic posture. The deficit developed rapidly (within 1 week post-SCI) and remained steadily for at least 2–3 months by exceeding on average the level 1 on the Ashworth rating scale and lowering the level 7 on the BBB score ($p < 0.001$; Fig. 1a). The regression analysis demonstrated a strong correlation between the BBB and the Ashworth scores that gradually increased with a time post-SCI: the Pearson correlation coefficient was −0.54 ($p < 0.01$) at week 1 and −0.86 at week 5 post-SCI ($p < 0.001$, n = 32; Fig. 1b). Consistent to the increased muscle tone observed in the SCI-injured rats, the H-reflex recordings (Fig. 1c) demonstrated the impaired sensorimotor integration post-SCI. The ratio of the H- to the M-waves was markedly increased on the ipsilateral side in the SCI-injured rats at ~1 month post-SCI (by ~33% compared with contralateral side, $p < 0.001$, paired t-test, n = 27 rats and by ~29% compared with average ratio on the ipsilateral side of the sham-operated group, n = 8 animals, $p < 0.001$, unpaired t-test; Fig. 1c).

Experimental SCI was reported to increase peripheral sensitivity to various stimulus modalities[17–19] that may give rise to chronic pain. Therefore, we next examined changes in peripheral sensitivity of each hindlimb in the SCI-injured rats. We observed peripheral nociceptive hypersensitivity to thermal stimulation on the ipsilateral (Fig. 1d) and contralateral sides (Fig. S1) that developed shortly (within 1 week) and persisted over time post-SCI (the thermal threshold decreased by ~30%, n = 15 SCI-injured rats, $p < 0.001$ compared with the sham-operated group, unpaired t-test, n = 14). Moreover, the thermal pain hypersensitivity correlated with changes in the H-reflex (the Spearman correlation coefficient was −0.48, $p < 0.01$ n = 10 rats of the sham-operated group and n = 18 animals post-SCI; Fig. 1e). Chronic pain post-SCI could develop into unceasing, debilitating pain becoming intolerable, as suggested here by a self-mutilatory behaviour (autotomy), which some animals (about 15%) displayed later (2–3 months) postoperatively (Fig. S1B). Autotomy was directed ipsilaterally and typically proceeded with morphological changes, including skin reddening, tissue swelling, and tumour; it was associated with severe muscle spasm state and has been suggested to reflect intolerable chronic pain in animal studies[17,20]. Neither sham-operated nor control animals exhibited mutilation (Fig. S1B). However, we failed to evidence peripheral mechanical hypersensitivity and allodynia post-SCI when measured the mechanical threshold with von Frey monofilaments; peripheral responses to plantar mechanical stimulation in the SCI-injured animals were comparable to those of the sham-operated group regardless innocuous or noxious stimuli were applied (Fig. S2).

The DH hyperexcitability post-SCI. The DH lamina I–II is the primary area for nociceptive input integration and pain processing. The hyperexcitability of motoneurons after SCI has been associated with changes in sensory transmission[8]. To test if spasticity and pain post-SCI are associated with the hyperexcitability of the DH, the voltage-clamp recordings were made in lamina II interneurons from adult rats experiencing long-lasting (1–2-month) spasticity (only animals with the level 3 to 4 on the Ashworth score were taken, with a clear spasm state). In total, 17320 sEPSCs were recorded in 36 interneurons from control (n = 7 rats), whereas 20304 events – in 22 ipsilateral interneurons from spastic animals (n = 6 rats). The median inter-event interval of sEPSCs was 205 ms in control, but 78 ms in spasticity ($p < 0.001$, the KS- and U-tests; Fig. 2a), indicating the increased frequency post-SCI (from 1.8 Hz to 3.8 Hz, increase by ~116%; Fig. 2b). There were predominant high-frequency sEPSCs in spasticity while the low-frequency sEPSCs in control (Fig. 2a, right). The median amplitude of sEPSCs was increased (from 11.2 pA in control to 17.5 pA in spasticity, increase by ~56%, $p < 0.001$, the KS- and U-tests; Fig. 2b). Changes in both frequency and amplitude were correlated ($p < 0.05$, the Fisher r-to-z transformation compared to control): the Spearman's rank correlation coefficient was 0.76 in spasticity (n = 21, $p < 0.001$) *vs.* 0.48 in control (n = 34, $p < 0.01$, the Spearman's test; Fig. 2c). Thus, spasticity and pain are associated with the activity-dependent boosting of synaptic excitation in sensory circuits. The changes were similar to those observed in the DH in neuropathic[21] and chronic inflammatory pain conditions[22].

The DH hyperexcitability originates from changes in both excitation and inhibition. Loss of inhibition within the DH accompanied abnormal pain sensation and chronic pain of different origins[23–25]. To test if this is the case in spasticity, we recorded inhibitory currents in lamina II interneurons. Disinhibition was manifested as an increase in the inter-event interval of sIPSCs ($p < 0.001$, the KS- and U-tests; Fig. 2d insert) – reflecting the decreased sIPSC frequency (by ~52%; Fig. 2e) – as a reduction in the sIPSC density (Fig. 2d), and as a drop in the current amplitude (from 22 pA in control to 18 pA in spasticity, decrease by ~18%, $p < 0.001$, U-test; Fig. 2e). The correlation profile of excitatory and inhibitory inputs received by individual interneurons further demonstrated boosted excitatory drive while reduced inhibitory control post-SCI (Fig. 2f).

The SCI-induced changes in excitatory drive and postsynaptic AMPARs in specific types of DH interneurons. *Heterogeneous excitatory drive to DH interneurons in control.* The interneuron-type-specific changes in excitatory DH transmission were reported in neuropathic[21] and inflammatory pain conditions[22]. To test if the SCI-induced changes are uniform or different between types of interneurons, we examined two principal neuronal populations: AFNs (Fig. 3a) and TFNs (Fig. 4a), distinguishable by their electrophysiological properties. Consistent with our previous observations[22], AFNs and TFNs revealed distinct excitatory drive in control ($p < 0.001$, the KS- and U-tests for the sEPSC inter-event interval and amplitude, data not shown). Changes in neuronal excitation post-SCI were also different; moreover, they were bidirectional.

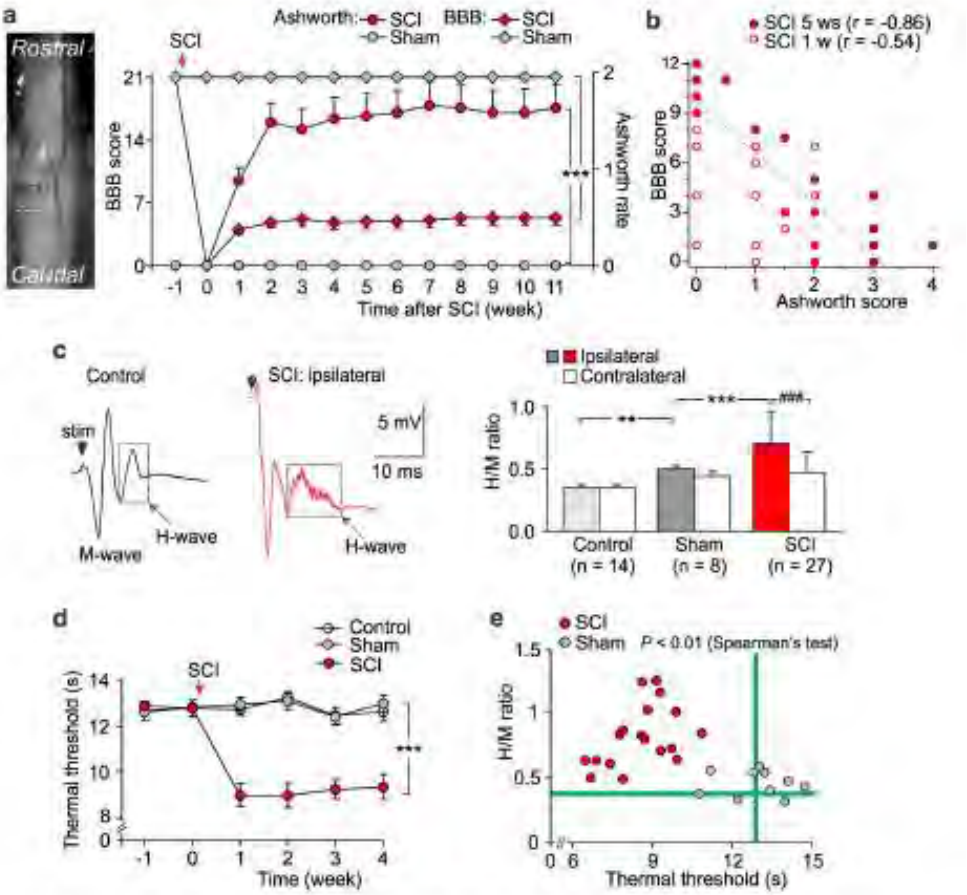

Figure 1. The SCI-induced spasticity correlates with chronic pain. (**a**) Left, image of the spinal cord immediately after the lesion (white box indicates the lesion site, Th_{11}). Right, summary of the BBB (left Y axis) scaling of animal locomotion and the Ashworth rate (right Y axis) of long-lasting impairments in muscle tone on the ipsilateral side postoperatively (n = 32 SCI-injured rats, n = 14 sham-operated animals). $^{***}p < 0.001$ (two-way repeated analysis of variance and Bonferroni post-hoc test). (**b**) The BBB score estimated for each animal at week 1 and week 5 post-SCI (n = 32 animals) plotted against its Ashworth scoring value. The Pearson correlation coefficients (r) are indicated. (**c**) Left, examples of the H-reflex recordings, demonstrating the M- and the H-wave responses in control and post-SCI at ~1 month postoperatively. Right, the ratio of the H- to the-M-wave amplitudes in different experimental groups. $^{\#\#\#}P < 0.001$ (paired *t*-test), $^{**}p < 0.01$, $^{***}p < 0.001$ (unpaired *t*-test). (**d**) The time course of changes in the thermal nociceptive threshold of the ipsilateral hindpaw in different groups of animals, demonstrating experiencing of the long-lasting pain post-SCI (n = 11 control, n = 14 sham-operated rats and n = 15 animals post-SCI). $^{***}P < 0.001$ (ANOVA with Bonferroni post-hoc test). (**e**) The H-reflex measurements (the H/M ratio) plotted against the thermal nociceptive threshold estimated for a respective animal at the time-point of ~1 month postoperatively for the sham-operated (n = 10 animals) and the SCI groups (n = 18 animals). The Spearman's test significance is indicated. Green lines indicate the average parameters in control animals (no surgery). Data are expressed as mean; error bars, SEM.

Boosted drive and upregulated postsynaptic AMPARs in AFNs post-SCI. Excitatory drive was boosted to AFNs post-SCI. The inter-event interval of sEPSCs was decreased (up to 3-fold, $p < 0.001$, the KS-test), reflecting the increased frequency (from 0.83 Hz in control to 7.60 Hz in spasticity, increase in the median frequency up to 9-fold, $p < 0.001$, U-test; Fig. 3b). The median sEPSC amplitude was also increased (from 7.2 pA in control to 16.6 pA in spasticity, $p < 0.05$, U-test; Fig. 3b). Changes in both median frequency and amplitude (analysed for individual neurons) were correlated: the Spearman's correlation coefficient was 0.83 in spasticity (n = 11, $p < 0.001$) *vs.* 0.38 in control (n = 17, $p = 0.12$, Spearman's non-parametric test; Fig. 3c), implying the activity-dependent upregulation of receptors at glutamatergic synapses.

Postsynaptic AMPARs mediate the majority of glutamatergic transmission in sensory circuits[26]. For the assessment of the SCI-induced changes in postsynaptic AMPARs we recorded the AMPAR-mediated postsynaptic currents (see Methods). In AFNs, AMPARs were upregulated post-SCI, as revealed by the dramatically augmented current amplitude (Fig. 3d) and changes in other current parameters (Fig. S3). The median current amplitude was

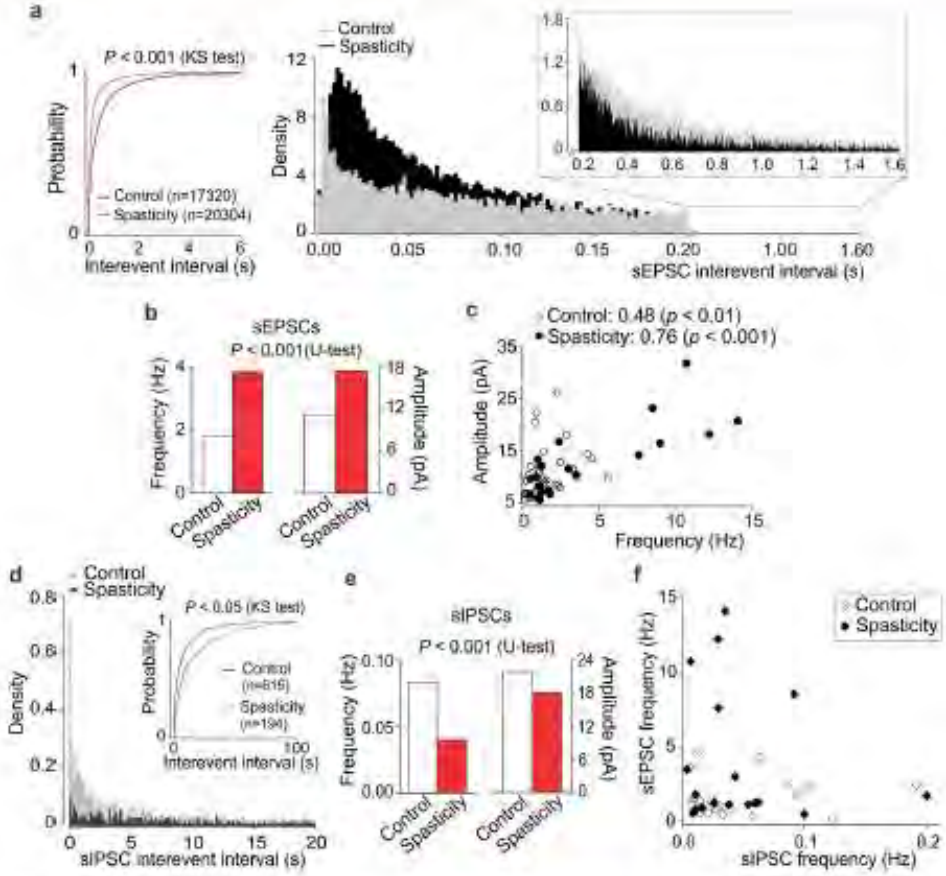

Figure 2. The SCI-induced hyperexcitability of the DH results from boosted excitation and synaptic disinhibition. (**a**) Voltage-clamp recordings in the DH interneurons (Vh = −70 mV) unveiled boosted circuitry excitation post-SCI. Cumulative probability plots (left) and the probability density functions for the inter-event interval of sEPSCs (right) demonstrate the high-frequency sEPSCs post-SCI and opposite the low-frequency sEPSCs in control (insert). (**b**) Summary for the median frequency (left Y axis) and the median amplitude (right Y axis) of sEPSCs in control and spasticity. (**c**) The median sEPSC frequency plotted against its median amplitude, estimated for each individual neuron (n = 34 cells from control and n = 21 cells from spastic animals). The Spearman correlation coefficients and the Spearman's non-parametric test significance are indicated. (**d**) Voltage-clamp recordings of sIPSCs in the DH interneurons (Vh = 0 mV) revealed the decreased density of inhibitory currents post-SCI. Cumulative probability plots for the sIPSC inter-event interval in experimental groups (insert). (**e**) Summary for the median frequency (left Y axis) and the median amplitude (right Y axis) of sIPSCs in different conditions. (**f**) The median frequency of sEPSCs plotted against the median frequency of sIPSCs recorded from the same neurons in control (n = 24 cells) and spasticity (n = 18 cells). The Kolmogorov-Smirnov (KS) or the Mann-Whitney U-test significance is indicated.

increased by ~60%, the current area by ~113%, the decay kinetics by ~71% ($p < 0.001$, U-test for either parameter; Fig. 3d). The pool of AMPAR-currents rearranged (Fig. 3e) such that proportion of the AMPAR-mediated currents with fast decay kinetics (≤2.5 ms) became reduced ($p < 0.001$, the KS-test), with a shift towards the AMPAR-currents with slower decay kinetics (>2.5 ms, $p < 0.05$, the KS-test). There were similar rearrangements in the pooled AMPAR-conductance: a drop in the density of AMPARs of smaller conductance along to the increased density of receptors of larger conductance ($p < 0.001$, the KS-test; Fig. 3f). Together it points to the AMPAR subunit re-composition at glutamatergic synapses post-SCI. Given that either slower desensitization or larger channel conductance characterizes the GluA2-containing AMPARs[27], a drop in the density of both fast-decayed currents and smaller conductance indicates the loss of GluA2-lacking AMPARs. Consistently, the increased proportion of both AMPAR-currents of slower decay kinetics and larger channel conductance reflects the increased proportion of GluA2-containing AMPARs and suggests a promoted insertion of these receptors into glutamatergic synapses that is in line with the augmented current amplitude.

PS-NSFA revealed a drop in the single-channel AMPAR-conductance (γ): from 19.9 ± 3.7 pS (n = 6 AFNs, 453 AMPAR-currents) in control to 6.05 ± 1.32 pS (n = 4 cells, 670 AMPAR-currents) in spasticity ($p < 0.001$,

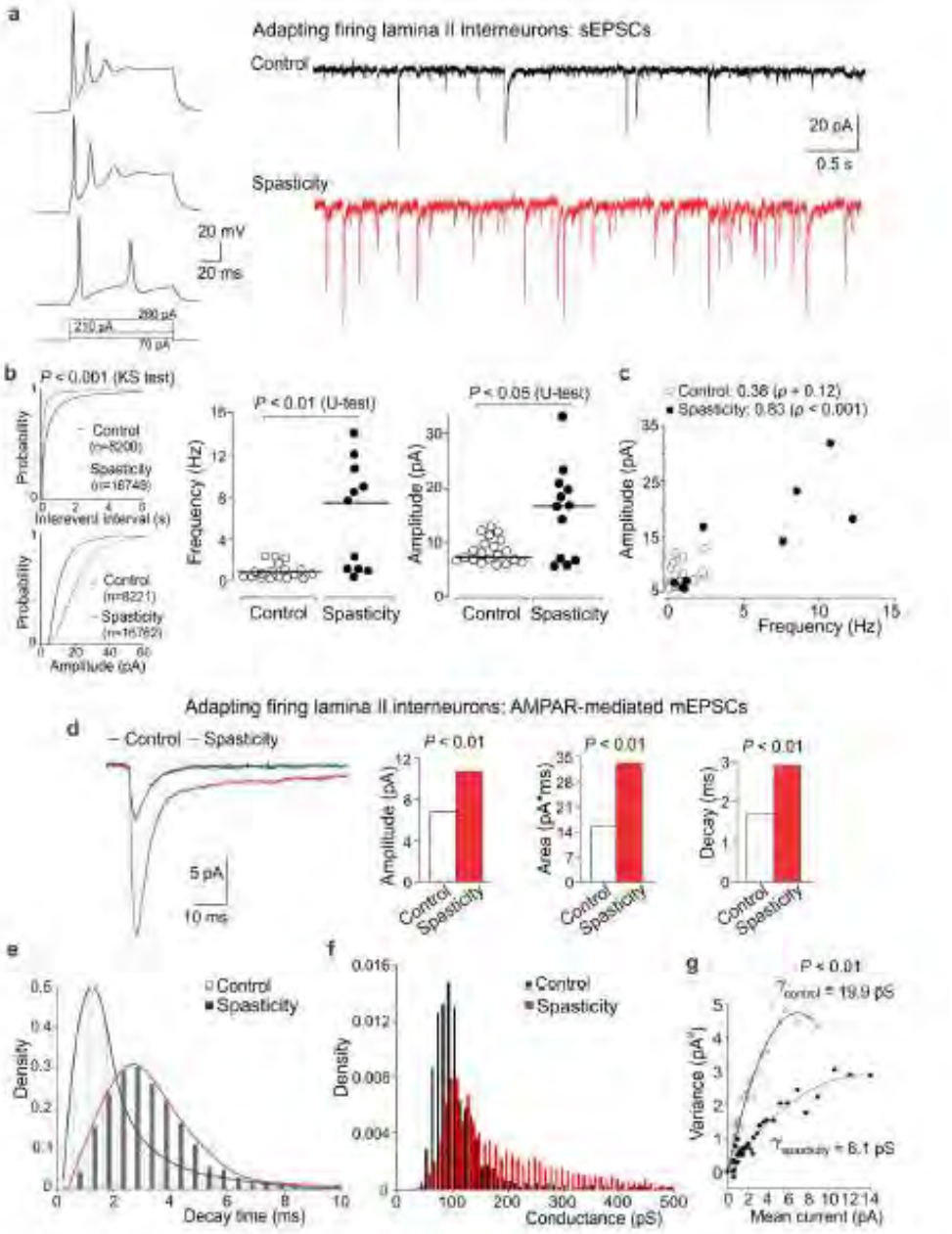

Figure 3. Boosted excitatory drive and upregulated postsynaptic AMPARs in AFNs post-SCI. (**a**) Examples of the current-clamp recordings of typical firing pattern of AFNs (left) in response to depolarizing currents (indicated on the bottom) and the voltage-clamp recordings of sEPSCs (Vh = −70 mV) in control and spastic animals (right). (**b**) Left, cumulative probability plots for the inter-event interval and the amplitude of sEPSCs in control and spasticity. Right, scatter plots of the median sEPSC frequency and the median current amplitude estimated for individual AFNs in control (n = 18 cells) and spasticity (n = 11 neurons). The Kolmogorov-Smirnov (KS) or the Mann-Whitney U-test significance is indicated. (**c**) The median sEPSC frequency plotted against the median current amplitude for individual AFNs in control and spasticity. The Spearman correlation coefficients with the Spearman's non-parametric test significance are indicated. (**d**) The averaged AMPAR-mediated mEPSCs (left) and summary for the median current amplitude, area, and the decay kinetics (right) in control and spasticity. The Mann-Whitney U-test significance is indicated. (**e**,**f**) The probability density functions for the decay kinetics of postsynaptic AMPAR-mediated currents (**e**) and the estimated AMPAR-conductance (**f**) in AFNs in control and spasticity. (**g**) The single-channel conductance of postsynaptic AMPARs in AFNs in control (n = 6 cells, 453 currents) and spasticity (n = 4 cells, 670 currents). The bootstrap hypothesis test for two-sample problem is indicated.

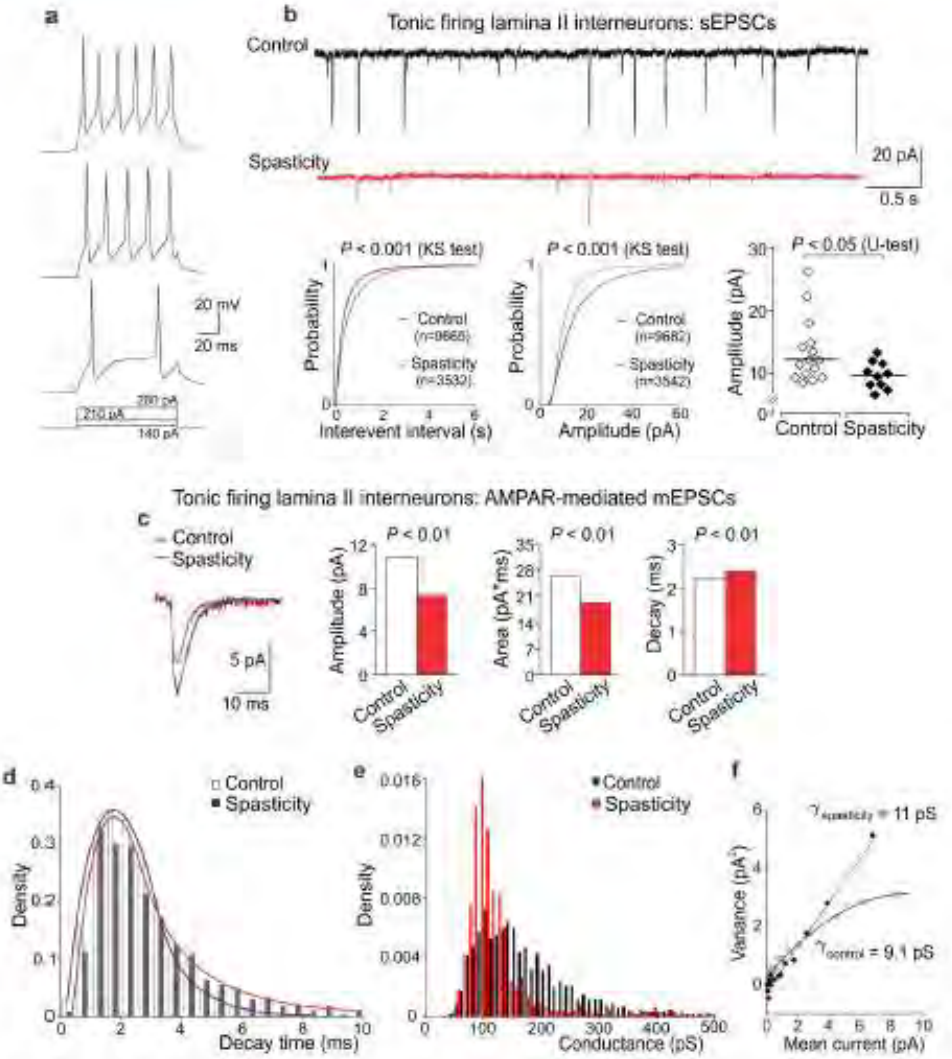

Figure 4. The reduced excitatory drive and diminished postsynaptic AMPAR-currents in TFNs post-SCI. (**a**) Examples of the current-clamp recordings of typical firing discharge of TFNs in response to depolarizing currents of increased intensity (indicated on the bottom). (**b**) Representative voltage-clamp recordings of sEPSCs (Vh = −70 mV) in control and spasticity (upper rows) and cumulative probability plots for the inter-event interval and the amplitude of sEPSCs (lower left) with the Kolmogorov-Smirnov (KS) test significance indicated. The scatter plots for the median current amplitude (lower right) in control and spasticity, estimated for each individual TFN (n = 15 cells in control and 10 cells in spasticity). The Mann-Whitney U-test significance is indicated. (**c**) The averaged AMPAR-mediated mEPSCs (left) and summary of the median current amplitude, the area, and the decay kinetics (right) in TFNs in control and spasticity. The Mann-Whitney U-test significance is indicated. (**d**,**e**) The probability density functions of the decay time of AMPAR-mediated currents (**d**) and the estimated AMPAR-conductance (**e**) in TFNs in control and spasticity. (**f**) The single-channel conductance of postsynaptic AMPARs in TFNs in control (n = 5 cells, 711 mEPSCs) and spasticity (n = 6 cells, 120 mEPSCs).

bootstrap hypothesis test; Fig. 3g), confirming the lack of GluA2-lacking AMPARs from synapses of AFNs post-SCI.

Reduced excitatory drive and diminished AMPAR-currents in TFNs post-SCI. In contrast to AFNs, excitation of TFNs was reduced post-SCI. The inter-event interval of sEPSCs was increased (by −49%, $p < 0.001$, the KS-test; Fig. 4b), reflecting the decreased frequency. The median current amplitude was also decreased (by −20%, $p < 0.05$, U-test; Fig. 4b). This accompanied with the reduced AMPAR- current amplitude (Fig. 4c) and changes in other parameters (Fig. S4). The median current amplitude decreased by −32% and the current area by −26%;

the decay kinetics prolonged by ~9% ($p < 0.01$, U-test for either parameter; Fig. 4c,d). Rearrangements in the AMPAR pool in TFNs were opposite to those in AFNs post-SCI. Whilst the density of fast-decayed currents remained unchanged ($p = 0.72$, the KS-test; Fig. 4d), the density of AMPAR-currents of smaller conductance increased in TFNs in spasticity ($p < 0.001$, the KS-test; Fig. 4e). The average γ also increased (from 9.1 ± 2.1 pS, $n = 5$ cells, 711 mEPSCs in control to 11 ± 2 pS, $n = 6$ cells, 120 mEPSCs in spasticity), though difference did not reach a significance with the bootstrap hypothesis test for two-sample problem ($p = 0.67$; Fig. 4f). Given that the AMPAR-current amplitude decreased in spasticity, such rearrangements may reflect a downregulation of post-synaptic AMPARs with a shift in the proportions of GluA2-containing to GluA2-lacking AMPARs.

Remarkably, γ was different between AFNs and TFNs in control: 19.9 ± 3.7 pS *vs.* 9.1 ± 2.1 pS, respectively ($p < 0.01$, bootstrap hypothesis test). A large difference in the conductance implies distinct receptor subunit composition between neuronal types that is consistent to heterogeneous synaptic drive[22].

The SCI-induced changes in synaptic inhibition in specific types of DH interneurons. *Heterogeneous inhibitory control of DH interneurons in control.* It emerges that inhibitory control is heterogeneous for distinct populations of DH interneurons. Therefore, we first examined synaptic inhibition of AFNs and TFNs in control. The parameters of sIPSCs were significantly different between neuronal types ($p < 0.01$, the KS-test for inter-event interval, $p < 0.001$, the KS-test for either current amplitude or decay; Fig. 5a). Analysts of the decay kinetics of sIPSCs unveiled a large difference in the proportion of fast ($\tau < 13$ ms) to slow currents ($\tau > 13$ ms) between neuronal types ($p < 0.001$, Fischer's test; Fig. 5b), reflecting glycinergic and GABAergic inhibition, respectively [the characteristic decay time of glycine receptor (GlyR)-mediated postsynaptic currents in DH interneurons is 8.4 ms while 26.9 ms for the GABA receptor (GABAR)-mediated ones[25]]. The predominant fast sIPSCs [counted up to 77% of the entire pool of inhibitory events in AFNs] indicate that AFNs receive major glycinergic inhibitory control, with much less GABAergic inhibition [slow sIPSCs counted ~23%]. In contrast, TFNs demonstrated prevailing GABAergic inhibition (58%) balanced with glycinergic one (42%). Our data are consistent with two distinct populations of glycine- or GABA-dominant DH interneurons in lamina I-III[25].

Having observed the difference in both excitatory drive and inhibitory control of DH interneurons, we then estimated the relative balance between synaptic excitation and inhibition that neurons receive simultaneously (see Methods for details). The ratio of the median sEPSC frequency to the median sIPSC frequency was 19.8 ($n = 14$) for AFNs but 113.0 ($n = 10$) for TFNs ($p < 0.001$, U-test; Fig. 5c), demonstrating a moderate synaptic drive to excitatory interneurons while boosted excitatory drive to inhibitory interneurons in control.

As in the case of synaptic excitation, changes in neuronal inhibition post-SCI were neuronal-type-specific; moreover, they were opposite to excitatory ones.

The SCI-induced disinhibition of AFNs. There was a disinhibition of AFNs post-SCI, manifested as an increase in the inter-event interval of sIPSCs ($p < 0.001$, the KS- and U-tests) – reflecting the decreased sIPSC frequency (by ~43%) – and as a decrease in the current amplitude (by ~25%, $p < 0.001$, the KS- and U-tests; Fig. 6a). GABAergic and glycinergic inhibition were both dramatically reduced in AFNs (up to 4-fold; Fig. 6b) and the slow [GABAR-mediated] inhibitory currents became rarely detectable post-SCI. The median amplitude of fast [GlyR-mediated] inhibitory currents dropped (from 23 pA in control to 16 pA in spasticity, $p < 0.001$, the KS- and U-tests) and the current decay became faster (7.6 ms in control *vs.* 5.2 ms in spasticity, $p < 0.01$, U-test; Fig. 6d). The changes correlated ($p < 0.05$, the Fisher r-to-z transformation compared to control): the Spearman's correlation coefficient was 0.38 in spasticity ($p < 0.05$, Spearman's non-parametric test) and 0.60 in control ($p < 0.01$, Spearman's non-parametric test; Fig. 6c). Besides, we observed the lack of currents of large amplitude (above 30 pA) and slower decay kinetics (8–13 ms).

The SCI-induced changes in both synaptic excitation and inhibition resulted in largely amplified excitability of AFNs (above 11-fold): the balance shifted from 19.8 ($n = 14$) in control to 228.2 ($n = 10$, $p < 0.01$, U-test) in spasticity (Fig. 6c).

The SCI-induced reshuffle in GABAergic and glycinergic inhibition of TFNs. Neither median frequency ($p = 0.8$) nor median amplitude of sIPSCs ($p = 0.4$, U-test) was changed in TFNs post-SCI, though cumulative distributions revealed a significant difference between experimental conditions ($p < 0.001$, the KS-test; Fig. 7a). Analysis of the fast and slow inhibitory currents unveiled their rearranged proportion: a drop in the slow [GABAR-mediated] currents (from 58% in control to 13% in spasticity, $p < 0.001$, Fischer's test) while an opposite increase in the fast [GlyR-mediated] currents (from 42% in control to 87% in spasticity, $p < 0.001$, Fischer test; Fig. 7b). Thus, inhibitory control of TFNs reshuffled post-SCI by eliminating GABAergic whilst potentiating glycinergic inhibition. Such potentiation was associated with the increased amplitude of GlyR-currents ($p < 0.05$, the KS test; Fig. 7c) correlated with the prolonged current decay kinetics: the Spearman's rank correlation coefficient was 0.44 in spasticity ($p < 0.001$, Spearman's non-parametric test) and 0.09 in control ($p = 0.6$, Spearman's non-parametric test; Fig. 7d). The correlation profile (Fig. 7d) revealed appearance of fast currents of large amplitude (40–120 pA) and slower decay kinetics (7–13 ms) that suggests GlyR upregulation at inhibitory synapses post-SCI.

Potentiated synaptic inhibition of TFNs together with the reduced AMPAR-mediated excitation resulted in suppressing of TFNs (up to 2-times): the balance dropped from 113 ($n = 10$) in control to 54.6 ($n = 9$) in spasticity ($p = 0.079$, U-test; Fig. 7e). The overall balance between excitation and inhibition within the DH was re-directed from driving of inhibitory interneurons in control to boosting of excitatory interneurons post-SCI (Fig. 7f).

Discussion

This is the first study of central mechanisms underlying chronic pain associated with spasticity that reveals the SCI-induced shifts in neuronal excitation and inhibition resulted in the DH circuit hyperexcitability. We provide

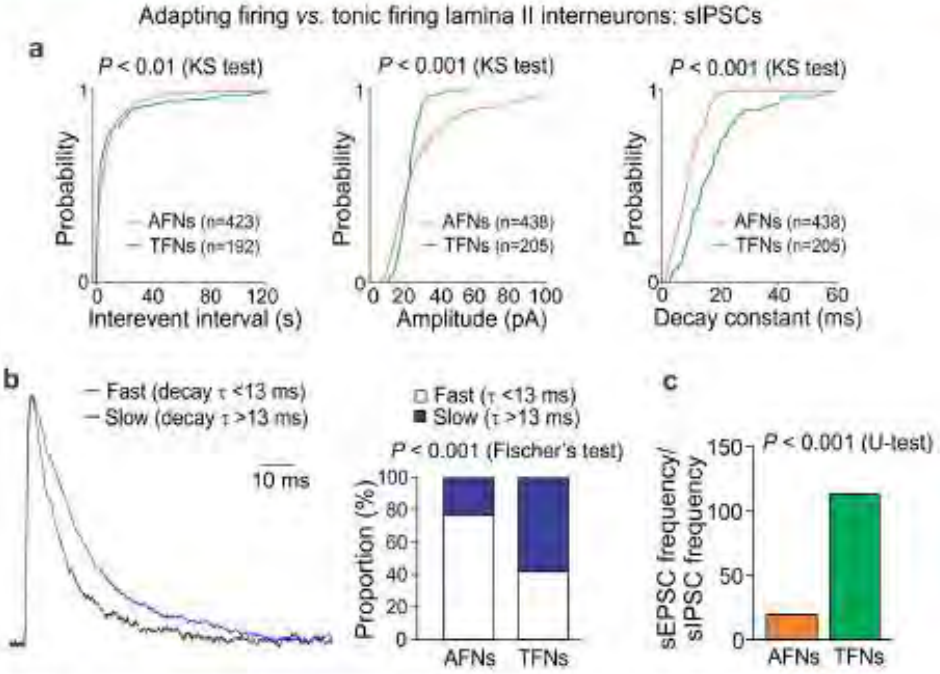

Figure 5. Heterogeneous inhibitory control of DH interneurons. (**a**) Cumulative probability plots for the inter-event interval, the amplitude and the decay constant of sIPSCs in AFNs and TFNs in control. The Kolmogorov Smirnov (KS) test significance with the number of events for analysis is indicated. (**b**) Left, the fast sIPSCs ($\tau < 13$ ms, black line) and slow sIPSCs ($\tau > 13$ ms, blue line) in AFNs in control. The currents are average from 112 fast ($\tau = 10.5$ ms) and 44 slow ($\tau = 19.6$ ms) events recorded in 15 cells. Right, the relative proportions of fast to slow inhibitory currents in AFNs and TFNs in control. The Fisher's exact test significance is indicated. (**c**) The average balance between neuronal excitation and inhibition, estimated as the ratio of the median sEPSC frequency to the median sIPSC frequency recorded from individual AFNs (n = 14 cells) or TFNs (n = 10 cells) in control. The Mann-Whitney U-test significance is indicated.

here quantitative counting of synaptic excitation and inhibition in the DH lamina II interneurons, demonstrating the reciprocal changes occurring in the interneuron-type-specific manner to elucidate how nociceptive processing changes in both spasticity and pain, the most challenging complications post-SCI.

A high occurrence of chronic pain after SCI (up to 80% cases) has been reported by clinical studies[5,6]. This pain could develop through diverse clinical features with a low capability to be cured. In animal studies, the SCI-induced nociceptive hypersensitivity was correlated with severity of injury[18,28]. In our modelling of unilateral SCI, animals displayed severe motor deficit that exceeded on average the level 1 on the Ashworth rating scale and lowered the level 7 on the BBB scale. Recordings of the H-reflex, a physiological marker of spasticity[3,29], revealed the increased ratio of H/M-wave responses in the SCI-injured animals, evidencing the hyperexcitability within sensorimotor pathways. Consistently, animals exhibited pain hypersensitivity in response to thermal stimulation of hindpaw (both ipsilateral and contralateral) detected with a semi-automated method of measuring the thermal threshold[22,30,31]. The hypersensitivity persisted over weeks post-SCI, evidencing chronic pain, which correlated with the degree of spasticity (the H/M ratio). This pain can exacerbate to unceasing chronic pain and become intolerable, as suggested here by a self-mutilatory behaviour in some of the rats, which has been proposed as a readout of neuropathic pain[17,23]. However, our plantar testing with von Frey monofilaments failed to directly demonstrate the mechanical hyperalgesia and allodynia post-SCI that very likely relates to a restricted motility of hindlimbs in the SCI-injured animals since applications of the classical behavioural methodology for studying tactile sensation are less accurate or impractical in animals with severe motor dysfunction and limited weight support[19,28].

The present study focuses on central mechanisms of chronic pain and permanent changes in sensory input integration in the DH for pain processing. To achieve this, patch-clamping of lamina II interneurons, which process input integration from both primary sensory afferents and other interneurons, was performed in the spinal cord below lesion from the SCI-injured animals experiencing long-term spasticity (1–2-month) that yields benefits of the direct recordings from vulnerable DH interneurons (2–3-month-old) following chronic pathology. The present study demonstrates the DH hyperexcitability in conditions of both spasticity and pain post-SCI. Although we cannot rule out that the DH hyperexcitability exaggerated with a tissue damage produced by surgical procedure as no sham-operated control was tested electrophysiologically, the DH hyperexcitability post-SCI has been emerged from the hyperexcitation of the dorsal root ganglion neurons and the augmented primary afferent

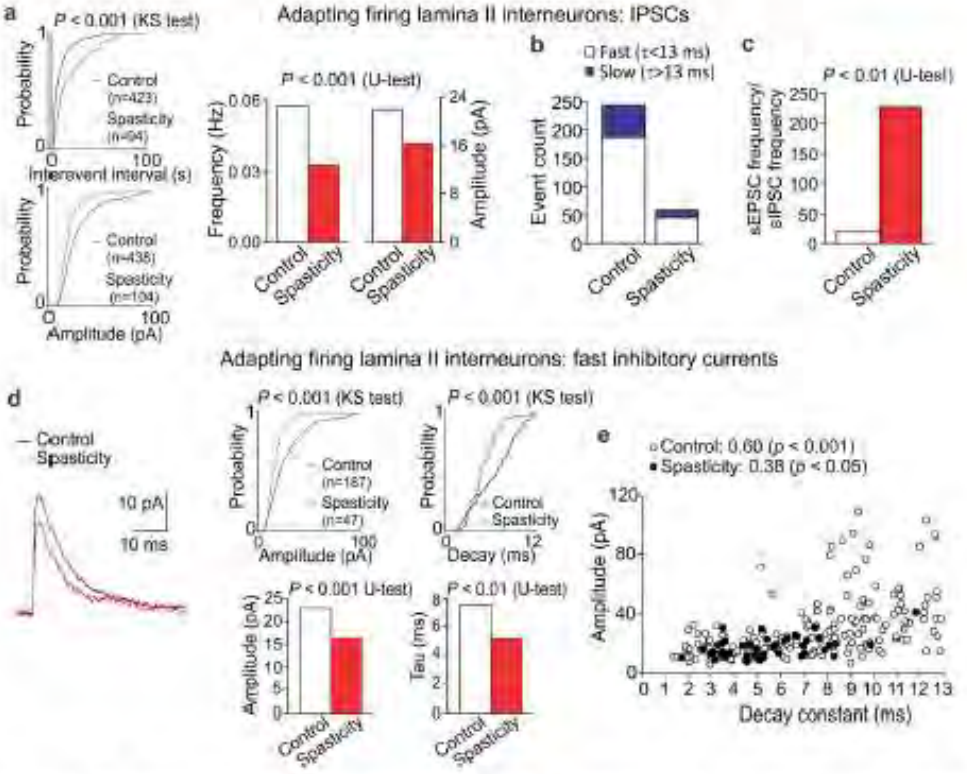

Figure 6. The SCI-induced loss of inhibition in AFNs. (**a**) Cumulative probability plots for the inter-event interval and the amplitude of sIPSCs (left) and summary of the median frequency and the median current amplitude (right) in AFNs in control and spasticity. (**b**) Occurrence of the fast (τ< 13 ms) and the slow (τ > 13 ms) inhibitory currents in different experimental conditions. (**c**) The average balance between synaptic excitation and inhibition of AFNs, estimated as the median frequency of sEPSCs to the median frequency of sIPSCs for each individual AFN in control (n = 14 cells) and spasticity (n = 10 cells). (**d**) Left, examples of the fast inhibitory currents in control (black line, average of 112 fast currents recorded in 15 AFNs) and in spasticity (red line, average of 25 fast currents recorded in 10 AFNs). Right, cumulative probability plots (upper raw) and summary of the median current amplitude and the decay time constant (lower raw) in AFNs in control and spasticity. (**e**) The amplitude of fast IPSCs (τ < 13 ms) plotted against its current decay constant in AFNs in control and spasticity. The Spearman correlation coefficients and the Spearman's non-parametric test significance are indicated. The Kolmogorov-Smirnov (KS) or the Mann-Whitney U-test significance is indicated.

inputs[8], and the increased interneuron firing in response to noxious or innocuous stimuli[15,32], arguing for both peripheral and central sensitization below and above lesion causing aberrant pain processing. Our recordings of excitatory and inhibitory currents in lamina II interneurons demonstrate that the DH circuit hyperexcitability results from two mechanisms – boosted excitation and synaptic disinhibition – those contribute to the hyperexcitability of the DH post-SCI. Most attention through studies of chronic pain of different origins has hitherto been given to the loss of GABAergic inhibition[23,33,34], with a possible death of GABAergic interneurons[35]. A shift in chloride gradient due to a downregulation of the chloride transporter after SCI has been also demonstrated to reverse potential for GABA[16,36], a mechanism attenuating GABAergic inhibition in DH interneurons[37].

Central to this study is the interneuron-type-specific changes in synaptic excitation and inhibition, occurring in the bidirectional and reciprocal manners in two principal types of DH interneurons, AFNs and TFNs, those differ by electrophysiological properties[38–42], synaptic drive[22,41], and neurochemical phenotype[39]. A moderate synaptic drive to excitatory AFNs in control has been boosted following SCI, opposite to a promoted excitatory drive to inhibitory TFNs in control, which has been reduced after SCI. These changes were similar to those in chronic inflammatory pain[22], arguing for similar mechanisms of chronic pain. Boosting of AFNs was mirrored by the activity-dependent upregulation of postsynaptic AMPARs, though the AMPAR-mediated currents were decelerated and the single-channel conductance was reduced post-SCI. The slower decay kinetics, a prominent characteristics of GluA2-containing AMPARs[42,43], may reflect a promoted insertion of GluA2-containing AMPARs into glutamatergic synapses – coherent with the augmented current amplitude – while a drop in the single-channel conductance very likely relates to a loss of GluA2-lacking AMPARs (only fast AMPAR-currents [decay from 1 to 5 ms] were analyzed). The rearranged pool of postsynaptic AMPAR-currents indicates the AMPAR subunit re-composition post-SCI, with a few mechanisms involved whose biophysical and molecular basis remain to

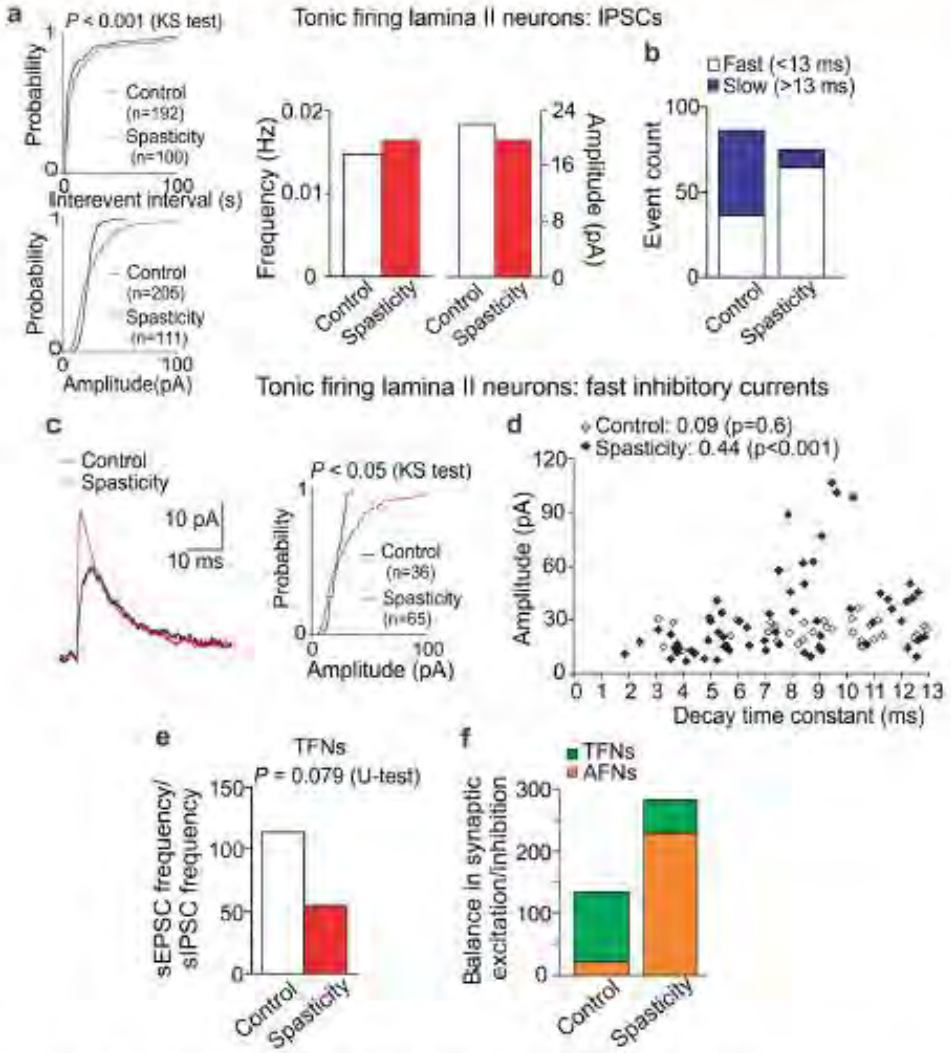

Figure 7. The SCI-induced reshuffle between GABAergic and glycinergic inhibition in TFNs. (**a**) Cumulative probability plots for the inter-event interval and the amplitude of sIPSCs (left) and summary of the median frequency and the median current amplitude (right) in TFNs in control and spasticity. (**b**) Occurrence of the fast ($\tau < 13$ ms) and the slow ($\tau > 13$ ms) inhibitory currents in TFNs in control and spasticity. (**c**) Examples of the fast inhibitory currents (left) and cumulative probability plots for the current amplitude (right) in TFNs in control and spasticity. The currents are average from 25 fast sIPSCs recorded in 11 TFNs in control (black line) and 53 fast sIPSCs recorded in 11 cells in spastic animals (red line). (**d**) The amplitude of fast sIPSCs plotted against the correspondent decay constant in TFNs from control and spastic animals. The Spearman correlation coefficients with the Spearman's non-parametric test significance are indicated. (**e**) The average balance between synaptic excitation and inhibition of TFNs, estimated as the median frequency of sEPSCs to the median frequency of sIPSCs for each individual TFN in control (n = 10 cells) and spasticity (n = 9 cells). (**f**) The relative balance between excitatory drive and synaptic inhibition of AFNs and TFNs in control and post-SCI. The Kolmogorov-Smirnov (KS) or the Mann-Whitney U-test significance is indicated.

be elucidated. Changes in TFNs (e.g., the decreased AMPAR-current amplitude, rearranged pools of the decay kinetics and the single-channel conductance) were opposite to AFNs, indicating differential mechanisms of the AMPAR subunit re-composition between neuronal types. The decreased amplitude may relate to internalization of GluA2-containing AMPARs, demonstrated for the synapses between primary afferents and DH interneurons in chronic inflammatory pain conditions[44], although TFNs lost the GluA2-lacking AMPARs in the peripheral injury-induced neuropathic pain[21]. Remarkably, the single-channel conductance of postsynaptic AMPARs was different between AFNs and TFNs even in physiological conditions (19.9 pS *vs.* 9.1 pS, respectively) that further

proves a distinct receptor subunit composition and is consistent to the distinct synaptic drive to AFNs and TFNs[22] and to the higher surface expression of GluR1 in inhibitory DH interneurons while GluR2 in excitatory ones[45,46].

The present study stresses the SCI-induced shifts in synaptic excitation and inhibition occurring in the bidirectional and reciprocal manner in two principal types of sensory interneurons, excitatory and inhibitory, such that changes in neuronal inhibition opposed changes in their excitation. Such contraposition resulted in a shifted balance of neuronal excitation and inhibition, suggesting a phenomenon of the reciprocal reshuffle between excitatory and inhibitory transmission as a neurophysiological mechanism of amplifying nociceptive processing. The SCI-induced disinhibition of AFNs (major excitatory interneurons) through diminishing of both GABAergic and glycinergic controls contrasted with inhibition of TFNs (inhibitory interneurons) despite of their loss of GABAergic control post-SCI. Whilst loss of GABAergic inhibition is abundantly evidenced in the DH after SCI[16,34,37], a reshuffle between GABAergic and glycinergic inhibition has not been to the date reported. Potentiation at glycinergic synapses on inhibitory interneurons would promote their inhibition, retard inhibitory control of sensory circuits, and cause the DH disinhibition[47]. Notably, the fast inhibitory currents became often in TFNs post-SCI, with larger amplitude and slower decay kinetics that may reflect GlyR upregulation, though changes in biophysical properties of the receptors and/or the number of functional synapses cannot be also excluded. The SCI-induced potentiation of glycinergic inhibition at inhibitory synapses together with the reduced AMPAR-mediated excitation at glutamatergic synapses represent two coherent mechanisms of reciprocal retardation of inhibitory interneurons for circuitry disinhibition and central sensitization mediating chronic pain.

The bidirectional and opposite changes in excitatory and inhibitory transmission in two types of interneurons underlyi the DH hyperexcitability post-SCI that could, in turn, contribute to hyperexcitability of the ventral horn. This may include interconnections between the lamina II interneurons with interneurons of deeper laminae, e.g. involving the laminae IV–V interneurons projecting ipsilaterally to motoneurons of the ventral horn[48]. Whilst we did not attempt to focus on components of the motor circuit control, extensive studies over years demonstrated the reduced intrinsic excitability of motoneurons with normalization of uncontrolled circuit function following pharmacological targeting of sensory transmission to motoneurons[49,50] or electrical stimulation of spinal circuitry[51,52] that ultimately improved management of spasticity post-SCI. This is also consistent to the microsurgical dorsal root entry zone (DREZ)-tomy relief in neurogenic pain and hyperspastic states in patients with severe spasticity and pain, implemented in clinics over decades ago[53]. Although the nature of spasticity is complex and not finally explained, we provide here a central mechanism of unbalancing the sensory circuit component relying on the bidirectional and reciprocal changes in excitatory and inhibitory transmission in DH interneurons in conditions of spasticity and pain, the most severe complications post-SCI.

Methods

All animal procedures were approved by the Animal Ethics Committee in Bogomoletz Institute of Physiology and were in accordance with the European Commission Directive (86/609/EEC). All efforts were made to avoid or minimize animal suffering and to reduce the number of animals used.

Experimental SCI. For modelling of experimental SCI hemisection of the spinal cord was used in 21–25-day-old male Wistar rats. For the surgery a rat was deeply anesthetized with ketamine and xylazine (70 mg/kg and 15 mg/kg, respectively, intraperitoneal injection), confirmed with the lack of the corneal reflex. After surgical area was prepared and treated with antiseptics, one longitudinal skin incision was made around Th_8–L_2 segments and muscles were retracted to expose the spinal column. Laminectomy was carried out at Th_{10}–Th_{11} segments, pre-determined by palpation of the dorsal surface and by counting spinous processes to locate the laminae. Hemisection of the spinal cord was performed transversally at Th_{11} on the left side, with extra care taken to avoid any damage to the dorsal vessel or its branches (Fig. 1a). To ensure that hemisection carried out completely, one branch of ophthalmologic tweezers was pulled through the spinal cord incision. The muscles and fascia were sutured and wound closed. Animals received postoperatively bicillin (1 million U/kg) and dexamethazon (6 mg/kg). Post-hoc histology confirmed hemisection not crossing the midline in transverse spinal cord sections. Sham surgery was performed by exposing the spinal cord to a similar procedure without hemisection.

Only animals revealing motor deficit ipsilateral to the hemisection side were included into the study; in case of sparse animals revealed neurological deficit on the contralateral side post-SCI, they were discarded. We also discarded animals if their scoring exceeded the level 7 on the Basso, Beattie, and Bresnahan (BBB) rating scale and was level 0 on the Ashworth scale on day 2–3 post-lesion (less than 15% animals).

Behavioural assessments post-SCI. For the assessment of motor deficit and muscle tone of hindlimb post-SCI we used behavioural tests – the BBB and the Ashworth rating scales, respectively. For the assessment of pain hypersensitivity of each hindlimb post-SCI we utilized a semi-detected method of measuring the latency of paw withdrawal (the Hargreaves technique) and the method of von Frey monofilaments (Extended Experimental Procedures). Animals were also monitored for a self-mutilatory behaviour (Extended Experimental Procedures), which has been proposed as a readout of neuropathic pain in animal studies[17,20]. Behavioural assessments were performed in a quiet room by the same experimenter for a given test.

The BBB rating scale. The BBB scale was used for the assessment of motor function of hindlimbs in each animal. The test is widely utilized for evaluation of animal locomotion, with some modifications. Our scoring was based on the BBB rating scale for the incompletely spinal cord injury in rats[54,55]. Tested animal was allowed to freely move and evaluated for its hindlimb joint movements, paw placement, weight support, and limb coordination according to the scoring criteria described in details in Table 1. Each animal was evaluated before lesion, on day

Score	Criteria	
	BBB	Ashworth
0	no hindlimb movement	no increase in muscle tone
1	slight (less than half movement) of one or two joints (the hip and/or the knee)	slight increase in tone when hindlimb is moved in flexion or extension
2	extensive movement of one joint (more than half of the normal range of joint motion)	more marked increase in tone, with limb still easily flexed
3	extensive movement of two joints	considerable strength of tone with difficult passive movement
4	slight movement of all three joints	hindlimb rigid in flexion or extension
5	slight movement of two joints and extensive movement of the third	
6	extensive movement of two joints and slight movement of the third	
7 and above	extensive or full movement of all joints, including additional levels of plantar foot placement and/or weight support	

Table 1. Scoring for the BBB and the Ashworth rating scales in unilateral SCI in rats.

2–3 post-lesion and then consistently scored for at least 3 months postoperatively. Only scores of hindlimb on the hemisected side (left side) are presented.

The Ashworth scale. The Ashworth rating scale was used for the assessment of muscle tone and hindlimb rigid post-SCI according to the adapted Ashworth scale for rats[56,57]. We evaluated positioning of hindlimb ipsilateral to the hemisected side as described in details in Table 1. Each animal was evaluated before lesion, on day 2–3 post-lesion and then for at least 3 months postoperatively.

Hargreaves plantar test for thermal pain hypersensitivity. Peripheral sensitivity to the thermal (heat) stimulus was measured in rats with Hargreaves technique as described previously[30,31,58]. Briefly, after an animal habituated to the Plexiglas chamber located above a light box (Ugo Basile Model 7370 Plantar Test), a radiant heat was applied to the middle of the plantar surface of one hind paw. The light beam was automatically turned off when animal lifted its paw. Trial was repeated 3–5 times with an interval between measurements 3 to 5 minutes. The time between the start of stimulus and animal lifted its paw, the withdrawal latency, was measured, which represents the thermal nociceptive threshold.

Hoffman (H)-reflex measurement. The H-reflex measurements were performed using a multimodality stimulator system (Neurosoft, Russia) as described in details elsewhere[29]. After a rat was anaesthetized, the longitudinal incision was made along the femoral surface of a tested hindlimb to expose sciatic nerve. Stimulating bipolar hook electrode was placed on the nerve surroundings; recording needle electrode was placed into the gastrocnemius muscle. The nerve was stimulated using square pulses (1–2 mA, 5-ms duration, 0.2 Hz) of increased stimulus intensity (1-mA-increment). Several trials (5 sweeps/trial) were recorded with at least 5-min-rest intervals between trials. The M- and the H-waveform peak amplitudes were measured and the ratio of H- to M-wave amplitudes was calculated. In the case of the end of M-wave and the beginning of H-wave overlapped, the M- and the H-wave currents were summated since the M-wave amplitude and the latency remained stable, not affecting the H-wave amplitude comparison[29]. The H-reflex measurements were performed at the time period of 4–5 weeks postoperatively.

Spinal cord slice preparation. Spinal cord slices were prepared from 2–3-month-old rats as described previously, with minor modifications[22,38]. The spinal cord below hemisection (lumbar segments) was removed and placed in an ice-cold dissection solution that contained (in mM) 250 sucrose, 2 KCl, 1.2 NaH_2PO_4, 0.5 $CaCl_2$, 7 $MgCl_2$, 26 $NaHCO_3$, 11 glucose, oxygenated with 95% O_2 and 5% CO_2. Transverse slices (350–400 μm thickness) were cut with a HA752 vibratome (Campden Instruments, Loughborough, UK) and maintained in a physiologic Krebs solution that contained (in mM) 125 NaCl, 2.5 KCl, 1.25 NaH_2PO_4, 2 $CaCl_2$, 1 $MgCl_2$, 26 $NaHCO_3$, 10 glucose, oxygenated with 95% O_2 and 5% CO_2.

Electrophysiology. Whole-cell recordings were made from lamina II interneurons ipsilateral to hemisection, using a Multipatch 700B amplifier controlled with pClamp 9.2 software (Molecular Devices, USA). Neurons were visualized with infrared optics using a 60× water-immersion objective on an Olympus BX50WI upright microscope (Olympus, Japan). Recording pipettes (resistance 4–5 MΩ) were filled with an internal solution containing (in mM) 133 K-gluconate, 5 NaCl, 0.5 $MgCl_2$, 10 HEPES-Na, 2 MgATP, 0.1 GTP-Na, 0.5 EGTA (pH 7.2, osmolarity 290 mOsM). Interneurons were categorized according to their discharge patterns in response to the series of depolarizing current of 0.5–1-s duration[22,36,38]. Tonic-firing, adapting-firing, transient (initial burst)-firing, and single-spiking discharge patterns were recorded. Because all these patterns except the tonic-firing are adapting due to the A-type potassium-current-related pattern of discharge, we grouped them together that neurons were divided in two groups: "adapting-firing" (AFN) and "tonic-firing" neurons (TFN)[22,30,38]. TFNs were defined as those able to support continuous firing during depolarizing current and increase firing frequency with increasing the stimulus intensity (Fig. 4A); this neuronal type represents putative inhibitory interneurons[39,40].

Spontaneous excitatory postsynaptic currents (sEPSCs) were recorded in interneurons at −70 mV for at least 5 minutes. The membrane potential was then switched to 0 mV to record spontaneous inhibitory postsynaptic currents (sIPSCs) from the same neuron for the next 5 minutes (after baseline stabilization at 0 mV)[32]. To isolate the AMPA receptor (AMPAR)-mediated component, miniature EPSCs (mEPSCs) were recorded at −70 mV in the continuous presence of a cocktail of antagonists, which consisted of TTX (200 nM), APV (50 μM), bicuculline (5 μM), strychnine (2 μM), $CdCl_2$ (100 μM), administered 10 min prior to the recording. Only neurons with a stable baseline during the entire recording were included into analysis.

Data analysis. Mini Analysis Program (Synaptosoft, Decatur, GA) was used for analysis as described previously[32]. The kinetics of EPSCs were analysed within the time frame of 10% to 90% of current for rise time and 100% to 37% of current for decay time. The area of currents was calculated as an integral within the time frame of current initiation until 37% of current decay. The decay kinetics of sIPSCs (τ) was calculated within the time frame of 100% to 37% of current decay fitted with the mono-exponential function. The balance between synaptic excitation and inhibition received by individual neurons simultaneously was estimated as the ratio of excitatory inputs [the median sEPSC frequency] to inhibitory inputs [the median sIPSC frequency] recorded in the same neurons. The AMPAR-conductance was calculated according to the following equation:

$$G = I_{max}/(V_{rev} - V_m)$$

where I_{max} is the peak of AMPAR-mediated current, V_{rev} is the reversal potential, V_m is the membrane potential.

The data sets were probed for normality using the Shapiro-Wilk test. Data sets not normally distributed were compared using a nonparametric Mann-Whitney U-test and results were presented as medians with interquartile ranges (IQR). The Kolmogorov-Smirnov two-sample test (KS-test) was used to compare the distributions in parameters between groups. Correlations between variable, non-parametrically distributed parameters were assessed using a Spearman non-parametric rank correlation. The Fisher exact test was used to determine statistical difference between two categorical variables. A P value less than 0.05 was considered as statistically significant for either test.

Peak-scaled non-stationary fluctuation analysis. The single-channel conductance (γ) of postsynaptic AMPARs was estimated using the peak-scaled non-stationary fluctuation analysis (PS-NSFA)[59]. Only AMPAR-mediated mEPSCs with the decay time from 1 to 5 ms were used for the analysis if displayed a stable baseline with no overlapping events during decay. Selected currents were averaged to obtain the mean mEPSC and then individual currents were scaled to the mean to obtain the peak scaled current according to the Equation (1)

$$I_i^{peak-scaled} = I_i - \langle I \rangle \frac{\max(I_i)}{\max \langle I \rangle}, \quad (1)$$

where I_i is an individual current, $\langle I \rangle$ is the mean mEPSC.

Variance of the peak-scaled mEPSCs, $\sigma^2(I^{peak-scaled})$, was plotted versus mean and fitted with parabola described by the Equation (2), using the weighted least squares method with weights $\omega^2 = \frac{1}{\text{variance}(\sigma_i^2)}$,

$$\sigma^2(I^{peak-scaled}) = i_{ch}\langle I \rangle - \frac{\langle I \rangle^2}{N} + \sigma_0^2, \quad (2)$$

where $\langle I \rangle$ is the mean mEPSC, N is the functional number of channels, σ_0^2 is the variance of background noise and i_{ch} is the single-channel current. Finally, γ was calculated from the equation

$$\gamma = \frac{i_{ch}}{V - E_{rev}}, \quad (3)$$

where V is the holding potential, E_{rev} is the reversal potential (0 mV).

The accuracy of the estimated γ was calculated using bootstrap method where 1000 bootstrap samples were generated for each group; significant difference was assessed with the bootstrap hypothesis test for two-sample problem.

References

1. Biering-Sorensen, F., Nielsen, J. B. & Klinge, K. Spasticity-assessment: a review. *Spinal cord* **44**, 708–722, doi:10.1038/sj.sc.3101928 (2006).
2. Skold, C., Levi, R. & Seiger, A. Spasticity after traumatic spinal cord injury: nature, severity, and location. *Archives of physical medicine and rehabilitation* **80**, 1548–1557 (1999).
3. Nielsen, J. B., Crone, C. & Hultborn, H. The spinal pathophysiology of spasticity–from a basic science point of view. *Acta physiologica (Oxford, England)* **189**, 171–180, doi:10.1111/j.1748-1716.2006.01652.x (2007).
4. Adams, M. M. & Hicks, A. L. Spasticity after spinal cord injury. *Spinal cord* **43**, 577–586, doi:10.1038/sj.sc.3101757 (2005).
5. Andresen, S. R. *et al.* Pain, spasticity and quality of life in individuals with traumatic spinal cord injury in Denmark. *Spinal cord* doi:10.1038/sc.2016.46 (2016).
6. Finnerup, N. B. *et al.* Phenotypes and predictors of pain following traumatic spinal cord injury: a prospective study. *The journal of pain: official journal of the American Pain Society* **15**, 40–48, doi:10.1016/j.jpain.2013.09.008 (2014).
7. D'Amico, J. M., Condliffe, E. G., Martins, K. J., Bennett, D. J. & Gorassini, M. A. Recovery of neuronal and network excitability after spinal cord injury and implications for spasticity. *Frontiers in integrative neuroscience* **8**, 36, doi:10.3389/fnint.2014.00036 (2014).
8. Norton, J. A., Bennett, D. J., Knash, M. E., Murray, K. C. & Gorassini, M. A. Changes in sensory-evoked synaptic activation of motoneurons after spinal cord injury in man. *Brain: a journal of neurology* **131**, 1478–1491, doi:10.1093/brain/awn050 (2008).

9. Bedi, S. S. *et al.* Chronic spontaneous activity generated in the somata of primary nociceptors is associated with pain-related behavior after spinal cord injury. *The Journal of neuroscience: the official journal of the Society for Neuroscience* **30**, 14870–14882, doi:10.1523/jneurosci.2428-10.2010 (2010).
10. Gwak, Y. S. & Hulsebosch, C. E. Neuronal hyperexcitability: a substrate for central neuropathic pain after spinal cord injury. *Current pain and headache reports* **15**, 215–222, doi:10.1007/s11916-011-0186-2 (2011).
11. Walters, E. T. Neuroinflammatory contributions to pain after SCI: roles for central glial mechanisms and nociceptor-mediated host defense. *Experimental neurology* **258**, 48–61, doi:10.1016/j.expneurol.2014.02.001 (2014).
12. Hains, B. C. *et al.* Upregulation of sodium channel Nav1.3 and functional involvement in neuronal hyperexcitability associated with central neuropathic pain after spinal cord injury. *The Journal of neuroscience: the official journal of the Society for Neuroscience* **23**, 8881–8892 (2003).
13. Lampert, A., Hains, B. C. & Waxman, S. G. Upregulation of persistent and ramp sodium current in dorsal horn neurons after spinal cord injury. *Experimental brain research* **174**, 660–666, doi:10.1007/s00221-006-0511-x (2006).
14. Xu, G. Y., Hughes, M. G., Ye, Z., Hulsebosch, C. E. & McAdoo, D. J. Concentrations of glutamate released following spinal cord injury kill oligodendrocytes in the spinal cord. *Experimental neurology* **187**, 329–336, doi:10.1016/j.expneurol.2004.01.029 (2004).
15. Gwak, Y. S., Crown, E. D., Unabia, G. C. & Hulsebosch, C. E. Propentofylline attenuates allodynia, glial activation and modulates GABAergic tone after spinal cord injury in the rat. *Pain* **138**, 410–422, doi:10.1016/j.pain.2008.01.021 (2008).
16. Boulenguez, P. *et al.* Down-regulation of the potassium-chloride cotransporter KCC2 contributes to spasticity after spinal cord injury. *Nature medicine* **16**, 302–307, doi:10.1038/nm.2107 (2010).
17. Christensen, M. D., Everhart, A. W., Pickelman, J. T. & Hulsebosch, C. E. Mechanical and thermal allodynia in chronic central pain following spinal cord injury. *Pain* **68**, 97–107 (1996).
18. Kramer, J. L. *et al.* Neuropathic pain following traumatic spinal cord injury: Models, measurement, and mechanisms. *Journal of neuroscience research* **95**, 1295–1306, doi:10.1002/jnr.23881 (2017).
19. Mills, C. D., Hains, B. C., Johnson, K. M. & Hulsebosch, C. E. Strain and model differences in behavioral outcomes after spinal cord injury in rat. *Journal of neurotrauma* **18**, 743–756, doi:10.1089/089771501316919111 (2001).
20. Abdulla, F. A. & Smith, P. A. Changes in Na(+) channel currents of rat dorsal root ganglion neurons following axotomy and axotomy-induced autotomy. *Journal of neurophysiology* **88**, 2518–2529, doi:10.1152/jn.00913.2001 (2002).
21. Chen, Y., Derkach, V. A. & Smith, P. A. Loss of Ca(2+)-permeable AMPA receptors in synapses of tonic firing substantia gelatinosa neurons in the chronic constriction injury model of neuropathic pain. *Experimental neurology* **279**, 168–177, doi:10.1016/j.expneurol.2016.03.001 (2016).
22. Kopach, O., Krotov, V., Belan, P. & Voitenko, N. Inflammatory-induced changes in synaptic drive and postsynaptic AMPARs in lamina II dorsal horn neurons are cell-type specific. *Pain* **156**, 428–438, doi:10.1097/01.j.pain.0000460318.65734.00 (2015).
23. Moore, K. A. *et al.* Partial peripheral nerve injury promotes a selective loss of GABAergic inhibition in the superficial dorsal horn of the spinal cord. *The Journal of neuroscience: the official journal of the Society for Neuroscience* **22**, 6724–6731, doi:20026611 (2002).
24. Sandkuhler, J. Models and mechanisms of hyperalgesia and allodynia. *Physiological reviews* **89**, 707–758, doi:10.1152/physrev.00025.2008 (2009).
25. Takazawa, T. & MacDermott, A. B. Glycinergic and GABAergic tonic inhibition fine tune inhibitory control in regionally distinct subpopulations of dorsal horn neurons. *The Journal of physiology* **588**, 2571–2587, doi:10.1113/jphysiol.2010.188292 (2010).
26. Tong, C. K. & MacDermott, A. B. Both Ca2+ -permeable and -impermeable AMPA receptors contribute to primary synaptic drive onto rat dorsal horn neurons. *The Journal of physiology* **575**, 133–144, doi:10.1113/jphysiol.2006.110072 (2006).
27. Liu, S. Q. & Cull-Candy, S. G. Synaptic activity at calcium-permeable AMPA receptors induces a switch in receptor subtype. *Nature* **405**, 454–458, doi:10.1038/35013064 (2000).
28. Detloff, M. R., Fisher, L. C., Delbert, R. J. & Basso, D. M. Acute and chronic tactile sensory testing after spinal cord injury in rats. *Journal of visualized experiments: JoVE* e3247, doi:10.3791/3247 (2012).
29. Tan, A. M., Chakrabarty, S., Kimura, H. & Martin, J. H. Selective corticospinal tract injury in the rat induces primary afferent fiber sprouting in the spinal cord and hyperreflexia. *The Journal of neuroscience: the official journal of the Society for Neuroscience* **32**, 12896–12908, doi:10.1523/jneurosci.6451-11.2012 (2012).
30. Kopach, O. *et al.* PKCalpha is required for inflammation-induced trafficking of extrasynaptic AMPA receptors in tonically firing lamina II dorsal horn neurons during the maintenance of persistent inflammatory pain. *The journal of pain: official journal of the American Pain Society* **14**, 182–192, doi:10.1016/j.jpain.2012.10.015 (2013).
31. Kopach, O., Viatchenko-Karpinski, V., Belan, P. & Voitenko, N. Development of inflammation-induced hyperalgesia and allodynia is associated with the upregulation of extrasynaptic AMPA receptors in tonically firing lamina II dorsal horn neurons. *Frontiers in physiology* **3**, 391, doi:10.3389/fphys.2012.00391 (2012).
32. Hao, J. X., Kupers, R. C. & Xu, X. J. Response characteristics of spinal cord dorsal horn neurons in chronic allodynic rats after spinal cord injury. *Journal of neurophysiology* **92**, 1391–1399, doi:10.1152/jn.00121.2004 (2004).
33. Zhang, Z., Cai, Y. Q., Zou, F., Bie, B. & Pan, Z. Z. Epigenetic suppression of GAD65 expression mediates persistent pain. *Nature medicine* **17**, 1448–1455, doi:10.1038/nm.2442 (2011).
34. Drew, G. M., Siddall, P. J. & Duggan, A. W. Mechanical allodynia following contusion injury of the rat spinal cord is associated with loss of GABAergic inhibition in the dorsal horn. *Pain* **109**, 379–388, doi:10.1016/j.pain.2004.02.007 (2004).
35. Ferguson, A. R. *et al.* Cell death after spinal cord injury is exacerbated by rapid TNF alpha-induced trafficking of GluR2-lacking AMPARs to the plasma membrane. *The Journal of neuroscience: the official journal of the Society for Neuroscience* **28**, 11391–11400, doi:10.1523/jneurosci.3708-08.2008 (2008).
36. Hasbargen, T. *et al.* Role of NKCC1 and KCC2 in the development of chronic neuropathic pain following spinal cord injury. *Annals of the New York Academy of Sciences* **1198**, 168–172, doi:10.1111/j.1749-6632.2010.05462.x (2010).
37. Lu, Y., Zheng, J., Xiong, L., Zimmermann, M. & Yang, J. Spinal cord injury-induced attenuation of GABAergic inhibition in spinal dorsal horn circuits is associated with down-regulation of the chloride transporter KCC2 in rat. *The Journal of physiology* **586**, 5701–5715, doi:10.1113/jphysiol.2008.152348 (2008).
38. Kopach, O. *et al.* Inflammation alters trafficking of extrasynaptic AMPA receptors in tonically firing lamina II neurons of the rat spinal dorsal horn. *Pain* **152**, 912–923, doi:10.1016/j.pain.2011.01.016 (2011).
39. Punnakkal, P., von Schoultz, C., Haenraets, K., Wildner, H. & Zeilhofer, H. U. Morphological, biophysical and synaptic properties of glutamatergic neurons of the mouse spinal dorsal horn. *The Journal of physiology* **592**, 759–776, doi:10.1113/jphysiol.2013.264937 (2014).
40. Yasaka, T., Tiong, S. Y., Hughes, D. I., Riddell, J. S. & Todd, A. J. Populations of inhibitory and excitatory interneurons in lamina II of the adult rat spinal dorsal horn revealed by a combined electrophysiological and anatomical approach. *Pain* **151**, 475–488, doi:10.1016/j.pain.2010.08.008 (2010).
41. Chen, Y., Balasubramanyan, S., Lai, A. Y., Todd, K. G. & Smith, P. A. Effects of sciatic nerve axotomy on excitatory synaptic transmission in rat substantia gelatinosa. *Journal of neurophysiology* **102**, 3203–3215, doi:10.1152/jn.00296.2009 (2009).
42. Coombs, I. D. *et al.* Cornichons modify channel properties of recombinant and glial AMPA receptors. *The Journal of neuroscience: the official journal of the Society for Neuroscience* **32**, 9796–9804, doi:10.1523/jneurosci.0345-12.2012 (2012).
43. Burnashev, N., Monyer, H., Seeburg, P. H. & Sakmann, B. Divalent ion permeability of AMPA receptor channels is dominated by the edited form of a single subunit. *Neuron* **8**, 189–198 (1992).

44. Park, J. S. *et al.* Persistent inflammation induces GluR2 internalization via NMDA receptor-triggered PKC activation in dorsal horn neurons. *The Journal of neuroscience: the official journal of the Society for Neuroscience* **29**, 3206–3219, doi:10.1523/jneurosci.4514-08.2009 (2009).
45. Engelman, H. S., Allen, T. B. & MacDermott, A. B. The distribution of neurons expressing calcium-permeable AMPA receptors in the superficial laminae of the spinal cord dorsal horn. *The Journal of neuroscience: the official journal of the Society for Neuroscience* **19**, 2081–2089 (1999).
46. Polgar, E., Watanabe, M., Hartmann, B., Grant, S. G. & Todd, A. J. Expression of AMPA receptor subunits at synapses in laminae I–III of the rodent spinal dorsal horn. *Molecular pain* **4**, 5, doi:10.1186/1744-8069-4-5 (2008).
47. Chirila, A. M. *et al.* Long-term potentiation of glycinergic synapses triggered by interleukin 1beta. *Proceedings of the National Academy of Sciences of the United States of America* **111**, 8263–8268, doi:10.1073/pnas.1401013111 (2014).
48. Bannatyne, B. A., Edgley, S. A., Hammar, I., Jankowska, E. & Maxwell, D. J. Differential projections of excitatory and inhibitory dorsal horn interneurons relaying information from group II muscle afferents in the cat spinal cord. *The Journal of neuroscience: the official journal of the Society for Neuroscience* **26**, 2871–2880, doi:10.1523/jneurosci.5172-05.2006 (2006).
49. Li, Y., Li, X., Harvey, P. J. & Bennett, D. J. Effects of baclofen on spinal reflexes and persistent inward currents in motoneurons of chronic spinal rats with spasticity. *Journal of neurophysiology* **92**, 2694–2703, doi:10.1152/jn.00164.2004 (2004).
50. Krach, L. E. Pharmacotherapy of spasticity: oral medications and intrathecal baclofen. *Journal of child neurology* **16**, 31–36 (2001).
51. Gerasimenko, Y. P. *et al.* Noninvasive Reactivation of Motor Descending Control after Paralysis. *Journal of neurotrauma* **32**, 1968–1980, doi:10.1089/neu.2015.4008 (2015).
52. Dietz, V. & Fouad, K. Restoration of sensorimotor functions after spinal cord injury. *Brain: a journal of neurology* **137**, 654–667, doi:10.1093/brain/awt262 (2014).
53. Sindou, M. Microsurgical DREZotomy (MDT) for pain, spasticity, and hyperactive bladder: a 20-year experience. *Acta neurochirurgica* **137**, 1–5 (1995).
54. Webb, A. A. & Muir, G. D. Compensatory locomotor adjustments of rats with cervical or thoracic spinal cord hemisections. *Journal of neurotrauma* **19**, 239–256, doi:10.1089/089771502506883 (2002).
55. Martinez, M., Brezun, J. M., Bonnier, L. & Xerri, C. A new rating scale for open-field evaluation of behavioral recovery after cervical spinal cord injury in rats. *Journal of neurotrauma* **26**, 1043–1053, doi:10.1089/neu.2008.0717 (2009).
56. Haas, B. M., Bergstrom, E., Jamous, A. & Bennie, A. The inter rater reliability of the original and of the modified Ashworth scale for the assessment of spasticity in patients with spinal cord injury. *Spinal cord* **34**, 560–564 (1996).
57. Hahm, S. C., Yoon, Y. W. & Kim, J. High-frequency transcutaneous electrical nerve stimulation alleviates spasticity after spinal contusion by inhibiting activated microglia in rats. *Neurorehabilitation and neural repair* **29**, 370–381, doi:10.1177/1545968314545172 (2015).
58. Kopach, O., Krotov, V., Goncharenko, J. & Voitenko, N. Inhibition of Spinal Ca(2+)-Permeable AMPA Receptors with Dicationic Compounds Alleviates Persistent Inflammatory Pain without Adverse Effects. *Frontiers in cellular neuroscience* **10**, 50, doi:10.3389/fncel.2016.00050 (2016).
59. Traynelis, S. F., Silver, R. A. & Cull-Candy, S. G. Estimated conductance of glutamate receptor channels activated during EPSCs at the cerebellar mossy fiber-granule cell synapse. *Neuron* **11**, 279–289 (1993).

Acknowledgements

This work was supported by the NAS Ukraine (grants to NV). The authors thank Ms E. Ischenko for the help in animal pain testing, Mr. M. Tatarchuk for his help with the H-reflex recordings, Dr. A. Stepanyuk for the PS-NSF analysis, Prof. D.A. Rusakov for the helpful comments and discussion.

Author Contributions

O.K.: research design, electrophysiological recordings, data analysis and interpretation, manuscript preparation. V.M.: surgery, the H-reflex recordings, assessment of motor dysfunctions. V.K.: peripheral sensitivity measurements, data analysis and interpretation. A.B.: analysis of the AMPAR conductance. V.T. and N.V.: conceiving the study, manuscript revision.

Additional Information

Supplementary information accompanies this paper at doi:10.1038/s41598-017-06049-7

Competing Interests: The authors declare that they have no competing interests.

Publisher's note: Springer Nature remains neutral with regard to jurisdictional claims in published maps and institutional affiliations.

3.3. Гіперзбудливість сенсорних нейронів, спричинена збільшенням внутрішньоклітинного входу Ca^{2+}, призводить до виникнення больового синдрому при хворобі Фабрі

Neuroscience Letters 594 (2015) 163–168

Contents lists available at ScienceDirect

Neuroscience Letters

journal homepage: www.elsevier.com/locate/neulet

Plenary article

The Fabry disease-associated lipid Lyso-Gb3 enhances voltage-gated calcium currents in sensory neurons and causes pain

L. Choi [a,1], J. Vernon [a,1], O. Kopach [a,1], M.S. Minett [a], K. Mills [a,2], P.T. Clayton [a,2], T. Meert [a,3], J.N. Wood [a,b,*]

[a] Molecular Nociception Group, Wolfson Institute for Biomedical Research, University College London, Gower St., London, WC1E 6BT, UK
[b] BK21 Programme, Department of Molecular Medicine, Seoul National University, South Korea

HIGHLIGHTS

- Gb3 and Lyso-Gb3, plasma lipids accumulating in Fabry disease, cause mechanical allodynia in mice.
- Lyso-Gb3 elevates intracellular calcium level in sensory neurons.
- Lyso-Gb3 enhances voltage-dependent calcium currents in small-diameter DRG neurons.
- Direct effects of lyso-Gb3 on sensory neurons may contribute to the pain of Fabry disease.

ARTICLE INFO

Article history:
Received 3 January 2015
Received in revised form 22 January 2015
Accepted 25 January 2015
Available online 16 February 2015

Keywords:
Pain
Calcium imaging
Voltage-dependent Ca^{2+} channels
Fabry disease
Dorsal root ganglia

ABSTRACT

Fabry disease is an X-linked lysosomal storage disorder characterised by accumulation of glycosphingolipids, and accompanied by clinical manifestations, such as cardiac disorders, renal failure, pain and peripheral neuropathy. Globotriaosylsphingosine (lyso-Gb3), a deacylated form of globotriaosylceramide (Gb3), has emerged as a marker of Fabry disease. We investigated the link between Gb3, lyso-Gb3 and pain. Plantar administration of lyso-Gb3 or Gb3 caused mechanical allodynia in healthy mice. *In vitro* application of 100 nM lyso-Gb3 caused uptake of extracellular calcium in 10% of sensory neurons expressing nociceptor markers, rising to 40% of neurons at 1 μM, a concentration that may occur in Fabry disease patients. Peak current densities of voltage-dependent Ca^{2+} channels were substantially enhanced by application of 1 μM lyso-Gb3. These studies suggest a direct role for lyso-Gb3 in the sensitisation of peripheral nociceptive neurons that may provide an opportunity for therapeutic intervention in the treatment of Fabry disease-associated pain.

1. Introduction

Fabry disease (OMIM 301500) is a lysosomal storage disorder caused by a deficiency or absence of the enzyme α-galactosidase A, due to mutations of the X-linked gene *GLA* [1]. As a result, unmetabolised glycosphingolipids accumulate in various types of cells including neurons of the dorsal root ganglia (DRG) [2]. Accumulation in the lysosomes of vascular endothelial cells contributes to a characteristic renal and cardiovascular pathology. Neuropathic pain, typically a sensation of burning, itching or shooting pain in the hands and feet, is an early symptom of Fabry disease [2–4]. However, little is known about the direct effects of accumulated lipids on neuronal function.

Among the glycosphingolipids which are found to be elevated in patients with Fabry disease, globotriaosylceramide (Gb3) has been recognised as a diagnostic and predictive marker [5]. However, recent studies suggest the existence of other factors in addition to Gb3, since GLA enzyme replacement therapy for clearance of excessive Gb3 does not result in remission, and Gb3 levels do not always correlate with severity [6]. Globotriaosylsphingosine (lyso-Gb3), a deacylated form of Gb3, has emerged as a good biomarker for Fabry disease since a robust increase in plasma in both patients and animal models has been reported [7]. Lyso-Gb3 has been proposed to play a causative role in Fabry disease

Abbreviations: Gb3, globotriaosylceramide; Lyso-Gb3, lyso-globotriaosylceramide; GLA, gene encoding alpha galactosidase A; HBSS, HEPES buffered saline; PBS, phosphate buffered saline.

* Corresponding author at: BK21 Programme, Department of Molecular Medicine, Seoul National University, South Korea. Tel.: +44 207 679 6954; fax: +44 207 679 6619.
E-mail address: j.wood@ucl.ac.uk (J.N. Wood).
[1] Equal first authors.
[2] Biochemistry Research Group, Clinical and Molecular Genetics Unit, Institute of Child Health, University College London, WC1N 1EH, United Kingdom
[3] Janssen Pharmaceutica, Turnhoutseweg 30 2340, Beerse, Belgium

http://dx.doi.org/10.1016/j.neulet.2015.01.084

pathogenesis by accelerating Gb3 storage [7]. In GLA null mutant mice and in Fabry patients, the drug migalastat-HCl lowers plasma levels of lyso-Gb3, which suggests that the lyso marker is clinically relevant [8,9], although phase III drug trial endpoints were not met [10]. Migalastat both mimics the terminal galactose on Gb3, and stabilises the structure of mutant GLA, while it is targeted to the lysosome where Gb3 can be metabolised. However, the contribution of lyso-Gb3 to Fabry pain is uncertain.

Pain is a response to noxious stimuli, such as cold or heat, mechanical stress or the signals arising during inflammation. The noxious stimulus is detected by peripheral damage-sensing neurons (nociceptors). The depolarisation of the nociceptor is usually linked to an increase in cytosolic Ca^{2+} levels [19]. Although accumulation of lipids in DRG has been reported in Fabry patients [2], the effect of elevated glycosphingolipids on sensory neuron function has not been investigated. We therefore, examined whether lyso-Gb3 functionally affects nociceptive neurons to determine if there is a causal link between the marker lyso-Gb3 and pain in Fabry disease.

2. Material and methods

2.1. Animals

All experiments were approved by the UCL ethics board with prior approval by the UK home office. C57/BL6 mice (Charles River, UK) were treated in accordance with the UK Animal (Scientific Procedures) Act 1986.

2.2. Von Frey test

Mechanical withdrawal thresholds were measured by applying von Frey hairs (Stoelting, Wood Dale, USA) to the plantar surface of the hindpaw. The 50% paw withdrawal threshold was calculated using the up-and-down method [11]. Animals received a plantar injection of Gb3, lyso-Gb3 or saline (20 μl) 30 min prior to testing. All experiments were performed blind to treatment.

2.3. Adult DRG neuronal culture

DRG from all spinal levels were dissected from adult 7–8 week old mice and cultured as previously described [12]. Dissociated cells were plated on 1 μg/ml poly-L-lysine and 0.02 mg/ml laminin pre-coated either 15 mm cover slips (for calcium imaging) or 35 mm petri dishes (for whole-cell patch clamp recording).

2.4. Calcium imaging

Plated DRG cells were washed with Ca^{2+} recording buffer consisting of (in mM) 140 $NaCl_2$, 4 KCl, 2$CaCl_2$, 1 $MgCl_2$, 10 HEPES, 10 glucose adjusted to pH 7.4 and osmolality 320 mOsm/l using NaOH and sucrose, respectively. Cells were incubated in recording buffer with 2.5 μM Fura-2AM (Invitrogen, UK) for 30 min at room temperature. In some experiments, cells were pre-treated with 5 μg/l IB4-FITC (Sigma, UK) in culture medium at 37 °C for 20 min before Fura-2AM loading. Cells were washed twice with Ca^{2+} recording buffer for 5 min each time at room temperature to remove excess Fura-2AM. A coverslip of cells was placed over the window of a SA-NIK stage adapter (Warner Instruments). The perfusing chamber was tightened onto the adapter, with vacuum grease silicone (Beckman, USA) to enhance the seal. 0.5 ml of Ca^{2+} recording buffer was loaded onto the perfusing chamber before the whole assembly was mounted onto the stage of a Nikon Eclipse TE300 microscope. The inlet tube of a perfusing system (cFlow 8 Channel Flow Controller, Cell Micro Controls, USA) was connected to the recording chamber, and the speed of superfusate was set to 250 μl/min. Images were obtained using either a 20× or 40× (oil immersion) Nikon objective, equipped with fluorescent filter sets. A Till polychrome II monochromator was used to excite the fluorescence of Fura-2 at 340 nm and 380 nm, and data were acquired using OptoFluor software (Cairn Research, UK). Fura-2AM emission was collected at 505 nm.

2.5. Electrophysiology

Whole-cell patch-clamp recordings were performed at room temperature using an Axopatch 200B amplifier and Digidata board 1320A controlled by pClamp v9.0 software (Axon Instruments, Molecular Devices Inc.). Recording pipettes were pulled from borosilicate glass microcapillaries (Intracel Ltd., Herts, UK) with a range of pipette resistances between 2 and 4 MΩ after filling with intracellular solution consisting of (in mM) 146 $CsCl_2$, 1 $CaCl_2$, 4 $MgCl_2$, 10 HEPES–Na, 10 EGTA, 4.5 MgATP and 0.4 GTP–Na, adjusted to pH 7.3 and osmolarity 300 mOsm/l using CsOH and sucrose, respectively. Recordings were performed in voltage-clamp mode and currents were low-pass filtered at 5 kHz and sampled at 10 kHz. Values for series resistance (Rs) and capacitance (Cm) were read directly from the amplifier after subtraction of capacitative transients. Series resistances were compensated to the maximum extent possible (usually 60–75%) and voltages were not corrected for liquid junction potentials. External solution consisting of (in mM) 162.5 tetraethylammonium (TEA)–Cl, 5 $CaCl_2$, 1 $MgCl_2$, 10 glucose and 10 HEPES with pH adjusted to 7.4 using TEA–OH was used to isolate calcium currents. Lyso-Gb3 was applied to cells *via* a perfusing system and the speed of perfusing solution was set at 1 ml/min. Only small-diameter DRG neurons (with capacitance less than 25 pF) were chosen for recording. Off-line data analysis was performed using ClampFit v9.0 software (Axon Instruments, Molecular Devices Inc.).

Drugs stocks of Fura-2AM (Invitrogen, UK) and lyso-Gb3 (Sigma, UK) were dissolved in DMSO and HBSS containing 2 mM Ca^{2+} and 1 mM Mg^{2+}, respectively. Stocks of capsaicin (8-methyl-*N*-vanillyl-*trans*-6-nonenamide, Sigma, UK) were prepared in ethanol. For intraplantar administration, Gb3 or lyso-Gb3 (Matreya LLC, UK) were prepared in saline. 50 mM KCl was prepared in Ca^{2+} recording buffer on the same day for use.

2.6. Statistical analysis

One way ANOVA was followed by a Bonferroni *post-hoc* test when statistical significance was observed. Comparison between two groups was performed with independent samples *T*-test, and a Student's paired *T*-test was used to compare two different conditions in the same cell unless otherwise stated. Data were presented as the mean ± SEM. All statistical analyses were performed using Prism 5 for Windows.

3. Results

3.1. Treatment with Gb3 or lyso-Gb3 induces mechanical allodynia in healthy mice

We administered 20 μl of 30 μM Gb3 or lyso-Gb3 to the hind paws of wild type mice and tested sensitivity at different time points. As seen in Fig. 1A, both Fabry lipids significantly reduced pain thresholds compared to saline ($P < 0.05$). The increased sensitivity lasted up to 6 h. All the mice completely recovered from the acute mechanical allodynia 24 h post injection.

3.2. Exogenous lyso-Gb3 increases intracellular Ca^{2+} in sensory neurons

We next examined the cellular actions of lyso-Gb3 on DRG sensory neurons in culture. We investigated the effect of apply-

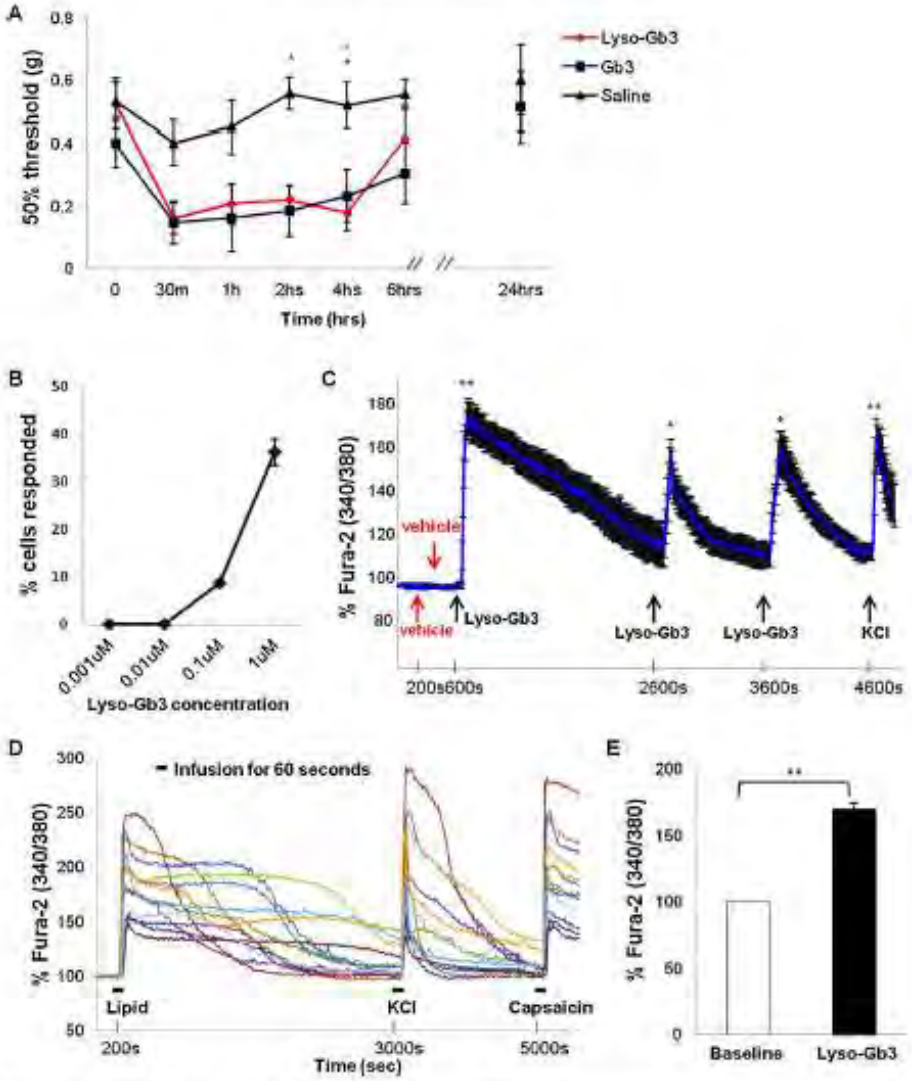

Fig. 1. Effects of lyso-Gb3 on pain sensitivity and intracellular Ca^{2+} levels in nociceptive DRG neurons.
(A) Either Gb3 or lyso-Gb3 injected into mice hind paws significantly enhanced pain sensitivity to mechanical stimuli over several hours post injection ($n = 6$–9 per group). Sensitivity resolved to a normal level within 24 h. Repeated measures ANOVA revealed effects of time: $F(6,126) = 7.551$, $P < 0.0001$, and of Fabry lipids ($F(21,126) = 3.089$, $P < 0.001$) but no difference between the two lipids (effect of lipid type: $F(2,126) = 6.179$, $P < 0.05$).
(B) Lyso-Gb3 evoked an increase in cytoplasmic Ca^{2+} levels in DRG neurons in a dose-dependent manner. The concentration of lyso-Gb3 producing changes in Ca^{2+} levels is plotted against the percentage of responsive DRG neurons. (C) Repetitive applications of lyso-Gb3 (1 μM), but not vehicle evoked transient increases in Ca^{2+} levels in DRG neurons. (D) Representative real time recordings of the changes in Fura-2 ratio acquired every 10 s in individual DRG neurons during bath applications of 1 μM Lyso-Gb3, 50 mM KCl and 1 μM capsaicin. (E) Statistical summary of the changes in Fura-2 ratio before and after application of 1 μM of lyso-Gb3 ($n = 74$). *$P < 0.05$ and **$P < 0.0001$.

ing lyso-Gb3 on the levels of intracellular Ca^{2+} of DRG neurons. Increased Ca^{2+} levels were observed following lyso-Gb3 application at concentrations higher than 0.1 μM (Fig 1B). Concentrations between 0.1 and 1 μM are found in Fabry disease patients with clinical manifestations [13,14]. Our results indicate that clinical lyso-Gb3 concentrations cause a concentration-dependent increase in Ca^{2+} levels in the cytoplasm of sensory neurons. We then used 1 μM lyso-Gb3 to test if repetitive application of lipid could trigger a repetitive rise in intracellular Ca^{2+} level in DRG neurons. Fig. 1C demonstrates that whilst applications of vehicle alone did not affect basal Ca^{2+} levels, 1 μM lyso-Gb3 applied three times evoked transient increases in Ca^{2+} levels. Administration of high-potassium-containing medium (KCl, 50 mM) evoked a depolarization-mediated rise in intracellular Ca^{2+} level in every tested neuron (Fig. 1C and D). All DRG neurons showing an increase in Ca^{2+} levels following lyso-Gb3 application and responding to 50 mM of KCl were capsaicin-sensitive as shown by an increase in cytoplasmic Ca^{2+} levels during application of 1 μM capsaicin (Fig. 1D).

3.3. *Lyso-Gb3 increases intracellular Ca^{2+} in capsaicin-sensitive peptidergic neurons*

Sensory neurons can be classified using a range of morphological and functional criteria. Small diameter sensory neurons, many of which are nociceptors, can be subdivided into peptidergic neurons

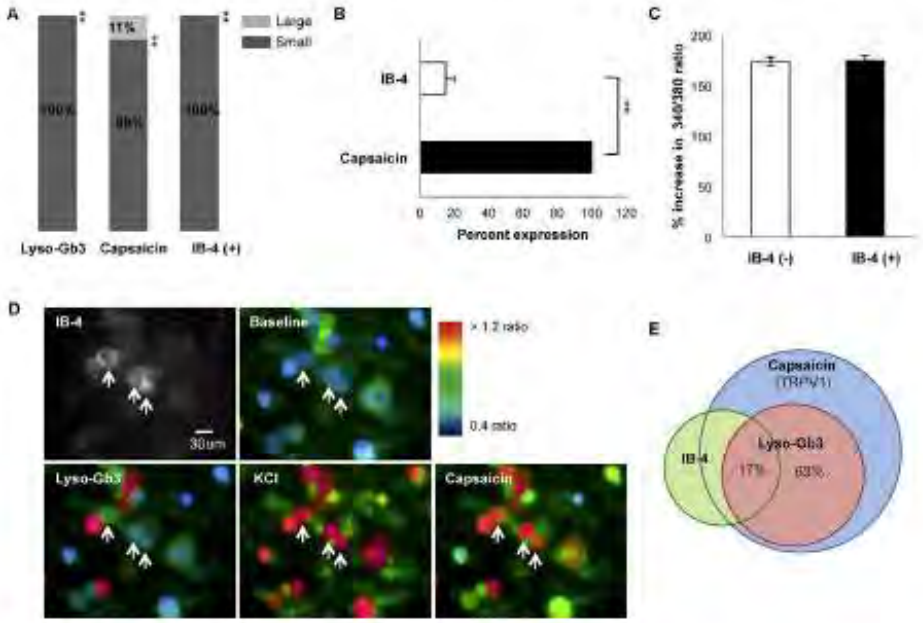

Fig. 2. Identification of the DRG neuron population responsive to lyso-Gb3.
(A) Distribution of cells according to diameter; lyso-Gb3 responders were all small-diameter cells, as were 89 % of capsaicin-responsive cells. The third bar of the histogram signifies that IB-4 positive cells were all small-diameter neurons. (B) Lyso-Gb3 responsive cells were all stimulated by 1 μM capsaicin, but only 17 % of these bound IB-4. (B) Other lyso-Gb3 responsive capsaicin-sensitive cells were IB-4 negative. (C) Statistical summary of the lyso-Gb3-induced changes in Fura-2 ratio in neuronal subgroups shows no significant difference between IB4-positive and IB4-negative DRG neurons. (D) Representative images showing the changes in Fura-2 fluorescence during application of lyso-Gb3, KCl or capsaicin in IB4-positive DRG neurons. Arrows point to the IB4-positive neurons. (E) Subpopulation of lyso-Gb3-responding neurons represents approximately 63% of capsaicin-sensitive DRG neurons, only 17% of those were positive for IB-4 binding. **P< 0.0001.

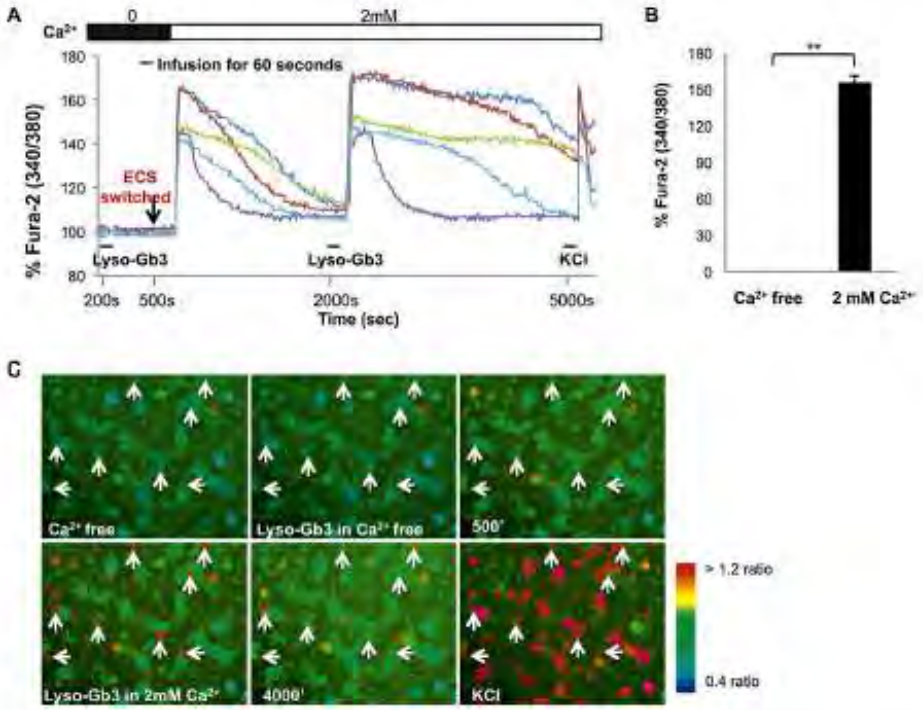

Fig. 3. Requirement for extracellular calcium in the Fura-2 response to lyso-GB3.
(A) Representative real time traces showing intracellular Ca^{2+} levels following superfusion with lyso-Gb3 in either Ca^{2+} free or standard recording buffer containing 2 mM Ca^{2+}. (B) Peak Fura-2AM 340/380 ratio between baseline and lyso-Gb3. Cells appear red in accordance with Ca^{2+} levels. (C) Representative fluorescent images showing changes in Ca^{2+} levels.
Note: Data sampled every 10 s during calcium imaging. ** P< 0.0001.

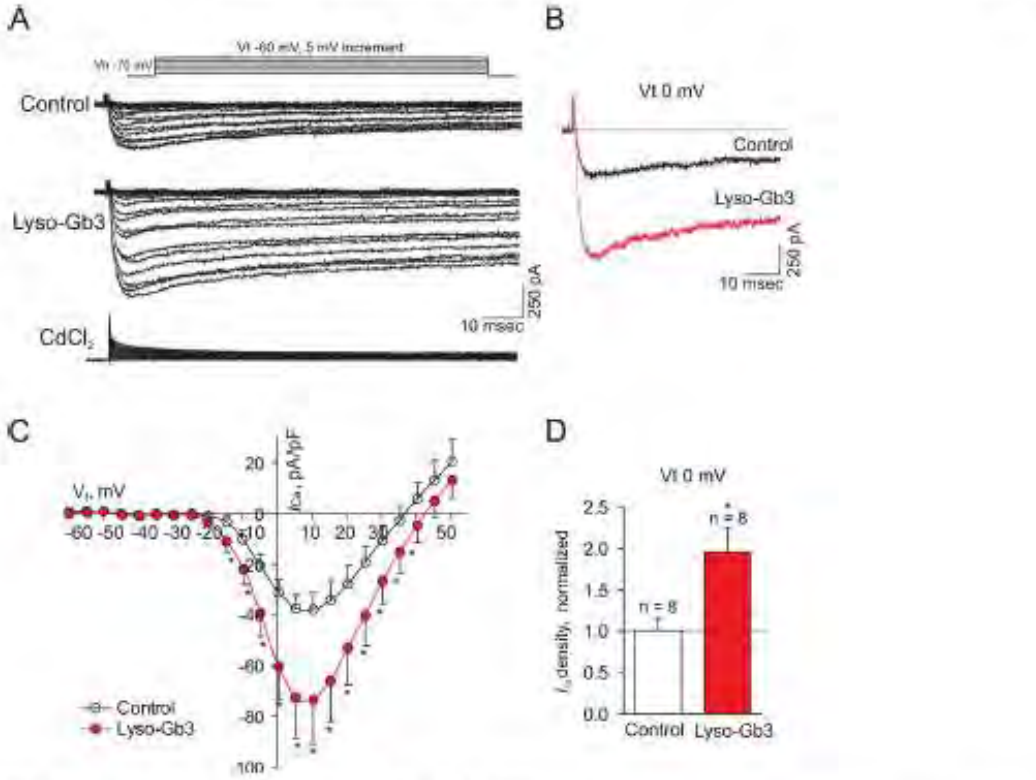

Fig. 4. Effects of lyso-Gb3 on Ca^{2+} influx and current density of voltage-activated Ca^{2+} channels in DRG neurons.
(A) Representative traces of Ca^{2+} currents evoked in the same small-diameter DRG neuron by voltage steps from holding potential (V_h) – 70 mV to test potential (V_t) from −60 mV to +50 mV in 5 mV increments before (top) or during (medium) application of 1 μM lyso-Gb3 via a perfusion system. Ca^{2+} currents (bottom) in the presence of lyso-Gb3 were completely inhibited by 50 μM $CdCl_2$. Inset illustrates the voltage-clamp protocol used to elicit currents. (B) Representative Ca^{2+} currents recorded at V_t 0 mV before (control) and after lyso-Gb3 application. (C) Average current–voltage relationships of Ca^{2+} currents before and during an application of 1 μM lyso-Gb3. The peak current amplitudes at each V_t were normalized to cell capacitance and expressed as the current density. (D) A statistical summary of the current densities at V_t 0 mV before and during lyso-Gb3 application. Changes in current density were normalized to control. $^*P < 0.05$ (paired t-test).

that do not bind the lectin IB4 and another subset that express c-Ret that do bind IB4, [15,16]. These two subsets of sensory neurons have been found to show functional differences [15]. We examined the subgroups of lyso-Gb3 responsive DRG neurons using calcium imaging combined with IB4 labelling. We measured the size of cells which showed at least a 30% increase in Fura-2 ratio following a 1 min superfusion with lyso-Gb3. The lipid responsive cells were identified as small-diameter neurons (Fig. 2A), responsive to 1 μM capsaicin and predominantly negative for IB4 staining – in other words peptidergic neurons (Fig. 2B). However, the average lyso-Gb3-evoked changes in Fura-2 ratio did not differ between IB4-positive and IB4-negative small-diameter DRG neurons (Fig. 2C). Fig. 2E illustrates the overlapping subpopulations detected in these experiments.

Fig. 3A shows that increased intracellular Ca^{2+} influx occurred only in the presence of Ca^{2+} in the recording buffer, indicating that the source for increased cytoplasmic Ca^{2+} was the extracellular solution and not intracellular stores.

3.4. Lyso-Gb3 increases the current density of voltage-dependent Ca^{2+} channels in small-diameter DRG neurons

Next we examined whether the lyso-Gb3-evoked increases in cytoplasmic Ca^{2+} levels were mediated by effects on voltage-activated Ca^{2+} channels, known to control Ca^{2+} entry during neuronal depolarisation [17]. To assess how lyso-Gb3 affects voltage-activated Ca^{2+} currents in nociceptive DRG neurons, we recorded inward Ca^{2+} currents in small-diameter DRG before (control) and during application of lyso-Gb3 by eliciting currents with a set of 250-ms voltage steps from −60 to +50 mV (V_t) in 5 mV increments (holding potential: −70 mV, see Fig. 4A top). In the presence of 1 μM lyso-Gb3, Ca^{2+} currents were significantly augmented in small-diameter DRG neurons at most of the tested membrane potentials (Fig. 4A and B). Furthermore, the current density of voltage-activated Ca^{2+} currents was significantly increased from V_t −15 mV to +35 mV ($n = 8$/membrane potential; $P < 0.05$; Fig. 4C and D). In the presence of vehicle for lyso-Gb3 there was no significant change in current before and during the application (data not shown).

4. Discussion

This study investigated a potential link between high levels of the Fabry lipid lyso-Gb3 and pain. In healthy mice administration of lyso-Gb3 induced mechanical allodynia. In peptidergic DRG neurons, lyso-Gb3 evoked an increase in intracellular Ca^{2+} levels associated with the functional upregulation of voltage-activated Ca^{2+} channels.

Plasma circulation of lyso-Gb3 and the concomitant lysosomal accumulation of Gb3 have been proposed to lead to pain in Fabry disease [7], and our study provides evidence consistent with this, by showing that healthy mice receiving plantar injections of Gb3

or lyso-Gb3 developed mechanical allodynia. This observation is consistent with direct sensitization of DRG neurons following infiltration of lysoGb3 into plasma. We found that lyso-Gb3 triggers a rise in intracellular Ca^{2+} levels in a subpopulation of DRG neurons that express markers associated with damage sensing. The origin of excessive lysoGb3 is not clearly identified, although drugs that stabilise the GLA enzyme also reduce the levels of lyso-Gb3 in plasma [9] suggesting that lyso-Gb3 is a direct product of normal lipid catabolism rather than the outcome of degradation.

This study is the first to show a direct link between lyso-Gb3, intracellular changes in peripheral sensory neurons and pain. The pain syndrome in Fabry disease was thought to arise from small fibre dysfunction, such as length dependent neuropathy which is typically linked to a loss or decrease of myelinated Aδ fibres and unmyelinated C fibres [4]. However, it is not known whether the exposure to or accumulation of lipids directly causes small nerve fiber damage [18], and our study did not investigate any neuropathic effects of lyso-Gb3. Nevertheless the possibility of small nerve fibre damage by lyso-Gb3 exists, given that promoted Ca^{2+} influx may cause Ca^{2+}-dependent excitotoxicity [19]. Our study showed that only high concentrations of lyso-Gb3 equivalent to the level in pre-treated Fabry patients evoked Ca^{2+} rises in small-diameter DRG neurons of the IB4 nonbinding, peptidergic sub-class.

Intracellular Ca^{2+} signalling regulates many cellular functions. In the present study, 1 μM lyso-Gb3, a possible concentration reported in patients with Fabry disease [13], was shown to induce a promoted membrane Ca^{2+} influx. Further, the lipid enhanced voltage-dependent Ca^{2+} current densities, indicating functional upregulation of voltage-dependent Ca^{2+} channels as a plausible mechanism of functional changes in peripheral nociceptors. Voltage-dependent Ca^{2+} channels in DRG neurons play a role in transmission of nociceptive signals from the periphery, and neuropathic manifestations including increased pain sensitivity have also been shown to be associated with increased Ca^{2+} entry in disease states, such as diabetes [20].

This is the first report showing the onset of mechanical allodynia, and augmented Ca^{2+} influx mediated by upregulated voltage-dependent Ca^{2+} channels in nociceptive DRG neurons, following lyso-Gb3 administration. This study shows that Fabry lipids may cause pain through direct actions on sensory neurons, and that promoted Ca^{2+}-dependent excitability of nociceptors is a possible mechanism. These observations support further investigation of the effects of Fabry-disease associated lipids on ion fluxes in sensory neurons and their potential significance in the pain associated with this condition.

Acknowledgements

We thank J and J, as well as the MRC, The Wellcome Trust, the BK21 programme, and the EU IMI for supporting our work.

References

[1] H. Fabry, Angiokeratoma corporis diffusum- Fabry disease: historical review from the original description to the introduction of enzyme replacement therapy, Acta Paediatr. 91 (2002) 3–5.
[2] E.M. Kaye, E.H. Kolodny, E.L. Logigian, M.D. Ullman, Nervous system involvement in Fabry's disease: clinicopathological and biochemical correlation, Ann. Neurol. 23 (1988) 505–509.
[3] A.T. Møller, T.S. Jensen, Neurological manifestations in Fabry's disease, Nat. Clin. Pract. Neurol. 3 (2007) 95–106.
[4] M. Dütsch, H. Marthol, B. Stemper, M. Brys, T. Haendl, M.J. Hilz, Small fiber dysfunction predominates in Fabry neuropathy, J. Clin. Neurophysiol. 19 (2002) 575–586.
[5] K. Mills, P. Morris, P. Lee, A. Vellodi, S. Waldek, E. Young, B. Winchester, Measurement of urinary CDH and CTH by tandem mass spectrometry in patients hemizygous and heterozygous for Fabry disease, J. Inherit. Metab. Dis. 28 (2005) 35–48.
[6] E. Young, K. Mills, P. Morris, A. Vellodi, P. Lee, S. Waldek, B. Winchester, Is globotriaosylceramide a useful biomarker in Fabry disease? Acta Pediatr. Suppl. 94 (2005) 51–54.
[7] J.M. Aerts, J.E. Groener, S. Kuiper, W.E. Donker-Koopman, A. Strijland, R. Ottenhoff, C. van Roomen, M. Mirzaian, F.A. Wijburg, G.E. Linthorst, A.C. Vedder, S.M. Rombach, J. Cox-Brinkman, P. Somerharju, R.G. Boot, C.E. Hollak, R.O. Brady, B.J. Poorthuis, Elevated globotriaosylsphingosine is a hallmark of Fabry disease, Proc. Natl. Acad. Sci. U. S. A. 105 (2008) 2812–2817.
[8] T. Ohshima, G.J. Murray, W.D. Swaim, G. Longenecker, J.M. Quirk, C.O. Cardarelli, Y. Sugimoto, I. Pastan, M.M. Gottesman, R.O. Brady, A.B. Kulkarni, Alpha-galactosidase A deficient mice: a model of Fabry disease, Proc. Natl. Acad. Sci. U. S. A. 94 (1997) 2540–2544.
[9] B. Young-Gqamana, N. Brignol, H.H. Chang, R. Khanna, R. Soska, M. Fuller, S.A. Sitaraman, D.P. Germain, R. Giugliani, D.A. Hughes, A. Mehta, K. Nicholls, P. Boudes, D.J. Lockhart, K.J. Valenzano, E.R. Benjamin, Migalastat HCl reduces globotriaosylsphingosine (lyso-Gb3) in Fabry transgenic mice and in the plasma of Fabry patients, PLoS One 8 (2013) e57631.
[10] T. Kierkegaard, Emerging therapies and therapeutic concepts for lysosomal storage diseases, Expert Opin. Orphan Drugs 1 (2013) 385–404.
[11] S.R. Chaplan, F.W. Bach, J.W. Pogrel, J.M. Chung, T.L. Yaksh, Quantitative assessment of tactile allodynia in the rat paw, J. Neurosci. Methods 53 (1994) 55–63.
[12] M.S. Minett, M.A. Nassar, A.K. Clark, G. Passmore, A.H. Dickenson, F. Wang, M. Malcangio, J.N. Wood, Distinct Nav1.7-dependent pain sensations require different sets of sensory and sympathetic neurons, Nat. Commun. 3 (2012) 791.
[13] F.O. Dupont, R. Gagnon, M. Boutin, C. Auray-Blais, A metabolomic study reveals novel plasma lyso-Gb3 analogs as Fabry disease biomarkers, Curr. Med. Chem. 20 (2013) 280–288.
[14] V. Manwaring, M. Boutin, C. Auray-Blais, A metabolomic study to identify new globotriaosylceramide-related biomarkers in the plasma of Fabry disease patients, Anal. Chem. 85 (2013) 9039–9048.
[15] C.L. Stucky, G.R. Lewin, Isolectin B(4)-positive and -negative nociceptors are functionally distinct, J. Neurosci. 19 (1999) 6497–6505.
[16] S. Dirajlal, L.E. Pauers, C.L. Stucky, Differential response properties of IB(4)-positive and -negative unmyelinated sensory neurons to protons and capsaicin, J. Neurophysiol. 89 (2003) 513–524.
[17] W.A. Catterall, Voltage-gated calcium channels, Cold Spring Harb. Perspect. Biol. 3 (2011) 1–23.
[18] S. Gupta, M. Ries, S. Kotsopoulos, R. Schiffmann, The relationship of vascular glycolipid storage to clinical manifestations of Fabry disease: a cross-sectional study of a large cohort of clinically affected heterozygous women, Med. (Baltimore) 84 (2005) 261–268.
[19] M. Arundine, M. Tymianski, Molecular mechanisms of calcium-dependent neurodegeneration in excitotoxicity, Cell Calcium 34 (2003) 325–337.
[20] N.V. Voitenko, I.A. Kruglikov, E.P. Kostyuk, P.G. Kostyuk, Effect of streptozotocin-induced diabetes on the activity of calcium channels in rat dorsal horn neurons, Neuroscience 95 (2000) 519–524.

3.4. Роль натрієвих каналів підтипу 1.9 у розвитку хронічного нейропатичного болю при невралгії трійчастого нерва

Luiz et al. Mol Pain (2015) 11:72
DOI 10.1186/s12990-015-0076-4

Molecular Pain

RESEARCH Open Access

The role of $Na_v1.9$ channel in the development of neuropathic orofacial pain associated with trigeminal neuralgia

Ana Paula Luiz[1*†], Olga Kopach[1†], Sonia Santana-Varela[1] and John N. Wood[1,2]

Abstract

Background: Trigeminal neuralgia is accompanied by severe mechanical, thermal and chemical hypersensitivity of the orofacial area innervated by neurons of trigeminal ganglion (TG). We examined the role of the voltage-gated sodium channel subtype $Na_v1.9$ in the development of trigeminal neuralgia.

Results: We found that $Na_v1.9$ is required for the development of both thermal and mechanical hypersensitivity induced by constriction of the infraorbital nerve (CION). The CION model does not induce change on $Na_v1.9$ mRNA expression in the ipsilateral TG neurons when evaluated 9 days after surgery.

Conclusions: These results demonstrate that $Na_v1.9$ channels play a critical role in the development of orofacial neuropathic pain. New routes for the treatment of orofacial neuropathic pain focussing on regulation of the voltage-gated $Na_v1.9$ sodium channel activity should be investigated.

Keywords: $Na_v1.9$ sodium channels, Trigeminal ganglion (TG) neurons, Constriction of the infraorbital nerve, Trigeminal neuralgia, Neuropathic pain

Background

Trigeminal neuralgia is an excruciating pain syndrome characterized by severe facial pain that can be triggered by light touch of the orofacial surface area producing stabbing, shooting or burning sensations. Trigeminal neuralgia is accompanied by mechanical, thermal and/or chemical hypersensitivities of the orofacial area and is maintained by impaired signaling in sensory neurons of trigeminal ganglion (TG) [1]. However, little is known about the intracellular mechanisms or altered functioning of TG nociceptors underling the development of orofacial pain.

Voltage-gated sodium channels play a central role in nociception, being key determinants of neuronal excitability. Specific expression of tetrodotoxin-resistant (TTX-R) voltage-gated sodium channels $Na_v1.8$ and $Na_v1.9$ subtypes was found for a restricted population of peripheral nociceptors in TG [2–4], dorsal root ganglion (DRG) [5–9], nodose ganglion [10], unmyelinated afferent fibres and nerve terminals [8, 9, 11, 12]. While $Na_v1.8$ channels carry the majority of inward current during the upstroke of the action potentials (AP) [13–15], $Na_v1.9$ channels sustain repetitive firing and plateau potentials [16, 17] due to their characteristic activation at relatively negative membrane potentials as well as slow and incomplete inactivation, producing "persistent" Na^+ flow at subthreshold voltages [18–20].

Studies of the role of $Na_v1.9$ channels showed that SCN11A null mutant mice developed reduced hyperalgesia in different inflammatory pain models [formalin, carrageenan, complete freund's adjuvant (CFA), prostaglandin E_2] [21, 22] as well as diminished nociceptive sensitivity triggered by inflammatory mediators [bradykinin, serotonin, adenosine triphosphate (ATP)] [2]. In contrast, $Na_v1.9^{-/-}$ mice showed unaltered pain-related behaviour in models of DRG-related neuropathic pain of various origins (partial sciatic nerve injury [2], chronic

*Correspondence: a.luiz@ucl.ac.uk
†Ana Paula Luiz and Olga Kopach contributed equally to this work
[1] Molecular Nociception Group, Wolfson Institute for Biomedical Research, University College London, Gower St, London WC1E 6BT, UK
Full list of author information is available at the end of the article

constriction injury (CCI) [23] and spinal nerve transaction [24]). Recent studies of human SCN11A gene mutations demonstrated that several mutations in this gene are associated with either, peripheral neuropathy and episodic chronic pain [25] or congenital inability to experience pain [26]. Despite the established role of $Na_v1.9$ channels in pain perception, the contribution of this channel subtype to the development of orofacial pain remains unknown, and how cephalic neuropathic pain develops with loss of $Na_v1.9$ channels has not been studied.

Using global $Na_v1.9$ knockout mice, we show for the first time that loss of $Na_v1.9$ channels is associated with the failure to develop orofacial pain in a model of trigeminal neuralgia.

Results

Basal orofacial sensitivity in $Na_v1.9^{+/+}$ and $Na_v1.9^{-/-}$ mice

To examine if the loss of $Na_v1.9$ channels could influence the sensitivity of the orofacial area, basal mechanical and thermal sensitivities were examined in $Na_v1.9^{+/+}$ and $Na_v1.9^{-/-}$ mice. Mechanical orofacial sensitivity was evaluated as a functional reaction in response to 0.04 g von Frey filament applied to the animal forehead innervated by the trigeminal nerve (Fig. 1a). A filament of 0.04 g intensity was chosen since I have been found to evoke nociceptive responses in the orofacial area after unilateral constriction of the infraorbital nerve (CION), but present almost no effect in control mice [27]. No differences in basal responses to mechanical stimulation were observed between genotypes ($n = 13–14$ mice, $p > 0.05$; Fig. 1c). Groups did not differ with regard to basal thermal sensitivity, measured as a latency of response to radiant heat applied to the vibrissal pad surface ($n = 13–14$ mice, $p > 0.05$; Fig. 1b, d). Thus, loss of $Na_v1.9$ channels does not affect basal orofacial sensitivity, either mechanical or thermal, in mice.

We next examined the responses of control and knockout mice to a sham surgical inflammation without nerve damage. No major differences in mechanical and thermal sensitivities were found between $Na_v1.9^{+/+}$ and $Na_v1.9^{-/-}$ mice, submitted to this sham surgical procedure with no CION, at different time-points (on days 2, 5, 7, 14, 21 and 28 post-surgery; $n = 13–14$ mice; Fig. 1e, f). Although, the orofacial area was sensitised after the sham surgical procedure, the surgery-induced changes were similar between $Na_v1.9^{+/+}$ and $Na_v1.9^{-/-}$ sham-operated mice for either threshold mechanical (by 26 %, $p < 0.01$ and by 31 %, $p < 0.001$ in $Na_v1.9^{+/+}$ and $Na_v1.9^{-/-}$ mice, respectively; $n = 13–14$ mice; Fig. 1g) or threshold thermal sensitivities (by 29 % and by 31 %, $n = 13–14$ mice, $p < 0.01$ in $Na_v1.9^{+/+}$ and $Na_v1.9^{-/-}$ mice, respectively; Fig. 1h).

Loss of $Na_v1.9$ channels alleviates CION-induced orofacial hypersensitivity

Constriction of the infraorbital nerve [25] led to a development of long-lasting mechanical hypersensitivity in $Na_v1.9^{+/+}$. This hypersensitivity developed 7 days after surgery, reached a peak at 2 weeks, and remained persistent until 3 weeks (Fig. 2a). CION-induced mechanical hypersensitivity was robust, showing a significantly increased reaction in response to von Frey filament applied to the forehead of $Na_v1.9^{+/+}$ and $Na_v1.9^{-/-}$ mice. The increase in the response frequency was 26 % ($p < 0.05$), 35 % ($p < 0.01$) and 31 % ($p < 0.01$) on day 7, 14 and 21 after CION respectively compared to sham-operated mice ($n = 13–14$ mice; Fig. 2a). Strikingly, in $Na_v1.9^{-/-}$ mice, CION was not accompanied by the development of hypersensitivity of the orofacial area. The responses of $Na_v1.9^{-/-}$ mice were similar to those observed in the littermates of the sham-operated group over all periods tested. Thus, loss of $Na_v1.9$ channels abolished the development of CION-induced mechanical hypersensitivity.

Loss of $Na_v1.9$ channels also abolished the development of CION-induced thermal hypersensitivity. Consistent with previous studies [28], CION produced a long-lasting thermal hypersensitivity in $Na_v1.9^{+/+}$ mice, which developed within 1 week after surgery. The CION-induced decrease in thermal latency in $Na_v1.9^{+/+}$ mice was 10 % ($p < 0.05$) on day 7 and 12 % ($p < 0.001$) on day 14 post-surgery. However, the latency was not changed in $Na_v1.9^{-/-}$ mice following CION over all period tested ($n = 13–14$ mice; Fig. 2b). Together, these results indicate that the $Na_v1.9$ channel is required for the development of neuropathic orofacial pain.

Expression of $Na_v1.9$ mRNA in TG on Sham and CION $Na_v1.9^{+/+}$ mice

As the $Na_v1.9^{-/-}$ mice did not develop mechanical or thermal hypersensitivity after CION, the next step was to evaluate if the CION model induced any change in the expression of $Na_v1.9$ mRNA in TG neurons. Sample from ipsilateral TG was processed on day 9 after surgery, for extraction of mRNA. As showed on Fig. 3, no $Na_v1.9$ mRNA expression difference was observed between the CION (1.06 ± 0.42) and Sham (1.12 ± 0.28) groups in $Na_v1.9^{+/+}$ mice ($p = 0.9026$).

Discussion

Considerable evidence suggests participation of $Na_v1.9$ channels in the perception of pain. Both gain of function and loss of function pain conditions have been associated with point mutations in $Na_v1.9$ [25, 26]. Two of those mutations led to a reduction in the current threshold and increased firing frequency in response to suprathreshold

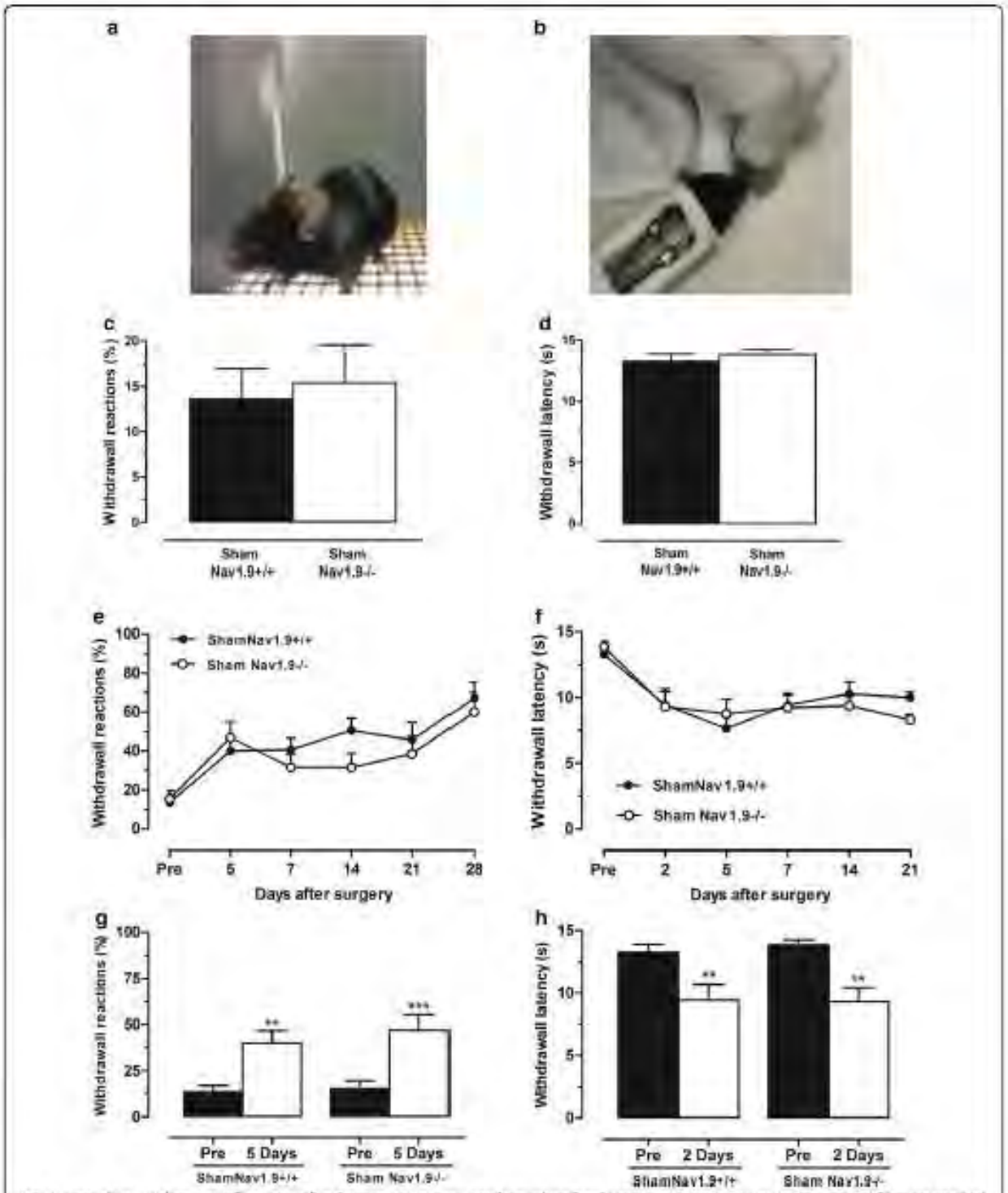

Fig. 1 Loss of $Na_v1.9$ does not influence orofacial sensitivity in mice. Mechanical orofacial sensitivity in response to 0.04 g von Frey filament applied to the forehead (**a**) and thermal orofacial sensitivity in response to radiant heat applied to a vibrissal pad (**b**) in sham-operated $Na_v1.9^{+/+}$ and $Na_v1.9^{-/-}$ mice. Mechanical (**c**) and thermal (**d**) orofacial sensitivities baselines. Mechanical (**e**) and thermal (**f**) orofacial sensitivities evaluated before (pre) and at different time-points after surgery. Changes in mechanical (**g**) and thermal (**h**) orofacial sensitivities after sham-operation. Values represent mean ± SEM analysed for 13–14 mice. **p < 0.01, ***p < 0.001 compared to that before surgery (pre) (Student paired t test)

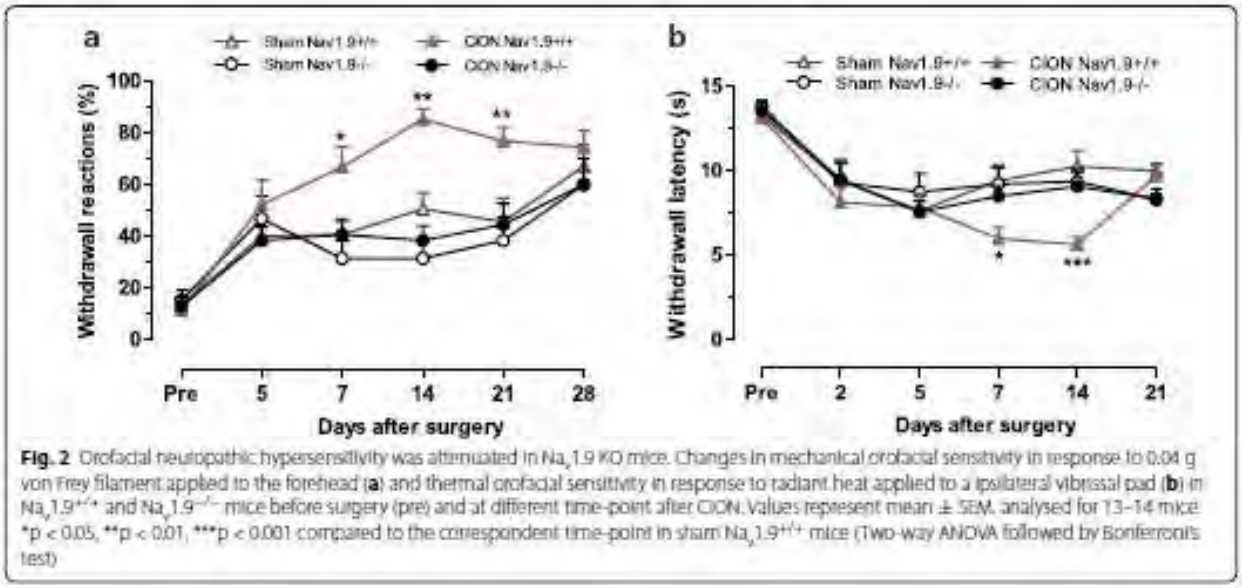

Fig. 2 Orofacial neuropathic hypersensitivity was attenuated in $Na_v1.9$ KO mice. Changes in mechanical orofacial sensitivity in response to 0.04 g von Frey filament applied to the forehead (**a**) and thermal orofacial sensitivity in response to radiant heat applied to a ipsilateral vibrissal pad (**b**) in $Na_v1.9^{+/+}$ and $Na_v1.9^{-/-}$ mice before surgery (pre) and at different time-point after CION. Values represent mean ± SEM, analysed for 13–14 mice. $^*p < 0.05$, $^{**}p < 0.01$, $^{***}p < 0.001$ compared to the correspondent time-point in sham $Na_v1.9^{+/+}$ mice (Two-way ANOVA followed by Bonferroni's test)

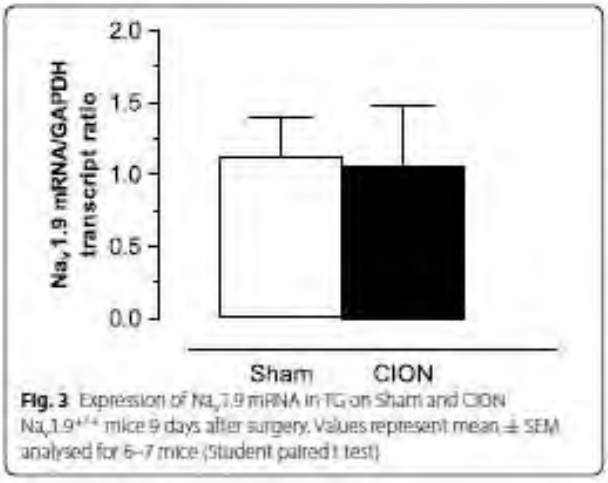

Fig. 3 Expression of $Na_v1.9$ mRNA in TG on Sham and CION $Na_v1.9^{+/+}$ mice 9 days after surgery. Values represent mean ± SEM analysed for 6–7 mice (Student paired t test)

stimuli [25]. Mutations in SCN11A (R225C and A808G), reported in patients experienced episodic chronic pain, caused an increase in the $Na_v1.9$ channels-mediated current density and hyperexcitability of nociceptive DRG neurons without changes in the resting membrane potential [29]. Other gain of function mutations lead $Na_v1.9$ channels to display excessive activity at resting voltages, causing sustained depolarization of nociceptors, impaired generation of action potentials and resulting in a pain-free state [26]. The principal mechanism by which $Na_v1.9$ channels contribute to painful states includes sensitization of nociceptors triggered by generation of persistent Na^+ currents at subthreshold voltages that promotes depolarization near the resting membrane potential, reduces the current threshold required to trigger an action potential, and results in hyperexcitability of sensory neurons [7, 16, 18–20, 30]. Here using $Na_v1.9^{-/-}$ mice, we show that $Na_v1.9$ channels are also involved in sustained (tonic) firing of nociceptive TG neurons and are required for the development of orofacial neuropathic pain.

The role of the $Na_v1.9$ channel in maintaining peripheral inflammatory pain has been demonstrated in different studies [21, 22, 30]. Inflammatory pain of different origins (induced by formalin, carrageenan, CFA, capsaicin, ATP, IL-1β or prostaglandin-E2) was substantially reduced in $Na_v1.9^{-/-}$ mice [21, 22, 30], while neuropathic pain, produced by CCI or spinal nerve transection, still developed, showing mechanical allodynia of the hind paw of $Na_v1.9^{-/-}$ mice [24, 31]. Using CION-induced model of orofacial neuropathic pain [28, 32], we demonstrate here the absence of both mechanical and thermal hypersensitivity of the orofacial area in $Na_v1.9^{-/-}$ mice after CION. Loss of $Na_v1.9$ channels did not change basal orofacial sensitivity (mechanical or thermal), indicating no major effects of $Na_v1.9$ deletion on normal nociceptive pathways. Our findings of a crucial role for $Na_v1.9$ channels in the development of neuropathic orofacial pain are in contrast with reports showing no critical involvement of these channels in the development of neuropathic pain in other somatic neuropathic pain models [24, 31]. This may reflect distinct mechanisms of neuropathic pain.

$Na_v1.9$ channels enhance sustained repetitive (tonic) firing in TG neurons. Previous studies showing that $Na_v1.9$ channels maintain sustained repetitive firing in DRG nociceptors and modulate patterns of firing discharge, including plateau potentials, active

hyperpolarizing responses, and sustained oscillatory bursting discharges [16, 18, 33]. It is intriguing that gain of function $Na_v1.9$ mutations in humans may result in enhanced pain or a complete loss of pain sensation [25, 26]. In transgenic mice, inflammatory pain is associated with enhanced $Na_v1.9$ persistent sodium channel activity [30]. In the present study, neuropathic pain is dependent on the activity of $Na_v1.9$ in a model of trigeminal neuralgia. A critical role for $Na_v1.9$ in regulating pain thresholds is thus clear, but the precise mechanisms that contribute to the different pain phenotypes remains to be established.

Conclusions

Our study demonstrates for the first time that the $Na_v1.9$ channel plays a critical role in the development of neuropathic orofacial pain associated with trigeminal neuralgia. Understanding how orbital nerve damage leads to myofascial pain through the modulation of $Na_v1.9$ activity may provide new approaches to the treatment of trigeminal neuralgia.

Methods

Animals

C57Bl/6 mice (2–3 month-old) were used in accordance with the protocols approved by the UK Home Office and UCL ethics committee under a Home Office project license. All efforts were made to minimise animal suffering and to reduce the number of animals used. Experiments were conducted using both male and female wild type littermate and global $Na_v1.9$ knockout mice bred from heterozygous ($Na_v1.9^{+/-}$) animals. The generation and characterization of the $Na_v1.9$ null mutant line was previously described [34]. Mouse colonies were genotyped by PCR using ear biopsy samples. Only homozygous $Na_v1.9$-null ($Na_v1.9^{-/-}$) and wild type ($Na_v1.9^{+/+}$) mice were used in these studies. Genomic DNA was extracted using a lysis buffer containing (in mM) 67 Tris, 16 $(NH_4)_2SO_4$, 6.7 $MgCl_2$, 100 β-mercaptoethanol, and 0.5 % Triton X-100 and 0.05 mg/ml proteinase K. The primers used were: 5′-AAC AGTCTTACGCTGTTCCGATG-3′ (sense), 5′-ATGTG GCACTGGGCTTGAACTC-3′ (antisense), 5′-CTCGTC GTGACCCATGGCGAT-3′ (Neomycin FW). PCR was performed in one reaction and resulted in a 276 bp fragment product for WT and a 600 bp band for knockout mice.

Infraorbital nerve constriction

To produce the painful condition of trigeminal neuralgia, we used a model of unilateral CION [25] according to a method previously described for rats [28, 35] with some modifications. Briefly, mice were anesthetized with an intramuscular (i.m.) injection of a mixture of ketamine (Fort Dodge Animal Health LTD, UK) and medetomidine (Orion Pharma, UK) in the doses of 50 and 0.5 mg/kg, respectively. One incision was made below the right eye 1 mm caudal to the myofascial (vibrissal) pads. The superior lip elevator and anterior superficial masseter muscles were dissected to expose the rostral end of the infraorbital nerve, as it emerges from the infraorbital fissure. Extra care was taken to prevent facial nerve damage. Two silk ligatures (No. 8.0, Ethicon) were loosely tied at a distance of 2 mm around the infraorbital nerve, producing a development of orofacial hypersensitivity and preventing infraorbital nerve destruction [35]. The incision was closed with polypropylene sutures (No. 6.0, Ethicon). After surgery, all animals were injected i.m. with atipamezole (5 mg/kg, Orion Pharma) and were maintained in a warmed area until full recovery from anaesthesia. Animals operated on an identical manner with no ligature applied to the nerve were used as control (sham).

Behavioral tests

Measurement of mechanical hyperalgesia

Mice were acclimatized in an individual animal enclosure (4″ × 4″) chamber for at least 1 h. Sham-operated or CION-injured animals were submitted to a repeated mechanical stimulus (0.04 g von Frey filament) applied to the forehead surface innervated by the trigeminal nerve (Fig. 1a). Each trial was repeated 10 times at 30-s interval at least. The occurrence of head reactions (attack/escape or head withdrawal) was expressed for each trial as the mean of percentage reactions that represents an index of mechanical nociceptive sensitivity [27]. To determine basal mechanical sensitivity, the mechanical stimulus was applied to the forehead of animals 1 day before surgery. A development of mechanical hyperalgesia following CION was estimated at different days after surgery.

Measurement of thermal hyperalgesia

Thermal hyperalgesia of the orofacial area was measured as previously described [28, 36]. Each animal was held in front of a radiant heat source positioned 1 cm from the vibrissal pad surface (Fig. 1b). The intensity of thermal stimulus applied to the vibrissal pad skin was adjusted to temperature of ~50 °C (15 s cut off). Once the animal started to withdraw its head or vigorously flick a snout, the heat beam was turned off. The time between the start of the beam and a functional response was defined as a latency of response. A reduction in the response latency reflected thermal hyperalgesia. To determine basal thermal sensitivity, a heat stimulus was applied to the ipsilateral side of the snout 1 day before surgery. Basal latency of responses was typically from 10 to 15 s. The

development of thermal hyperalgesia following CION was measured at different days after surgery.

$Na_v1.9$ expression analysis real-time PCR

After animal euthanasia (with a CO_2 chamber following by cervical dislocation), TG was quickly removed and placed in buffer RTL and RNA was isolated using RNeasy mini kit (Quiagen) according to the manufacturer instructions. The RNA was quantified by Nanodrop and converted to cDNA using iScript™ reverse transcription supermix for qRT-PCR (BioRad) according to the manufacturer instructions. PCR amplifications were performed using a Mastercycler ep realplex (Eppendorf). All samples were run in triplicate in a final volume of 20 µl containing 10 ng of cDNA, 1 µM of primers and SsoAdvanced™ universal SYBR® Green supermix (BioRad), according to manufacturer protocol. Prior to PCR, an 8 min enzyme activation step was done at 95 °C. The PCR protocol consisted of 10 s denaturation at 95 °C, 5 s at annealing temperature at 63 °C, 10 s elongation at 72 °C for 40 cycles. The annealing temperature was confirmed by melting curve. The primers sequences used were the following: TTCCACTCTACGTACCTTCCGAGT (forward) and ATTCCCATGAAGAGCTGCTGACCA (reverse) for $Na_v1.9$; TGCGACTTCAACAGCAACTC (forward) and CTTGCTCAGTGTCCTTGCTG (reverse) for GAPDH.

$Na_v1.9$ and GAPDH cDNA relative amounts were calculated function of the samples cycle threshold (Ct) using a standard concentration curve constructed with a serial dilution (10 times) from 100 to 0.01 ng of cDNA mix. For each sample, the relative amount of $Na_v1.9$ cDNA was normalized by the GAPDH cDNA amount.

Statistical analysis

Data were analyzed using GraphPad Prism 5. The results are presented as mean ± SEM with *n* referring to the number of animals tested. Multiple groups were compared using two-way analysis of variance [37] followed by Bonferroni post hoc test or Student paired t test as indicated.

Values of p less than 0.05 was considered as statistically significant for either test used.

Abbreviations

AP: action potential; ATP: adenosine triphosphate; CCI: chronic constriction injury; CFA: complete freund adjuvant; CION: constriction of the infraorbital nerve; DRG: dorsal root ganglion; IL-1β: interleukin-1 beta; mRNA: messenger ribonucleic acid; Nav1.8: voltage-gated sodium channel 1.8 subtype; Nav1.9: voltage-gated sodium channel 1.9 subtype; qRT-PCR: quantitative reverse transcription polymerase chain reaction; SCN11A: gene coding voltage-gated sodium channel 1.9 subtype; TG: trigeminal ganglion; TTX-R: tetrodotoxin-resistant.

Authors' contributions

APL: research concept, animal surgery and behavioural studies, data analysis and interpretation, drafting of the manuscript; OK: research concept, drafting of the manuscript; SS-V: animal surgery and pictures; JNW: research concept, supervision of studies, critical revision of the manuscript. All authors read and approved the final manuscript.

Author details

[1] Molecular Nociception Group, Wolfson Institute for Biomedical Research, University College London, Gower St, London WC1E 6BT, UK. [2] Department of Molecular Medicine and Biopharmaceutical Sciences, College of Medicine, Seoul National University, Seoul, South Korea.

Acknowledgements

This work was supported by Brazilian National Research Council Grant (CNPq), Brazilian Government Scholarship Programme Science without Border (A.P.L.), Wellcome Trust, the MRC and Arthritis UK Grants (J.N.W.). The authors thank Dr. Michael S. Minett for advice in behavioural studies.

Competing interests

The authors declare that they have no competing interests.

Received: 7 May 2015 Accepted: 12 November 2015
Published online: 25 November 2015

References

1. Wilcox SL, et al. Trigeminal nerve anatomy in neuropathic and non-neuropathic orofacial pain patients. J Pain. 2013;14(8):865–72.
2. Amaya F, et al. Diversity of expression of the sensory neuron-specific TTX-resistant voltage-gated sodium ion channels SNS and SNS2. Mol Cell Neurosci. 2000;15(4):331–42.
3. Padilla F, et al. Expression and localization of the Nav1.9 sodium channel in enteric neurons and in trigeminal sensory endings: implication for intestinal reflex function and orofacial pain. Mol Cell Neurosci. 2007;35(1):138–52.
4. Scroggs RS. The distribution of low-threshold TTX-resistant Na^+ currents in rat trigeminal ganglion cells. Neuroscience. 2012;222:205–14.
5. Akopian AN, Sivilotti L, Wood JN. A tetrodotoxin-resistant voltage-gated sodium channel expressed by sensory neurons. Nature. 1996;379(6562):257–62.
6. Black JA, et al. Changes in the expression of tetrodotoxin-sensitive sodium channels within dorsal root ganglia neurons in inflammatory pain. Pain. 2004;108(3):237–47.
7. Coste B, Crest M, Delmas P. Pharmacological dissection and distribution of NaN/Nav1.9, T-type Ca^{2+} currents, and mechanically activated cation currents in different populations of DRG neurons. J Gen Physiol. 2007;129(1):57–77.
8. Dib-Hajj S, et al. NaN/Nav1.9: a sodium channel with unique properties. Trends Neurosci. 2002;25(5):253–9.
9. Dib-Hajj SD, et al. NaN, a novel voltage-gated Na channel, is expressed preferentially in peripheral sensory neurons and down-regulated after axotomy. Proc Natl Acad Sci USA. 1998;95(15):8963–8.
10. Matsumoto S, et al. Effect of 8-bromo-cAMP on the tetrodotoxin-resistant sodium (Nav 1.8) current in small-diameter nodose ganglion neurons. Neuropharmacology. 2007;52(3):904–14.
11. Hang X, et al. Intense isolectin-B4 binding in rat dorsal root ganglion neurons distinguishes C-fiber nociceptors with broad action potentials and high Nav1.9 expression. J Neurosci. 2006;26(27):7281–92.
12. Persson AK, et al. Sodium–calcium exchanger and multiple sodium channel isoforms in intra-epidermal nerve terminals. Mol Pain. 2010;6:84.
13. Blair NT, Bean BP. Roles of tetrodotoxin (TTX)-sensitive Na^+ current, TTX-resistant Na^+ current, and Ca^{2+} current in the action potentials of nociceptive sensory neurons. J Neurosci. 2002;22(23):10277–90.
14. Cummins TR, et al. Glial-derived neurotrophic factor upregulates expression of functional SNS and NaN sodium channels and their currents in axotomized dorsal root ganglion neurons. J Neurosci. 2000;20(23):8754–61.
15. Suwanchai A, et al. NaV 1.8, but not NaV 1.9, is upregulated in the inflamed dental pulp tissue of human primary teeth. Int Endod J. 2012;45(4):372–8.

16. Mairiger F, et al. Inflammatory mediators increase Nav1.9 current and excitability in nociceptors through a coincident detection mechanism. J Gen Physiol. 2008;131(3):211–25.
17. Chorio N, Keroged S, Delmas P. Specialized functions of Nav1.5 and Nav1.9 channels in electrogenesis of myenteric neurons in intact mouse ganglia. J Neurosci. 2014;34(15):5233–44.
18. Coste B, et al. Gating and modulation of presumptive NaV1.9 channels in enteric and spinal sensory neurons. Mol Cell Neurosci. 2004;26(1):123–34.
19. Cummins TR, et al. A novel persistent tetrodotoxin-resistant sodium current in SNS-null and wild-type small primary sensory neurons. J Neurosci. 1999;19(24):RC43.
20. Maruyama H, et al. Electrophysiological characterization of the tetrodotoxin-resistant Na+ channel, Na(v)1.9, in mouse dorsal root ganglion neurons. Pflugers Arch. 2004;449(1):76–87.
21. Lolignier S, et al. Nav1.9 channel contributes to mechanical and heat pain hypersensitivity induced by subacute and chronic inflammation. PLoS One. 2011;6(8):e23083.
22. Priest BT, et al. Contribution of the tetrodotoxin-resistant voltage-gated sodium channel NaV1.9 to sensory transmission and nociceptive behavior. Proc Natl Acad Sci USA. 2005;102(26):9382–7.
23. Hillsley K, et al. Dissecting the role of sodium currents in visceral sensory neurons in a model of chronic hyperexcitability using Nav1.8 and Nav1.9 null mice. J Physiol. 2006;576(Pt 1):257–67.
24. Minett MS, et al. Pain without nociceptors? Nav1.7-independent pain mechanisms. Cell Rep. 2014;6(2):301–12.
25. Huang J, et al. Gain-of-function mutations in sodium channel Na(v)1.9 in painful neuropathy. Brain. 2014;137(Pt 6):1627–42.
26. Leipold E, et al. A de novo gain-of-function mutation in SCN11A causes loss of pain perception. Nat Genet. 2013;45(11):1399–404.
27. Luiz AP, et al. Contribution and interaction of kinin receptors and dynorphin A in a model of trigeminal neuropathic pain in mice. Neuroscience. 2015;300:189–200.
28. Luiz AP, et al. Kinin B(1) and B(2) receptors contribute to orofacial heat hyperalgesia induced by infraorbital nerve constriction injury in mice and rats. Neuropeptides. 2010;44(2):87–92.
29. Zhang XY, et al. Gain-of-function mutations in SCN11A cause familial episodic pain. Am J Hum Genet. 2013;93(5):957–66.
30. Amaya F, et al. The voltage-gated sodium channel Na(v)1.9 is an effector of peripheral inflammatory pain hypersensitivity. J Neurosci. 2006;26(50):12852–60.
31. Lee S, D'Hooge R, Meert T. Exploring the role of nociceptor-specific sodium channels in pain transmission using Nav1.8 and Nav1.9 knockout mice. Behav Brain Res. 2010;208(1):149–57.
32. Krzyzanowska A, Avendano C. Behavioral testing in rodent models of orofacial neuropathic and inflammatory pain. Brain Behav. 2012;2(5):678–97.
33. Baker MD, et al. GTP-induced tetrodotoxin-resistant Na+ current regulates excitability in mouse and rat small diameter sensory neurones. J Physiol. 2003;548(Pt 2):373–82.
34. Ostman JA, et al. GTP up-regulated persistent Na+ current and enhanced nociceptor excitability require NaV1.9. J Physiol. 2008;586(4):1077–87.
35. Vos BP, Strassman AM, Maciewicz RJ. Behavioral evidence of trigeminal neuropathic pain following chronic constriction injury to the rat's infraorbital nerve. J Neurosci. 1994;14(5 Pt 1):2708–23.
36. Almeida TF, Roizenblatt S, Tufik S. Afferent pain pathways: a neuroanatomical review. Brain Res. 2004;1000(1–2):40–56.
37. Bergamaschi G, et al. Saporin, a ribosome-inactivating protein used in prepare immunotoxins, induces cell death via apoptosis. Br J Haematol. 1996;93(4):789–94.

РОЗДІЛ 4

РОЗРОБКА НОВИХ ПІДХОДІВ ДЛЯ ТЕРАПІЇ БОЛЬОВИХ СИНДРОМІВ: ФАРМАКОЛОГІЧНІ ПІДХОДИ ТА ЗАСТОСУВАННЯ ГЕННОЇ ТЕРАПІЇ І НАНОТЕХНОЛОГІЙ

4.1. Хронічна імплантація катетеру у субарахноїдальний простір поперекового відділу спинного мозку через атланто-окципітальну мембрану як метод цільової доставки терапевтичних сполук

Journal of Neuroscience Methods 290 (2017) 125–132

Contents lists available at ScienceDirect

Journal of Neuroscience Methods

journal homepage: www.elsevier.com/locate/jneumeth

Atlanto-occipital catheterization of young rats for long-term drug delivery into the lumbar subarachnoid space combined with *in vivo* testing and electrophysiology *in situ*

Olga Kopach [a,b,*], Volodymyr Krotov [a], Nana Voitenko [a]

[a] Bogomoletz Institute of Physiology, Bogomoletz str. 4, Kyiv 01024, Ukraine
[b] Institute of Neurology, University College London, Queen Square, London WC1N 3BG, UK

HIGHLIGHTS

- A method of lumbar catheterization of young rats (3-week-old) is described.
- The high catheterization success rate was demonstrated for young rats (about 80%).
- No adverse effects on peripheral sensitivity, animal locomotion or anxiety were found after spinal catheterization.
- Whole-cell recordings from sensory interneurons *in situ* were obtained after spinal treatment with genetic material *in vivo*.
- The technique is feasible and useful for studies both *in vivo* and *in situ*.

ARTICLE INFO

Article history:
Received 11 April 2017
Received in revised form 30 July 2017
Accepted 1 August 2017
Available online 2 August 2017

Keywords:
Spinal catheterization
Intrathecal delivery
Young animals
Genetic material
Oligodeoxynucleotides
Local treatment
Spinal cord electrophysiology
Sensory interneurons
Behavioral testing
Peripheral sensitivity

ABSTRACT

Background: Catheterization has been widely used in neuroscience and pain research for local drug delivery. Though different modifications were developed, the use of young animals for spinal catheterization remains limited because of a little success rate. A reliable technique is needed to catheterize young animals aimed for *in vivo* testing combined with spinal cord electrophysiology, often limited by animal age, to facilitate pain research.
New methods: We describe intrathecal catheterization of young rats (3-week-old) through atlanto-occipical approach for long-lasting drug delivery into the lumbar subarachnoid space. The technique represents a surgical approach of minimized invasiveness that requires PE-10 catheter and few equipment of standard laboratory use.
Results: Behavioral assessments revealed that spinal catheterization does not change peripheral sensitivity of different modalities (thermal and mechanical) and gives no rise to locomotive deficit or anxiety-like behavior in young rats. The long-term administration of genetic material (oligodeoxynucleotides given up to 4 days), examined both *in vivo* and *in situ*, produced no adverse effects on basal peripheral sensitivity, but changed the AMPA receptor-mediated currents in sensory interneurons of the spinal cord.
Comparison with existing methods: Dissimilar to already described methods, the method is designed for the use of young rats for behavioral testing *in vivo* and/or spinal cord electrophysiology *in situ*.
Conclusions: A practical method for spinal catheterization of young animals designed for studies *in vivo* and *in situ* is proposed. The method is rapid and effective and should facilitate investigation of therapeutic effects on both systemic and subcellular levels, as an advantage over the existing methods.

1. Introduction

Intrathecal catheterization has been widely used for local delivery of compounds of interest into the spinal cord and different methodological modifications were developed to prompt higher success rate in various species (Yamashita et al., 2003; Malkmus and Yaksh, 2004; Federici et al., 2012; Lambertini et al., 2015; Hou et al., 2016; Mazur et al., 2017). The main benefits of the technique

* Corresponding author at: Institute of Neurology, University College London, Queen Square, London, WC1N 3BG, UK.
E-mail address: o.kopach@ucl.ac.uk (O. Kopach).

http://dx.doi.org/10.1016/j.jneumeth.2017.08.001
0165-0270/

Fig. 1. Photographs of PE-10 tubing used in the study (A) and a fabricated catheter of 10-cm long cut (B) with a knot made approximately at the middle (C), tightened then out (D).

is local delivery of a drug to avoid systemic blood circulation and reduce high doses required to achieve efficient drug concentrations associated with a risk of developing side effects (Humphreys et al., 2005; O'Donnell and Iohom, 2008). Among advantages, there is a capability for delivery of genetic materials, which could not cross the blood brain barrier due to a large molecular weight (hundred thousand Da). Catheterization also yields long-term delivery of a drug whenever repeated injections needed in much less invasive way as compared with technically challenging punctures into the subarachnoid area, associated with a risk of damage to the spinal cord.

Despite advantages, the procedure of spinal catheterization via atlanto-occipital membrane could cause postoperative mortality and neurological deficits that prompted up methodological excellence through modifying catheters (Pogatzki et al., 2000) or using needles for a catheter guidance in rodents (Storkson et al., 1996; Wu et al., 2004). A high catheterization success rate has been demonstrated for adult rats (LoPachin et al., 1981; Malkmus and Yaksh, 2004), whereas it remains considerably low for young and small animals, e.g., mice (Wu et al., 2004; Oladosu et al., 2016). The young animals, however, are of a particular interest for electrophysiological studies of the spinal cord where recordings become limited with aging of experimental animals (e.g., whole-cell recordings from vulnerable sensory interneurons in slices or the whole spinal cord demand by up to 3–4-week-old rats (Voitenko et al., 2004; Szucs et al., 2009). Though the emerging call, a technique for spinal catheterization of young animals has not yet been described whilst would benefit pain research with intracellular recordings from spinal interneurons following-up behavioral assessments *in vivo* after local treatment.

Here we provide the detailed description of intrathecal catheterization of young rats (3-week-old) through the atlanto-occipital membrane and figure out few technical improvements how to avoid typical complications that could arise upon and following the procedure when catheterizing the small-sized animals. The method does not require special equipment and can be readily implemented for routine use to facilitate studies of central pain processing.

2. Methods

2.1. Animals

Male Wistar rats (20 ± 3 day-old) were used in this study (Fig. 2A), whose body weight was 40 ± 10 g (n = 114 rats in total, including 18 control, non-catheterized animals). All animal procedures were approved by the local Animal Ethics Committee in Bogomoletz Institute of Physiology (Kyiv, Ukraine) and were in accordance with the European Commission Directive (86/609/EEC) and ethical guidelines of the International Association for the Study of Pain.

2.2. Materials and tools for intrathecal catheterization

For the procedure of intrathecal catheter implantation following tools and instruments are required:

- PE-10 polyethylene tube (ID 0.11″, OD 0.24″),
- scales for laboratory animals,
- stereotaxis or head holder,
- shaver (cream) for removing fur,
- scalpel (blade size #11 or #15),
- 2 forceps (one with wide branches, another with tiny ones),
- slant tip tweezer,
- silk suture,
- scissors,
- cotton (or cotton-tipped applicators),
- ethanol and betadine (or other antiseptics of choice).

2.3. Pre-surgical preparation

Standard PE-10 polyethylene tubing (Instech Solomon, PA, USA; Fig. 1A) was used in the study. We cut PE-10 tubing to make a near 10 cm long catheter; tube cuts of blunt ends are more preferable than those of slant shapes to reduce a risk of stabbing tissue when inserting catheter (Fig. 1B). A knot was tied at approximately the middle of the tube and tightened up to have one arm of the catheter of slightly longer length (near 6 cm long that is an external part) and a shorter another one (~4 cm long – an internal part; Fig. 1C–D). In such length, the internal part of catheter would reach lumbar spinal segments, as confirmed in young rats (n = 96 catheterized animals) with the caudal end of the catheter located within Th_{13}-L_2 spinal segments. Before implantation, we used to stretch the internal arm of the catheter to make tube straight that enables managing its insertion in less compressive and more controllable manner. To check out that there is no leakage or any occlusion, catheters were flushed with saline before implantation.

2.4. Anesthesia

Animals were weighed and individual doses of anesthetics were prepared (Fig. 2). For anesthesia of young rats we used a mixture

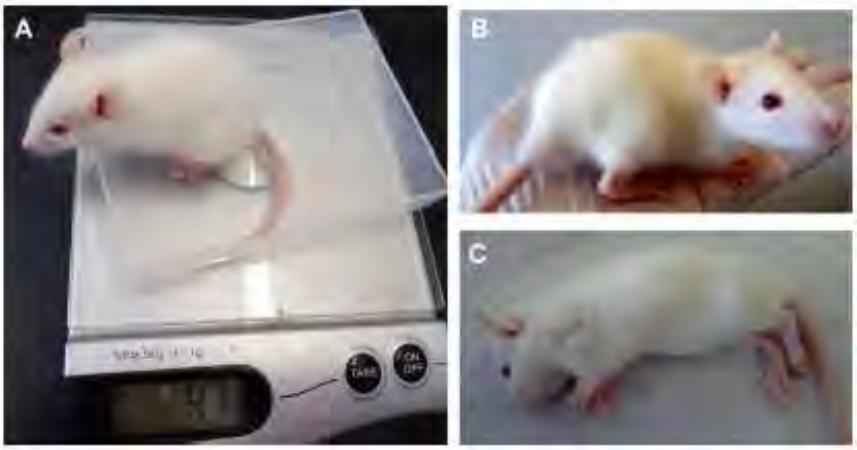

Fig. 2. Photographs of a 19 day-old rat with weight of 47 g (A) before (B) and after intraperitoneal injection of a mixture of ketamine and xylazine (C).

of ketamine (70 mg/kg) and xylazine (15 mg/kg) given intraperitoneally. Other anesthetics, either liquids or inhalators, are a subject of choice. The depth of anesthesia was confirmed with the loss of corneal reflex. At this point, it might be helpful to double verify that the length of the internal part of catheter fits an anesthetized animal, reaching 0,5 cm caudally the last ribs (measured from the atlanto-occipital membrane on the neck) and adjust the length, if needed (note that the internal arm has to be stretched up when fitting on animal's back).

2.5. Intrathecal catheterization

Anesthetized rat was placed in a stereotaxic frame and animal's head was securely fixed with the ear bars. For spinal catheterization the fixation is secured when animal's head is positioned symmetrically, allowing head movements only in up and down directions without any lateral move; the body trunk locates perpendicularly, in a right angle with animal's head. Fixation in other way may increase a risk of damage to spinal cord upon implantation, resulting in neurological deficits post-operatively. To prevent animal's eyes to get dry, an ophthalmic ointment was applied. Skin on the animal's head back was shaved out (3 × 2 cm area) and swiped with ethanol. A 1-cm longitudinal incision was made through skin below the nape where the occipital bone terminates, caudal to the neck (Fig. 3A–B). The occipital crest muscles were gently retracted out to expose the atlanto-occipital membrane. For muscle retraction we use sharp forceps, not cutting muscles with a scalpel. Once the atlanto-occipital membrane had been exposed, surrounding tissues were kept using the wide-branch forceps in left hand (Fig. 3C) while small incision was made in the membrane (1–2 mm long) with a scalpel in right hand. We prefer to make incision in very caudal part of the membrane since inserting catheter at that area diminishes a risk of damage to the spinal cord. In young animals, the atlanto-occipital membrane is thin and gentle, therefore no hook is needed for opening dura, in opposite to adult animals (Malkmus and Yaksh, 2004). Opening of the atlanto-occipital membrane is confirmed with a cerebro-spinal fluid coming up immediately through incised membrane. Then, the catheter was placed into the subarachnoid space at the rostral level of the spinal cord. The procedure of intrathecal insertion requires catheter to be kept in a straight position, parallel to the spinal cord, as close to the dorsal side as possible (Fig. 3D). A proper insertion into the thecal space is fairly validated by a cerebrospinal fluid flow through tube following-up insertion. A sudden resistance might be felt at any point – no forced pressure should be applied there to avoid any damage to the spinal cord. In a case of resistance, the catheter needs to be taken up to a previ-

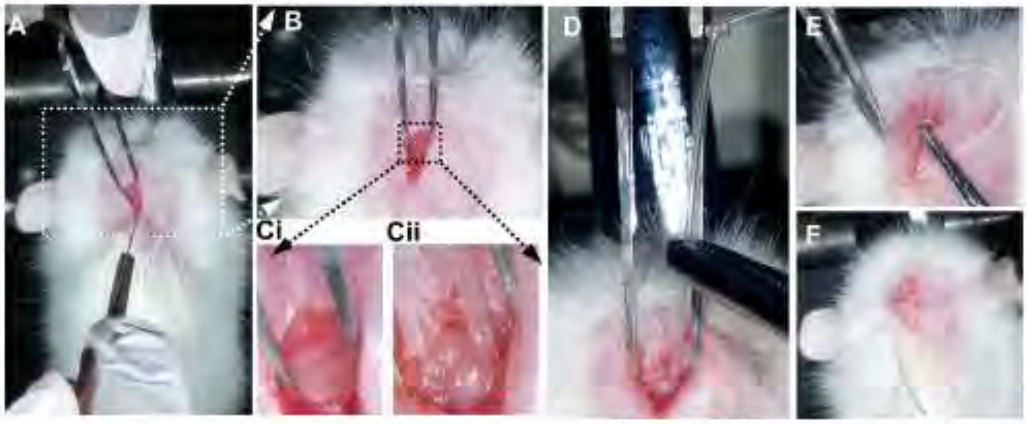

Fig. 3. Photographs depicting the procedure of intrathecal catheterization of a 19 day-old rat. After an animal's head was fixed, one incision in skin was made as shown in A, and muscles were retracted to expose the atlanto-occipital membrane, as demonstrated (B-Ci). A small cut was made in the caudal part of the membrane, where catheter was inserted intrathecally down (Cii-D) until a knot reached muscles (E). Catheter was anchored beneath skin, leading its external part through skin to exit out (F).

ous position and further inserted down in a slightly different angle. Catheter should be inserted until a knot reached the neck muscles (Fig. 3E). Afterwards, suture ligatures were applied to tighten muscles, but catheter knot shall remain right above the muscles to prevent any damage to the atlanto-occipital membrane. Finally, the external part of the catheter was tunneled throughout skin to exit on animal's head (between ears) using sharp forceps or a needle (20G or others) to puncture skin. Incised skin is closed (2–3 suture ligatures usually suffice; Fig. 3F) and treated with betadine (Egis Pharmaceutical PLC, Hungary).

The surgery typically takes 10–15 min for each animal. The surgical approach is bloodless – appearance of blood at any step indicates tissue damage upon operation. Animals were kept postoperatively on a warm surface (28–30 °C) until fully recovered from anesthesia. Catheterized animals were housed separately and monitored for their behavior and health conditions before being taken into experiments. A period for full animal recovery, including complete wound healing, typically takes 3 days. From the day 1 post-surgery, catheter has to be flushed with sterile saline once a day, daily, to avoid possible occlusion.

2.6. The Hargreaves plantar test for measuring the thermal peripheral sensitivity

The Hargreaves technique was used to measure peripheral sensitivity of rats to the thermal stimulus (heat) as described recently (Kopach et al., 2016). Briefly, after an animal habituated to a Plexiglas chamber, a radiant heat was applied to the middle of the plantar surface of one hind paw (Ugo Basile Model 7370 Plantar Test). The light beam was automatically turned off when animal lifted its paw. The time between starting the stimulus and animal lifted its paw – the withdrawal latency – was measured, which reflects the thermal nociceptive threshold. Trial was repeated 3–5 times with an interval between measurements 3–5 min and values were averaged. We examined catheterized animals for their peripheral sensitivity on the day 5 post-surgery. The age-matched naïve animals, quasi-randomly sampled, were used as control. Animals were eliminated after termination of experiments with overdose of anesthetics.

2.7. Assessment of mechanical peripheral sensitivity with von Frey's monofilaments

The method of von Frey monofilaments was used to measure mechanical peripheral sensitivity in rats, as described earlier (Kopach et al., 2016). Briefly, after an animal was habituated to an experimental chamber located on an elevated mesh screen, von Frey monofilaments of different intensity of stimulus (Bioseb) were applied to each hind paw. Applications were repeated 10 times for each hind paw with an interval between stimulations for at least 2 min for each tested filament. The percentage of responses was calculated for every trial and averaged; it was defined as the paw withdrawal threshold. Catheterized animals were examined for peripheral mechanical sensitivity on the day 5 post-surgery. The age-matched naïve animals, quasi-randomly sampled, were used as control.

2.8. The open-field test for animal locomotion and anxiety

For the assessment of general activity and locomotion of young animals after spinal catheterization the open-field test was performed, as described in details recently (Kopach et al., 2016). Briefly, an animal was placed in the open-field arena, a 75 × 75 × 40 cm wooden box with a digital camera (Logitech C270) attached above to record animal relocations within the box. The total distance explored by an animal for the defined period of time (5 min) was calculated.

Anxiety is a commonly used readout of side effects, which could rise following treatment. Anxiety in rodents is typically characterized by suppressed exploratory activity of animals those avoid entering the arena center (open area) whilst keep within the box corners or travel close to the walls (Kopach et al., 2016). We measured both parameters of anxiety-like behavior – the number of crossing the arena center and the time spent within the central area. Catheterized animals were examined for their locomotive activity on the day 5 post-surgery. The aged-matched naïve animals were used as control.

Tests were performed within the same daily period for different experimental groups to avoid (or minimize) an influence on behavior assessment with daily activity of laboratory animals.

2.9. Dye injection

To validate the delivery of a drug into the subarachnoid space in lumbar segments through implanted catheter we used morphological dye Alexa Fluor 594 (Molecular Probes, USA). Catheterized animals were given a single injection of Alexa (10 μl, 100 μM), flushed with saline (10 μl). The spinal cord was examined for the Alexa-mediated fluorescence shortly after injection of the dye (~15 min post).

2.10. Spinal administration of genetic material

For long lasting spinal treatment with genetic material the antisense (AS) oligodeoxynucleotides (ODN) specific to PKC subtype α were used with the following sequence, 5′-GACATCCCTTTCCCCCTCGG-3′. Missense (MS) oligodeoxynucleotides with the sequence of 5′-CGTCCTCAGTCGTCCCTCAC-3′ were used as control. Genetic material was intrathecally delivered through implanted catheter with a 25-gauge needle connected to a 25 μl Hamilton syringe. Animals received intrathecal injections of AS ODN or MS ODN (10 μg/10 μl) once a day for 3 days. The reduced expression of PKCα protein at the lumbar enlargement segment following such a treatment has been confirmed in our previous studies (Kopach et al., 2013).

Animals were assessed for their peripheral sensitivity before initiating a treatment with genetic material and then every day following (treatment of a 3 day-duration), with measurements performed once a day, daily.

2.11. Spinal cord slice preparation

Spinal cord slices were prepared from catheterized animals those received spinal treatment with genetic material (see above Section 2.10) according to methodology described in details previously (Kopach et al., 2013; Kopach et al., 2015). Briefly, the spinal cord was quickly dissected out and placed in an ice-cold dissection solution that contained (in mM) 250 sucrose, 2 KCl, 1.2 NaH_2PO_4, 0.5 $CaCl_2$, 7 $MgCl_2$, 26 $NaHCO_3$, 11 glucose, oxygenated with 95% O_2 and 5% CO_2. Transverse slices (350-μm thick) were cut with a HA 752 vibratome (Campden Instruments, Loughborough, UK). Slices were maintained at room temperature in a physiological Krebs bicarbonate solution that contained (in mM) 125 NaCl, 2.5 KCl, 1.25 NaH_2PO_4, 2 $CaCl_2$, 1 $MgCl_2$, 26 $NaHCO_3$, 10 glucose, oxygenated with 95% O_2 and 5% CO_2 (pH 7.4).

2.12. Electrophysiology in situ

Whole-cell recordings were made from lamina II DH interneurons using an Axopatch 200 B amplifier controlled with pClamp 9.2 software (Molecular Devices, USA). Neurons were visualized with

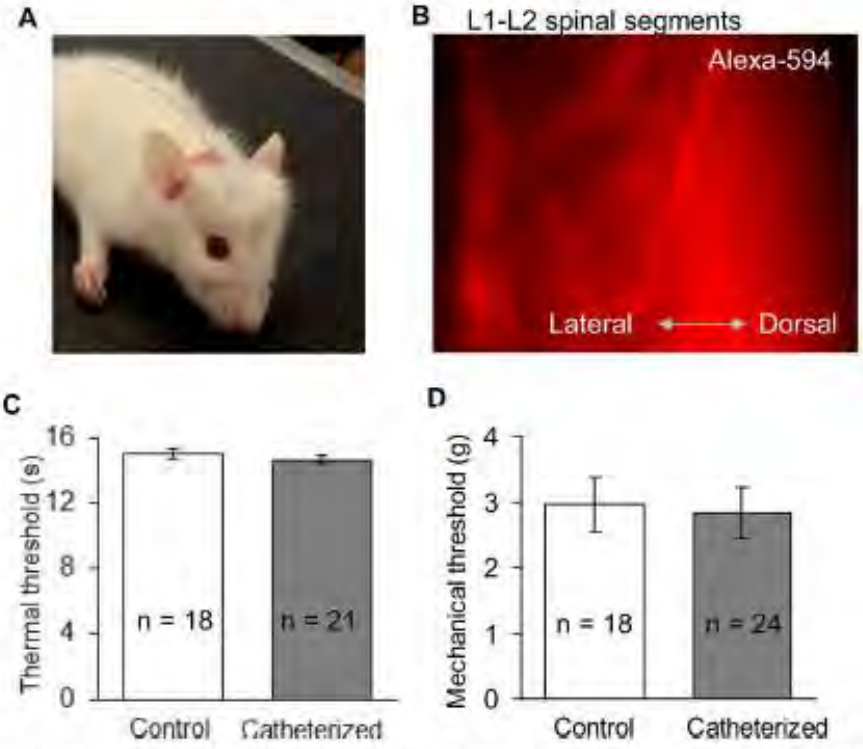

Fig. 4. Spinal catheterization changes neither thermal nor mechanical basal sensitivities of young animals. (A) Photograph of a 19 day-old young rat shortly after intrathecal catheterization. (B) Epifluorescence imaging of the lumbar spinal cord after dye injection (Alexa-594, 100 μM/10 μl). (C) Measuring of the thermal nociceptive threshold revealed no changes in the peripheral thermal sensitivity between catheterized animals (n = 21 rats) and the age-matched control (n= 18 rats). (C) The plantar measurements of the mechanical threshold with von Frey monofilaments showed no difference in the peripheral mechanical sensitivity between catheterized animals (n = 24 rats) and control (n = 18 rats). Data are expressed as mean ± SEM.

an infrared optics using a × 60.09 water-immersion objective on an Olympus BX50WI upright microscope (Olympus, Japan). Patch pipettes (resistance of 5 MΩ) were filled with an internal solution containing (in mM) 130 Cs-methylsulfonate, 10 NaCl, 10 EGTA, 2 $CaCl_2$, 10 HEPES, 5 QX-314, 0.1 spermine tetrahydrochloride, 2 Mg-ATP, and 0.1 Na-GTP (pH 7.2). The membrane resistance was constantly monitored by applying a short hyperpolarizing pulse (−5 mV).

The AMPA receptor (AMPAR)-mediated currents were induced by a selective receptor agonist, AMPA, bath applied in the continuous presence of TTX (0.5 μM), cadmium chloride (100 μM), APV (50 μM), bicuculline methiodide (10 μM), and strychnine hydrochloride (2 μM). To prevent a fast desensitization of AMPARs, the agonist was applied in the continuous presence of cyclothiazide (20 μM). Typically, one neuron was studied per slice. For quantification of changes in the current-voltage relationship of the AMPAR-mediated currents the rectification index (RI) was calculated as the peak current amplitude at +30 mV to the peak current amplitude recorded at −50 mV, as we described in details earlier (Kopach et al., 2013).

2.13. Statistics; power analysis

The data sets were probed for normality using the Shapiro-Wilk test. Since the data sets have been normally distributed, the results are presented as mean ± standard error of the mean (SEM) with n referring to the number of animals/cells tested. Student's *t*-test was used to determine statistical difference between experimental groups using OriginPro software and Excel package. A *p* value of less than 0.05 was considered as statistically significant.

Power analysis was performed to determine the sample size required to detect an effect of spinal catheterization on peripheral sensitivity and/or animal locomotion, if any, in young animals. The analysis determined that in order to detect 10% changes in either thermal threshold value (peripheral sensitivity) or total distance value (animal locomotion), the group size required to be 21 and 30, respectively, to give a degree of confidence 90%.

3. Results

The group of catheterized animals in this study consisted of 53 rats, including 3 animals those did not recover from surgery/anesthesia (~6%) and 7 rats those developed neurological deficits post-operatively (~13%). Neurological deficits were forelimb paresis, chromodacryorhea ('bloody' eyes) or tremor, which animals displayed post-surgery. Examination of those animals revealed compression, in some cases lesion in the spinal cord, produced by catheter. Therefore, the effectiveness of intrathecal catheterization of young rats counted ~ 81% (43 catheterized animals without any deficit out of 53). None animal withdrew the catheter after implantation.

3.1. The lumbar catheter location for intrathecal delivery

For the assessment of lumbar placement of catheter in young rats and local delivery of a drug into the subarachnoid space we used morphological dye Alexa Fluor 594 (see Methods for details). A robust Alexa-mediated fluorescence was observed within the lumbar spinal cord, the area where implanted catheter ended, when

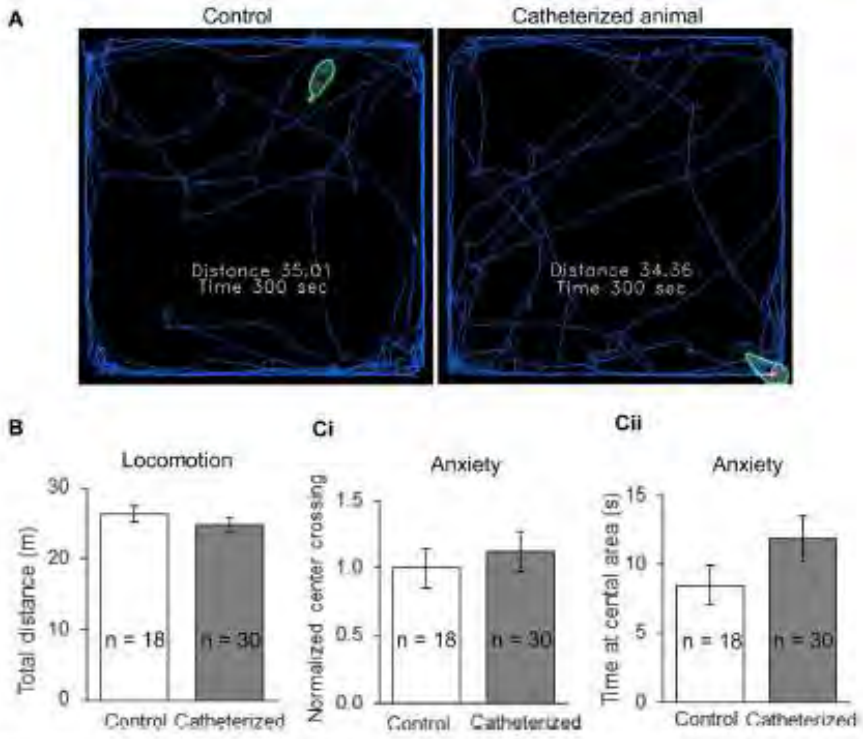

Fig. 5. Spinal catheterization gives no rise to locomotion deficit or anxiety-like behavior of young rats. (A) The open-field test analysis snapshots taken from a control animal (left) and a catheterized rat (right) demonstrate no difference in locomotor activity between animals. Sketches of the animal movement trajectory and the total distance indicated are for 5 min-duration recordings. (B) Average distance explored by animals during the open-field test demonstrates no difference between catheterized animals (n = 30 rats) and their age-matched control (n = 18 rats). Data are expressed as mean ± SEM. (C) The parameters for anxiety-like behavior, the crossing of arena center (Ci) and the time spent within the central area (Cii), are similar between catheterized animals (n = 30 rats) and control (n = 18 rats), indicating no anxiety after catheterization. Data are normalized to control for Cii and present as mean ± SEM for Cii.

examining the spinal cord shortly after dye injection (n = 3 rats; Fig. 4B).

Necroscopic analysis confirmed the catheter location within the lumbar thecal space (n = 50 catheterized animals for post-euthanasia analysis). The catheter was predominantly positioned within the lateral spinal cord that counted up ~62% (31 out of 50 animals), with less occurring placement at the dorsal area that estimated ~24% (12 out of 50 animals).

3.2. Catheterization changes neither thermal nor mechanical peripheral sensitivity of young rats

To examine if spinal catheterization could give rise to adverse effects and impair the peripheral sensitivity of young animals, we tested out basal peripheral sensitivity of different modalities – thermal and mechanical. The Hargreaves plantar test demonstrated no differences in the thermal nociceptive sensitivity of animal's hind paw between catheterized animals and control group. The average thermal threshold was 14.6 ± 0.3 s (n = 21) for catheterized animals and 15.0 ± 0.3 s (n = 18; $p > 0.3$) for their age-matched control on the day 5 post-surgery (Fig. 4C).

The method of von Frey monofilaments demonstrated no changes in peripheral sensitivity to mechanical stimulation between catheterized animals and control group. The average mechanical threshold was 2.8 ± 0.4 g (n = 24) for catheterized animals and 3.0 ± 0.4 (n = 18) for their age-matched control ($p > 0.8$; Fig. 4D). Thus, spinal catheterization does not change basal peripheral sensitivity of different modalities in young rats.

3.3. Catheterization gives no rise to locomotive deficit and animal anxiety

Next, we performed the open-field test to examine if spinal catheterization gives a rise to locomotive deficit and/or anxiety in young animals. No changes in general activity of young animals were observed after catheterization. There was no difference in animal locomotion between catheterized and control animals (Fig. 5A). The total distance of animal's movement was 25 ± 1 m (n = 30) for catheterized rats and 26 ± 1 m (n = 18, $p > 0.3$) for control group (Fig. 5B). There were also no signs of anxiety in young animals after catheterization. Catheterized rats actively explored novel surroundings and freely entered the center of arena (Fig. 5A, see Video recording). There were no significant changes in any tested parameters for the anxiety-like behavior – the number of animal crossing the arena center ($p > 0.5$; Fig. 5Ci) and the time spent within the central area ($p > 0.1$; Fig. 5Cii) – after catheterization.

3.4. Long term spinal administration of genetic material does not change basal peripheral sensitivity

Given that spinal catheterization of young animals produces no changes in their basal peripheral sensitivity and gives no rise to common side effects (e.g., locomotive deficit and/or anxiety), we finally examined whether intrathecal drug administration through implanted catheter would affect peripheral sensitivity of catheterized animals following treatment with genetic material for a prolonged period of time (3-day-duration treatment, see Methods

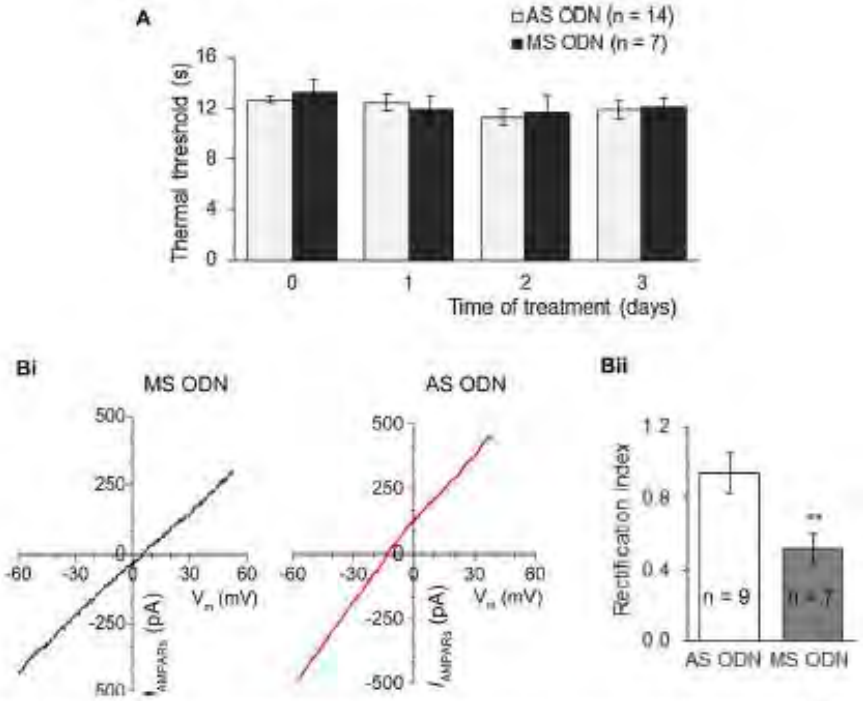

Fig. 6. Long-lasting intrathecal administration of genetic material does not influence basal peripheral sensitivity *in vivo*, but changes the AMPA-induced currents in sensory interneurons. (A) The thermal nociceptive threshold in catheterized animals remains at similar level before and following spinal treatment with antisense (AS) or missense (MS) oligodeoxynucleotides (ODN) specific to PKCα. Data are expressed as mean ± SEM, n = 14 rats treated with AS ODN and n = 7 rats for MS ODN. (Bi) Whole-cell recordings from the lamina II dorsal horn interneurons in spinal cord slices *in situ* revealed the difference in the current-voltage relationships of the AMPAR-mediated currents between experimental groups given spinal treatment with MS ODN (left) and AS ODN (right). (Bii) The difference in current-voltage relationships was expressed by quantifying the rectification index of the currents at different membrane potentials (+30 mV to −50 mV). Data are expressed as mean ± SEM, n = 9 neurons from AS ODN-treated group and n = 7 neurons from MS ODN-treated groups. ** $P < 0.01$ (unpaired *t*-test).

for details). Intrathecal administration of AS ODN or MS ODN (daily injections for 3 days) did not change basal peripheral sensitivity of young animals for the whole period. There were no changes in the thermal threshold in both experimental groups at every time-point tested, as compared with "0" time (before initiating a treatment) or between groups (n = 14 rats treated with AS ODN and n = 7 rats treated with MS ODN, $p > 0.01$; Fig. 6A).

3.5. Genetic inhibition of spinal PKCα changes the AMPAR-mediated currents in sensory interneurons

Finally, a capability of catheterized animals after prolonged spinal treatment *in vivo* for the reliable spinal cord preparation aimed for electrophysiological studies *in situ* was validated with acute spinal cord slices prepared from catheterized animals following long-lasting genetic treatment with AS ODN or MS ODN. We enabled the acute spinal cord slice preparation for the intracellular recordings made from lamina II DH interneurons in whole-cell configuration (see Methods for details). Consistent to our previous findings (Kopach et al., 2013), electrophysiological parameters of the DH interneurons did not differ between AS ODN- and MS ODN-treated groups for the resting membrane potential, input resistance, capacitance, and series resistance of patched interneurons (data nor shown). However, we found changes in the AMPA-induced currents in lamina II interneurons after spinal administration of AS ODN (genetic inhibition of PKCα). The AMPA-induced currents demonstrated a linear current-voltage relationship in the AS ODN-treated group, whereas the opposite inward rectification was observed at positive potentials in the MS ODN-treated group (Fig. 6Bi). The rectification index of the AMPAR-mediated currents (see Methods for details) was 0.94 ± 0.11 (n = 9 cells) for the AS ODN-treated group, but 0.51 ± 0.08 (n = 7 cells; $p < 0.01$) for the MS ODN-treated group (Fig. 6Bii). The difference indicates changes in the proportion between Ca^{2+}-permeable and Ca^{2+}-impermeable AMPARs in DH interneurons by local genetic inhibition (knocking down) of spinal PKCα. These results are consistent with our previous findings of the role of PKCα in AMPARs trafficking in DH interneurons, demonstrated for both synaptic (Park et al., 2009) and extrasynaptic pools of AMPARs (Kopach et al., 2013).

4. Discussion

The present study described in details the technique of spinal catheterization of young rats (3-week-old) aimed for combined use of the animals for both *in vivo* (testing the therapeutic effects of a drug) and *in situ* studies (electrophysiology of the spinal cord), as advantage over the existing methods. The technique represents a surgical approach of minimized invasiveness, which is simple and prompt, bloodless and could be performed without specialized equipment (for instance, monitoring the cardiorespiratory parameters that could be implemented, if necessary). The effectiveness of the described methodology is high (more than 80% catheterization success rate). This rate is similar to that reported for mice (Oladosu et al., 2016), although it remains lower comparing with the modified methods for catheterization of adult rats where success rate may raise up to 95–98% (Malkmus and Yaksh, 2004). Such discrepancy is due to a little thecal space in young animals

that complicates catheter placement by challenging the procedure with highly increased risk of spinal cord damage in the small-sized animals. In order to boost catheterization success rate, the use of smaller gauge catheter might be helpful, as suggested (Pogatzki et al., 2000). Nevertheless, we routinely use standard PE-10 tubing for catheterization of young rats, achieving a success rate about 80%. To obtain this rate, we elaborated few technical improvements for the atlanto-occipital catheterization, those have been particularly essential for implanting catheter into young animals, as described in the study. In the atlanto-occipital approach, it is crucial positioning of the animal's head in right angle to body trunk with further catheter insertion in a very straight direction, and towards the dorsal side. The insertion should follow without any sharp pressure applied over the entire procedure.

Behavioral assessments *in vivo* using different tests for measuring peripheral sensitivity of different modalities (thermal, mechanical) and locomotive activity (locomotion, anxiety-like behavior) confirmed that spinal catheterization gives no rise to development of any deficit in young animals. Neither thermal nor mechanical peripheral sensitivity changed after spinal catheterization. The open-field test, a robust assay for the assessment of general activity and anxiety (as a readout of side effects that could develop following treatment), demonstrated no changes in locomotion and exploratory behavior of young animals after catheterization. Thus, no evidence for locomotive deficit and/or anxiety status has been found in catheterized rats. Furthermore, the fluorescence detection within the lumbar spinal cord confirmed localized delivery of a compound of interest through implanted catheter into the thecal space. Altogether, our results prove that the described technique is reliable for testing fine therapeutic effects of localized drug treatment *in vivo*.

Our whole-cell recordings from sensory interneurons in acute spinal cord slices prepared from catheterized animals after prolonged spinal treatment *in vivo* have also confirmed the use of the animals for reliable spinal cord preparation and following-up electrophysiological studies *in situ*. Interneurons of the superficial dorsal horn (lamina I–II) represent a highly vulnerable population for *in situ* preparation, often limited by aging of experimental animals that compromised obtaining of intracellular recordings from elder animals (Voitenko et al., 2004; Szucs et al., 2009). Therefore, the demonstrated capability of acute spinal cord preparations from catheterized animals to obtain whole-cell recordings from sensory interneurons provides substantial advantages of the described technique over the existing methods since enables investigations on subcellular level after long-term spinal treatment *in vivo*. The changes observed in sensory interneurons *in situ* (the AMPAR-mediated currents) following treatment with genetic material *in vivo* (knocking down of spinal PKCα) are consistent with our previous findings of the role of spinal PKCα in AMPAR trafficking in DH interneurons in persistent inflammatory pain conditions (Kopach et al., 2013). Together this confirms the use of catheterized animals for localized treatment (e.g., gene silencing of spinal PKCα (Kopach et al., 2013) to investigate the precise intracellular mechanisms of pain processing in central pathways.

Summarizing, our data demonstrate that the described technique of spinal catheterization of young animals provides the reliable use of animals for combined testing of therapeutic effects *in vivo* and consistent electrophysiological studies *in situ* to yield benefits of exploring effects on both systemic and subcellular levels to facilitate pain research and beyond.

Acknowledgment

This work was supported by the National Academy of Science of Ukraine Biotechnology Grant (to NV). The authors declare no conflict of interests.

Appendix A. Supplementary data

Supplementary data associated with this article can be found, in the online version, at http://dx.doi.org/10.1016/j.jneumeth.2017.08.001.

References

Federici, T., Taub, J.S., Baum, G.R., Gray, S.J., Grieger, J.C., Matthews, K.A., Handy, C.R., Passini, M.A., Samulski, R.J., Boulis, N.M., 2012. Robust spinal motor neuron transduction following intrathecal delivery of AAV9 in pigs. Gene Ther. 19, 852–859.

Hou, Y., Wang, L., Gao, J., Jin, X., Ji, F., Yang, J., 2016. A modified procedure for lumbar intrathecal catheterization in rats. Neurol. Res. 38, 725–732.

Humphreys, N., Bays, S.M., Parry, A.J., Pawade, A., Heyderman, R.S., Wolf, A.R., 2005. Spinal anesthesia with an indwelling catheter reduces the stress response in pediatric open heart surgery. Anesthesiology 103, 1113–1120.

Kopach, O., Viatchenko-Karpinski, V., Atianjoh, F.E., Belan, P., Tao, Y.X., Voitenko, N., 2013. PKCalpha is required for inflammation-induced trafficking of extrasynaptic AMPA receptors in tonically firing lamina II dorsal horn neurons during the maintenance of persistent inflammatory pain. J. Pain: Off. J. Am. Pain Soc. 14, 182–192.

Kopach, O., Krotov, V., Belan, P., Voitenko, N., 2015. Inflammatory-induced changes in synaptic drive and postsynaptic AMPARs in lamina II dorsal horn neurons are cell-type specific. Pain 156, 428–438.

Kopach, O., Krotov, V., Goncharenko, J., Voitenko, N., 2016. Inhibition of spinal Ca(2+)-Permeable AMPA receptors with dicationic compounds alleviates persistent inflammatory pain without adverse effects. Front. Cell. Neurosci. 10, 50.

Lambertini, C., Ventrella, D., Barone, F., Sorrentino, N.C., Dondi, F., Fraldi, A., Giunti, M., Surace, E.M., Bacci, M.L., Romagnoli, N., 2015. Transdermal spinal catheter placement in piglets: description and validation of the technique. J. Neurosci. Methods 255, 17–21.

LoPachin, R.M., Rudy, T.A., Yaksh, T.L., 1981. An improved method for chronic catheterization of the rat spinal subarachnoid space. Physiol. Behav. 27, 559–561.

Malkmus, S.A., Yaksh, T.L., 2004. Intrathecal catheterization and drug delivery in the rat. Methods Mol. Med. 99, 109–121.

Mazur, C., Fitzsimmons, B., Kamme, F., Nichols, B., Powers, B., Wancewicz, E., 2017. Development of a simple, rapid, and robust intrathecal catheterization method in the rat. J. Neurosci. Methods 280, 36–46.

O'Donnell, B.D., Iohom, G., 2008. Regional anesthesia techniques for ambulatory orthopedic surgery. Curr. Opin. Anaesthesiol. 21, 723–728.

Oladosu, F.A., Ciszek, B.P., O'Buckley, S.C., Nackley, A.G., 2016. Novel intrathecal and subcutaneous catheter delivery systems in the mouse. J. Neurosci. Methods 264, 119–128.

Park, J.S., Voitenko, N., Petralia, R.S., Guan, X., Xu, J.T., Steinberg, J.P., Takamiya, K., Sotnik, A., Kopach, O., Huganir, R.L., Tao, Y.X., 2009. Persistent inflammation induces GluR2 internalization via NMDA receptor-triggered PKC activation in dorsal horn neurons. J. Neurosci.: Off. J. Soc. Neurosci. 29, 3206–3219.

Pogatzki, E.M., Zahn, P.K., Brennan, T.J., 2000. Lumbar catheterization of the subarachnoid space with a 32-gauge polyurethane catheter in the rat. Eur. J. Pain 4, 111–113 (London, England).

Storkson, R.V., Kjorsvik, A., Tjolsen, A., Hole, K., 1996. Lumbar catheterization of the spinal subarachnoid space in the rat. J. Neurosci. Methods 65, 167–172.

Szucs, P., Pinto, V., Safronov, B.V., 2009. Advanced technique of infrared LED imaging of unstained cells and intracellular structures in isolated spinal cord, brainstem, ganglia and cerebellum. J. Neurosci. Methods 177, 369–380.

Voitenko, N., Gerber, G., Youn, D., Randic, M., 2004. Peripheral inflamation-induced increase of AMPA-mediated currents and Ca2+ transients in the presence of cyclothiazide in the rat substantia gelatinosa neurons. Cell Calcium 35, 461–469.

Wu, W.P., Xu, X.J., Hao, J.X., 2004. Chronic lumbar catheterization of the spinal subarachnoid space in mice. J. Neurosci. Methods 133, 65–69.

Yamashita, A., Matsumoto, M., Matsumoto, S., Itoh, M., Kawai, K., Sakabe, T., 2003. A comparison of the neurotoxic effects on the spinal cord of tetracaine, lidocaine, bupivacaine, and ropivacaine administered intrathecally in rabbits. Anesth. Analg. 97, 512–519 (table of contents).

4.2. Терапевтичний ефект селективного блокування Ca^{2+}-проникних AMPA-рецепторів інгібіторами нового покоління на полегшення хронічного больового синдрому при тривалому периферичному запаленні не супроводжується виникненням побічних ефектів

frontiers in Cellular Neuroscience

ORIGINAL RESEARCH
published: 29 February 2016
doi: 10.3389/fncel.2016.00060

Inhibition of Spinal Ca^{2+}-Permeable AMPA Receptors with Dicationic Compounds Alleviates Persistent Inflammatory Pain without Adverse Effects

Olga Kopach[1,2], Volodymyr Krotov[1], Julia Goncharenko[1†] and Nana Voitenko[1,3]**

[1] Laboratory of Sensory Signaling, Bogomoletz Institute of Physiology, Kyiv, Ukraine, [2] Laboratory of Synaptic Imaging, Institute of Neurology, University College London, London, UK, [3] International Center for Molecular Physiology, Bogomoletz Institute of Physiology, Kyiv, Ukraine

OPEN ACCESS

Edited by:
Andrea Nistri,
Scuola Internazionale Superiore di Studi Avanzati, Italy

Reviewed by:
Pascal Darbon,
University of Strasbourg, France
Jing Wang,
NYU School of Medicine, USA

***Correspondence:**
Olga Kopach
kopach@biph.kiev.ua,
o.kopach@ucl.ac.uk;
Nana Voitenko
nana@biph.kiev.ua

†Present address:
Julia Goncharenko,
University of Hertfordshire, UK

Received: 18 September 2015
Accepted: 13 February 2016
Published: 29 February 2016

Citation:
Kopach O, Krotov V, Goncharenko J and Voitenko N (2016) Inhibition of Spinal Ca^{2+}-Permeable AMPA Receptors with Dicationic Compounds Alleviates Persistent Inflammatory Pain without Adverse Effects. Front. Cell. Neurosci. 10:60. doi: 10.3389/fncel.2016.00060

Upregulation of Ca^{2+}-permeable AMPA receptors (CP-AMPARs) in the dorsal horn (DH) neurons of the spinal cord has been causally linked to the maintenance of persistent inflammatory pain. Therefore, inhibition of CP-AMPARs could potentially alleviate an, otherwise, poorly treatable chronic pain. However, a loss of CP-AMPARs could produce considerable side effects because of the crucial role of CP-AMPARs in synaptic plasticity. Here we have tested whether the inhibition of spinal CP-AMPARs with dicationic compounds, the open-channel antagonists acting in an activity-dependent manner, can relieve inflammatory pain without adverse effects being developed. Dicationic compounds, *N*1-(1-phenylcyclohexyl)pentane-1,5-diaminium bromide (IEM-1925) and 1-trimethylammonio-5-1-adamantane-methyl-ammoniopentane dibromide (IEM-1460) were applied intrathecally (i.t.) as a post-treatment for inflammatory pain in the model of complete Freund's adjuvant (CFA)-induced long-lasting peripheral inflammation. The capability of dicationic compounds to ameliorate inflammatory pain was tested in rats *in vivo* using the Hargreaves, the von Frey and the open-field tests. Treatment with IEM-1460 or IEM-1925 resulted in profound alleviation of inflammatory pain. The pain relief appeared shortly after compound administration. The effects were concentration-dependent, displaying a high potency of dicationic compounds for alleviation of inflammatory hyperalgesia in the micromolar range, for both acute and long-lasting responses. The period of pain maintenance was shortened following treatment. Treatment with IEM-1460 or IEM-1925 changed neither thermal and mechanical basal sensitivities nor animal locomotion, suggesting that inhibition of CP-AMPARs with dicationic compounds does not give rise to detectable side effects. Thus, the ability of dicationic compounds to alleviate persistent inflammatory pain may provide new routes in the treatment of chronic pain.

Keywords: dicationic compounds, Ca^{2+}-permeable AMPA receptors, the activity-dependent inhibition, dorsal horn, persistent inflammatory pain, antinociception

INTRODUCTION

Persistent or chronic pain is a prominent healthcare problem worldwide, which is defined by the International Association for the Study of Pain (IASP) as a disease on its own, without apparent biological value that needs to be utterly eliminated after its appearance. Despite considerable efforts, chronic pain remains poorly treatable, attended with side effects and adaptation to a treatment, representing a growing clinical problem that requires new routes based on a mechanism-targeted therapy.

It is known that upregulation of AMPA receptors (AMPARs) in the dorsal horn (DH) neurons causes central sensitization, a specific form of synaptic plasticity in the DH sustainable for a long period of time (Woolf and Salter, 2000; Ji et al., 2003). Peripheral inflammatory pain induces upregulation of Ca^{2+}-permeable AMPARs (CP-AMPARs) both at the synapses (Hartmann et al., 2004; Vikman et al., 2008; Park et al., 2009) and the extrasynaptic membranes of DH interneurons (Park et al., 2009; Kopach et al., 2011, 2013), two of those are causally linked to the persistent pain maintenance (Kopach and Voitenko, 2013). Preventing the upregulation of CP-AMPARs in DH interneurons through the interference with molecular mechanisms of AMPAR trafficking has been demonstrated as an effective way to alleviate persistent inflammatory pain at the periphery (Park et al., 2009; Kopach et al., 2013). However, inhibition of central receptors with genetic approaches remains restricted in practical treatment: the preferred focus is the use of conventional compounds.

A substantial variety of blockers inhibiting CP-AMPARs is currently available. They can be divided in two principal groups of: (i) organic toxins (philanthotoxin, joro spider toxin, argiotoxin; Blaschke et al., 1993; Herlitze et al., 1993; Go et al., 1996) and (ii) dicationic compounds (IEM-1460, IEM-1754, IEM-1925; Magazanik et al., 1997; Tikhonov et al., 2000; Zaitsev et al., 2011). Studies of the effects of organic toxins on pain showed the attenuated development of injury-evoked allodynia when organic toxins (joro spider toxin, philanthotoxin) were used as a pre-treatment (Sorkin et al., 1999, 2001; Pogatzki et al., 2003). However, pain maintenance was unchanged when they were administered as a post-treatment, even in comparatively high doses (Jones and Sorkin, 2004). Strikingly, the effects of dicationic compounds on pain management have not been investigated. In the meantime, they are of special interest since the revealed capability to inhibit CP-AMPARs in the voltage- and the use-dependent manner (Magazanik et al., 1997; Tikhonov et al., 2000; Tikhonova et al., 2008; Zaitsev et al., 2011). The use-dependent inhibition might be the key to impede the development of adverse effects because it "switches off" only functionally active (upregulated) receptors rather than blocking the entire receptor pool. Cumulatively, the effectiveness of use-dependent inhibition correlates with the number of activated receptors/open channels (Zaitsev et al., 2011). Previously, we have demonstrated the increased number of functional CP-AMPARs in DH interneurons in persistent pain conditions: this resulted from promoted insertion of GluR1-containing AMPARs into extrasynaptic plasma membrane (Kopach et al., 2011, 2013) and internalization of GluR2-containing AMPARs from synapses between primary afferents and DH interneurons (Park et al., 2009). In addition, we have shown the capability of dicationic compound IEM-1460 to reverse the inflammatory-induced changes in the AMPAR-mediated currents in DH interneurons (Kopach et al., 2011). Despite the evidenced effects of dicationic compounds at the cellular level, their effects on chronic pain *in vivo* have not been tested yet.

MATERIALS AND METHODS

Animal Care

Animals used in the study were 3–5 weeks-old male Wistar rats. All animal procedures were approved by the local Animal Ethics Committee (Bogomoletz Institute of Physiology, Kyiv, Ukraine) and were performed in accordance with ethical guidelines of the IASP and the European Commission Directive (86/609/EEC). Great care was taken to avoid or minimize any discomfort of the animals with all efforts made to reduce the number of animals used.

Intrathecal Catheter Implantation

For local delivery of dicationic compounds into the spinal cord we used intrathecal catheter implantation according to a method previously described for rats (Kopach et al., 2013). Briefly, a rat was anesthetized with an intraperitoneal (i.p.) injection of a mixture of ketamine (Farmak, Ukraine) and xylazine (Farmak, Ukraine) in the doses of 70 mg kg^{-1} and 25 mg kg^{-1}, respectively. Anesthetized rat was placed in a stereotaxic frame with the head securely fixed between ear bars. One incision was made below the nape 1 cm caudal to the neck. The external occipital crest muscles were retracted with extra care to expose the atlanto-occipital membrane. A polyethylene tube (PE-10) was inserted into the subarachnoid space at the rostral level of the spinal cord region around Th_{10}-L_2 spinal segments through an incision at the atlanto-occipital membrane (**Figure 1A**). Extra care was taken to avoid any damage of the spinal cord. The incision was closed with silk sutures and treated with Betadine (Gedeon Richter Ltd, Budapest, Hungary). Animals received postoperatively bicillin (0.6 million U kg^{-1}, i.p., Farmak, Ukraine) and dexamethazon (60 mg kg^{-1}, i.p., Farmak, Ukraine) and were maintained in a warmed area until full recovery from anesthesia. Animals were housed postoperatively in a temperature-controlled environment with food and water *ad libitum*. They were recovered postoperatively for several days before being used in experiments (typically 5 days or until the complete healing of surgical incision if needed). Animals showing any neurological deficits were discarded. The position of the catheter has been confirmed in each animal after termination of an experiment.

Induction of Peripheral Inflammation

To produce unilateral peripheral inflammation and nociceptive hypersensitivity, 50–100 µl of complete Freund's adjuvant (CFA, *Mycobacterium tuberculosis*) suspended in an oil-saline (1:1)

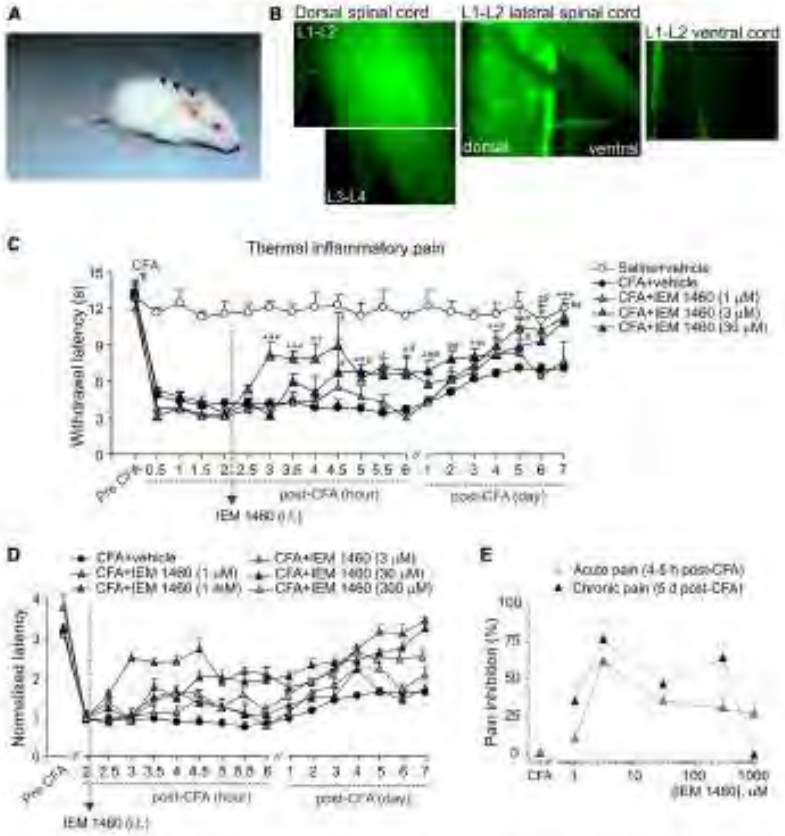

FIGURE 1 | The concentration-dependent alleviation of thermal nociceptive hypersensitivity by the dicationic compound IEM-1460. (A) Photograph of a rat with implanted catheter into spinal cord column. **(B)** Fluorescent images of different areas of freshly dissected spinal cord after i.t. injection of morphological dye Alexa-594 (100 μM, 10 μl) into the lumbar spinal cord showing the fluorescence in the dorsal spinal cord (lumbar segments), but not in the ventral spinal cord with notably dim fluorescent signal along the attached roots. **(C)** Hargreaves pain behavioral test in different groups of animals demonstrates that post-treatment of complete Freund's adjuvant (CFA)-induced inflammatory pain with the dicationic compound IEM-1460 alleviates thermal pain hypersensitivity in rats. Data are expressed as mean ± SEM. $^{*}p < 0.05$, $^{**}p < 0.01$, $^{***}p < 0.001$ for 3 μM of IEM-1460 vs. the correspondent time-point in the CFA-inflamed group. $^{\#}p < 0.05$, $^{\#\#}p < 0.01$ for 30 μM of IEM-1460 vs. the correspondent time-point in the CFA-inflamed group. One-way analysis of variance (ANOVA) and Bonferroni *post hoc* tess. **(D)** The paw withdrawal latencies in different groups of animals treated with IEM-1460 were normalized to the correspondent value prior to starting the treatment (2 h) to demonstrate the time-dependence of pain relief on the compound concentration. **(E)** The concentration-inhibition curves of IEM-1460-induced inhibition of inflammatory pain for the acute and the long-lasting responses.

emulsion was injected subcutaneously into the plantar side of one hind paw of the rats. Saline (0.9%; 100 μl) injection was used as a control.

Intrathecal Drug Administration

Dicationic compounds were delivered intrathecally (i.t.) into the dorsal spinal cord as confirmed with the Alexa-596-mediated fluorescence detected preferentially at the dorsal lumbar spinal cord (L_1–L_3 segments), but not at the ventral lumbar spinal cord or along the attached roots (**Figure 1B**). Different groups of animals (non-inflamed, CFA-inflamed) received a treatment with saline (control), IEM-1460 or IEM-1925 at indicated concentrations. Injection of a drug (10 μl, diluted in saline) was followed by administration of saline (10 μl) to flush the catheter. Dicationic compounds were used as a post-treatment of peripheral hypersensitivity developed after the induction of peripheral inflammation. After validation that peripheral nociceptive hypersensitivity had profoundly developed following an intraplantar injection of CFA, animals were given a single drug injection (at 2 h post-CFA) or two drug injections (at 2 h and at 5 h after injection of CFA). Timing of starting a treatment was based on our earlier studies of the time-dependent inflammatory changes in the DH GluR2 phosphorylation (Park et al., 2009) and the AMPAR-mediated currents in lamina II DH interneurons (Kopach et al., 2012) in the same model of long-lasting peripheral inflammation in rats.

For assessment of possible side effects of the compounds animals were thoroughly observed for the signs of motor deficit, impaired/irregular movement, stress and anxiety over

the entire period of testing an animal. In addition, groups of animals, which received dicationic compounds alone (without induction of peripheral inflammation), were tested for their behavioral responses to peripheral stimulation of different modality (thermal, mechanical) and for sings of possible locomotive deficit and/or the anxiety-like behavior following treatment.

Behavioral Testing

Behavioral tests were performed in a quiet room, by the experimenter evaluating the animal's behavior in a blind manner (the experimenter did not know if the animals were treated with saline or drug).

Hargreaves Plantar Test

The paw withdrawal responses to thermal stimuli were measured using the Hargreaves technique as described in details previously (Park et al., 2009; Kopach et al., 2013). Briefly, after an animal was habituated to a Plexiglas chamber located above a light box, a radiant heat was applied to the middle of the plantar surface of one hind paw. The intensity of thermal stimulus applied to the plantar skin was adjusted to temperature of ~46°C (30 s cut off). The light beam was automatically turned off when the animal lifted its paw. The time between starting the stimulus and lifting the paw was defined as the paw withdrawal latency. The trial was repeated 3–5 times for each paw with intervals between measurements for at least 3–4 min. For representation of the time-dependent changes produced by dicationic compounds in various concentrations (**Figure 1D**), the paw withdrawal responses in different experimental groups were normalized to the correspondent value measured prior to starting the treatment (2 h post-CFA) as indicated.

Method of von Frey's Monofilaments

The paw withdrawal responses to the repeated mechanical stimuli were measured using the method of von Frey monofilaments as described previously (Park et al., 2009; Kopach et al., 2013). Briefly, after an animal was habituated to a Plexiglas chamber on an elevated mesh screen (at least 10–15 min prior to testing), the von Frey monofilaments of different intensity of stimulus (Bioseb) were applied to each hind paw. The monofilaments were chosen according to our previous studies of the development and maintenance of the mechanical hypersensitivity and allodynia in the CFA-induced model of peripheral inflammation in rats (Kopach et al., 2012, 2013). The trial was repeated 10 times for each hind paw with an interval between filament applications for at least 1 min. The percentage of responses was calculated for each trial and was defined as the paw withdrawal frequency.

Open-Field Test

For assessment of changes in locomotion and general activity of animals in the persistent pain conditions or during an experimental treatment, the open-field test was performed. The open-field test (open-field arena) represents a robust assay for an integrative analysis of animal activity (such as exploratory behavior, sedation, stress/anxiety etc.) as described in detail elsewhere (Bellavance and Beitz, 1996; Bailey and Crawley, 2009). We assessed the animal locomotion and the anxiety-like behavior (which is commonly used to represent side effects) by testing animals in an open-field arena during the defined period of time. For this, a rat was placed in the open-field arena representing a 75 cm × 75 cm × 40 cm wooden box with a digital camera (Logitech C270) attached above a center of the arena to record relocations of animal through the box. Tested animal was allowed to move freely within box during 5 min, often used session duration to sufficiently capture the critical components of animal' behavior. The total distance traveled by an animal horizontally was analyzed offline and defined as the index of locomotion. The anxiety-like behavior (Buccafusco, 2009) was assessed by the animal movement with regard to the time spent in the box corners, traveling close to the walls (indicating increased anxiety) and crossing the central area (representing the innate behavior of animals to explore novel environments). Testing was typically performed at the same period of time to minimize influencing of animal behavior with a daily activity of laboratory animals.

Statistical Analysis

All data are presented as mean ± standard error of the mean (SEM) with *n* referring to the number of animals tested. The statistical difference between experimental groups was analyzed by one-way or two-way analysis of variance (ANOVA) followed by Bonferroni *post hoc* test where appropriate. A p value of less than 0.05 was considered as statistically significant.

Experimental Drugs

CFA was purchased from Sigma-Aldrich Company Ltd. (St. Louis, MO, USA and Dorset, UK). 1-trimethylammonio-5-1-adamantane-methyl-ammoniopentane dibromide (IEM-1460) was purchased from Tocris Bioscience (Ellisville, MO, USA). *N*1-(1-phenylcyclohexyl)pentane-1,5-diaminium bromide (IEM-1925) was provided by Prof. L. Magazanik and Dr. D. Tikhonov (I.M. Sechenov Institute of Evolutionary Physiology and Biochemistry RAS, Saint-Petersburg, Russia) and purchased also from Insight Biotechnology (Wembley Middlesex, UK).

RESULTS

For assessment of a capability of dicationic compounds to alleviate nociceptive hypersensitivity during persistent pain conditions, two different compounds, IEM-1460 and IEM-1925, those high-potent ability to inhibit CP-AMPARs in the use-dependent manner has been proved *in vitro* and *in situ* (Magazanik et al., 1997; Buldakova et al., 1999; Tikhonov et al., 2000; Tikhonova et al., 2008; Zaitsev et al., 2011), were tested *in vivo* in a model of the CFA-induced long-lasting peripheral inflammation. Dicationic compounds were used as a post-treatment of inflammatory pain that had developed after induction of peripheral inflammation. The compounds were administered i.t. at different concentrations to figure out their

efficacy in alleviating the inflammatory pain hypersensitivity of different modalities (thermal, mechanical) and in recovering the locomotive deficit and depressed activity of inflamed animals.

Dicationic Compound IEM-1460 Efficiently Alleviates Inflammatory Hyperalgesia

First we tested whether the dicationic compound IEM-1460 could produce antinociceptive effect on thermal pain hypersensitivity that had developed after the induction of CFA-induced unilateral inflammation in rats. Consistent with our previous studies and those of others (Park et al., 2008, 2009; Kopach et al., 2012, 2013), intraplantar injection of CFA into a rat hind paw produced a robust thermal hypersensitivity on the ipsilateral (but not on the contralateral) side, which developed rapidly (30 min to 1 h after injection), maintained at a peak level for next hours and persisted over several weeks ($n = 20$, $p < 0.01$), representing the period of CFA-induced inflammatory pain maintenance (**Figures 1C,D**). IEM-1460 given i.t. as a post-treatment of CFA-induced inflammatory pain markedly alleviated the inflammatory-induced thermal hypersensitivity. Relief in inflammatory pain appeared shortly after the compound administration (within 1–2 h after i.t. IEM-1460 application that was 3–4 h post-CFA) and was manifested as the increase in the paw withdrawal latency of inflamed paw, reduced after the induction of inflammation. This increase produced by IEM-1460 reflects the reduction in thermal hyperalgesia; it has been observed within hours after starting the treatment (acute effect) and lasted for at least seven consecutive days after treatment, reflecting the long-lasting antinociceptive effects of the compound (**Figures 1C,D**). The relief in pain was concentration-dependent, displaying the profound antihyperalgesic effect produced by IEM-1460 at the micromolar concentration range, 3–300 μM, for both acute and chronic responses (**Figure 1E**). The fastest outcome for pain relief following IEM administration was observed when IEM-1460 was administered at the concentration of 3 μM (**Figure 1D**), a concentration very close to the estimated IC50 for blocking specifically CP-AMPARs (Buldakova et al., 1999). In particular, the paw withdrawal latency in inflamed-animals, which received 3 μM of IEM-1460 ($n = 7$ per group), has been recovered by approximately 60% of its pre-inflammatory level after 2 h of starting the treatment. After 5 days of treatment with 3 μM IEM-1460, the thermal pain sensitivity of inflamed paw was comparable with those of non-inflamed animals (saline-treated, $n = 6$ per group, $p > 0.05$; **Figures 1C–E**). Lowering concentration of IEM-1460 to 1 μM or on the contrary increasing it to 1 mM (the estimated IC50 value for blocking GluR2-containing Ca^{2+}-impermeable AMPARs; Buldakova et al., 1999) resulted in a short-term reduction in thermal hyperalgesia, observed as a peak increase of the paw withdrawal latency (or a plateau of 1-2 h duration), which steadily declined returning back to the CFA-inflamed level (**Figures 1C,D**).

The capability of dicationic compound IEM-1460 to alleviate persistent inflammatory pain *in vivo* was next tested for the inflammatory-induced mechanical hypersensitivity using the method of von Frey monofilaments. Consistent with previous results (Park et al., 2008, 2009; Kopach et al., 2012, 2013), injection of CFA produced a profound allodynia and the robust mechanical hypersensitivity in response to the von Frey monofilaments of different intensity (**Figure 2A**) that revealed on the ipsilateral (but not on the contralateral) side. IEM-1460 alleviated the CFA-induced allodynia and mechanical hypersensitivity when applied at a micromole concentration range according with the sufficiently alleviated chronic thermal hypersensitivity, demonstrated above. IEM-1460 at the concentration 30 μM or 300 μM substantially reduced the inflammatory-induced mechanical hypersensitivity in response to the 2 g and 4 g von Frey monofilaments, which produced around 50% of responses in inflamed rats (the mechanical pain threshold), after 2–3 days of treatment ($n = 5$ per group; **Figure 2B**). After 3 days of treatment, mechanical sensitivity of inflamed paw was indistinguishable from those of non-inflamed animals ($p > 0.05$; **Figures 2B,C**), indicating that IEM-1460 markedly shortened mechanical pain maintenance. Together, these data demonstrate that dicationic compound IEM-1460 efficiently alleviates inflammatory hyperalgesia of different modalities (thermal, mechanical) and shortens chronic pain maintenance acting within the micromole concentration range.

The Recovered Locomotion and Diverted Anxiety-Like Behavior of Inflamed Animals After Treatment with IEM-1460

The open-field test is based on the innate behavior of rodents to explore novel area/surroundings, allowing monitoring and assessment of locomotion, exploratory behavior and general activity of tested animals for integrative analysis of sensorimotor function upon a treatment (Bellavance and Beitz, 1996; Bailey and Crawley, 2009). For assessment of the inflammatory-induced locomotive deficit and the impaired activity of animals in persistent pain conditions, we tested animals prior to the induction of peripheral inflammation and at different time-points following the developed inflammatory pain to compare animal locomotion and explorative behavior between conditions. The robust reduction in animal locomotion together with the profoundly suppressed general activity of animals have been seen shortly after the induction of inflammation (within first few hours), which declined further and maintained at a stably low level for a long period of time (**Figures 3A,B**; for at least few weeks). For instance, the total distance traveled by an inflamed animal on day 1 after CFA injection was reduced up to ninefold as compared to the distance traveled by the animal prior to the inflammation ($n = 28$ per group, $p < 0.001$; **Figure 3B**) or to that one in the saline-treated group ($n = 11$ per group, $p < 0.001$; **Figure 3B**). Typically, the animals with inflamed paw spent a time by predominantly sitting in the arena corners with no attempts to explore surroundings over the entire recording session, displaying the anxiety-like behavior during the persistent pain syndrome (**Figures 3A,B**).

Further studying a capability of dicationic compound IEM-1460 to alleviate persistent inflammatory pain, we have tested whether the pain relief produced by IEM-1460 would

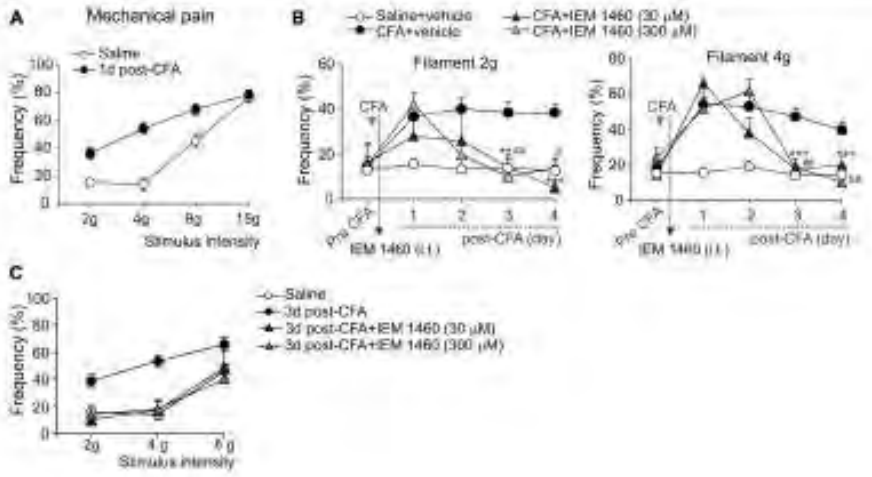

FIGURE 2 | Analgesic effect of IEM-1460 on the inflammatory-induced mechanical hypersensitivity. (A) von Frey behavioral test demonstrates tactile allodynia in the CFA-inflamed rats in response to von Frey monofilaments of different stimulus intensity. **(B)** Treatment with IEM-1460 recovered the paw withdrawal frequency in response to the 2 g (left graph) and 4 g (right graph) von Frey monofilaments. Results are presented as mean ± SEM. $^{**}p < 0.01$, $^{***}p < 0.001$ for 30 μM of IEM-1460 vs. the correspondent time-point in the CFA-inflamed group. $^{\#}p < 0.05$, $^{\#\#}p < 0.01$ for 300 μM of IEM-1460 vs. the correspondent time-point in the CFA-inflamed group. One-way ANOVA and Bonferroni post hoc test. **(C)** Post-treatment with IEM-1460 recovered tactile allodynia in the CFA-inflamed rats after 3 days of treatment.

accompany by alleviation in the locomotive deficit developed in inflamed animals. We first verified that the impairments had developed after the induction of inflammation and then tested the animals following treatment once a day until the parameters reached a complete recovery (**Figure 3C**). Treatment with IEM-1460 improved the locomotion of inflamed animals, revealing the increase in the total distance traveled by an animal with inflamed paw (**Figures 3C,D**). This improvement has been observed even after 1 day of treatment; it further progressed following next days, showing the restored ability of inflamed animals to travel as much as prior to the induction of inflammation after 3 days of treatment with IEM-1460 at either tested concentration (n = 5–6 per group; **Figure 3D**). This is consistent with the time-course of recovery in the CFA-induced mechanical hypersensitivity by IEM-1460, demonstrated above. The alleviated locomotive deficit was accompanied by facilitated exploratory behavior of inflamed animals that was revealed as their increased crossing of the central area of arena (**Figure 3E**). Such behavior indicates the recovered general activity of inflamed animals after treatment with IEM-1460 along with the diverted stress and anxiety, which had been developed in persistent pain conditions.

Assessment of Possible Side Effects Developed by Treatment with IEM-1460

For assessment of possible side effects developed upon inhibition of spinal CP-AMPARs with dicationic compound IEM-1460, animals were tested for their responses to thermal and mechanical peripheral stimulations as well as their locomotive and the anxiety-like behavior before and after the treatment with IEM-1460 at different concentrations.

To thoroughly evaluate if an acute and/or a delayed adverse effect might develop upon a treatment, we tested the basal thermal nociceptive sensitivity by measuring the paw withdrawal latency before and every next hour (a 6 h-duration) after starting the treatment and then once a day over a week afterwards. Groups of animals, which received IEM-1460 at different concentrations, did not differ in their withdrawal latency at any time-point tested (within hours or days after treatment) as compared to the value prior to starting the treatment or that value in control littermates (saline; $p > 0.05$; **Figure 4A**). Similar to this, groups of animals did not also differ with regard to their basal mechanical sensitivity following treatment with IEM-1460 (n = 5–6 per group, $p > 0.05$; **Figure 4B**).

Further, no significant changes were observed in the animal locomotion (n = 5, $p > 0.05$; **Figure 4C**) after inhibition of spinal CP-AMPARs with 3 μM IEM-1460, which produced the fastest outcome for modulating pain *in vivo* and also represents the estimated IC50 for blocking CP-AMPARs (Buldakova et al., 1999). Finally, IEM-1460 (3 μM) did not give rise to the anxiety-like behavior, the commonly used readout of side effects, since none of three parameters tested for the signs of increased anxiety were significantly different between the IEM-1460-treated animals and the control (saline-treated) group (n = 5 per group for 3 μM IEM-1460, n = 11 per group for saline; $p > 0.05$; **Figure 4D**). We have analyzed: (i) the total time of running along the walls; (ii) time spent within the central area of arena; and (iii) crossing the arena center (**Figure 4D**). Notably, animals of both tested groups demonstrated promoted attempts to explore the open-field arena over the entire period of testing (for several days) by crossing the central area rather than running along the walls when

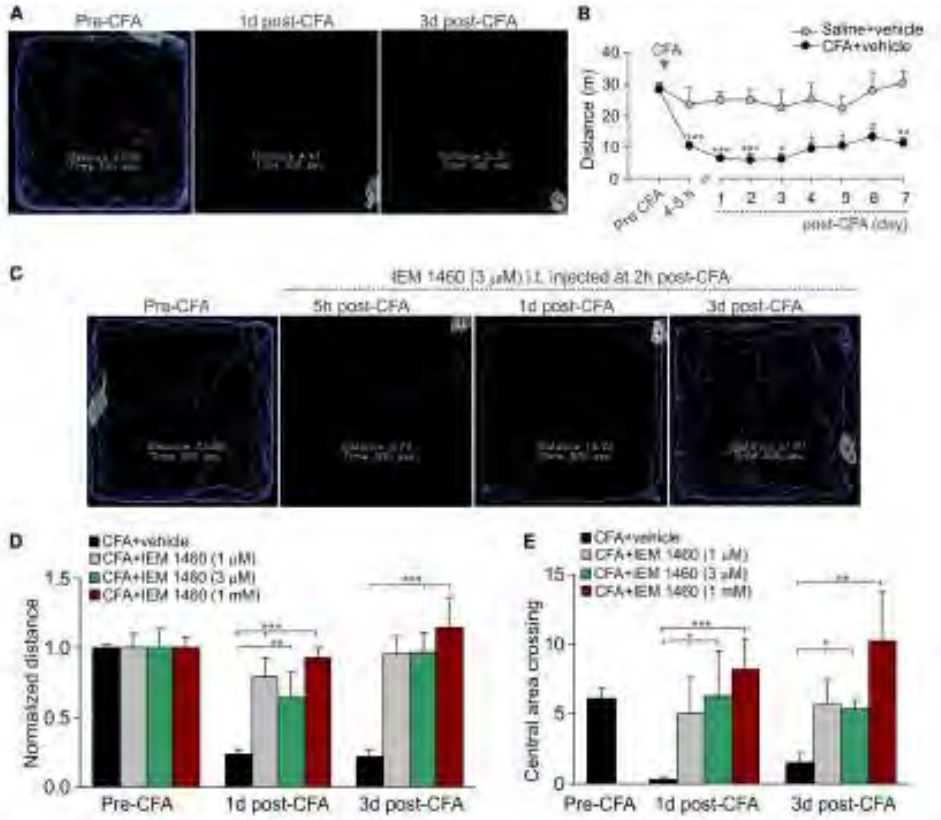

FIGURE 3 | The IEM-1460-induced relief in locomotive deficit and the anxiety-like behavior of inflamed animals. (A) The open-field test snapshots demonstrate the severe locomotive deficit in rats with developed peripheral pain syndrome. Sketches of the animal movements taken from the same animal before and at different time-points after induction of inflammation indicating the total distance traveled by an animal for 5 min of recording. **(B)** Summary of the total distance traveled (a 5 min duration) by the saline-treated and the CFA-inflamed animals over the time. Data are expressed as mean ± SEM. $^{*}p < 0.05$, $^{**}p < 0.01$, $^{***}p < 0.001$ vs. the correspondent time-point in saline. One-way ANOVA and Bonferroni *post hoc* test. **(C–E)** Treatment with IEM-1460 recovered the inflammatory-induced locomotive deficit **(D)** and the anxiety-like behavior **(E)** as seen from the representing open-filed recordings taken from the same animal before and after the induction of peripheral inflammation followed by IEM-1460 treatment **(C)**. $^{*}p < 0.05$, $^{**}p < 0.01$, $^{***}p < 0.001$ vs. the indicated bar. One-way ANOVA and Bonferroni *post hoc* test.

compared both parameters at different time-points to those ones taken from starting testing (**Figure 4D**). Together these data demonstrate that treatment with IEM-1460 produces no adverse effects on basal peripheral sensitivity (neither thermal nor mechanical), the locomotive behavior and on none of tested parameters representing the anxiety-like behavior of tested animals.

Antinociceptive Effects of Dicationic Compound IEM-1925 on Inflammatory Hypersensitivity and Locomotive Deficit

Despite the proven high-potent capability of dicationic compound IEM-1925 to inhibit CP-AMPARs in the activity-dependent manner (Tikhonov et al., 2000; Zaitsev et al., 2011), the effects of such inhibition *in vivo* have not been tested yet. Here we have studied a capability of the compound to alleviate thermal and mechanical hypersensitivities and to restore the locomotive deficit and suppressed activity of animals with persistent peripheral inflammation when inhibit spinal CP-AMPARs with dicationic compound IEM-1925 *in vivo*. As in the case of IEM-1460, IEM-1925 markedly alleviated the inflammatory-induced thermal hypersensitivity when used as a post-treatment of CFA-induced inflammatory pain (**Figure 5A**). The effect of IEM-1925 was dose-dependent, displaying a profound relief in thermal hyperalgesia (either acute or chronic responses) when drug was applied at a micromole concentration range, 5–300 μM (**Figure 5B**). I.t. administration of IEM-1925 (5–300 μM) resulted in attenuated thermal hypersensitivity, which lasted over the entire period of testing (at least 7 days; $n = 5$ per group for 5 μM IEM-1925; $n = 15$ per group for 20 μM IEM-1925; $n = 9$ per group for 300 μM IEM-1925). Relief in pain produced by IEM-1925 appeared faster than for IEM-1460 used at the similar concentration range. In particular, thermal pain sensitivity of inflamed paw was indistinguishable from that in non-inflamed animals after 3 days of treatment

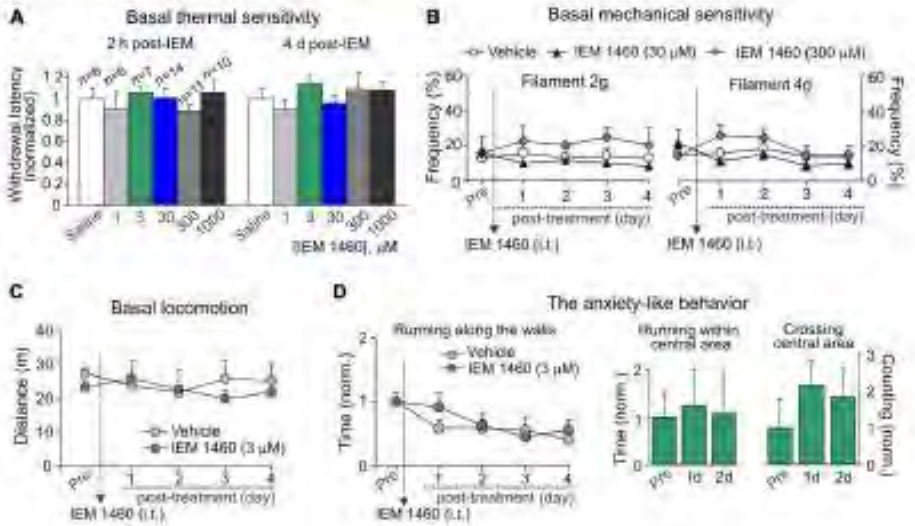

FIGURE 4 | Dicationic compound IEM-1460 does not give rise to detectable side effects. (A) The Hargreaves test demonstrates that treatment with IEM-1460 at different concentrations produces neither acute nor delayed changes in thermal peripheral sensitivity. Data are expressed as the mean paw withdrawal latencies normalized to the correspondent time-point in the saline-treated group. **(B)** The von Frey behavioral test shows no changes in the mechanical peripheral sensitivity in response to the 2 g (left graph) and 4 g (right graph) von Frey monofilaments in rats treated with IEM-1460. Results are presented as mean ± SEM. **(C,D)** The open-field test demonstrates no significant changes in animal locomotion **(C)** and the anxiety-like behavior **(D)** after treatment with 3 μM IEM-1460. The anxiety-like behavior was assessed by changes in the time of running along the walls (left graph in **D**), the time spent within the central area of arena (middle bars in **D**) and crossing by animal the arena center (right bars in **D**); results are presented as mean values normalized to the correspondent time-point prior to the treatment (Pre).

with IEM-1925 ($p > 0.05$; **Figure 5A**), indicating the profound shortening of the inflammatory pain maintenance by IEM-1925 (**Figures 5A,B**). Similar to IEM-1460, lowering concentration of IEM-1925 to 1 μM or opposite increasing it to 1 mM (the highest drug concentration tested) produced the reduction of thermal hypersensitivity for a short period of time, which lasted within hours (for 1 μM IEM-1925) or for a few days only (for 1 mM IEM-1925) after treatment with following decline of the paw withdrawal latency back to the CFA-inflamed level ($n = 6$ per both groups; **Figure 5A**).

IEM-1925 also alleviated the CFA-induced mechanical hypersensitivity and allodynia in inflamed rats. As in the case of thermal hyperalgesia, IEM-1925 alleviated mechanical hypersensitivity faster than IEM-1460. The CFA-induced mechanical hypersensitivity in response to either 2 g or the 4 g von Frey filaments was substantially alleviated even after 2 days of treatment with 20 μM IEM-1925 ($n = 5$ per group; **Figures 5C,D**); after 3 days of treatment the withdrawal frequency of inflamed paw was comparable to its basal (pre-inflammatory) level (**Figure 5C**), indicating a complete recovery in peripheral mechanical sensitivity by treatment with IEM-1925.

Finally, the locomotive deficit that had developed in the inflamed animals along to the persistent pain syndrome has been effectively eliminated by treatment with IEM-1925. Again, the outcome in relief produced by the treatment with IEM-1925 revealed faster than that for IEM-1460. In particular, the total distance traveled by inflamed animals was recovered to its pre-inflammatory level even after 1 day of treatment with IEM-1925 at the concentration 1 μM or 5 μM, but not at a high concentration, 1 mM ($n = 5$ per group; **Figures 6A,B**). This was accompanied by a promoted exploratory behavior of inflamed animals, demonstrating the increased crossing the central area of arena (**Figure 6C**). The latter indicates that treatment with IEM-1925 declines the anxiety-like behavior in CFA-inflamed animal.

Dicationic Compound IEM-1925 Affects None of Tested Parameters for Possible Side Effects

For assessment of possible side effects developed upon inhibition of spinal CP-AMPARs with dicationic compound IEM-1925, we first tested whether IEM-1925 could influence peripheral sensitivity of animals to different stimulus modalities (thermal, mechanical). No detectable changes in thermal nociceptive sensitivity were found in rats following i.t. administration of IEM-1925 within hours (acute effect) and during next several days after treatment (delayed effect) as compared to their sensitivity prior to starting the treatment or to this sensitivity in the control (saline-treated) group ($p > 0.05$; **Figure 7A**). Neither of tested concentration of the compound affected the animals' thermal nociceptive sensitivity over the time. Treatment with IEM-1925 did not also change the basal mechanical sensitivity of animals in response to the 2 g or 4 g von Frey filaments following next

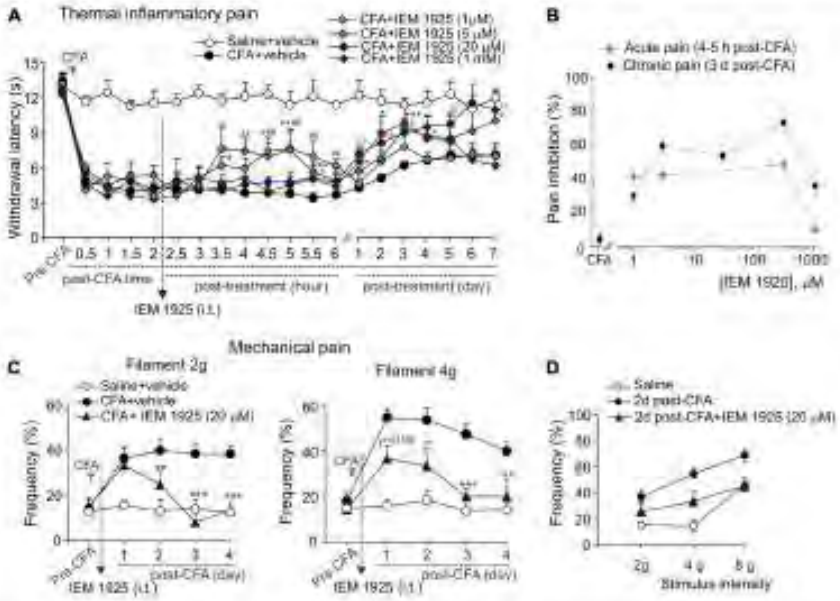

FIGURE 5 | Antinociception produced by dicationic compound IEM-1925 on the inflammatory-induced thermal and mechanical hypersensitivities. **(A)** The Hargreaves pain behavioral test demonstrates the reduced thermal inflammatory hypersensitivity following treatment with IEM-1925 at different concentrations. Data are expressed as mean ± SEM. *$p < 0.05$, **$p < 0.01$, ***$p < 0.001$ for 5 μM of IEM-1925 vs. the correspondent time-point in the CFA-inflamed group. $^{\$}p < 0.05$, $^{\$\$}p < 0.01$ for 1 μM of IEM-1925 vs. the correspondent time-point in the CFA-inflamed group. $^{\S}p < 0.05$, $^{\S\S}p < 0.01$, $^{\S\S\S}p < 0.001$ for 20 μM of IEM-1925 vs. the correspondent time-point in the CFA-inflamed group. One-way ANOVA and Bonferroni *post hoc* test. **(B)** The concentration-inhibition curves of the IEM-1925-mediated inhibition of the thermal inflammatory hypersensitivity for the acute and long-lasting inhibitory effects. **(C,D)** The von Frey behavioral test demonstrates the alleviated mechanical hypersensitivity by IEM-1925 (20 μM) in response to the 2 g (left graph) and 4 g (right graph) von Frey filaments **(C)** and the IEM-1925-mediated relief in the inflammatory-induced tactile allodynia in CFA-inflamed animals on day 2 after treatment **(D)**. Results are presented as mean ± SEM. *$p < 0.05$, **$p < 0.01$, ***$p < 0.001$ for 20 μM of IEM-1925 vs. the correspondent time-point in the CFA-inflamed group. One-way ANOVA and Bonferroni *post hoc* test.

several days after treatment ($n = 6$ per group, $p > 0.05$; **Figure 7B**).

Consistent with these results and those reported above for dicationic compound IEM-1460, IEM-1925 did not change the animal locomotion as determined by the unaltered total distance traveled by an animal following treatment with 5 μM IEM-1925 ($n = 5$ per group, $p > 0.05$; **Figure 7C**). Treatment with IEM-1925 did not also give rise to the anxiety-like behavior, since the time of running along the walls remained indistinguishable from that in the saline-treated animals (**Figure 7D**, left graph) and each of tested parameters reflecting the animal exploratory behavior did not decline over the time of treatment with IEM-1925 (**Figure 7D**, right bars). Thus, IEM-1925 did not give rise to detectable acute and/or delayed side effects in rats.

DISCUSSION

Cumulative evidence indicates the key role of AMPARs in central sensitization of the DH, a specific form of plasticity in the spinal cord underlying the central mechanism by which peripheral pain develops and is maintained (Woolf and Salter, 2000; Ji et al., 2003). Inhibition of spinal AMPARs with conventional antagonists (NBQX, CNQX, GYKI 52466, CFM-2) reversed mechanical allodynia and both thermal and mechanical hypersensitivities during the development and maintenance of pain of various origins (Sorkin et al., 2001; Nozaki-Taguchi and Yaksh, 2002; Jones and Sorkin, 2004; Park et al., 2008). However, inhibition of AMPARs with competitive antagonists affected the basal peripheral sensitivity and caused sedation (Hao and Xu, 1996; Park et al., 2008) that makes this approach impractical. Studies of the molecular mechanisms of persistent pain maintenance demonstrated the upregulation of CP-AMPARs either at the synapses (Hartmann et al., 2004; Vikman et al., 2008; Park et al., 2009) or at the extrasynaptic membranes of DH interneurons (Park et al., 2009; Kopach et al., 2011, 2013), both of those are causally linked to the maintenance of persistent inflammatory pain, since prevention of the CP-AMPAR upregulation in DH interneurons through targeted genetic interfering with the receptor trafficking machinery has effectively alleviated persistent inflammatory pain at the periphery (Park et al., 2009; Kopach et al., 2013). However, usage of genetic approaches remains restricted in treatment, with preferred focus on commercially available drugs.

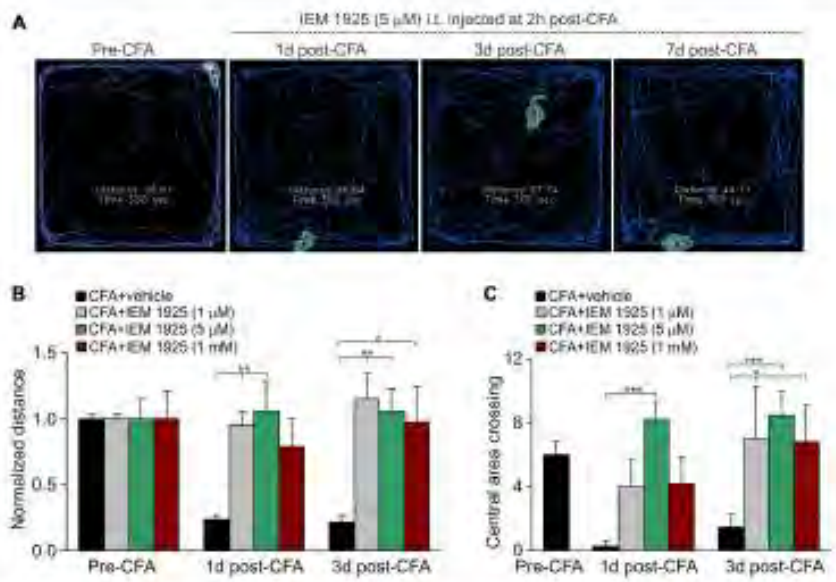

FIGURE 6 | The IEM-1925-induced relief in locomotive deficit and the anxiety-like behavior in CFA-inflamed animals. (A) The representative sketches of the open-field test, taken from the same animal, show the distance traveled by the animal before and after the induction of peripheral inflammation, followed by treatment with 5 μM IEM-1925. **(B–C)** Summary of the restored both locomotive deficit **(B)** and suppressed activity of the animals with inflamed paw **(C)** after treatment with IEM-1925. Data are expressed as mean ± SEM. *$p < 0.05$, **$p < 0.01$, ***$p < 0.001$ vs. the indicated bar (the correspondent time-point in CFA-inflamed group without treatment). One-way ANOVA and Bonferroni *post hoc* test.

Among two principal groups of the selective antagonists of CP-AMPARs, the group of organic toxins has been extensively explored for their effectiveness in managing pain in various pain models (Sorkin et al., 1999, 2001; Pogatzki et al., 2003; Jones and Sorkin, 2004), whereas the effects of dicationic compounds have not been studied *in vivo* at all, leaving the whole class of blockers open for further considerations. In the meantime, a capability of dicationic compounds (IEM-1460, IEM-1754, IEM-1925) to block CP-AMPARs in the activity-dependent manner (Magazanik et al., 1997; Tikhonov et al., 2000; Zaitsev et al., 2011) may provide their potential effectiveness in pain relief. As the open-channel antagonists acting in the use-dependent manner, dicationic compounds inhibit CP-AMPARs only if receptor is open that the effectiveness of blockage correlates with the number of open channels (Zaitsev et al., 2011). Therefore, we have tested two dicationic compounds, IEM-1460 and IEM-1925, which capability to inhibit neuronal CP-AMPARs in the use-dependent manner had been proved already (Magazanik et al., 1997; Tikhonov et al., 2000; Tikhonova et al., 2008; Zaitsev et al., 2011) to figure out their effectiveness in managing persistent inflammatory pain *in vivo*. Dicationic compounds were applied i.t. as a post-treatment of persistent inflammatory pain that had developed in the CFA-induced model of long-lasting peripheral inflammation. Either IEM-1460 or IEM-1925 produced profound alleviation of inflammatory hypersensitivity. Firstly, relief in pain appeared shortly after compound administration (within hours). Secondly, the reduction in inflammatory hypersensitivity lasted for a long period of time, resulting thirdly, in a marked shortening of the period of pain maintenance after treatment with dicationic compounds. The effects obtained with using dicationic compounds here are consistent with those demonstrated previously when we prevented the upregulation of CP-AMPARs in DH interneurons by utilizing a gene-targeted strategy (Park et al., 2009; Kopach et al., 2013). However, the effects of dicationic compounds on inflammatory pain maintenance contrast with those reported for organic toxins (joro spider toxin, philantotoxin), which attenuated the development of thermal injury-evoked mechanical allodynia (Sorkin et al., 1999, 2001), carrageenan-induced hyperalgesia (Sorkin et al., 2001) and mechanical allodynia in the postincision pain model (Pogatzki et al., 2003), but failed to alleviate the pain maintenance (Sorkin et al., 2001; Jones and Sorkin, 2004). Such discrepancy very likely relates to different pain models and reflects also a different involvement of CP-AMPARs in mechanisms underlying development and maintenance of pain of various origins. Consistent with this assumption, the acute effects of dicationic compounds on thermal hypersensitivity were similar to those produced by organic toxins (Sorkin et al., 1999, 2001; Pogatzki et al., 2003).

Dicationic compounds alleviated inflammatory pain in the concentration-dependent manner, displaying the fastest and maximal pain relief when IEM-1460 or IEM-1925 was used at the concentration very close to the value estimated

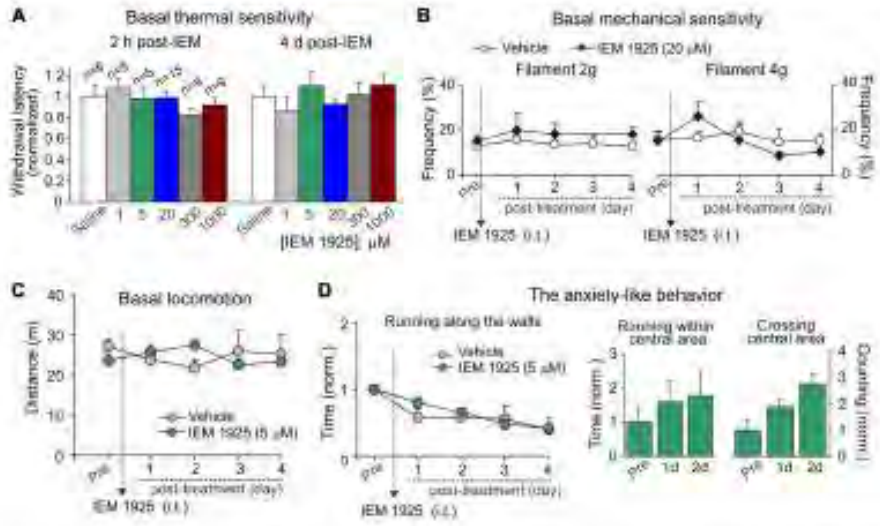

FIGURE 7 | IEM-1925 does not give rise to detectable side effects. (A) The Hargreaves test demonstrates neither acute nor delayed changes of thermal peripheral sensitivity in rats after treatment with dicationic compound IEM-1925 at different concentrations. Data are expressed as the mean paw withdrawal latencies normalized to the correspondent time point in the saline-treated group. **(B)** The von Frey behavioral test shows no changes in the mechanical peripheral sensitivity in response to the 2 g (left graph) and 4 g (right graph) von Frey monofilaments in rats treated with 20 μM IEM-1925. Results are presented as mean ± SEM. **(C,D)** The open-field test shows no changes in animal locomotion **(C)** and no rise in the anxiety-like behavior **(D)** following treatment with 5 μM IEM-1925. Assessment of the anxiety-like behavior was similar as in **Figure 4D**; results are presented as mean values normalized to the correspondent time-point prior to the treatment (Pre) for all parameters tested.

as IC50 for blocking CP-AMPARs (Buldakova et al., 1999). Either compound produced alleviation in persistent inflammatory pain, which: (i) appeared shortly after starting the treatment; (ii) maintained for a long period of time (at least 7 days); and (iii) results in a marked shortening of inflammatory pain maintenance. However, relief in pain produced by IEM-1925 appeared faster than by IEM-1460 (for either thermal or mechanical hypersensitivity) when compared antinociceptive effects between the compounds. Our *in vivo* observation is consistent with the reported higher potency of IEM-1925 to inhibit CP-AMPARs *in vitro* comparing to the potency of other blockers (IEM-1460, IEM-1754) within the group of dicationic compounds (Magazanik et al., 1997; Tikhonov et al., 2000; Zaitsev et al., 2011). Notably, lowering concentration of drug to 1 μM or increasing it to a milimolar range (1 mM, the concentration representing the estimated IC50 value for blocking GluR2-containing Ca^{2+}-impermeable AMPARs; Buldakova et al., 1999) resulted in the short-lasted alleviation of inflammatory pain with a negligible effect produced by compounds on the inflammatory pain maintenance. This is in agreement with the causally linked upregulation of CP-AMPARs in the DH interneurons of spinal cord to the persistent inflammatory pain maintenance (Park et al., 2009; Kopach et al., 2011, 2013).

However, a loss of CP-AMPARs may cause adverse effects because of the crucial role of CP-AMPARs in synaptic plasticity that would make the prominent analgesic effects produced by dicationic compounds impractical. Therefore, we have thoroughly tested whether inhibition of spinal CP-AMPARs with dicationic compounds could develop side effects by utilizing a set of different behavioral tests to find out if any one among a set of parameters tested is altered following treatment with dicationic compounds. Our behavioral studies demonstrated that neither peripheral sensitivity of different modalities (thermal, mechanical) nor the animal locomotive behavior was changed following treatment. Further, dicationic compounds did not give rise to side effects developed in tested animals since none of the commonly used parameters representing the anxiety-like behavior had been altered (the time of running along the walls, within the central area of arena, crossing of the arena center). Our *in vivo* results are consistent with the absent changes in basal transmission in the brain *in situ* when dicationic compounds were continuously present (Zaitsev et al., 2011). Cumulatively, it indicates that the activity-dependent inhibition of CP-AMPARs with dicationic compounds does not lead to detectable adverse effects.

Summarizing, dicationic compounds, the open-channel antagonists acting in the activity-dependent manner, effectively relieve persistent pain syndrome by alleviating a repertoire of the inflammatory symptoms, including the peripheral hypersensitivity of different modalities (thermal and mechanical pain), the locomotor deficit and the suppressed activity of injured animals in persistent inflammatory pain conditions. The ability of dicationic compounds to provide relief in chronic inflammatory pain represents a new reliable route for pain management and further perspectives in a mechanism-targeted therapy of chronic pain.

AUTHOR CONTRIBUTIONS

OK: research concept; design of experiments; animal surgery and behavioral studies; data analysis and interpretation; drafting and revision of the manuscript. VK: design of experiments; animal surgery and behavioral studies; data analysis and interpretation. JG: design of experiments; animal surgery and behavioral studies; drafting of the manuscript. NV: research concept; design of experiments; supervision of studies; critical revision of the manuscript.

FUNDING

This work was supported by the National Academy of Sciences of Ukraine (NASU) Biotechnology, Functional Genomics and DFFD F47/066 Grants to NV, and NASU Grant for Young Scientists to OK.

ACKNOWLEDGMENTS

The authors thank Prof. Lev G. Magazanik and Dr. Denis Tikhonov (Sechenov Institute of Evolutionary Physiology and Biochemistry of the Russian Academy of Sciences, Saint Petersburg, Russia) for dicationic compounds. The authors would like to gratefully acknowledge Mr. Arseniy Bozhenko for technical assistance with the open-field test analysis. The authors thank Prof. Dmitri Rusakov (Institute of Neurology, University College London, UK) for helpful comments and discussion and Prof. Neil Davey (University of Hertfordshire, Hatfield, UK) for editorial assistance.

REFERENCES

Batley, K. R., and Crawley, J. N. (2009). "Anxiety-related behaviors in mice," in *Methods of Behavior Analysis in Neuroscience*, 2nd Edn, ed. J. J., Buccafusco (Boca Raton, FL: CRC Press, Taylor and Francis Group, LLC), 78–82.

Bellavance, L. L., and Beitz, A. J. (1996). Altered c-fos expression in the parabrachial nucleus in a rodent model of CFA-induced peripheral inflammation. *J. Comp. Neurol.* 366, 431–447. doi: 10.1002/(sici)1096-9861(19960311)366:3<431::aid-cne5>3.0.co;2-5

Blaschke, M., Keller, B. U., Rivosecchi, R., Hollmann, M., Heinemann, S., and Konnerth, A. (1993). A single amino acid determines the subunit-specific spider toxin block of alpha-amino-3-hydroxy-5-methylisoxazole-4-propionate/kainate receptor channels. *Proc. Natl. Acad. Sci. U S A.* 90, 6528–6532. doi: 10.1073/pnas.90.14.6528

Buccafusco, J. J. (2009). *Methods of Behavior Analysis in Neuroscience*. 2nd Edn. Boca Raton, FL: CRC Press/Taylor and Francis.

Bukdakova, S. L., Vorobjev, V. S., Sharonova, I. N., Samotlova, M. V., and Magazanik, L. G. (1999). Characterization of AMPA receptor populations in rat brain cells by the use of subunit-specific open channel blocking drug, IEM-1460. *Brain Res.* 846, 52–58. doi: 10.1016/s0006-8993(99)01970-8

Gu, J. G., Albuquerque, C., Lee, C. J., and MacDermott, A. B. (1996). Synaptic strengthening through activation of Ca^{2+}-permeable AMPA receptors. *Nature* 381, 793–796. doi: 10.1038/381793a0

Hao, J. X., and Xu, X. J. (1996). Treatment of a chronic allodynia-like response in spinally injured rats: effects of systemically administered excitatory amino acid receptor antagonists. *Pain* 66, 279–285. doi: 10.1016/0304-3959(96)03019-9

Hartmann, B., Ahmadi, S., Heppenstall, P. A., Lewin, G. R., Schott, C., Borchardt, T., et al. (2004). The AMPA receptor subunits GluR-A and GluR-B reciprocally modulate spinal synaptic plasticity and inflammatory pain. *Neuron* 44, 637–650. doi: 10.1016/j.neuron.2004.10.029

Herlitze, S., Raditsch, M., Ruppersberg, J. P., Jahn, W., Monyer, H., Schoepfer, R., et al. (1993). Argiotoxin detects molecular differences in AMPA receptor channels. *Neuron* 10, 1131–1140. doi: 10.1016/0896-6273(93)90061-a

Ji, R. R., Kohno, T., Moore, K. A., and Woolf, C. J. (2003). Central sensitization and LTP: do pain and memory share similar mechanisms? *Trends Neurosci.* 26, 696–705. doi: 10.1016/j.tins.2003.09.017

Jones, T. L., and Sorkin, L. S. (2004). Calcium-permeable alpha-amino-3-hydroxy-5-methyl-4-isoxazolepropionic acid/kainate receptors mediate development, but not maintenance, of secondary allodynia evoked by first-degree burn in the rat. *J. Pharmacol. Exp. Ther.* 310, 223–229. doi: 10.1124/jpet.103.064741

Kopach, O., Kao, S. C., Petralia, R. S., Belan, P., Tao, Y. X., and Voitenko, N. (2011). Inflammation alters trafficking of extrasynaptic AMPA receptors in tonically firing lamina II neurons of the rat spinal dorsal horn. *Pain* 152, 912–923. doi: 10.1016/j.pain.2011.01.016

Kopach, O., Viatchenko-Karpinski, V., Attanjoh, F. E., Belan, P., Tao, Y. X., and Voitenko, N. (2013). PKCα is required for inflammation-induced trafficking of extrasynaptic AMPA receptors in tonically firing lamina II dorsal horn neurons during the maintenance of persistent inflammatory pain. *J. Pain* 14, 182–192. doi: 10.1016/j.jpain.2012.10.015

Kopach, O., Viatchenko-Karpinski, V., Belan, P., and Voitenko, N. (2012). Development of inflammation-induced hyperalgesia and allodynia is associated with the upregulation of extrasynaptic AMPA receptors in tonically firing lamina II dorsal horn neurons. *Front. Physiol.* 3:391. doi: 10.3389/fphys.2012.00391

Kopach, O., and Voitenko, N. (2013). Extrasynaptic AMPA receptors in the dorsal horn: evidence and functional significance. *Brain Res. Bull.* 93, 47–56. doi: 10.1016/j.brainresbull.2012.11.004

Magazanik, L. G., Buldakova, S. L., Samotlova, M. V., Gmiro, V. E., Mellor, I. R., and Usherwood, P. N. (1997). Block of open channels of recombinant AMPA receptors and native AMPA/kainate receptors by adamantane derivatives. *J. Physiol.* 505, 655–663. doi: 10.1111/j.1469-7793.1997.655ba.x

Nozaki-Taguchi, N., and Yaksh, T. L. (2002). Pharmacology of spinal glutamatergic receptors in post-thermal injury-evoked tactile allodynia and thermal hyperalgesia. *Anesthesiology* 96, 617–626. doi: 10.1097/00000542-200203000-00018

Park, J. S., Voitenko, N., Petralia, R. S., Guan, X., Xu, J. T., Steinberg, J. P., et al. (2009). Persistent inflammation induces GluR2 internalization via NMDA receptor-triggered PKC activation in dorsal horn neurons. *J. Neurosci.* 29, 3206–3219. doi: 10.1523/JNEUROSCI.4514-08.2009

Park, J. S., Yaster, M., Guan, X., Xu, J. T., Shih, M. H., Guan, Y., et al. (2008). Role of spinal cord alpha-amino-3-hydroxy-5-methyl-4-isoxazolepropionic acid receptors in complete Freund's adjuvant-induced inflammatory pain. *Mol. Pain* 4:67. doi: 10.1186/1744-8069-4-67

Pogatzki, E. M., Niemeier, J. S., Sorkin, L. S., and Brennan, T. J. (2003). Spinal glutamate receptor antagonists differentiate primary and secondary mechanical hyperalgesia caused by incision. *Pain* 105, 97–107. doi: 10.1016/s0304-3959(03)00169-6

Sorkin, L. S., Yaksh, T. L., and Doom, C. M. (1999). Mechanical allodynia in rats is blocked by a Ca^{2+} permeable AMPA receptor antagonist. *Neuroreport* 10, 3523–3526. doi: 10.1097/00001756-199911260-00011

Sorkin, L. S., Yaksh, T. L., and Doom, C. M. (2001). Pain models display differential sensitivity to Ca^{2+}-permeable non-NMDA glutamate receptor antagonists. *Anesthesiology* 95, 965–973. doi: 10.1097/00000542-200110000-00028

Tikhonov, D. B., Samotlova, M. V., Buldakova, S. L., Gmiro, V. E., and Magazanik, L. G. (2000). Voltage-dependent block of native AMPA receptor channels by dicationic compounds. Br. *J. Pharmacol.* 129, 265–274. doi: 10.1038/sj.bjp.0703043

Tikhonova, T. B., Barygin, O. I., Gmiro, V. E., Tikhonov, D. B., and Magazanik, L. G. (2008). Organic blockers escape from trapping in the AMPA receptor channels by leaking into the cytoplasm. *Neuropharmacology* 54, 653–664. doi: 10.1016/j.neuropharm.2007.11.014

Vikman, K. S., Rycroft, B. K., and Christie, M. J. (2008). Switch to Ca^{2+}-permeable AMPA and reduced NR2B NMDA receptor-mediated

neurotransmission at dorsal horn nociceptive synapses during inflammatory pain in the rat. *J. Physiol.* 586, 515–527. doi: 10.1113/jphysiol.2007.145581

Woolf, C. J., and Salter, M. W. (2000). Neuronal plasticity: increasing the gain in pain. *Science* 288, 1765–1769. doi: 10.1126/science.288.5472.1765

Zaitsev, A. V., Kim, K. K., Fedorova, I. M., Dorofeeva, N. A., Magazanik, L. G., and Tikhonov, D. B. (2011). Specific mechanism of use-dependent channel block of calcium-permeable AMPA receptors provides activity-dependent inhibition of glutamatergic neurotransmission. *J. Physiol.* 589, 1587–1601. doi: 10.1113/jphysiol.2011.204362

Conflict of Interest Statement: The authors declare that the research was conducted in the absence of any commercial or financial relationships that could be construed as a potential conflict of interest.

4.3. Роль PKCα у порушеному обігу AMPA-рецепторів у нейронах ДР спинного мозку при тривалому периферичному запаленні: застосування генної терапії для лікування хронічного болю

American Pain Society
RESEARCH
EDUCATION
TREATMENT
ADVOCACY
PUBLISHED BY ELSEVIER

The Journal of Pain, Vol 14, No 2 (February), 2013: pp 182-192
Available online at www.jpain.org and www.sciencedirect.com

PKCα Is Required for Inflammation-Induced Trafficking of Extrasynaptic AMPA Receptors in Tonically Firing Lamina II Dorsal Horn Neurons During the Maintenance of Persistent Inflammatory Pain

Olga Kopach,* Viacheslav Viatchenko-Karpinski,* Fidelis E. Atianjoh,† Pavel Belan,* Yuan-Xiang Tao,† and Nana Voitenko*

*State Key Laboratory of Molecular and Cellular Biology, Bogomoletz Institute of Physiology, Kiev, Ukraine.
†Department of Anesthesiology and Critical Care Medicine, Johns Hopkins University School of Medicine, Baltimore, Maryland.

Abstract: Persistent inflammation promotes internalization of synaptic GluR2-containing, Ca^{2+}-impermeable AMPA receptors (AMPARs) and insertion of GluR1-containing, Ca^{2+}-permeable AMPARs at extrasynaptic sites in dorsal horn neurons. Previously we have shown that internalization of synaptic GluR2-containing AMPARs requires activation of spinal cord protein kinase C alpha (PKCα), but molecular mechanisms that underlie altered trafficking of extrasynaptic AMPARs are unclear. Here, using antisense (AS) oligodeoxynucleotides (ODN) that specifically knock down PKCα, we found that a decrease in dorsal horn PKCα expression prevents complete Freund's adjuvant (CFA)-induced increase in functional expression of extrasynaptic Ca^{2+}-permeable AMPARs in substantia gelatinosa (SG) neurons of the rat spinal cord. Augmented AMPA-induced currents and associated $[Ca^{2+}]_i$ transients were abolished, and the current rectification 1 day post-CFA was reversed. These changes were observed specifically in SG neurons characterized by intrinsic tonic firing properties, but not in those that exhibited strong adaptation. Finally, dorsal horn PKCα knockdown produced an antinociceptive effect on CFA-induced thermal and mechanical hypersensitivity during the maintenance period of inflammatory pain, indicating a role for PKCα in persistent inflammatory pain maintenance. Our results indicate that inflammation-induced trafficking of extrasynaptic Ca^{2+}-permeable AMPARs in tonically firing SG neurons depends on PKCα, and that this PKCα-dependent trafficking may contribute to persistent inflammatory pain maintenance.

Perspective: *This study shows that PKCα knockdown blocks inflammation-induced upregulation of extrasynaptic Ca^{2+}-permeable AMPARs in dorsal horn neurons and produces an antinociceptive effect during the maintenance period of inflammatory pain. These findings have potential implications for use of PKCα gene-silencing therapy to prevent and/or treat persistent inflammatory pain.*

Key words: *Extrasynaptic AMPA receptors, PKCα, inflammatory pain, substantia gelatinosa neurons.*

Received March 17, 2012; Revised August 29, 2012; Accepted October 31, 2012.
Supported by NASU Biotechnology STCU #5510, DMD #46.2/001 Grants (N.V.); by NASU Grant for Young Scientists (O.K.); by Mr. David Koch and the Patrick C. Walsh Prostate Cancer Research Fund, the Blaustein Pain Research Fund, the Rita Allen Foundation, and NIH Grants NS 058886 and NS072206 (Y.-X.T.); and by the NIH Biobehavioral Pain Research Fellowship (F.E.A.).
The authors declare no conflicts of interest.
Address reprint requests to Dr. Nana Voitenko, Bogomoletz Institute of Physiology, 4 Bogomoletz Str., Kiev 01024, Ukraine. E-mail: nana@biph.kiev.ua
1526-5900/$36.00

http://dx.doi.org/10.1016/j.jpain.2012.10.015

Persistent or chronic pain, which may result from inflammation, infection, or injury to tissue or nerve, is a major public health problem worldwide. Its treatment success is limited by our incomplete understanding of the molecular mechanisms that underlie the transmission and perception of chronic pain. It is generally believed that spinal cord dorsal horn central sensitization contributes to the induction and maintenance of chronic pain.[1]

Activity-dependent trafficking of α-amino-3-hydroxy-5-methyl-4-isoxazolepropionic acid receptors (AMPARs), which mediate fast excitatory transmission, has emerged

as a key mechanism underlying synaptic plasticity in the brain[26,32,33] and central sensitization (a specific form of plasticity) in spinal cord dorsal horn.[16,22,27,35] This activity-dependent trafficking represents regulated functional expression of the receptor subunits GluR1–GluR4, the composition of which determines the functional properties of AMPARs.[34] Recent evidence indicates that altered AMPAR trafficking in dorsal horn neurons is causally linked to peripheral inflammatory pain maintenance.[16,19,20,27] It has been shown that complete Freund's adjuvant (CFA)-induced inflammation activates dorsal horn protein kinase C alpha (PKCα), which is required for phosphorylation of GluR2 at the S880 residue.[3,27,39] This phosphorylation disrupts interaction between GluR2 and its synaptic anchoring protein, ABP/GRIP, and promotes GluR2 endocytosis from the postsynaptic membrane of dorsal horn neurons.[3,27,39] As a result, GluR2-containing AMPARs switch to GluR2-lacking AMPARs, and Ca^{2+} permeability of synaptic AMPARs increases in dorsal horn neurons.[16,19,27,36]

Our recent studies of extrasynaptic AMPAR trafficking in dorsal horn neurons have shown that functional expression of GluR2-lacking, GluR1-containing, Ca^{2+}-permeable AMPARs increases in the extrasynaptic plasma membrane of substantia gelatinosa (SG) neurons during the maintenance period of CFA-induced inflammatory pain.[20] Despite the significant role that extrasynaptic Ca^{2+}-permeable AMPARs play in synaptic plasticity[7,18] and nociception,[12,20,21] molecular mechanisms that underlie extrasynaptic AMPAR trafficking during the maintenance period of inflammatory pain have not been studied. Recently, it has been shown that phosphorylation of GluR1 by PKC promotes activity-dependent GluR1 membrane insertion in hippocampal neurons to maintain an extrasynaptic pool of GluR1-containing AMPARs for recruitment to postsynaptic densities during sustained synaptic potentiation.[6,24] These findings suggest that inflammation-induced activation of PKCα[3,27,39] may be involved in functional expression of extrasynaptic Ca^{2+}-permeable AMPARs[20] and may contribute to inflammatory pain maintenance.

In this work, we used PKCα antisense (AS) oligodeoxynucleotide (ODN) to knock down PKCα locally in spinal cord of rats. With this approach, we show that PKCα contributes to inflammation-induced upregulation of extrasynaptic Ca^{2+}-permeable AMPAR in dorsal horn neurons and plays a role in the maintenance of persistent inflammatory pain.

Methods

Animal Preparation

Male rats (18–30 days old) were housed in cages on a standard 12:12 hour light/dark cycle, with water and food available ad libitum. The animals were used in accordance with protocols that were approved by the Animal Care and Use Committees at the Bogomoletz Institute of Physiology and Johns Hopkins University and were consistent with the ethical guidelines of the National Institutes of Health and the International Association for the Study of Pain. All efforts were made to minimize animal suffering and to reduce the number of animals used.

Experimental Drugs

CFA was purchased from Sigma Chemical Co (St. Louis, MO). Fura-2 was obtained from Invitrogen (Carlsbad, CA); tetrodotoxin (TTX) was from Alomone Labs Ltd (Jerusalem, Israel). APV, AMPA, cyclothiazide (CTZ), bicuculline, strychnine, and 1-trimethylammonio-5-(1-adamantane-methyl-ammoniopentane dibromide) (IEM-1460) were purchased from Tocris Bioscience (Ellisville, MO). AS and missense (MS) ODNs were obtained from ISIS Pharmaceuticals Inc (Carlsbad, CA).

Intrathecal Administration of PKCα ODN

To specifically and selectively knock down the expression of PKC subtype α, we designed and synthesized AS ODN and MS ODN with the following sequences: AS, 5′-GACATCCCTTTCCCCCTCGG-3′ and MS, 5′-CGTCCTCAGTCGTCCCTCAC-3′ as described previously.[10] ODNs were dissolved in saline and stored at −20°C.

For chronic local delivery of ODNs to the L4-5 spinal cord region, a polyethylene (PE-10) tube was inserted into the subarachnoid space at the rostral level of the spinal cord lumbar enlargement segment through an incision at the atlanto-occipital membrane, as described previously.[28,40] The rats were allowed to recover for at least 3 to 5 days before being used experimentally. Rats showing any neurologic deficits postoperatively were excluded. The position of the catheter was confirmed in each animal after behavioral experiments and before electrophysiologic recording.

Once daily for 4 days, the rats were administered saline (10 μL; control), AS ODN (10 μg/10 μL), or MS ODN (10 μg/10 μL) through the intrathecal catheter, followed by 10 μL of saline to flush the catheter. On the third day of injections, the rats received an intraplantar injection of CFA or saline as described below.

Induction of Peripheral Inflammation

To produce unilateral peripheral inflammation and nociceptive hypersensitivity in rats, 100 μL of CFA (*Mycobacterium tuberculosis*) suspended in an oil-saline (1:1) emulsion was injected subcutaneously into the plantar side of 1 hind paw. Saline injection (.9%; 100 μL) was used as a control. Because studies from our laboratory and those of others have shown that CFA produces a significant change in synaptic AMPAR trafficking in dorsal horn neurons 24 hours after injection,[27,28] we carried out Western blot analysis or electrophysiologic recording at that time point.

Western Blot Analysis

Soluble proteins were prepared according to procedures described previously.[27,28] In brief, after the rats (n = 4/group) were euthanized by an overdose of isoflurane, the tissues from the dorsal portions of lumbar spinal cord were dissected and rapidly frozen in

liquid nitrogen. The tissues were then homogenized in homogenization buffer (50 mM Tris-HCl, .1 mM EDTA, .1 mM EGTA, 1 mM phenylmethylsulfonyl fluoride, 1 μM leupeptin, 2 μM pepstatin A). The crude homogenate was centrifuged at 4°C for 15 minutes at 1,000 g, and the supernatants were collected. After protein concentration was measured, the protein was heated for 5 minutes at 98°C and loaded onto 4% stacking/7.5% separating SDS-polyacrylamide gels. After separation, the protein was electrophoretically transferred onto a nitrocellulose membrane. The membrane was blocked with 3% nonfat dry milk and subsequently incubated for 2 hours with polyclonal rabbit primary antibody to PKCα (1:1,000; Santa Cruz Biotechnology, Santa Cruz, CA) or PKCγ (1:1,000,000; Santa Cruz Biotechnology), and with monoclonal mouse primary antibody to β-actin (1:2,000; Santa Cruz Biotechnology). The proteins were detected by horseradish peroxidase-conjugated anti-rabbit or anti-mouse secondary antibody and visualized by chemiluminescence reagents provided with the ECL kit (Amersham Pharmacia Biotech, Piscataway, NJ) and exposure to film. The blot density from naive rats was set as 100%. The relative density values from other groups were determined by dividing the optical density values from these groups by the value from naive rats after they were normalized to the corresponding β-actin.

Behavioral Testing

Animals were acclimatized to the experimental venue before the testing. The experimenters were blinded to the treatment groups during behavioral testing.

Paw withdrawal responses to thermal stimuli were measured in rats by using the Hargreaves technique.[15] For measurement of paw withdrawal responses to noxious heat stimuli, the animal was placed in a Plexiglas chamber on a glass plate located above a light box. Radiant heat was applied by focused infrared beam through a hole in the light box through the glass plate to the middle of the plantar surface of each hind paw. When the animal lifted its foot, the light beam was automatically turned off. The length of time between the start of the beam and the foot lift was defined as the paw withdrawal latency. Each trial was repeated 5 times at 5-minute intervals for each paw. A cut-off time of 30 seconds was used to avoid tissue damage. Behavioral tests were performed before ODN injection, at 1, 2, and 3 days after the first ODN injection, and then at 1, 2, 3, 4, 5, 6, and 7 days after CFA injection.

We used the von Frey method to measure paw withdrawal responses to repeated mechanical stimuli. A rat was placed in a Plexiglas chamber on an elevated mesh screen, and each von Frey monofilament (Bioseb, Vitrolles, France) was applied to the hind paw for approximately 1 to 2 seconds. Trials of each hind paw were repeated 10 times at 1-minute intervals. The occurrence of paw withdrawal in each of these trials was expressed as a percentage response frequency.

Spinal Cord Slice Preparation

Spinal cord slices were prepared from 18- to 30-day-old male rats as described previously.[20,37] Briefly, after rats were deeply anesthetized with an overdose of isoflurane, the L4-5 spinal segments were removed. Transverse slices (300 μm thick) were cut on a vibratome in an ice-cold solution that was continuously bubbled with 95% O_2 and 5% CO_2 and contained (in mM) 250 sucrose, 2 KCl, 1.2 NaH_2PO_4, .5 $CaCl_2$, 7 $MgCl_2$, 26 $NaHCO_3$, and 11 glucose (pH 7.4). Slices were maintained at room temperature in a physiologic Krebs bicarbonate solution that contained (in mM) 125 NaCl, 2.5 KCl, 1.25 NaH_2PO_4, 2 $CaCl_2$, 1 $MgCl_2$, 26 $NaHCO_3$, and 10 glucose (pH 7.4, 310–320 mOsM) and was equilibrated with 95% O_2 and 5% CO_2.

Simultaneous Ca^{2+} Imaging and Patch-Clamp Recording

Simultaneous Ca^{2+} imaging and whole-cell electrophysiologic recordings were obtained from the lamina II SG neurons of the spinal L4-5 dorsal horn as described previously.[20] Briefly, the neurons were visually identified with a video microscope (Olympus Corp, Tokyo, Japan). The patch pipettes with resistance of 6 to 10 MΩ were filled with an internal solution containing (in mM) 133 K-gluconate, 5 NaCl, .5 $MgCl_2$, 10 HEPES-Na, 2 MgATP, .1 GTP-Na, and .2 fura-2 pentapotassium salt (pH 7.2, 290 mOsM). The membrane potential of SG neurons was held at −60 mV. Only data from neurons that exhibited a resting membrane potential ≤ −60 mV were included in the analysis.

All SG neurons were categorized according to their discharge pattern in response to a series of 1-second current pulses, as described previously.[20] SG neurons were predominantly divided into "tonic" and "transient" groups. Tonic neurons were defined as those able to support continued discharge of action potentials during 1-second depolarizing inward current and an increased frequency of discharge with increasing current intensity. Transient neurons were those that exhibited a strong adaptation by generating short bursts of spikes or a single spike regardless of depolarizing current intensity.[20]

To isolate AMPAR-mediated current and associated increase in $[Ca^{2+}]_i$, we performed recordings in the continuous presence of APV (50 μM), bicuculline (5 μM), and strychnine (2 μM) to block NMDA, $GABA_A$, and glycine receptors, respectively. In addition, TTX (.5 μM) and cadmium chloride (100 μM) were added to Krebs bicarbonate solution to block corresponding voltage-activated sodium and calcium channels. To prevent desensitization of AMPARs during bath application of the agonist, we applied AMPA in the continuous presence of CTZ (20 μM). Typically, 1 neuron was studied per slice.

Fura-2 fluorescent signal was collected from SG neurons located between 50 and 100 μm below the surface of the slice by using a 60×, NA .9 water-immersion objective (Olympus Corp) and a 12-bit cooled CCD camera and capturing board (Sensicam; PCO, Kelheim, Germany). Fluorescence intensity was measured at wavelengths >

510 nm when excited at 380 nm and 340 nm by a PolyChrome IV monochromator (Till Photonics, Gräfelfing, Germany) using Imaging Workbench software (INDEC System, Santa Clara, CA). The fluorescence intensities for soma and dendrites were expressed as changes in the ratio of fura-2 fluorescence at 340 and 380 nm, as ratio is proportional to $[Ca^{2+}]_i$.[13] The amplitude of the AMPA-induced $[Ca^{2+}]_i$ transient was calculated as the difference between the fura-2 fluorescence ratio before AMPA application and the ratio at the maximum $[Ca^{2+}]_i$ rise during AMPA stimulation.

To study the current-voltage (I-V) relationship, we used an internal solution that contained (in mM) 130 Cs-methylsulfonate, 10 NaCl, .5 EGTA, 10 HEPES, .2 spermine tetrahydrochloride, 2 Mg-ATP, and .1 Na-GTP (pH 7.2, 290 mOsM). I-V curves were constructed by holding neurons at −70 mV in a voltage clamp and ramping for 100 to 300 milliseconds every 5 seconds initially to +50 mV and then to −70 mV. A short hyperpolarizing voltage step to −75 mV was applied before every ramp to monitor input and access resistance. To inhibit K^+-channel currents, we perfused patched neurons with this internal solution for at least 10 minutes before recording. To isolate AMPA-induced current, we subtracted the ramp currents recorded before AMPA application from the currents recorded during the bath AMPA application at each membrane potential. The rectification index (RI) of the AMPA-induced current was determined by dividing the current amplitude at +30 mV by the current amplitude at −50 mV. The RI was also estimated by dividing the AMPAR conductance at −30 mV by the conductance at −50 mV; a reversal potential of AMPA-induced current, which is necessary for conductance calculation, was determined for each I-V curve. Clampfit 8.0 software (Molecular Devices, Sunnyvale, CA) was used to analyze the currents.

Statistical Analysis

All data are presented as mean ± SEM with n referring to the number of cells analyzed. Student t-tests were used to determine statistically significant differences. A P value of less than .05 was considered statistically significant.

Results

Effect of Intrathecal PKCα AS ODN on Spinal Cord PKCα Protein Expression

We first examined whether intrathecal administration of PKCα AS ODN selectively and specifically altered dorsal horn PKCα expression. MS ODN was used as a control. Consistent with a previous report,[10] 4 once-daily intrathecal injections of PKCα AS ODN, but not MS ODN, significantly reduced PKCα protein expression in the dorsal horn of spinal cord lumbar enlargement segment (Fig 1). The level of PKCα in the AS ODN-treated group (n = 4) was reduced by 43% ($P < .05$) compared to the level in the naive group (n = 4; Fig 1). Neither AS ODN nor MS ODN affected the expression of PKCγ (Fig 1).

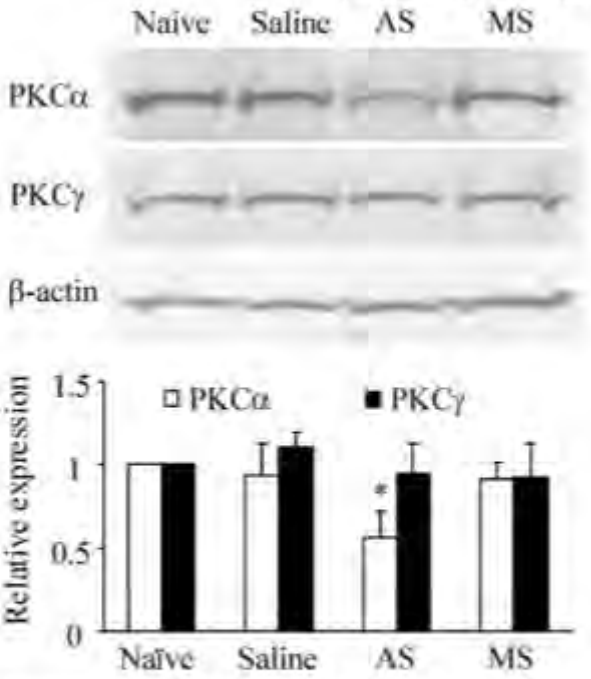

Figure 1. Effect of PKCα AS ODN on PKCα protein expression in spinal cord. Intrathecal injection of 10 μg PKCα AS ODN, but not saline or 10 μg MS ODN, significantly reduced expression of PKCα in the dorsal horn of spinal cord lumbar enlargement segments compared to that in naive rats. Expression of PKCγ was unaffected. Top: Representative Western blots. Bottom: Statistical summary of the densitometric analysis expressed relative to naive rats after normalization to corresponding β-actin. *$P < .05$.

Effect of Intrathecal PKCα AS ODN on CFA-Induced Augmentation of Extrasynaptic AMPAR-Mediated Currents and $[Ca^{2+}]_i$ Transients in Tonically Firing SG Neurons

Previously we showed that CFA-induced peripheral inflammation substantially increases functional expression of Ca^{2+}-permeable AMPARs in the extrasynaptic plasma membrane of tonically firing SG neurons.[20] In this work, we investigated whether downregulation of dorsal horn PKCα by AS ODN affects this increase by simultaneously recording AMPA-induced transmembrane currents and associated $[Ca^{2+}]_i$ changes in soma and dendrites of SG neurons. Consistent with previous reports,[20,37] bath administration of AMPA (5 μM, 60 seconds) to the spinal cord slices evoked an inward current in all SG neurons at a holding potential of −60 mV. The current was characterized by a slow rising phase followed by a plateau level. Although bath applied AMPA activates a total pool of plasma membrane AMPARs, extrasynaptic AMPARs are the predominant contributor to AMPA-induced current because they are relatively more abundant than synaptic AMPARs.[2,14,20] Differences in functional properties between the total pool of AMPARs and synaptic AMPARs (eg, rectification properties of the current in dorsal horn and hippocampal neurons and sensitivity to polyamine derivatives)[13,20,27] additionally confirm the

major contribution of extrasynaptic AMPARs to AMPA-induced current.

We found that acute transient knockdown of dorsal horn PKCα was sufficient to significantly attenuate CFA-induced augmentation of AMPAR-mediated current in tonically firing SG neurons (Figs 2A and 2B). Consistent with our previous study,[20] CFA injection markedly increased the amplitude of AMPA-induced currents in the saline-treated group (−460 ± 48 pA; n = 20 versus −204 ± 18 pA; n = 35 in control; $P < .001$; Fig 2C), indicating a dramatic upregulation of extrasynaptic AMPARs during CFA-induced inflammation. However, CFA-induced inflammatory insult did not alter the amplitude of evoked AMPAR-mediated excitatory postsynaptic currents (eEPSCs) in dorsal horn neurons as we[27] and others[19,36] have reported previously, additionally supporting the premise that extrasynaptic AMPARs are the major contributor to AMPA-induced currents.

After 4 days of AS ODN injections, the average amplitude of AMPA-induced current was −191 ± 32 pA (n = 9) in neurons from the CFA-treated group of animals, a value that was close to that obtained in the saline-treated noninflamed animals (−204 ± 18 pA; n = 35; $P > .7$; Fig 2C). As expected, MS ODN did not affect the CFA-induced increase in current amplitude (MS ODN: −454 ± 44 pA, n = 13; $P > .4$ compared to the saline-treated CFA-inflamed animals). One day after CFA injection, no significant differences were observed between AS ODN- and MS ODN-treated groups in resting membrane potential of tonic neurons (AS ODN: −52 ± 2 mV, n = 13; MS ODN: −54 ± 2 mV, n = 23; $P = .5$), input resistance (AS ODN: 709 ± 77 MΩ, n = 26; MS ODN: 528 ± 85 MΩ, n = 23; $P > .1$), membrane capacitance (AS ODN: 26 ± 2 pF, n = 26; MS ODN: 25 ± 1 pF, n = 25; $P > .7$), or series resistance (AS ODN: 30 ± 2 MΩ, n = 26; MS ODN: 34 ± 2 MΩ, n = 23; $P > .2$).

The AMPA-induced current was associated with a synchronous rise in $[Ca^{2+}]_i$ observed in both soma and dendrites of tonic neurons. This change in $[Ca^{2+}]_i$ consisted of an initial fast rise followed by a slow decay to baseline within a few minutes. In line with our previous results,[20,37] CFA-induced inflammatory insult markedly increased the amplitude of AMPA-induced $[Ca^{2+}]_i$ transients in soma (by 92 ± 11%, n = 11) and dendrites (by 96 ± 17%, n = 11) of tonically firing SG neurons ($P < .05$), indicating a dramatic upregulation of extrasynaptic Ca^{2+}-permeable AMPARs during CFA-induced inflammation. As with the AMPA-induced currents, knockdown of dorsal horn PKCα also significantly reversed augmented $[Ca^{2+}]_i$ transients 1 day after CFA injection. In soma, the average amplitudes of AMPA-induced $[Ca^{2+}]_i$ transients in CFA-inflamed rats were .91 ± .10 (n = 11) after saline treatment but .22 ± .05 (n = 10; $P < .05$) after AS ODN treatment (Fig 2C). Likewise in the dendrites, the average amplitudes of AMPA-induced $[Ca^{2+}]_i$ transients in these rats were 1.17 ± .21 (n = 11) after saline treatment, but .32 ± .06 (n = 14; $P < .05$) after AS ODN treatment (Fig 2C). It is interesting to note that the average amplitude of AMPA-induced

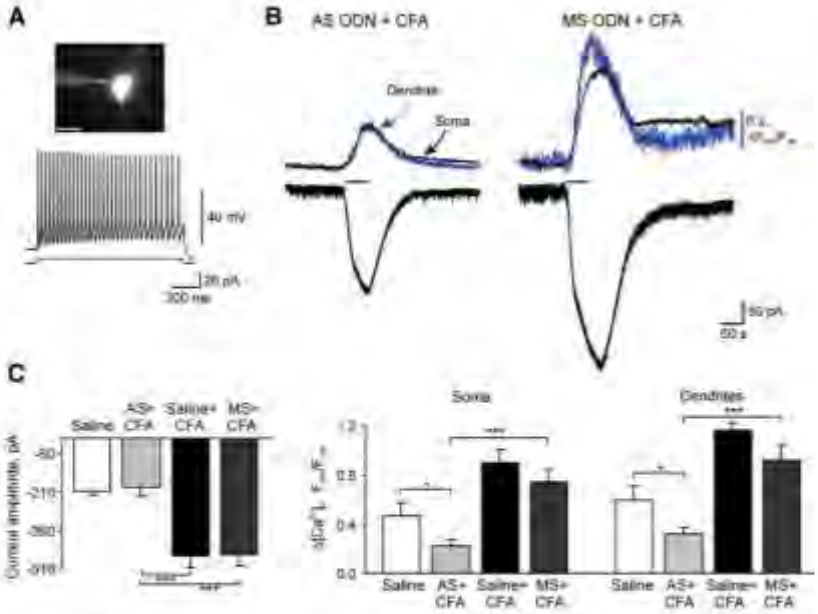

Figure 2. Knockdown of dorsal horn PKCα attenuates CFA-induced augmentation of AMPA-induced current and $[Ca^{2+}]_i$ transients in tonically firing SG neurons. **(A)** *Top*: fluorescent image of a SG neuron loaded with fura-2 (200 μM); scale bar = 20 μm. *Bottom*: typical firing pattern for tonic neurons in response to sustained depolarizing current. **(B)** One day after rats were administered intraplantar CFA injections, neurons were collected for electrophysiologic recordings. Representative examples of a somatic membrane current (*bottom trace*) and associated $[Ca^{2+}]_i$ transients (*upper traces*) recorded from the soma (*black trace*) and dendrites (*blue trace*) of tonic neurons during AMPA bath application (5 μM, 60 seconds) in the AS ODN- (right) and MS ODN-treated (left) groups. **(C)** Statistical summary of the amplitudes of AMPA-induced current (left graph) and associated $[Ca^{2+}]_i$ transients in soma and dendrites (right graph) of tonic SG neurons from the saline-, AS ODN- and MS ODN-treated groups 1 day after saline or CFA injection. $^*P < .05$, $^{***}P < .001$.

$[Ca^{2+}]_i$ transients in the AS ODN-treated CFA-inflamed group was lower than that in the saline-treated noninflamed group (in soma: .22 ± .05; n = 10 versus .47 ± .10; n = 21; $P < .05$; in dendrites: .32 ± .06; n = 14 versus .60 ± .12; n = 14; $P < .05$; Fig 2C). No significant difference was observed in the amplitudes of somatic and dendritic $[Ca^{2+}]_i$ transients between the MS ODN- and saline-treated groups 1 day post-CFA (in soma: .91 ± .10 for saline, n = 11 versus .75 ± .09 for MS ODN, n = 9; $P > .4$; in dendrites: 1.17 ± .21 for saline, n = 11 versus .93 ± .12 for MS ODN, n = 9; $P > .3$, respectively; Fig 2C).

Taken together, our results show that knockdown of dorsal horn PKCα efficiently abolishes CFA-induced augmentation of extrasynaptic AMPAR-mediated current and associated $[Ca^{2+}]_i$ transients in tonically firing SG neurons. These findings indicate that CFA-promoted upregulation of extrasynaptic Ca^{2+}-permeable AMPAR in these neurons is PKCα-dependent.

It should be noted that knockdown of dorsal horn PKCα did not affect AMPAR-mediated current or somatic or dendritic $[Ca^{2+}]_i$ transients in SG neurons that adapted to sustained membrane depolarization by generating short bursts of spikes or a single spike, regardless of depolarizing current intensity (transient neurons). No significant difference was observed in the average amplitudes of AMPA-induced currents and $[Ca^{2+}]_i$ transients among saline-treated (n = 28), AS ODN-treated (n = 7), and MS ODN-treated (n = 13) groups 1 day after injection of CFA or saline. Average amplitudes of AMPA-induced currents were −173 ± 19 pA ($n = 28$) in the saline-treated group and −150 ± 17 pA (n = 21; $P > .37$) in the CFA-treated group. One day after CFA injection, they were −180 ± 56 pA (n = 7) in the AS ODN-treated group and −196 ± 41 pA (n = 13; $P > .8$) in the MS ODN-treated group. Average amplitudes of $[Ca^{2+}]_i$ transients in soma were .48 ± .09 and .47 ± .08 for the saline- and CFA-treated groups, respectively ($P > .9$), and were .46 ± .09 and .29 ± .08 for the AS ODN- and MS ODN-treated groups, respectively ($P > .2$), 1 day after CFA injection. Dendritic $[Ca^{2+}]_i$ transients were .52 ± .09 and .59 ± .10 for the saline- and CFA-treated groups, respectively ($P > .6$), and were .52 ± .10 and .40 ± .10 for the AS ODN- and MS ODN-treated groups, respectively ($P > .4$). No significant differences were observed in the transient SG neurons between the AS ODN- and MS ODN-treated groups 1 day post-CFA in electrophysiologic properties of input resistance (AS ODN: 1096 ± 215 MΩ, n = 21; MS ODN: 932 ± 170 MΩ, n = 31; $P > .6$), membrane capacitance (AS ODN: 18 ± 3 pF, n = 21; MS ODN: 22 ± 1 pF, n = 31; $P > .2$), and series resistance (AS ODN: 30 ± 2 MΩ, n = 21; MS ODN: 32 ± 2 MΩ, n = 31; $P > .4$). These results demonstrate that functional expression of extrasynaptic AMPAR is not altered during the maintenance of peripheral inflammation in SG neurons that exhibit strong adaptation. The results also indicate that PKCα does not play a significant role in AMPAR functioning in this type of SG neuron.

Effect of Intrathecal PKCα AS ODN on CFA-Induced Increase in the Proportion of Ca^{2+}-Permeable AMPARs in the Total Pool of Extrasynaptic AMPARs

Persistent inflammation increases the proportion of Ca^{2+}-permeable AMPARs within the total extrasynaptic AMPAR pool in tonically firing SG neurons during the maintenance period of CFA-induced inflammatory pain.[20] To examine whether the knockdown of dorsal horn PKCα affects this increase, we compared the I-V relationship of the AMPA-induced currents in SG neurons 1 day after saline or CFA injection in saline-, AS ODN-, and MS ODN-treated groups. The relative proportion of Ca^{2+}-permeable AMPARs can be estimated based on the prominent inwardly rectifying properties of Ca^{2+}-permeable AMPARs.[9] To obtain I-V curves, we used a previously described protocol[20] in which a neuron was held at −70 mV and ramped every 5 seconds initially to +50 mV, and then to −70 mV before and during the bath application of AMPA (Fig 3A). The AMPAR-mediated component of the recorded current was isolated by subtracting the ramp currents recorded before and during the agonist application.

I-V curves obtained from the tonic neurons in the AS ODN-treated group were linear and did not show any rectification at positive membrane potentials on day 4 of AS ODN infusion (Fig 3A). In contrast, extrasynaptic AMPAR-mediated currents displayed weak inward rectification in neurons from the MS ODN- and saline-treated animals (Fig 3A). Rectification of AMPAR-mediated currents was quantitatively expressed as a rectification index ($RI_{+30/-50}$). RI values were 1.02 ± .10 (n = 8) in the AS ODN-treated group and .79 ± .05 (n = 8; $P = .07$; Figs 3B and 3C) in the MS ODN-treated group. In the saline-treated rats, RI was .74 ± .07 (n = 11),[20] a value 38 ± 4% lower than that in the AS ODN-treated group ($P < .05$). Given that an increase in RI value after dorsal horn PKCα knockdown indicates a decrease in the proportion of extrasynaptic Ca^{2+}-permeable AMPARs, our findings suggest that PKCα participates in trafficking of extrasynaptic Ca^{2+}-permeable AMPARs in tonically firing SG neurons under normal conditions.

Consistent with our previous report,[20] CFA-induced peripheral inflammation led to a strong inward rectification of the AMPA-induced currents. On day 1 after CFA injection, RI was .28 ± .05 (n = 5; $P < .001$ compared to control; Figs 3C and 3D) and .27 ± .05 (n = 12; $P < .001$ compared to control) in the MS ODN- and saline-treated groups, respectively. CFA-induced inward rectification of AMPAR-mediated currents could be reversed by a selective blocker of Ca^{2+}-permeable AMPARs, the polyamine derivative IEM-1460.[6] In the MS ODN-treated group, IEM-1460 (40 μM) increased RI value by 67 ± 7% (n = 3; $P < .05$; Figs 3C and 3E). However, we did not observe a significant inward rectification of AMPA-induced currents in tonic SG neurons from the AS ODN-treated group 1 day post-CFA (Fig 3C). RI value, which was .90 ± .07 (n = 8), did not differ significantly from that in the AS ODN-treated noninflamed animals

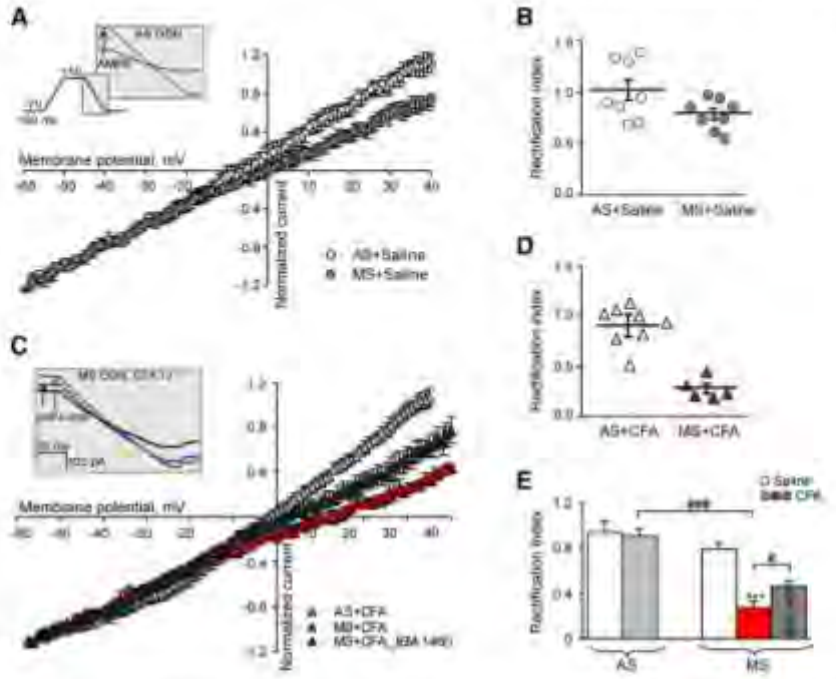

Figure 3. Effect of dorsal horn PKCα knockdown on the I-V relationship of AMPAR-mediated currents in tonically firing SG neurons. **(A)** I-V curves obtained in tonic SG neurons of the AS ODN- and MS ODN-treated groups 1 day after intraplantar saline injection. Inset illustrates the protocol for reconstruction of the I-V relationship from ramp recordings. **(B)** The scatter plot illustrates a spread in rectification index ($RI = I_{+40\,mV}/I_{-50\,mV}$) in tonic SG neurons after AS ODN or MS ODN treatment for 4 days. **(C–D)** I-V curves **(C)** and a scatter plot of rectification index **(D)** in tonic SG neurons from the AS ODN- and MS ODN-treated groups 1 day after CFA injection. **(E)** A statistical summary for rectification index in tonic neurons from the AS ODN- and MS ODN-treated groups 1 day after intraplantar injection of saline or CFA. Rectification index was calculate before (*red bar*) and after (*gray bar*) application of IEM-1460 (40 μM), a selective blocker of Ca^{2+}-permeable AMPARs. ***$P < .001$ versus the saline-injected group, #$P < .05$, ###$P < .001$ versus indicated group.

($P > .35$) or the saline-treated noninflamed rats ($P > .1$). Taking into account that a reversal potential of the AMPA-induced currents could be potentially right-shifted in the neurons of inflamed animals because of the greater contribution of Ca^{2+} influx to the total current, we also calculated RI based on the measurements of AMPAR conductance (not currents) at positive and negative potentials (+30 mV and −50 mV, respectively). The RI values obtained in this way were also significantly different in the AS ODN- and MS ODN-treated groups 1 day post-CFA (1.61 ± .23, n = 8 versus .59 ± .13, n = 6; $P < .01$), but no significant differences were found between the AS ODN- and MS ODN-treated groups 1 day post-saline (1.18 ± .13, n = 8 versus 1.09 ± .15, n = 9; $P = .64$). These results indicate that dorsal horn PKCα knockdown was sufficient to significantly abolish the CFA-induced increase in proportion of extrasynaptic Ca^{2+}-permeable AMPARs in tonic SG neurons.

Effect of Intrathecal PKCα AS ODN on CFA-Induced Inflammatory Pain Maintenance

Thus far, our findings indicate that spinal cord PKCα is required for inflammation-induced increases in Ca^{2+}-permeable AMPARs at extrasynaptic sites of dorsal horn neurons. Finally, we examined whether spinal cord PKCα was also required for the maintenance of CFA-induced inflammatory pain. Therefore, we evaluated the effect of knocking down spinal cord PKCα on CFA-induced thermal and mechanical pain hypersensitivity. Consistent with previous reports,[27,28] subcutaneous injection of CFA into a hind paw led to development of long-term thermal pain hypersensitivity, as evidenced by a decrease in ipsilateral paw withdrawal latency (n = 10; Fig 4). This hypersensitivity reached a peak on day 1 and persisted for at least 5 days in the saline-treated group. Intrathecal AS ODN significantly alleviated CFA-induced thermal pain hypersensitivity 1 day post-CFA injection. Paw withdrawal latency was 47 ± 3% greater in the AS ODN-treated group than in the saline-treated group (n = 18; $P < .001$; Fig 4A). In addition, the maintenance period of CFA-induced thermal pain hypersensitivity was markedly reduced in the AS ODN-treated group (Fig 4A). Paw withdrawal latencies on days 2 and 3 after CFA injection (that is, on days 2 and 3 after the final AS ODN injection) were 57 ± 5% greater (n = 11; $P < .01$) and 42 ± 2% greater (n = 7; $P < .05$), respectively, than those in the saline-treated group (Fig 4A). In contrast, MS ODN (n = 14) did not affect the CFA-induced thermal pain hypersensitivity during the observation period (Fig 4A). AS ODN by itself did not change basal response to thermal stimulation (Fig 4A).

We also assessed the effect of intrathecal PKCα AS ODN on CFA-induced mechanical pain hypersensitivity.

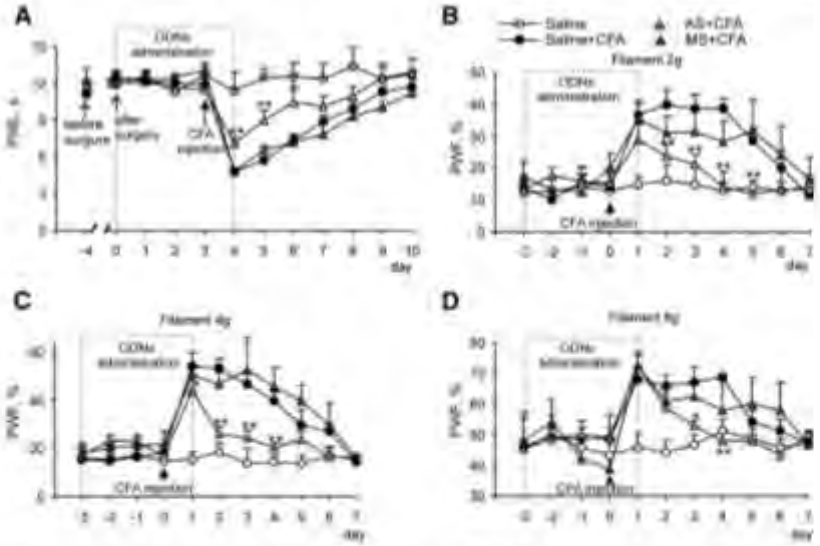

Figure 4. Knockdown of dorsal horn PKCα reduces CFA-induced thermal and mechanical pain hypersensitivity. **(A)** Intrathecal injections with 10 μg PKCα AS ODN, but not saline or 10 μg MS ODN, significantly attenuated the CFA-induced decrease in paw withdrawal latency (PWL) in response to thermal stimulation. **(B–D)** Intrathecal injections with PKCα AS ODN ameliorated the CFA-induced increase in PWF in response to 2-g **(B)**, 4-g **(C)**, and 8-g **(D)** von Frey filaments at the time points shown. $^{*}P < .05$, $^{**}P < .01$ compared to the corresponding time point in the saline-treated, CFA-inflamed group.

Consistent with previous studies,[5,27,28] CFA injection led to mechanical pain hypersensitivity that manifested as a marked increase in paw withdrawal frequency (PWF) in response to von Frey filaments applied to the injected hind paw (Figs 4B–D). The basal PWFs in response to 2-g, 4-g, and 8-g von Frey filaments were similar among the saline-, AS ODN-, and MS ODN-treated groups (Figs 4B–D), indicating no effect on basal response to mechanical stimuli. However, CFA-induced increases in PWF were significantly lower in the AS ODN-treated group than in the saline-treated group 1 day after CFA injection (2-g filament: 29 ± 5% lower, n = 10; 4-g filament: 19 ± 1% lower, n = 10; $P < .05$, Figs 4B–D). In addition, the response frequencies to the 2-g von Frey filament were reduced in the AS ODN-treated group (n = 10) by 47 ± 7%, 52 ± 7%, 64 ± 23%, and 58 ± 10% ($P < .01$, Fig 4B) on days 2, 3, 4, and 5 post-CFA injection, respectively, compared to those in the saline-treated group. The response frequencies to the 4-g von Frey filament were reduced in the AS ODN-treated group (n = 10) by 51 ± 14%, 48 ± 6%, and 50 ± 8% ($P < .01$; Fig 4C) on days 2, 3, and 4 post-CFA injection, respectively, compared to those in the saline-treated group. The response frequencies to the 8-g filament were reduced by 21 ± 1% on day 3 and by 30 ± 2% on day 4 (both $P < .01$ versus saline treatment; Fig 4D). Together, these findings indicate a functional role of PKCα in the maintenance of CFA-induced inflammatory pain.

Discussion

Activity-dependent trafficking of Ca^{2+}-permeable AMPARs at synaptic and extrasynaptic plasma membranes plays a critical role in synaptic plasticity and spinal central sensitization associated with development and maintenance of pain.[4,22,27,35] However, the molecular mechanisms that underlie the regulation of extrasynaptic Ca^{2+}-permeable AMPAR trafficking in persistent pain are still elusive. Utilizing a gene-silencing approach, we have demonstrated that spinal cord PKCα is required for the upregulation of Ca^{2+}-permeable AMPARs at extrasynaptic sites of tonically firing dorsal horn SG neurons during persistent inflammatory pain. This altered PKCα-dependent AMPAR trafficking in dorsal horn neurons is associated with inflammation-induced pain hypersensitivity and might be involved in the maintenance of persistent inflammatory pain.

Our findings and those of others[10] show that gene silencing by local intrathecal administration of AS ODN specific for PKCα significantly and selectively downregulates PKCα protein expression in the dorsal horn of spinal cord lumbar enlargement segment. This downregulation of PKCα was able to significantly attenuate the upregulation of extrasynaptic Ca^{2+}-permeable AMPARs in SG neurons during CFA-evoked peripheral inflammation. Extrasynaptic AMPAR expression is high in the dorsal horn,[28,29] and studies have shown substantial differences in the functional properties of extrasynaptic and synaptic AMPARs (eg, sensitivity to polyamine blockers and RI of the current).[20,27,28] Normally, most dorsal horn AMPARs are Ca^{2+} impermeable, whether they are located at the postsynaptic membrane[19,27,36] or at extrasynaptic sites.[20] Using patch-clamp recording combined with Ca^{2+} imaging, we showed that Ca^{2+}-permeable AMPARs are dramatically upregulated during CFA-induced persistent inflammation, a finding that is consistent with previous reports.[20,28] We can attribute the increase in currents induced by bath-applied AMPA to upregulation of the extrasynaptic pool of Ca^{2+}-permeable AMPARs, because we[27] and others[19,36]

have previously shown that the amplitude of synaptically evoked AMPAR-mediated eEPSCs in dorsal horn neurons does not change significantly 1 day after CFA injection. Our previous electron microscopy and biochemical data support this conclusion by demonstrating an inflammation-induced increase in GluR1-containing, Ca^{2+}-permeable AMPARs in extrasynaptic membranes of dorsal horn neurons.[20,28] Our current work illustrates that PKCα is required for this inflammation-induced receptor upregulation, as knockdown of spinal PKCα significantly attenuated CFA-induced augmentation of the amplitudes of both AMPA-induced current and $[Ca^{2+}]_i$ transients. Additionally, PKCα knockdown significantly reversed inward rectification of AMPA-induced currents, indicating that PKCα-dependent upregulation of extrasynaptic Ca^{2+}-permeable AMPARs is due to altered AMPAR trafficking during persistent inflammation.

The changes in AMPAR-mediated currents and $[Ca^{2+}]_i$ transients might also be mediated by other mechanisms, such as PKCα-dependent modulation of single channel conductance, channel gating, or agonist affinity. However, GluR2-containing, Ca^{2+}-impermeable AMPARs mainly contribute to AMPA-induced currents in the control group.[20] Changes in the receptor's affinity to AMPA and in its conductance during inflammation do not affect Ca^{2+} permeability. Nevertheless, the increase in $[Ca^{2+}]_i$ transient amplitudes (Fig 2) illustrates the fact that Ca^{2+} permeability of AMPARs was increased. Moreover, the significant changes in rectification of AMPA-induced currents (Fig 3) and the increased sensitivity of the receptor to the polyamine,[20] both of which are prominent features of GluR2-lacking Ca^{2+}-permeable AMPARs,[9] directly indicate that the proportion of GluR2-lacking, Ca^{2+}-permeable AMPARs increases during persistent inflammation.

Inflammation-induced, PKCα-dependent trafficking of extrasynaptic AMPARs occurs specifically in SG neurons that exhibit intrinsic tonic firing. Neither CFA-induced increase in functional expression of Ca^{2+}-permeable AMPARs[20] nor PKCα-dependent extrasynaptic AMPAR trafficking have been observed in neurons that exhibit strong adaptation. Under normal conditions, the AMPA-induced currents and associated $[Ca^{2+}]_i$ transients were similar in tonic and transient SG neurons,[20] suggesting similar patterns of extrasynaptic AMPAR expression. Thus, PKCα plays an essential role in inflammation-induced AMPAR trafficking only in tonically firing SG neurons. Knockdown of dorsal horn PKCα did not significantly change the electrophysiologic properties of either tonic or transient SG neurons, suggesting that PKCα silencing does not substantially modulate neuronal excitability. Since AMPAR trafficking is required for the maintenance of persistent inflammatory pain,[19,27] our data suggest that the transient SG neurons might not contribute to the maintenance of persistent pain. Taking into account that the overwhelming majority of tonic SG interneurons are excitatory,[10] our results suggest that spinal cord PKCα activation in tonically firing excitatory dorsal horn SG neurons is specifically required for inflammation-induced upregulation of extrasynaptic Ca^{2+}-permeable AMPARs during the maintenance period of inflammatory pain.

Dorsal horn PKCα may also play a functional role in Ca^{2+}-permeable AMPAR trafficking in SG neurons under physiologic conditions. For example, the amplitudes of somatic and dendritic AMPA-induced $[Ca^{2+}]_i$ transients in the AS ODN-treated CFA-inflamed group were lower than those in the saline-treated noninflamed group. Hence, knockdown of PKCα is sufficient to suppress Ca^{2+}-permeability of extrasynaptic AMPARs to a level even lower than in control, indicating a reduction in the pool of extrasynaptic Ca^{2+}-permeable AMPARs under normal conditions. Moreover, in AS ODN-treated noninflamed rats, the I-V relationship of the AMPA-induced currents was linear (RI = 1.02), unlike the slightly rectified I-V curves in the MS ODN-treated (RI = .79) and saline-treated (RI = .74) groups. Therefore, under normal conditions, PKCα might regulate trafficking of Ca^{2+}-permeable AMPARs in tonic SG neurons.

Phosphorylation of GluR1 by PKCα may underlie the observed CFA-induced trafficking of extrasynaptic, Ca^{2+}-permeable AMPARs in dorsal horn neurons during inflammatory pain maintenance. As we have demonstrated previously, CFA-induced peripheral inflammatory insult promotes insertion of GluR1 into extrasynaptic membrane of SG neurons.[20] A few serine residue sites on GluR1 in hippocampal neurons are phosphorylated by PKC: S831, S818, and S816.[8,6,17,28] S831 is a substrate for both PKC and CaMKII. It undergoes phosphorylation during long-term potentiation,[5] increasing the single channel conductance of synaptic AMPARs.[35] Phosphorylation of S831 does not influence membrane insertion.[17] In contrast, phosphorylation at S818 by PKC promotes synaptic incorporation of GluR1-containing AMPARs and facilitates AMPAR interaction with protein 4.1N, a downstream actin-binding protein; this interaction stabilizes GluR1.[6,31] Recent studies also have shown that protein 4.1N is required for activity-dependent GluR1 insertion at extrasynaptic sites. Phosphorylation of GluR1 at S816 and S818 enhances 4.1N binding and facilitates GluR1-containing AMPAR insertion in extrasynaptic plasma membrane.[24] Thus, it is likely that the increase in extrasynaptic Ca^{2+}-permeable AMPARs during the maintenance phase of inflammatory pain results from PKCα-dependent phosphorylation of GluR1 S816 and S818 and subsequent insertion of GluR1-containing AMPARs in extrasynaptic plasma membrane of dorsal horn neurons. This conclusion could be further confirmed if specific and selective antibodies against GluR1 S816 and S818 phosphorylation sites were available.

PKCα-dependent trafficking of extrasynaptic Ca^{2+}-permeable AMPARs in dorsal horn SG neurons might be involved in the maintenance of CFA-induced persistent inflammatory pain. Our results show that acute downregulation of dorsal horn PKCα significantly attenuates thermal and mechanical pain hypersensitivity during the maintenance phase of CFA-induced inflammatory pain. Moreover, PKCα also appeared to substantially shorten the maintenance period of inflammatory pain. However, AS ODN alone did not produce any

significant effects on basal responses to thermal and mechanical stimuli. Our behavioral results contrast with those of Zhao et al,[41] who reported that PKCβ, γ, and δ, but not PKCα, are involved in CFA-induced thermal hyperalgesia and that none of the PKC isoforms are required for development of CFA-induced mechanical allodynia in mice that lacked those genes. The differences between our findings and those of Zhao et al may relate to differences in species used and in the age of the animals. Furthermore, the gene knockout approach that they used is limited by the potential development of multiple compensatory mechanisms. Therefore, knockdown strategies that use inducible and localized gene knockout can be more reliable for deciphering nociceptive pathways.

The extrasynaptic AMPAR pool must be replenished to enable synaptic insertion of Ca^{2+}-permeable AMPARs[17] during the maintenance of inflammatory pain.[27,36] Thus, the antihyperalgesic effect produced by PKCα knockdown might result from the prevention of PKCα-dependent insertion of Ca^{2+}-permeable AMPARs into the extrasynaptic membrane. Furthermore, during injury or inflammation, when primary afferent input is strong, glutamate release from primary afferents of presynaptic neurons and glia is excessive. The resulting glutamate spillover from nearby primary afferent terminals[1,21,38] activates extrasynaptic AMPARs, thus strengthening glutamatergic transmission. Membrane insertion of GluR1 promotes Ca^{2+} permeability of AMPARs first at extrasynaptic sites. The GluR1-containing receptors then are delivered to synaptic sites, increasing Ca^{2+} influx and activating intracellular Ca^{2+}-dependent cascades. Such events might contribute to the maintenance of inflammatory pain. Other mechanisms may also be involved in the observed antihyperalgesic effect of dorsal horn PKCα knockdown. Internalization of synaptic GluR2-containing Ca^{2+}-impermeable AMPARs in dorsal horn neurons[19,27,36] also involves activation of PKCα as an upstream trigger, with subsequent GluR2 phosphorylation at S880, disruption of GluR2 binding to its synaptic anchoring protein, and GluR2 internalization.[37] Targeted mutation of GluR2 PKCα phosphorylation at S880 prevents GluR2 internalization and facilitates CFA-induced thermal and mechanical pain hypersensitivity in animals during the maintenance period of inflammatory pain.[16,27] Thus, PKCα-dependent phosphorylation of GluR1 and GluR2 AMPAR subunits in tonically firing excitatory SG neurons contributes to long-lasting changes in functional expression of synaptic and extrasynaptic AMPARs, which may in turn contribute to the maintenance of persistent inflammatory pain.

In conclusion, our study demonstrates that dorsal horn PKCα knockdown significantly attenuates the inflammation-induced upregulation of extrasynaptic Ca^{2+}-permeable AMPARs in tonically firing SG neurons during the maintenance period of inflammatory pain. This attenuation is associated with a substantial antinociceptive effect during persistent peripheral inflammation. Our findings reveal that PKCα functions as an intracellular trigger for trafficking of extrasynaptic Ca^{2+}-permeable AMPARs in dorsal horn neurons. These findings have potential implications for the use of PKCα gene-silencing therapy in the treatment of persistent inflammatory pain.

Acknowledgments

The authors thank Claire F. Levine, MS, for her editorial assistance.

References

1. Allan SM, Rothwell NJ: Cytokines and acute neurodegeneration. Nat Rev Neurosci 2:734-744, 2001

2. Arendt KL, Royo M, Fernandez-Monreal M, Knafo S, Petrok CN, Martens JR, Esteban JA: PIP3 controls synaptic function by maintaining AMPA receptor clustering at the postsynaptic membrane. Nat Neurosci 13:36-44, 2010

3. Atianjoh FE, Yaster M, Zhao X, Takamiya K, Xia J, Gauda EB, Huganir RL, Tao YX: Spinal cord protein interacting with C kinase 1 is required for the maintenance of complete Freund's adjuvant-induced inflammatory pain but not for incision-induced post-operative pain. Pain 151: 226-234, 2010

4. Barria A, Derkach V, Soderling T: Identification of the Ca2+/calmodulin-dependent protein kinase II regulatory phosphorylation site in the alpha-amino-3-hydroxyl-5-methyl-4-isoxazole-propionate-type glutamate receptor. J Biol Chem 272:32727-32730, 1997

5. Barria A, Muller D, Derkach V, Griffith LC, Soderling TR: Regulatory phosphorylation of AMPA-type glutamate receptors by CaM-KII during long-term potentiation. Science 276:2042-2045, 1997

6. Boehm J, Kang MG, Johnson RC, Esteban J, Huganir RL, Malinow R: Synaptic incorporation of AMPA receptors during LTP is controlled by a PKC phosphorylation site on GluR1. Neuron 51:213-225, 2006

7. Borgdorff AJ, Choquet D: Regulation of AMPA receptor lateral movements. Nature 417:649-653, 2002

8. Buldakova SL, Kim KK, Tikhonov DB, Magazanik LG: Selective blockade of Ca^{2+} permeable AMPA receptors in CA1 area of rat hippocampus. Neuroscience 144:88-99, 2007

9. Burnashev N, Monyer H, Seeburg PH, Sakmann B: Divalent ion permeability of AMPA receptor channels is dominated by the edited form of a single subunit. Neuron 8: 189-198, 1992

10. Butler M, Hayes CS, Chappell A, Murray SF, Yaksh TL, Hua XY: Spinal distribution and metabolism of 2'-O-(2-methoxyethyl)-modified oligonucleotides after intrathecal administration in rats. Neuroscience 131:705-715, 2005

11. Choquet D, Triller A: The role of receptor diffusion in the organization of the postsynaptic membrane. Nat Rev Neurosci 4:251-265, 2003

12. Ferguson AR, Christensen RN, Gensel JC, Miller BA, Sun F, Beattie EC, Bresnahan JC, Beattie MS: Cell death after spinal

cord injury is exacerbated by rapid TNF alpha-induced trafficking of GluR2-lacking AMPARs to the plasma membrane. J Neurosci 28:11391-11400, 2008

13. Grynkiewicz G, Poenie M, Tsien RY: A new generation of Ca^{2+} indicators with greatly improved fluorescence properties. J Biol Chem 260:3440-3450, 1985

14. Guire ES, Oh MC, Soderling TR, Derkach VA: Recruitment of calcium-permeable AMPA receptors during synaptic potentiation is regulated by CaM-kinase I. J Neurosci 28: 6000-6009, 2008

15. Hargreaves K, Dubner R, Brown F, Flores C, Joris J: A new and sensitive method for measuring thermal nociception in cutaneous hyperalgesia. Pain 32:77-88, 1988

16. Hartmann B, Ahmadi S, Heppenstall PA, Lewin GR, Schott C, Borchardt T, Seeburg PH, Zeilhofer HU, Sprengel R, Kuner R: The AMPA receptor subunits GluR-A and GluR-B reciprocally modulate spinal synaptic plasticity and inflammatory pain. Neuron 44:637-650, 2004

17. Hayashi Y, Shi SH, Esteban JA, Piccini A, Poncer JC, Malinow R: Driving AMPA receptors into synapses by LTP and CaMKII: requirement for GluR1 and PDZ domain interaction. Science 287:2262-2267, 2000

18. Heine M, Groc L, Frischknecht R, Beique JC, Lounis B, Rumbaugh G, Huganir RL, Cognet L, Choquet D: Surface mobility of postsynaptic AMPARs tunes synaptic transmission. Science 320:201-205, 2008

19. Katano T, Furue H, Okuda-Ashitaka E, Tagaya M, Watanabe M, Yoshimura M, Ito S: N-ethylmaleimide-sensitive fusion protein (NSF) is involved in central sensitization in the spinal cord through GluR2 subunit composition switch after inflammation. Eur J Neurosci 27:3161-3170, 2008

20. Kopach O, Kao SC, Petralia RS, Belan P, Tao YX, Voitenko N: Inflammation alters trafficking of extrasynaptic AMPA receptors in tonically firing lamina II neurons of the rat spinal dorsal horn. Pain 152:912-923, 2011

21. Kullmann DM: Spillover and synaptic cross talk mediated by glutamate and GABA in the mammalian brain. Prog Brain Res 125:339-351, 2000

22. Latremoliere A, Woolf CJ: Central sensitization: A generator of pain hypersensitivity by central neural plasticity. J Pain 10:895-926, 2009

23. Leonoudakis D, Zhao P, Beattie EC: Rapid tumor necrosis factor alpha-induced exocytosis of glutamate receptor 2-lacking AMPA receptors to extrasynaptic plasma membrane potentiates excitotoxicity. J Neurosci 28:2119-2130, 2008

24. Lin DT, Makino Y, Sharma K, Hayashi T, Neve R, Takamiya K, Huganir RL: Regulation of AMPA receptor extrasynaptic insertion by 4.1N, phosphorylation and palmitoylation. Nat Neurosci 12:879-887, 2009

25. Luthi A, Wikstrom MA, Palmer MJ, Matthews P, Benke TA, Isaac JT, Collingridge GL: Bi-directional modulation of AMPA receptor unitary conductance by synaptic activity. BMC Neurosci 5:44, 2004

26. Malinow R, Malenka RC: AMPA receptor trafficking and synaptic plasticity. Annu Rev Neurosci 25:103-126, 2002

27. Park JS, Voitenko N, Petralia RS, Guan X, Xu JT, Steinberg JP, Takamiya K, Sotnik A, Kopach O, Huganir RL, Tao YX: Persistent inflammation induces GluR2 internalization via NMDA receptor-triggered PKC activation in dorsal horn neurons. J Neurosci 29:3206-3219, 2009

28. Park JS, Yaster M, Guan X, Xu JT, Shih MH, Guan Y, Raja SN, Tao YX: Role of spinal cord alpha-amino-3-hydroxy-5-methyl-4-isoxazolepropionic acid receptors in complete Freund's adjuvant-induced inflammatory pain. Mol Pain 4:67, 2008

29. Petralia RS, Wang YX, Mayat E, Wenthold RJ: Glutamate receptor subunit 2-selective antibody shows a differential distribution of calcium-impermeable AMPA receptors among populations of neurons. J Comp Neurol 385: 456-476, 1997

30. Santos SF, Rebelo S, Derkach VA, Safronov BV: Excitatory interneurons dominate sensory processing in the spinal substantia gelatinosa of rat. J Physiol 581:241-254, 2007

31. Shen L, Liang F, Walensky LD, Huganir RL: Regulation of AMPA receptor GluR1 subunit surface expression by a 4. 1N-linked actin cytoskeletal association. J Neurosci 20: 7932-7940, 2000

32. Shepherd JD, Huganir RL: The cell biology of synaptic plasticity: AMPA receptor trafficking. Annu Rev Cell Dev Biol 23:613-643, 2007

33. Shi SH, Hayashi Y, Petralia RS, Zaman SH, Wenthold RJ, Svoboda K, Malinow R: Rapid spine delivery and redistribution of AMPA receptors after synaptic NMDA receptor activation. Science 284:1811-1816, 1999

34. Swanson GT, Kamboj SK, Cull-Candy SG: Single-channel properties of recombinant AMPA receptors depend on RNA editing, splice variation, and subunit composition. J Neurosci 17:58-69, 1997

35. Tao YX: Dorsal horn alpha-amino-3-hydroxy-5-methyl-4-isoxazolepropionic acid receptor trafficking in inflammatory pain. Anesthesiology 112:1259-1265, 2010

36. Vikman KS, Rycroft BK, Christie MJ: Switch to Ca^{2+}-permeable AMPA and reduced NR2B NMDA receptor-mediated neurotransmission at dorsal horn nociceptive synapses during inflammatory pain in the rat. J Physiol 586:515-527, 2008

37. Voitenko N, Gerber G, Youn D, Randic M: Peripheral inflammation-induced increase of AMPA-mediated currents and Ca^{2+} transients in the presence of cyclothiazide in the rat substantia gelatinosa neurons. Cell Calcium 35:461-469, 2004

38. Weng HR, Chen JH, Cata JP: Inhibition of glutamate uptake in the spinal cord induces hyperalgesia and increased responses of spinal dorsal horn neurons to peripheral afferent stimulation. Neuroscience 138:1351-1360, 2006

39. Xia J, Chung HJ, Wihler C, Huganir RL, Linden DJ: Cerebellar long-term depression requires PKC-regulated interactions between GluR2/3 and PDZ domain-containing proteins. Neuron 28:499-510, 2000

40. Zhang B, Tao F, Liaw WJ, Bredt DS, Johns RA, Tao YX: Effect of knock down of spinal cord PSD-93/chapsin-110 on persistent pain induced by complete Freund's adjuvant and peripheral nerve injury. Pain 106:187-196, 2003

41. Zhao C, Leitges M, Gereau RW: Isozyme-specific effects of protein kinase C in pain modulation. Anesthesiology 115:1261-1270, 2011

4.4. Застосування наноінженерії для лікування хронічного болю при тривалому периферичному запаленні: полімерні мікрокапсули

DRUG DELIVERY, 2018
VOL. 25, NO. 1, 435–447
https://doi.org/10.1080/10717544.2018.1431981

Taylor & Francis
Taylor & Francis Group

RESEARCH ARTICLE

OPEN ACCESS

Nano-engineered microcapsules boost the treatment of persistent pain

Olga Kopach[a], Kayiu Zheng[a], Luo Dong[b], Andrei Sapelkin[c], Nana Voitenko[d], Gleb B. Sukhorukov[b] and Dmitri A. Rusakov[a]

[a]Department of Clinical and Experimental Epilepsy, UCL Institute of Neurology, University College London, London, UK; [b]School of Engineering and Materials Science, Queen Mary University of London, London, UK; [c]Centre for Condensed Matter and Materials Physics, Queen Mary University of London, London, UK; [d]Department of Sensory Signaling, Bogomoletz Institute of Physiology, Kyiv, Ukraine

ABSTRACT

Persistent pain remains a major health issue: common treatments relying on either repeated local injections or systemic drug administration are prone to concomitant side-effects. It is thought that an alternative could be a multifunctional cargo system to deliver medicine to the target site and release it over a prolonged time window. We nano-engineered microcapsules equipped with adjustable cargo release properties and encapsulated the sodium-channel blocker QX-314 using the layer-by-layer (LbL) technology. First, we employed single-cell electrophysiology to establish *in vitro* that microcapsule application can dampen neuronal excitability in a controlled fashion. Secondly, we used two-photon excitation imaging to monitor and adjust long-lasting release of encapsulated cargo in target tissue *in situ*. Finally, we explored an established peripheral inflammation model in rodents to find that a single local injection of QX-314-containing microcapsules could provide robust pain relief lasting for over a week. This was accompanied by a recovery of the locomotive deficit and the amelioration of anxiety in animals with persistent inflammation. *Post hoc* immunohistology confirmed biodegradation of microcapsules over a period of several weeks. The overall remedial effect lasted 10–20 times longer than that of a single focal drug injection. It depended on the QX-314 encapsulation levels, involved TRPV1-channel-dependent cell permeability of QX-314, and showed no detectable side-effects. Our data suggest that nano-engineered encapsulation provides local drug delivery suitable for prolonged pain relief, which could be highly advantageous compared to existing treatments.

ARTICLE HISTORY
Received 8 December 2017
Revised 16 January 2018
Accepted 21 January 2018

KEYWORDS
Biodegradable microcapsules; persistent pain; Na^+ channels; drug diffusion; neuronal excitability; pain relief; locomotive deficit and anxiety

Introduction

Persistent or chronic pain remains largely resistant to treatment. In practice, the analgesics of choice have been opiates and Na^+-channel blockers, such as lidocaine. However, their use has been restricted by side-effects, such as sedation for opiates and cardiotoxicity for lidocaine and its derivatives. These factors curtail the amount administered, mainly due to the risk of a rapid systemic escape from the target site or from a drug depot. Furthermore, existing methods of focal drug application have principal limitations: singular injections provide poor control over the application kinetics whereas chronic injecting devices are invasive, costly, and are prone to the infection risk.

Over the years, various medicine cargo systems have been explored and tested for their capability of targeted drug delivery (Sukhorukov et al., 2005; Tanbour et al., 2016), including pain treatment. Some notable attempts utilized hydrogels involving steroid treatment (Liu et al., 2016), photo-triggered liposomes carrying Na^+-channel blocker tetrodotoxin (Rwei et al., 2015; Zhan et al., 2016), or immunoliposomes for opioid delivery (Hua & Cabot, 2013). A major challenge has been, however, to incorporate multiple functionalities into a single entity, which would deliver medicine to the target site and release it over a relatively long period, in a controllable fashion (Sukhorukov et al., 2005; Sukhorukov & Mohwald, 2007; Stuart et al., 2010). One promising direction has been biodegradable polyelectrolyte-based microcapsule systems constructed with the layer-by-layer (LbL) method (Decher, 1997; Stuart et al., 2010). Such systems could incorporate different polyelectrolytes and charged nanoparticles in a single-LbL capsule combining several functionalities. A wide variety of substances have successfully been tried as cargo for encapsulation (De Cock et al., 2010).

In brief, the LbL microcapsules could be made controllably to a size of >0.3 μm, with the outer layers providing their functional features, such as varied permeability (cargo release rate) or sensitivity to the external stimuli (pH, temperature, osmolarity, light, etc.) (Munoz Javier et al., 2008; Antipina & Sukhorukov, 2011; Delcea et al., 2011; Pavlov et al., 2011, 2013; Gao et al., 2016). The microcapsules are routinely made

CONTACT Dmitri A. Rusakov d.rusakov@ucl.ac.uk Department of Clinical and Experimental Epilepsy, UCL Institute of Neurology, University College London, London, UK; Olga Kopach o.kopach@ucl.ac.uk Department of Clinical and Experimental Epilepsy, UCL Institute of Neurology, University College London, London, UK; Gleb B. Sukhorukov g.sukhorukov@qmul.ac.uk School of Engineering and Materials Science, Queen Mary University of London, London, UK

Supplemental data for this article can be accessed here.

of biodegradable components and show no toxicity or appreciable inflammation or apoptotic effects when injected in tissue or internalized by cultured cells (Pavlov et al., 2011).

Among the analgesics used for local pain treatment there has been a growing interest in the Na^+-channel blocker QX-314, which appears to produce relatively long-lasting analgesic effects, at relatively higher potency, in animal models (Lim et al., 2007; Roberson et al., 2011; Zhao et al., 2014). Whilst QX-314 is membrane-impermeable and blocks Na^+ channels from the cytoplasm side, studies *in situ* have established that it enters nerve cells through the transient receptor potential (TRP) receptors TRPV1 and TRPA1 (Binshtok et al., 2007; Leffler et al., 2011; Stueber et al., 2016), which are strongly expressed in peripheral nociceptors (pain-signaling neurons), but also through a TRP-independent mechanism (Brenneis et al., 2014; Hofmann et al., 2014). These findings have prompted calls for further validation of this potentially efficient analgesic (Roberson et al., 2011; Stueber et al., 2016).

Notwithstanding the promise of LbL encapsulation technology, there have been no systematic attempts to adapt it to the explorative studies of therapeutic intervention pertinent to neuropathologies such as peripheral pain. We therefore set out to test whether drug delivery via nano-engineered LbL microcapsules has a therapeutic potential in the context of pain treatment. Here, we encapsulate QX-314 in biodegradable microcapsules made of poly-L-arginine (PArg) and dextran sulfate, adjust and test its release action *in vitro* and *in situ*, and document the effects of encapsulated QX-314 (injected subcutaneously) in a persistent inflammatory pain model in rodents *in vivo*.

Materials and methods

Design and fabrication of microcapsules

Polymer-based multilayer microcapsules were fabricated in accord with the previously established LbL assembly technique (Sukhorukov & Mohwald, 2007; Stuart et al., 2010). Quaternary lidocaine derivative QX-314 chloride, the membrane-impermeable blocker of voltage-gated Na^+ channels, was encapsulated at variable amounts (4–10 pg/capsule). Briefly, $CaCO_3$ was used as sacrificial templates, and PArg was deposited as the first layer and incubated for 15 min, then washed three times; the oppositely charged dextran sulfate sodium salt (DXS) was assembled as the second layer with the same procedure. In order to encapsulate QX-314 into the capsule shells, two of the DXS layers were substituted by QX-314 during the assembly process. Polymer solutions and QX-314 solutions were prepared at 2 mg/ml. For fluorescent visualization, one of the PArg layers was labeled with TRITC. After the assembly of eight layers, the CaCO3 cores were removed with 0.2 M EDTA. The resulting microcapsule architecture was PArg/DXS/QX-314/DXS/QX-314/DS/PArg-TRITC/DXS. Empty microcapsules (no payload) were used as control. The concentration of capsules in suspension was determined by a hemocytometer, Labtech International, Heathfield, UK (density range $1.1–2.2 \times 10^8$ 1/ml). The QX-314 encapsulation rate was calculated by measuring the remaining QX-314 in supernatants. The suspension of microcapsules was stored at 4 °C. To assess the encapsulated cargo release rate, the microcapsules of a similar configuration were made, with one of the DXS layer substituted by Alexa Fluor 488 hydrazide (ThermoFisher Scientific, Paisley, UK).

Primary neuron cultures

Hippocampal neurons were isolated from the Sprague-Dawley rat pups (P0–P2 day-old), in accordance with the European Commission Directive (86/609/EEC) and the United Kingdom Home Office (Scientific Procedures) Act (1986). Neurons were cultured in NeuroBasal A/B27-based medium on a rat astrocyte feeder layer at 37 °C as described (Ermolyuk et al., 2013). Cultured neurons were placed in a recording chamber mounted on the stage of an Olympus BX51WI upright microscope (Olympus, Tokyo, Japan) equipped with a LUMPlanFL/IR 40 × 0.8 objective coupled to an infrared DIC imaging system.

Electrophysiology

Electrophysiological recordings were carried out using a Multipatch 700B amplifier controlled by the pClamp 10.2 software package (Molecular Devices, Silicon Valley, CA). Recordings were made in a bicarbonate-buffered solution (aCSF) containing (in mM) 126 NaCl, 3 KCl, 2 $MgSO_4$, 2 $CaCl_2$, 26 $NaHCO_3$, 1.25 NaH_2PO_4, 10 D-glucose saturated with 95% O_2 and 5% CO_2 (pH 7.4; 300–310 mOsmol) at 31–33 °C. The recording electrode resistance was 2.5–5 MΩ when filled with the intracellular solution containing (in mM) 126 K-gluconate, 10 HEPES, 4 KCl, 4 $MgCl_2$, 2 BAPTA, 4 Mg-ATP and 0.4 GTP-Na (pH 7.2 with KOH, osmolarity ~290 mOsmol). For the intracellular delivery of microcapsules, the glass electrode tip was back-filled with a suspension of microcapsules supplemented to the intracellular solution. The presence of microcapsules at the pipette tip was confirmed by visualizing their TRITC (FITC) fluorescence (conjugated to the capsule shell) prior to the breaking into whole-cell mode. Once in whole-cell, neurons were monitored for changes in their intrinsic active and passive membrane properties using fast sampling (20 kHz) every 1–3 min, until the baseline had stabilized (40–50 min). The series of sub- and supra-threshold rectangular current pulses (500–1000 ms duration) of the gradually (stepwise) increased stimulus intensity were applied. The steady-state input resistance (R_{input}) was estimated from the measured current–voltage relationship at various time points during the experiment. The maximal firing frequency and the corresponding (minimal) membrane voltage were monitored throughout. Changes in the action potentials (AP) shape were analyzed using the first AP spike responding to a slow-ramp input current (ramp slope 480 pA/s).

Acute skin tissue preparation

Peripheral tissue was taken from the plantar surface of the hind paw of Sprague-Dawley rats (21 to 25-day-old) following animal sacrifice. Tissue sections (300–350 μm thickness)

consisting of skin layers and the tissue beneath were cut using a tissue chopper (McIlwain Model TC752, Mickle Laboratory Engineering Co., Guilford, Surrey, UK). Acute slices were placed in the recording chamber mounted on the stage of an Olympus upright microscope (Olympus) and maintained in HEPES-based physiological buffer.

Imaging of encapsulated drug release

Microcapsules containing Alexa Fluor-488 (similar molecular weight to QX-314) were delivered into acute skin tissue *in situ* with a glass pipette positioned between epidermal and dermal layers. One-photon (confocal) or two-photon (2P) excitation fluorescent imaging was carried out with either a Radiance 2000 (Zeiss-Bio-Rad, Jena, Germany) or a Femto2D (Femtonics, Budapest, Hungary) system optically linked to a Ti:Sapphire Mai-Tai femtosecond pulse laser (SpectraPhysics-Newport, Santa Clara, CA, USA), with various digital zooms, appropriate emission filters, and excitation at λ_{ex}^{2P}=800 nm, as detailed earlier (Zheng et al., 2015; Mishra et al., 2016). The *z*-stacks of fluorescent images were collected every 5–10 min using 512 × 512 pixel frames (typically 30–50 optical sections in 1-μm *z*-steps) for time-lapse monitoring of Alexa Fluor 488 fluorescence upon microcapsule injection (overall, 5–8 h *in situ*). To provide a direct *in situ* comparison of the diffusion escape rates between non-capsulated and encapsulated Alexa Fluor 488, the former was injected between epidermal and dermal layers with another glass pipette near the microcapsules. In a separate set of experiments, microcapsules carrying Alexa Fluor 488 were placed in glycerol (99%) and monitored using a fast-scanning confocal fluorescence microscope (750–1000 lines/sec) in a photon-count mode, as described.

Animals in behavioral studies

The animals used for behavioral studies were 2.5- to 3-month-old male Wistar rats. All animal procedures were approved by the local Animal Ethics Committee (Bogomoletz Institute of Physiology, Kyiv, Ukraine): there were performed in full compliance with the ethical guidelines of the International Association for the Study of Pain and the United States Public Health Service's Policy on Humane Care and Use of Laboratory Animals, as detailed in our previous works (Park et al., 2009b; Kopach et al., 2012, 2016). Animal procedures were fully compliant with the European Commission Directive (86/609/EEC) and the United Kingdom Home Office (Scientific Procedures) Act (1986).

Experimental design of pain models in vivo

To produce unilateral peripheral inflammation and persistent nociceptive hypersensitivity, 50–100 μl of complete Freund's adjuvant (CFA; Sigma Chemicals, St. Louis, IL) suspended in an oil:saline (1:1) emulsion was injected subcutaneously into the plantar side of one hind paw of rats (Kopach et al., 2013; Kopach et al., 2015, 2016). Encapsulated QX-314 was injected as a post-treatment of nociceptive hypersensitivity (after induction of the CFA-induced peripheral inflammation). Different groups of animals received a single-intraplantar injection of microcapsules (carrying QX-314 at various concentrations, or empty capsules) into the inflamed tissue of the hind paw, in a total volume of 50 μl (diluted in saline) at 1 day post-CFA, the time point indicating inflammatory pain maintenance (Kopach et al., 2013, 2016). A control group of the CFA-inflamed animals received a similar injection of non-capsulated QX-314 or 2% lidocaine. In a separate set of experiments, groups of non-inflamed animals (no CFA) received encapsulated QX-314 or empty microcapsules. To produce unilateral acute peripheral hypersensitivity of neurogenic origin, 50 μl of capsaicin (1.5 μg/μl, Sigma Chemicals) was injected intradermally into the plantar side of one hind paw.

Pain assessment

The peripheral thermal pain threshold was measured using the Hargreaves technique, as we described previously (Kopach et al., 2012, 2016). Briefly, after an animal was habituated to a Plexiglas chamber (Biological Research Apparatus, Ugo Basile, Italy), an infrared heat stimulus was applied to the middle of the plantar surface of the hind paw. The heat beam was automatically turned off when the animal lifted its paw. The time between the stimulus onset and the paw withdrawal was automatically recorded: it represented the latency of nociceptive response (thermal pain threshold). Measurements were repeated 3–5 times for each hind paw, the values were averaged.

Open-field test for explorative behavior and anxiety

To assess the sensorimotor function and animal locomotive behavior, an open-field test (open-field arena) was used as detailed previously (Kopach et al., 2016). In brief, animals were placed in an open-field arena (a 75 × 75 × 40 cm wooden box with a digital camera attached above) and allowed to move freely over a predefined time period (10 min). Recordings were analyzed with MATLAB software using in-house scripts. The following parameters were monitored and recorded to assess locomotion: the total distance traveled by an animal, the maximal speed, and the acceleration. The anxiety level was assessed by computing the ratio between the fractions of time spent in the arena center versus corners.

Immunohistology

The localization of microcapsules injected *in vivo* was examined with *post hoc* immunohistology of the glabrous skin samples collected from the hind paw at different time points post-injection. The dissected glabrous skin tissue (~1 cm) was fixed in 3% PFA (1–2 days at 4 °C). After fixation, samples were replaced into PBS containing 0.02% sodium azide and underwent a cryo-protection treatment (10% sucrose for 2 h, then 20% for 2 h, followed by 30% for overnight). Tissue was mounted in OCT and stored at −80 °C until processed for cryo-sectioning. The transverse

tissue sections (30–60 μm thick) were cut and collected as an ordered series. Floating tissue sections were rinsed with PBS at least 3 times/5' each section and blocked with 1% BSA, 5% Donkey serum in 0.2% Triton X-100 PBS for 4 h. The primary antibodies were mouse anti-PGP9.5, neuron cytoplasmic protein 9.5 (1:500; Merck Millipore U.K, Feltham, UK). After incubation with primary antibodies (2 days at 4 °C), tissue sections were incubated with the secondary antibodies (overnight at 4 °C). Secondary antibodies were Alexa Fluor 488 from the same host (1:200 or 1:400; Invitrogen, Paisley, UK). The following-day sections were washed, unrolled and mounted on glass slides using Vectashield H-1400 (Vector

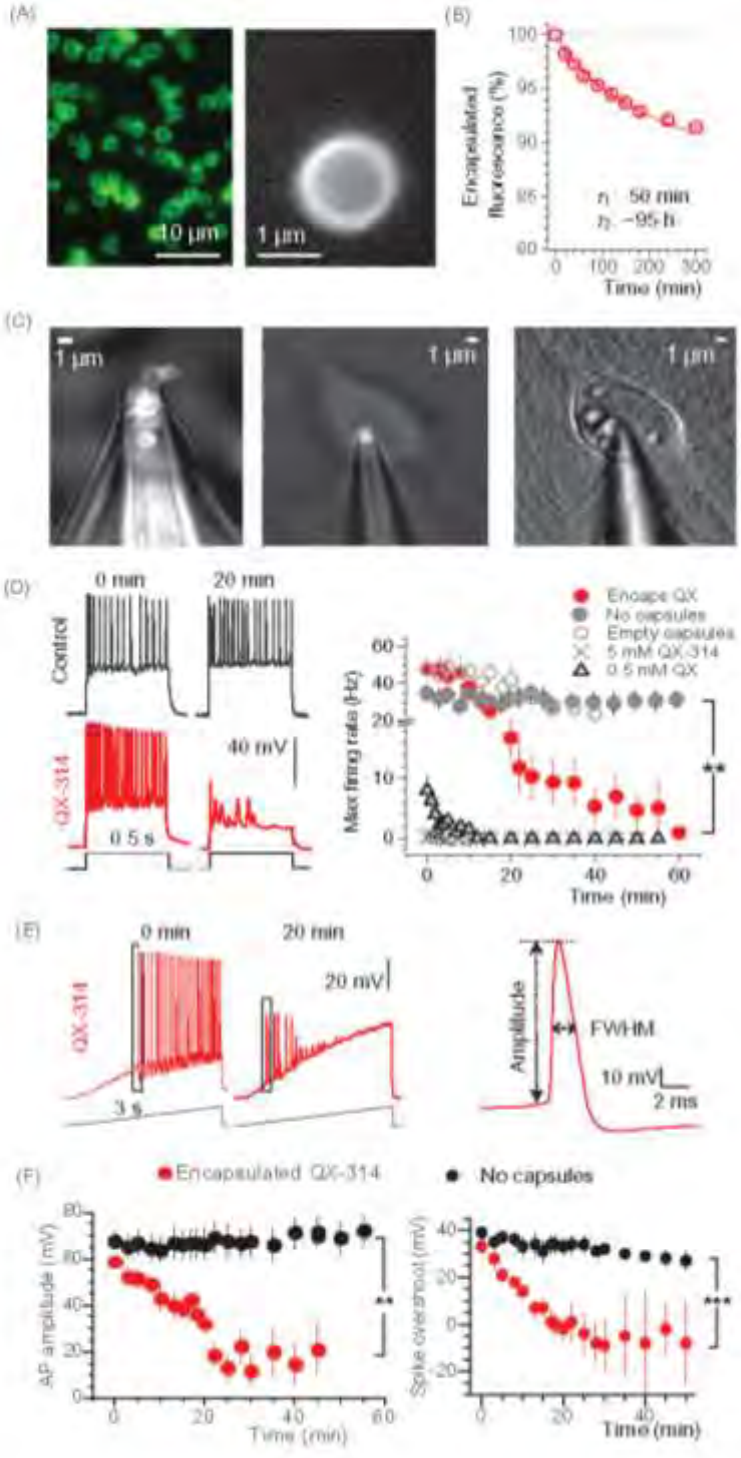

Labs, Burlingame, CA, USA). Tissue sections were scanned for both PGP9.5-positive structures and microcapsules using a Radiance 2000 imaging system (Zeiss-Bio-Rad) or Femto2D (Femtonics) imaging system using various digital zooms.

Microcapsule biodegradability assay

Tissue samples were collected at various time points post-injection (at 1, 5, and 10 weeks), fixed and processed for immunohistology (see above). Special care was taken to make sure that the microcapsule injection parameters (microcapsule concentration in suspension, pressure pulse, etc.) were uniform across the tested samples. To gauge the spatial distribution of microcapsules across the peripheral tissue, we scanned the entire tissue volume (transverse tissue sections cut and collected in a serial order) containing all detectable capsules in a *z*-stack of individual focal *x*–*y* planes (3-μm *z*-step, total scanned volume of ~370 μm^3) using a Femto2D (Femtonics) imaging system. The fluorescence distributed in the *z*-direction thus reported the amount of fluorescently labeled capsules in the tissue volume.

Statistics

Unless indicated otherwise, summary data are presented as mean ± SEM (standard error of the mean) with *n* referring to the number of cells (*in vitro* experiments) or animals (*in vivo* experiments) in the group. Student's *t*-test (two-tailed unpaired) was used to determine statistical difference between experimental groups. The statistical difference between groups of experimental animals was analyzed by one-way or two-way analysis of variance (ANOVA) followed by Bonferroni *post hoc* test or Fisher's test where appropriate. A *p* value of $<.05$ was considered as statistically significant for either test.

Results

Encapsulated QX-314 can gradually suppress neuronal excitability in vitro

We fabricated polymeric LbL microcapsules and encapsulated the membrane-impermeable Na^+-channels blocker QX-314 within the penultimate shell layer (4–10 pg/capsule; Figure 1(A)). The latter was to enable controllable shell permeability for the encapsulated compound. After initial trials, the capsule shell composition was adjusted to provide a cargo release rate of 4–5%/h (decay constant ~20 h), which was gauged by monitoring the escape of encapsulated fluorescent dye (Alexa Fluor 488, a similar molecular weight to QX-314, Figure 1(B)).

To examine how the encapsulated QX-314 suppresses neuronal excitability, we delivered the microcapsules inside individual hippocampal neurons (primary culture) using a patch pipette in whole-cell configuration (Figure 1(C)). Thus, we monitored cell excitability in real time starting shortly upon microcapsule injection, and compared test groups with control (i.e. cells injected with empty microcapsules, or no capsules, Figure 1(D–F)). We found a gradual suppression of neuronal excitability, which progressed within 15–20 min after injecting encapsulated QX-314, leading to a sharp drop in the maximum firing rate ($n = 18$ cells, $p < .01$ compared with either empty microcapsules, $n = 12$, or no capsules, $n = 17$; Figure 1(D)). In parallel, encapsulated QX reduced the spike amplitude and the spike overshoot (amplitude above 0 mV; $n = 9$, $p < .001$ compared to that with no capsules, $n = 9$; Figure 1(E,F)).

We also confirmed that the cell input resistance remained stable over time and was not affected by the injection of empty capsules (Figure 2(A,B)). However, it gradually increased following injection of encapsulated QX-314, reflecting major ion channel blockade ($n = 14$, difference at $p < .05$ with the empty-microcapsule group, $n = 15$, or no-capsules group, $n = 14$; Figure 2(C,D)). In contrast, adding QX-314 directly to the intracellular solution (0.5 mM, and especially 5 mM, a commonly used concentration in whole-cell) suppressed spike generation almost immediately (Figure 2(E,F)). To replicate the slow progression of excitability blockade under encapsulated QX-314, intracellular concentration of non-encapsulated QX-314 had to be reduced at least 10^3–10^4-fold (to ~500 nM; Figure 2(F)).

Microcapsule cargo release rate in skin tissue in situ

Because our ultimate goal was to test the pain-relieving effects of encapsulated QX-314, we first sought to establish the microcapsule cargo release properties in peripheral skin tissue *in situ*. To achieve this, we employed an acute skin tissue preparation from glabrous skin of the rat hind paw. Microcapsules with encapsulated Alexa Fluor 488 were delivered through a micropipette between epidermal and dermal layers and monitored using two-photon excitation (2PE)

Figure 1. Encapsulated QX-314 delivered intracellularly gradually suppresses neuronal excitability *in vitro*. (A) A snapshot showing the suspension of nano-engineered microcapsules (magnified on the right), with encapsulated Alexa Fluor 488; confocal imaging ($\lambda_{ex} = 488$ nm). (B) Monitoring gradual release of encapsulated Alexa Fluor 488 from microcapsules; ordinate, time course of average capsule fluorescence normalized to the initial value; solid line, best-fit bi-exponential approximation (with 0.04 and 0.96 partial weights, respectively; decay constants as shown; $n = 1.6 \times 10^5$ microcapsules). (C) Snapshots displaying the patch pipette tip filled with microcapsules (TRITC fluorescence) prior to patching (left), when targeting a cultured neuron (middle), and in whole-cell configuration, 25 min following intracellular delivery of microcapsules (right; DIC + fluorescence images of the same cell). (D) Traces, examples of current-clamp recordings of neuronal firing in control condition and after injection of encapsulated QX-314 (immediately after breaking-in and 20 min later, as indicated). Graph, statistical summary: time course of the maximal neuronal firing rate in control cells (no microcapsules; $n = 17$), with empty microcapsules injected ($n = 12$), encapsulated QX-314 injected ($n = 18$), with non-capsulated QX-314 injected at 0.5 mM ($n = 6$) and 5 mM ($n = 4$), as indicated. (E) Left, examples of neuronal firing in response to a slow-ramp current after infusion of encapsulated QX-314 (left, 0 and 20 min post-injection in the same cell; dotted boxes indicate first spikes selected for comparisons); right, example of single AP evoked in hippocampal neurons, with the estimated parameters indicated (FWHM, full width at half maximum). (F) Time course of the relative spike amplitude (left) and the spike overshoot (amplitude above 0 mV; right) in control condition (no capsules, black dots) and after intracellular delivery of encapsulated QX-314 (red dots), as indicated; spike sampling as shown in panel E (left); control, $n = 9$ neurons, encapsulated QX-314, $n = 9$ neurons. All data are shown as mean ± SEM. $^{**}p < .01$, $^{***}p < .001$ (unpaired *t*-test).

fluorescence microscopy (Figure 3(A)). Microcapsules showed a release rate constant of ~14 h (slow component), as evaluated by the time-lapse fluorescence emission monitoring of the encapsulated Alexa Fluor 488 *in situ* (Figure 3(B)). In contrast, Alexa Fluor 488 in a free solution injected nearby, directly into the tissue via a micropipette, was escaping at a rate of ~4.12 s (slow component; Figure 3(C)), i.e. ~10^4 times faster. In addition, we used photon counting (within ~1 µm focal plane), in line with procedures detailed earlier (Zheng et al., 2015), to document a build-up of the diffuse fluorescence profile in the vicinity of individual microcapsules (Figure 3(D)). Within ~7 h post-injection *in situ*, this profile was consistent with the slow cargo diffusion escape from the microcapsules reported above (Figure 3(E)).

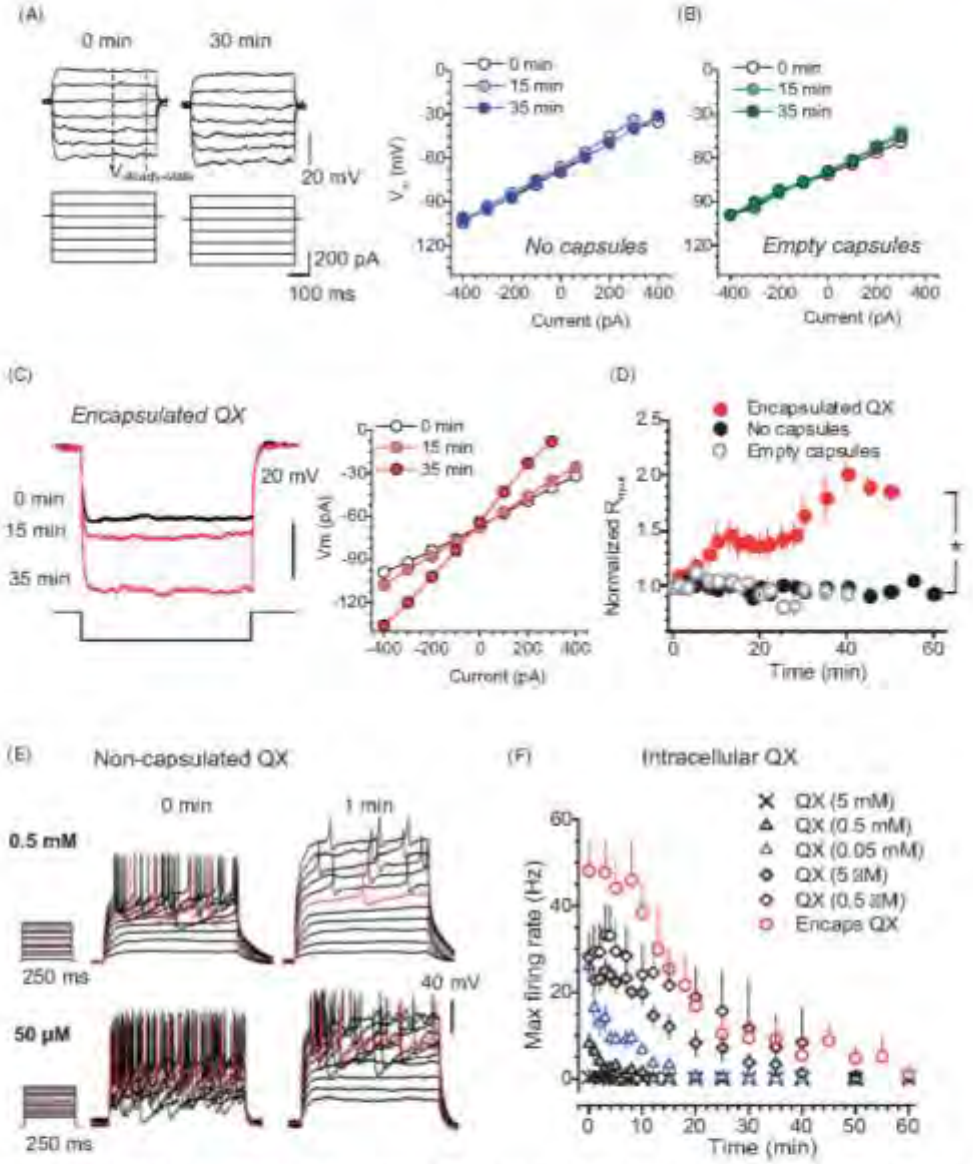

Figure 2. Encapsulated QX-314 gradually increases cell input resistance of neurons while reducing their firing rate in a dose-dependent manner. (A) Traces, examples of the membrane potential response (top) to current step pulses (bottom) in the same neuron (control condition, no microcapsules) at two time points, as indicated. Dashed lines, time window (stable response) where the input resistance was estimated. Graph, examples of the current-voltage relationship at three time points, as indicated, in control conditions. (B) Examples of the current-voltage relationship at three time points, as indicated, after the injection of empty microcapsules. (C) Traces, examples of the membrane potential response (top) to a current injection (bottom) at three time points after intracellular delivery of encapsulated QX-314, as indicated. Graph, examples of the current-voltage relationship at three time points, as indicated, for the same cell. (D) Time course of the cell input resistance in control ($n = 14$ neurons), post-infusion of empty microcapsules ($n = 15$) or encapsulated QX-314 ($n = 14$), as indicated. (E) Traces, representative recordings of neuronal firing after whole-cell dialysis with different concentrations of QX-314, at two time points, as indicated. (F) Time course of the maximum cell firing rate for different concentrations of free QX-314, compared with encapsulated QX-314, added to the intracellular medium, as indicated. Data are mean ± SEM. $^*p < .05$ (unpaired *t*-test).

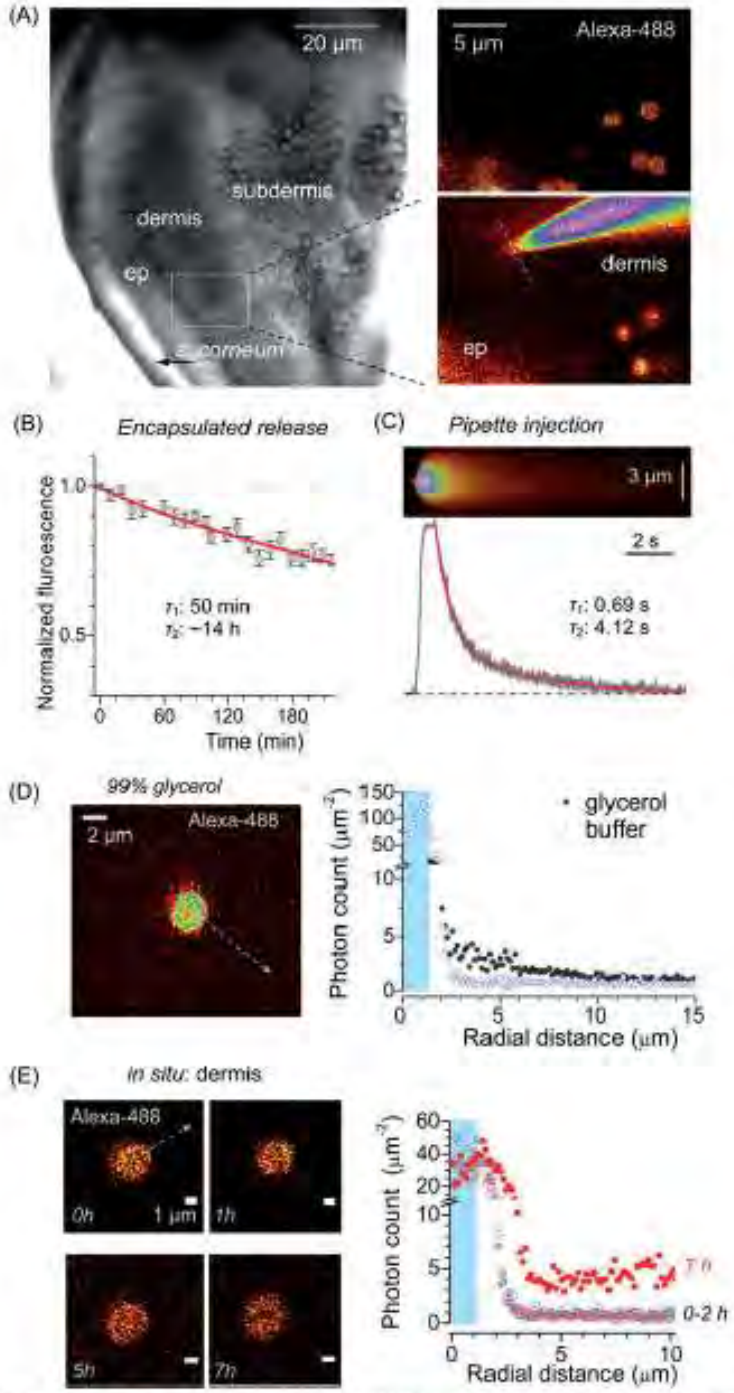

Figure 3. Long-lasting release of encapsulated cargo inside glabrous skin *in situ*. (A) Left image, acute skin tissue preparation from plantar surface of the rat hind paw (DIC image) depicting region of interest (ROI, dotted rectangle). Right images, ROI enlarged and shown in fluorescence channel ($\lambda_x^{2P} = 800$ nm), depicting injected microcapsules (top, encapsulated Alexa Fluor 488), and the subsequently positioned micropipette tip filled with free Alexa Fluor 488 (bottom); dotted line: line-scan position. (B) Concentration kinetics of encapsulated Alexa Fluor 488 release from microcapsules *in situ* (mean ± SEM, $n = 10$); red line, best fit bi-exponential approximation (τ_1, τ_2: decay constants, 0.04 and 0.96 partial weights partial weights, respectively). (C) Image, example of line-scan (position in A, right bottom image; $\lambda_x^{2P} = 800$ nm) depicting the escape of non-capsulated Alexa Fluor 488 injected from the micropipette. Graph, concentration kinetics of free Alexa Fluor 488 injected from the micropipette (0.75 s pressure pulse) *in situ*; red line, best fit bi-exponential approximation (τ_1, τ_2: decay constants, 0.08 and 0.92 partial weights, respectively). (D) Image, experimental arrangement for photon-counting of spatial Alexa Fluor 488 fluorescence escape a single microcapsule shown in 99% glycerol (arrow, depiction of the radial profile calculation). Graph, radial profiles of Alexa Fluor 488 generated photon counts in two experimental conditions, as indicated (shaded area: capsule radius). (E) Image, example of a microcapsule in the epidermal–dermal area at different time-points (0–7 h, as indicated) following injection into acute skin tissue *in situ* (arrow, depiction of the radial profile calculation). Graph, radial profiles of Alexa Fluor 488 generated photon counts in the epidermal–dermal area, at different time points after injection, as indicated (shaded area: capsule radius).

Encapsulated QX-314 provides long-lasting pain relief in vivo

To explore therapeutic potential of encapsulated QX-314, we turned to a well-established experimental paradigm of the CFA-induced unilateral persistent peripheral inflammation (Park et al., 2009b; Kopach et al., 2012, 2016). Following the intraplantar injection of CFA, animals displayed robust thermal hypersensitivity on the ipsilateral (but not contralateral) side, as evaluated by measuring the thermal pain threshold (see 'Materials and methods' section). If left untreated, the hypersensitivity persisted for at least 11 days (Figure 4(A)), and a single focal subcutaneous injection of the common analgesic lidocaine had no long-lasting effect (Supplementary Figure S1).

The CFA-inflamed animals were quasi-randomly sampled to receive a single injection of either encapsulated QX-314 or empty microcapsules into the sites of inflammation at 1 day post-CFA. Animals that received encapsulated QX-314 showed substantially alleviated hypersensitivity, with a progressive recovery of the thermal pain threshold back to the pre-inflammatory level by the next day ($n = 6$ rats, $p < .01$ compared with the CFA-inflamed group injected either empty microcapsules, $n = 5$, or no capsules, $n = 27$; Figure 4(A,B)). Injecting empty capsules had no detectable effect ($n = 6$ rats, Figure 4(A) and Supplementary Figure S1(A)) whereas a single-focal injection of 100 mM non-encapsulated QX-314 had only a brief and marginal relief of the thermal nociceptive hypersensitivity ($n = 5$ rats, $p < .05$ compared with no treatment at 2 days post-CFA; Figure 4(A)). We could routinely confirm with *post hoc* immunohistology that microcapsules were scattered within the epidermal–dermal area as targeted (Figure 4(C)). Importantly, the therapeutic effect of encapsulated QX-314 remained significant for at least 12 days ($p < .01$ between the CFA-inflamed group injected with 3 mM encapsulated QX and that with empty microcapsules, over the experiment duration; Figure 4(A)) and its time course depended on the concentration of encapsulated QX-314 (Figure 4(B); $p < .001$ between the effects of 7.5 mM encapsulated QX-314, $n = 7$ rats, and empty microcapsules, over 11 days post-CFA; but no difference between 0.01 mM encapsulated QX-314, $n = 5$ and empty microcapsules over the 7–11-day period). Separate experiments showed how the effect depended on the amount of QX-314 encapsulated per capsule (lasting over 12 days post-CFA for microcapsules containing 10 pg of encapsulated QX-314: $n = 8$ rats, $p < .01$ compared with empty microcapsules, but up to 7 days for 4.5 pg of encapsulated QX-314, $n = 5$ rats; Figure 4(D)) and on the capsule size (Figure 4(E); $n = 6$ rats, $p < .01$ for 2 μm microcapsules containing 3 mM of encapsulated QX-314 and $n = 5$ rats, $p < .05$ for 1 μm microcapsules compared with empty ones over the time of experiment).

Control experiments confirmed that in healthy animals (no induced inflammation or pain), neither empty microcapsules (Supplementary Figure 2(A)) nor encapsulated QX-314 (Supplementary Figure 2(B)) affected the peripheral thermal sensitivity, thus ruling out the concomitant effects of microcapsules *per se*. There were no acute (within hours) or delayed (days) effects on thermal sensitivity of the ipsilateral hind paw following intraplantar injection of microcapsules as compared with the contralateral hind paw (no capsules) or with the zero time-point (before injection; Supplementary Figure S2).

Encapsulated QX-314 rescues locomotive deficit and animal anxiety produced by peripheral inflammation

We next examined whether the anti-nociceptive effect of encapsulated QX-314 influences the locomotor deficit and the heightened anxiety, which is often associated with painful states (Kopach et al., 2016). We thus implemented an open-field test, a well-established assay for an integrative analysis of animal behavior, including anxiety (Figure 5(A)). The group of animals with the CFA-induced inflammatory pain showed a dramatic reduction in the traveled distance ($n = 5$ rats, $p < .01$ for each recorded post-CFA time point compared with zero time-point; Figure 5(B)) that persisted for at least 10 days after CFA injection. An integrative analysis of animal behavior demonstrated that encapsulated QX-314 progressively rescued the impaired locomotion in inflamed animals within 2–4 days post-treatment ($n = 5$ rats, $p < .05$ compared with empty microcapsules; Figure 5(B)), in a dose-dependent manner (Figure 5(C)). This was consistent with the improved speed (Figure 5(D)) and acceleration (Supplementary Figure 3(A)). The effect was paralleled by a decline in the anxiety-like behavior, which was monitored as the proportion of time spent near the arena center, as opposed to corners (Figure 5(E)).

Anti-nociceptive effect of encapsulated QX-314 involves TRPV1 receptors

Because QX-314 acts on Na^+ channels from the intracellular side, it has to be transported into nerve fibers once released inside the tissue. The key established mechanism of this permeation involves TRP-dependent receptors TRPV1 (Binshtok et al., 2007; Peters et al., 2014) and TRPA1 (Roberson et al., 2011; Brenneis et al., 2014), although the Toll-like receptor-5 could also contribute (Xu et al., 2015). First, we confirmed that the injected microcapsules rest near the peripheral nerve fibers (identified with neuron-specific PGP9.5 staining) innervating skin tissue layers (Figure 6(A)). To determine whether the QX-314 action involves the TRP-mediated pathway, we next used a model of neurogenic pain induced by capsaicin, a prototypic TRPV1 agonist (Frias & Merighi, 2016).

Capsaicin (1.5 μg/μl) produced thermal hyperalgesia within a minute ($n = 6$ rats, $p < .01$), with an immediate adverse reaction of the animal (licking, shaking the injected hind paw); the thermal hypersensitivity lasted up to 2–3 h, reversing back to control values (Figure 6(B)). QX-314 (7.4 mM, non-capsulated) co-injected with capsaicin rapidly produced anesthesia, which gradually developed into analgesia to a heat stimulus within 3–5 h post-injection ($n = 6$ rats, $p < .05$ compared with capsaicin at the corresponding time-points), fully consistent with previous observations (Binshtok et al., 2007). The anti-nociceptive effect of QX-314 remained for several days ($n = 6$ rats, $p < .05$ compared with

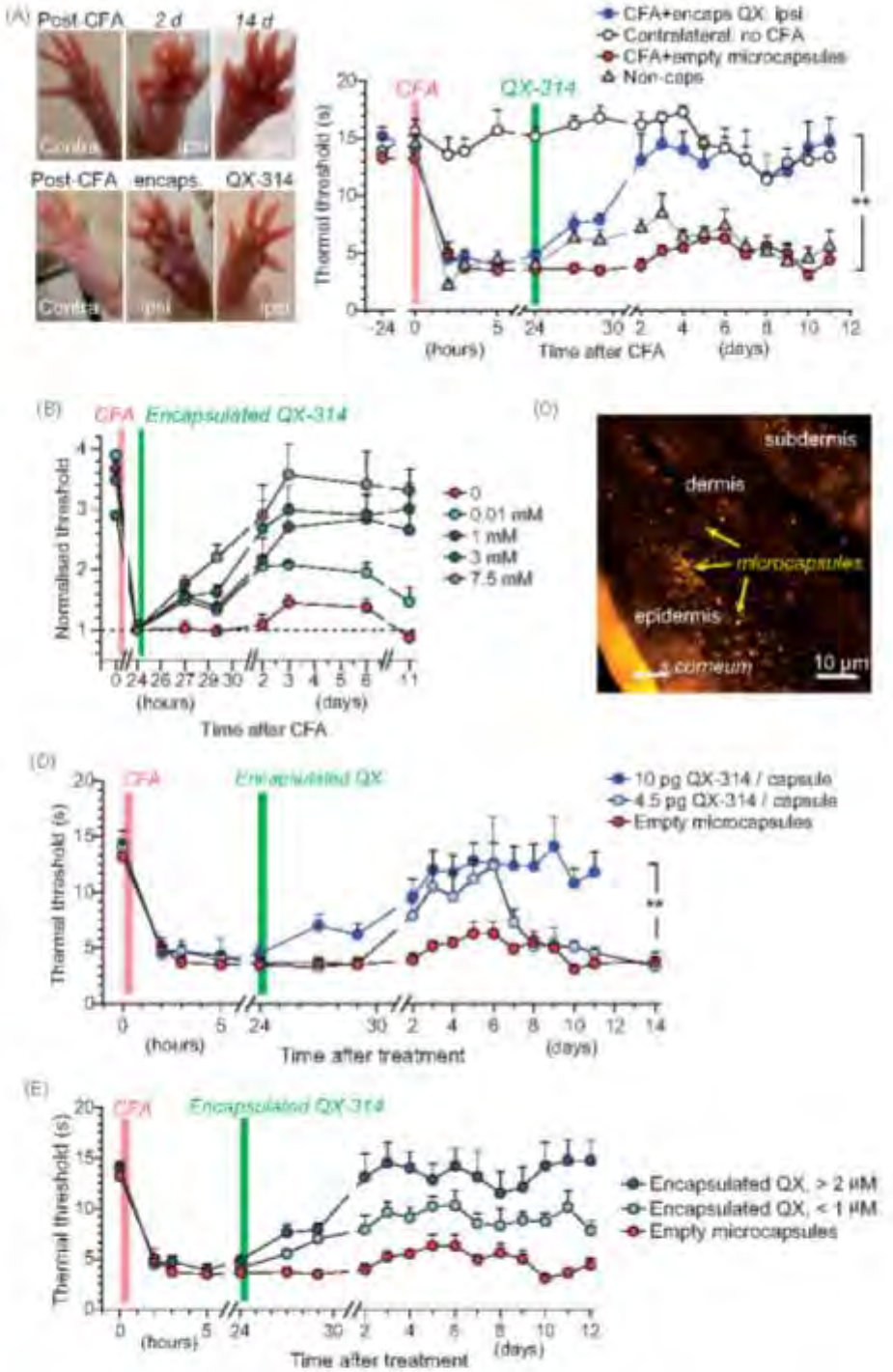

Figure 4. The anti-nociceptive effect of encapsulated QX-314 in a persistent pain model in rodents. (A) Image panels, examples of rat hind paw following injection of CFA with no treatment (top row) and with encapsulated QX-314 (~3 mM; bottom row) at different time points, as indicated; ipsi, ipsilateral, inflammatory side; contra: contralateral, non-inflamed, side. Graph, time course of the thermal nociceptive threshold in control (contralateral, $n = 5$ rats) and CFA-inflamed animals injected with empty microcapsules ($n = 5$) or encapsulated QX-314 (~3 mM, $n = 6$) or non-capsulated QX-314 (100 mM, $n = 5$), as indicated. (B) Time course of the thermal nociceptive threshold (normalized to that at the treatment onset, which is 24 h post-CFA), for different dosage of encapsulated QX-314, as indicated: 10 µM ($n = 6$ rats), 1 mM ($n = 8$), 3 mM ($n = 6$), and 7.5 mM ($n = 7$). (C) Fluorescent image (FITC fluorescence, transverse skin tissue section) displaying the epidermal–dermal area (the rat hind paw) with scattered microcapsules on Day 1 after microcapsule injection. (D) Time course of inflammatory hypersensitivity in rats with persistent peripheral inflammation following treatment with different amounts of QX-314 per capsule, as indicated (animals received the same overall dose of QX-314, 1 mM): 4.5 pg ($n = 6$ rats), 10 pg ($n = 8$) and 0 pg (empty, $n = 5$). (E) Time course of inflammatory hypersensitivity with QX-314 in microcapsules of different sizes (animals received the same overall dose of encapsulated QX-314, 3 mM): 2 µm diameter ($n = 6$ rats), 1 µm ($n = 9$) and empty (varied size, $n = 5$). Data are shown as mean ± SEM. **$p < .01$ (one-way ANOVA with Bonferroni *post hoc* test for encapsulated QX-314 compared with empty microcapsules).

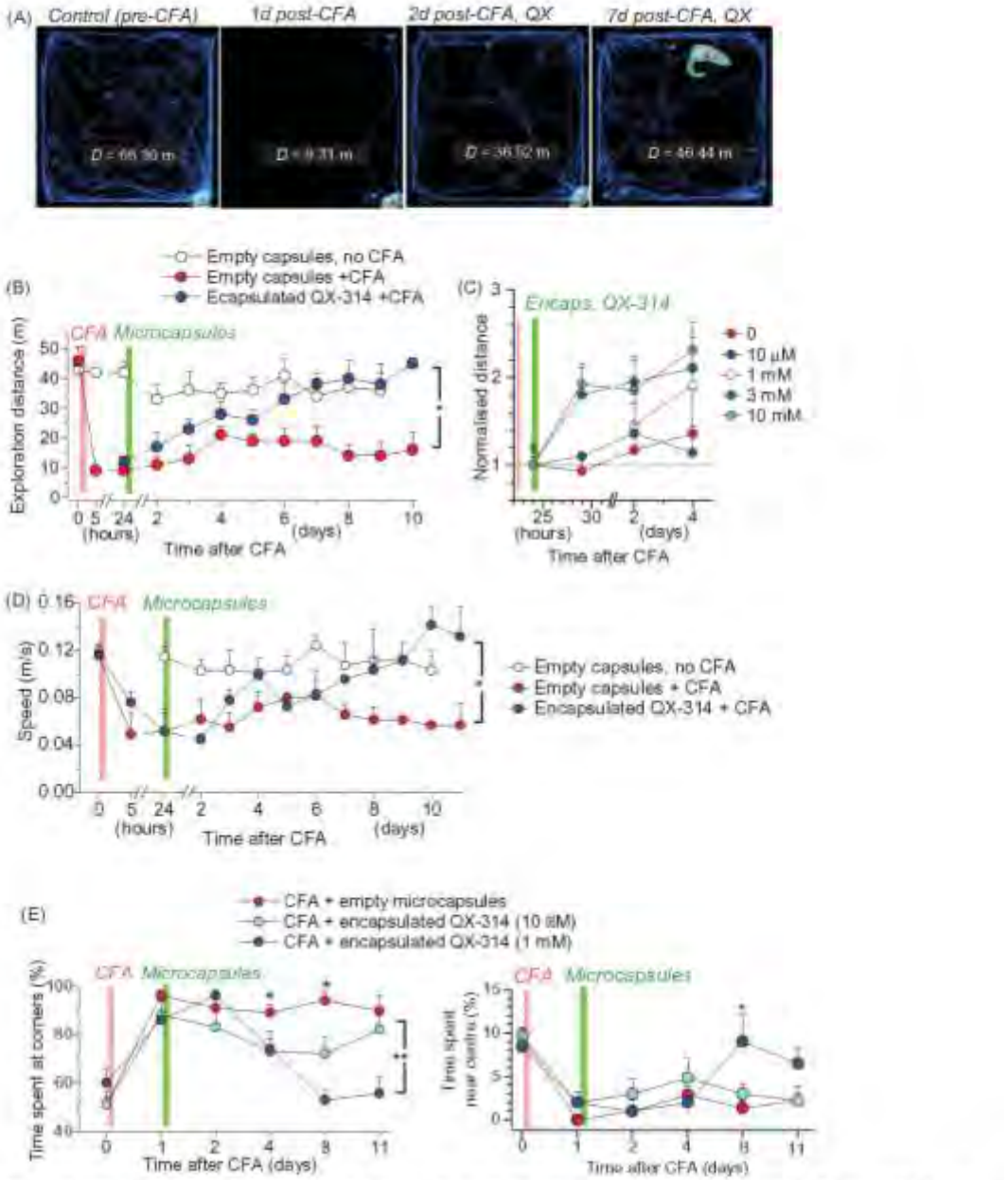

Figure 5. Encapsulated QX-314 abolishes locomotive deficit and anxiety in animals with persistent peripheral inflammation. (A) Examples of the open-field test trajectory records taken from one animal at different time-points following CFA injection and treatment with encapsulated QX-314 (1 mM, 1 day post-CFA), as indicated; *D*, overall distance (m) traveled over 10.0 min. (B) The effect of encapsulated QX-314 on animal locomotion: time course of the average exploration distance traveled by CFA-inflamed animals injected with encapsulated QX-314 (1 mM) or empty microcapsules, and by healthy animals (no CFA) injected with empty microcapsules. (C) The dose-effect of encapsulated QX-314 on exploratory activity in CFA-inflamed animals: time course of the average distance (normalized by that 1 day post-CFA) traveled by CFA-inflamed rats; treatment with empty capsules ($n = 5$ rats), 10 µM encapsulated QX-314 ($n = 5$), 1 mM encapsulated QX-314 ($n = 5$), 3 mM encapsulated QX-314 ($n = 9$), 10 mM encapsulated QX-314 ($n = 6$), as indicated. (D) The effect of encapsulated QX-314 on the average speed that animals could develop following treatment; notations as in (B). (E) The effect of encapsulated QX-314 on the animal's anxiety, estimated as the average fraction (%) of time spent in the arena corners (correlative anxiety indicator; left) versus the arena center (anti-correlative anxiety indicator; right). Treatment with empty capsules ($n = 5$ rats), 10 µM encapsulated QX-314 ($n = 5$), 1 mM encapsulated QX-314 ($n = 5$). Data are shown as mean ± SEM. *$p < .05$, **$p < .01$ (one-way ANOVA with Bonferroni *post hoc* test).

capsaicin at 1–5 days post-injection; Figure 6(B)). In contrast to the complex cellular signaling mechanisms mediating the CFA-induced persistent inflammatory pain, the capsaicin-induced neurogenic pain should specifically involve TRPV1 activation at primary nociceptor afferents. Therefore, the most parsimonious explanation of the prolonged analgesic effect observed in this study is that QX-314, once injected subcutaneously, gets into the primary nociceptors through the activated TRPV1 receptors and retained inside nerve fibers.

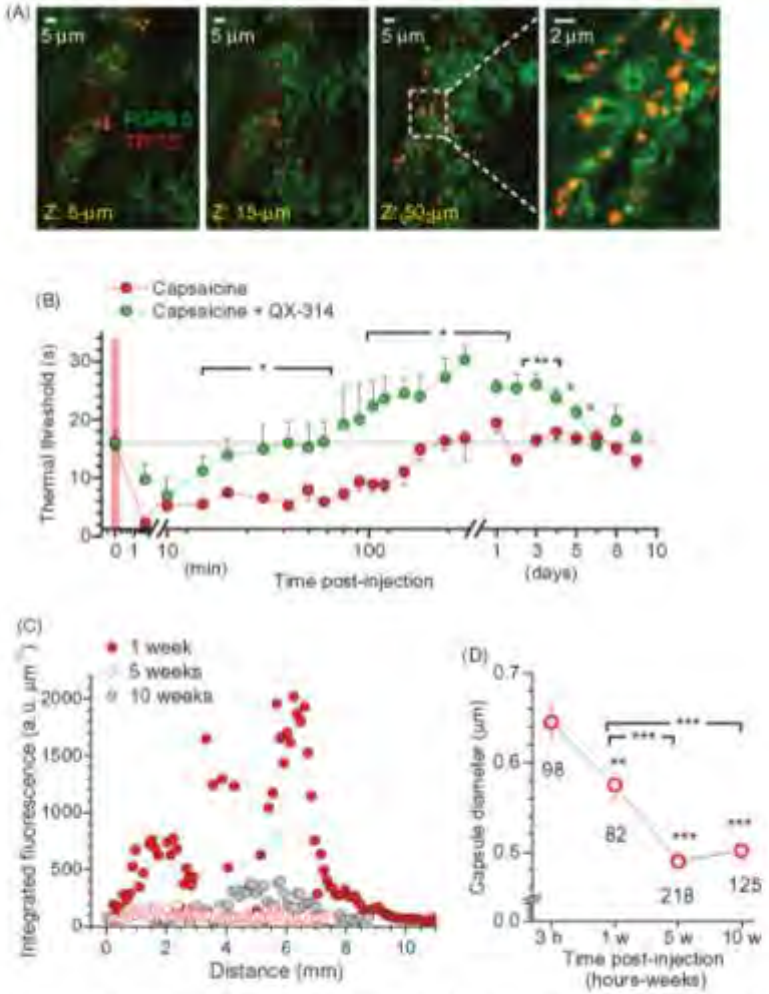

Figure 6. Microcapsules co-localize with peripheral nerve fibers, engage TRPV1-mediated analgesic effect of QX-314, and degrade with a time. (A) Examples of immunohistology of glabrous skin tissue (individual focal planes shown) for microcapsules carrying encapsulated QX-314 (3 mM; TRITC fluorescence, red) surrounding peripheral nerve fibers (neuron-specific PGP9.5 staining, green). Transverse skin sections (30 µm thick). (B) Time course of the thermal pain threshold in animals injected with capsaicin (1.5 µg µl^{-1}, $n = 6$ rats) or with capsaicin together with 3.4 mM QX-314 (non-capsulated, $n = 6$). Data are mean ± SEM. *$p < .05$, **$p < .01$ (one-way ANOVA with Bonferroni *post hoc* test). (C) The *z*-axis profile of the microcapsule fluorescence (TRITC, $\lambda_{ex}^{TF} = 820$ nm; 3 mM encapsulated QX-314, integrated fluorescence) inside the skin tissue from the rat hind paw at different times post-injection *in vivo*, as indicated. Total scanned volume ~370 µm^3; 3 µm *z*-steps. (D) Averaged diameter of microcapsules inside the skin tissue from the rat hind paw at different time points post-injection *in vivo*, as indicated. The reduced diameter reflects progressive degradation of the outer capsule shell. Total number of analyzed capsules is indicated; **$p < .01$, ***$p < .001$ (one-way ANOVA with Fisher's test).

Microcapsules undergo progressive biodegradation post-injection in vivo

The progressive and nontoxic biodegradation of the fabricated microcapsules is important for their safe biomedical use. The capsules of a similar design and polymer composition have already been validated for biodegradability and decomposition in human cell lines (De Cock et al., 2010; Pavlov et al., 2011; Gao et al., 2016). The constituent nanomaterials have also been tested for their low-toxicity biodegradation *in vivo* (Park et al., 2009a; Chiappini et al., 2015). To confirm the satisfactory biodegradation of microcapsules used here, a *post hoc* immunohistology was carried out in tissue samples collected at different time-points after injecting microcapsules *in vivo*.

We assembled the integrated microcapsule fluorescence distributed in the *z*-direction to gauge the amount of fluorescently labeled capsules in the tissue volume (total scanned volume of ~370 µm^3). Five weeks or later post-injection, this distribution was reduced dramatically (Figure 6(C); there was no detectable photo-bleaching of TRITC in individual remaining capsules at these time-points). In parallel, we monitored the average diameter of the remaining microcapsules (those with a distinguishable shape). As biodegradation of the multiple layers comprising the capsule shell is expected to start from the outer layer, it should gradually reduce the visible capsule size—this we precisely observed ($p < .01$ or $p < .001$ compared with the initial time-point, 3 h post-injection; Figure 6(D)) as a confirmation of robust enzymatic

decomposition of the microcapsule shell material within live tissue over a time post-injection.

Discussion

Improving the treatment of persistent pain is amongst the most challenging tasks in clinical practice today, directly affecting the lives of millions. Systemic administration of established painkillers over a prolonged period of time tends to have serious side effects and is therefore considered sub-optimal. When the peripheral source of pain can be localized, the existing methods of local anesthesia rely either on a direct repetitive drug injection or on the permanent drug-administering devices. Both methods have serious limitations pertinent to the patient's discomfort, the costs involved, and a possible systemic escape of the drug.

The present study was prompted by the recent breakthroughs in the nano-engineering LbL technology, which enables micro-encapsulation and subsequent controllable release for the medicine of choice. A wide variety of substances have successfully been used as a payload for encapsulation (De Cock et al., 2010). The capsule size could be adjusted between 0.3 μm and >10 μm (determined by their template), whilst the surface functionality is provided by the outer layers. Crucially, the capsule shell permeability can be made sensitive to environmental variations (pH, temperature, osmolarity) (Delcea et al., 2011) or a remote physical stimulus (light, magnetic field, ultrasound) (Antipina & Sukhorukov, 2011), which is achieved through the incorporation of sensitive elements into the multilayer capsule wall (Munoz Javier et al., 2008; Pavlov et al., 2011, 2013; Gao et al., 2016). The LbL microcapsules normally show no toxicity or appreciable inflammation effects (Pavlov et al., 2011) and in most cases they are fabricated using standard biodegradable components (e.g. hyaluronic acid, dextran derivatives and other polysaccharides, gelatin and other peptides) approved by the FDA and equivalent European regulatory authorities for use in humans (Zhang et al., 2013). They therefore generally meet the requirements for a safe drug delivery platform suitable for use in humans.

In parallel, there has been a growing interest in the Na^+-channel blocker QX-314, which appears to be more potent and longer-lasting in its analgesic effects in mammals, compared to the more traditional painkillers (Lim et al., 2007; Roberson et al., 2011; Zhao et al., 2014). It is also routinely used in experimental neurophysiology research for dampening neuronal excitability. Although QX-314 is a membrane-impermeable compound which blocks Na^+ channels from the cytoplasm side, studies *in situ* have established that it enters nerve cells through the TRP receptors subtypes TRPV1 and TRPA1 (Binshtok et al., 2007; Leffler et al., 2011; Stueber et al., 2016) and possibly also through a TRP-independent mechanism (Brenneis et al., 2014; Hofmann et al., 2014).

Our research strategy sought to combine these two recent lines of enquiry, aiming to test it in a case study in rats whether encapsulated QX-314 could improve peripheral pain treatment compared to more traditional approaches. This strategy achieved several objectives. Firstly, we nano-engineered encapsulated QX-314, injected the microcapsules into individual nerve cells (in culture) and documented gradual suppression of excitability in individual neurons under whole-cell electrophysiological control. Secondly, we evaluated and adjusted the microcapsule properties in the target tissue areas *in situ* to ensure relatively slow, long-term local release of the encapsulated cargo. Thirdly, and perhaps most importantly, we found that a single local injection of encapsulated QX-314 had a robust anti-nociceptive effect in an animal model of persistent inflammatory pain *in vivo*. The effect, which lasted for more than 1 week, was documented using the semi-automated measurements of the pain threshold and camera-traced quantification of the animal locomotion and explorative behavior. The results were gauged against the groups of inflamed animals which received a single injection of either empty microcapsules or non-encapsulated QX-314, and also the control groups of non-inflamed animals or those with an injection of empty microcapsules. Finally, we established that, consistent with the previous observations, the prevalent cellular mechanism enabling intracellular QX-314 action is likely to involve TRPV1 receptors and that the microcapsules undergo robust biodegradation from Week 5 post-injection onwards.

Clearly, although the LbL microcapsules are proving themselves as a highly flexible method of drug encapsulation and delivery, the injection method described here provides relatively limited control over their precise positioning, dosage, and spread in the target tissue. Remote control of microcapsule movement inside tissue could further improve the coordinate precision of drug delivery. Another promising objective for the future development is to equip the surface of microcapsules with physicochemical properties that would help to recognize target tissue or cells. In terms of practical application, further tests are needed to establish the stability and the storage requirements for the microencapsulated medicine, including the costs involved. Nonetheless, the present results suggest that LbL microcapsules represent a promising approach to provide long-lasting, efficient and controllable focal delivery of anti-nociceptive drugs, with limited side effects on the systemic level.

Acknowledgements

The authors thank Prof. Martin Koltzenburg and Dr. Mona AlQatary for valuable comments and technical guidance.

Disclosure statement

No potential conflict of interest was reported by the authors.

Funding

This work was supported by the Wellcome Trust Principal Fellowship [101896], European Research Council Advanced Grant [323113 NETSIGNAL], Russian Science Foundation Grant [15-14-30000, computing cluster setup], FP7 ITN [606950 EXTRABRAIN] and European Research Council Proof-of-Concept Grant [767372 NEUROCLOUD].

References

Antipina MN, Sukhorukov GB. (2011). Remote control over guidance and release properties of composite polyelectrolyte based capsules. Adv Drug Deliv Rev 63:716–29.

Binshtok AM, Bean BP, Woolf CJ. (2007). Inhibition of nociceptors by TRPV1-mediated entry of impermeant sodium channel blockers. Nature 449:607–10.

Brenneis C, Kistner K, Puopolo M, et al. (2014). Bupivacaine-induced cellular entry of QX-314 and its contribution to differential nerve block. Br J Pharmacol 171:438–51.

Chiappini C, De Rosa E, Martinez JO, et al. (2015). Biodegradable silicon nanoneedles delivering nucleic acids intracellularly induce localized *in vivo* neovascularization. Nat Mater 14:532–9.

De Cock LJ, De Koker S, De Geest BG, et al. (2010). Polymeric multilayer capsules in drug delivery. Angew Chem Int Ed Engl 49:6954–73.

Decher G. (1997). Fuzzy nanoassemblies: toward layered polymeric multicomposites. Science 277:1232–7.

Delcea M, Mohwald H, Skirtach AG. (2011). Stimuli-responsive LbL capsules and nanoshells for drug delivery. Adv Drug Deliv Rev 63:730–47.

Ermolyuk YS, Alder FG, Surges R, et al. (2013). Differential triggering of spontaneous glutamate release by P/Q-, N- and R-type Ca2+ channels. Nat Neurosci 16:1754–63.

Frias B, Merighi A. (2016). Capsaicin, nociception and pain. Molecules 21:pii:E797.

Gao H, Goriacheva OA, Tarakina NV, et al. (2016). Intracellularly biodegradable polyelectrolyte/silica composite microcapsules as carriers for small molecules. ACS Appl Mater Interfaces 8:9651–61.

Hofmann ME, Largent-Milnes TM, Fawley JA, et al. (2014). External QX-314 inhibits evoked cranial primary afferent synaptic transmission independent of TRPV1. J Neurophysiol 112:2697–706.

Hua S, Cabot PJ. (2013). Targeted nanoparticles that mimic immune cells in pain control inducing analgesic and anti-inflammatory actions: a potential novel treatment of acute and chronic pain condition. Pain Physician 16:E199–216.

Kopach O, Krotov V, Belan P, et al. (2015). Inflammatory-induced changes in synaptic drive and postsynaptic AMPARs in lamina II dorsal horn neurons are cell-type specific. Pain 156:428–38.

Kopach O, Krotov V, Goncharenko J, et al. (2016). Inhibition of Spinal Ca^{2+}-permeable AMPA receptors with dicationic compounds alleviates persistent inflammatory pain without adverse effects. Front Cell Neurosci 10:50.

Kopach O, Viatchenko-Karpinski V, Atianjoh FE, et al. (2013). PKCalpha is required for inflammation-induced trafficking of extrasynaptic AMPA receptors in tonically firing lamina II dorsal horn neurons during the maintenance of persistent inflammatory pain. J Pain 14:182–92.

Kopach O, Viatchenko-Karpinski V, Belan P, et al. (2012). Development of inflammation-induced hyperalgesia and allodynia is associated with the upregulation of extrasynaptic AMPA receptors in tonically firing lamina II dorsal horn neurons. Front Physiol 3:391.

Leffler A, Lattrell A, Kronewald S, et al. (2011). Activation of TRPA1 by membrane permeable local anesthetics. Mol Pain 7:62.

Lim TK, Macleod BA, Ries CR, et al. (2007). The quaternary lidocaine derivative, QX-314, produces long-lasting local anesthesia in animal models *in vivo*. Anesthesiology 107:305–11.

Liu Q, Zhan C, Barhoumi A, et al. (2016). A supramolecular shear-thinning anti-inflammatory steroid hydrogel. Adv Mater Weinheim 28:6680–6.

Mishra A, Reynolds JP, Chen Y, et al. (2016). Astrocytes mediate neurovascular signaling to capillary pericytes but not to arterioles. Nat Neurosci 19:1619–27.

Munoz Javier A, Del Pino P, Bedard MF, et al. (2008). Photoactivated release of cargo from the cavity of polyelectrolyte capsules to the cytosol of cells. Langmuir 24:12517–20.

Park JH, Gu L, Von Maltzahn G, et al. (2009a). Biodegradable luminescent porous silicon nanoparticles for *in vivo* applications. Nat Mater 8:331–6.

Park JS, Voitenko N, Petralia RS, et al. (2009b). Persistent inflammation induces GluR2 internalization via NMDA receptor-triggered PKC activation in dorsal horn neurons. J Neurosci 29:3206–19.

Pavlov AM, De Geest BG, Louage B, et al. (2013). Magnetically engineered microcapsules as intracellular anchors for remote control over cellular mobility. Adv Mater Weinheim 25:6945–50.

Pavlov AM, Sapelkin AV, Huang X, et al. (2011). Neuron cells uptake of polymeric microcapsules and subsequent intracellular release. Macromol Biosci 11:848–54.

Peters CM, Ilinle D, Houle TT, et al. (2014). Nociceptor-selective peripheral nerve block induces delayed mechanical hypersensitivity and neurotoxicity in rats. Anesthesiology 120:976–86.

Roberson DP, Binshtok AM, Blasi F, et al. (2011). Targeting of sodium channel blockers into nociceptors to produce long-duration analgesia: a systematic study and review. Br J Pharmacol 164:48–58.

Rwei AY, Lee JJ, Zhan C, et al. (2015). Repeatable and adjustable on-demand sciatic nerve block with phototriggerable liposomes. Proc Natl Acad Sci USA 112:15719–24.

Stuart MA, Huck WT, Genzer J, et al. (2010). Emerging applications of stimuli-responsive polymer materials. Nat Mater 9:101–13.

Stueber T, Eberhardt MJ, Hadamitzky C, et al. (2016). Quaternary lidocaine derivative QX-314 activates and permeates human TRPV1 and TRPA1 to produce inhibition of sodium channels and cytotoxicity. Anesthesiology 124:1153–65.

Sukhorukov GB, Mohwald H. (2007). Multifunctional cargo systems for biotechnology. Trends Biotechnol 25:93–8.

Sukhorukov GB, Rogach AL, Zebli B, et al. (2005). Nanoengineered polymer capsules: tools for detection, controlled delivery, and site-specific manipulation. Small 1:194–200.

Tanbour R, Martins AM, Pitt WG, et al. (2016). Drug delivery systems based on polymeric micelles and ultrasound: a review. Curr Pharm Des 22:2796–807.

Xu ZZ, Kim YH, Bang S, et al. (2015). Inhibition of mechanical allodynia in neuropathic pain by TLR5-mediated A-fiber blockade. Nat Med 21:1326–31.

Zhan C, Wang W, Mcalvin JB, et al. (2016). Phototriggered local anesthesia. Nano Lett 16:177–81.

Zhang Y, Chan HF, Leong KW. (2013). Advanced materials and processing for drug delivery: the past and the future. Adv Drug Deliv Rev 65:104–20.

Zhao Y, Zhou C, Liu J, et al. (2014). The quaternary lidocaine derivative QX-314 produces long-lasting intravenous regional anesthesia in rats. PLoS One 9:e89704.

Zheng K, Bard L, Reynolds JP, et al. (2015). Time-resolved imaging reveals heterogeneous landscapes of nanomolar Ca^{2+} in neurons and astroglia. Neuron 88:277–88.

4.5. Наноінженерні полімерні плівки для депонування та індукованого вивільнення біологічно активних сполук

Biomaterials Science

PAPER

View Article Online

Cite this: Biomater. Sci., 2019, 7, 2358

Polymer microchamber arrays for geometry-controlled drug release: a functional study in human cells of neuronal phenotype

Olga Kopach,[a] Kayiu Zheng,[a] Olga A. Sindeeva,[a,c] Meiyu Gai,[b] Gleb B. Sukhorukov[a,b] and Dmitri A. Rusakov[a]

Polyelectrolyte multilayer (PEM) microchambers can provide a versatile cargo delivery system enabling rapid, site-specific drug release on demand. However, experimental evidence for their potential benefits in live human cells is scarce. Equally, practical applications often require substance delivery that is geometrically constrained and highly localized. Here, we establish human-cell biocompatibility and on-demand cargo release properties of the PEM or polylactic acid (PLA)-based microchamber arrays fabricated on a patterned film base. We grow human N2A cells (a neuroblastoma cell line widely used for studies of neurotoxicity) on the surface of the patterned microchamber arrays loaded with either a fluorescent indicator or the ubiquitous excitatory neurotransmitter glutamate. The differentiating human N2A cells show no detrimental effects on viability when growing on either PEM@PLA or PLA-based arrays for up to ten days *in vitro*. Firstly, we use two-photon (2P) excitation with femtosecond laser pulses to open individual microchambers in a controlled way while monitoring release and diffusion of the fluorescent cargo (rhodamine or FITC fluorescent dye). Secondly, we document the increases in intracellular Ca^{2+} in local N2A cells in response to the laser-triggered glutamate release from individual microchambers. The functional cell response is site-specific and reproducible on demand and could be replicated by applying glutamate to the cells using a pressurised micropipette. Time-resolved fluorescence imaging confirms the physiological range of the glutamate-evoked intracellular Ca^{2+} dynamics in the differentiating N2A cells. Our data indicate that the nano-engineering design of the fabricated PEM or PLA-based patterned microchamber arrays could provide a biologically safe and efficient tool for targeted, geometrically constrained drug delivery.

Received 17th November 2018,
Accepted 17th March 2019

DOI: 10.1039/c8bm01499j

rsc.li/biomaterials-science

Introduction

Over the past decade, various nano-engineering designs have been explored for their capability for micro-packaging, targeted delivery, and controlled release of bioactive compounds. Among such systems, the most prominent were nanoparticles and microcapsules,[1–3] hydrogels,[4] and nanocomposite films fabricated with the polyelectrolyte-based multilayer (PEM) assembly using the layer-by-layer (LbL) technique.[5,6] Nanostructured PEMs combine multiple functionalities to provide control over cargo release: their shell permeability could be changed by external triggering using either an altered environment (pH, osmolarity) or a physical stimulus (light, temperature, or ultrasound).[7–10] A broad range of functional properties, together with a relatively small size of capsules (nano- to micrometer range), ultimately provided such cargo systems with numerous benefits, prompting growing interest towards translating fundamental studies into practical implementations.[3,8,11,12] Whilst successful encapsulation has been implemented for a wide variety of substances,[13] microscopic targeting of cargo release along predetermined space trajectories or geometric patterns has remained elusive. This targeting could be particularly important, for instance, for guiding cell growth or dealing with geometrically defined tissue areas.

Recent advances in PEM films fabricated on patterned surfaces appear to overcome the issue of capsule scattering, by enabling an array of micro-wells or microchambers of predetermined size and spatial distribution.[5,6,14] Composed as LbL-assembled PEM films, this novel strategy of housing bio-

[a]Department of Clinical and Experimental Epilepsy, UCL Queen Square Institute of Neurology, University College London, London WC1N 3BG, UK. E-mail: d.rusakov@ucl.ac.uk
[b]School of Engineering and Materials Science, Queen Mary University of London, Mile End Road, London E1 4NS, UK. E-mail: g.sukhorukov@qmul.ac.uk
[c]Remote Controlled Theranostic Systems Lab, Saratov State University, 83 Astrakhanskaya Street, Saratov 410012, Russia

active compounds combines all functionalities of PEM nanostructures with having a layer of hydrophobic polymer such as polylactic acid (PLA) to increase load capacity. The efficient entrapment and storage of various compounds in PEM microchambers have recently been demonstrated,[15,16] including the use of wall nanocomposites sensitive to external triggering for payload release.[14,17] Clearly, the predetermined patterns of microchambers could provide an opportunity to control the localised release of active compounds in space, time, and dosage. Films containing microchambers could also be deposited as a microscopic coating on the surfaces of stents or implants. It would seem therefore important to understand whether and how this delivery system can be used in the conditions of live cells and their networks.

To address this issue, we grew human N2A cells differentiating to neuronal phenotype on the surface of either PEM@polylactic acid (PLA)-based or PLA-based films to test biocompatibility (neurotoxicity) and safe preservation of low molecular weight substances as the cargo inside the square grid distributed microchambers for up to two weeks *in vitro*. We probed the efficient release of the cargo, the excitatory neurotransmitter glutamate, using a focused laser beam and established the glutamate-induced physiological effects on the adjacent N2A cells. Our results provide evidence for the safe and efficient use of the fabricated microchamber arrays for a pharmacological action on human cells.

Methods

Fabrication of microchamber arrays

Patterned microchamber array production was performed as detailed in our previous studies,[6,14,15,17,18] with some modifications. Generally, a patterned microchamber array was composed of two nanocomposite films (Fig. 1A and B), each printed separately and joined after loading a cargo (Fig. 1C). The first film represents a patterned layer containing microwells, while the second is flat, without wells, made of the same composite materials.

Patterned PDMS stamps. To fabricate patterned films with micro-wells, poly(dimethylsiloxane) (PDMS) stamps were used (Sylgard 184, Dow-Corning, Midland, USA). PDMS stamps were printed out from silicon masters with micropillars. For this, a mixture of a pre-polymer and a curing agent was prepared in a ratio of 10 : 1 and poured on silicon masters, then degassed in a vacuum for 30 min and cured at 70 °C for 3 h. The silicon master was prepared by conventional photolithography. The fabricated micropillars had a cylindrical shape of 10 μm in diameter and 5 μm height.

PEM@PLA and PLA production. Different types of microchamber arrays were fabricated, variable by the nanocomposite assembly (PEM@PLA and PLA) and/or the cargo payload (glutamate and its analogue, fluorescent dyes, or empty ones (no payload)), for further functional testing of either array. PEM films were fabricated with the LbL assembly method,[5,6] using a dip-coating robot. Before starting, both PDMS stamp and cover glass (for a flat film production) were submerged in a positively charged poly(ethylenimine) (PEI, Sigma, St Louis, USA) solution for 10 min, followed by washing with ddH_2O 3 times for 1 min each. Subsequently, two opposite-charged polyelectrolytes, poly(sodium 4-styrenesulfonate) (PSS, Sigma, St Louis, USA) and poly(diallyldimethylammonium chloride) (PDDA, Sigma, St Louis, USA), were layered with the same procedure. Either compound was used at the concentration of 2 g L^{-1} (in 0.5 M NaCl) for each layer. In total, 40 layers of PSS/PDDA were applied on the PDMS stamp and 20 layers of PSS/PDDA on the cover glass. For hydrophobization, the PEM films were immersed in 0.5% polylactic acid (PLA, 3 mm nominal granule size, Sigma, St Louis, USA) for 3 s and dried afterwards (typically, 10 min in air) (Fig. 1A). For fabrication of the PLA-based films, the procedure includes the immersion of both the PDMS stamp and the cover glass in a 0.75% PLA solution for 3 s, followed by drying (Fig. 1B).

Cargo loading and microchamber sealing. Several water-soluble, low molecular weight substances were loaded inside the microchambers, including fluorescent dyes (FITC, rhodamine) and the most common excitatory neurotransmitter glutamate (glutamic acid or its pharmacological analogue, L-glutamic acid hydrochloride). Each compound was diluted at a required concentration (near its maximal solubility) and applied onto the surface of the patterned film to fill micro-wells. The compound concentration was as follows: 0.5 μg ml^{-1} for rhodamine and FITC (Sigma, St Louis, USA), 10 μg ml^{-1} for glutamic acid, and 300 μg ml^{-1} for L-glutamic acid hydrochloride (Sigma, St Louis, USA). After filling the micro-wells with the solution, the film was allowed to dry until cargo crystals were formed (Fig. 1D). Finally, the patterned microfilm with the crystals inside the microchambers was sealed to a flat film with a pressure (~2 kg cm^{-2}) to make one single unit (Fig. 1C).

To optimise filing of the microchambers, L-glutamic acid hydrochloride (diluted at 300 μg ml^{-1} in ddH_2O) was applied onto the patterned film surface in 200–300 μl volume batches to fill all microchambers across a sample; the remaining medium was then carefully removed from the film surface (a process facilitated by the hydrophobic PLA surface). As a result, large crystals of L-glutamic acid hydrochloride (clearly visible at a magnification of ×20 and above) were filling the microchambers homogeneously across the sample and, importantly, were of a similar size between the microchambers, as evidenced by SEM images (Fig. 1D). Such a controlled cargo payload for individual microchambers is essential for further functional testing on live cells. The estimated amount of L-glutamic acid hydrochloride was ~20 pg per microchamber.

Scanning electron microscopy (SEM)

Scanning electron microscopy (SEM, FEI, Inspect-F) was used to visualize the microchamber morphology at different steps through the fabrication procedure (payload, sealing) and after opening the microchamber(s) to ensure appropriate samples. SEM was carried out using an accelerating voltage of 10 kV, a spot size of 3.5 nm, and a working distance of approximately 10 mm.

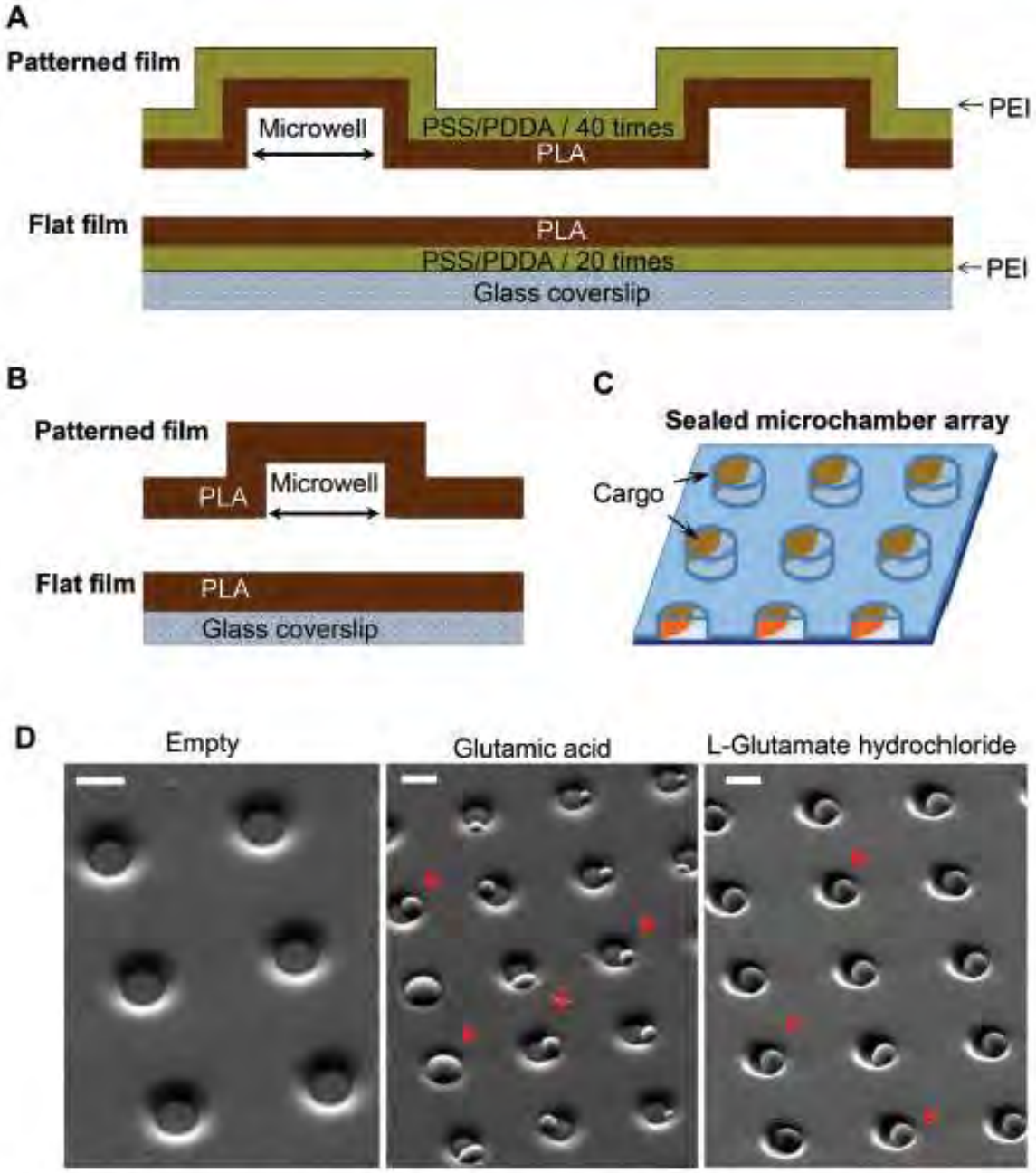

Fig. 1 Fabrication of polymer microchamber arrays containing low molecular weight substances as a cargo payload. (A) Fabrication of the PEM@PLA nanocomposite assembly: two films, patterned and flat, each printed separately, before sealing together to compose polymer microchambers. (B) For the PLA-based microchamber arrays, the fabrication process includes production of the patterned film with the microchambers and the flat film on a glass, which are then sealed together. (C) A schematic depicting the sealed microchamber array, with a cargo payload within the microchambers. (D) SEM images of the microchambers (before sealing) for the various types of the fabricated polymer arrays: empty microchambers (no cargo; left image) and microchambers filled with glutamic acid (at the middle) or L-glutamate hydrochloride (right image). Red arrows show a cargo crystal per microchamber. Scale bars, 10 μm.

Cell cultures

Human N2A cell line, a gift from the Prof. Stephen Hart's group (UCL, UK), was cultured in Dulbecco's modified Eagle medium (DMEM, Invitrogen, Carlsbad, CA, USA), containing high glucose and 2 mM L-glutamine, supplemented with 10% fetal bovine serum (FBS), 2% penicillin–streptomycin, and 1% non-essential amino acids at 37 °C (5% CO_2). The cells were harvested using 0.05% trypsin–EDTA (Gibco, USA) for 5–10 min, washed and plated on the surface of microchamber arrays placed individually in a 5 cm^2 Petri dish. The fabricated microchamber arrays were pre-treated with UV light for at least 2 h prior to plating the cells. For differentiation of the N2A cells to neuronal phenotype, the culturing medium was low serum DMEM (2% FBS instead of 10%). The differentiating N2A cells were maintained on the microchamber array samples until used. For each type of the microchamber arrays, there were at least three independent cell preparations tested.

Cell viability assessment

To monitor possible concomitant toxic effects of the microchamber arrays, we compared the density of the N2A cells growing on the surface of the PEM@PLA- and PLA-based arrays with that of those growing outside the microchamber area, at various time points of cell growth. Healthy cells were counted within the sampling areas chosen in a quasi-random fashion in the middle of the microchamber arrays, and outside the microchamber area (close to the film edge). Cell density was calculated as the number of viable cells per mm^2. An additional control group included N2A cells plated on glass coverslips, with no polymer (PLA) present. The other functional indicator of cell viability was the total length of cell neurites per cell. To this end, cell images (sampled as above) were analysed with NeuronJ (ImageJ, NIH).

Opening of individual microchambers with a femtosecond pulse laser

To optically address individual microchambers, we employed a Femto2D (Femtonics) multi-photon excitation microscope system optically linked to a Ti:Sapphire Mai-Tai femtosecond pulse laser (SpectraPhysics, Newport, ~220 fs pulses at 80 MHz). The two key advantages of two-photon (2P) excitation (or absorption) with near-infrared light were (i) high penetration (low scattering and absorption) in turbid media compared to visible or UV light and (ii) the 2P excitation effect within a thin (~1 μm) focal layer only. Another important advantage of femtosecond-pulse excitation in live tissues was that, despite a very high intensity delivered during the pulse, the time-average wattage delivered to the specimen was fully compatible with live function. Indeed, the range of laser power used here was similar to that routinely used by us and others for cell imaging in acute brain slices and in live animals.[19–21]

The empirically determined optimal wavelength was 740 nm (opening of the PEM@PLA films) or 780–790 nm (opening of the PLA-based microchambers). For microchamber opening, the laser beam was focused on the top of the microchamber cap (typically, within the cap edges), at a power of 26 mW over 3–5 ms. We ensured that no neighbouring cells were affected by the high-power laser pulses during microchamber opening, as evidenced by the images shown. Otherwise, cell imaging was carried out at a power under the objective of <3 mW, as detailed below. We found that the two protocols for microchamber formation, PEM@PLA and PLA, work equally well for cargo (glutamate) loading and for laser opening. Thus, the presence of the precursor PEM film did not appear to have an effect on the microchamber functionality, which was defined largely by the terminated PLA layer.

Two-photon (2P) excitation fluorescence imaging. Cells were bolus loaded with the cell-permeable Ca^{2+} indicator Oregon Green BAPTA-1 (OGB-1 AM; 5 μM, Invitrogen) in the presence of Pluronic F-127 (0.02%, Invitrogen) by incubation for 30 minutes at 37 °C. After loading, the cells were washed for approximately 30 minutes for de-etherification of the dye. A sample was placed in a recording chamber mounted on the stage of an Olympus BX51WI upright microscope (Olympus, Japan) equipped with an XLPlanN 25×/1.05 objective coupled to an infrared DIC imaging system. Imaging was carried out using a Femto2D (Femtonics, Budapest, Hungary) system optically linked to a Ti:Sapphire Mai-Tai femtosecond pulse laser (SpectraPhysics, Newport), and excitation at λ_{ex}^{2P} = 800 nm optimized for OGB-1. To minimize contaminating fluorescence (PEM/PLA autofluorescence), 2P excitation fluorescence images were taken from a thin focal excitation plane (~1 μm) within individual cells, which was held unchanged throughout the experiment (prior to and following opening a microchamber). For the time-lapse changes in OGB-1 fluorescence, images were collected using 512 × 512 pixel frames in the stream acquisition mode acquired in 20 s time sections for typically 1 minute before opening a microchamber (baseline) and for 2.5–5 min immediately after the microchamber opening. Changes in $[Ca^{2+}]_i$ were expressed as the changes in OGB-1 fluorescence at the maximum of the fluorescent signal over the baseline ($\Delta F/F_0$), as detailed previously.[22]

The sequence of laser-triggered microchamber opening (pulse 3–5 ms, 1–2 times; λ = 790 nm), including focal adjustment and fast scanning in line mode to identify opening, took typically ~30 s. Recordings were carried out in a HEPES-based medium containing (in mM) 135 NaCl, 5 KCl, 2 $CaCl_2$, 2 $MgCl_2$, 10 HEPES, 10 glucose (pH 7.4; 290–300 mOsm). In a separate set of experiments, glutamate (5 μM) was locally applied to the cells *via* a fabricated glass micropipette (~1 μm inner diameter of the tip) to provide a direct comparison of the effects between the triggered release of cargo from the microchambers and the locally applied agonist. To enable a brief, localised agonist application (200–400 ms duration), a pressurised micropipette was connected to the two-channel PDES-02DX pneumatic microejector (npi electronic GmbH) with compressed nitrogen. The fluorescent tracer Alexa Fluor-594 (100 μM) was added into the pipette to visualize the area of the agonist spread.

Time-resolved fluorescence lifetime imaging (FLIM)

In the context of intracellular Ca^{2+} monitoring, fluorescence lifetime imaging (FLIM) can provide readouts insensitive to

concomitant fluctuations in focus or in dye concentration.[21,23,24] FLIM was conducted using the in-house system based on the Femto2D microscope equipped with a Becker and Hickl FLIM detector (Femtonics, Budapest), as described earlier.[21,22] The FLIM duty cycle was driven by an 80 MHz infrared pulsed laser (SpectraPhysics, Newport Mai-Tai BB). Fluorescence images were acquired at 2 frames per second and stored as a data tensor representing x-y pixel images with a distribution of the nanosecond delay time (t) of photons at each pixel over the frame duration (T). Average image acquisition times were 240–300 s (maximum frame laser exposure time per acquisition trial of <6 s to minimize phototoxic damage), depending on the total photon count; the maximum photon count rate was on average $\sim 10^5$ s^{-1} which is well below the effect of photon pile-up. To monitor changes in $[Ca^{2+}]$, we minimized the sampled image area with various digital zooms to approximately 70 × 70 μm (x, y). Because of the relatively low photon counts per pixel, the photon data were accumulated over the selected ROI from the (t, x, y, T) tensor into the (t, T) matrix before the data analysis was used to estimate $[Ca^{2+}]$. To confirm changes in the OGB-1 fluorescence intensity, we also calculated the intensity from FLIM data, by integration of the photon counting data (non-normalized) at the same ROI (Fig. 6A).

Statistical analysis

All data are presented as mean ± standard error of the mean, with n referring typically to the number of cells analyzed within the experimental groups. For the cell viability analysis, n refers to the number of different areas/samples where the cell density was assessed or indicates the number of neurites measured for their length. To determine statistical difference between the experimental groups, Student's t-test (two-tailed paired or unpaired) was used where appropriate. A p value of less than 0.05 was considered as statistically significant.

Results and discussion

Biocompatibility and cargo preservation

The neuroblastoma cell line (N2A) was selected to provide fast cell growth, with the cells differentiating to neuronal phenotype.[25–27] We placed the stamped arrays of microchambers (Fig. 1) filled with either glutamate or fluorescent indicator, or left empty, in the cell culture medium, and subsequently plated the N2A cells to grow on the array surface, or entirely outside the arrays, during 7–10 days (Methods). The two array types tested were PEM@PLA (Fig. 2) and PLA (Fig. 3).

24 h post plating, the N2A cells developed typical axon-like processes and extended neurites (*e.g.*, Fig. 2B and 3B). To assess cell viability, we monitored the length of such processes, along with the cell density, throughout the preparation, for up to ten days *in vitro* (Methods). During that time, cell processes could reach up to 300 μm in length, suggesting no gross detrimental effects of having the fabricated arrays nearby. On a finer scale, we found no difference in the cell viability among the samples containing microchambers, with or without loaded glutamate, inside or outside the chamber areas (or with no polymer material present), for both array fabrication types, over 3–7 days *in vitro* (Fig. 2C and 3C). This observation is consistent with the reported biocompatibility of the constituent polymers, PSS and PLA.[29,30] Also, given that the differentiating N2A cells are highly sensitive to low glutamate levels,[25,31] this result also suggests the microchamber wall stability in preventing cargo escape.

Localised cargo release by optical targeting of individual microchambers

Next, we used laser pulses to open individual microchambers at selected sites (Methods). We thus tested varied beam trajectories (line, spiral, point) to open individual microchambers across the polymer surface, also exploring varied exposure areas (from 1 to 5 μm; Fig. 4). The successful opening of the targeted microchambers, with fully intact neighbours, was confirmed with SEM (Fig. 4B and D). Importantly, cultured N2A cells nearby remained unperturbed (Fig. 5 and 6). We next tested whether the payload inside the microchambers remained intact after loading and optical addressing (laser beam opening). First, we used a fluorescent dye, either rhodamine or FITC, as the cargo. The presence of fluorescent emission inside the microchambers was confirmed using 2P excitation imaging at the plane of microchambers, for either loaded dye (Fig. 4A for rhodamine and Fig. 5 for FITC). We were also able to visualise the release of the loaded dye upon microchamber opening, using the time-lapse imaging: a prompt and robust rise in the FITC-mediated fluorescence next to the opened microchamber could be detected over the regions of interest (ROIs, indicated in Fig. 5A and C) shortly after the laser pulse (Fig. 5B and D). Appearance of an air bubble (transmitted light channel) immediately after the pulse indicated microchamber opening (Fig. 5A and C), as reported in previous studies.[15] Control experiments confirmed that there was no rise in FITC fluorescence (no payload release) over the same ROI when no laser pulse was applied (Fig. 5B and D) or when repeatedly targeting the opened microchamber. Subsequent targeting of the intact microchambers triggered a similar rise in local FITC fluorescence over the neighbour area (Fig. 5C and D), confirming the repeatable effect on demand.

Laser-triggered glutamate release from individual microchambers mobilises intracellular Ca^{2+} in local N2A cells

Finally, we evaluated functional effects of the triggered cargo release on live cells. To this end, we used glutamate-loaded microchambers: in N2A cells, glutamate induces a prominent inward current through the Ca^{2+}-permeable *N*-methyl-D-aspartate (NMDA) receptors.[32] We therefore employed 2P excitation imaging of the Ca^{2+} indicator Oregon Green BAPTA-1 (OGB-1) bulk-loaded into the differentiated N2A cells growing (3–6 days) on the microchamber arrays filled with glutamate (L-glutamic acid hydrochloride, Methods, Fig. 1D). Imaging was carried out in continuous frame-scanning mode (~500 ms per frame),

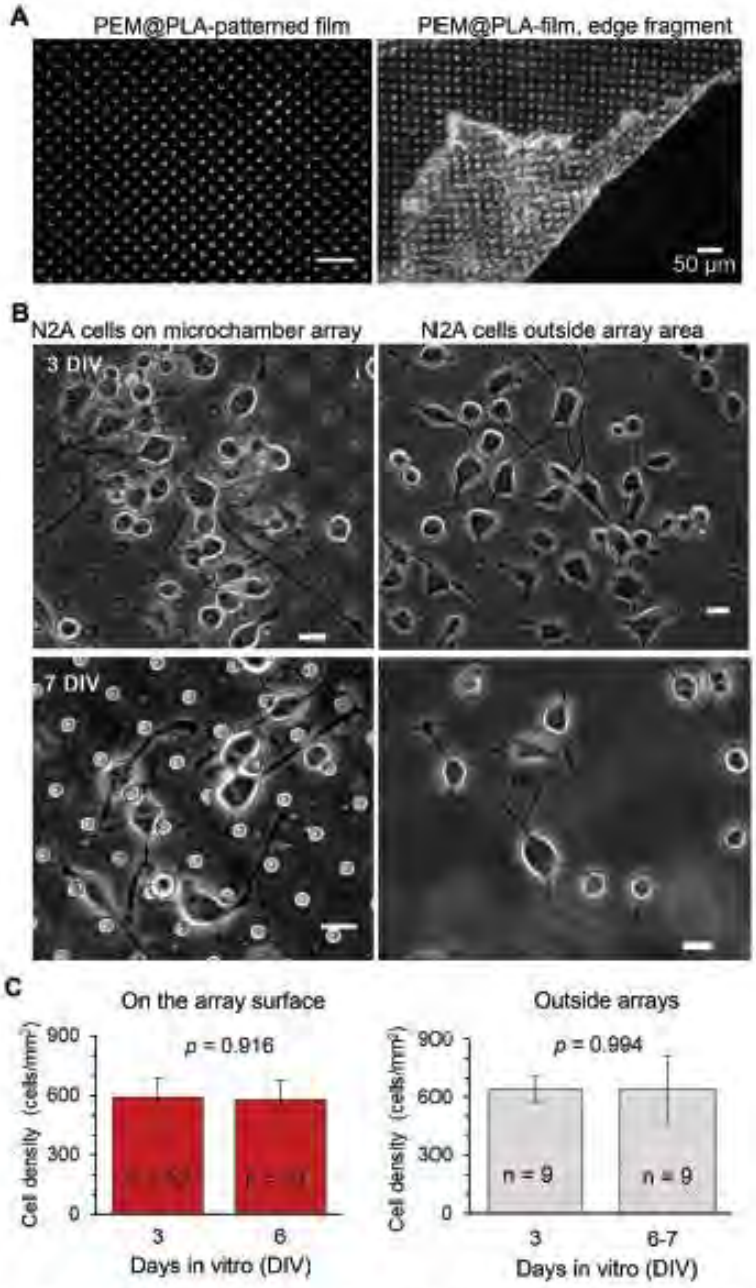

Fig. 2 Biocompatibility and cargo preservation within the microchambers: the fabricated PEM@PLA microchamber arrays. (A) Transmitted light images of PEM@PLA-patterned microchamber arrays, central area (left) and towards the edge, depicting the detached PEM film (right). Scale bars, 50 µm. (B) Representative images of the differentiating N2A cells growing on the surface of the microchambers loaded with glutamic acid (left row) or outside the microchamber area (right row) at different time points after cell plating. Green arrows, axon-like processes in the N2A cells of neuronal phenotype. Scale bars, 15 µm. (C) Statistical summary, cell density (mean ± s.e.m.) on top of the microchambers loaded with glutamate (left) and outside the microchambers (right), at three days *in vitro* (DIV3) and DIV6–7; *n*, number of sampled areas; *p*, two-tailed, unpaired *t*-test.

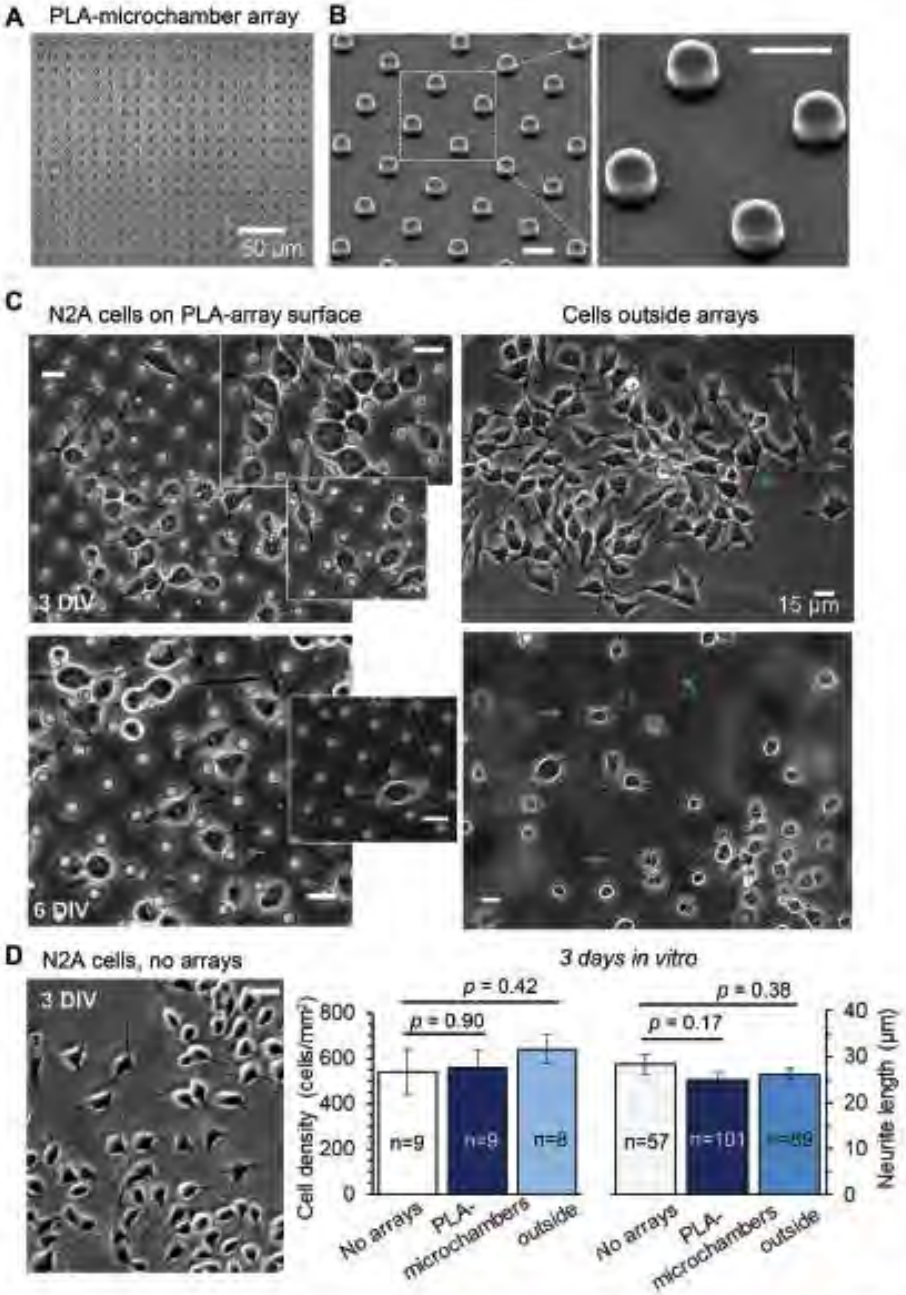

Fig. 3 The differentiating N2A cells show no signs of excitotoxicity when growing on the PLA-based microchamber arrays with the glutamate payload. (A–B) The representative transmitted light image (A) and SEM images (B) of the PLA-based microchamber array after sealing the microchambers with loaded glutamic acid inside. Scale bars in B, 10 µm. (C) Representative snapshots of the differentiating N2A cells growing on the surface of the PLA-based microchambers loaded with glutamate (left panels) and outside the microchamber area (right panels) at different times after cell plating. Green arrows, axon-like processes in the N2A cells of neuronal phenotype. Scale bars, 15 µm. (D) A snapshot of the differentiating N2A cells on a glass coverslip at DIV3. Plots, statistical summary, cell density (left) and neurite length (right, mean ± s.e.m.) for the cells growing on the coverslips, the PLA-based microchambers containing glutamate, in the area outside microchambers; *n*, number of sampled areas (left) or measured neurites (right); *p*, two-tailed, unpaired *t*-test.

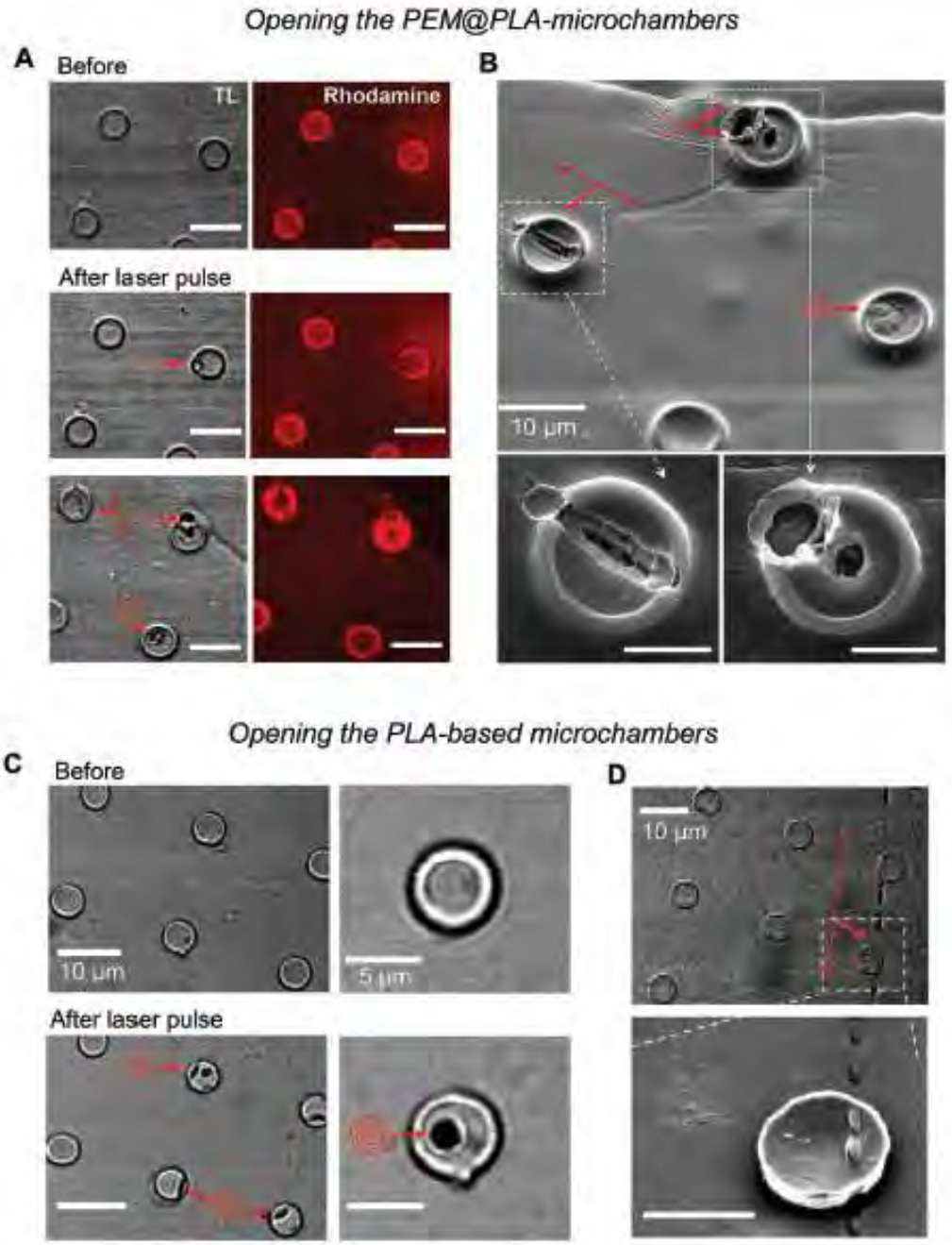

Fig. 4 Optical targeting of individual microchambers with a femtosecond infrared pulse. (A) Images of the PEM@PLA-microchambers (transmitted light, TL, and rhodamine fluorescence channels, λ_{exc}^{2P} = 800 nm) before and after applying a focused laser beam (λ = 740 nm) for opening the selected microchambers, using various trajectories (line or spiral) as indicated. Red arrows depict the pattern applied to open a microchamber. Scale bars, 10 μm. (B) SEM images of the microchamber morphology after opening with a femtosecond pulse laser. Images are taken from the same area as for the bottom row in A (microchambers match), showing successful opening with various patterns of a laser beam applied to the microchamber surface. Red arrows, patterns used for opening. Scale bars for bottom images, 5 μm. (C) Transmitted light images of the PLA-based microchamber arrays before and after applying a femtosecond pulse laser for microchamber opening (spiral trajectories, 3 μm wide). (D) SEM images of the opened microchamber, indicated in the top snapshot, using a line segment laser trajectory. Scale bars, 10 μm.

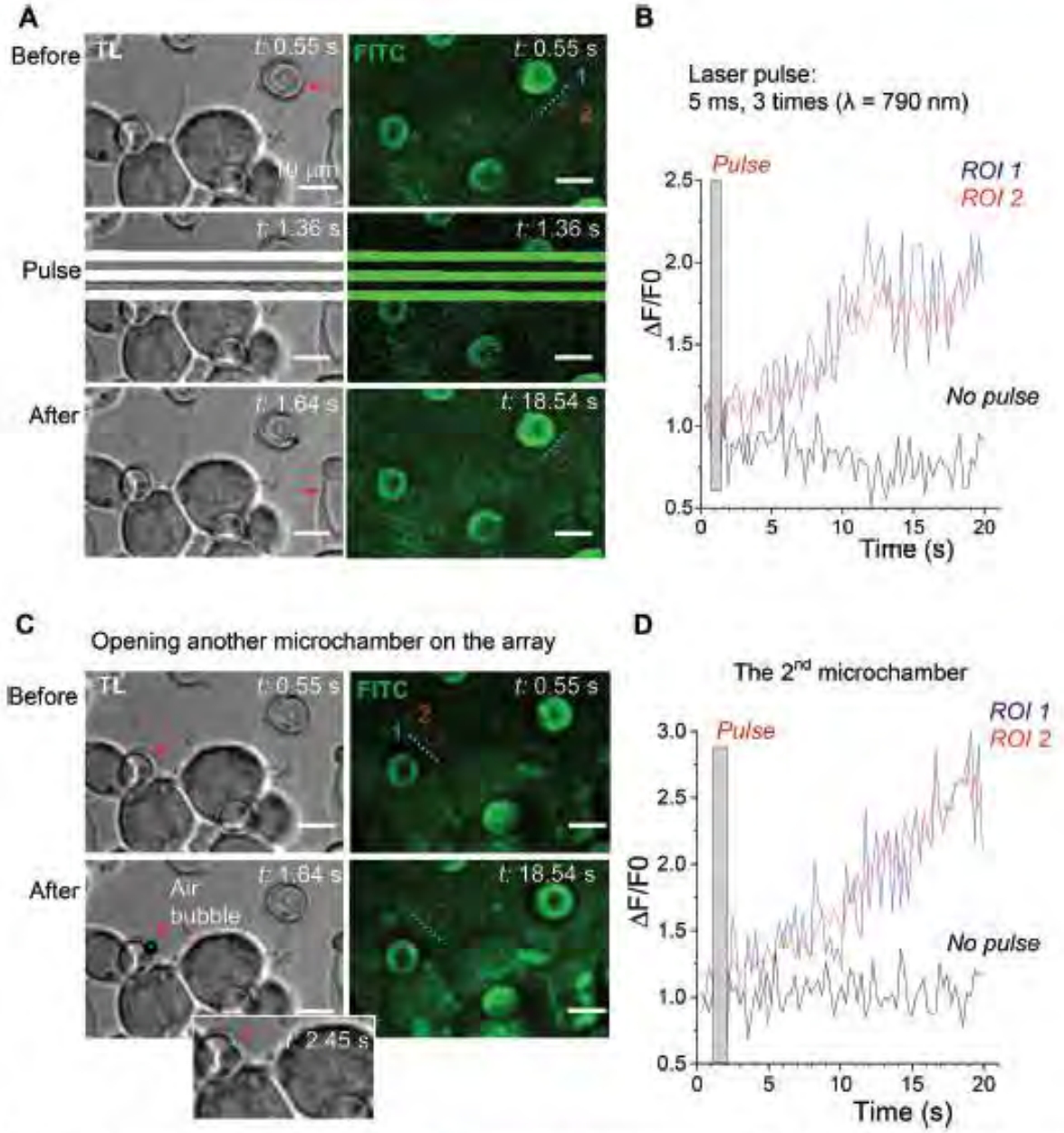

Fig. 5 Release of the fluorescent cargo from individual microchambers using optical targeting. (A) The PEM@PLA microchamber array with the FITC payload in microchambers (transmitted light, TL, and FITC fluorescence channels; λ_x^{2P} = 800 nm), before (top), during (middle), and after (bottom) optical targeting of a microchamber with a femtosecond laser beam (λ = 790 nm; 26 mW, 3 consequent pulses, for 5 ms each). An air bubble formed upon the laser pulse confirms the microchamber opening. Scale bars, 10 μm. (B) Time course of changes in FITC fluorescence over regions of interest (ROIs), as indicated in A. (C) The same PEM@PLA microchamber array as for A and B (FITC payload) while targeting another microchamber. Air bubble formation confirms the microchamber opening, followed by visualization of the opened (disfigured) microchamber. Scale bars, 10 μm. (D) Time course of changes in FITC fluorescence over various ROIs, as indicated in C.

before opening a microchamber (baseline) and immediately afterwards (up to several minutes; Fig. 6A). The chamber opening phase, including line scan (top middle image in Fig. 6A) and focal adjustment, took ~30 s (Methods). In the proximity of the glutamate-filled microchambers, we could detect clear Ca^{2+} rises inside the cells following local microchamber opening. The rises were transient and declined back close to the resting baseline level within minutes of micro-

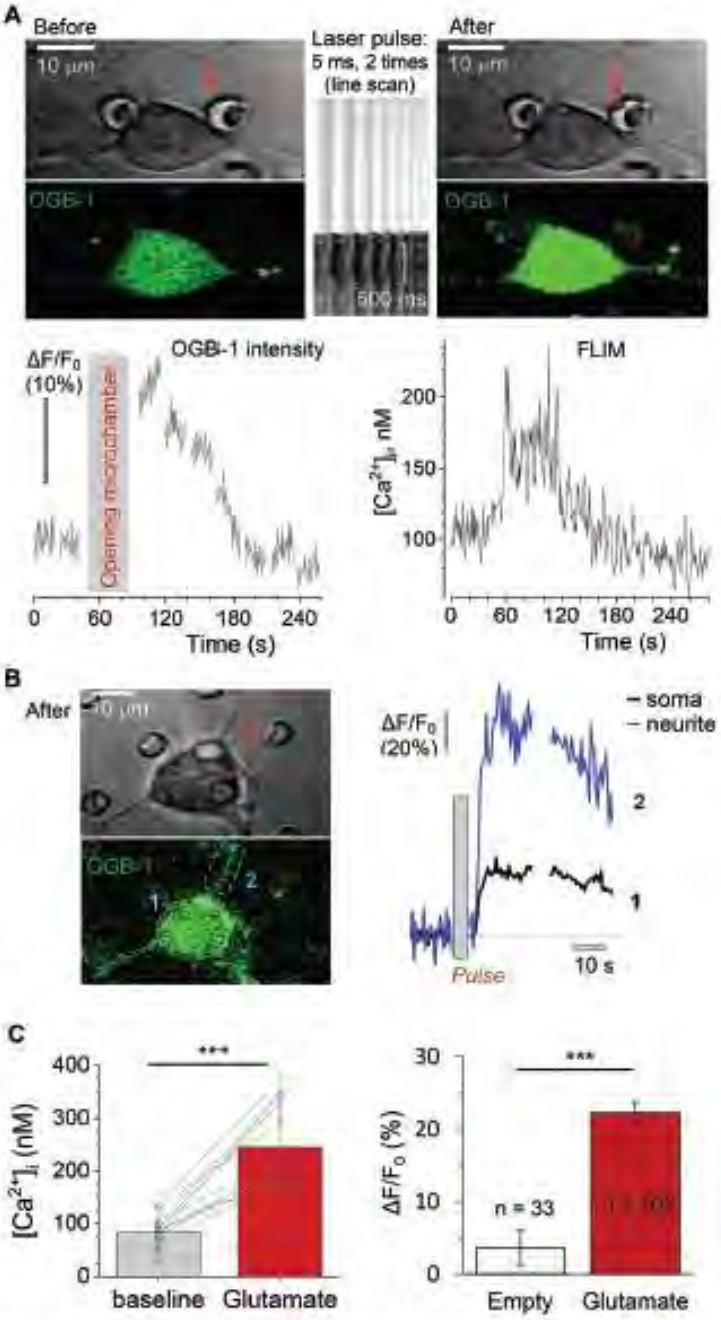

Fig. 6 Monitoring the intracellular Ca^{2+} rise in the differentiating N2A cells upon the triggered release of glutamate from the microchambers. (A) An example of a differentiated N2A cell grown on the PLA-based microchamber array loaded with glutamate before (left) and after (right) local microchamber opening (dotted line). Upper row, transmitted light images; bottom row images, the OGB-1 fluorescence channel (λ_{ex}^{2P} = 800 nm). Middle panel, line scan across the dotted line as shown in the left image, confirming the microchamber opening with a femtosecond pulse laser (λ = 790 nm; 26 mW); scale bars, 10 μm. Plots, time courses of the OGB-1 fluorescence intensity signal $\Delta F/F$ (left) and of $[Ca^{2+}]_i$ (FLIM readout, right), during chamber opening, as indicated. (B) Left panels: A DIC image (top) and OGB-1 channel snapshot (bottom); dotted areas, ROIs 1 and 2, for the soma and neurites, respectively; red arrow, the targeted microchamber. Plots: time course of the Ca^{2+} rise in the cell soma (ROI 1) and neurites (ROI 2), during the glutamate release from a microchamber, as indicated. (C) Statistical summary. Left, $[Ca^{2+}]_i$ levels in the N2A cells before and following microchamber opening (FLIM readout, n = 14 cells). Right, relative changes in OGB-1 fluorescence intensity in response to optical targeting of the PLA-based microchambers with no payload (empty) and loaded with glutamate (red); n, the total N2A cells analysed across four independent experiments for each type of fabricated arrays. ***, $p < 0.0001$ (two-tailed, paired and unpaired t-test for left and right plots, respectively).

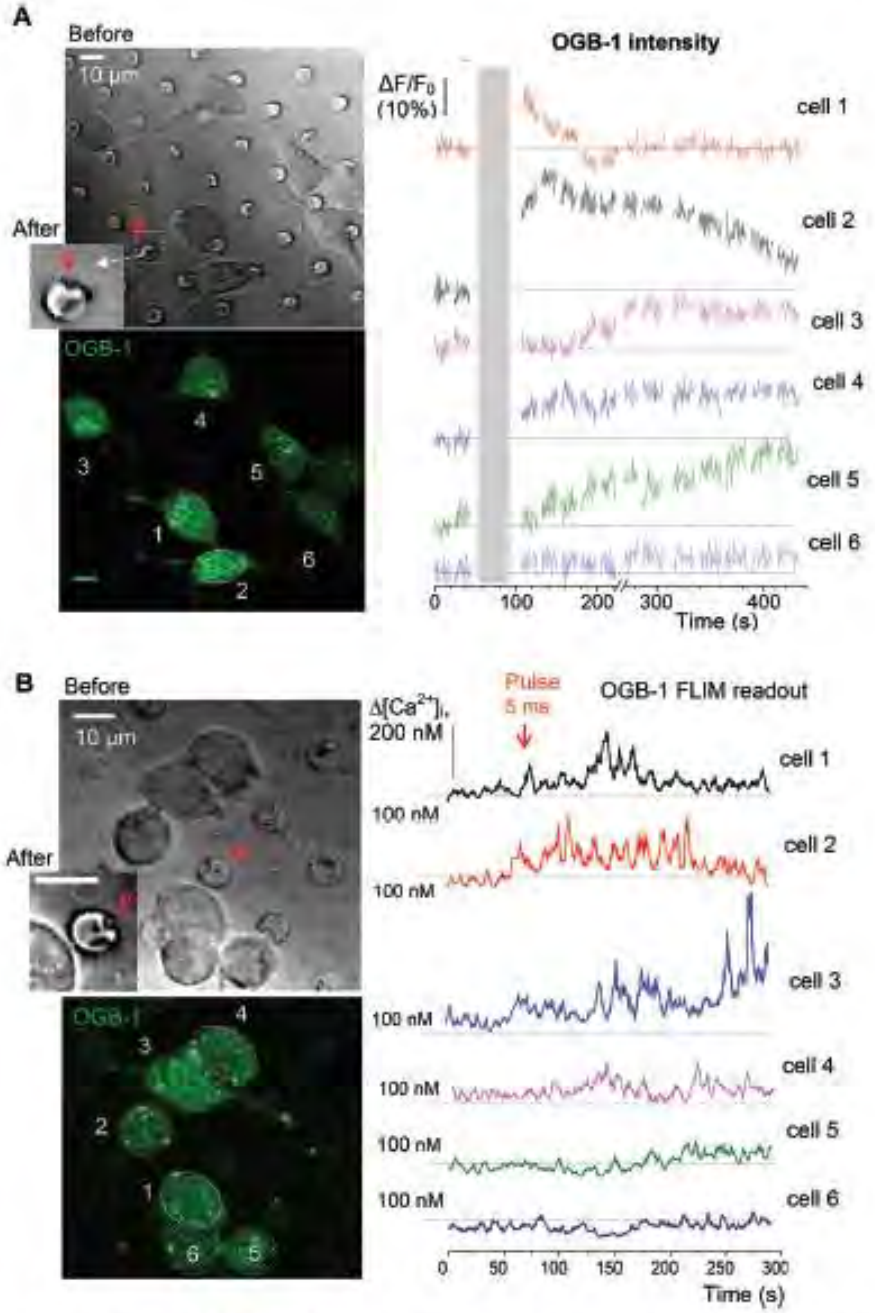

Fig. 7 Monitoring $[Ca^{2+}]_i$ dynamics in the adjacent N2A cells upon the triggered release of glutamate from individual microchambers. (A) Transmitted light (top) and fluorescence images (bottom, OGB-1 fluorescence channel; λ_x^{2P} = 800 nm) of the differentiating N2A cells growing on the surface of the PLA-based microchambers loaded with glutamate before and after opening the selected microchamber. Red arrow, a microchamber before and after opening. Plots, time course of changes in OGB-1 fluorescence intensity for individual cells as shown in the bottom left image. (B) Experiment as in A, but monitoring $[Ca^{2+}]_i$ in the N2A cells using the OGB-1 FLIM readout. Scale bars, 10 μm.

chamber opening (Fig. 6A, bottom). The time course of the Ca^{2+} rise detected in the N2A cell soma and neurites displayed comparable kinetic profiles (Fig. 6B). The functional effect was measured in 102 cells growing on top of the glutamate-loaded microchambers to be tested for opening (about 22 microchambers in total) across 4 PLA-microchamber array samples (n = 4 independent cell culture preparations; Fig. 6C). In contrast, there were no detectable changes in Ca^{2+} dynamics in the

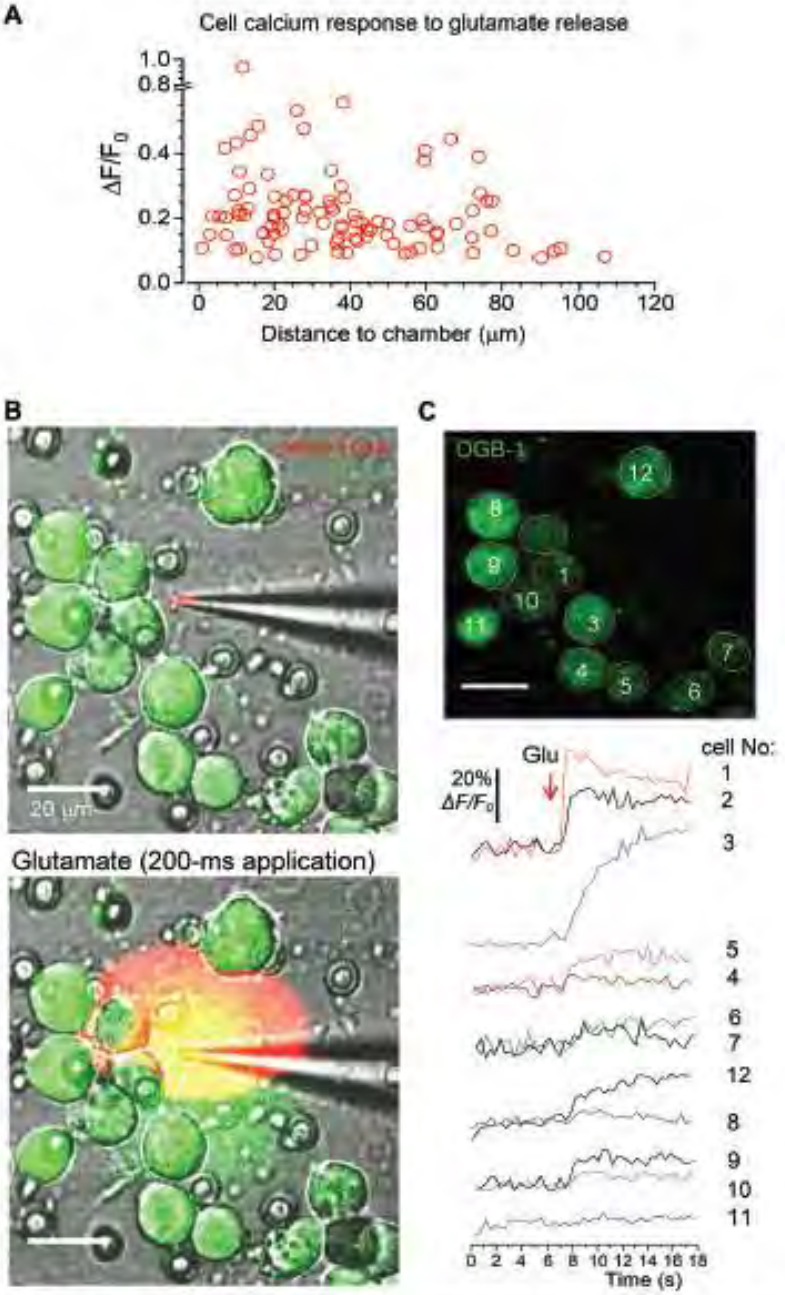

Fig. 8 Replicating the functional effect of the glutamate release from the microchambers with a focal agonist application onto the N2A cells. (A) Summary of the Ca^{2+} rise in individual N2A cells (n = 102) in response to the triggered glutamate release from the microchambers, plotted against the distance from the targeted microchambers. (B) Images of the differentiating N2A cells growing on the surface of the PLA-based microchamber array before (top) and after (bottom) a direct focal application of glutamate (5 μM, 200 ms duration) through a micropipette positioned in the close proximity of the cells. Images, combined transmitted light, OGB-1 (green), and Alexa Fluor-594 (red) channels (λ_x^{2P} = 800 nm). (C) The same area as in A, showing the N2A cells at the OGB-1 fluorescence channel (λ_x^{2P} = 800 nm); regions of interest (ROIs) are shown; red arrow, glutamate puff through the micropipette (dotted lines). Bottom plots, time course of the Ca^{2+} rise over indicated ROI before and after glutamate application (5 μM, 200 ms); red arrow, timing of glutamate puff.

N2A cells growing on the surface of the PLA arrays containing empty microchambers (no payload), upon their opening (n = 33; p < 0.001 compared with the group of cells on the glutamate-containing microchambers; Fig. 6C).

To verify that the observed Ca^{2+} transients were within the physiological range and not affected by focus fluctuations, cell deterioration, or concomitant laser pulse effects, we used a FLIM method to document the 'absolute' intracellular Ca^{2+} concentration ($[Ca^{2+}]_i$) dynamics, as shown earlier.[21,22] Thus, we obtained the direct readout of the intracellular Ca^{2+} concentration ($[Ca^{2+}]_i$) in the N2A cells before and after opening the microchambers (Fig. 6A bottom). Our data demonstrated a low resting $[Ca^{2+}]_i$ in the differentiated N2A cells (mean $[Ca^{2+}]_i$ value: 83 ± 8 nM, n = 14 cells; Fig. 6C), a fully relevant physiological level similar to the neuronal $[Ca^{2+}]_i$ reported *in situ*.[21,22] Glutamate release from the microchambers triggered a rapid $[Ca^{2+}]_i$ rise, in the 200–400 nm range, in each of the analysed cells (p < 0.001; Fig. 6C), which is consistent with the Ca^{2+} dynamics in neurons *in vivo*.[19]

Finally, to assess how far the released glutamate can spread following triggered microchamber opening, we monitored the $[Ca^{2+}]_i$ dynamics in N2A cells located at different distances from the targeted microchamber. We found transient changes in $[Ca^{2+}]_i$ (somata) only in cells located at <50 μm from the opened microchamber, across the targeted areas (Fig. 7 and 8A). Again, the functional effect could be detected using the OGB-1 fluorescence readout (Fig. 7A) and FLIM measurements (Fig. 7B). This was fully compatible with the spatial effects of glutamate which was applied *via* a pressurized micropipette (5 μM glutamate, Methods), with the fluorescent control of the puff (Alexa Fluor-594 inside the micropipette; Fig. 8B). These recordings demonstrated a prompt, site-specific $[Ca^{2+}]_i$ rise in differentiated N2A cells whose dynamics depended on the localization of cells towards the site of agonist release (Fig. 8C). It is noteworthy that, with a suitable adaptation of the microchamber properties, their opening could be, in principle, enacted along a moving trajectory of laser pulses, thus enabling a more comprehensive space–time control of substance release.

Conclusions

The present study provides experimental evidence indicating that the fabricated polymer microchamber arrays (PEM- and/or PLA-based) could be an efficient drug delivery system for the site-specific, geometry-bound targeting of human cells. Human N2A cells of neuronal phenotype, a highly environment-sensitive cell type, showed no detectable toxicity effects when grown on the PEM@PLA- or PLA-based film surfaces over at least ten days. This suggested (a) high biocompatibility of the film material and (b) reliable drug retention (no leakage) over days. One important advantage we observed was the successful optical addressing of individual microchambers with a focused laser beam, providing site targeting on the micron scale, without employing gold or other light-absorbing nanoparticles normally required to facilitate microchamber opening. Thus, having the precursor PEM film did not appear essential in microchamber fabrication, in the context, which should facilitate the fabrication process.

As a proof-of-concept, this study also demonstrates functional effects triggered by cargo release in live human cells of neuronal phenotype. The action was localised and repeatable on demand and could be reproduced by local puff application of the cargo. Further studies will be required to address the operational capability of polymer patterned arrays within organised tissue, *in situ* and *in vivo*, for their potential implementation towards controlled drug delivery throughout the tissue suitable for various therapeutic interventions.

Author contributions

D.A.R. and G.B.S. conceived the study and its research strategy; O.K. and K.Z. designed imaging experiments; O.K. carried out experiments and data analyses; K.Z. performed FLIM quantification; O.S. and M.G. fabricated polymer microchambers; O.S. performed SEM; all authors contributed to manuscript preparation.

Conflicts of interest

The authors declare no conflict of interests.

Acknowledgements

This work was supported by the Wellcome Trust Principal Fellowship (212251/Z/18/Z), European Research Council Advanced Grant (323113-NETSIGNAL), and Biology and Biotechnology Research Council (BB/J001473/1; all UK). Research visit of O.A.S. was funded by the Stipend of Ministry of Education and Science (Russian Federation). The authors thank Dr Andreas Lieb for a neuroblastoma cell line and valuable comments on cell cultures.

References

1 G. B. Sukhorukov and H. Mohwald, *Trends Biotechnol.*, 2007, **25**, 93–98.
2 H. Gao, O. A. Goriacheva, N. V. Tarakina and G. B. Sukhorukov, *ACS Appl. Mater. Interfaces*, 2016, **8**, 9651–9661.
3 J. H. Park, L. Gu, G. von Maltzahn, E. Ruoslahti, S. N. Bhatia and M. J. Sailor, *Nat. Mater.*, 2009, **8**, 331–336.
4 Q. Liu, C. Zhan, A. Barhoumi, W. Wang, C. Santamaria, J. B. McAlvin and D. S. Kohane, *Adv. Mater.*, 2016, **28**, 6680–6686.
5 M. N. Antipina, M. V. Kiryukhin, K. Chong, H. Y. Low and G. B. Sukhorukov, *Lab Chip*, 2009, **9**, 1472–1475.

6 M. V. Kiryukhin, S. M. Man, A. Tonoyan, H. Y. Low and G. B. Sukhorukov, *Langmuir*, 2012, **28**, 5678–5686.
7 M. Delcea, H. Mohwald and A. G. Skirtach, *Adv. Drug Delivery Rev.*, 2011, **63**, 730–747.
8 M. N. Antipina and G. B. Sukhorukov, *Adv. Drug Delivery Rev.*, 2011, **63**, 716–729.
9 A. Munoz Javier, P. del Pino, M. F. Bedard, D. Ho, A. G. Skirtach, G. B. Sukhorukov, C. Plank and W. J. Parak, *Langmuir*, 2008, **24**, 12517–12520.
10 A. M. Pavlov, B. G. De Geest, B. Louage, L. Lybaert, S. De Koker, Z. Koudelka, A. Sapelkin and G. B. Sukhorukov, *Adv. Mater.*, 2013, **25**, 6945–6950.
11 O. Kopach, K. Zheng, L. Dong, A. Sapelkin, N. Voitenko, G. B. Sukhorukov and D. A. Rusakov, *Drug Delivery*, 2018, **25**, 435–447.
12 G. B. Sukhorukov, A. L. Rogach, B. Zebli, T. Liedl, A. G. Skirtach, K. Kohler, A. A. Antipov, N. Gaponik, A. S. Susha, M. Winterhalter and W. J. Parak, *Small*, 2005, **1**, 194–200.
13 L. J. De Cock, S. De Koker, B. G. De Geest, J. Grooten, C. Vervaet, J. P. Remon, G. B. Sukhorukov and M. N. Antipina, *Angew. Chem., Int. Ed. Engl.*, 2010, **49**, 6954–6973.
14 M. V. Kiryukhin, S. R. Gorelik, S. M. Man, G. S. Subramanian, M. N. Antipina, H. Y. Low and G. B. Sukhorukov, *Macromol. Rapid Commun.*, 2013, **34**, 87–93.
15 M. Gai, J. Frueh, V. L. Kudryavtseva, A. M. Yashchenok and G. B. Sukhorukov, *ACS Appl. Mater. Interfaces*, 2017, **9**, 16536–16545.
16 H. H. Lau, R. Murney, N. L. Yakovlev, M. V. Novoselova, S. H. Lim, N. Roy, H. Singh, G. B. Sukhorukov, B. Haigh and M. V. Kiryukhin, *J. Colloid Interface Sci.*, 2017, **505**, 332–340.
17 M. Gai, J. Frueh, T. Tao, A. V. Petrov, V. V. Petrov, E. V. Shesterikov, S. L. Tverdokhlebov and G. B. Sukhorukov, *Nanoscale*, 2017, **9**, 7063–7070.
18 M. Gai, J. Frueh, V. L. Kudryavtseva, R. Mao, M. V. Kiryukhin and G. B. Sukhorukov, *Sci. Rep.*, 2016, **6**, 37000.
19 J. P. Reynolds, K. Zheng and D. A. Rusakov, *Neurosci. Lett.*, 2019, **689**, 26–32.
20 L. P. Savtchenko, L. Bard, T. P. Jensen, J. P. Reynolds, I. Kraev, N. Medvedev, M. G. Stewart, C. Henneberger and D. A. Rusakov, *Nat. Commun.*, 2018, **9**, 3554.
21 K. Zheng, L. Bard, J. P. Reynolds, C. King, T. P. Jensen, A. V. Gourine and D. A. Rusakov, *Neuron*, 2015, **88**, 277–288.
22 R. Scott, A. Ruiz, C. Henneberger, D. M. Kullmann and D. A. Rusakov, *J. Neurosci.*, 2008, **28**, 7765–7773.
23 T. P. Jensen, K. Zheng, O. Tyurikova, J. P. Reynolds and D. A. Rusakov, *Cell Calcium*, 2017, **64**, 102–108.
24 K. Zheng, T. P. Jensen and D. A. Rusakov, *Nat. Protoc.*, 2018, **13**, 581–597.
25 A. Elmann, A. Telerman, R. Ofir and Y. Kashman, *J. Mol. Neurosci.*, 2017, **62**, 99–105.
26 A. Rajabian, M. T. Boroushaki, P. Hayatdavoudi and H. R. Sadeghnia, *DNA Cell Biol.*, 2016, **35**, 666–679.
27 V. Reffatto, J. D. Rasinger, T. S. Carroll, T. Ganay, A. K. Lundebye, I. Sekler, M. Hershfinkel and C. Hogstrand, *Arch. Toxicol.*, 2018, **92**, 1189–1203.
28 Y. Fang, C. Y. Iu, C. N. Lui, Y. Zou, C. K. Fung, H. W. Li, N. Xi, K. K. Yung and K. W. Lai, *Sci. Rep.*, 2014, **4**, 7074.
29 J. Nicolas, S. Mura, D. Brambilla, N. Mackiewicz and P. Couvreur, *Chem. Soc. Rev.*, 2013, **42**, 1147–1235.
30 P. Tryoen-Toth, D. Vautier, Y. Haikel, J. C. Voegel, P. Schaaf, J. Chluba and J. Ogier, *J. Biomed. Mater. Res.*, 2002, **60**, 657–667.
31 X. Sun, X. Shi, L. Lu, Y. Jiang and B. Liu, *Mol. Med. Rep.*, 2016, **13**, 2215–2220.
32 J. B. van der Valk and H. P. Vijverberg, *Amino Acids*, 1991, **1**, 91–95.
33 O. Tyurikova, K. Zheng, A. Rings, A. Drews, D. Klenerman and D. A. Rusakov, *Brain Res. Bull.*, 2018, **136**, 85–90.

ВИСНОВКИ

У дисертаційній роботі представлені результати комплексного дослідження клітинних та молекулярних спінальних механізмів хронічного болю; ідентифіковано порушення динамічного обігу AMPA-рецепторів як центральний механізм, що опосередковує підтримання хронічного болю різного генезу, з'ясовано молекулярний механізм таких порушень та запропоновано нові підходи для полегшення хронічних больових синдромів із мінімальною кількістю побічних ефектів, які базуються на корекції виявлених порушень.

1. Тривале периферичне запалення викликає зменшення популяції GluR2-вмісних AMPA-рецепторів у синапсах між первинними аферентами та ноцицептивними нейронами спинного мозку. Показано, що в основі такого зменшення лежить вилучення (інтерналізація) GluR2-вмісних AMPA-рецепторів із постсинаптичної мембрани.
2. Описаний молекулярний механізм, що опосередковує інтерналізацію синаптичних GluR2-вмісних AMPA-рецепторів при периферичному запаленні, та охарактеризовано каскад внутрішньоклітинних білків (старгазин, ABP/GRIP, PICK1 та протеїнкіназа C підтипу α), залучених у цей процес.
3. У нейронах дорзального рогу (ДР) спинного мозку функціонує чисельна популяція позасинаптичних AMPA-рецепторів, у яких за фізіологічних умов домінують GluR2-вмісні рецептори, що визначає відносно низьку проникність позасинаптичних AMPA-рецепторів для іонів кальцію. Сенсорні нейрони різних типів у спинному мозку щурів експресують AMPA-рецептори подібного складу. При периферичному запаленні кількість Ca^{2+}-проникних AMPA-рецепторів у позасинаптичних мембранах збільшується.

4. Тривале периферичне запалення посилює вбудовування GluR1-вмісних Ca^{2+}-проникних AMPA-рецепторів у позасинаптичні ділянки мембрани нейронів ДР спинного мозку. Механізм такого вбудовування є PKCα-залежним.
5. Порушення динамічного обігу AMPA-рецепторів у нейронах ДР призводять до змін у балансі між збудженням та гальмуванням у нейронних мережах, що спричиняє сенситизацію ДР спинного мозку.
6. Порушення трафікінгу AMPA-рецепторів у найронах ДР мають місце при больових синдромах різного генезу (як периферичного, так і центрального походження). Гіперзбудливість (сенситизація) мереж ДР спинного мозку є результатом посилення збуджуючої синаптичної передачі та послаблення синаптичного гальмування. Такі зміни є клітинноспецифічними, а саме зміщення балансу у бік збудження адаптивних нейронів (переважно збуджуючі інтернейрони) та посилене синаптичне інгібування нейронів тонічного типу (гальмівні інтернейрони).
7. Розроблено метод цільової доставки у поперековий відділ спинного мозку для таргетування нейронів ДР з метою терапії хронічного болю. Отримані дані демонструють терапевтичний ефект фармакологічного блокування Ca^{2+}-проникних AMPA-рецепторів інгібіторами нового покоління (активаційно-залежними блокаторами) на полегшення больового синдрому з мінімальними побічними ефектами.
8. Показано терапевтичний вплив фармакологічного блокування PKCα як мішені для корегування порушеного трафікінгу AMPA-рецепторів у нейронах ДР спинного мозку та полегшення хронічного болю при тривалому периферичному запаленні.
9. Запропоновано застосування генної терапії хронічного болю. Продемонстровано терапевтичні ефекти нокдауну PKCα у поперековому відділі спинного мозку на полегшення запального болю у

експериментальних тварин та обґрунтовано ефективність такого підходу на клітинному рівні.

Отримані дані демонструють причинно-наслідкові зв’язки між порушеннями регуляції динамічного обігу AMPA-рецепторів у нейронах ДР спинного мозку та розвитком і підтриманням хронічного болю, а також науково обґрунтовують впровадження нових підходів у стратегію лікування хронічних больових синдромів із врахуванням ключової ролі центральних механізмів у підтриманні хронічного болю різного походження.

ДОДАТОК 1

СПИСОК ПУБЛІКАЦІЙ ЗА ТЕМОЮ ДИСЕРТАЦІЇ

1. Park JS, Voitenko N, Petralia RS, Guan X, Xu JT, Steinberg JP, Takamiya K, Sotnik A, **Kopach O**, Huganir RL, Tao YX. Persistent inflammation induces GluR2 internalization via NMDA receptor-triggered PKC activation in dorsal horn neurons. (2009). *Journal of Neuroscience,* 29(10), 3206-3219. (*Особисто дисертантом проведено частину електрофізіологічних досліджень, статистичну обробку та інтерпретування результатів*).
2. **Kopach O**, Kao SC, Petralia RS, Belan P, Tao YX, Voitenko N. (2011). Inflammation alters trafficking of extrasynaptic AMPA receptors in tonically firing lamina II neurons of the rat dorsal horn. *Pain*, 152(4), 912-923. (*Особисто дисертантом проведено електрофізіологічні та флуоресцентні дослідження, статистичний аналіз та інтерпретування результатів, формулювання висновків та підготовку матеріалів до друку*).
3. **Kopach O**, Viatchenko-Karpinski V, Belan P, Voitenko N. (2012). Development of inflammatory-induced hyperalgesia and allodynia is accompanied by upregulation of extrasynaptic AMPA receptors in tonically firing lamina II dorsal horn neurons. *Frontiers in Physiology,* 3: 391. doi:10.3389/fphys.2012.00391 (*Особисто дисертантом проведено експериментальні дослідження, статистичний аналіз результатів та оформлення статті*).
4. **Kopach O**, Viatchenko-Karpinski V, Atianjoh FE, Belan P, Tao YX, Voitenko N. (2013). PKCα is required for inflammation-induced trafficking of extrasynaptic AMPA receptors in tonically firing lamina II dorsal horn neurons during the maintenance of persistent inflammatory pain. *Journal of Pain,* 14(2), 182-192. (*Особисто дисертантом проведено електрофізіологічні та частину поведінкових експериментів, статистичний аналіз та інтерпретування результатів, оформлення статті*).

5. **Kopach O**, Voitenko N. (2013). Extrasynaptic AMPA receptors in dorsal horn: evidence and functional significance. *Brain Research Bulletin*. 93, 47-56. (*Особисто дисертантом проведено аналіз даних літератури, оформлення ілюстрацій та написання статті*).
6. **Kopach O**, Krotov V, Belan P, Voitenko N. (2015). Inflammatory-induced changes in synaptic drive and postsynaptic AMPARs in lamina II dorsal horn neurons are cell-type-specific. *Pain,* 156(3), 428-438. (*Особисто дисертантом проведено електрофізіологічні дослідження, інтерпретацію результатів та формулювання висновків, написання статті*).
7. Choi ML[1], Vernon J[1], **Kopach O**[1], Minett MS, Mills K, Clayton PT, Meert T, Wood JN. (2015). The Fabry disease-associated lipid Lyso-Gb3 enhances voltage-gated calcium currents in sensory neurons and causes pain. *Neuroscience Letters,* 594, 163-168. (*Особисто дисертантом проведено електрофізіологічні дослідження, їх аналіз та інтерпретування результатів, написання статті*). ([1] перший автор)
8. Luiz AP[1], **Kopach O**[1], Santana-Varela S, Wood JN. (2015). The role of Nav1.9 channels in the development of neuropathic orofacial pain associated with trigeminal neuralgia. *Molecular Pain,* 11(1), 72. (*Особисто дисертантом проведено частину експериментальних досліджень, аналіз отриманих результатів та написання статті*). ([1] перший автор)
9. **Kopach O**, Krotov V, Goncharenko J, Voitenko N. (2016). Inhibition of spinal Ca^{2+}-permeable AMPA receptors with dicationic compounds alleviates persistent inflammatory pain without adverse effects. *Frontiers in Cellular Neuroscience,* 10:50. (*Особисто дисертантом проведено частину експериментальнах досліджень, статистичний аналіз, формулювання висновків та написання статті*).
10. **Kopach O**, Medvediev V, Krotov V, Borisyuk A, Tsymbaliuk V, Voitenko N. (2017). Opposite, bidirectional shifts in excitation and inhibition in specific types of dorsal horn interneurons are associated with spasticity and pain post-

SCI. *Scientific Reports,* 7(1), 5884. doi: 10.1038/s41598-017-06049-7. (*Особисто дисертантом проведено електрофізіологічні дослідження, аналіз та інтерпретування результатів, написання статті*).

11. **Kopach O**, Krotov V, Voitenko N. (2017). Atlanto-occipital catheterization of young rats for long-term drug delivery into the lumbar subarachnoid space combined with in vivo testing and electrophysiology in situ. *Journal of Neuroscience Methods,* 290, 125-132. (*Особисто дисертантом проведено експериментальні дослідження, аналіз та інтерпретування отриманих результатів, оформлення статті*).
12. **Kopach O**, Zheng K, Dong L, Sapelkin A, Voitenko N, Sukhorukov GB, Rusakov DA. (2018). Nano-engineered microcapsules boost the treatment of peripheral pain. *Drug Delivery,* 25(1), 435-447. (*Особисто дисертантом проведено експериментальні дослідження, аналіз отриманих результатів та написання статті*).
13. **Kopach O**, Krotov V, Shysh A, Sotnic A, Viatchenko-Karpinski V, Dosenko V, Voitenko N. (2018). Spinal PKCα inhibition and gene-silencing for pain relief: AMPAR trafficking at the synapses between primary afferents and sensory interneurons. *Scientific Reports,* 8(1), 10285. doi: 10.1038/s41598-018-28512-9. (*Особисто дисертантом проведено електрофізіологічні дослідження та частину поведінкових експериментів, аналіз та інтерпретування отриманих результатів, написання статті*).
14. **Kopach O,** Zheng K, Sindeeva OA, Gai M, Sukhorukov GB, Rusakov DA. (2019). Polymer microchamber arrays for geometry-controlled drug release: a functional study in human cells of neuronal phenotype. *Biomaterials Science,* 7(6), 2358-2371. (*Особисто дисертантом проведено експериментальні дослідження, аналіз та інтерпретування отриманих результатів, оформлення статті*).

Апробація матеріалів дисертації:

1. **Kopach O**, Sindeeva O.A., Zheng K., Sukhorukov GB, Rusakov DA. Microchamber arrays for delivery of bioactive compounds: functional testing of cargo release on demand. *Main Meeting of the Physiological Society*. July 8-10, 2019, Aberdeen (United Kingdom). Публікація тез, постерна доповідь.
2. **Kopach O**, Esteras N., Rusakov DA, Abramov AY. Human stem cell models of tau-related dementia: how much are they credible for functional studies of human brain neurodegeneration? *8th Annual Meeting of the Ukrainian Biophysical Society*, Nov. 12-15 2019, Kyiv-Lutsk (Ukraine). Публікація тез, усна доповідь.
3. **Kopach O**, Esteras N., Rusakov DA, Abramov AY. Targeting glutamate receptors: a novel approach to frontotemporal dementia? *10th IBRO World Congress of Neuroscience*, 21-25 September, 2019, Daegu (Korea). Публікація тез, постерна доповідь.
4. **Kopach O**, Esteras N., Rusakov DA, Abramov AY. Electrophysiological study of the iPSC-derived cortical neurons from patients with frontotemporal dementia. UCL Queen Square Institute of Neurology, London/ICM, *Paris Conference*, October 24-26, 2018, Paris (France). Публікація тез, усна доповідь.
5. **Kopach O.**, Esteras N., Rusakov DA, Abramov AY. Pathophysiological excitability of the iPSC-derived cortical neurons from patients with frontotemporal dementia: the role of ionotropic glutamate receptors. *11th FENS Forum of Neuroscience*, July 7-11, 2018, Berlin (Germany). Публікація тез, постерна доповідь.
6. **Kopach O**., Zheng K., Dong L., Sapelkin A., Voitenko N., Sukhorukov G.B., Rusakov D.A. Nano-engineered drug encapsulation: a long-lasting, localised drug delivery in chronic pain treatment. 47th Annual Meeting of Society for Neuroscience, November 11-15, 2017, Washington, DC, USA. Публікація тез, постерна доповідь.

7. **Kopach O**., Medvediev V, Krotov V, Borisyuk A, Tsymbaliuk V, Voitenko N. Reshuffle between synaptic excitation and inhibition in specific types of the DH interneurons mediates chronic pain in the spinal cord injury-induced spasticity. VII Congress of the Ukrainian Society for Neuroscience, June 7-11, 2017, Kyiv, Ukraine. Публікація тез, усна доповідь.
8. **Kopach O.**, Pavlov A., Sanders A., Sapelkin A., Sukhorukov G.B., Rusakov D.A. Cell-targeted drug delivery to neurons using purpose-designed microcapsules. 9th IBRO World Congress of Neuroscience, July 7–11, 2015, Rio de Janeiro (Brazil). Публікація тез, постерна доповідь.
9. Belan P., Krotov V., **Kopach O.**, Voitenko N. Cell-type-specific inflammatory-induced changes in dorsal horn synaptic transmission. 44th Annual Meeting of the Society for Neuroscience, Washington, DC, USA, November 15-19, 2014. Публікація тез, постерна доповідь.
10. **Kopach O.,** Krotov V., Belan P., Voitenko N. Persistent peripheral inflammation rearranges synaptic drive and postsynaptic ampars in lamina II dorsal horn neurons in a cell-type-specific manner. 6th Congress of the Ukrainian Society for Neuroscience, Kiev, Ukraine, 4 - 8 June 2014. Публікація тез, усна доповідь.
11. Voitenko N., **Kopach O.**, Viatchenko-Karpinski V., Belan P. AMPA receptor trafficking in persistent pain: a basis for pain therapies. 6th Congress of the Ukrainian Society for Neuroscience, Kiev, Ukraine, 4 - 8 June 2014. Публікація тез, усна доповідь.
12. **Kopach O.**, Krotov V., Belan P., Voitenko N. Chronic peripheral inflammation increases excitability of neuronal network in substantia gelatinosa of spinal cord. *43nd Annual Meeting of SfN*, November 8-13, 2013, San Diego, CA (USA). Публікація тез, постерна доповідь.
13. Voitenko N., **Kopach O.**, Maistrenko A., Lushnikova I., Dosenko V., Skibo G. Anoxic preconditioning and blockage of HIF hydroxylation differently attenuates ischemia-induced changes in intracellular calcium signaling in CA1

and CA3 hippocampal neurons. *43nd Annual Meeting of SfN*, November 8-13, 2013, San Diego, CA (USA). Публікація тез, постерна доповідь.

14. **Kopach O.**, Sotnik A., Belan P., Voitenko N. Trafficking of AMPA receptors in dorsal horn neurons during persistent pain: the changes in synaptic and extrasynaptic receptor pools. *IUPS Congress 2013*. July 21-56, 2013, Birmingham (United Kingdom). Публікація тез, постерна доповідь.
15. Voitenko N., **Kopach O.**, Maistrenko A., Lushnikova I., Skibo G. Neuronal subtypes specificity of altered calcium signaling during ischemia, anoxia preconditioning, and blockage of HIF degradation in hippocampal organotypic slices. *42nd Annual Meeting of SfN*, October 13-17, 2012, New Orleans, LA (USA). Публікація тез.
16. Goncharenko Y., **Kopach O.**, Voitenko N. Selective inhibition of Ca^{2+}-permeable AMPA receptors attenuates persistent inflammatory pain and inflammatory-promoted AMPA receptors trafficking in dorsal horn neurons. *8th FENS Forum*, 14-18 July 2012, Barselona (Spain). Публікація тез, постерна доповідь.
17. **Kopach O.**, Maistrenko A., Lushnikova I., Skibo G., Voitenko N. Neuronal subtypes specificity of altered calcium signaling during ischemia, anoxia preconditioning, and blockage of HIF degradation in hippocampal organotypic slices. *8th FENS Forum*, 14-18 July 2012, Barselona (Spain). Публікація тез, постерна доповідь.
18. **Kopach O.**, Viatchenko-Karpinski V., Belan P., Tao Y.X., Voitenko N. Role of PKCα in adjusting of extrasynaptic AMPA receptors trafficking in dorsal horn neurons during persistent inflammatory pain. *Main Meeting of the Physiological Society*. July 2-5, 2012, Edinburg (United Kingdom). Публікація тез, постерна доповідь.
19. **Kopach O**., Lipina C., Vats J., Irving A., Fedirko N. Salivary acinar cells: functional expression of different cannabinoid receptor subtypes. *Main Meeting of the Physiological Society*. July 2-5, 2012, Edinburg (United

Kingdom). Публікація тез, постерна доповідь.

20. Гончаренко Ю., **Копач О.**, Войтенко Н. Використання селективних блокаторів Ca^{2+}-проникних АМПА-рецепторів для модуляції постійного периферичного болю. *VIII Міжнародна наукова конференція студентів і аспірантів "Молодь і поступ в біології"* 3-6 квітня 2012 року, Львів (Україна). Публікація тез, усна доповідь
21. Іщенко Є., Вятченко-Карпінський В., **Копач О.**, Войтенко Н. Роль протеїн кінази Cα у підтриманні хронічного запального болю, викликаного тривалим периферичним запаленням. *VIII Міжнародна наукова конференція студентів і аспірантів "Молодь і поступ в біології"* 3-6 квітня 2012 року, Львів (Україна). Публікація тез, усна доповідь.
22. Sotnic A., **Kopach O.**, Viatchenko-Karpinski V., Belan P., Voitenko N. Spinal cord protein kinase C blocking attenuates nociceptive hypersensitivity and increased Ca^{2+}-permeability of AMPARs at the synapses in dorsal horn neurons during persistent inflammation. *Young Scientists Conference "Physiology from molecules to the organisms"*, 20-21 October 2011, Kiev (Ukraine). Публікація тез.
23. **Kopach O.**, Petralia R.S., Tao Y.-X., Belan P., Voitenko N. Trafficking of extrasynaptic AMPA receptors in lamina II neurons of the spinal dorsal horn as a molecular mechanism for the persistent pain maintenance. *Научные труды III Съезда физиологов СНГ,* 1-6 октября 2011, Ялта (Украина). Публікація тез, усна доповідь.
24. **Kopach O.**, Petralia R.S., Tao Y.-X., Belan P., Voitenko N. Trafficking of AMPA receptors at extrasynaptic plasma membrane of spinal lamina II neurons during persistent inflammatory pain. *8th IBRO World Congress of Neuroscience 2011,* 14-18 July, 2011, Florence (Italy). Публікація тез, постерна доповідь.
25. Voitenko N., **Kopach O.**, Sotnic A., Viatchenko-Karpinski V., Tao Y.-X., Belan P. Trafficking of spinal AMPA receptors: a basis for future therapies of persistent pain. *8th IBRO World Congress of Neuroscience 2011,* 14-18 July,

2011, Florence (Italy). Публікація тез, постерна доповідь.

26. **Kopach O.**, Netsyk O., Voitenko N., Irving A., Fedirko N. Cannabinoid receptors activation: neurotransmition-related and unrelated peripheral effects. V Congress of the Ukrainian Society for Neuroscience. In memory of Platon Kostyuk, 6-10 June, 2011, Kiev (Ukraine). Публікація тез, постерна доповідь.
27. **Kopach O.**, Sotnic A., Viatchenko-Karpinski V., Tao Y.-X., Belan P., Voitenko N. *In vivo* silencing of spinal protein kinase Cα gene alleviates inflammation-induced hyperalgesia by adjusting a functional expression of $Ca2^{+}$-pearmeable AMPA receptors in Substantia Gelatinosa neurons. *40th Annual Meeting of SfN*, 12-17 November, 2010, San Diego (USA). 81.19/VV17. Публікація тез, постерна доповідь.
28. Voitenko N., **Kopach O.**, Sotnik A., Viatchenko-Karpinski V., Tao Y.-X., Belan P. AMPA receptor trafficking in persistent pain: a basis for future therapies. 9th International Conference on Fundamental Questions of Neuroscience “Gagra Talks”, October 13-16, 2010, Tbilisi (Georgia). Публікація тез, усна доповідь.
29. Нецик О.В., **Копач О.В.**, Федірко Н.В. Ендоканабіноїди регулюють процеси слиновиділення через модуляцію процесів кальцієвої сигналізації // *Матеріали X Українського біохімічного з’їзду*, 13-17 вересня 2010 р., м. Одеса. – *Укр. біохім. журн.* – 2010. – Т. 82, № 4 (додаток 1). – С.217–218. Публікація тез.
30. **Kopach O.,** Park J.-S., Petralia R.S., Belan P., Tao Y.-X., Voitenko N. Trafficking of extrasynaptic AMPA receptors in tonicaly firing dorsal horn neurons is involved in the maintenance of inflammatory pain. *7th FENS Forum of European Neuroscience.* July 3-7, 2009, Amsterdam (Netherlands). Публікація тез, постерна доповідь.
31. **Kopach O.**, Voitenko N., Fedirko N. Impaired mitochondria calcium signalling contributes to the development of diabetes-induced xerostomia. *Main Meeting*

of the Physiological Society. June 30-July 2, 2009, Manchester (United Kingdom). Публікація тез, постерна доповідь.

32. **Kopach O.,** Park J.-S., Petralia R.S., Sotnik A., Belan P., Tao Y.-X., Voitenko N. The extrasynaptic AMPA receptors functioning is altered under inflammatory pain. 39th Annual Meeting of SfN. Program #856.9. 17-21 October, 2009, Chicago (USA). Публікація тез, постерна доповідь.
33. Sotnik A., **Kopach O.,** Viatchenko-Karpinski V., Tao Y.-X., Belan P., Voitenko N. Protein kinase C α blocking or gene silencing in dorsal horn neurons demosntrates its major role in nociception. 39th Annual Meeting of SfN, Program #: 764.6. 17-21 October, 2009, Chicago (USA). Публікація тез, постерна доповідь.
34. **Kopach O.,** Sotnik A., Voitenko N. The extrasynaptic AMPA receptors functioning is altered under inflammatory pain. *9th International Congress of the Polish Neuroscience Society,* Warsaw, 9-12 Sept. 2009. Публікація тез, усна доповідь.
35. Voitenko N., **Kopach O.**, Sotnik A., Shang X., Belan P., Tao Y.-X.. Changes in Ca^{2+} permeability of AMPA receptors expressed on spinal dorsal horn neurons after peripheral inflammation. XXXVI Congress of Physiological Sciences, July 27-August 1, 2009, Kyoto (Japan). Публікація тез, постерна доповідь.
36. **Kopach O.,** Kruglikov I., Pivneva T., Voitenko N., Fedirko N. Mitochondria regulate Ca^{2+} influx and determine patterns of ER Ca^{2+} refilling in acinar cells. 7th European Biophysics Congress, July 11-15, 2009, Genoa, Italy. Публікація тез, постерна доповідь.
37. Sotnik A., **Kopach O.**, Belan P., Shang X., Tao Y.-X., Voitenko N.. Peripheral inflammation evokes an increase in Ca^{2+}-permeability of AMPA receptors of dorsal horn neurons due to GluR2 subunit loss. 6th FENS Forum, 12-16 July, 2008, Geneva, Switzerland. FENS Forum Abstract 189-26. Публікація тез, постерна доповідь.
38. **Kopach O.V.**, Kruglikov I.A., Voitenko N.V., Fedirko N.V. Neurotransmitter-

induced store-operated calcium entry is strictly dependent on the mitochondria functioning. *6th FENS Forum,* July, 12-16, 2008, Geneva, Switzerland. Публікація тез, постерна доповідь.

39. **Kopach O.**, Pivneva T., Kruglikov I., Voitenko N., Fedirko N. Mitochondria are essential for maintaining of store-operated Ca^{2+} influx and ER refilling under prolonged cells` stimulation. *Physiological Society International Workshop "Latest advances in ion channel techniques applied to physiological problems".* – Sept. 12-16, 2008, Shanghai, China. Публікація тез, усна доповідь.
40. Sotnik A., **Kopach O.**, Viatchenko-Karpinski V., Voitenko N.. Inflammatory hyperalgesia are accompanied by changes in AMPA receptor function. *IBRO-advanced Workshop "T-type calcium channels: from discovery to channelopathies, 25 years of research"*. June 5-7, 2008, Kiev, Ukraine. Публікація тез, усна доповідь.
41. Sotnik A., **Kopach O.,** Voitenko N. Changes in Ca^{2+}-permeability of AMPA receptors of dorsal horn neurons after peripheral inflammation. *Ukrainian-Poland Conference for Young Scientists in the frame Bogomoletz-Nencki collaboration*. Публікація тез, постерна доповідь.
42. Voitenko N., Shang X, **Kopach O.**, Sotnik A., Isaev D., Belan P., Tao Y.-X. "A switch of Ca^{2+}-impermeable AMPA receptors expressed on spinal dorsal horn neurons into Ca^{2+}-permeable AMPA receptors after peripheral inflammation", *SfN Meeting 2007* (Program #: 284.12). Публікація тез, постерна доповідь.